38 10-30-95 JS (2)

CONF-9402160--

ANL/APS/TM-15

Detectors for Third-Generation Synchrotron Sources: Workshop Report

Co-Chairs: B. Rodricks, E. M. Westbrook, P.A. Montano, and S. H. Barr

Advanced Photon Source

Argonne National Laboratory
operated by The University of Chicago for the U.S. Department of Energy under Contract W-31-109-Eng-38

Argonne National Laboratory, with facilities in the states of Illinois and Idaho, is owned by the United States government, and operated by The University of Chicago under the provisions of a contract with the Department of Energy.

Reproduced from the best available copy.

Available to DOE and DOE contractors from the
Office of Scientific and Technical Information
P.O. Box 62
Oak Ridge, TN 37831
Prices available from (615) 576-8401

Available to the public from the
National Technical Information Service
U.S. Department of Commerce
5285 Port Royal Road
Springfield, VA 22161

Distribution Category: Atomic,
Molecular, and Chemical Physics
(UC-411)

ARGONNE NATIONAL LABORATORY
9700 South Cass Avenue
Argonne, Illinois 60439

ANL/APS/TM-15

WORKSHOP ON DETECTORS FOR THIRD-GENERATION SYNCHROTRON SOURCES

Proceedings of a workshop held at
Argonne National Laboratory
February 14-15, 1994

Workshop Organizing Committee

Brian Rodricks
Edwin M. Westbrook
Pedro A. Montano
Susan H. Barr

December 1994

work sponsored by
U.S. DEPARTMENT OF ENERGY
Office of Energy Research

DISCLAIMER

Portions of this document may be illegible electronic image products. Images are produced from the best available original document.

FOREWORD

The Workshop on Detectors for Third-Generation Synchrotron Sources was hosted by the APS February 14-15, 1994. The aims of the workshop were (1) to acquaint APS users with current R&D being carried out on detectors, (2) to identify new detector systems possible during the next five years, (3) to identify new detectors theoretically possible in the future, (4) to stimulate interactions between user groups and detector developers, and (5) to obtain recommendations from expert panels on technical issues needing resolution. The two day workshop was attended by more than 100 scientists, with invited speakers from the ESRF, SPring-8, CERN, LBL, and BNL.

The organizing committee would like to thank Roy Clarke, Alain Fontaine, Sol Gruner, and Keith Moffat for chairing the discussion sessions; Dennis Mills and Gopal Shenoy for advice and suggestions; the APS User Office: (Linda Carlson, and Diane Sandberg) for local arrangements; Susan Picologlou for editing this Workshop Report; and finally, the speakers. Special thanks go to David Moncton for opening the workshop with a status report of the Advanced Photon Source. Support for the workshop was provided by the U.S Department of Energy BES-Material Science, under grant No. W-31-109-ENG-38.

CONTENTS

Progress in Detector Development at the ESRF
John Morse, ESRF 1

Detector Development at SPring-8
Masyo Suzuki and Tatzuo Ueki, RIKEN 53

Development of Gas and Silicon X-ray Detectors at BNL
Hobart Kraner and Graham Smith, Brookhaven National Laboratory 89

The Advanced Photon Source High Power Density X-ray Beam Position Monitor
Deming Shu and Tuncer M. Kuzay, Advanced Photon Source 113

Physical and Technological Aspects of Storage Phosphor Plates Made of $BaFBr:Eu^{2+}$
Andrew Harrison, Edinburgh University 153

Time-Resolved Experiments on Muscle Using Synchrotron Radiation
A. R. Faruqi, MRC Laboratory of Molecular Biology 187

CCD Area X-ray Detectors: Experiments and Possibilities
Sol M. Gruner, Princeton University 210

Amorphous Silicon-Based Imaging Detectors for Protein Crystallography
Istevan Naday, Argonne National Laboratory,
and Robert Sweet, Xerox 252

Crystallographic Data Handling and Reduction in Experiments with Extremely High Data-Acquisition Rates
Wladek Minor, Purdue University 279

Silicon Pixel Detector Development at CERN
Michael Campbell, CERN 297

APDs - Large Dynamic Range Detectors for Hard X-rays
Wolfgang Sturhahn, Advanced Photon Source 327

Application of Bulk-Grown $Cd_{1-x}Zn_xTe$ Alloys to Single-Photon X-ray Imaging
Richard C. Schirato, Raulf M. Polichar and John H. Reed,
Science Applications International Corporation 345

MBE CdTE Photoconductive Position Sensitive X-ray Detectors
Sung Shik Yoo, University of Illinois 371

Contents continued

Recent Work at Lawrence Berkeley Laboratory on Semiconductor Detectors for Synchrotron Applications
C. Rossington, B. Ludewigt, P. Luke, N. Derhacobian and J. Walton, Lawrence Berkeley Laboratory 398

The Multi-Element Mercuric Iodide Detector Array with Computer Controlled Miniaturized Electronics for EXAFS
B. E. Patt, J. S. Iwanctyk, R. Szczebiot and M. Wang, Xsirius Corporation, B. Hedman, K. O. Hodgson and T. Cox, Stanford Synchrotron Radiation Laboratory 420

Large Area Photodiodes
Marek Szawlowski and Ernesto Gramsch, Advanced Photonix 440

Agenda 461

Final List of Participants 465

John Morse

ESRF

Progress in Detector Development at the ESRF

In 1990, the ESRF Detector Group began work on scintillation detector schemes based upon i) medical X-ray Image Intensifiers (XIIs) for large sensitive areas (≈300 cm^2) and ii) scintillant screens <Ø100 mm for higher spatial resolution applications (≤50 μm FWHM). Both these approaches use the coupling of a visible light image to a CCD camera readout system. A development with Thomson Tubes Eléctroniques was funded to produce XIIs with beryllium input windows to extend their sensitive energy range down to 5 keV. The first XIIs with beryllium window and scintillator substrate have now been extensively tested at the ESRF: the absence of tails in the measured point spread function (≈150 μm FWHM, ≈1 mm FW0.1% M over a Ø200 mm input field) gives these an excellent capability to separate closely spaced diffraction peaks. An area detector of Ø110 mm input field has also been built and tested and is based upon a high resolution (PSF ≈50 μm FWHM) mammography x-ray screen directly coupled by a large aperture (f/0.87) relay lens to a CCD camera. A similar development is in progress to provide a time resolved (≈50 μsec) detector for the energy dispersive EXAFS beamline; this will be read out using a masked area-array CCD as a one-dimensional detector with fast internal-analogue buffering of data. Detailed measurements have been made on the problem of phosphor-screen-output decay times and afterglow over a dynamic range $\geq 10^4$, and this has resulted in the choice for this application of a novel low-lag ceramic phosphor. Work is in progress on evaluating new materials for high density and structured phosphor screens.

A 1Mpixel CCD camera to operate at up to 10 frames per second with a single-frame dynamic range ≥5000 is at an advanced stage of construction. The VXI electronic standard has been adopted for detector data acquisition and by March 1994, a camera interface and 256 Mbyte memory buffer will be completed. By using the VXI local bus feature, a continuous 40 Mbyte/sec update rate is available. The memory buffer will support several access modes including successive CCD frame integration and a histogramming function for other types of area detectors that are photon counters.

Photon-counting detectors under development for the ESRF include a two-dimensional microstrip gas detector, based on charge division readout in one dimension, and on a strip-by-strip basis in the second dimension at a pitch of 300 μm. The position interpolation scheme for this detector has been proven to a resolution of 1/500 over the microstrip length with readout rate >100 kcps/strip. For low-count-rate Compton scattering studies, monolithic, multielement germanium detectors are being developed, offering both good spatial resolution and energy resolution (≈1 keV) for background noise suppression for x-ray energies to >100 keV. A 30-strip test detector at 200-μm pitch is being studied to evaluate the consequences of interstrip dead zones and crosstalk; this will be followed by a 300-strip design.

ESRF

APS Detectors for 3rd Gen. Sources Workshop 14 - 15 February 1994

Developments within the ESRF Detector Group

1. X-ray Image Intensifiers: Ø215mm beryllium window device

2. Scintillant screen systems: 1-D detector for energy dispersive EXAFS
   Ø110mm camera for Microfocus beamline

3. Fast CCD camera head: 10 frames/sec 1024^2 pixels at 14 bits

4. Germanium multi-strip (200μm) high energy (30 -100 keV) detector

5. Rutherford Appleton Lab' - ESRF Area Gas Microstrip Detector

6. VXI-bus fast data acquisition: CCD interface; Histogramming Memory

J Morse, Detector Group, Experiments Division

ESRF Detector Group: *Personnel*

-Detector physics/engineering:	M Diot	
	S Gibney	
	A Koch	
	J Morse	
	J-P Moy	
- Electronics & software:	J Clément	
	P Habraken	
	J-C Labiche	
	T Mary	(ILL, until 5/94)
	J Segura	
	R Stephens	(RAL, Peak Load)
	D VanBrussel	

DETECTOR REQUIREMENTS: ESRF BEAMLINES

Detector types	BL 1 Micro focus	BL 2 Mat. Diff.	BL 3 White Beam	BL 4 High Brill.	BL 5 High Ener-gy	BL 6 Circ. Polar-ized dichro	BL 7 Surf' Diff.	BL 8 Disp-ersive. EX-AFS	BL 9 Troika Open Undul -ator	BL 10 Open BL	BL 11 Möss-bauer	BL 12 Magn' Scatt.	BL 13 Surf' SEX-AFS, Stand' Waves	BL 14 Med-ical angio' & tomo'	BL 15 Pow-der Diff.	BL 16 Topo-graphy	BL 17 Anom' Scatt.	BL 18 EX-AFS	BL 19 MAD	BL 20 Protein Macro. Cryst.	BL21 In-elastic Scatt'	BL22 X-ray Micro-scopy	BL23 Ultra-Dilute Spec'-scopy	BL24 Micro-fluore-scence
scintillator-PMT (counting mode)	*	*	*	*	*		*		*		*	*	*		*	*	*						*	
Photodiodes† (current mode)	*	*				*			*				*	*		*		*				*		
Scintillant screen - CCD	*						*	*					*			*								
X-Ray Intensifier- CCD		*	*	*													*		*	*				
1D-and-2D Gas MWPC or μstrip	*			*			*		*						*		*							
2D Image Plate	*	*	*	*	*									*	*		*		*	*				
Silicon-energy†† dispersive						*			*			*			*			*			*		*	
Germanium†† energy dispersive	*	*		*	*	*	*		*				*	*	*		*	*	*			*	*	*

† Photodiodes operating in current mode will also be used on many beamlines for beam intensity and/or position monitoring
††Includes single channel and multi-element systems (for higher counting rate or spatial resolution)
BL 11 alternative detectors are: i) avalanche diodes ii) scintillator/pulsed MCP

Last revision 8/2/94 - JM

ESRF Detector Group Developments

	X-ray Image Intensifier-CCD	Phosphor screen - CCD lens coupled camera	1D Phosphor screen- 'analog buffer' CCD camera	Multi-strip Germanium	RAL/ESRF Gas Microstrip charge division readout/strip
Application Areas	Diffraction and other 2D area imaging	Diffraction and other 2D high spatial resolution imaging	Energy Dispersive EXAFS, high intensity, fast 1D framing	Compton and high energy studies: spatial (1D) and energy resolution	Diffuse scattering: 2D, low noise, fast counting
Active Size *mm*	Al: to Ø400, Be: Ø200	Ø110	40 x (0.02 to > 0.1)	20 x 6 (30 element) 20 x 60 (300 element)	≈ 150 x 150
Number of elements	1024 x 1024 ('F3') 512 x 512 ('F4')	1000 x 1000	512	30 & 300	'y' axis: ≈300 strips 'x' axis: ≈500 fwhms
Optimum DQE %	≈90 at 15keV	≈30 for 10 to 20 keV	> 60 for 10 to25keV	>90 for 8 to 80keV	>90 at 8keV
Spatial resolution *input referred fwhm*	Be XII:180 µm, CCD: Nyquist	Screen/lens: 80 µm, CCD: Nyquist	Screen/lens: <40 µm, CCD: Nyquist	≈Nyquist(150µm active elements)	'y' axis: Nyquist-strip number 'x' axis: <500µm
Energy range *keV, >10% DQE*	Be: 6-60; Al: 20-200	6 - 30 keV	5 - 60 keV	6 to 150keV	6 - 20 (at 1 bar Xenon)
Energy resolution *keV fwhm*	none (integrating detector)	none (integrating detector)	none (integrating detector)	< 1	≈2
Exposure/sampling time *minimum, maximum seconds*	shutter limit to ≈20 ('F3')† shutter limit to ≈20 ('F4')†	shutter limit to >1000†	≈3E-6 to >1000*	<5E-8 (signal/preamp' risetime) to hours	<1E-6 to hours
Readout/dead time *seconds*	0.1 ('F3' frame readout) ≈2E-3 ('F4' frame transfer)	10 (CCD frame readout)	≈1E-5 (CCD line transfer)* 10 (CCD full frame readout)*	≈1E-6(signal shaping time)	≈1E-5 (signal processing time)
Noise	XII NEP: <0.1keV/mm2/sec	CCD readout ≈25keV/pixel	CCD readout ≈30keV/pixel	<1cpm/element	<1cpm/element
Dynamic range	>5000 ('F3') & ≈1000 ('F4')	≈50 000	≈100 000	'counting statistics'	'counting statistics'
Max. count rate per element	No limit††	No limit††	No limit††	≈10kcps (shaping time ~µsec)	≈100kcps per 'x' strip
Max. count rate 'global'	No limit††	No limit††	No limit††	≈300kcps (for 30 elements) ≈3Mcps (for 300 elements)	30Mcps (for 300 'x' strips)
Radiation tolerance	XII >>1E7 rads	phosphor screen to >1E11 rads	phosphor screen >1E7 rads	germanium crystal > 1E6 rads (?)	µstrip substrate >10Mrads (?)

Notes:

†minimum when used with µsec beam chopper, maximum is set by CCD dark current for F4 CCD (peltier cooled). F3, F4 refer to CCD camera systems under development in Detector Group.

††optical coupling to CCD adjustable by lens aperture and/or attenuating filters. Effective maximum count rate is set by dynamic range and readout time.

* area CCD operates as 1D sensor with 1 to 10 lines exposed, and fast analog signal buffer. Dead/readout time is limited by phosphor lag (1ms to 1E-3 of initial response),line transfer time and/or frame readout time. Last revision 3 Feb/94

EUROPEAN SYNCHROTRON RADIATION FACILITY
BP 22O
F - 38043 GRENOBLE CEDEX

FRANCE

X RAY IMAGE INTENSIFIER

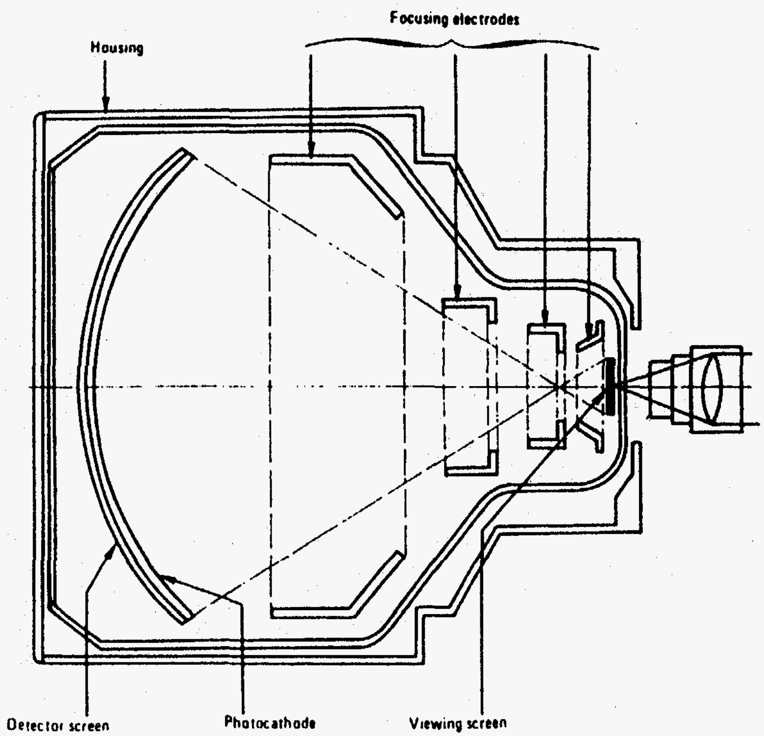

7

ESRF

COLUMNAR GROWTH OF SCINTILLATORS

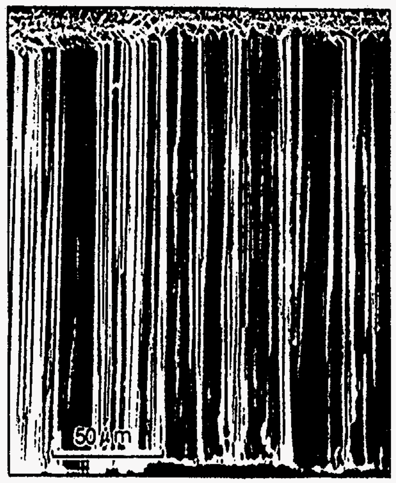

PHOTO: Electron Microscope Photograph (x 320) of CsI Input Phosphor Screen

	Be XRII, P20	Be XRII, P46	Standard 9" Al XRII, P20	Standard 9" Al XRII, P46	Standard 12" Al XRII, P20	Standard 12" Al XRII, P46
Energy range	5-25 keV	5-25 keV	20-80 keV	20-80 keV	20-80 keV	20-80 keV
useful input size	Ø200 mm	Ø200 mm	Ø200 mm	Ø200 mm	Ø270 mm	Ø270 mm
MTF @ 1.5 lp/mm	0.58	0.50 **	0.50	0.45 **	0.37 *	
MTF @ 4 lp/mm	0.10	0.08 **	0.06	0.04 **	0.02 *	
Ø of PSF @ 0.1%	1 mm	1 mm **	1.2 mm	1.4 mm**	1.5 mm**	
sensitivity (F/2 lens, CCD)	25 eV/ el.	100 eV/ el.	25 eV/ el.	100 eV/ el.	25 eV/ el.	100 eV/ el.
DQE	65% @ 10 keV	65% @ 10 keV	65% @ 40 keV*	65% @ 40 keV*	65% @ 40 keV*	65% @ 40 keV*
equiv. input dark signal	< 40 keV/s.cm^2	< 40 keV/s.cm^2	< 100 keV/s.cm^2	< 100 keV/s.cm^2	< 100 keV/s.cm^2	< 100 keV/s.cm^2
decay time to 10 %	< 1ms	< 10 µs	< 1ms	< 10 µs	< 1ms	< 10 µs
decay time to 0.1 %	500 ms	10 ms	500 ms	10 ms	500 ms	10 ms
integral distortion	< 4% *	< 4% *	< 4% *	< 4% *	< 8% *	< 8% *
recommended CCD camera	slow scan hi res fast moderate res	fast/ultra-fast	slow scan hi res fast moderate res	fast/ultra-fast	slow scan hi res fast moderate res	fast/ultra-fast
availability	mid 93	mid 93	off the shelf	custom	off the shelf	custom

All data result from measurements on real devices, except

* from THOMSON data sheet

** inferred from other measurements in different conditions; to be confirmed.

Table 1. Main characteristics of X-ray Image intensifiers to be used in the modular detectors

LAUE DIFFRACTION PATTERN
OF A LYSOSYME CRYSTAL

5 x 5 μm Beam from UNDULATOR, gap 50 mm
4 seconds exposure, Be XRII, full field, 1024^2 CCD
Log scale, 16000:1 dynamic range

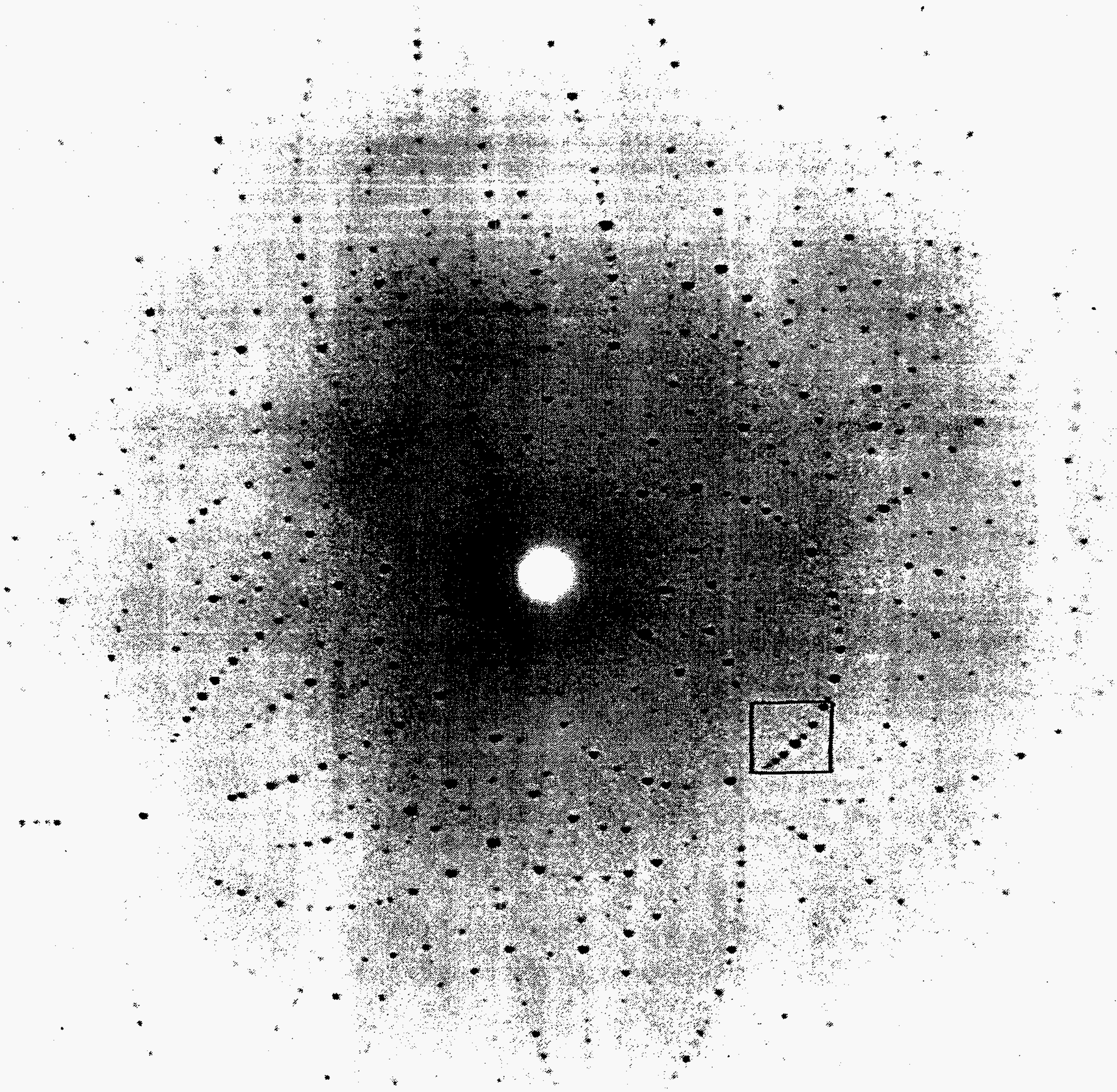

High Pressure ZrO_2 18 keV Al Be tube 1024^2 CCD
5 min exp time

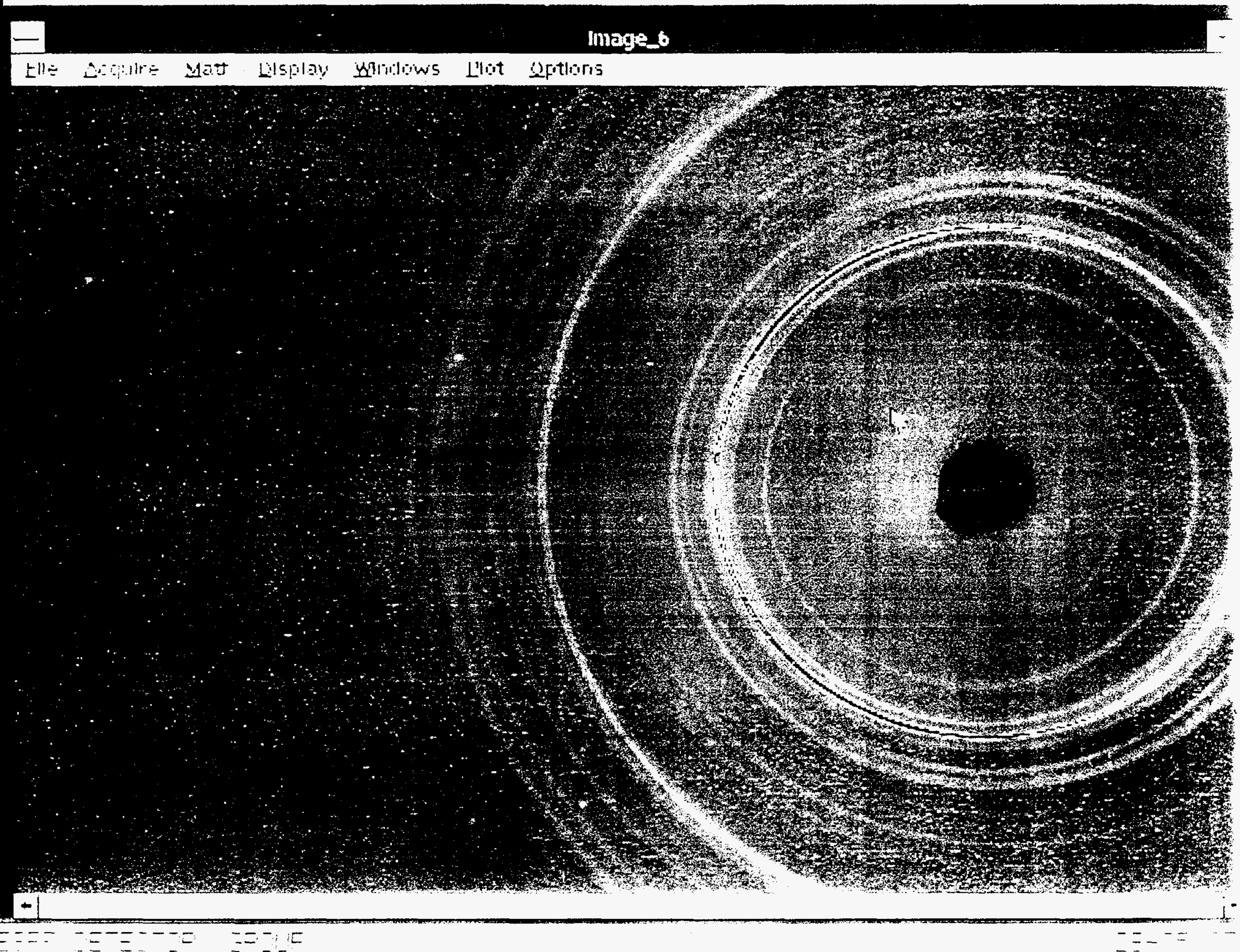

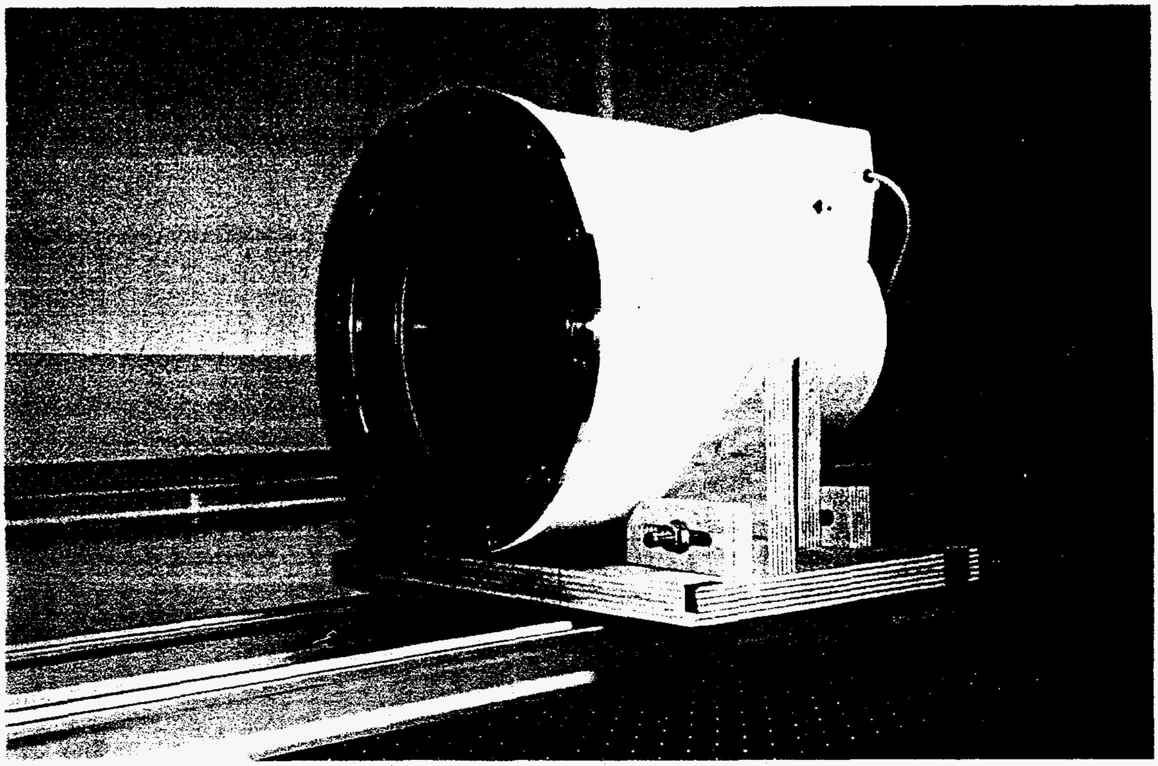

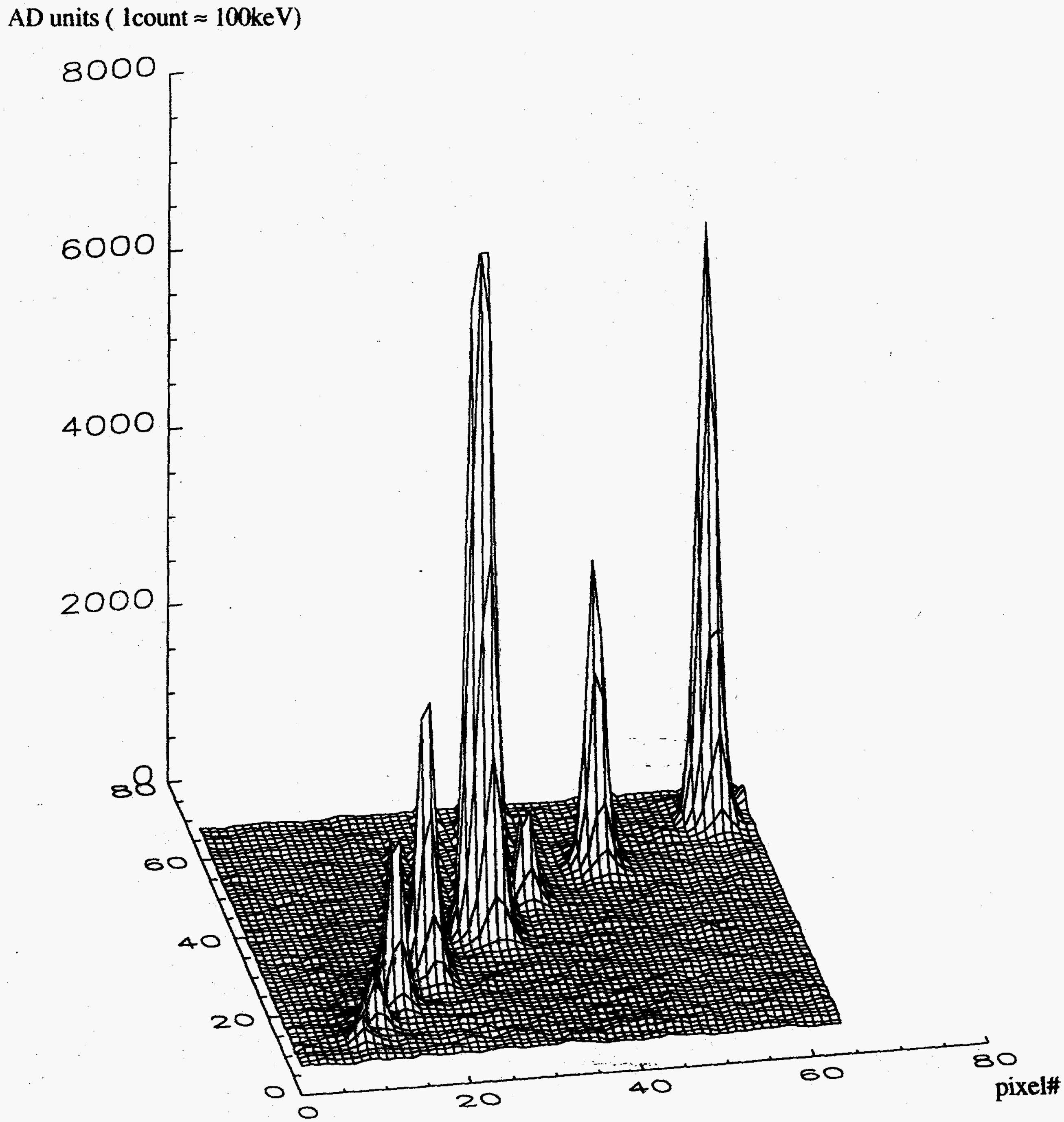

3-D plot of a 64 x 64 pixels region of the Laue diffraction pattern of a lysosyme crystal.
X-ray beam 5 x5 µm, undulator gap 50 mm, exposure time 4 seconds.

detector: Ø220 mm Be XRII optically coupled to a 1024^2 cooled CCD camera (14 bit, 200 kpel/s).

BL3, dec 94

RESOLUTION / DYNAMIC RANGE TEST

test pattern:

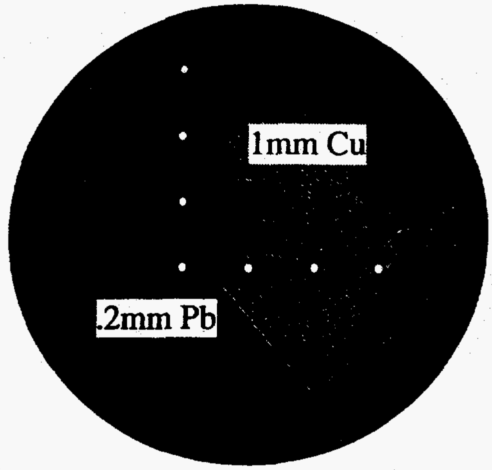

7 Ø 150 μm pinholes in 200 μm Pb foil, pitch: 1mm

Expanded 3D view from 0 to 0.5% of full scale.

central spot close to saturation, satellite spots ≈ 1/1000 of saturation contours at 0.15%, 0.10%, 0.05 %

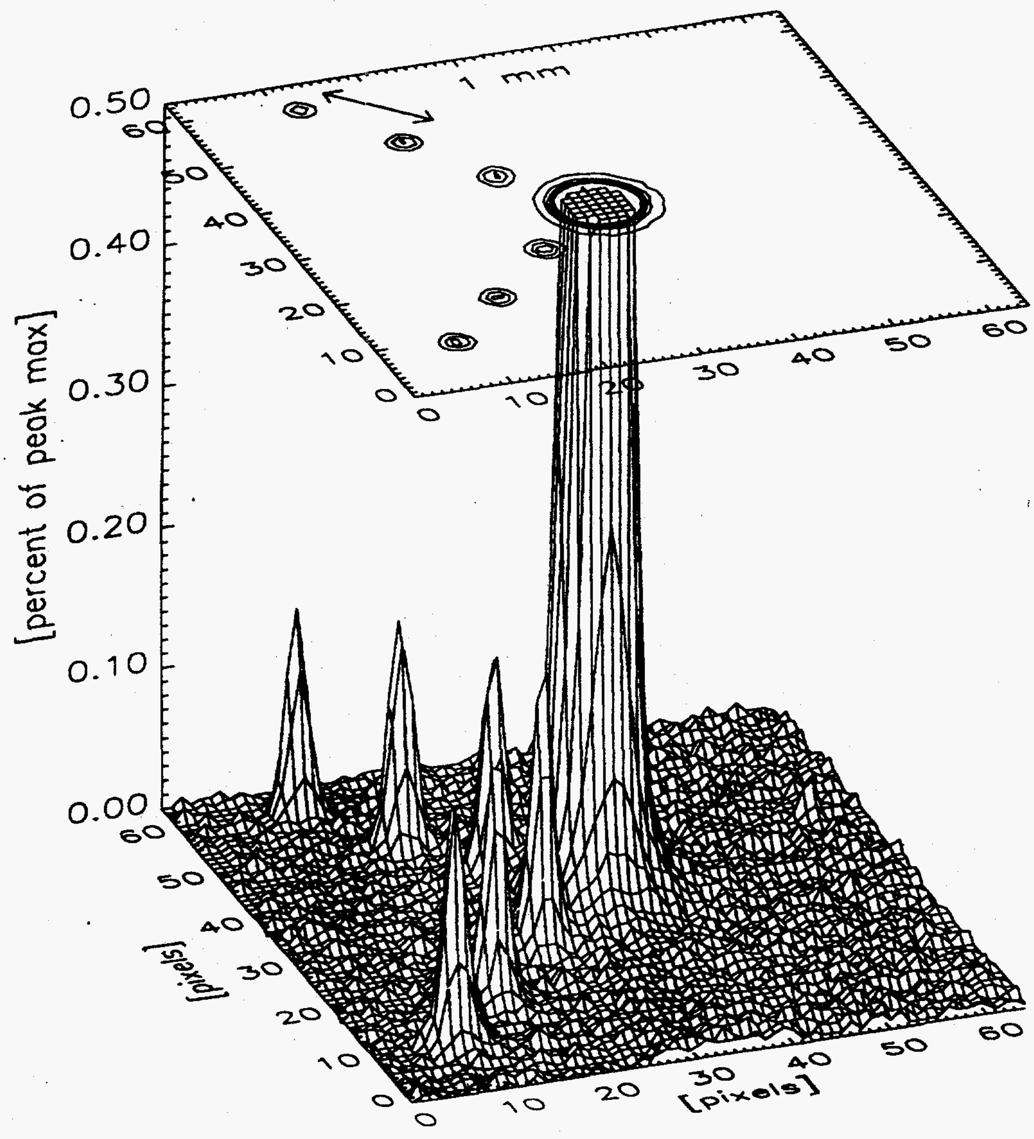

EUROPEAN SYNCHROTRON RADIATION FACILITY
BP 220
F - 38043 GRENOBLE CEDEX

COMPARED PSFs

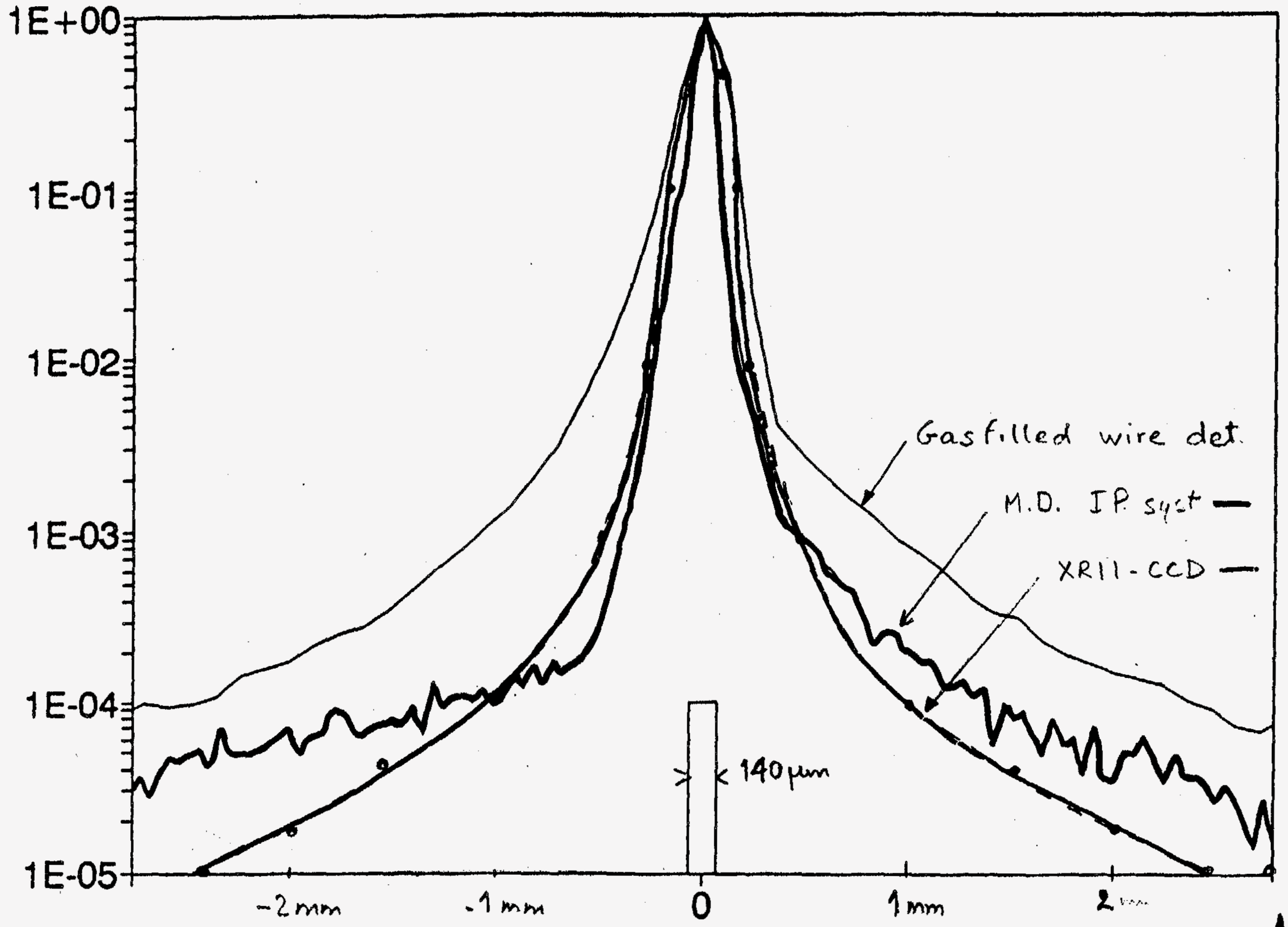

After Né, zemb ...

DISTORTION -
FIELD

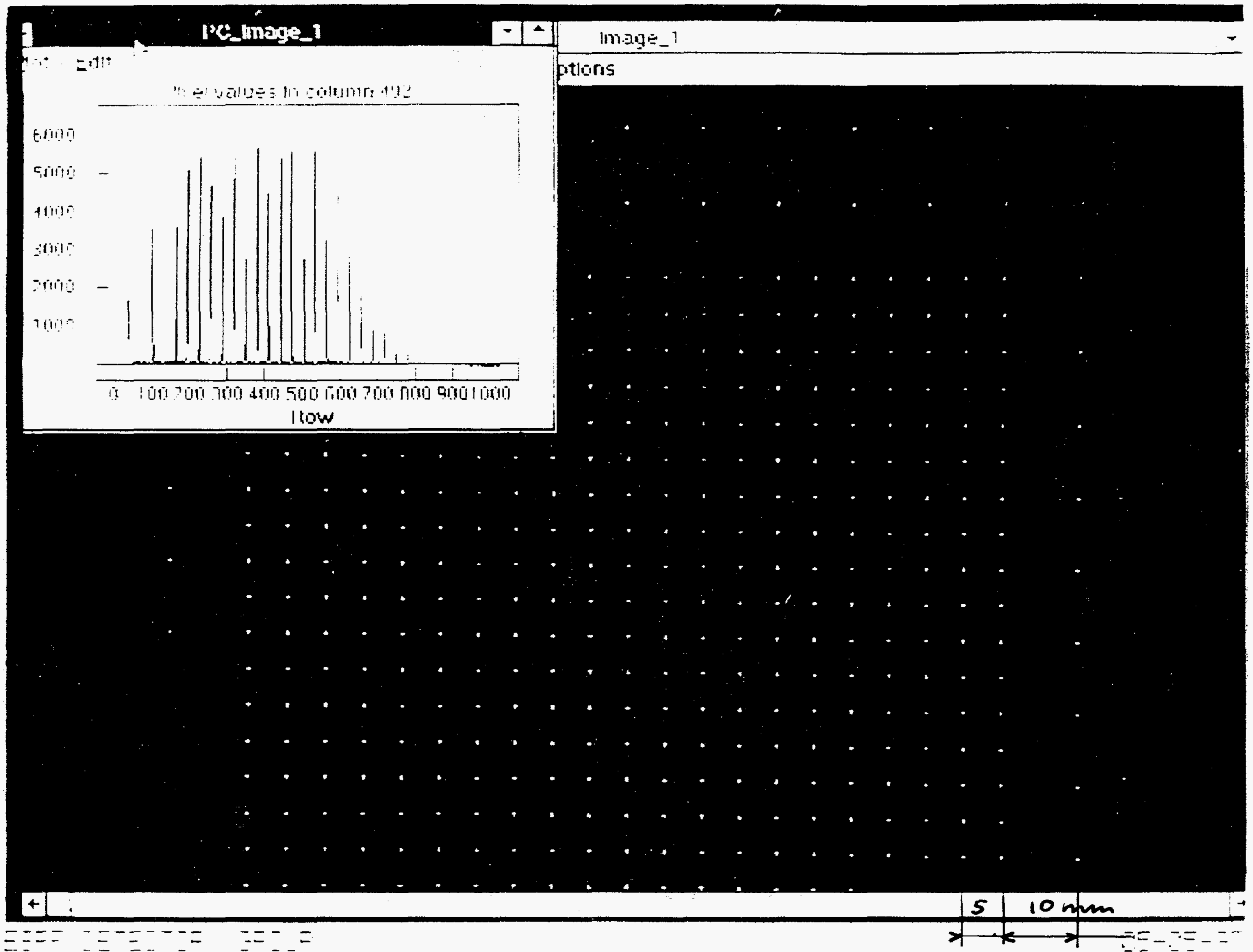

EUROPEAN SYNCHROTRON RADIATION FACILITY
BP 220
F - 38043 GRENOBLE CEDEX

FRANCE

MAIN DRAWBACKS OF THE XRII

- Convex input surface => limited diffraction angle, $< \pm 15°$,
  distortion depending on sample position
- Sensitivity to magnetic field => careful shielding required
- Non-uniformity of response => flat field correction mandatory
  (depending on sample position)
- CsI input => 33 and 36 keV edges.
  Gd based input available, but dramatic loss in resolution

EUROPEAN SYNCHROTRON RADIATION FACILITY
BP 220
F - 38043 GRENOBLE CEDEX

FRANCE

TIME RESPONSE

Governed by the CsI:Na input phosphor,
the P20 (slow, high resolution)
or P46 (fast, lower resolution) output phosphor

Typically, after a steplike excitation, fall time down to :

	10 %	0.1%
with P20	< 1ms	500 ms
with P46	< 10µs	10 ms

The P46 phosphor allows virtually lag free imaging even up to several thousand frames per second.

EUROPEAN SYNCHROTRON RADIATION FACILITY
BP 220
F - 38043 GRENOBLE CEDEX

FRANCE

FAST XRII TIME RESPONSE

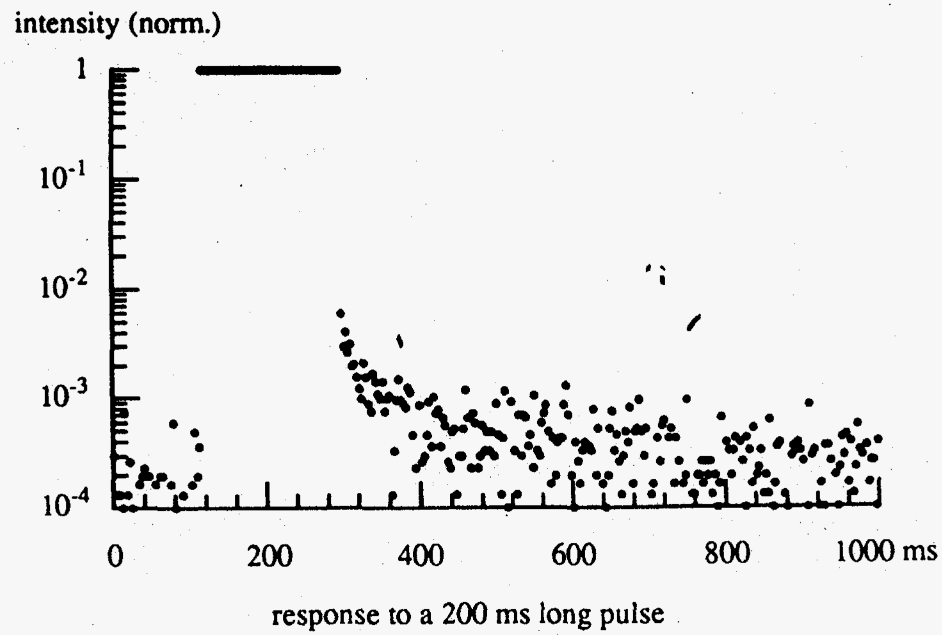

EUROPEAN SYNCHROTRON RADIATION FACILITY
BP 220
F - 38043 GRENOBLE CEDEX

FRANCE

SENSITIVITY , NOISE

Sensitivity is best expressed in number of electrons created in the CCD per input X-ray energy. It is essentially dependent on the optical coupling between the output screen and the CCD.

measured value : 170 electrons / keV
for F/D = 1
DQE ≈ 65% @ 10keV

The noise consists of a strongly non gaussian but very weak background and hot spots mainly due to cosmic rays and natural radioactivity:

background: 20-40 keV / s.cm^2 (input)

for short exposures (≈ seconds), the CCD readout noise is dominant.

Scintillant Screen-CCD cameras (A Koch)

Advantages: Flexibility of the system, scintillant screen may be easily exchanged:
- -efficiency vs. time response
- -efficiency vs. spatial resolution
- -absorption edges

No image intensifier gain stage:
- -source of additional noise removed
- -simple absorption corrections (flat detection surface)
- -rigorous image stability and simple geometric corrections, insensitive to **B** fields

High radiation tolerance possible
- -tests on ID11 wiggler white beam to >100Mrads

Disadvantages: Limited size of detector
- -light collection efficiency ~(demagnification)$^{-2}$ => practical size limit ~100cm^2
  e.g. for 10% efficient scintillator, CCD sensor at demagnification of 4, sensitivity ≈10keV/electron, field of view 80mm

Readout time ≈10 seconds for 1000 x 1000 pixels at low noise (≈5electron/pixel)

Prospects: Applications :µfocus beamline, DEXAFS, topography & microtomography (to 1µm)
radiation hard, online beam-profile monitors

structured (non isotropic) fabrication methods, low temperature scintillators

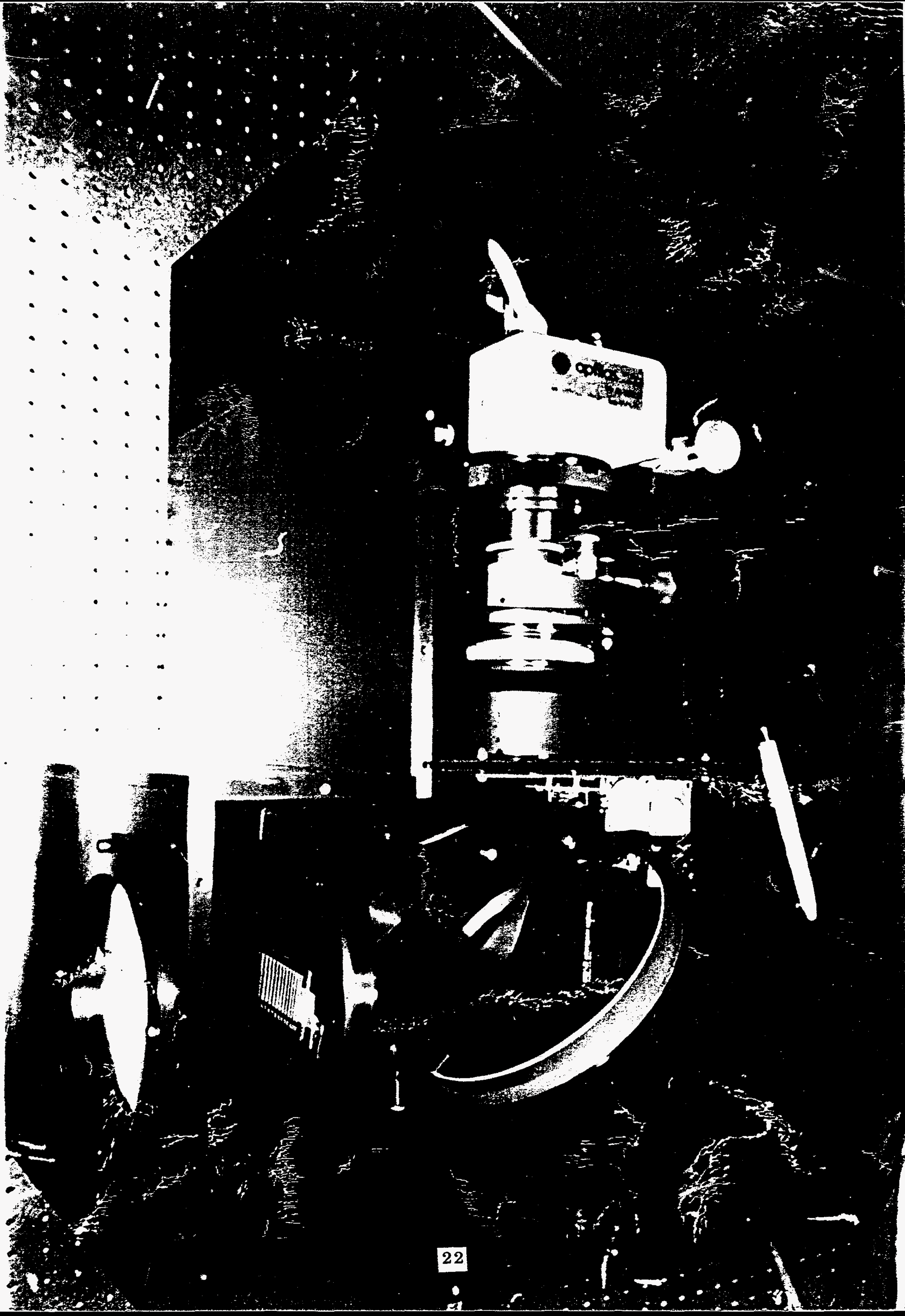

For Microfocus Beamline

ESRF

DETECTOR DESIGN

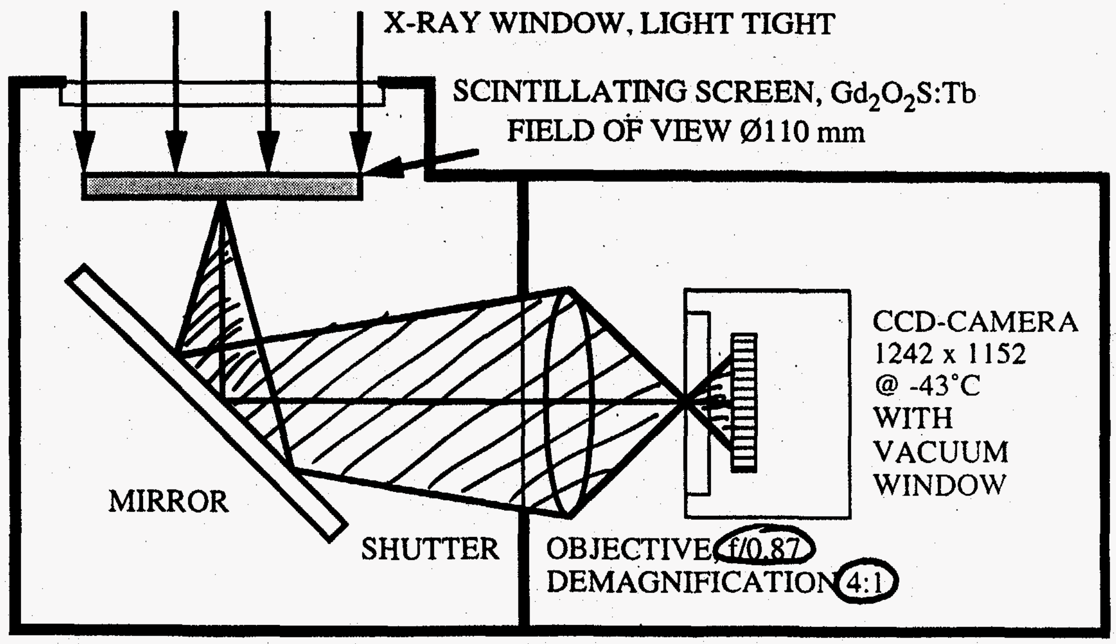

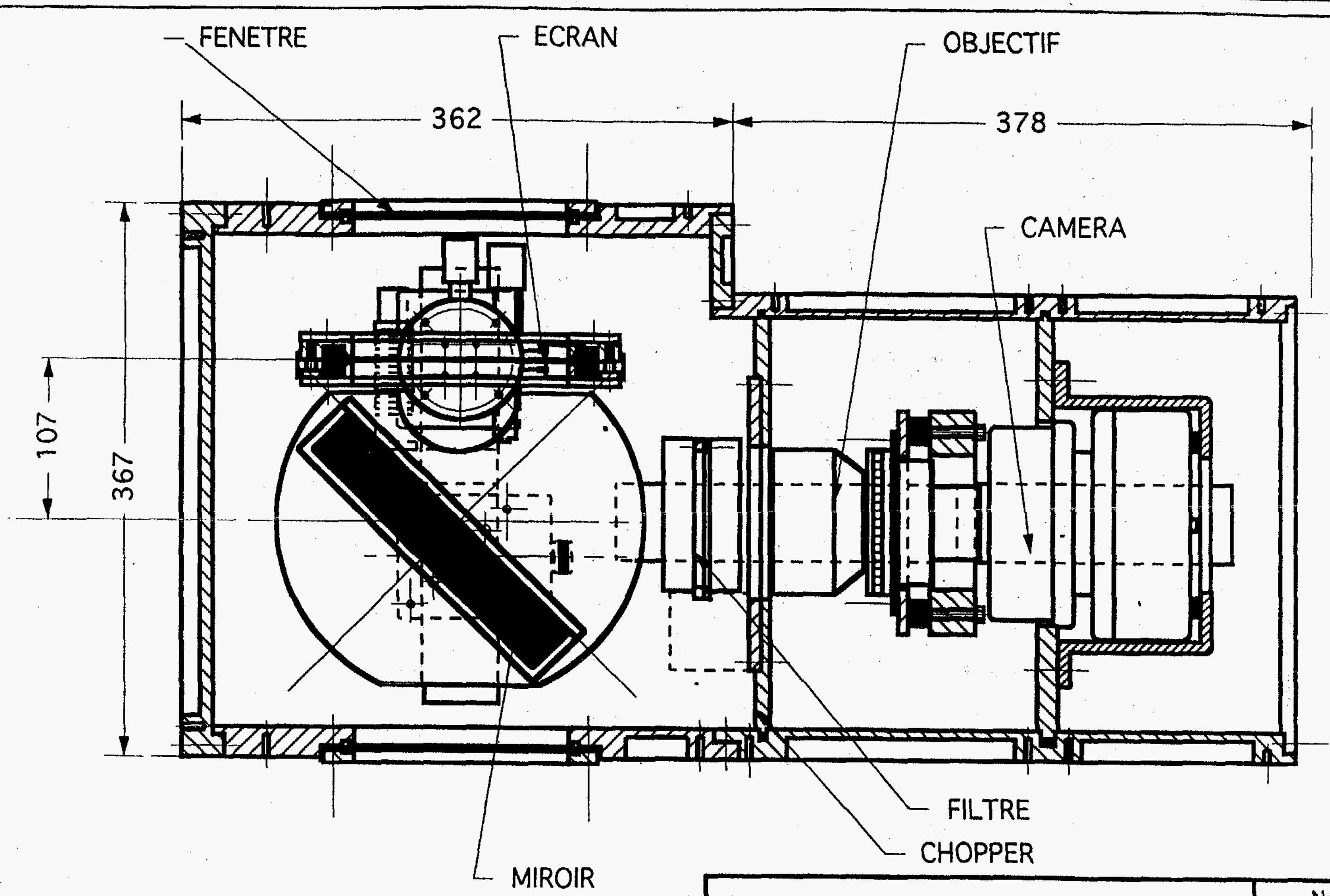

MICROFOCUS BEAMLINE CAMERA		NAME	DATE
		BEYNET	30/03/93
Ech:	EUROPEAN SYNCHROTRON RADIATION FACILITY *DETECTOR GROUP* BP 220 F-38043 GRENOBLE CEDEX TEL. 76-88-21-51 FAX 76-88-25-42	GEN.LINEAR TOL: GEN.ANGULAR TOL: GEN.SURF FINISH:	
Format: A4		N°: 001348	

ESRF

POINT SPREAD FUNCTION OF THE DETECTOR

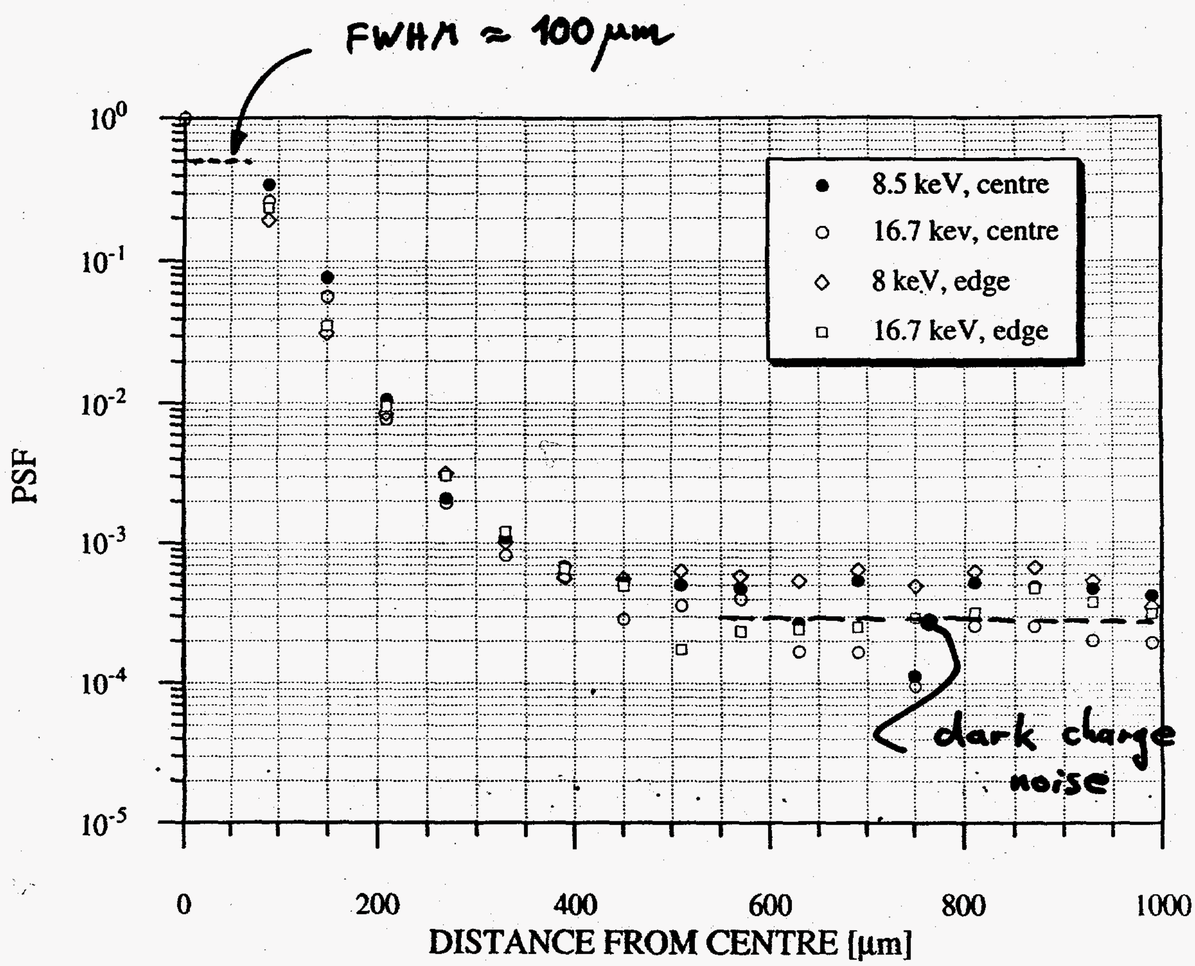

- no difference for tangential and sagittal PSF & MTF

ESRF

PERFORMANCE OF THE DETECTOR (µfocus camera)

energy range, optimized:	10 keV - 20 keV
DQE:	≈ 30% (10 keV - 20 keV) @ integrated intensity > 1×10^5 eV/mm^2/readout
equivalent input dark signal:	9×10^4 eV/mm^2/s
dynamic range:	10^4
sensitivity:	15 keV/e$^-$
field of view:	Ø110 mm
spatial resolution:	PSF @ FWHM: 100 µm, @ FW1%: 400 µm, @ FW0.1%: 650 µm MTF @ 3 lp/mm: 50%
distortion-integral:	0.4%
- differential:	<1%
pixel response non-uniformity:	1.5%, corrected by flatfielding
vignetting:	30%
readout time:	1 image/8s

<u>further potential improvements:</u>

- red emitting phosphor ----> better matched to quantum efficiency of CCD, higher DQE
- structured screens ----> better spatial resolution at higher energies
- lower temperature at CCD ----> lower dark charge, longer exposure times
- other deposition technique ----> higher density, better spatial resolution

CAMERA FOR DISPERSIVE EXAFS BEAMLINE

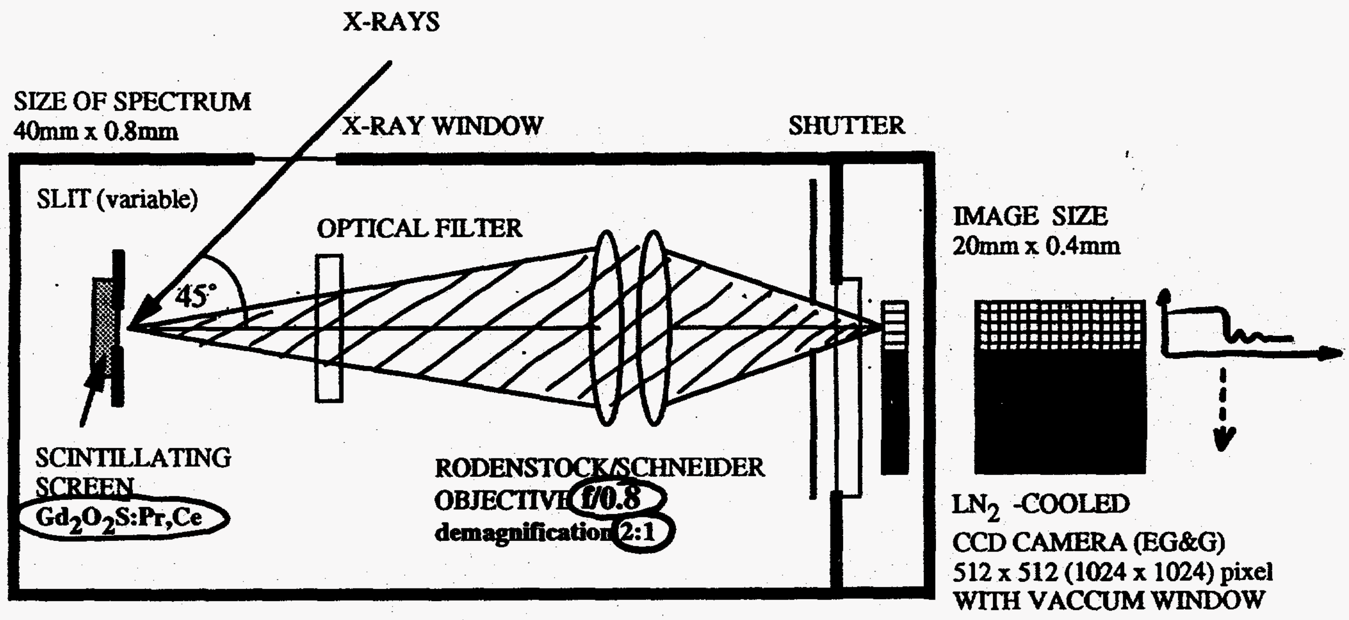

LIGHT TIGHT OPTICAL RELAY SYSTEM

essential characteristics:

- fast relay optics
- efficient phosphor
- fast luminescent decay of phosphor (--> high dynamic range)
- high spatial resolution of phosphor (--> high dynamic range)

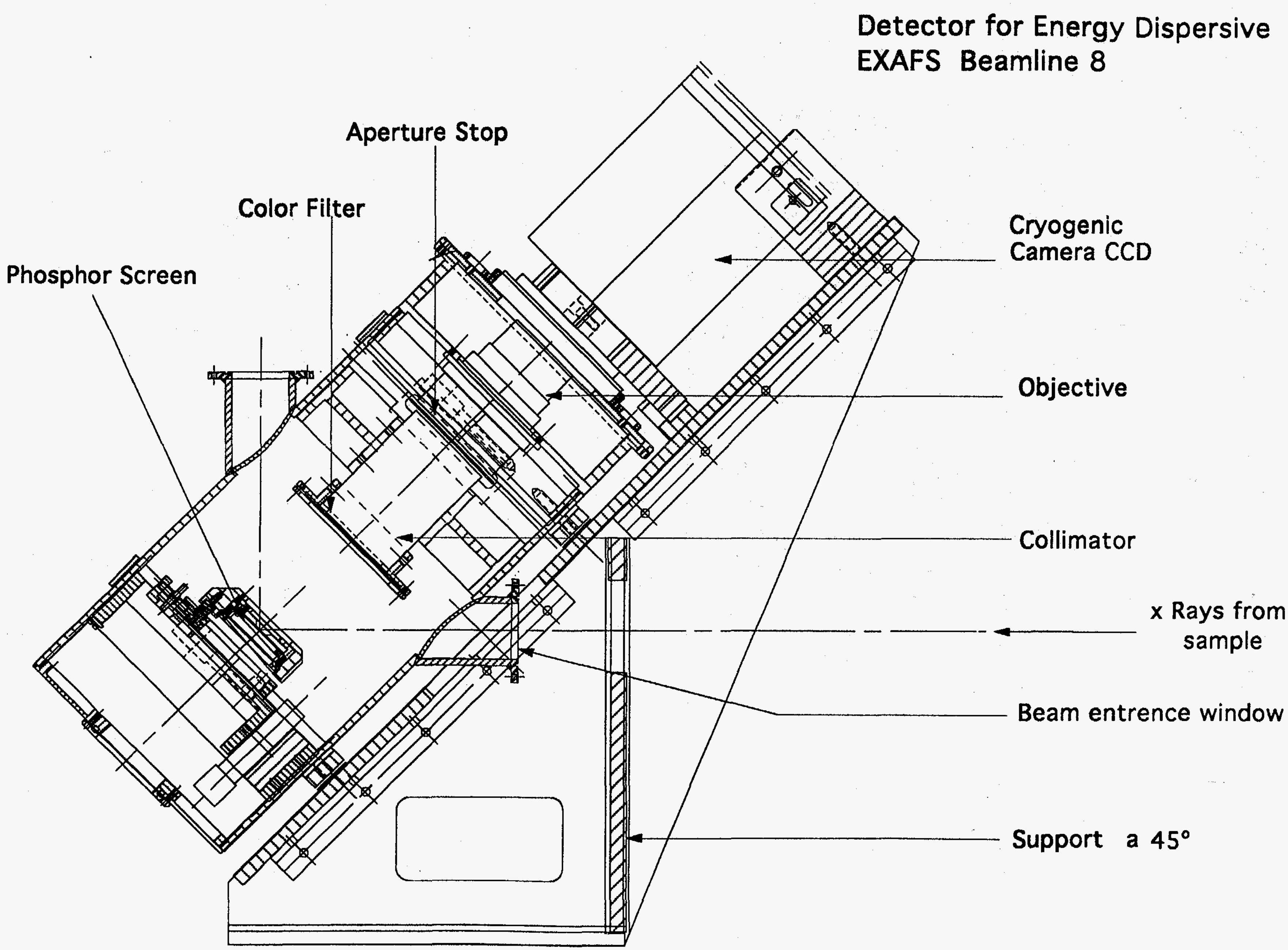
Detector for Energy Dispersive
EXAFS Beamline 8
Aperture Stop
Color Filter
Phosphor Screen
Cryogenic
Camera CCD
Objective
Collimator
x Rays from
sample
Beam entrence window
Support a 45°

TIME RESPONSE OF PHOSPHOR

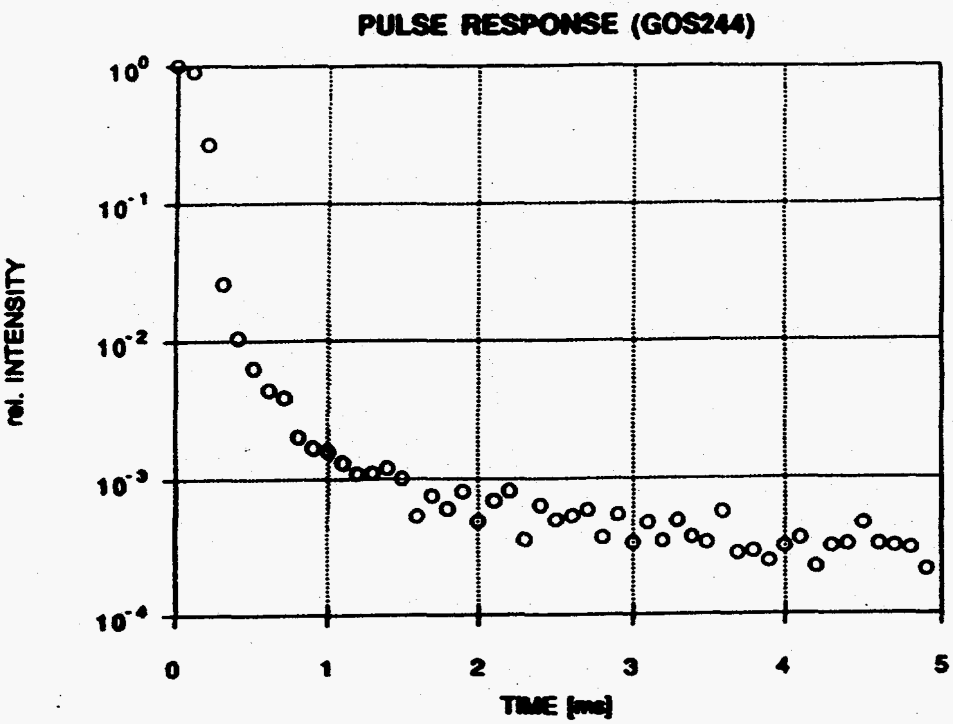

$\Delta t = 100 \mu s$

FWHM < $100 \mu s$

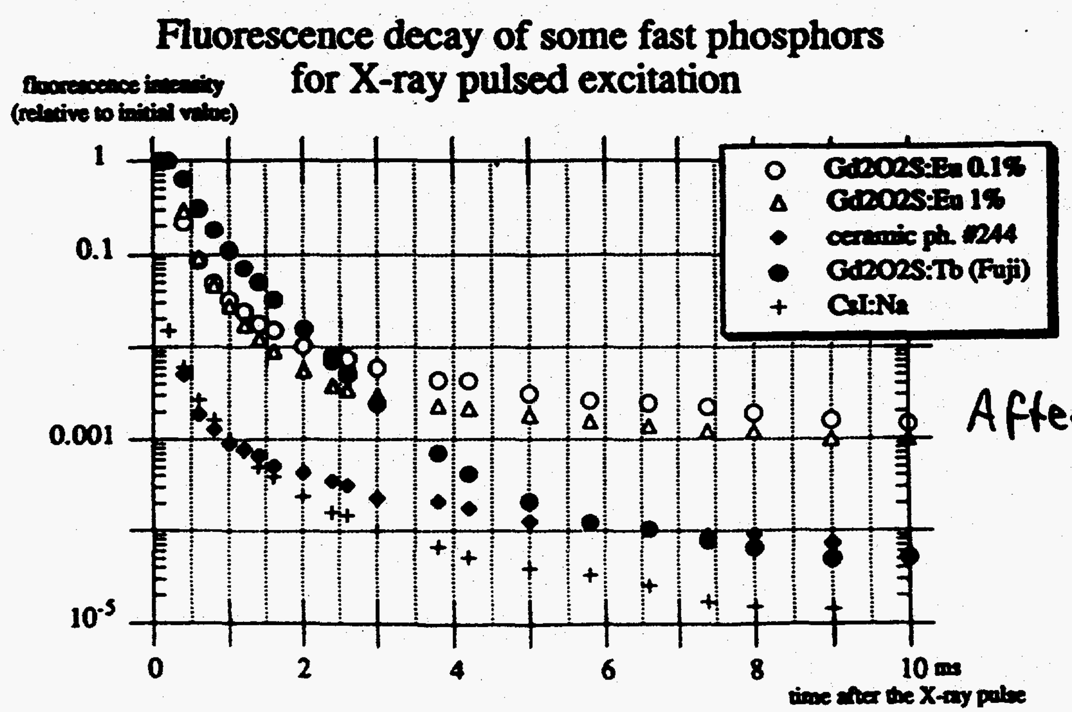

After-glow

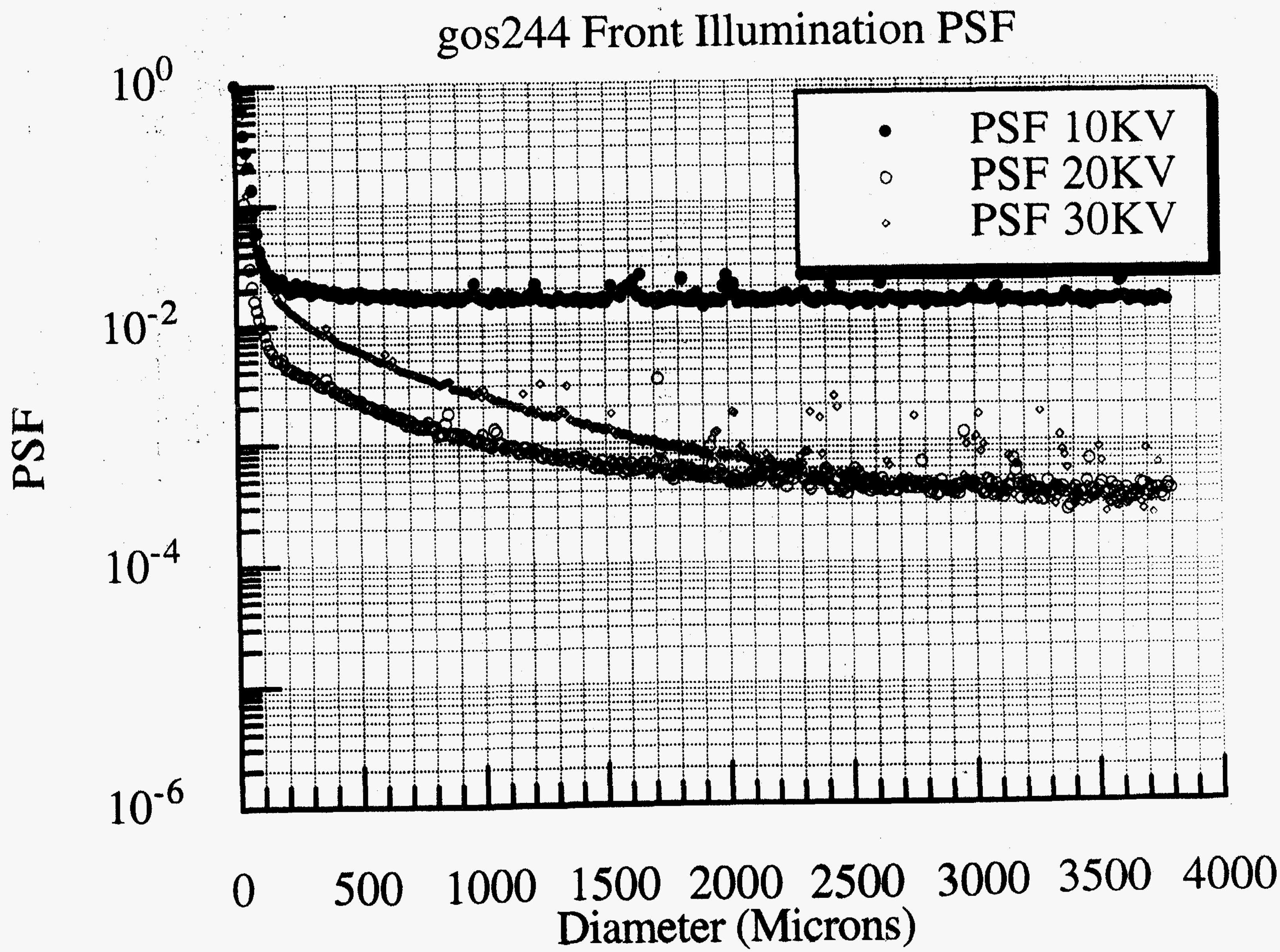
gos244 Front Illumination PSF
PSF
10^0
10^{-2}
10^{-4}
10^{-6}
PSF 10KV
PSF 20KV
PSF 30KV
0
500
1000
1500
2000
2500
3000
3500
4000
Diameter (Microns)

EXPECTED PERFORMANCE OF THE DETECTOR

- SUMMARY

energy range, optimized:	5 keV -30 keV
DQE:	≈ 50% (10 keV - 30 keV) @ integrated intensity > $6x10^5$ eV/pixel/readout
equivalent input dark signal:	20 eV/pixel/s
dynamic range:	10^4
sensitivity:	6 keV/e^-
field of view:	Ø40 mm
spatial resolution:	PSF @ FWHM: 40-50 µm
	MTF @ 12 lp/mm: 50%
distortion-integral:	0.2%
pixel response non-uniformity:	2%, to be corrected by flatfielding
vignetting:	30%
readout time:	1 image/5s

(1 pixel = 40 µm x 40 µm)

ESRF

CCD CAMERAS FOR X-RAY IMAGING

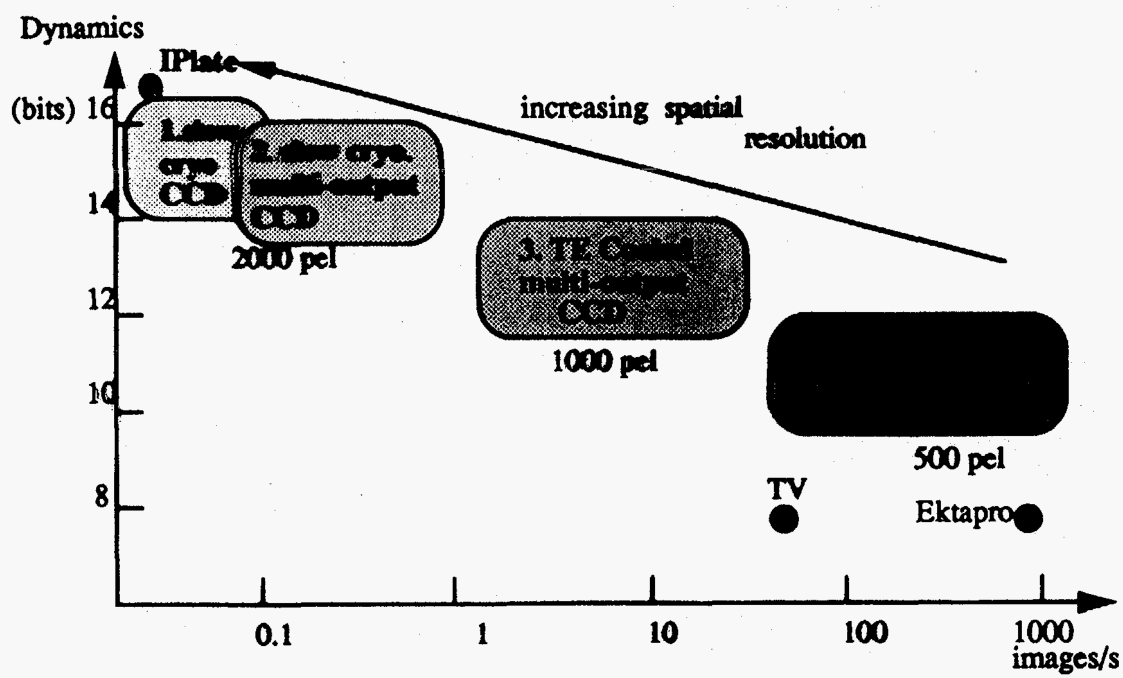

ESRF

Fast CCD Readout Projects

- 'Family 3' Thomson TH7896A
  - 4 output channels, 1024^2 full frame
  - 14 bit encoding/ 0.4µs/pixel --> 10 frames/sec

- 'Family 4' Sarnoff VCCD512H
  - 16 output channels, 512^2 frame transfer
  - 10 bit encoding/ 0.1µs/pixel --> 500 frames/sec

- Peltier-water cooled camera head, fibre-optic data transfer

- VXI : camera interface/controller and real-time monitor display
  - memory buffer 40 (400) Mbyte/sec update,
  - 256 (1024) Mbyte storage (32 bit address/data)

Sarnoff 512 x 512 16-Port CCD Imager Typical Specifications

Architecture:	512 x 512 Vertical frame transfer Back-side illumination	→ 1024 x 1024
Pixel Size:	18 x 18 µm	
Optical Fill Factor:	100%	
Quantum Efficiency:	400 nm, QE = 50% 600 nm, QE = 70% 700 nm, QE = 75% 800 nm, QE = 55%	
Output Ports:	16 output ports. Each port reads a subarray of 64(h) x 256(v) pixels	→ 32
Gamma:	1.0	
Frame Rate:	>500 fps	
Dark Readout Noise:	30 rms electrons per pixel	} DYNAMIC RANGE ~8000 AT 2mSec readout
Full Well Signal:	240,000 electrons	
Dark Current:	250 pa/cm^2 at 23 °C	
On-chip Amplifier:	Floating diffusion with correlated double sampling	
Output Impedance:	500 Ω	
Sensitivity:	3 µV/electron (C = 70 fF)	
Vertical Clock Rate:	2.5 MHz	
Horizontal Clock Rate:	>10 MHz	

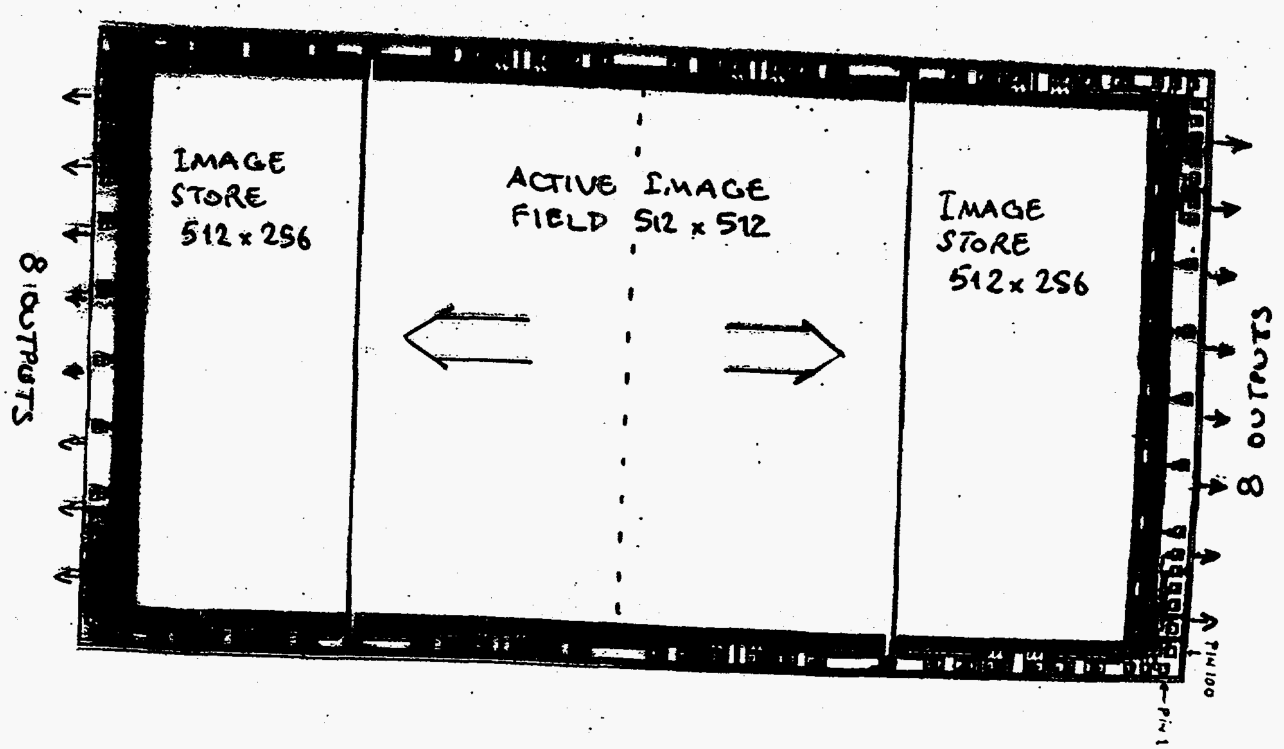

HDL512 Imager Architecture

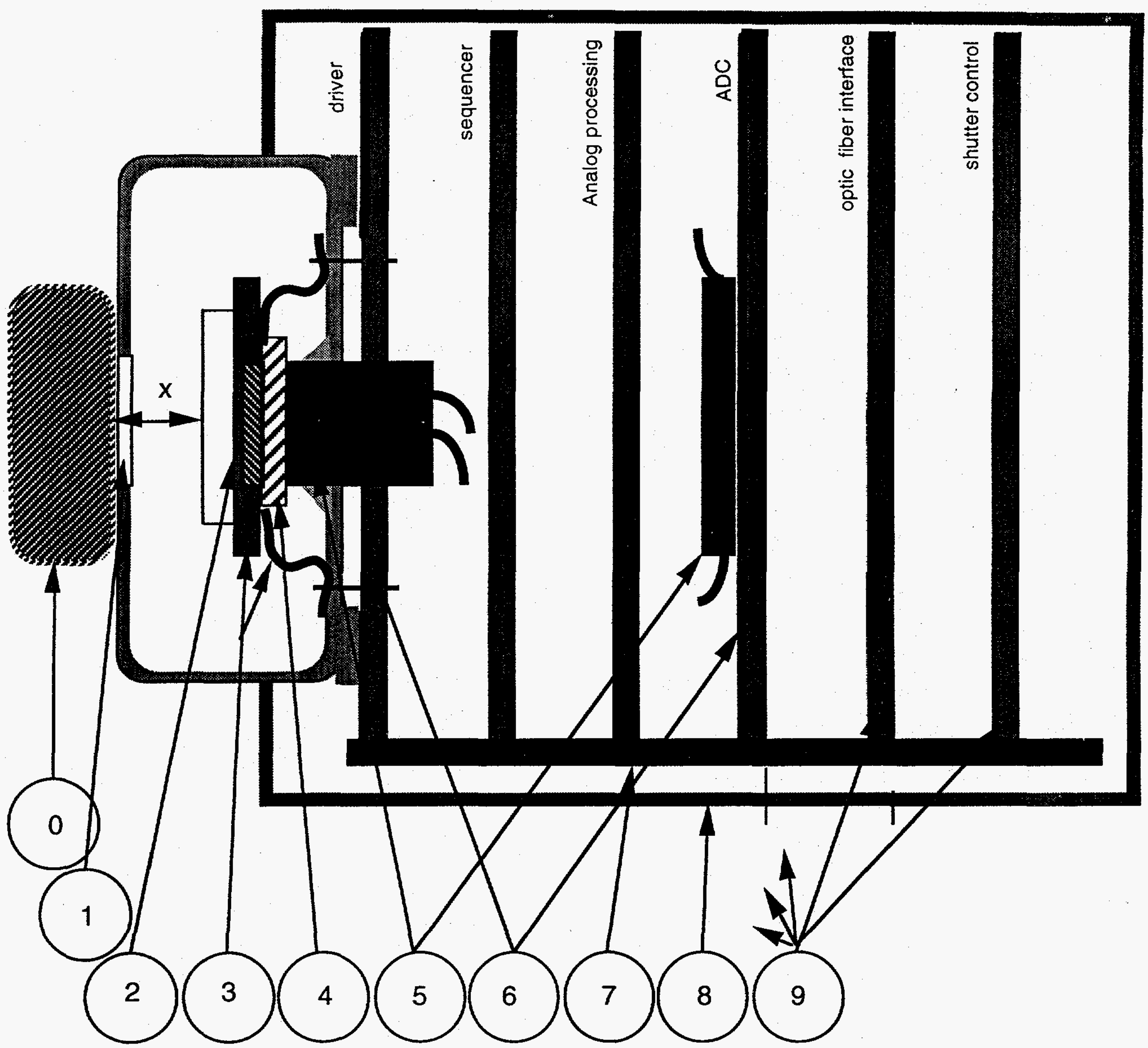

0 Ensemble optique. Fixé et alignable par rapport á la piéce 1
1 Chambre á vide ou á gaz inerte avec fenetre optique adaptable.
2 Plan du Capteur CCD.Pependicularité á l'axe < 10 µradians
3 Circuit imprimé en capton. Distance x <10mm (á préciser)
4 Etage refroidisseur peltier
5 Echangeurs de chaleur á eau
6 2 circuits imprimés avec drain thermique
7 Circuit imprimé de fond de panier
8 Chassis-boitier démontable. Protection électromagnétique
9 6 cartes circuits imprimés

ARCHITECTURE DE LA TETE DE CAMERA F3

SECTION AA

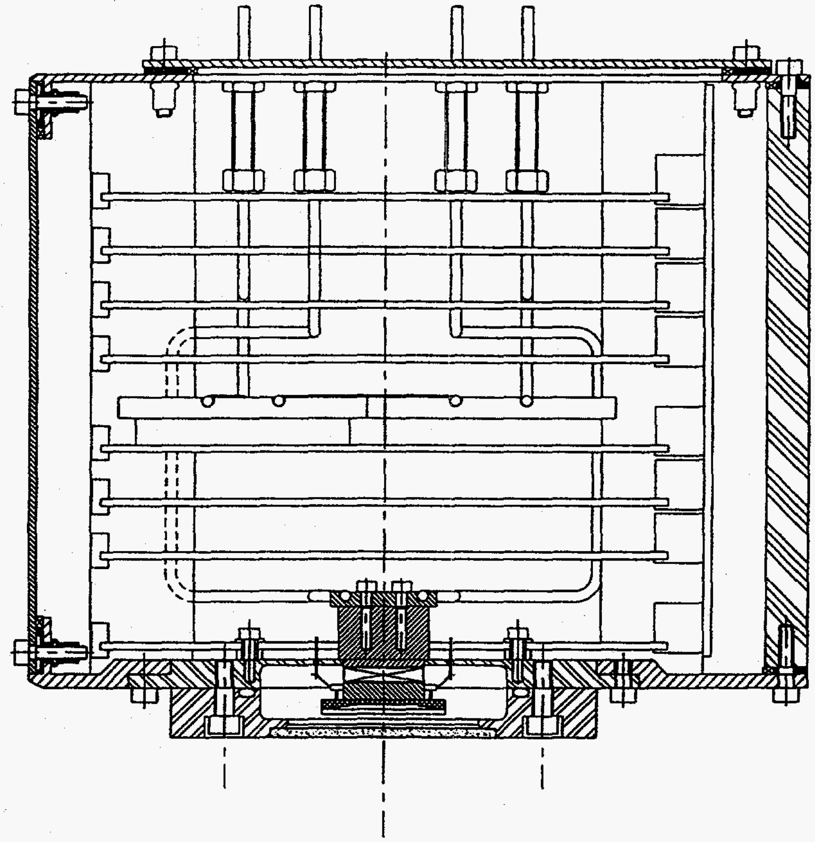

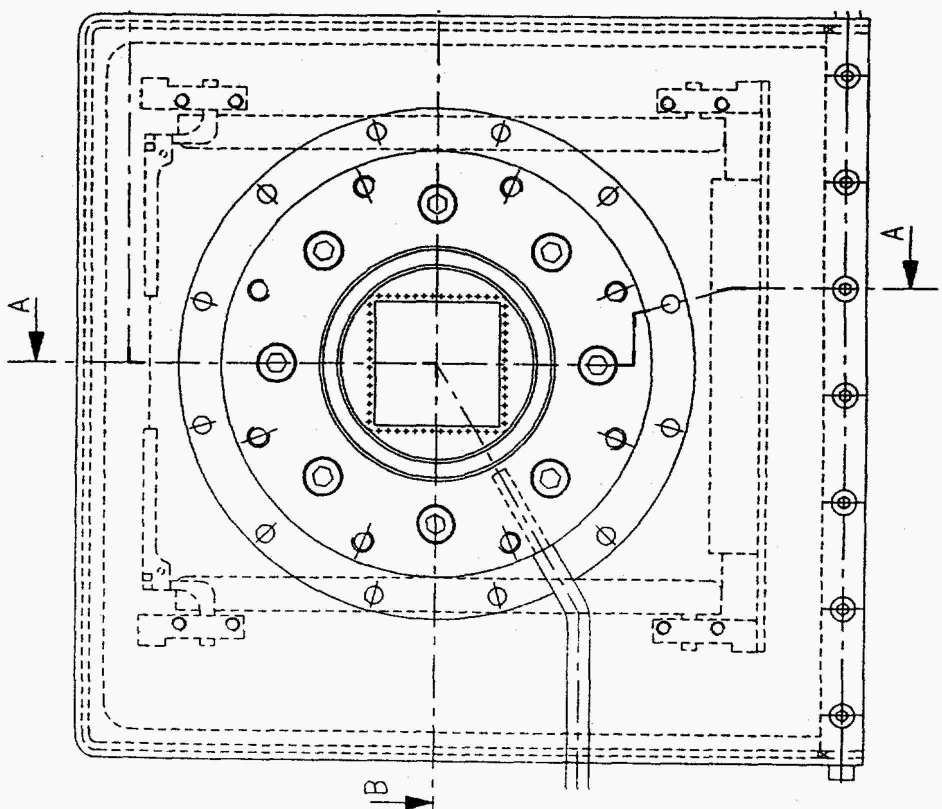

LEGEND :

1 = CCD INTERFACE BOARD
2 = LOWER FLANGE CD 307
3 = ALCATEL PIRANI SENSOR
4 = TH7896A CCD SENSOR
5 = WARM SUPPORT PIECE CD202
6 = AB31-1818 PELTIER COOLER
7 = COLD SUPPORT PIECE CD201
8 = BM12A RTD SENSOR
9 = CCD SOCKET BOARD

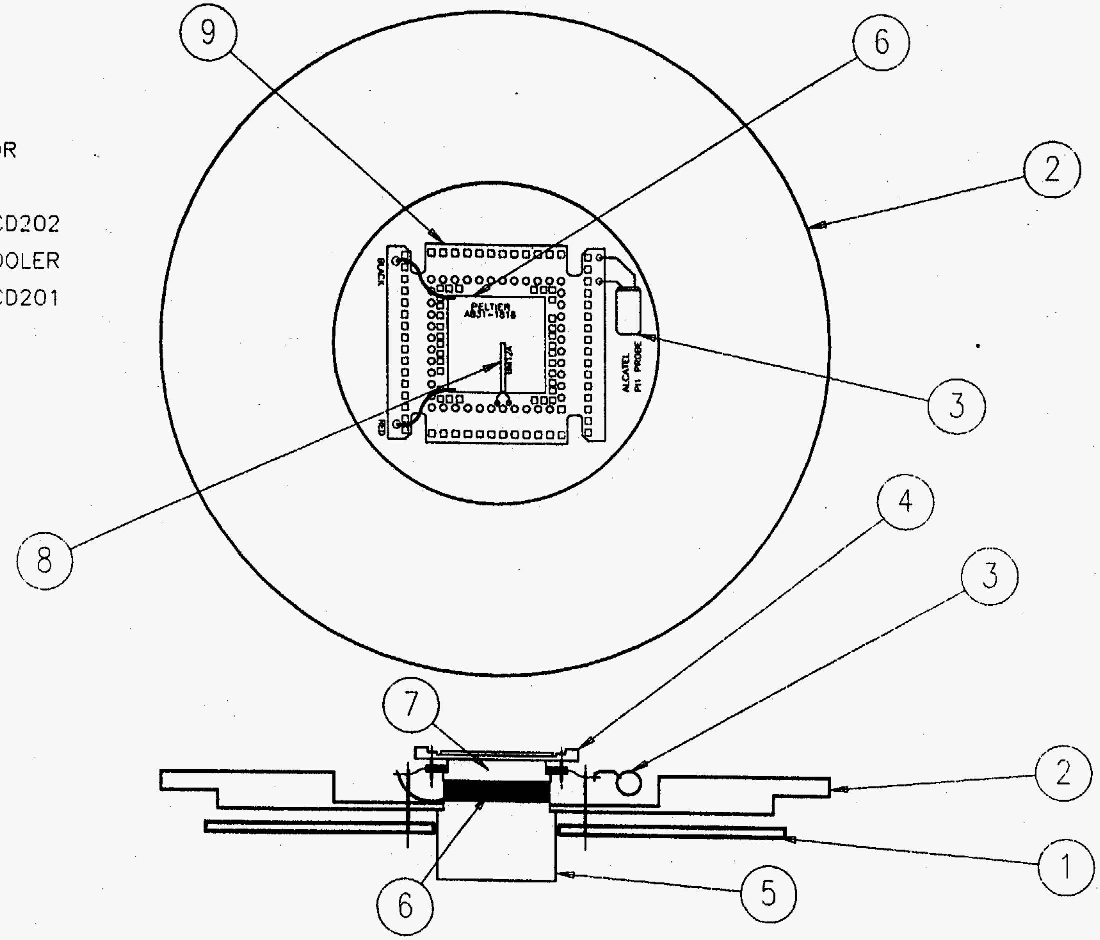

REVISIONS				UNLESS OTHERWISE SPECIFIED	SIGNATURES	DATE	E.S.R.F. DETECTORS GROUP
REV	DESCRIPTION	DATE	APPROVED	DIMENSIONS ARE IN			CCD SUPPORT BOARD
				TOLERANCES ON: 2 PL DECIMALS ± 3 PL DECIMALS ± ANGLES ± FRACTIONS ±	VANBRUSSEL	19/11/93	MECHANICAL ASSEMBLY
					ENGINEER	DATE	SIZE / DWG NO SHEET

Germanium Multi-element Semiconductor Detectors

Advantages:

- reliable fabrication of 1 sided *monolithic* detectors (2 sided?)
- established readout electronics and software for development work
- energy resolution (1% at 25keV)
- high density, high Z (=32, Silicon Z = 14)
  - --> wide energy range (300*eV* - 100 **keV**)
  - --> high spatial resolution ≈100μm at 30keV

Disadvantages:

- per channel count rate limit imposed by signal shaping (~μsec)
- crosstalk between channels --> spatial & energy resolution degradation
- need to develop integrated readout electronics and software for multi-channel (n>30) devices
- operation at ≈ 80° K (=> liquid nitrogen cryostat)

Prospects:

- large arrays (--> 150mm) using lithographic techniques and axially sliced boules
- integrated electronics within cryostat (eg preamplifiers, scalers, MUX...)
- alternative materials (CdZnTe for high energies, 'thick' Si --> 2mm)

Germanium Detectors: High energy Beamline 5

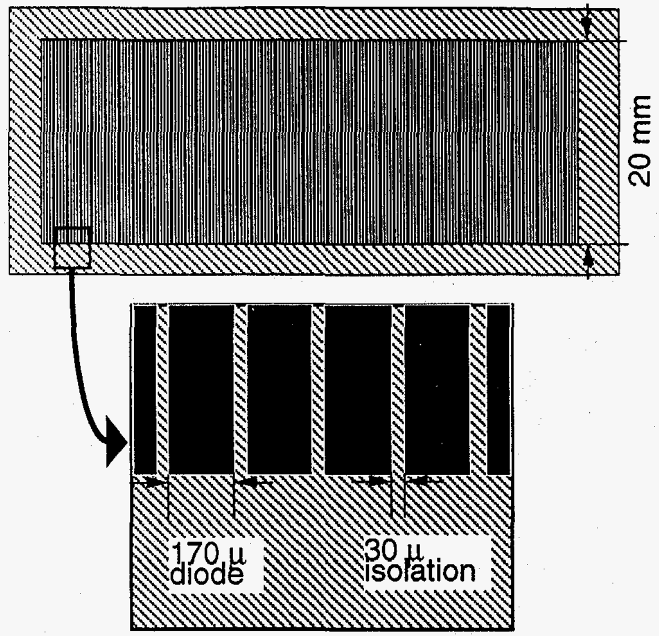

300 strip array,
≈1 keV @ 30keV,
1kcps/element
30 - 100 keV

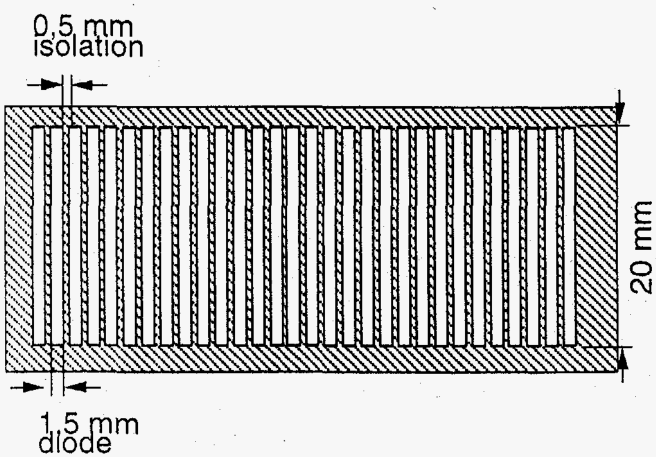

30 element array,
<600 eV @ 150keV,
50kcps/element
30 -150keV

Multielement Test Detector Program

- 28 strip Germanium test detector and cryostat (Intertechnique)
- preliminary measurements of resolution, spectral tailing/crosstalk using standard NIM etc. electronics (from 1/94)

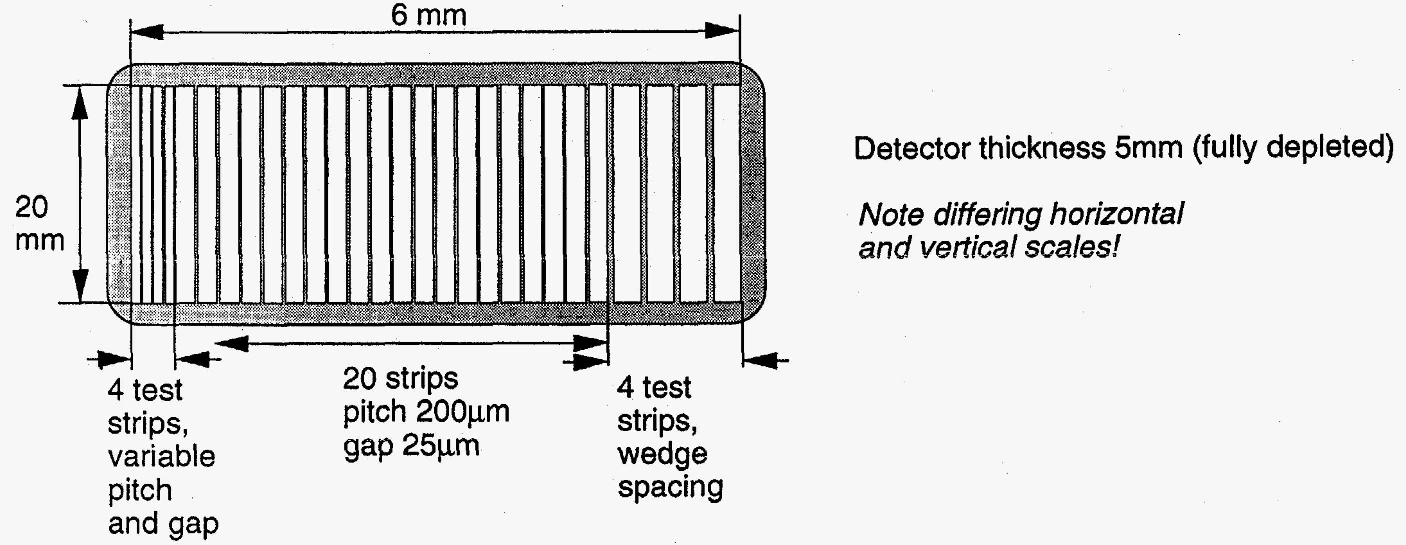

-optimisation of front-end electronics to minimize noise and suppress crosstalk (eg 3-channel sensing...)

- design for 300 channel system: cryostat/preamplifiers/data acquisition

Details of end strips (strips 5...24 are identical)

Not to scale!
dimensions in μm

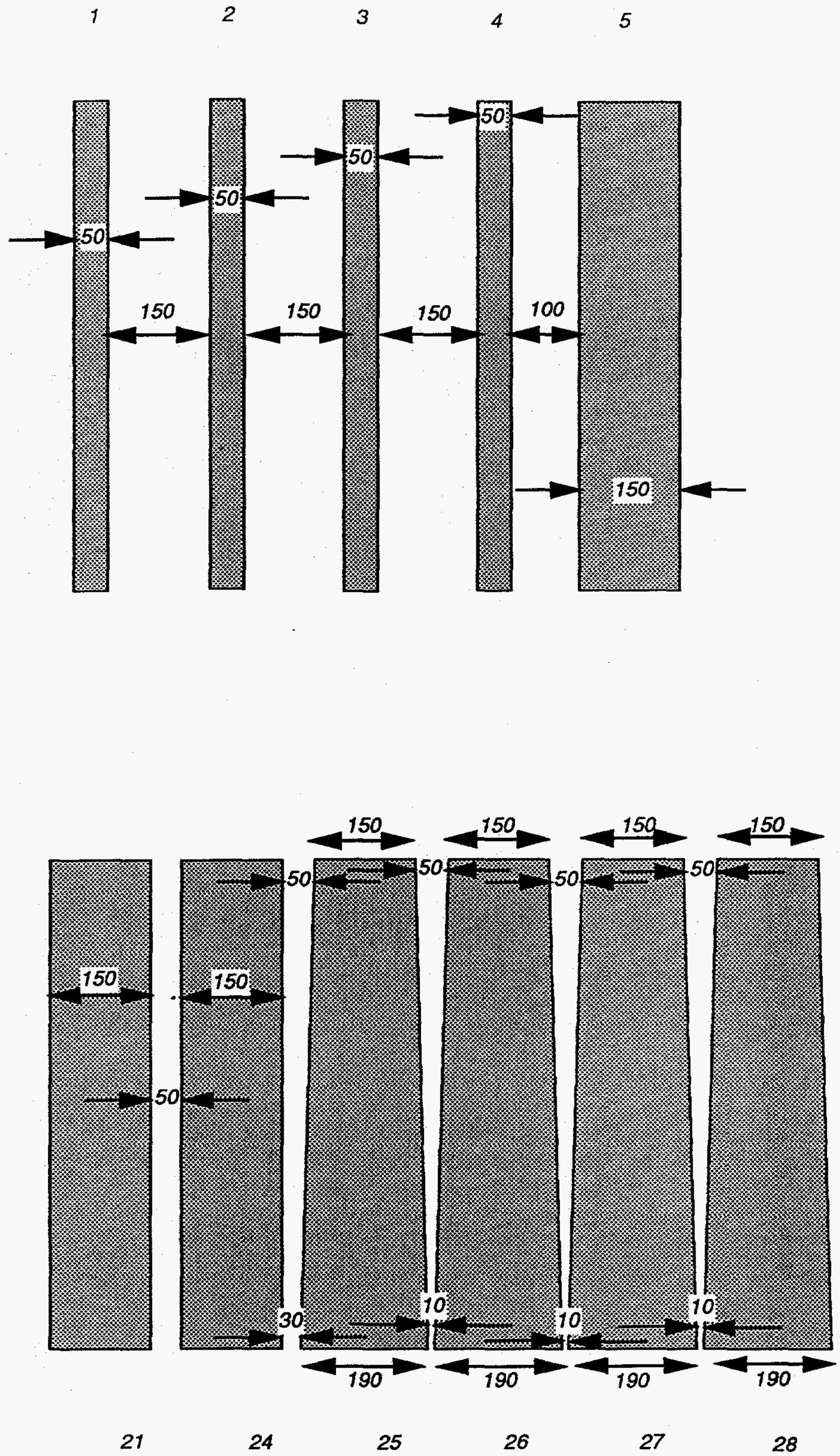

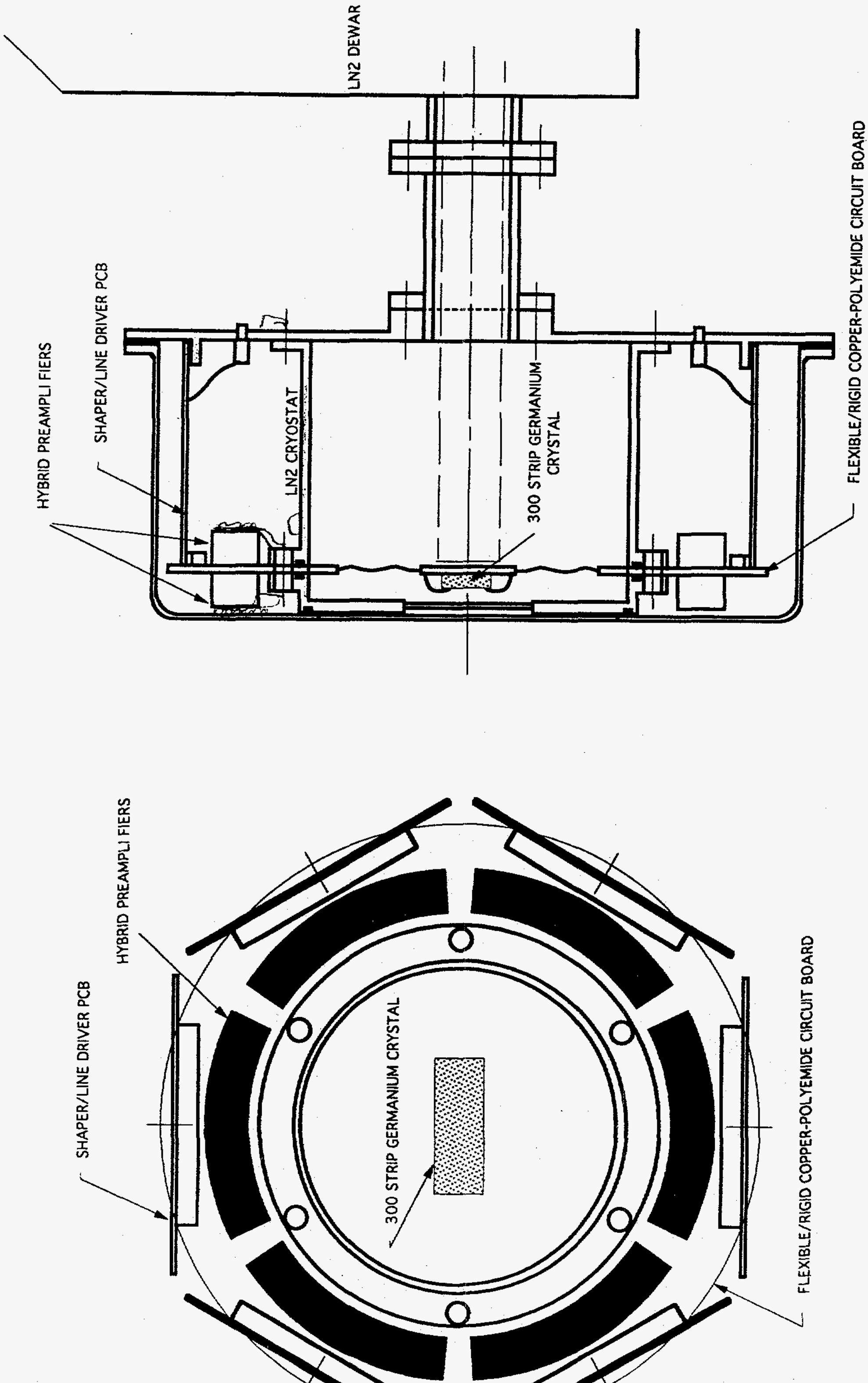

LN2 DEWAR
HYBRID PREAMPLI FIERS
SHAPER/LINE DRIVER PCB
LN2 CRYOSTAT
300 STRIP GERMANIUM CRYSTAL
FLEXIBLE/RIGID COPPER-POLYEMIDE CIRCUIT BOARD
SHAPER/LINE DRIVER PCB
HYBRID PREAMPLI FIERS
300 STRIP GERMANIUM CRYSTAL
FLEXIBLE/RIGID COPPER-POLYEMIDE CIRCUIT BOARD

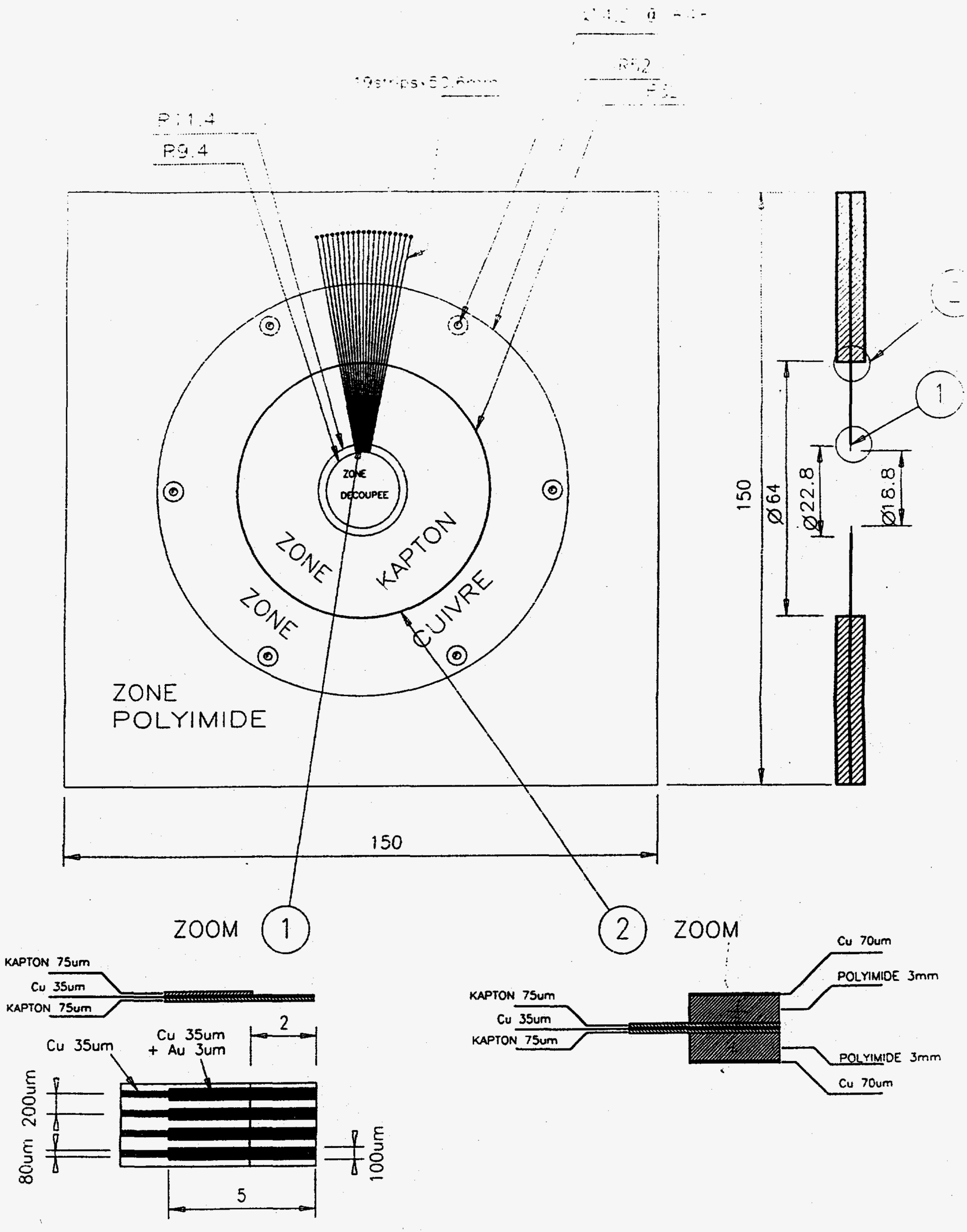

Low noise preamplifier mounting-cryostat feedthrough test assembly

40 000 pixel germanium detector for 'Cosy' at K.F.A. Jülich.

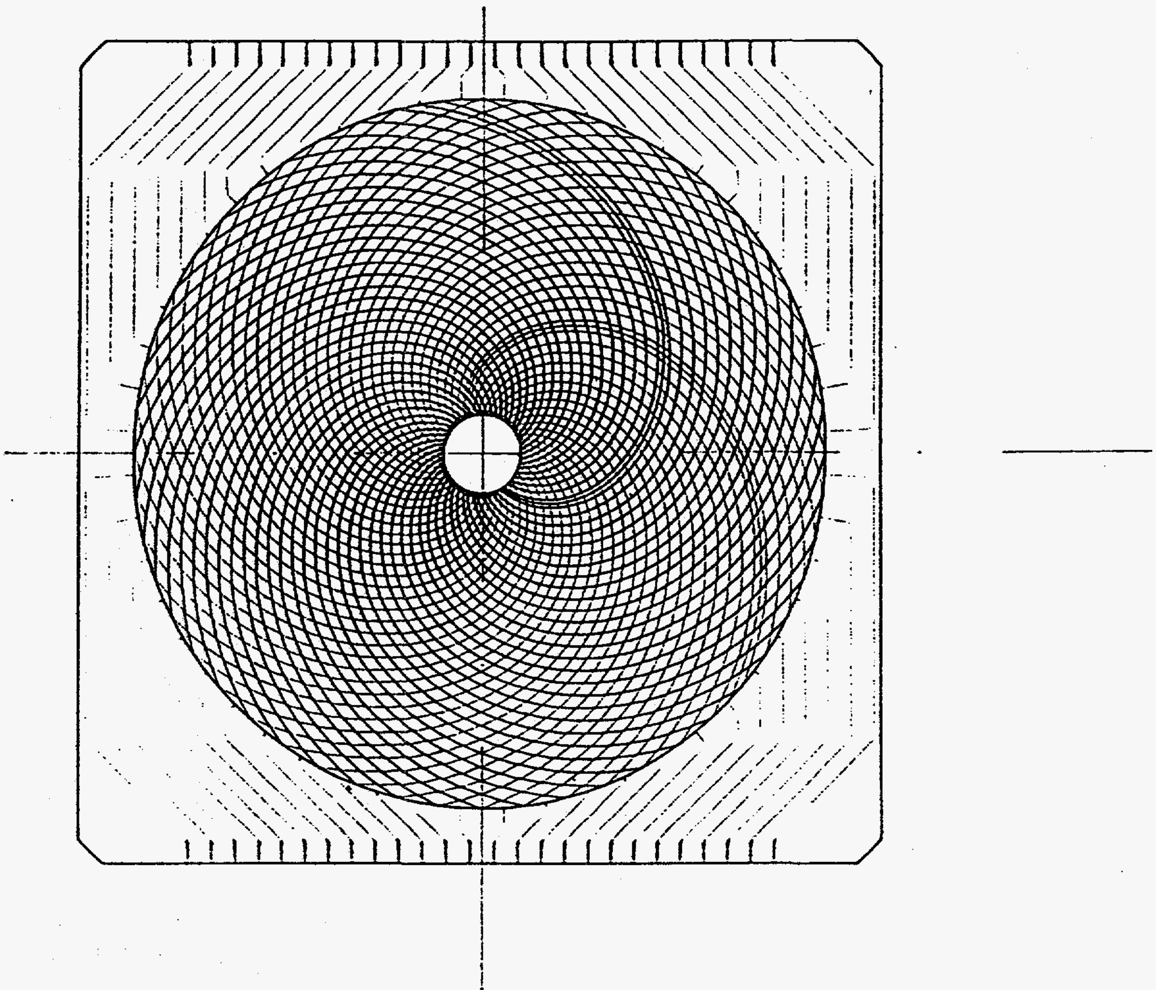

position structure of detector 1
only 52 elements (instead of 200) are shown

Riepe, KFA Jülich

Gas Microstrip Detectors

Advantages:

- lithographic production methods:
  - --> close spacing of anode lines (≈300μm)
  - --> non-rectilinear motifs possible
- fast ion transit => higher count rates (--> Mcps/cm)
- good intrinsic energy resolution (12% fwhm at 6keV)

Disadvantages:

- rate dependent gain drift effects (?)
- 'radiation' damage lifetime question: local effects
- gas absorption phase: parallax, photoelectron range and diffusion
- gain limit (eg 1000) --> analogue position encoding difficulties
- immature technology (semiconducting glasses, 'microgap'...) with expensive development cycle (materials R+D, mask designs...)

Prospects:

- very fast 1 and 2-dimensional counters (--> 100Mcps) with 'per strip' high density readout electronics

Rutherford-Appleton Laboratory - ESRF Gas µstrip Detector

Contract begun 1/91 for feasibility and design study for a ~300 strip detector with charge division readout on each strip at a rate >100kcps, to give a 'global' count rate ~100Mcps.

Objectives:

-substrate testing/manufacture to produce a gain stable µstrip detector of size ≥100cm^{2}
-design and test of charge division electronics for 16 strip prototype which can scale to a full size system of ≥300 channels at 300µm pitch.

Results:

-gain stability problems (with count rate, 'radiation' damage) preclude use of 'standard' glass substrates. Work now done on semiconducting glasses (Schott S-8900, 10^{11} ohm-cm) giving good rate stability; ageing tests in progress.
-hybrid/surface mount 16 channel preamplifiers suitable for 300µm pitch detector mounting.
-Double delay line NIM shaping modules designed which give position resolution (fwhm)<500µm on 80mm strips at >10^{5}cps.

Current status:

-studies of long term ageing effects
-measurements of neighbouring channel crosstalk effects on position resolution
-study of 300µm pitch <u>E</u>-field stress relieved bonding techniques

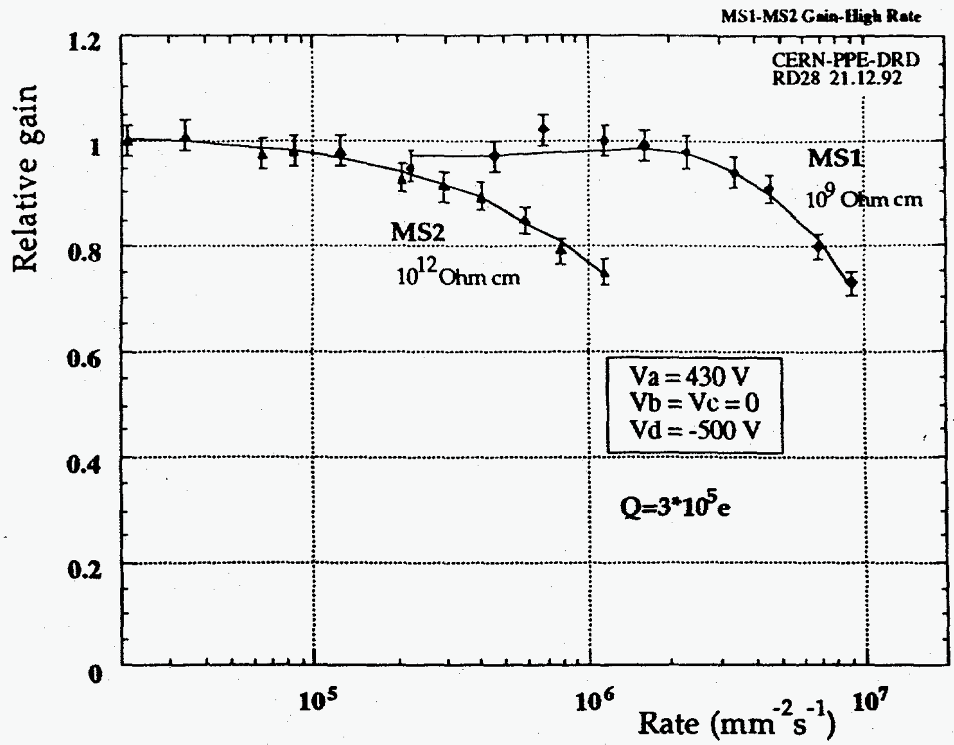

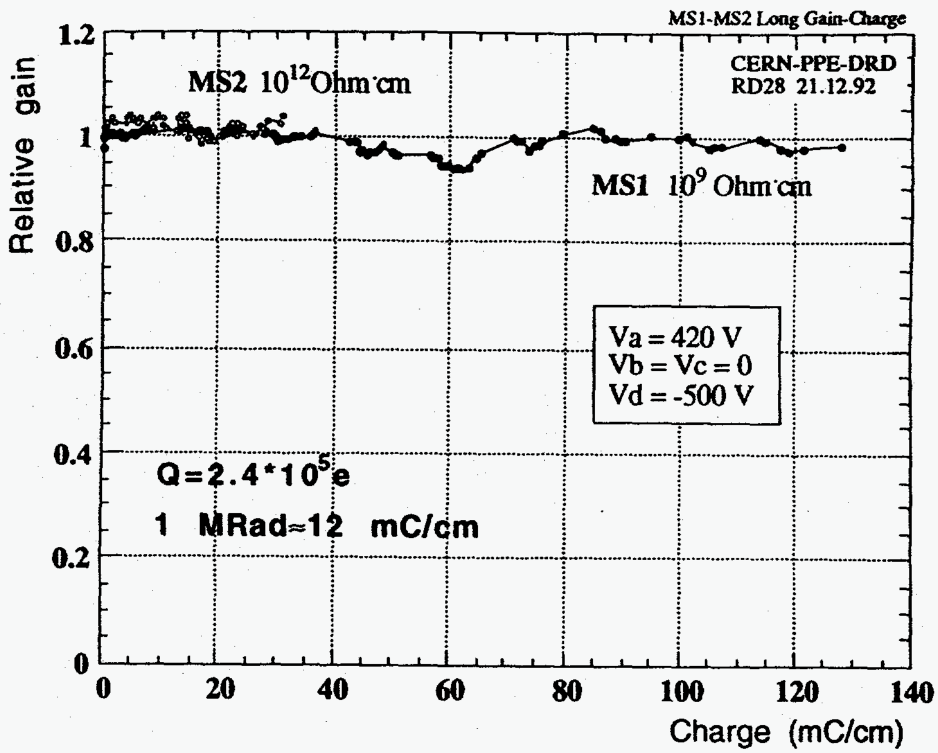

F. SAULI, CERN 1/93

A3

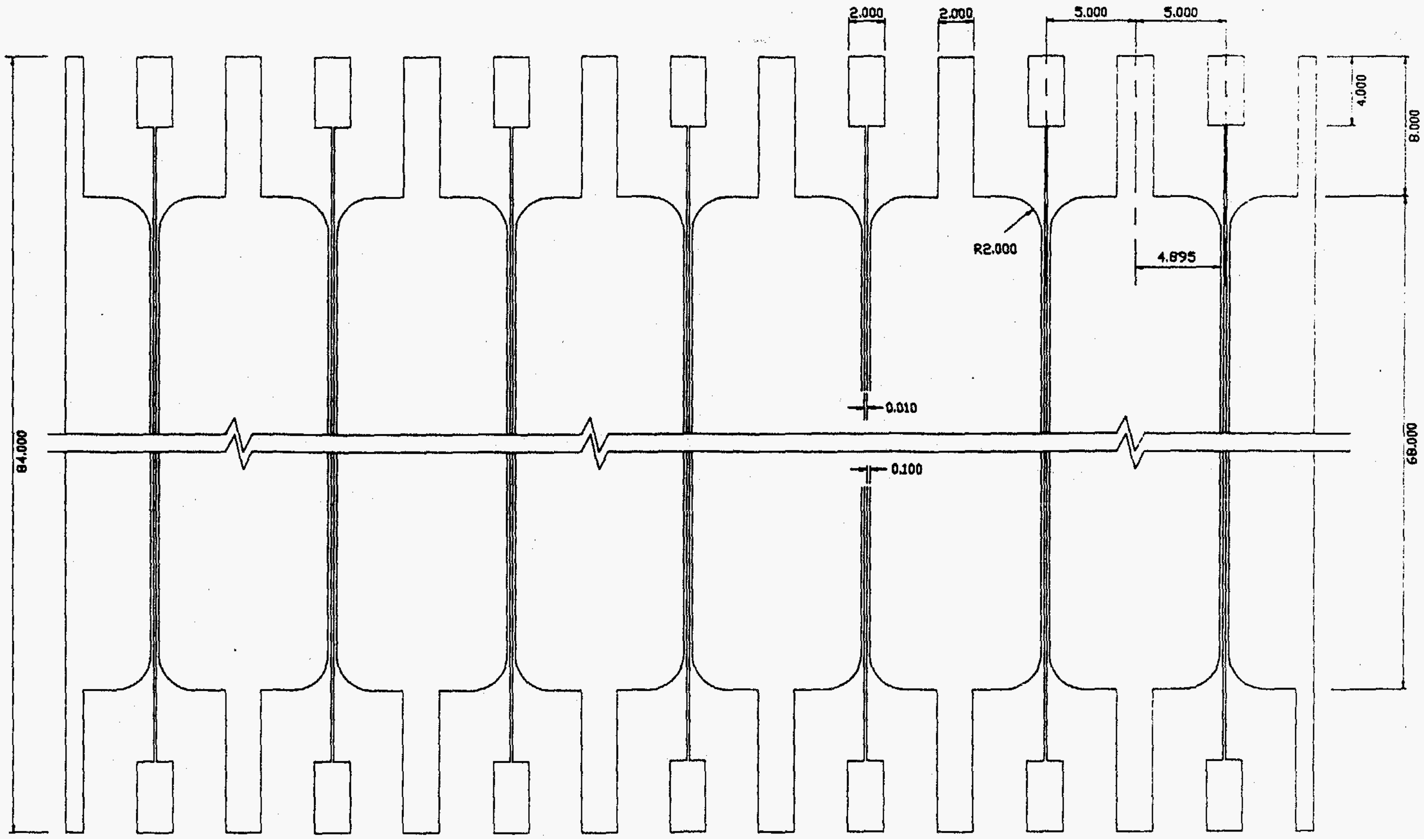

A	18AUG93					
ISSUE	DATE	MOD NO.	DRN. BY	CHKD.	APPD.	STATUS

USED ON

SCIENCE & ENGINEERING RESEARCH COUNCIL RUTHERFORD APPLETON LABORATORY, CHILTON, OXON OX11 0QX

TITLE MASK 2 CHARGE DIVISION TEST PATTERN

TOLERANCES UNLESS STATED	FINISH REMOVE ALL BURRS	ORIGINAL SCALE DO NOT SCALE
MATERIAL & SPEC.	SURFACE TEXTURE µm UNLESS STATED	0 mm

A3

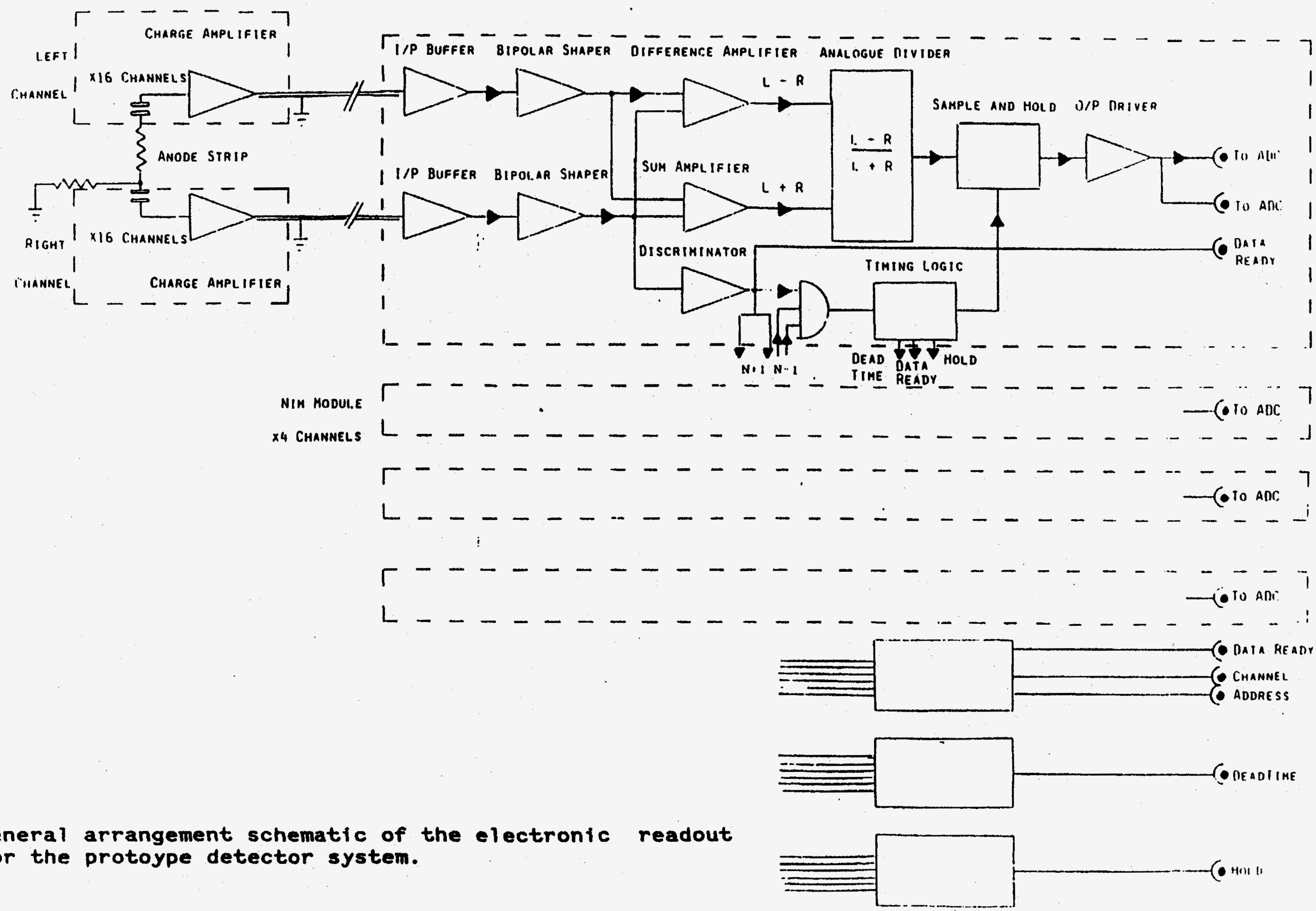

General arrangement schematic of the electronic readout for the protoype detector system.

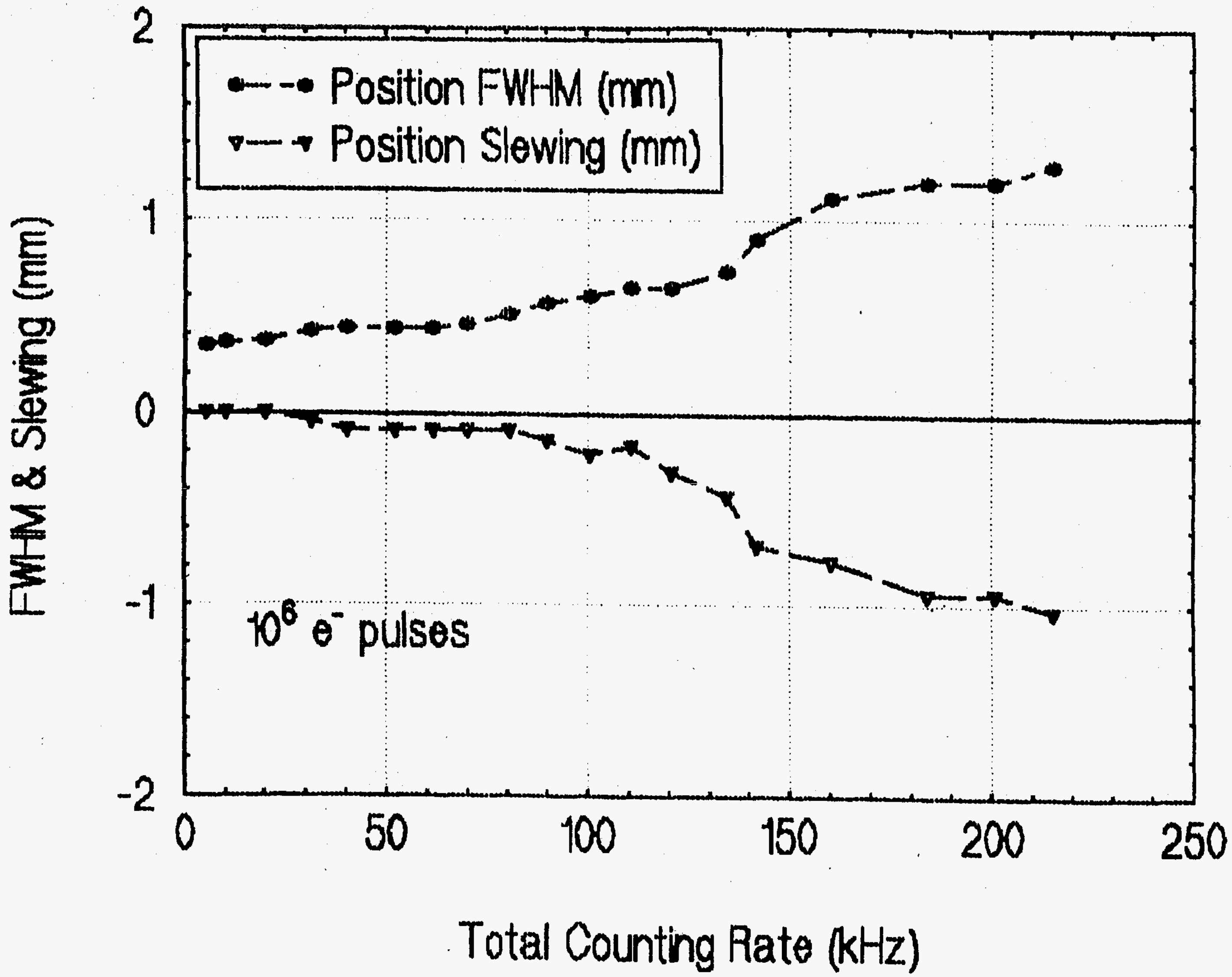

Rate peformance of the basic analogue processing system for finding the coordinate of an event along an anode strip.

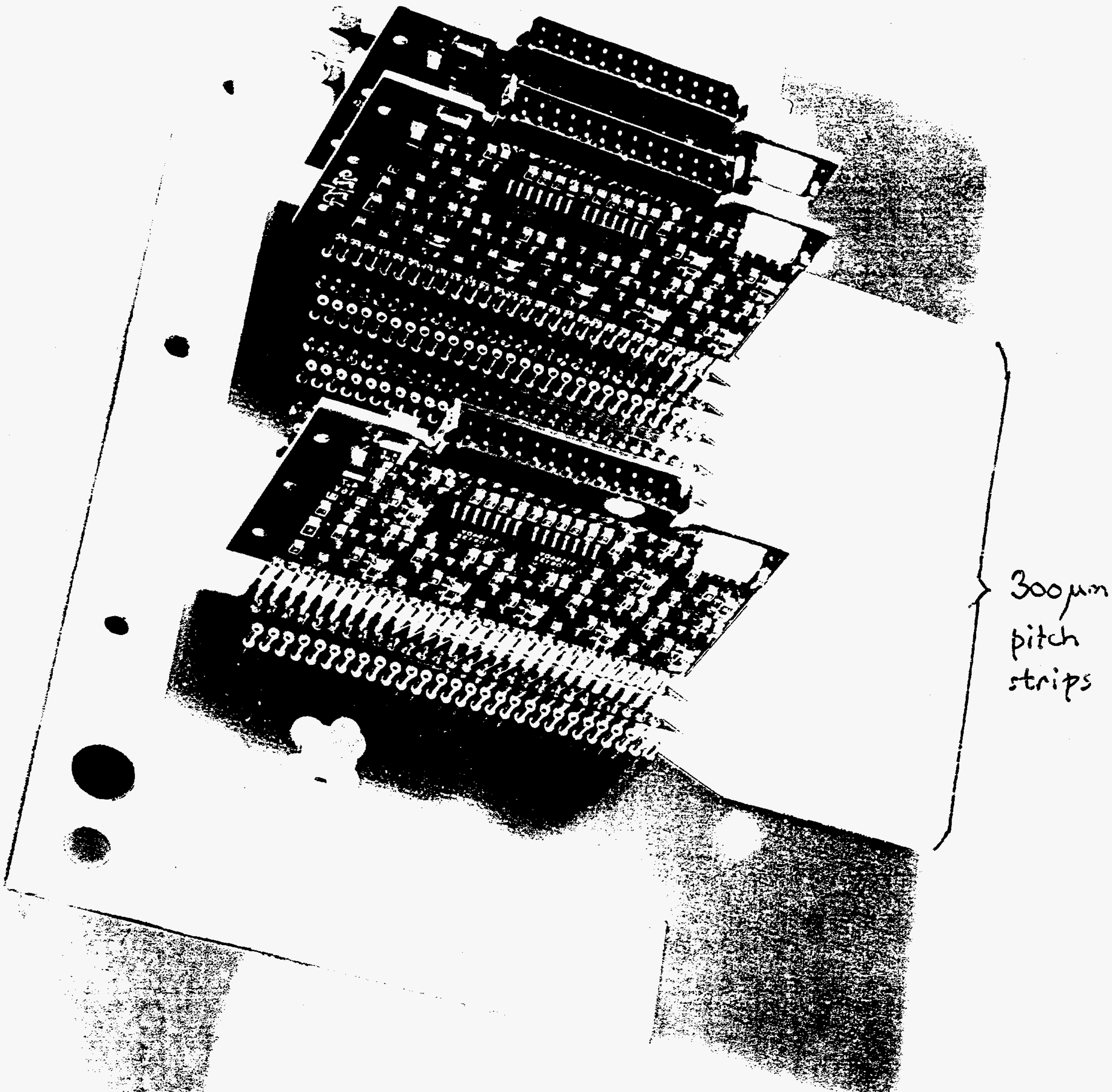

MOUNTING OF PREAMPLIFIERS (16 CHANNEL) AT 300µm PITCH

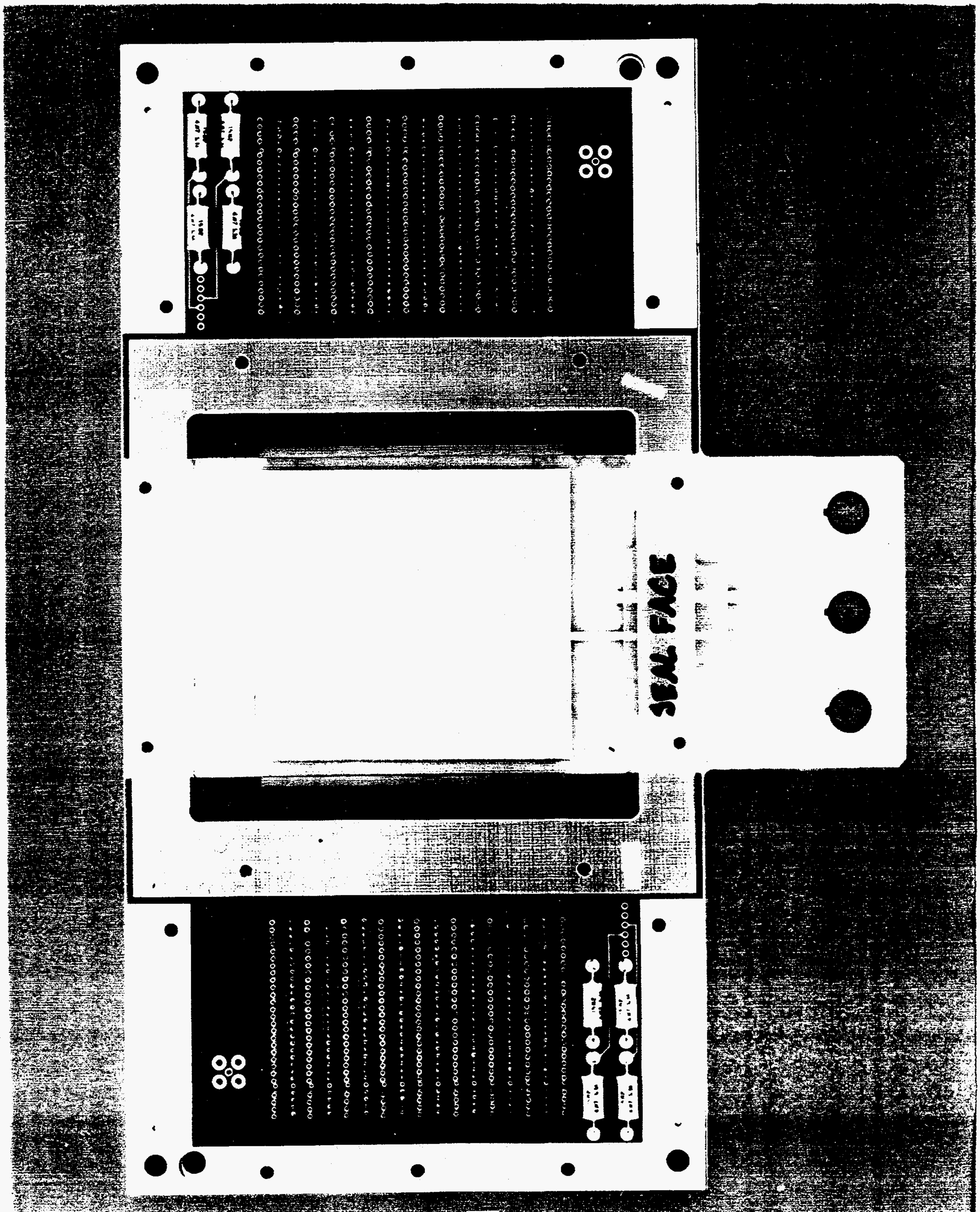
SEAL FACE

Masayo Suzuki

RIKEN

Detector Development at SPring-8

Masyo Suzuki and Tatzuo Ueki

The SPring-8 Project Team initiated a feasibility study of x-ray detectors in 1990. Having completed the study covering various types of detectors and evaluating the capability that each detector could attain, the SPring-8 Project Team decided to conduct R&D programs on the following detectors in 1992: [1] CdTe Solid State Detectors, [2] Ring-Cathode Proportional Detectors, [3] Image Plate Systems, [4] X-ray Image Intensifiers, [5] MicroStrip Gas Chambers, and [6] Proportional Scintillation X-ray Imaging Chambers. All of these R&D programs have successfully progressed, becoming one of the major ongoing efforts at the SPring-8 Project.

The R&D group for CdTe Detectors has developed a full-scale model, of a size 64 mm x 128 mm, having 512 independent channels, each composed of eight linearly arranged CdTe unit sensors (0.25 mm in width, 8 mm in length, and 0.8 mm in thickness). The unit sensor is associated with its own electronics consisting of a preamplifier, a lower-level discriminator, and a counter. The prototype has been tested with fluorescent x-rays (43 keV to 59 keV) from rare earth samples irradiated by hard synchrotron radiation at KEK/PF. The latest experimental data suggest that further optimization in terms of the wiring configuration and of the temperature regulation will result in improving its performance significantly.

The R&D group for Ring-Cathode Proportional Detectors has constructed a prototype with a newly designed delay-line having a delay time of 2.6 nsec/mm. The prototype has been installed in BL-10C at KEK/PF and attained a spatial resolution better than 800 μm. By carefully distributing the applied electric field over the ring-cathode, the prototype successfully operated at a counting rate of 2×10^5 without any discharge, above which distortion in scattering patterns began to be observed. The uniformity of response was found to be better than 10% with a scattering angle smaller than 30 degrees. The group will continue its effort in the direction of improving the high counting capability and the uniformity over the entire region of the detection area.

The R&D group for Image Plate Systems has introduced a new type of image plate Blue IP (Fuji film BAS-UR), originally designed for electron microscopy, to improve the spatial resolution. The preliminary test showed that the spatial resolution of Blue IP is twice as high as that of conventional image plates, such as White IP (Fuji film BAS-HR III). The group has also intensively studied a scanning mechanism associated with line-shaped laser light in order to shorten the readout time for large area image plates (400 mm x 600 mm). In this readout system, the photostimulated luminescence induced by the line-shaped laser light will be focused on a CCD through an optical lens system of large numerical aperture and will be read out one-dimensionally with a readout cycle of 500 kHz. Having completed the basic design, the group is currently constructing a prototype based upon this new readout mechanism.

The R&D group for X-ray Image Intensifiers has been successfully enlarging the detection area of the device. An x-ray image intensifier with a beryllium window having 150 mmϕ entrance field has been developed by the group on the basis of a technology for aluminum window medical x-ray image intensifiers. With the Be-window x-ray image intensifier, the photon gain is also improved by more than 10 times compared with the visible-light image intensifier. This improvement has enabled them to use standard CCDs to perform time-resolved measurements at a rate of 30 frames per second. Confirming that the x-ray image intensifier has a dynamic range wider than four orders of magnitude and a point spread function with a FWHM of 280 μm, the group has succeeded in observing time-resolved diffraction patterns from frog skeletal muscle during contraction under stretch.

The R&D group for MicroStrip Gas Chambers has developed a two-dimensional prototype chamber having an effective area of 50 mm x 50 mm with a very thin substrate by employing multi-chip module technology. It has 250 anode strips and 250 backplane strips orthogonal to each other with an expected spatial resolution of 60 μm. It is mounted on a large ceramic package with 600 connected pins, realizing easy and high-density connections. The x-ray images so far obtained are encouraging, although preamplifiers with a higher gain are required for better performance. The design of a full-scale model with an effective area of 100 mm x 100 mm is currently in progress, with which the group expects to extend the effective detection area up to 200 mm x 200 mm by combining four of these.

The R&D program on Proportional Scintillation X-ray Imaging Chambers has been the most challenging project among the programs, since it is based upon a new chamber technique. The detector system consists of a rare gas proportional scintillation chamber and an image-intensifier-associated CCD camera. The prototype constructed has demonstrated that this novel detector is capable of imaging single x-ray photons. The spatial resolutions attained in analogue mode and in digital mode were around 1 mm and better than 170 μm, respectively. The design of a full-scale detector is currently in progress.

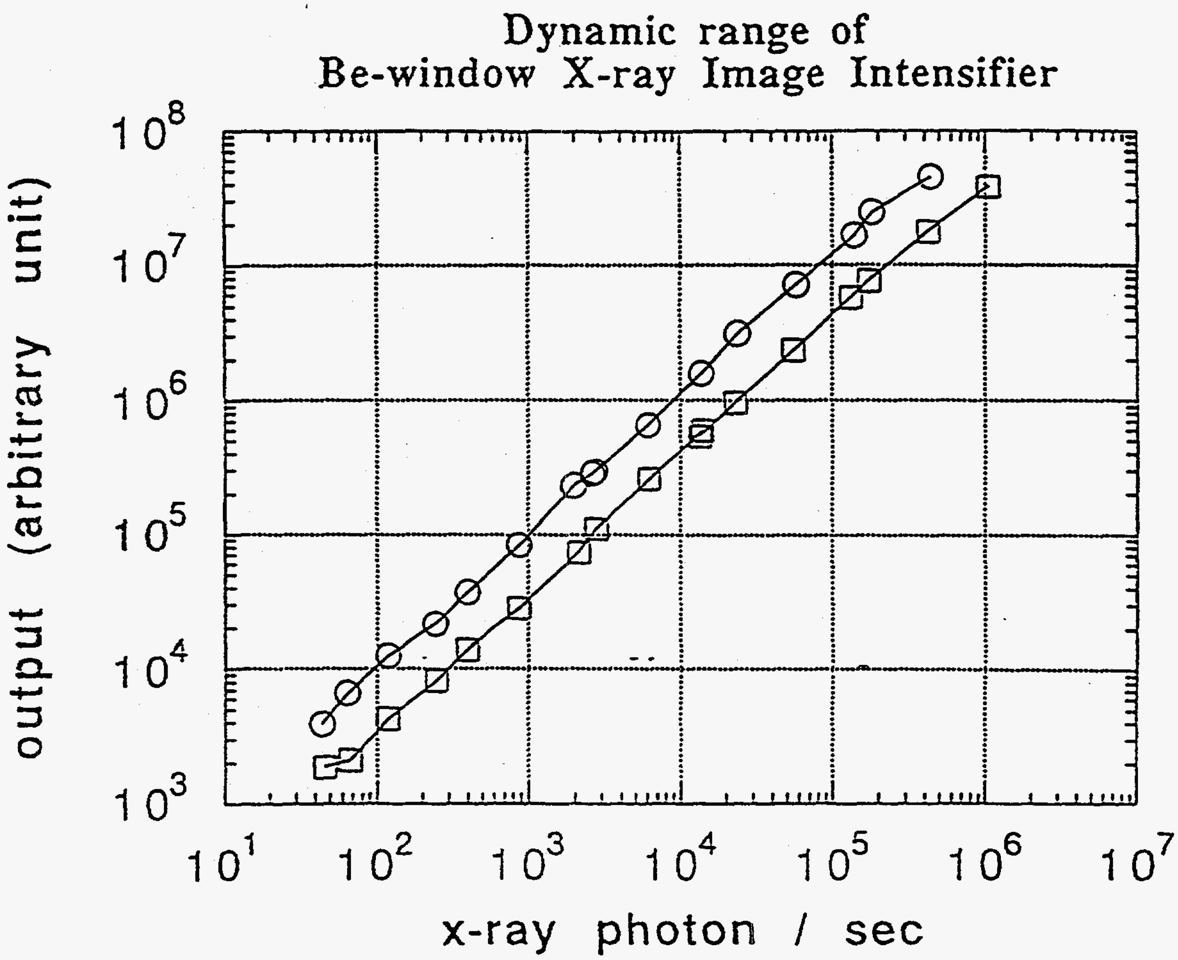

Dynamic range of
Be-window X-ray Image Intensifier
output (arbitrary unit)
10^8
10^7
10^6
10^5
10^4
10^3
10^1
10^2
10^3
10^4
10^5
10^6
10^7
x-ray photon / sec

D3
from
D1 & D2

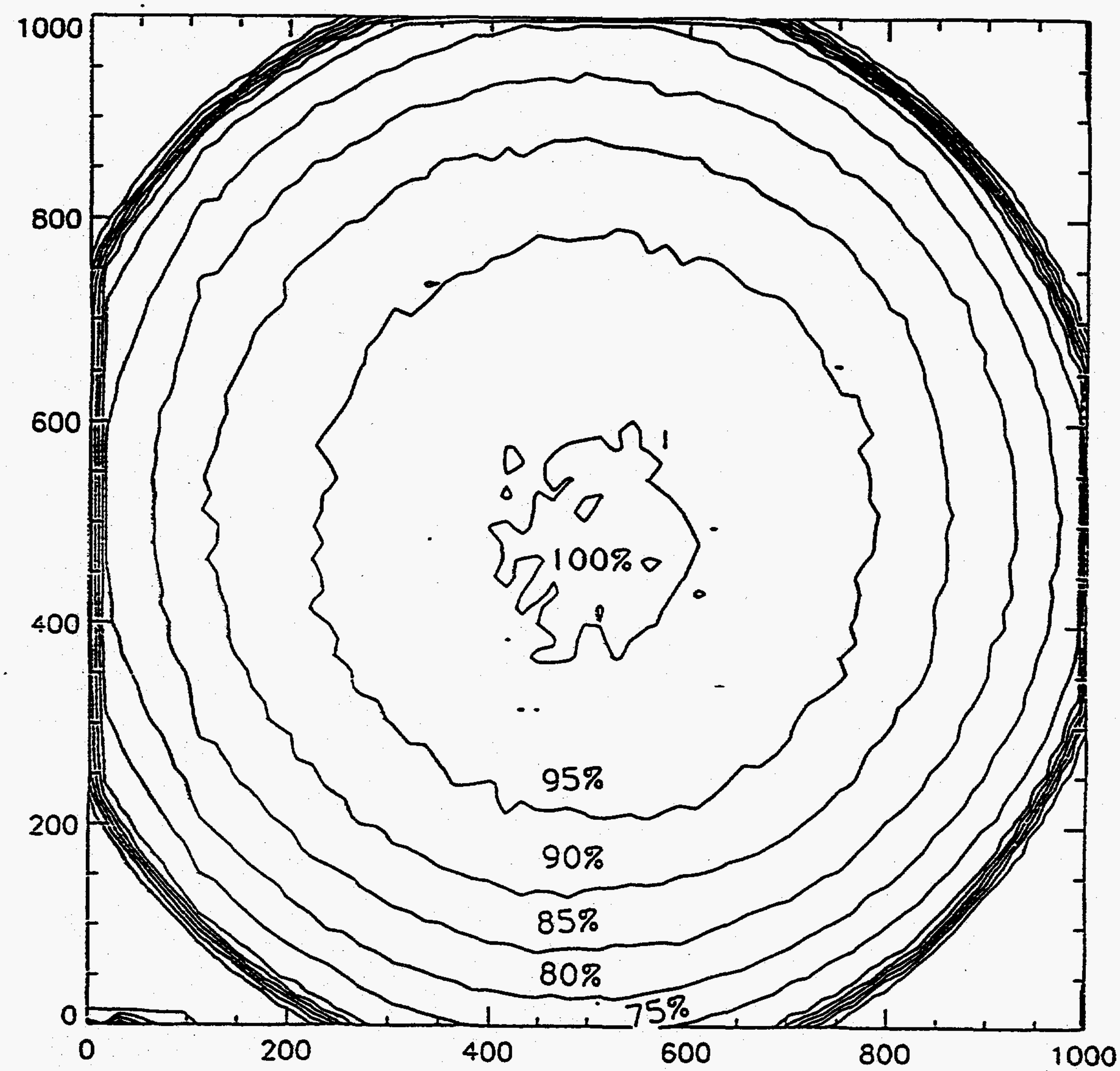

X-II with ^{241}Am

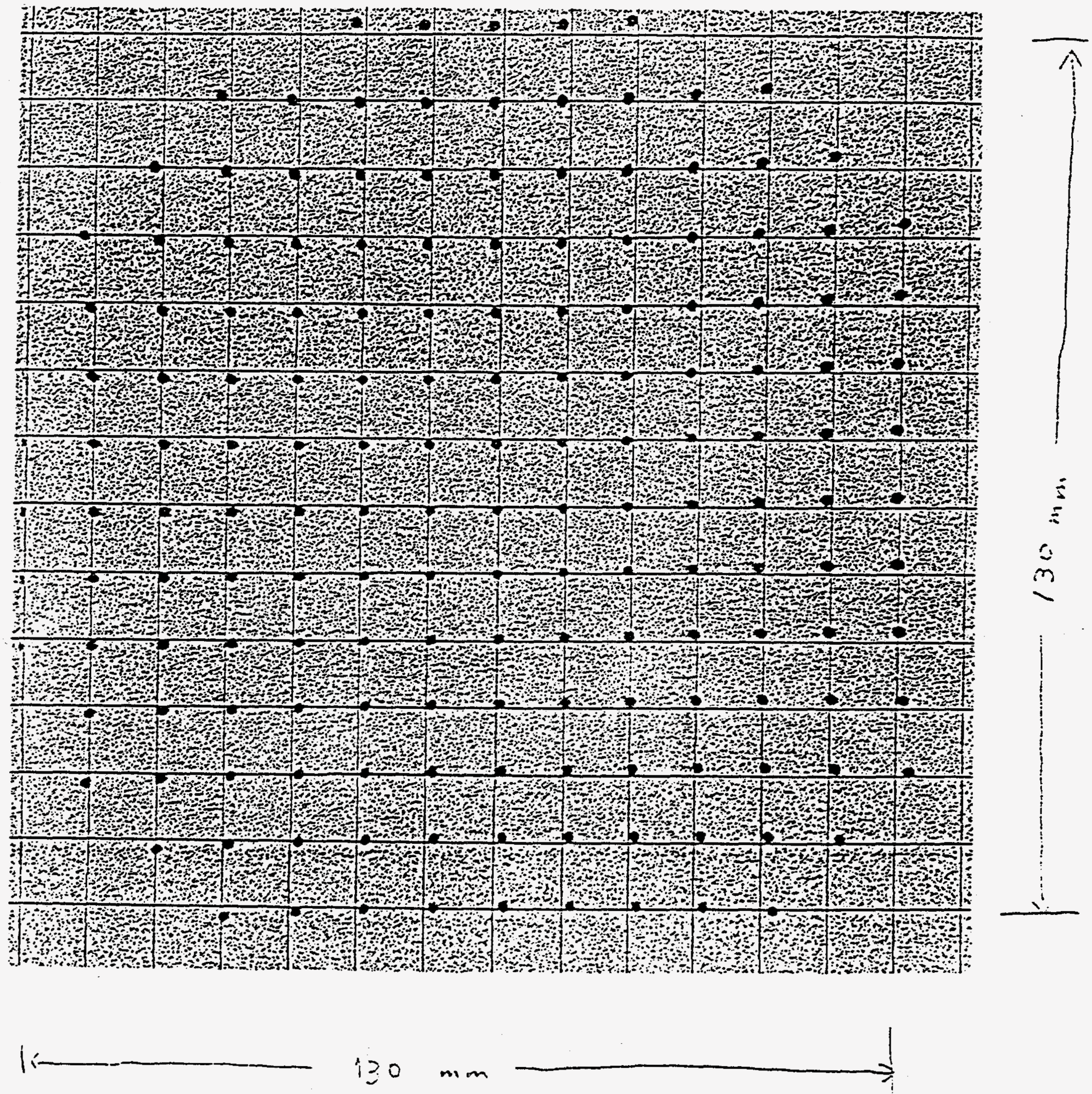
130 mm
130 mm

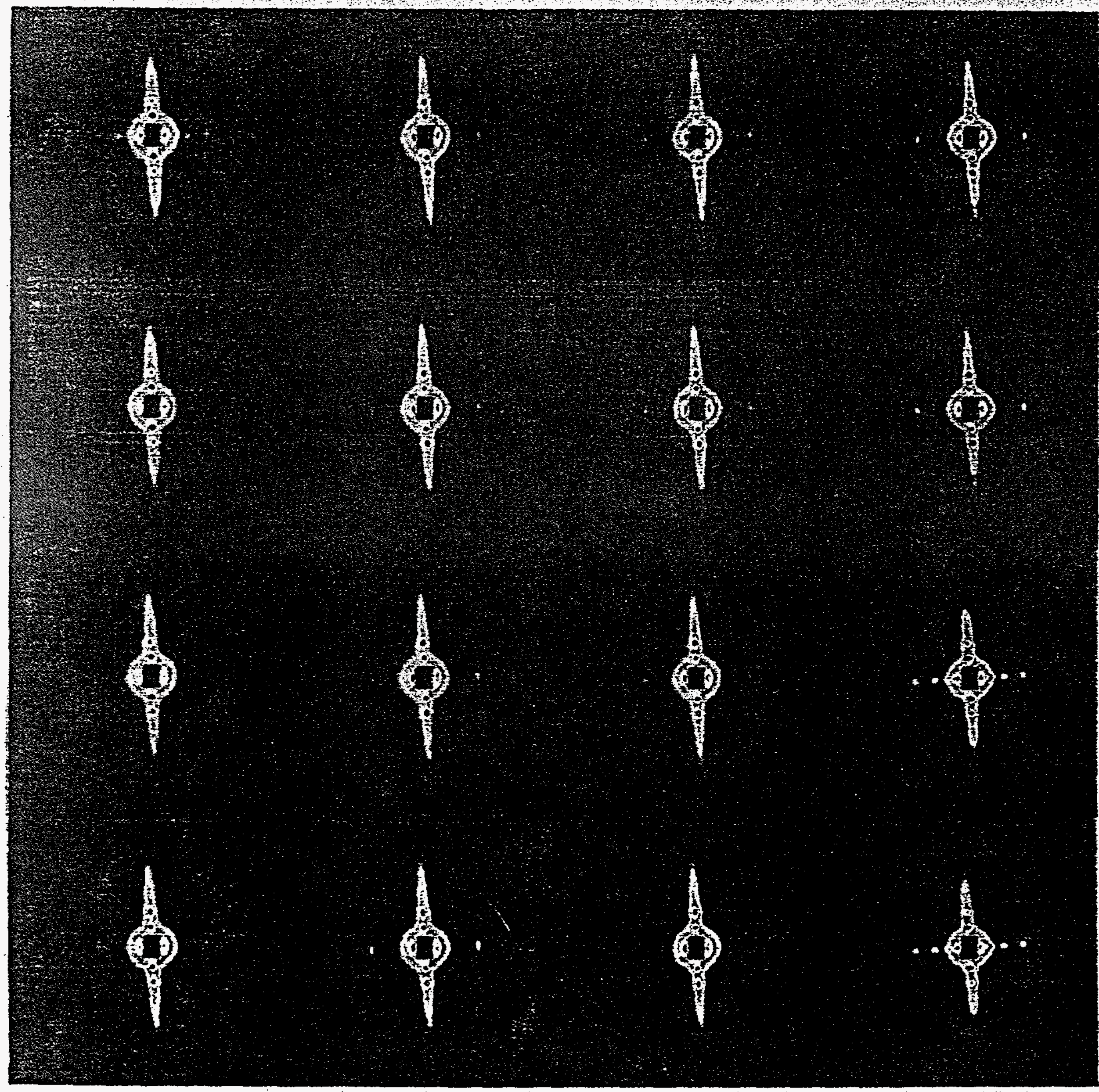

Feature of MicroStrip Gas Chamber (MSGS)

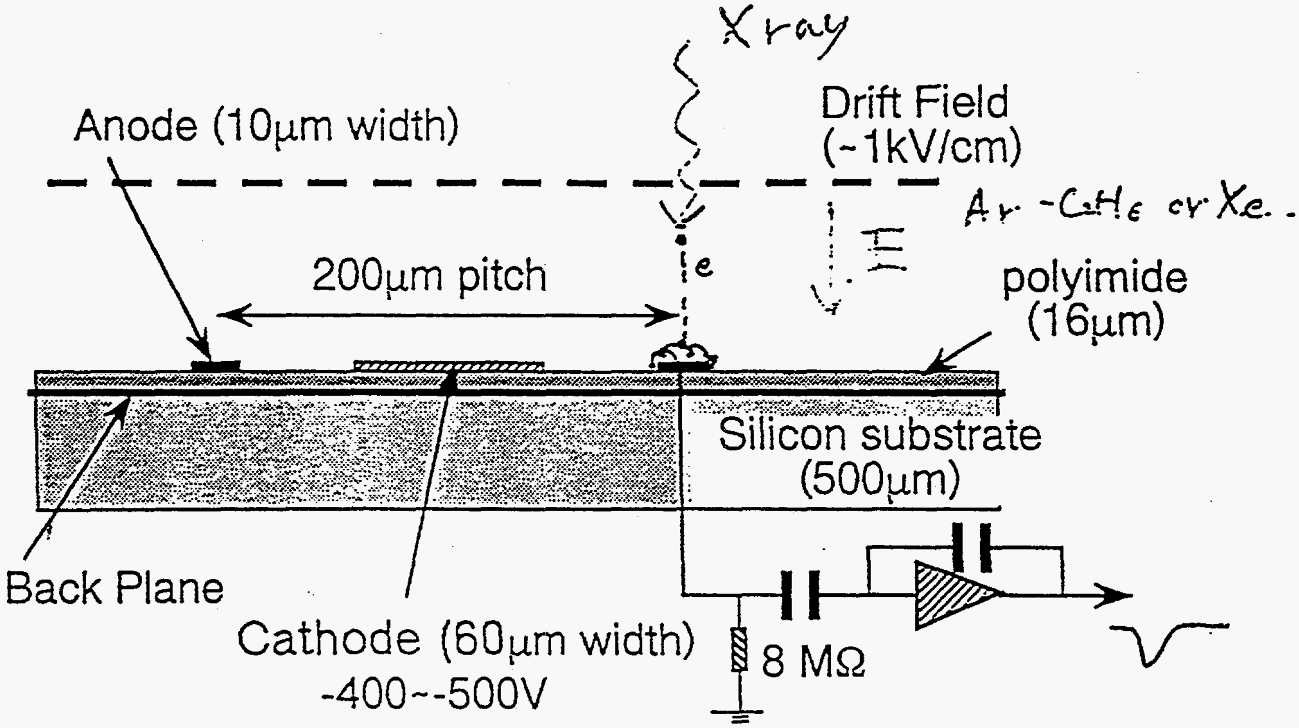

Skematic View of MicroStrip Gas Chamber(MSGC)

- Photon Counting Detector

Rigid Substrate &
Fine Precision Structure(<0.1μm)

↓

Fine Position Resolution (~60μm)

Fast Signal Processing (~10ns)

High Counting Rate ($\sim 10^{7}$ $Hz/mm^{-2}s^{-1}$)

Simple Fabrication

Structure of Two dimensional MSGC

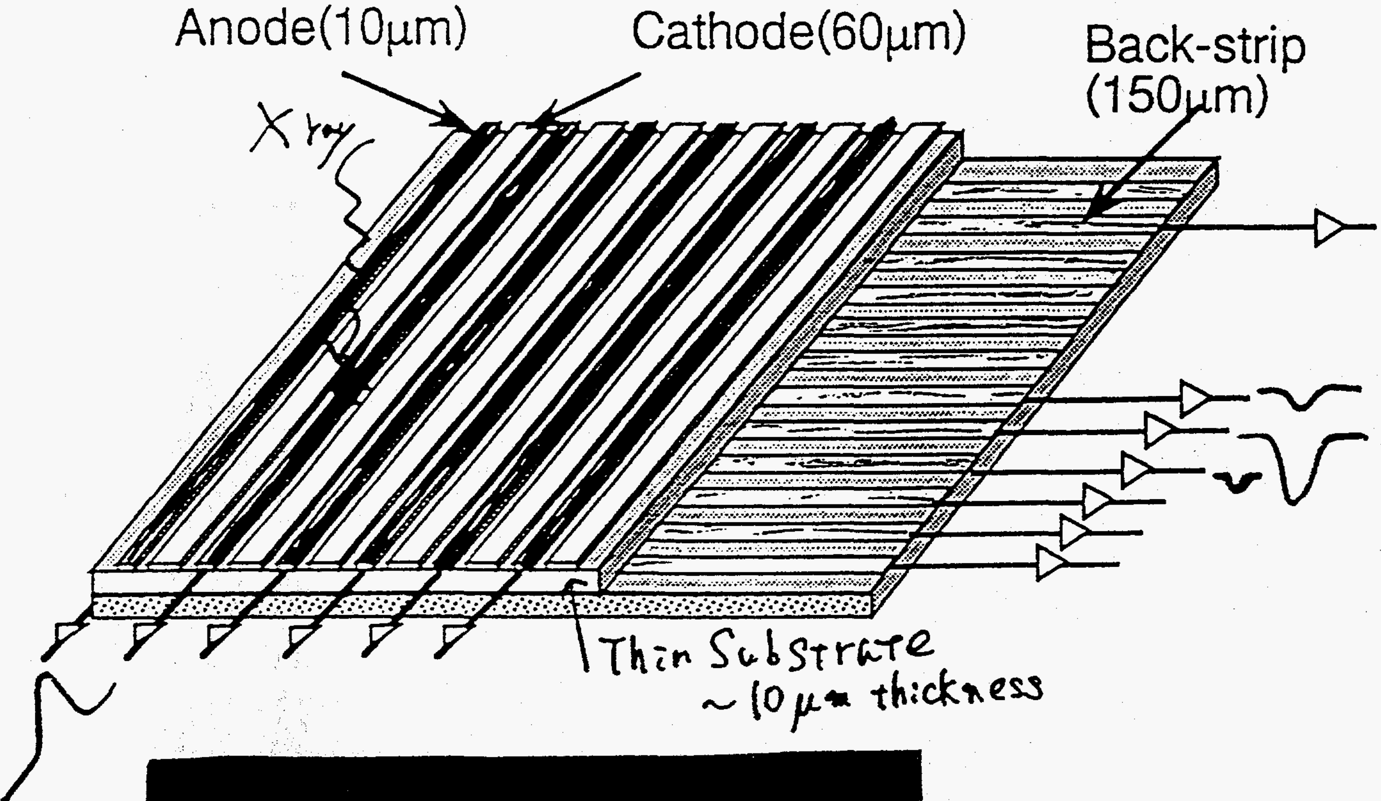

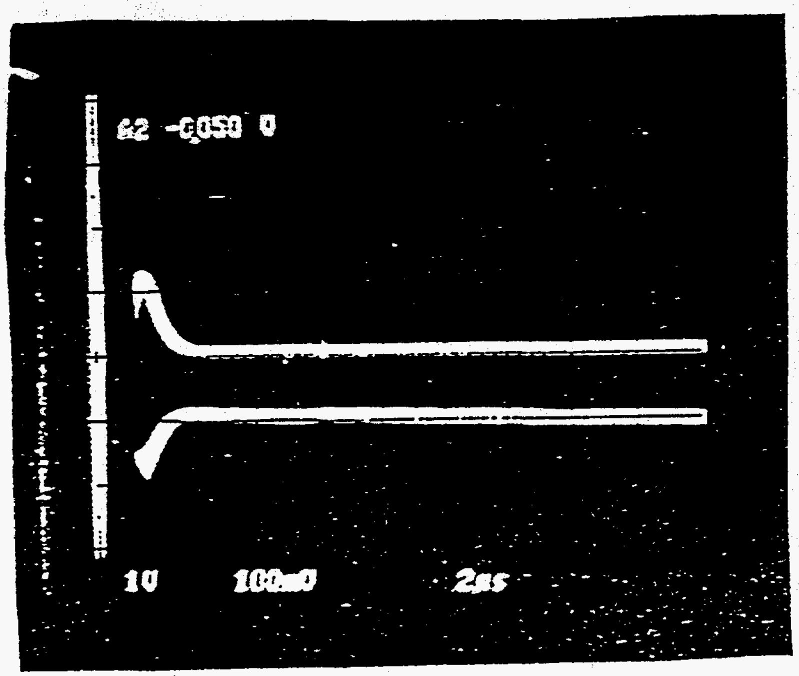

Anode signal

Back-Strip signal

Photograh of an anode signal (up) and a back-strip signal (down) of 50mm x 50mm two dimensional MSGC for 5.9 KeV Fe X-ray

MSGC Imaging System

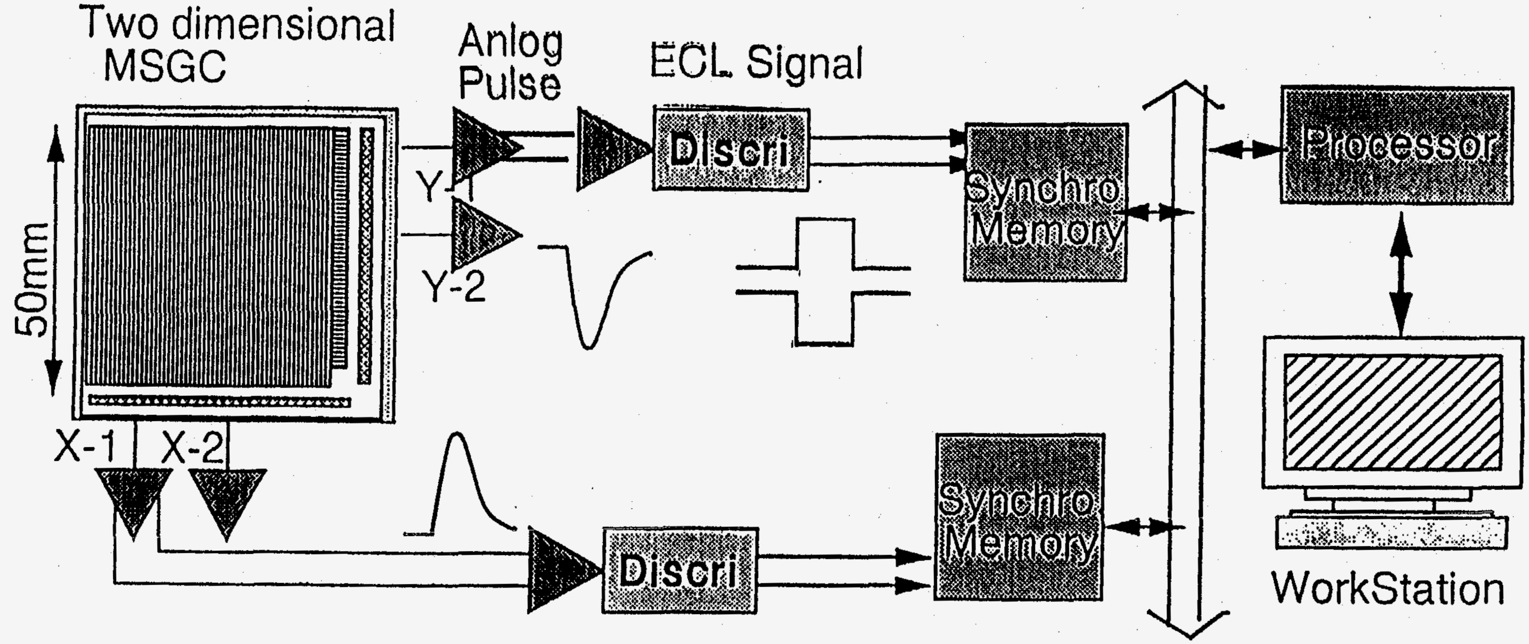

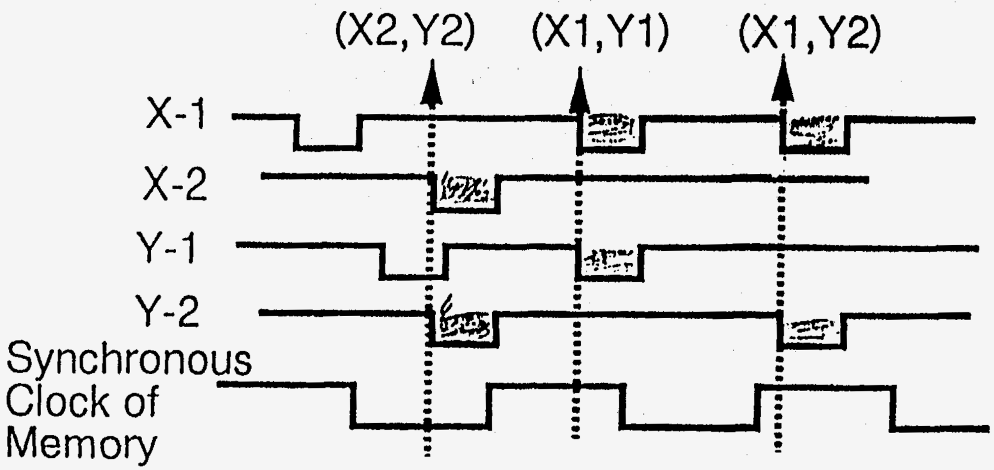

Schematic diagram of signal processing from MSGC.

Signal of MSGC is at first amplified and discriminated for every channel, and then pulse from dicriminator is latched in VME memory module synchronously with ~ 10 MHz clock.

Large area Two dimensional MSGC

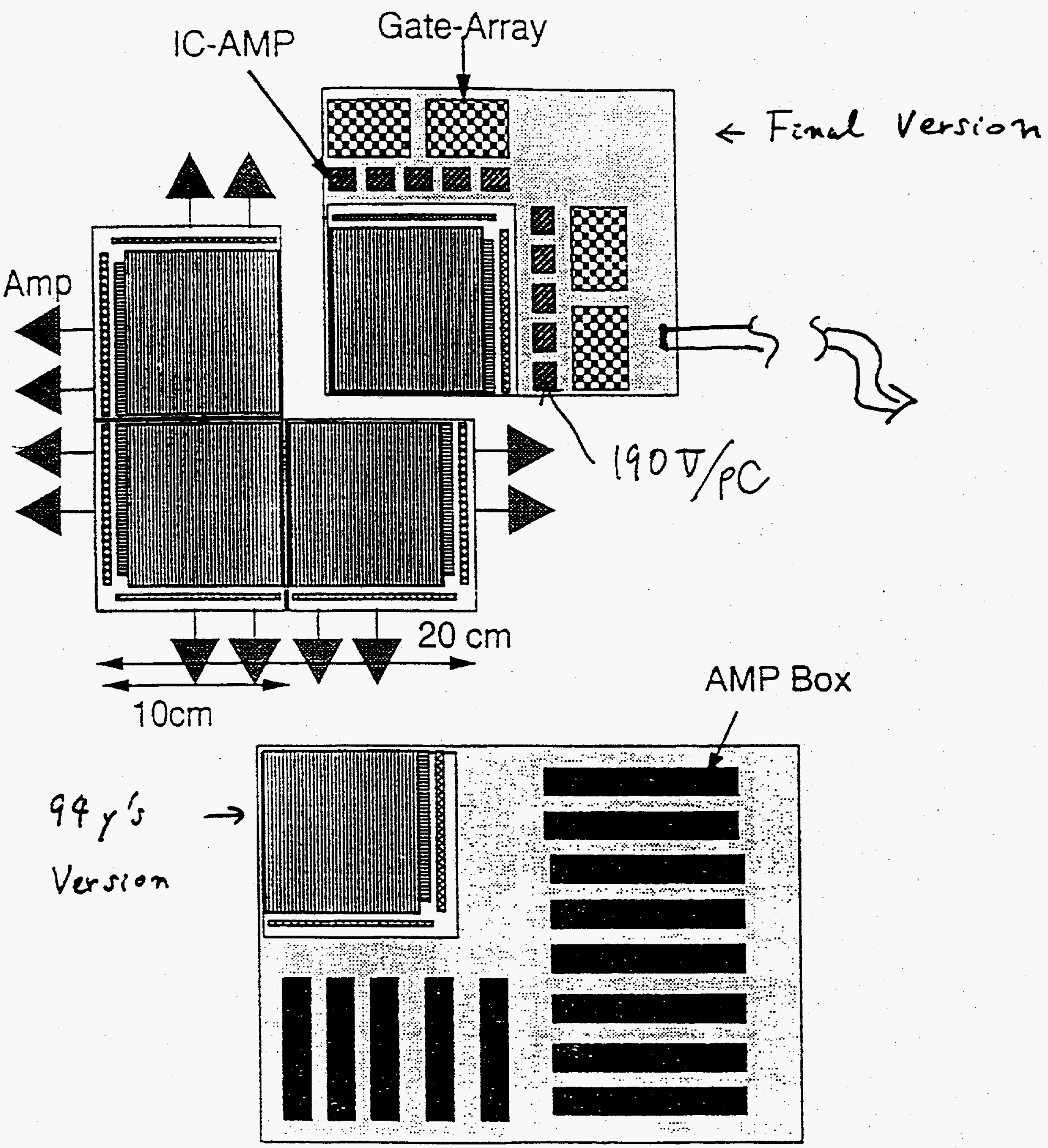

Large Imaging MSGC with 20cm x 20cm effective area, which consists of four MSGCs with 10cm x 10cm effective area

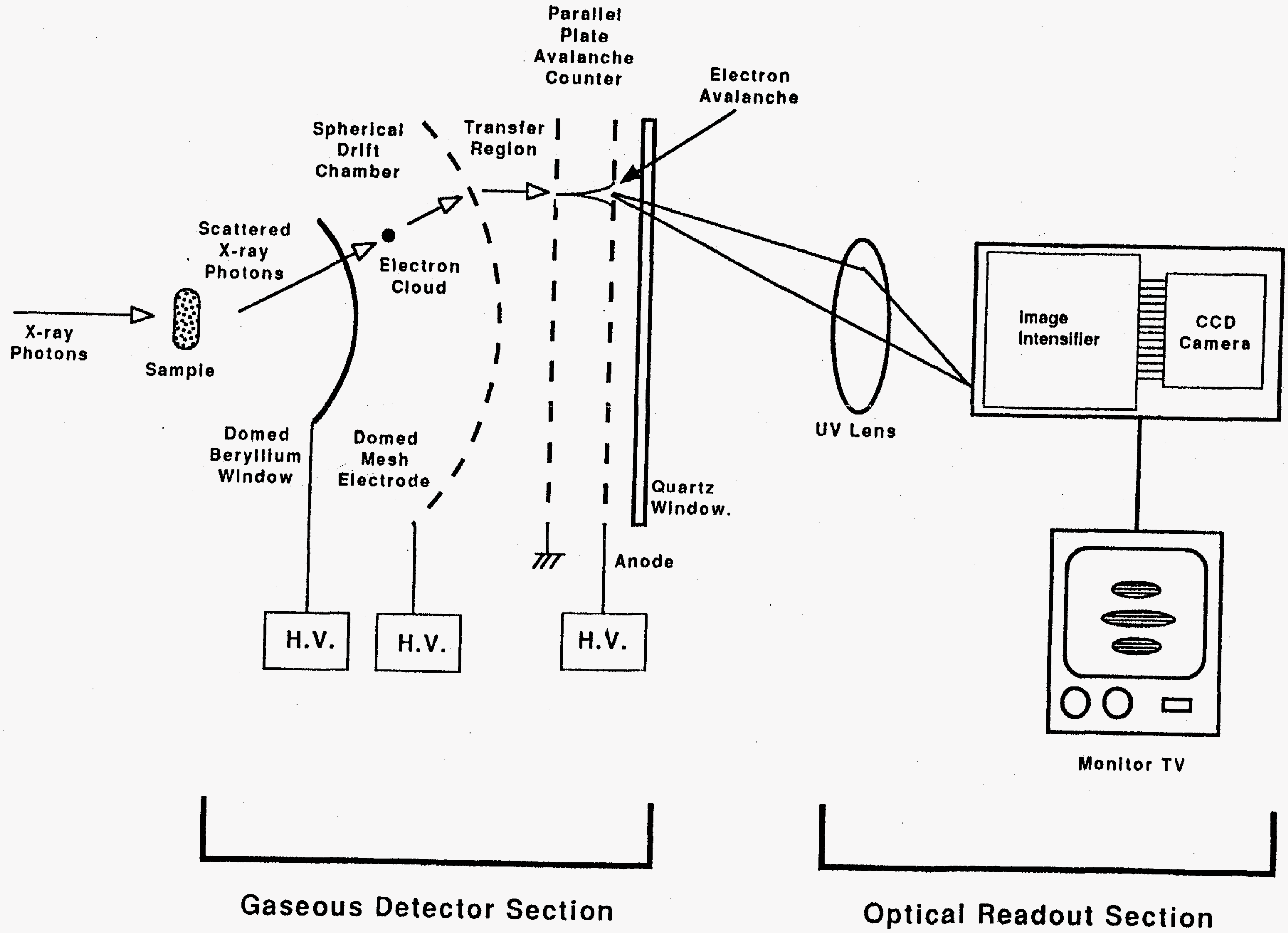
X-ray Photons
Sample
Scattered X-ray Photons
Domed Beryllium Window
Electron Cloud
Spherical Drift Chamber
Domed Mesh Electrode
Transfer Region
Parallel Plate Avalanche Counter
Electron Avalanche
Quartz Window.
Anode
H.V.
H.V.
H.V.
UV Lens
Image Intensifier
CCD Camera
Monitor TV
Gaseous Detector Section
Optical Readout Section

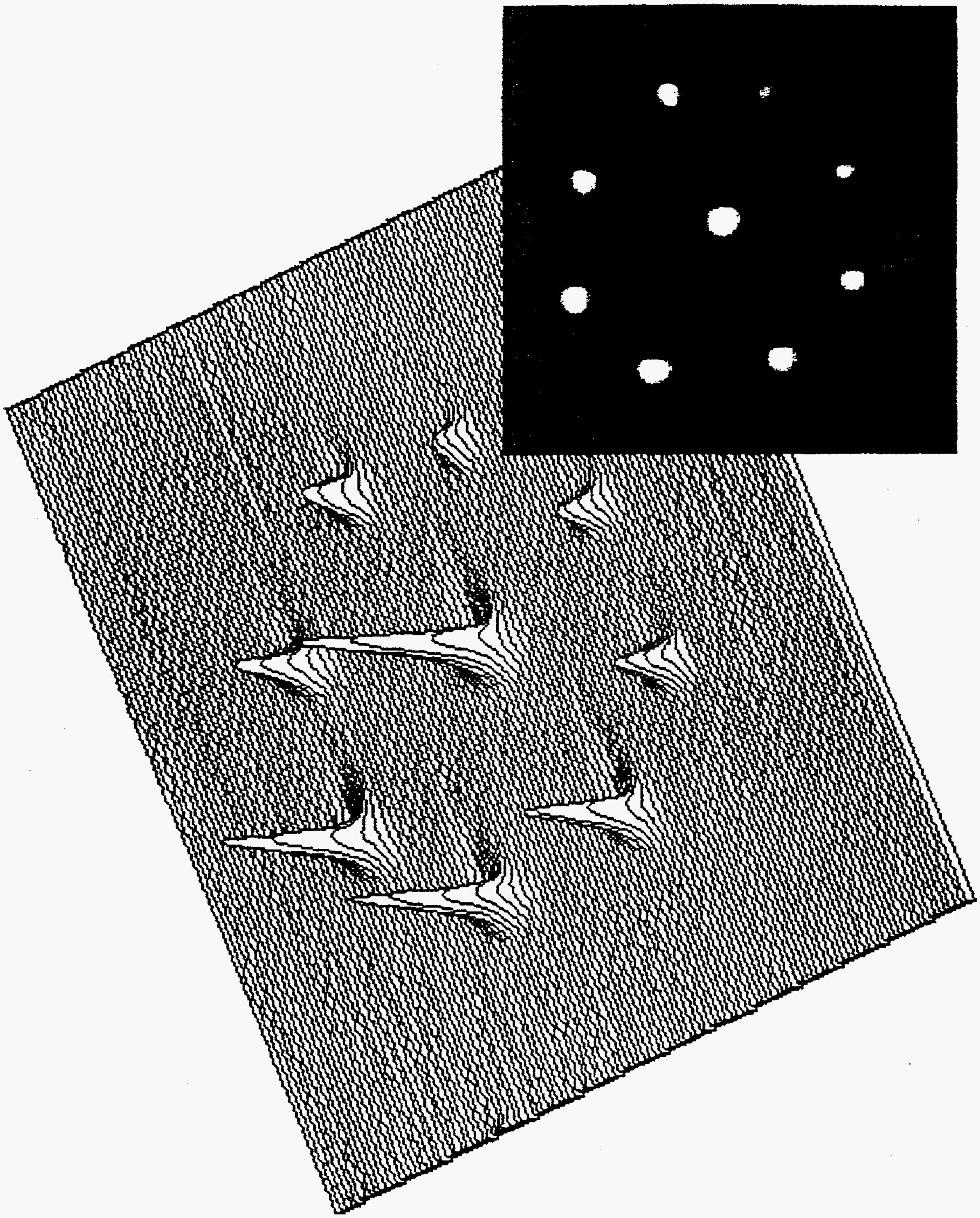

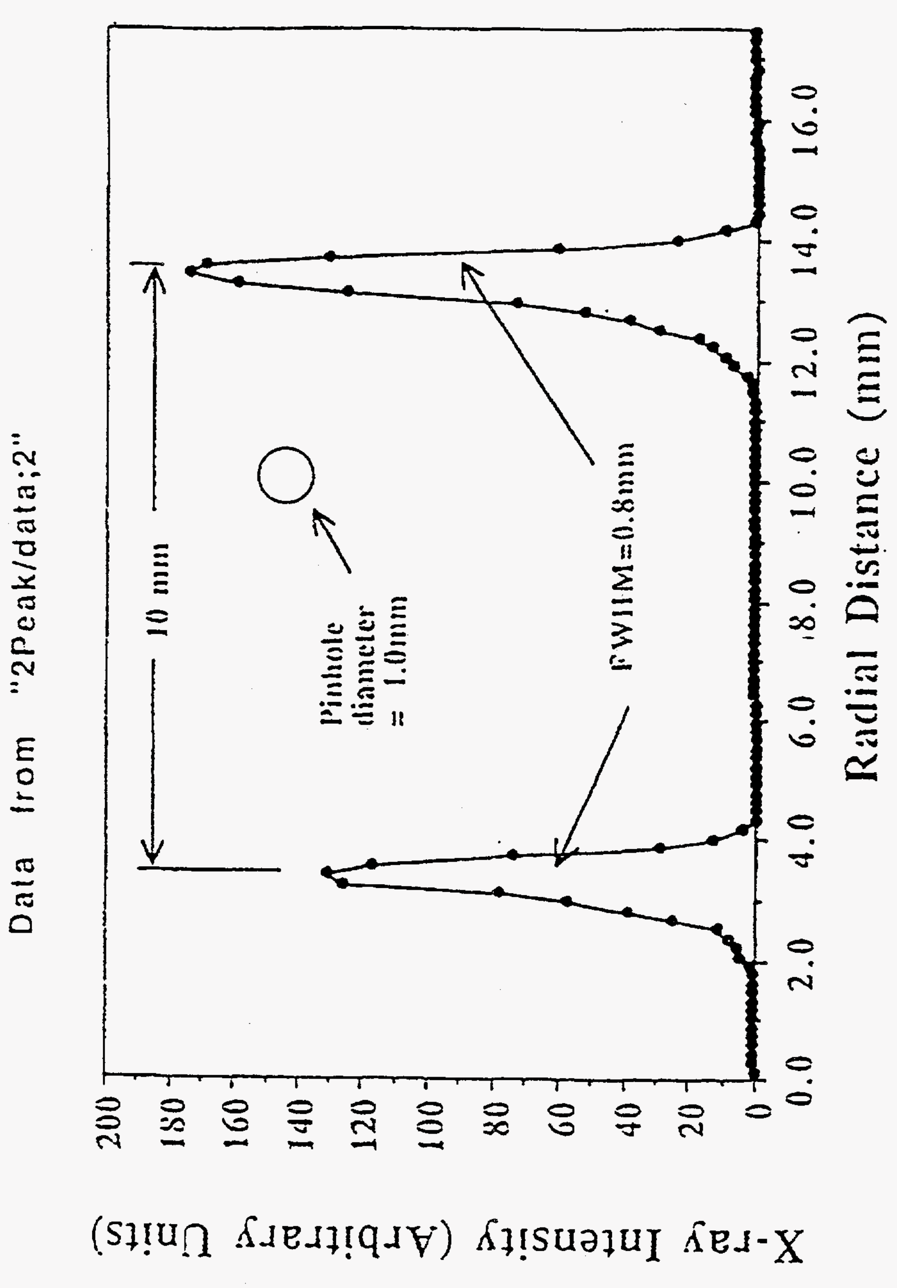
Data from "2Peak/data;2"
10 mm
Pinhole diameter = 1.0mm
FWHM=0.8mm
Radial Distance (mm)
X-ray Intensity (Arbitrary Units)
0.0 2.0 4.0 6.0 8.0 10.0 12.0 14.0 16.0
0 20 40 60 80 100 120 140 160 180 200

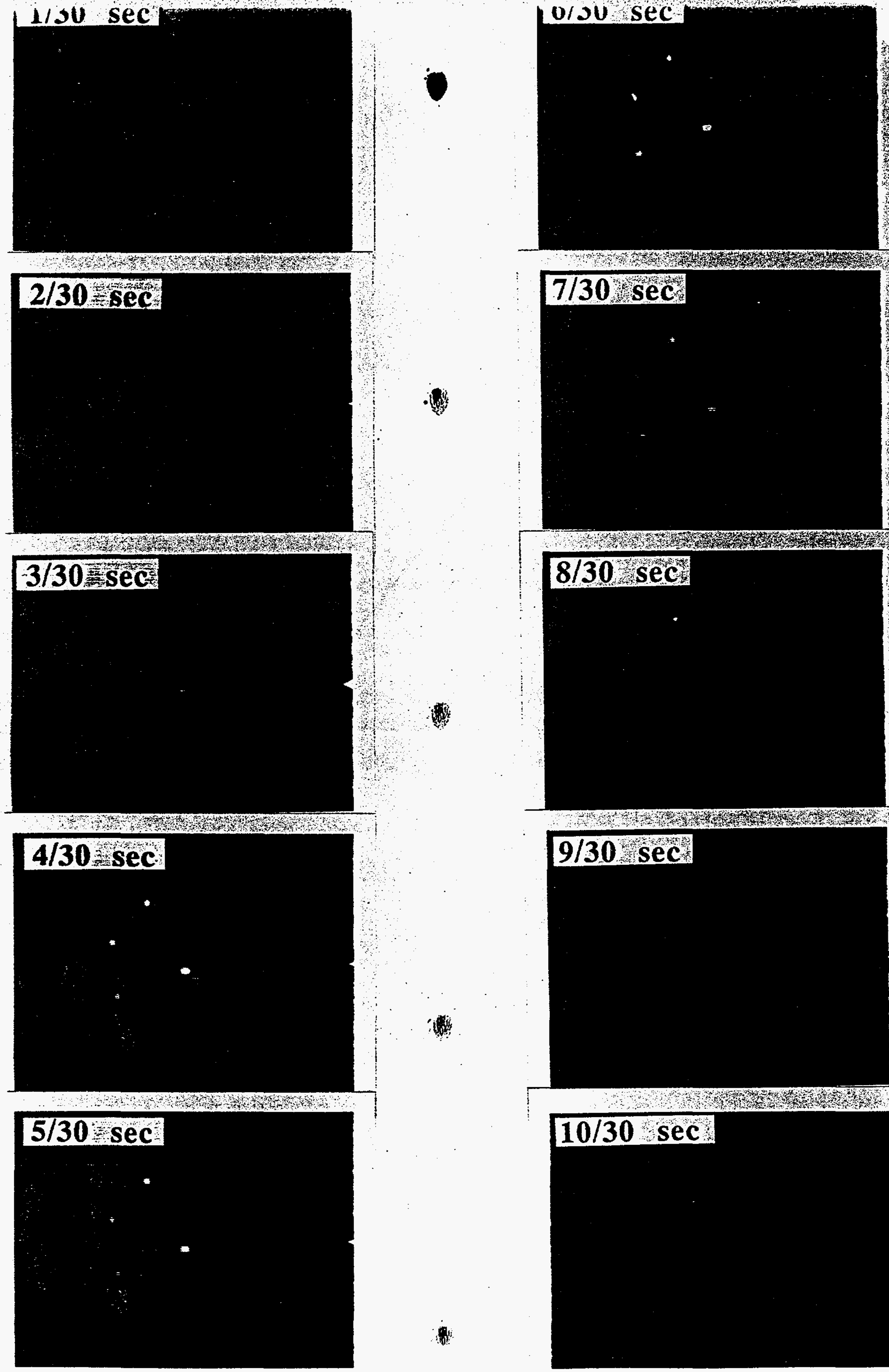
1/30 sec
2/30 sec
3/30 sec
4/30 sec
5/30 sec
6/30 sec
7/30 sec
8/30 sec
9/30 sec
10/30 sec

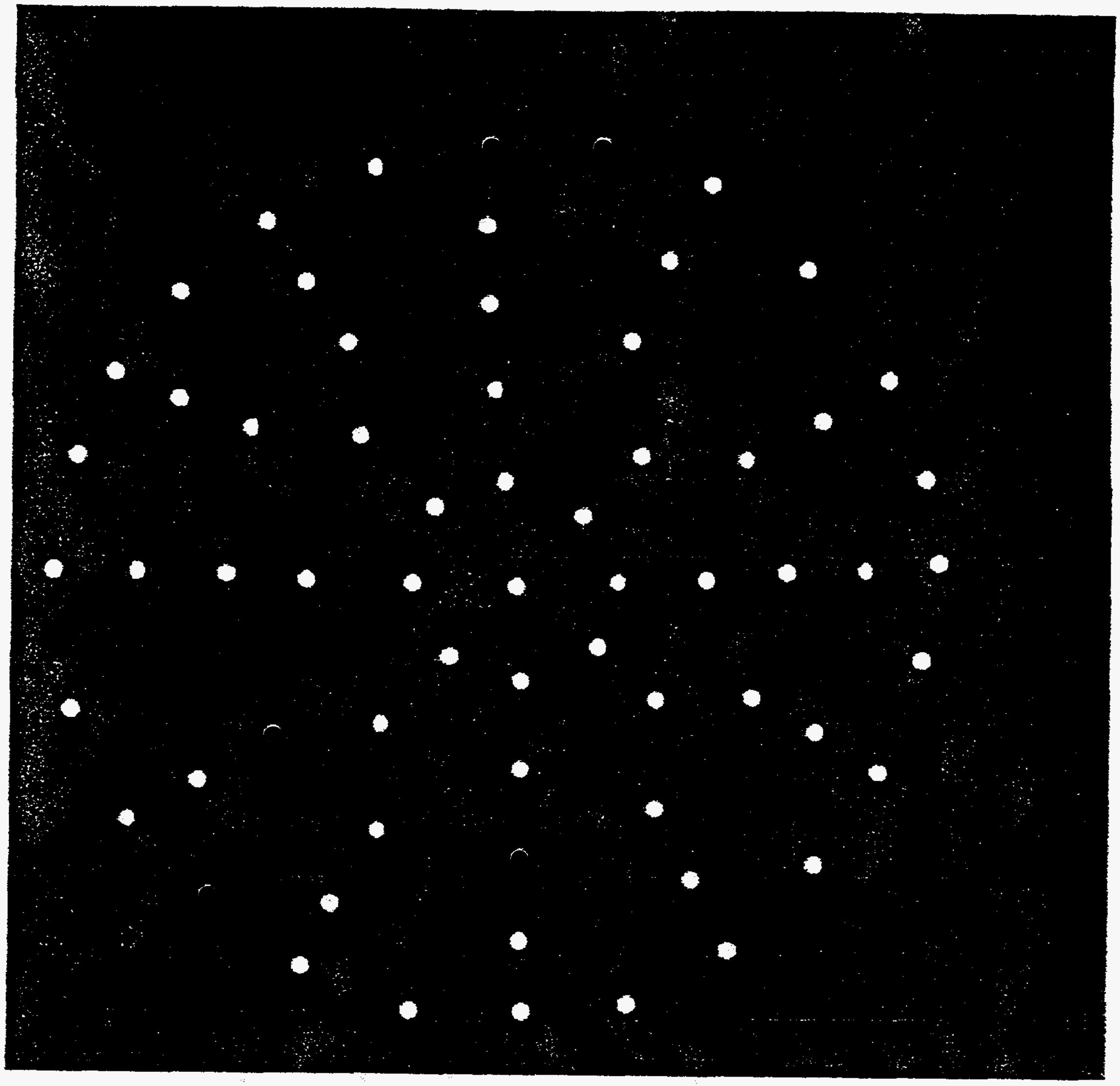

$\sigma_\theta < 170\ \mu m$

$\sigma_\phi < 100\ \mu m$

Detector Development at SPring-8

Masayo SUZUKI and Tatzuo UEKI

RIKEN, SPring-8 Project Team

[1] CdTe Solid State Detector

[2] Ring-Cathode Proportional Detector

[3] Image Plate System

[4] X-ray Image Intensifier

[5] MicroStrip Gas Chamber

[6] Proportional Scintillation X-ray Imaging Chamber

CdTe Array

by SHIMADZU Corporation

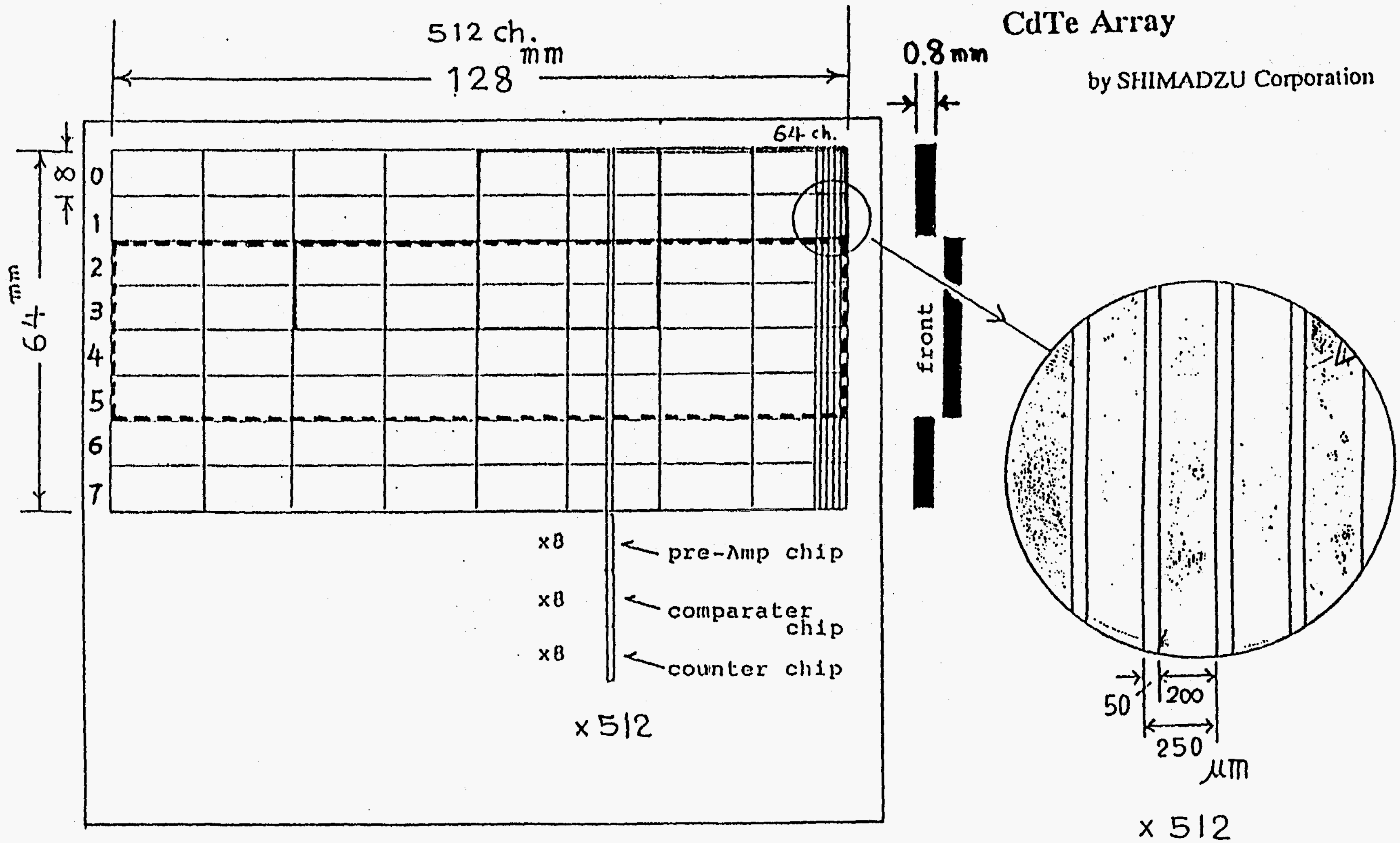

Cauchois Type Analyzer

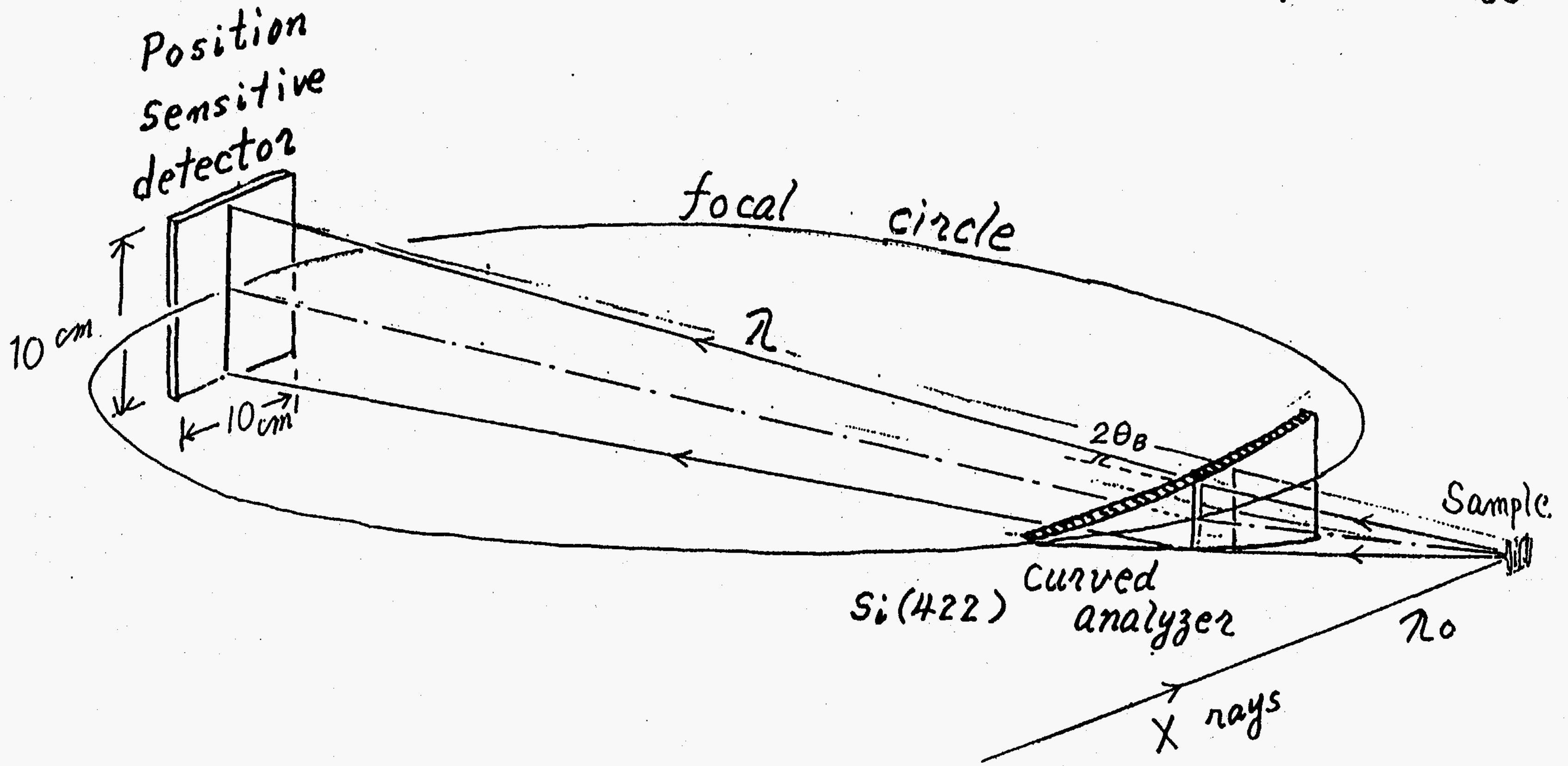

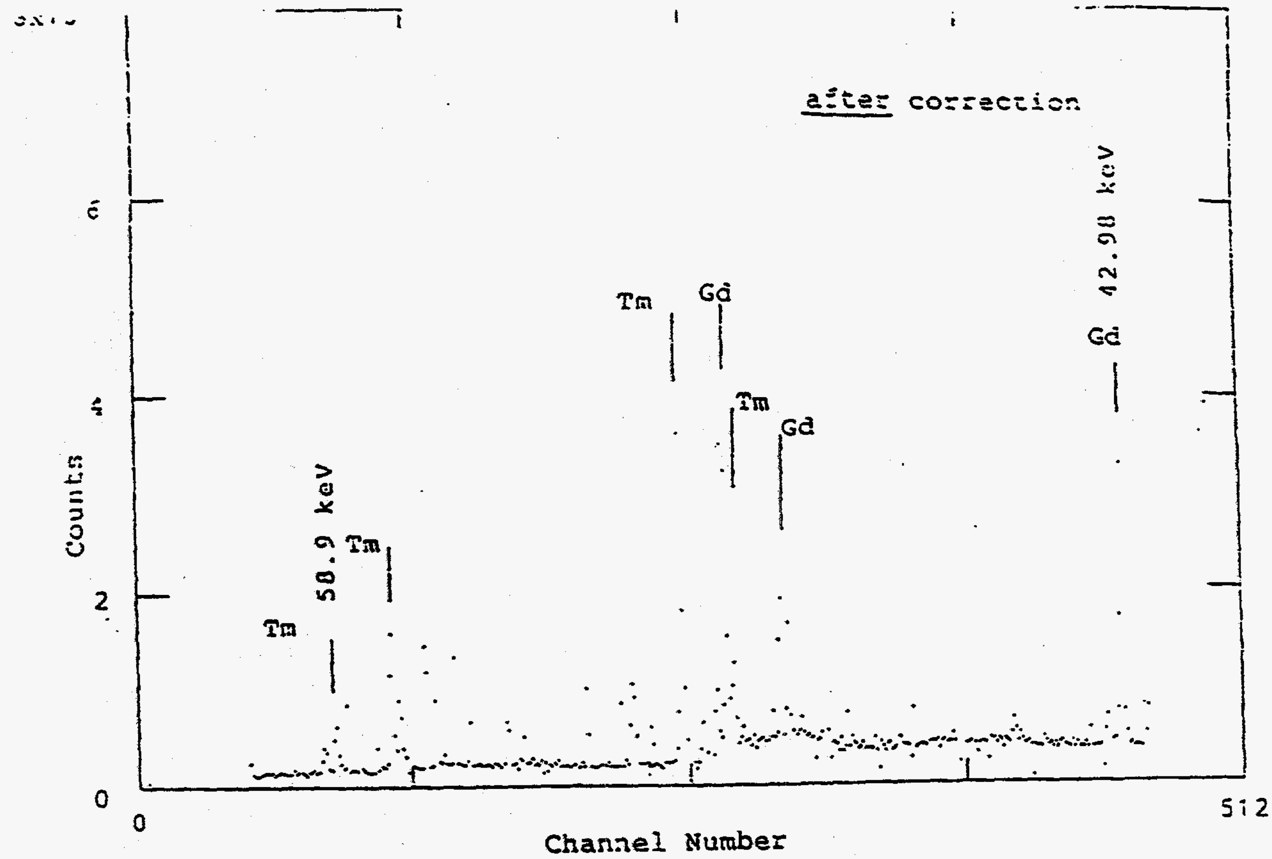
after correction
42.98 keV
Gd
Tm
Gd
Tm
Gd
58.9 keV
Tm
Tm
Counts
0
2
4
6
0
512
Channel Number

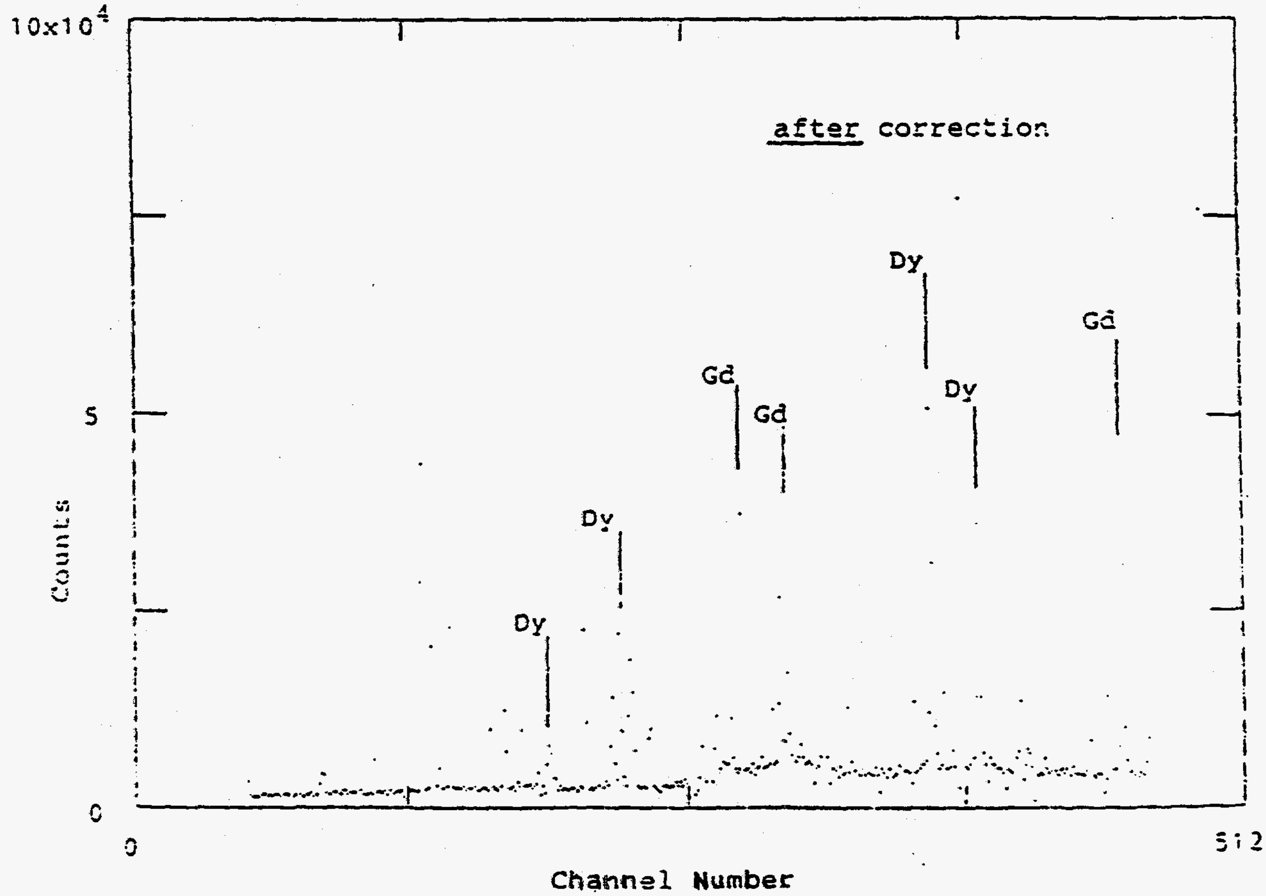
10x10^4
after correction
Dy
Gd
Gd
Gd
Dy
Dy
Dy
5
0
Counts
0
512
Channel Number

PSPCの動作原理

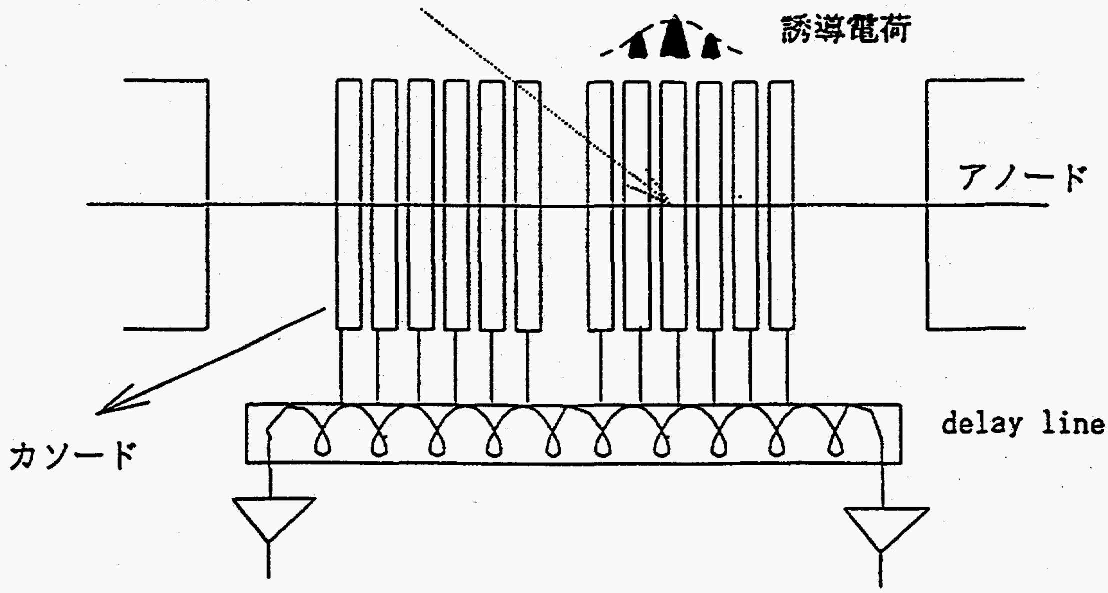

Ring detector

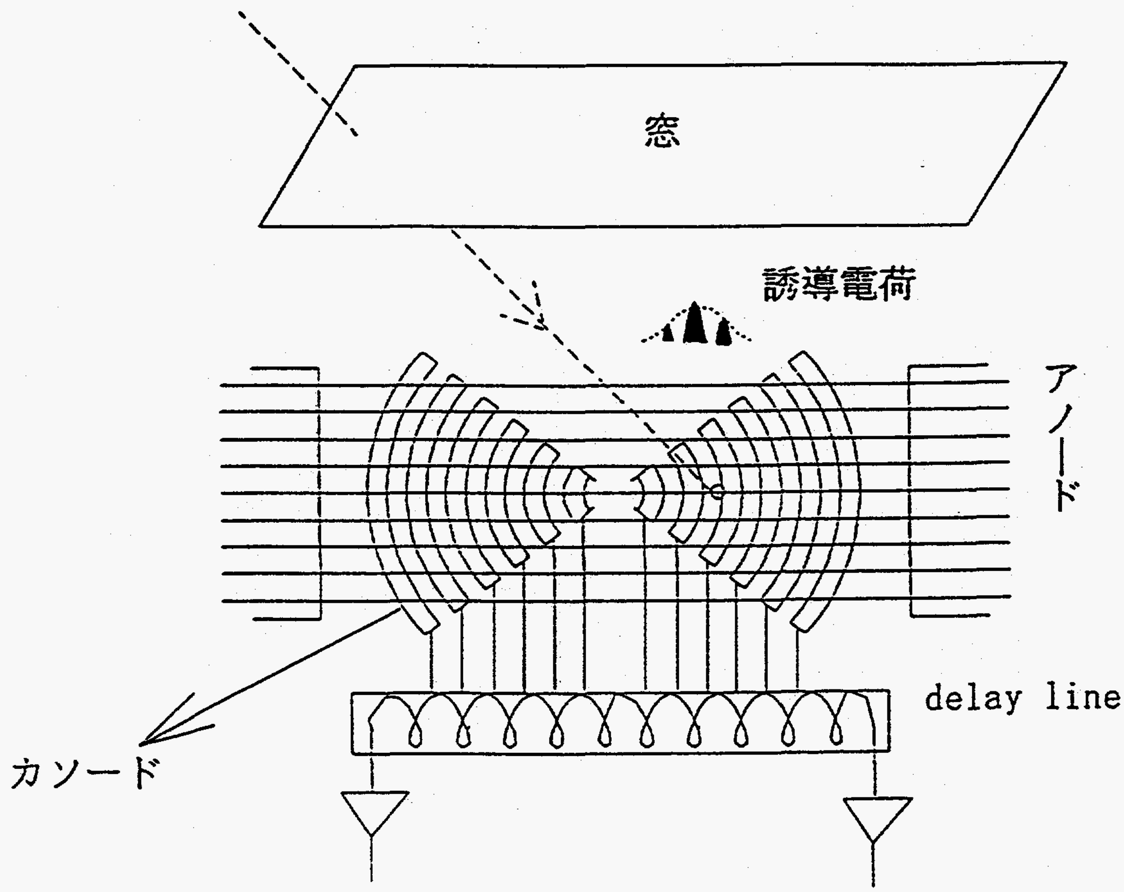

Ｒｉｎｇ－ｄｅｔｅｃｔｏｒの強度に対する感応性（補正後）

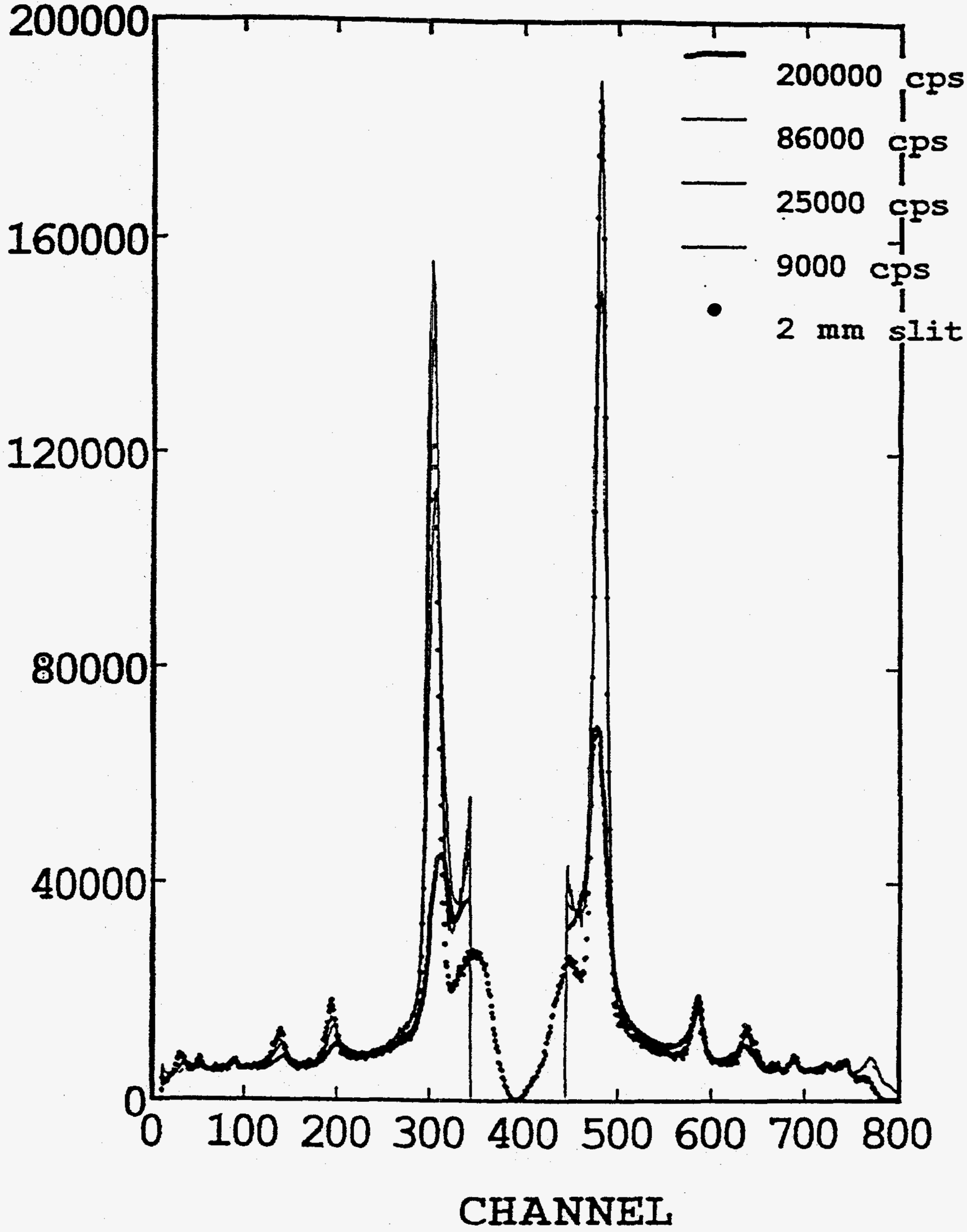

LDHの中広角散乱パターン

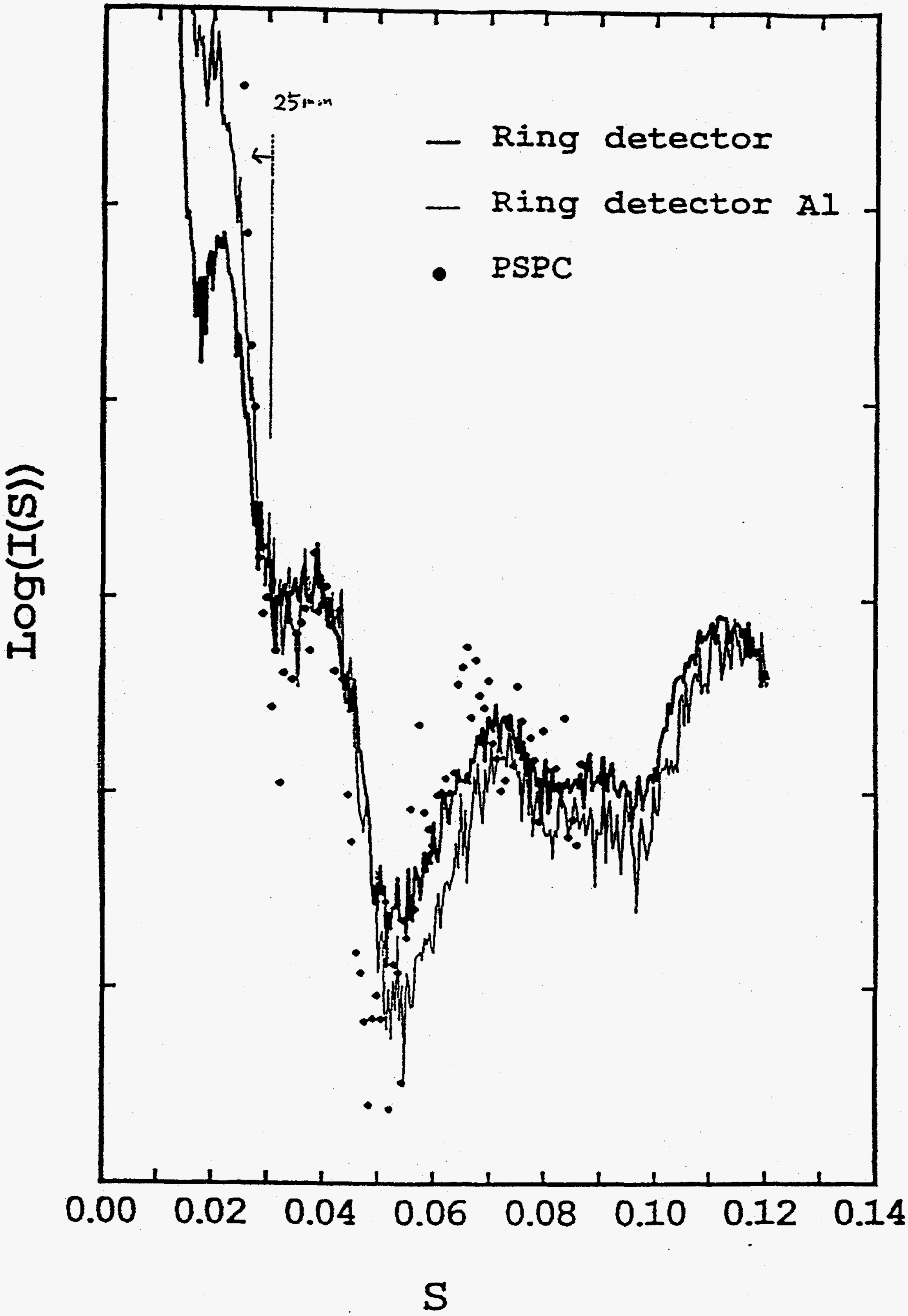

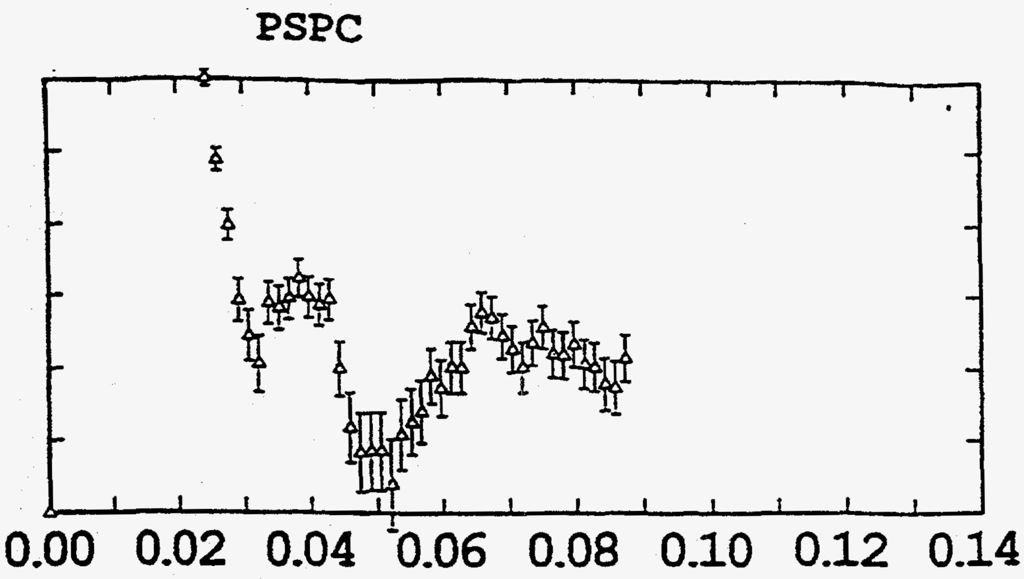
PSPC
0.00
0.02
0.04
0.06
0.08
0.10
0.12
0.14

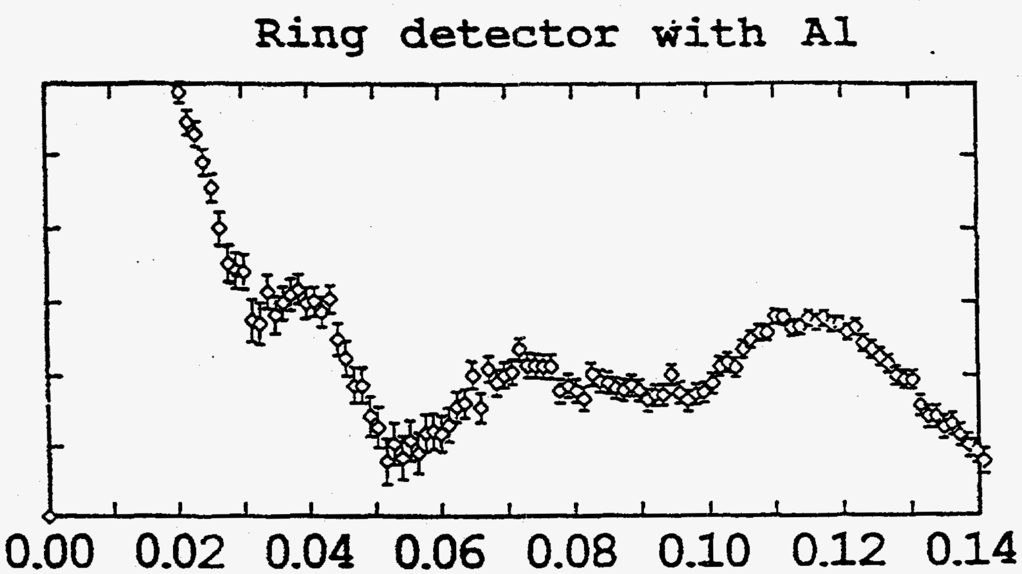
Ring detector with Al
0.00
0.02
0.04
0.06
0.08
0.10
0.12
0.14

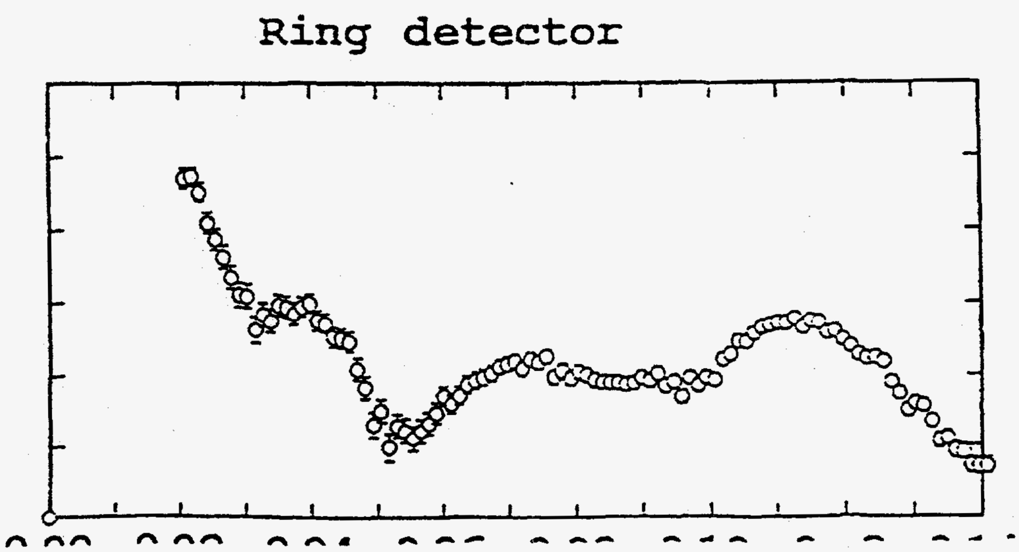
Ring detector

Imaging Plate Detector System Design

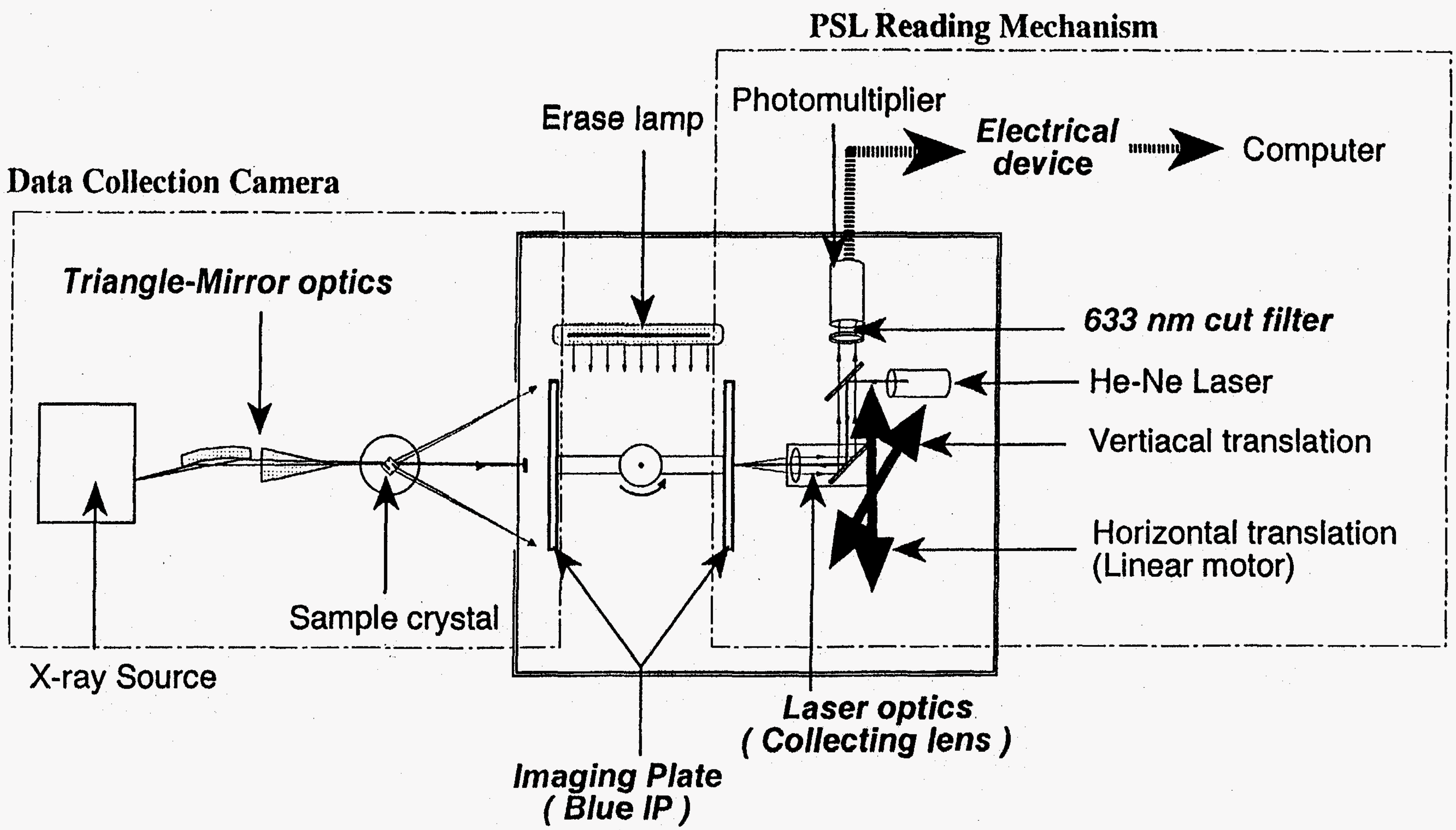

Preliminary Spatial Resolution TEST

Influence of Changing Imaging Plate and Readout Resolution

White IP (conventional type)
Fuji film BAS-HR III

Pixel Size	FWHM
100 µm	190 µm
50 µm	140 µm

Blue IP (high resolutional type)
Fuji film BAS-UR

Pixel Size	FWHM
100 µm	170 µm
50 µm	100 µm

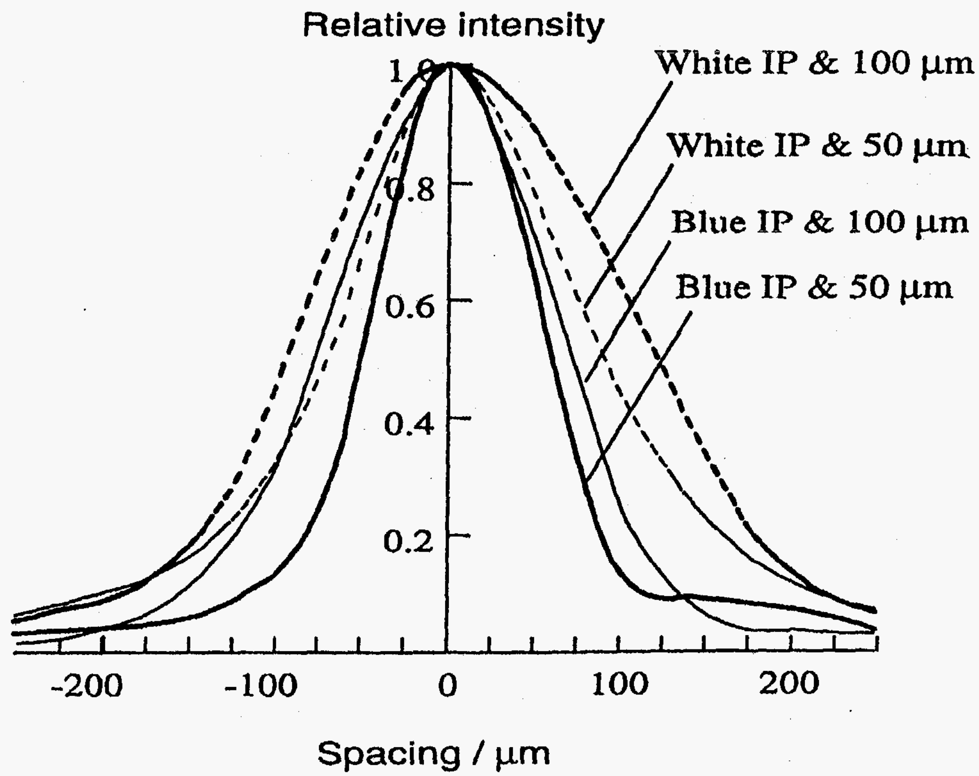

Performance of
The Imaging Plate Detector system

Spatial Resolution

Horizontal	53 μm (FWHM)
Vertical	73 μm (FWHM)

Sensitivity

The sensitivity of Blue IP is equal to that of White IP reading at 50 μm pixel size.

How to shorten the readout time

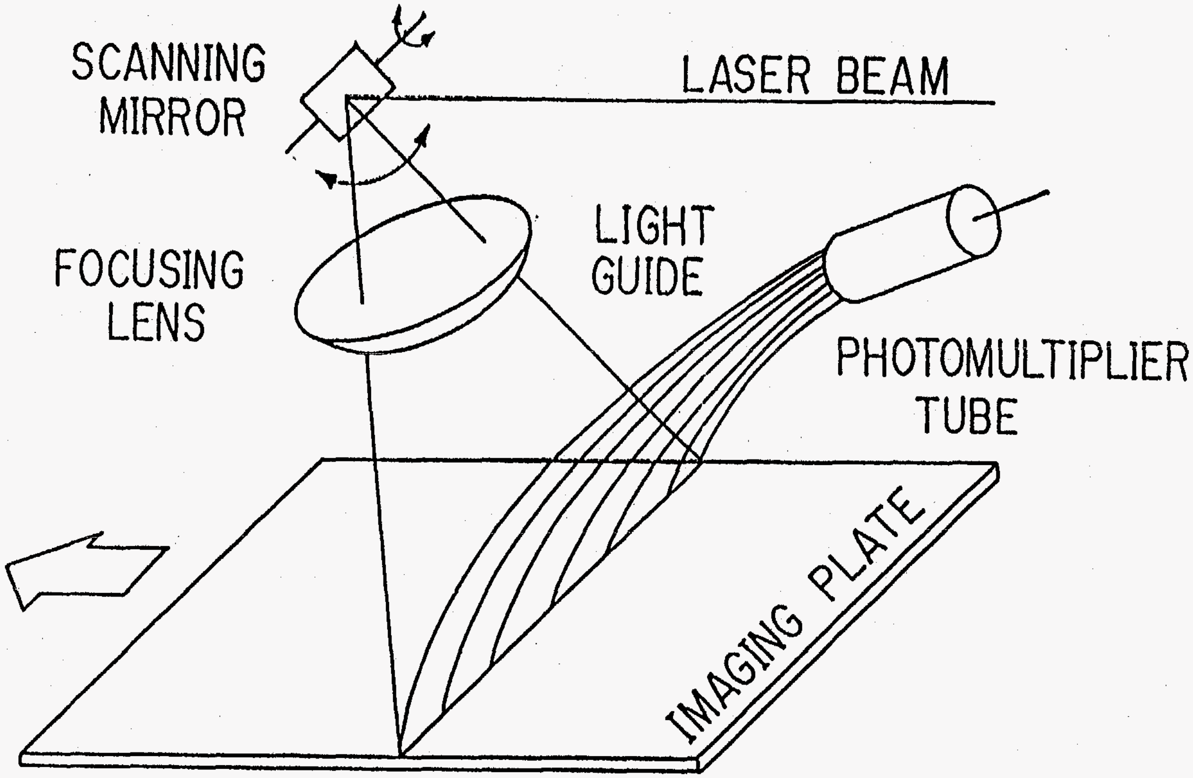

Lifetime of photostimulated luminescence (PSL) = 0.7 μsec

Readout time = 5 μsec/pixel (point by point mechanism)

How to make the line shaped laser light

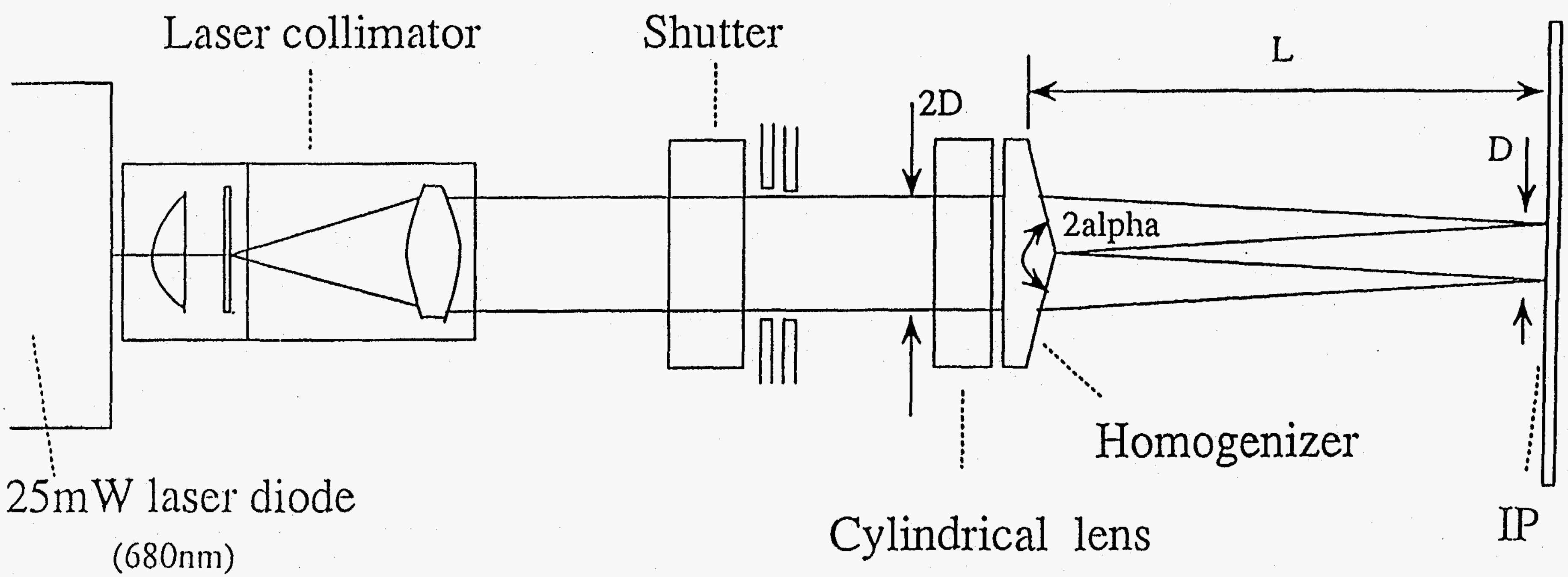

Specifications for optical lens system

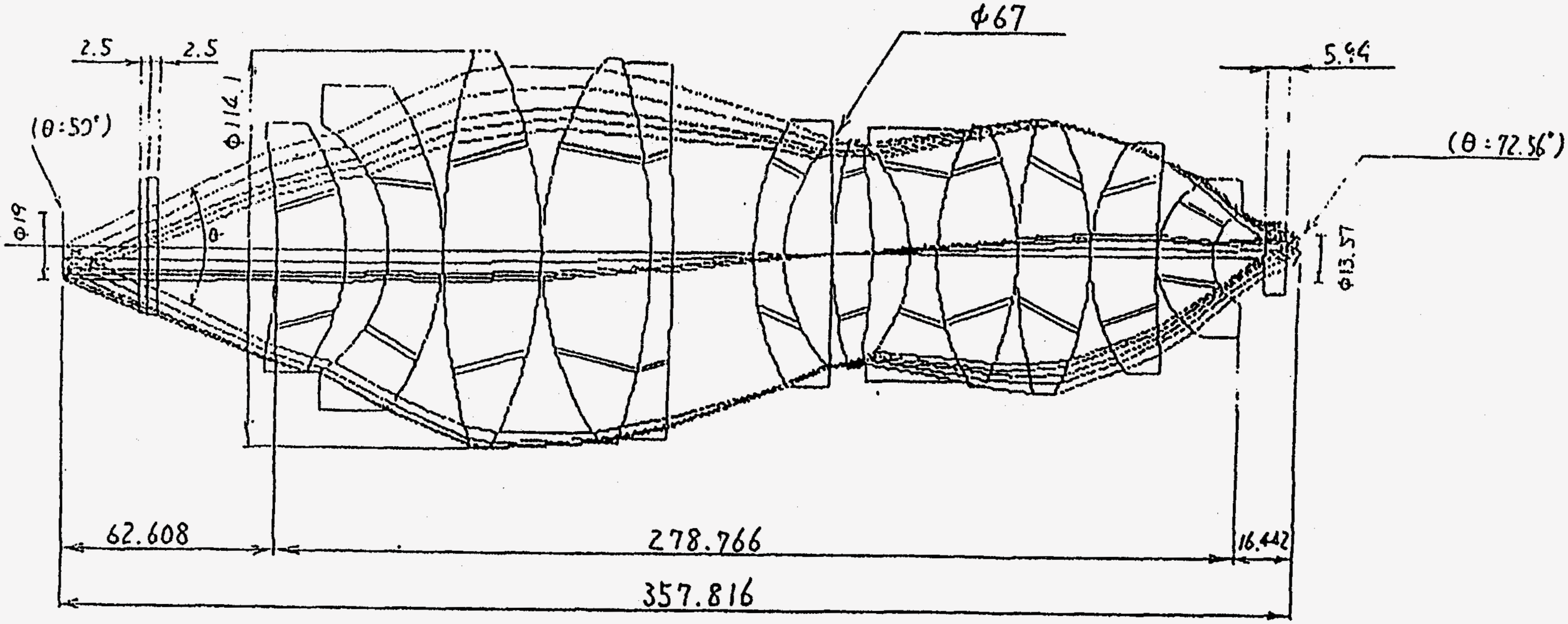

Wavelength : 380 ~ 410 nm

Magnification : 1/1.4

Numerical aperture : 0.65 (θ=50deg.)

Aberration : 10 lp/mm (MTF50%)

Transmittance : > 70%

Schematical drawing of prototype reader

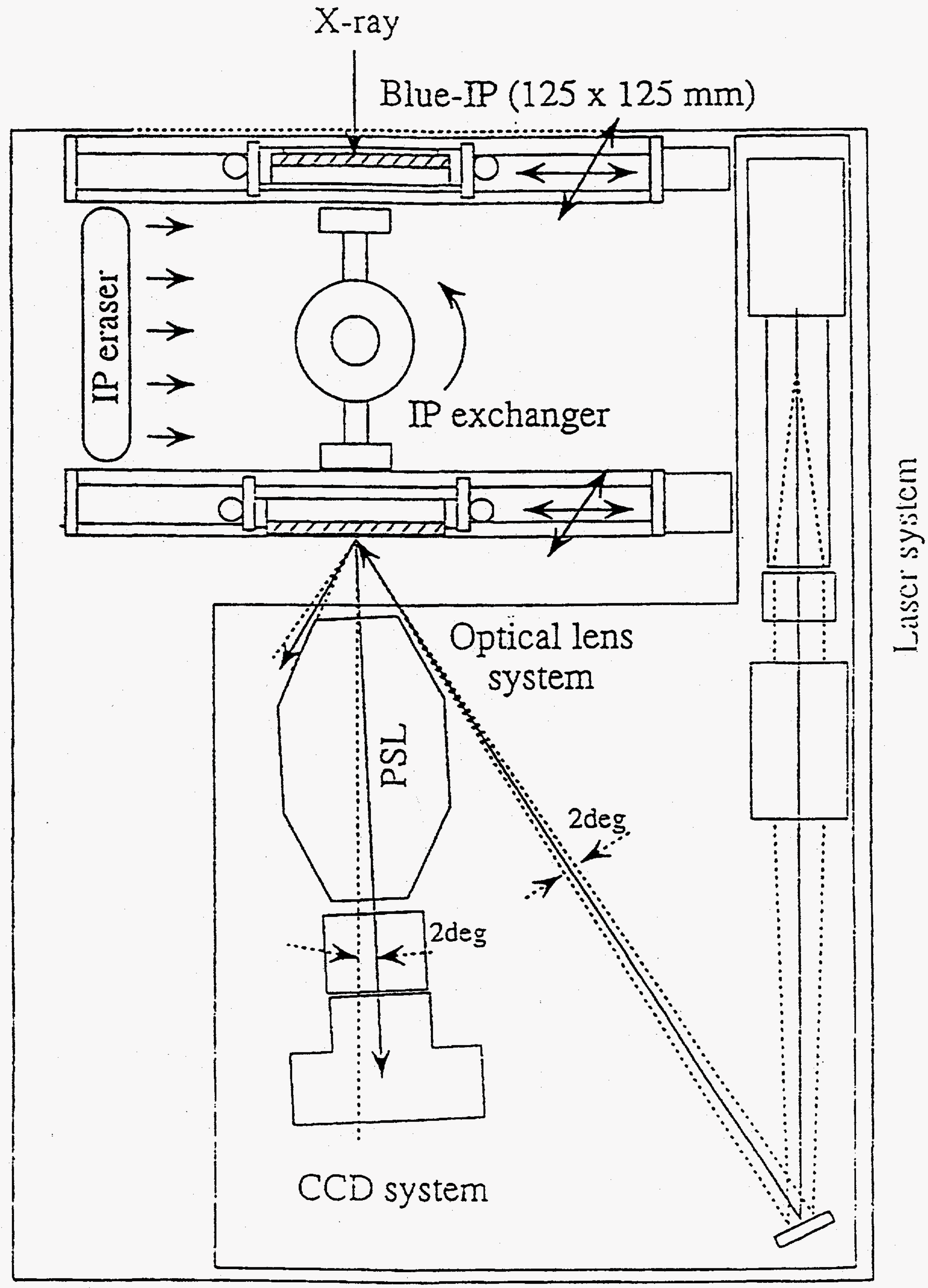

FEB-11-'94 FRI 00:52

TERM ID: XFD BLDG 362 P-9999

TEL NO.: (708) 252-3222

TRANSMIT RECORD

NO.	DATE	ST. TIME	TOTAL TIME	ABBR	ID	STATUS	#PGS	DEPT CODE	COMM. CODE
283	02-09	15:36	00°00'47		708 252 5753	OK	1		0688008000008800
284	02-09	16:13	00°00'42		TRA-CON INC	OK	1		0088008000009600
285	02-09	16:20	00°00'44		214 680 3331	OK	1		0688008000008400
286	02-09	16:25	00°00'53		712064851911	-	0		468C008100008C00
287	02-09	16:27	00°00'52		712064851911	OK	1		068C008000008C00
288	02-09	17:05	00°05'21		708 252 4500	OK	5		0688008000008810
289	02-10	08:47	00°01'44		715162823238	OK	3		068800800000A410
290	02-10	09:21	00°05'05		312 996 9016	OK	7		0688008000008810
291	02-10	09:26	00°01'23		1 708 252 5274	OK	2		0688008000009E13
292	02-10	10:00	00°00'48		708 252 5753	OK	1		0688008000008800
293	02-10	10:17	00°01'15		APS ASD DCC	OK	2		0088008000009611
294	02-10	10:29	00°01'25		312 996 9016	OK	2		0688008000008810
295	02-10	12:45	00°01'01		CTD TEL SVC	OK	1		0088008000009600
296	02-10	13:27	00°01'01		7082527305	OK	1		0688008000008800
297	02-10	14:18	00°00'53		25948	OK	1		0688008000009E00
298	02-10	14:23	00°00'45		048 462 4641	OK	1		0688008000008800
299	02-10	15:13	00°00'56		73497156	-	0		468C008020008816
300	02-10	15:21	00°01'02		7082527305	OK	1		0688008000008800
301	02-10	15:40	00°02'20		914 945 4407	OK	4		0688008000009011
302	02-10	15:59	00°01'01		7082527305	OK	1		0688008000008800
303	02-10	16:04	00°02'05		22948	OK	3		0688008000008810
304	02-10	16:24	00°00'48		7166343957	OK	1		0688008000003100
305	02-10	16:41	00°08'41		510 422 1370	OK	17		0688008000006610
306	02-10	16:52	00°01'43		7085623075	OK	3		068800800000A416
307	02-10	17:36	00°01'01		7082527305	OK	1		0688008000008800
						TOTAL #PGS	61		

RECEIVE RECORD

NO.	DATE	ST. TIME	TOTAL TIME	ABBR	ID	STATUS	#PGS	DEPT CODE	COMM. CODE
268	02-09	15:30	00°01'13		ARGONNE MSD-223	OK	2		0088008000009600
---	02-09	16:07	00°02'04		516 282 5773	OK	4		0788208000000000
---	02-09	16:22	00°01'00		815 753 8565	OK	1		0688008000000000
---	02-09	16:34	00°01'15		7082527305	OK	1		0788008000000000
---	02-09	17:22	00°00'58			OK	1		064C008000000000
---	02-09	22:23	00°04'35		708 972 9647	OK	6		068C008000000000
---	02-10	04:49	00°01'45		7087786615	OK	2		068C008000000000
---	02-10	07:04	00°00'57		031 650 4743	OK	1		0688008000000000
---	02-10	08:31	00°00'49		1 317 453 0460	OK	1		0688008000000000
---	02-10	09:29	00°00'33		-G3-	OK	1		0788008000000000
---	02-10	10:24	00°03'16		515 294 0689	OK	3		06E8008010000060
217	02-10	10:39	00°00'48		APS ASD DCC	OK	1		0088008000009600
---	02-10	11:15	00°01'08		615+483+2177	OK	2		0788008000000000
---	02-10	12:13	00°00'38		3137642193	OK	1		0788008000000000
---	02-10	12:19	00°01'06		619 562 3728	OK	1		068C008000000000
---	02-10	12:25	00°03'38		B E . -B.J.	OK	5		068C008000000070
---	02-10	12:52	00°03'35			OK	5		068C008000000000
---	02-10	13:12	00°00'56		13125673576	OK	1		0688008000000000
---	02-10	14:40	00°01'42			OK	3		068C008000000000
---	02-10	14:56	00°01'38		3174940706	-	0		46C80081100000F0
---	02-10	15:00	00°01'22		5019688645	OK	2		0688008000000000
---	02-10	15:08	00°00'54		+708 674 4133	OK	1		0688008000000000
---	02-10	15:23	00°08'42		7085623075	OK	7		07F8008010000000
---	02-10	16:21	00°00'49			OK	1		068C0080000000[illegible]
---	02-11	00:45	00°06'55		048 462 4641	OK	16		078800800000[illegible]
						TOTAL #PGS	69		

END PAGE

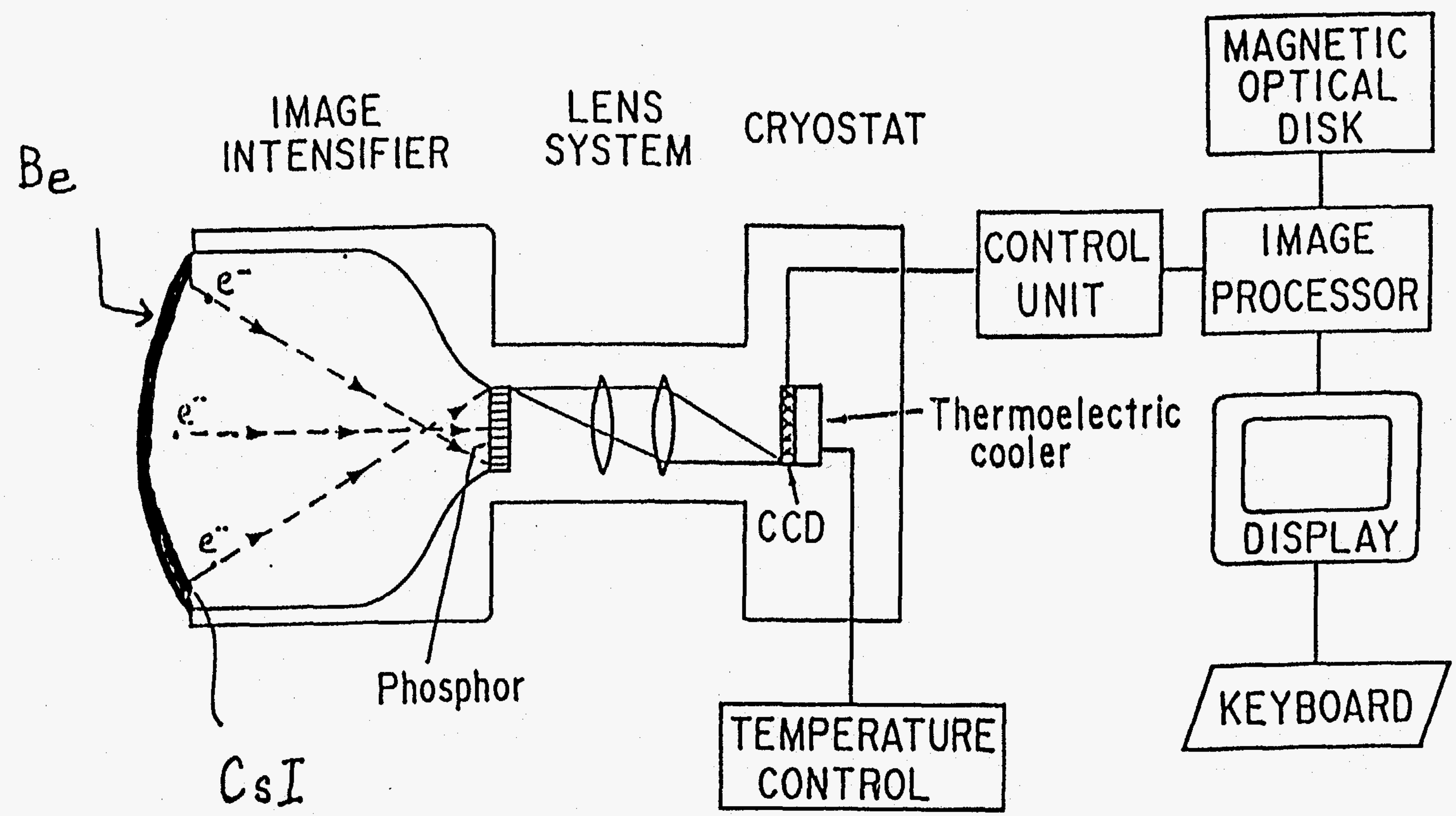

Schematics of the X-ray TV detector which utilizes the Be-window X ray image intensifier together with a cooled or a TV-rate CCD.

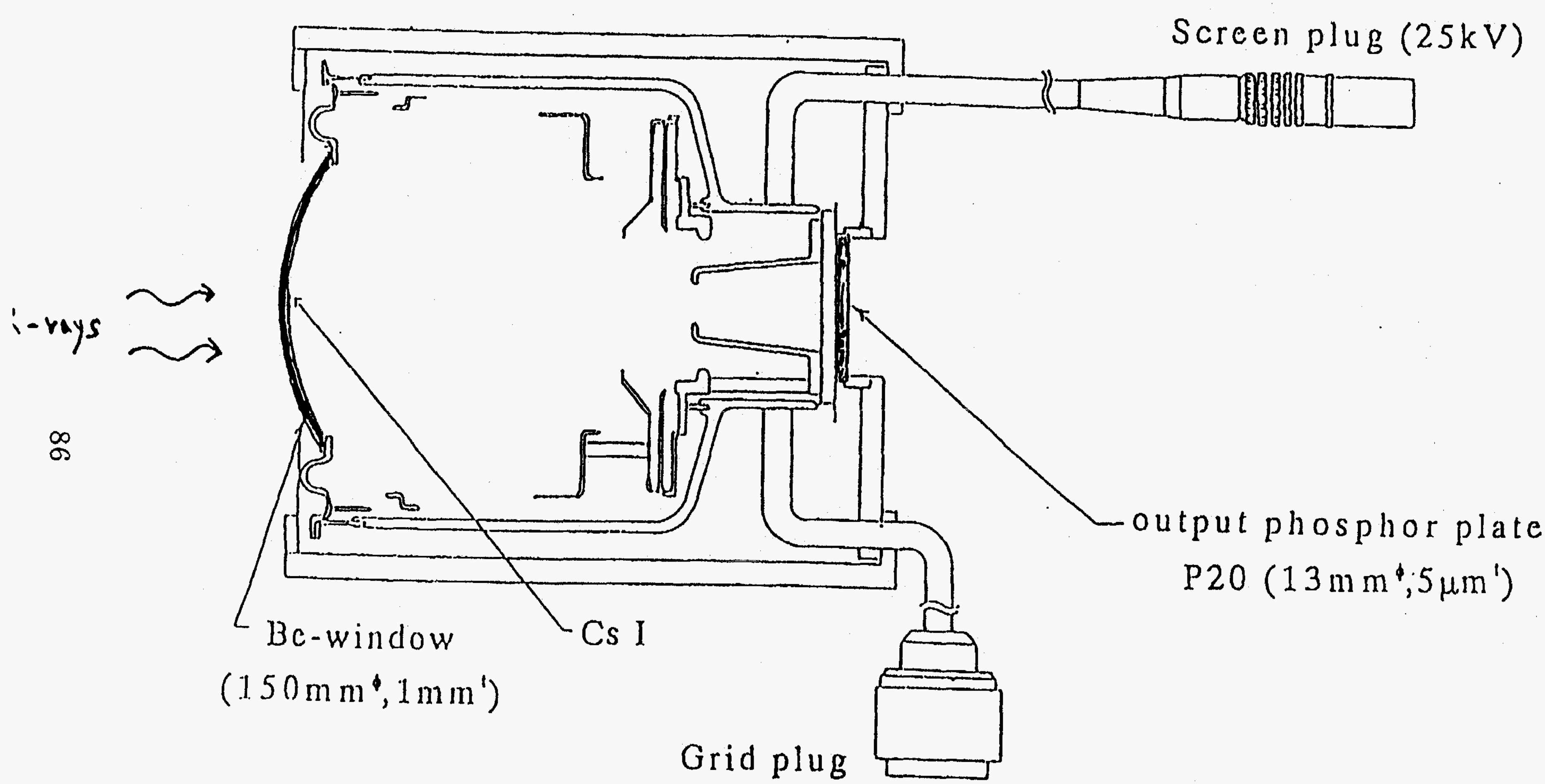

Be-windowed X-ray Image Intensifier

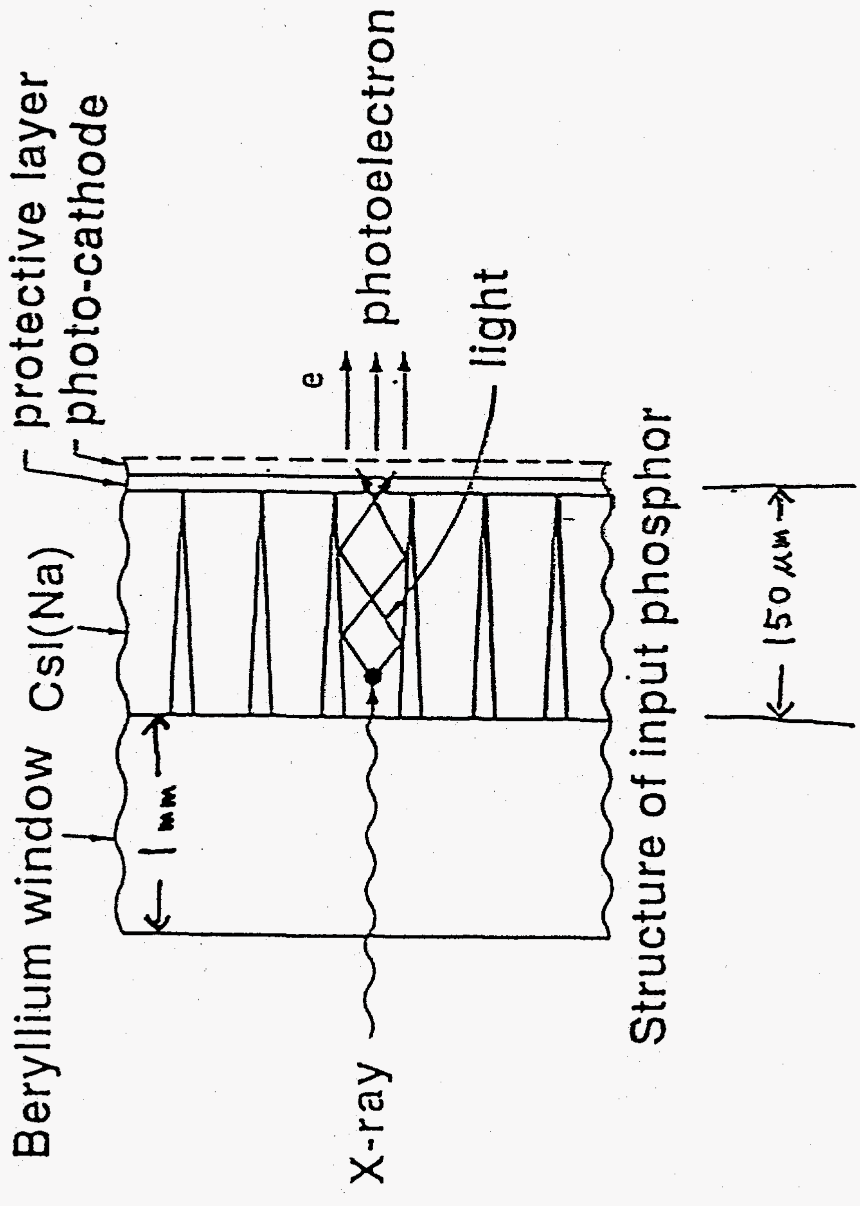

Structure of input phosphor

XII ⊕ レンズ ⊕ C4880

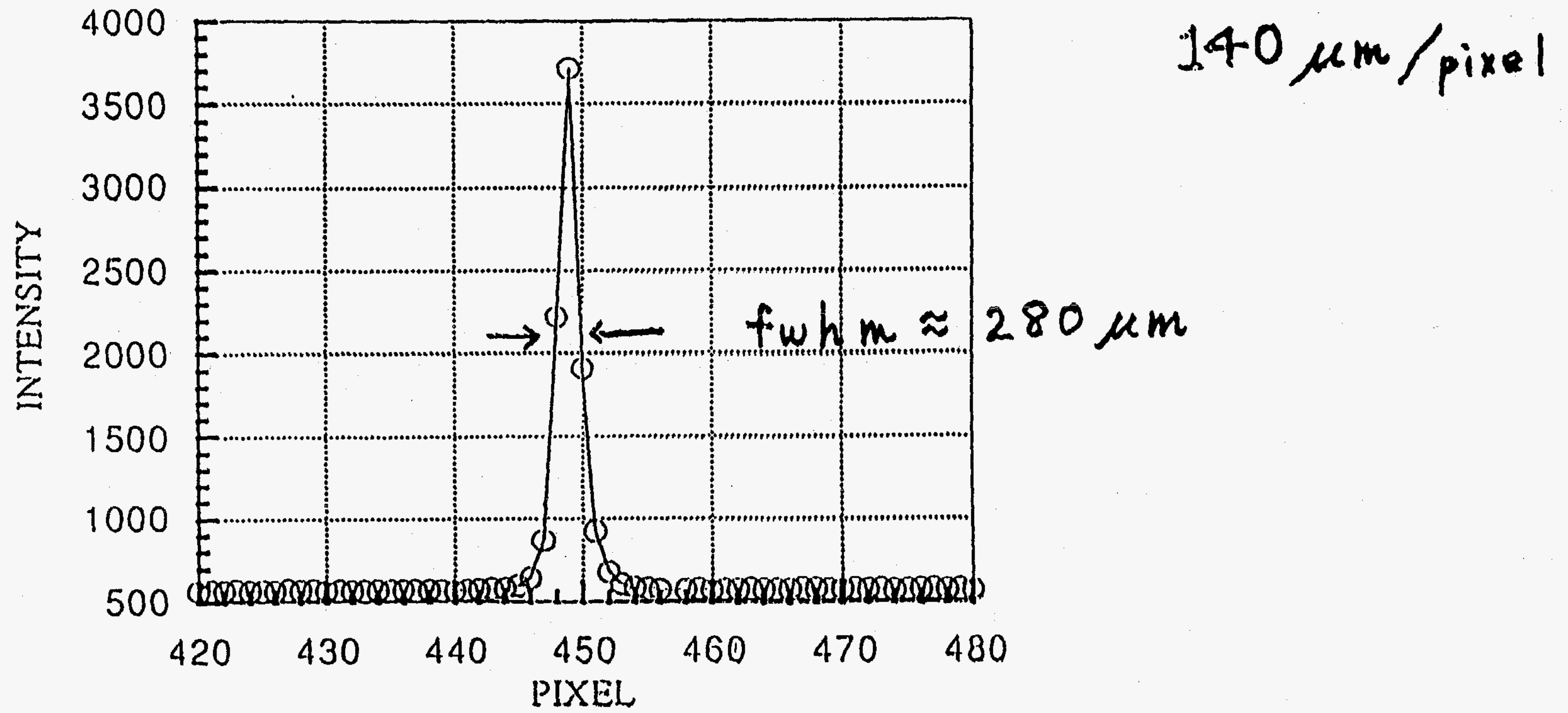

Hobart Kraner and Graham Smith

Brookhaven National Laboratory

Development of Gas and Silicon X-ray Detectors at BNL

Some basic characteristics of two-dimensional detectors based on multiwire proportional chambers, developed at BNL over the last several years, are presented, including position resolution (about 100 μm FWHM for 8 keV in xenon), counting rate capability (a few 10^5 s^{-1}) and differential nonlinearity (of order ±4%). The performance of a two-dimensional detector in combination with a purpose-built TDC, at the time-resolved beamline X12B of the NSLS, is described. A new generation of very high rate two-dimensional proportional chambers are now being developed in which the fundamental limit to position resolution will be achieved, but the limitations associated with counting one event at a time will be very much reduced. In this new class of device, based on similar principles to those being developed for multiparticle detection in high energy and nuclear physics experiments, position readout is carried out solely on the rear cathode, which is fabricated as an array of geometrically shaped pads. With close anode-wire spacing of less than one millimeter and compact low-noise preamplifiers fabricated in monolithic form, a detector of area 20 cm x 20 cm is being designed with over 10^8 s^{-1} rate capability.

Silicon drift chambers have been under development for about ten years; however, their main application so far has been as position-sensitive devices for high-energy physics. X-ray detection has, nevertheless, been demonstrated and several very attractive features of this concept should be noted. The potential for this structure in the synchrotron environment will be reviewed and results to date will be summarized.

SILICON DRIFT DETECTORS

H. W. Kraner, BNL

2/14/94

INTRODUCTION

- Operation, principles
- Fabrication considerations
- Survey of types, geometries
  - linear, cylindrical, spiral, CCD

SPECIFIC EXPERIENCE

- 3" cylindrical drift chamber
- 4x4cm STAR1 prototype linear

PHOTON DETECTORS

- cylindrical, 241Am
- windows

INVENTORS: P. Rehak and E. Gatti

MAJOR CONTRIBUTORS: MPI group, L. Struder, P. Holl
J. Kemmer, also J. Walton LBL

PRINCIPLES OF SILICON DRIFT DETECTOR

(Rehak et al)

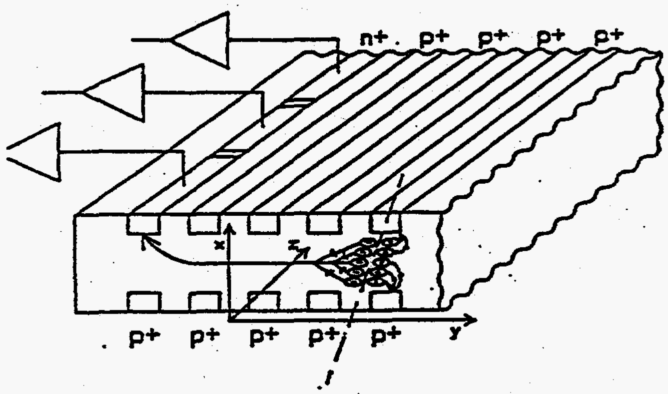

Figure 1: Perspective view (not to scale) of a semiconductor drift detector. Electrons created by an ionising particle are transported long distances parallel to the detector surface. The anode is divided into short segments to measure the coordinate perpendicular to the drift direction.

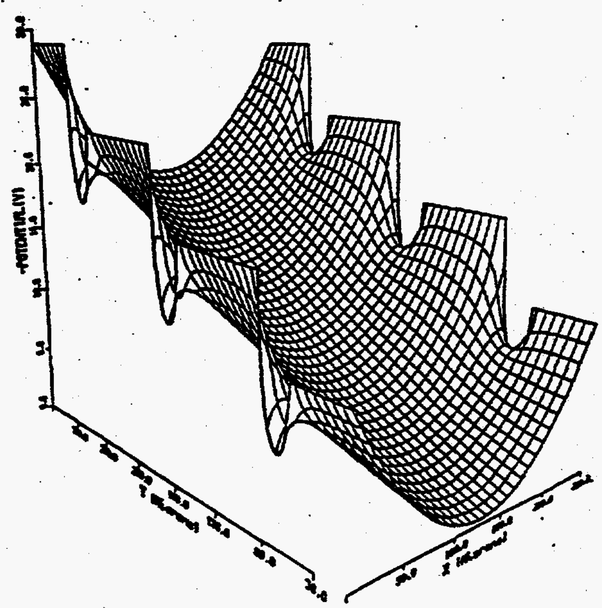

Figure 7: Negative potential in a radial cross section (called "Y") of the detector. Equipotentials imposed at both surfaces of the detector are the rectifying junctions. Surface between rectifying junctions is covered by SiO_2. Potential at this surface depends on the global design of the detector.

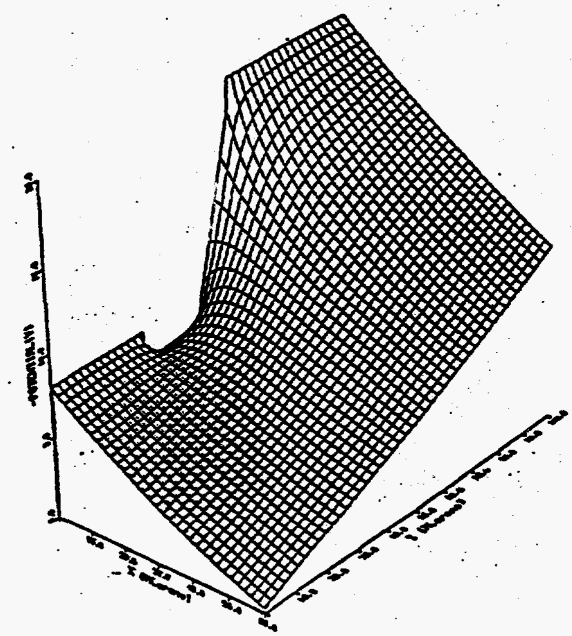

Figure 8: Detail of negative potential in a cross section of the detector close to the surface. The potential is defined in the p+ implants of two rings at both sides of the $Si - SiO_2$ interface. The secondary valley contains some electrons which form a conductive channel. There is still a barrier which prevents electrons generated on the $Si - SiO_2$ interface to reach the main valley of the detector.

FABRICATION CONSIDERATIONS

Silicon: ususally n-type, controllable surfaces
must be uniformly doped---NTD doped
Process should retain lifetime
Wacker cooperation

Complicated device structure (8-10 mask levels)
many process steps, continual inspection
considerable chance for fatal errors
(defects/wafer, not per die)
two-sided device, backside alignment
required, backside integrity to be
maintained

Limited interest by commercial firms
no US commercial fab

Desi gn requires serious simulation including Poisson

THE SEMICONDUCTOR DRIFT CHAMBER

"Progress in Semiconductor Drift Detectors", Rehak et al NIM A248, 367 (1986).

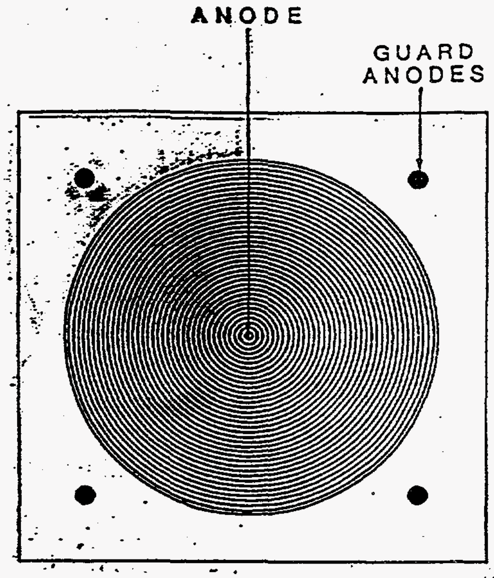

Fig. 6. Top view of the N-side of the circular SDC. The signal anode is the 200 m diameter circle in the center.

1 cm diam. Anode C ≈ 0.06 pf

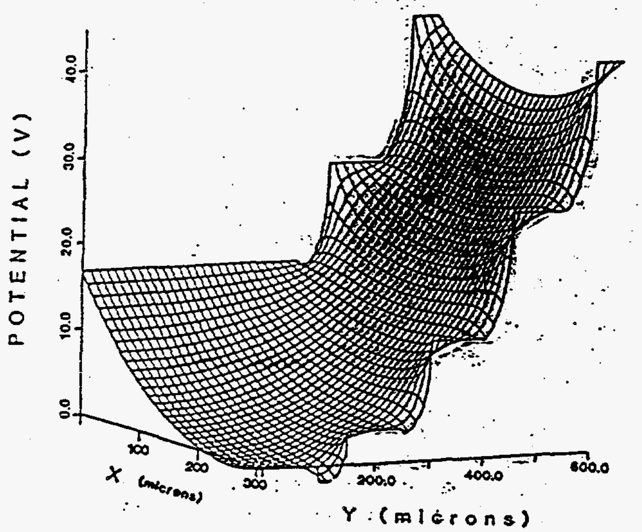

Fig. 9. Potential energy of electrons for the circular drift chamber.

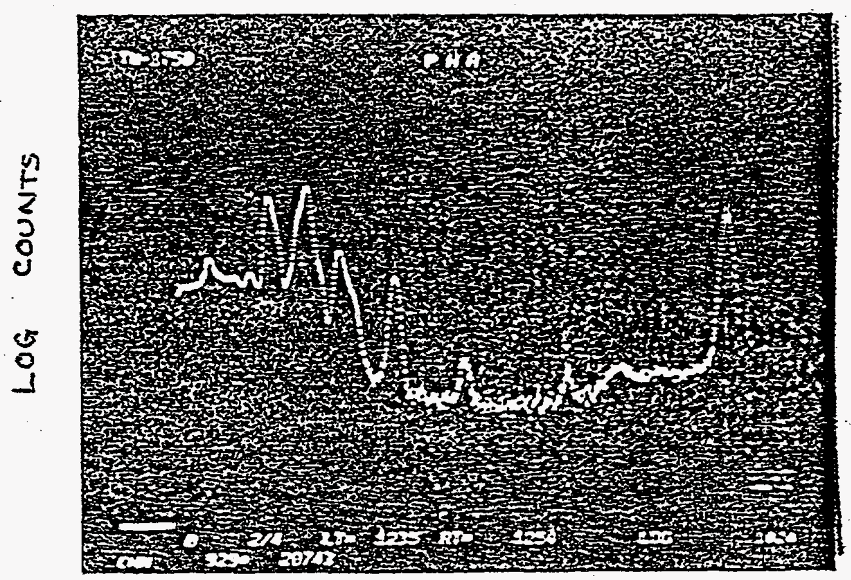

Total Input C (2N4416) ≈ 5pf

Noise 110 e rms (930 eV FWHM) @ 250 nsec shaping

$I_L \sim 3mA$

Various 10-20 keV L x-rays

60 keV 241 Am. γ

SPIRAL CYLINDRICAL DRIFT DETECTOR

Gatti et al IEEE TNS 36, 203 (1989)

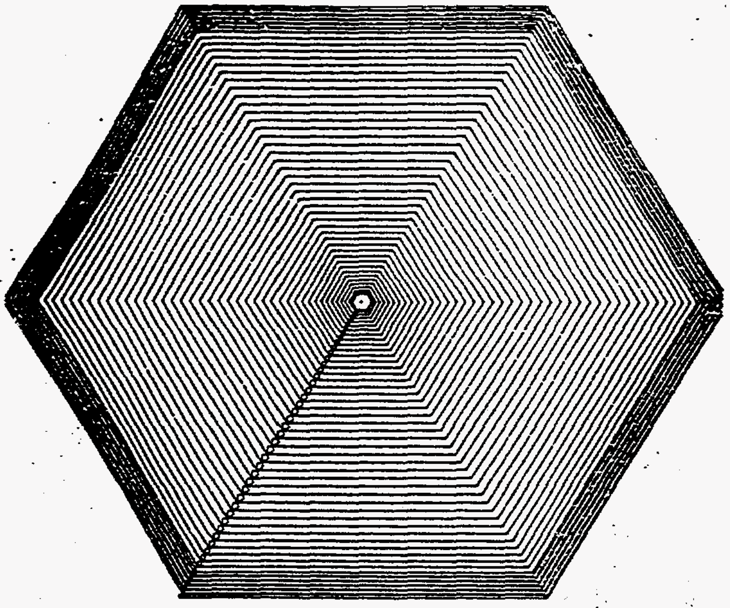

Fig. 2.2: *n*–side of the spiral detector. Two intertwined hexagonal spirals are visible. The wider spiral is a rectifying p+ implant; the narrower spiral is the thermally grown SiO_2. Both spirals are running from the outer radius to the center of the detector where the signal anode is located.

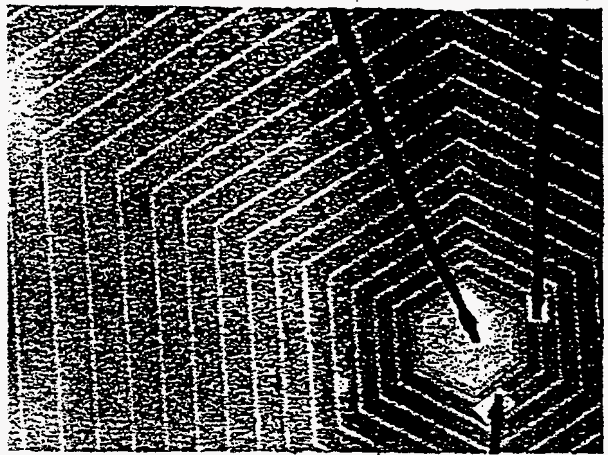

Fig. 2.4: Microphotograph of the central part of the detector. The large central hexagon is the anode. The lower bond is the connection to the final closed turn of the p^+ spiral. The bond at the right hand side is the connection to the guard sink.

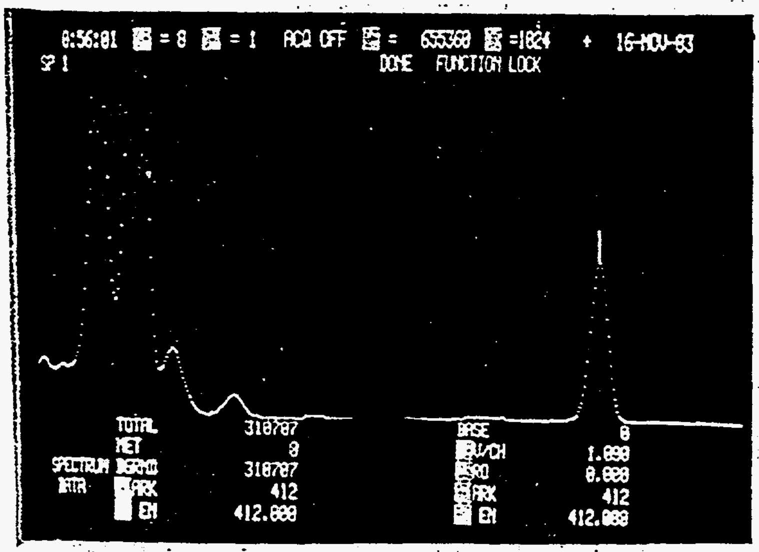

Fig. 4.3: Am^{241} X–ray spectrum obtained with a Silicon Spiral Detector and a commercially available preamplifier RL–791/1 (linear scale).

~1na I_L

190 e⁻ rms

(FWHM ~ 8x_

Gatti, Rehak

Chen, Kraner, Li

Silicon Drift Chamber

NA 45, WA 93

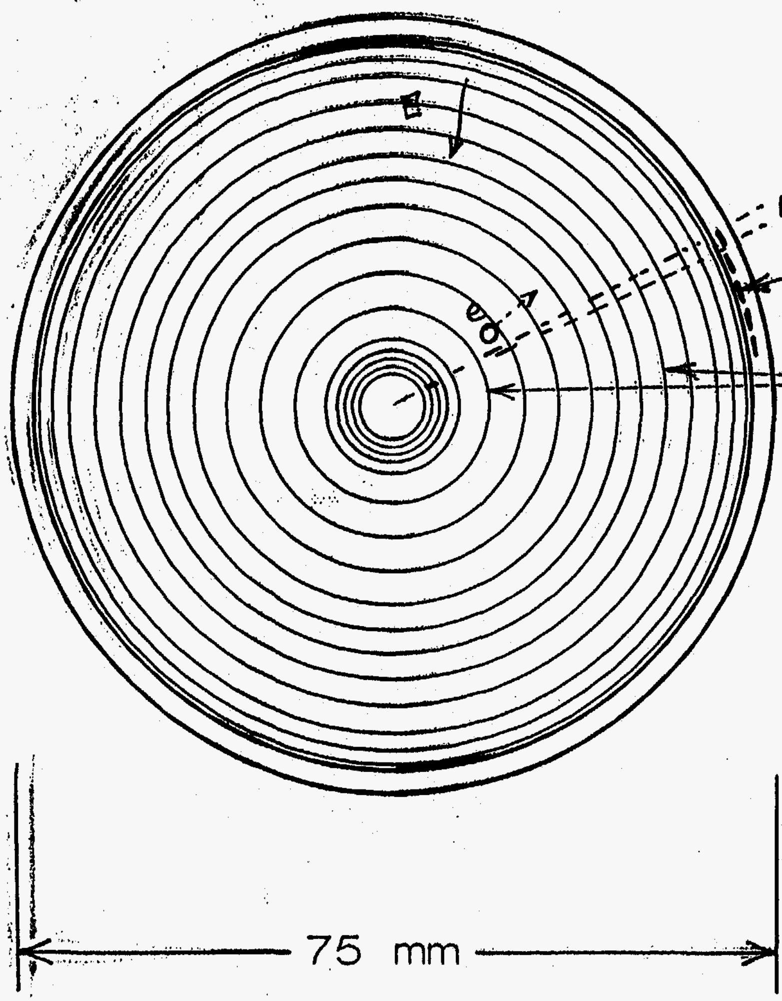

360 Anodes on Perifery

241 Rings, 3 cm radius
Note: Central Hole

250 um thick NTD

n-type silicon

$\sigma_r \approx 10\,\mu m$; $\frac{A}{\sigma_r \sigma_\Theta} \approx 10^6$ (X~10 due to ϕ INTER)

{Number of independent pixels ≈ ≈ 5×10^6}

~120 processing steps, inspections
8 Level Mask set. Double Sided

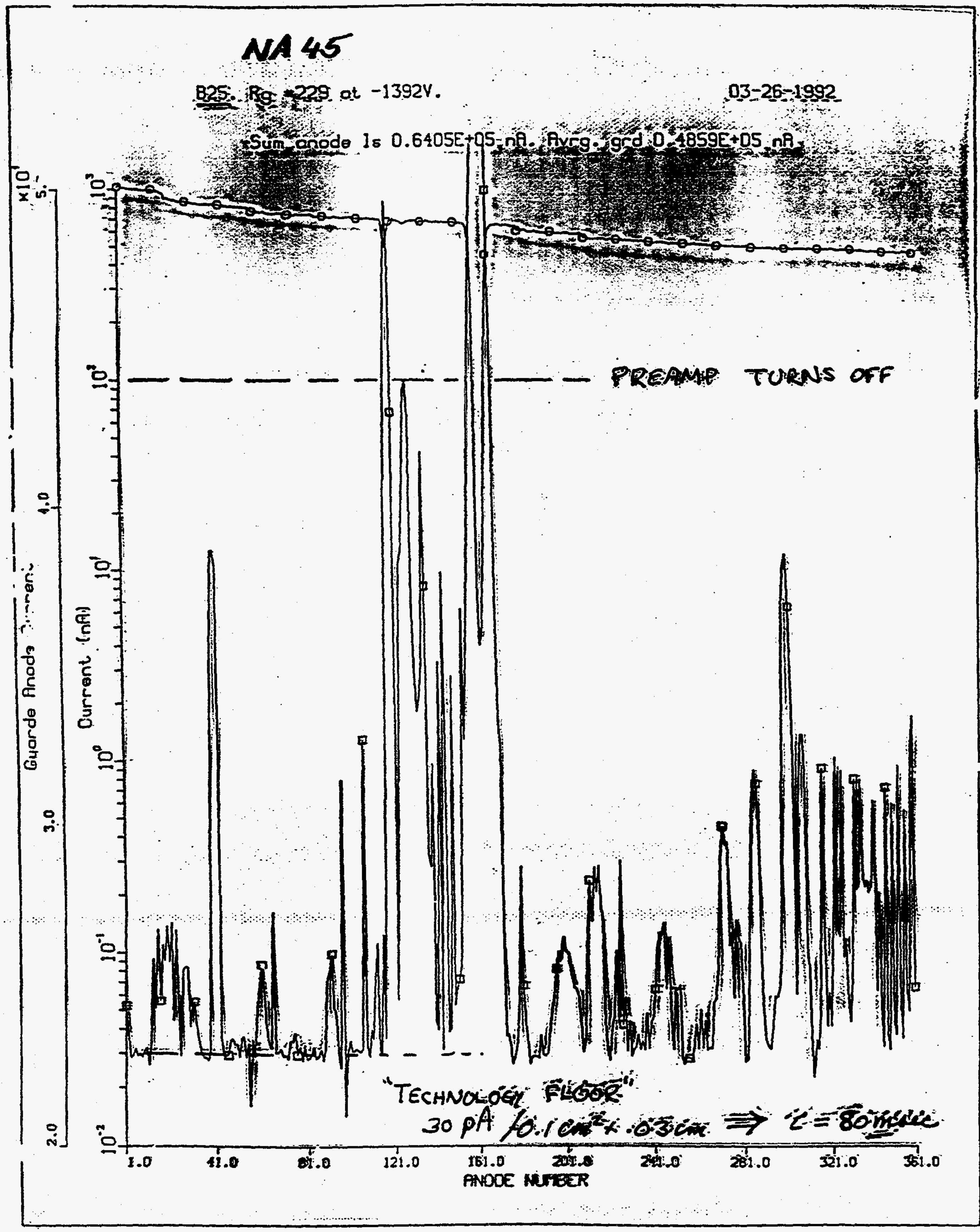

NA 45
B25. Rg. #229 at -1392V.
03-26-1992
*Sum anode is 0.6405E+05 nA. Avrg. grd 0.4859E+05 nA.
PREAMP TURNS OFF
"TECHNOLOGY FLOOR"
30 pA /0.1 cm² + 0.3 cm ⇒
Guarde Anode Current
Current (nA)
ANODE NUMBER
1.0
41.0
81.0
121.0
161.0
201.0
241.0
281.0
321.0
361.0
2.0
3.0
4.0

STAR PROTOTYPE DRIFT DETECTORS

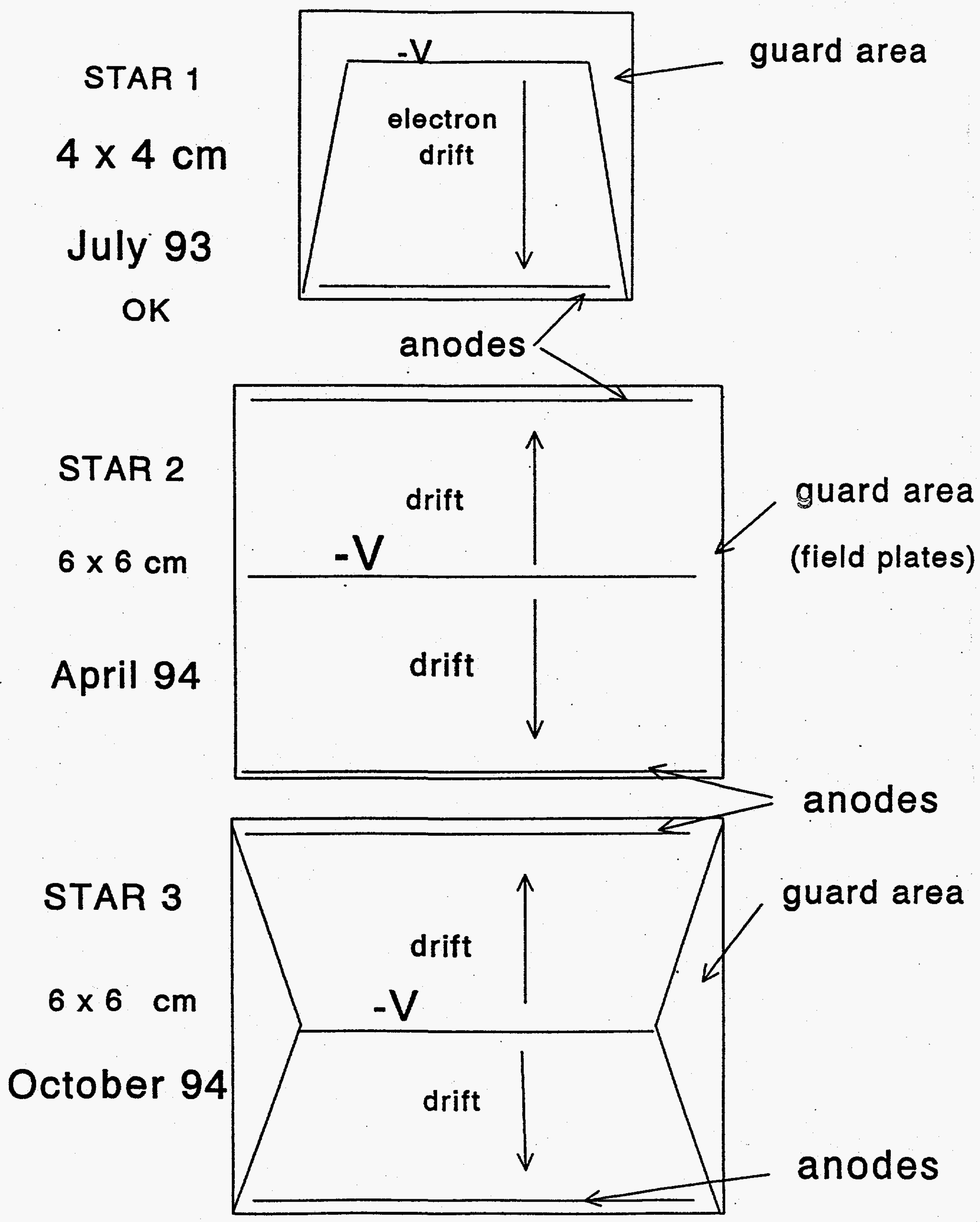

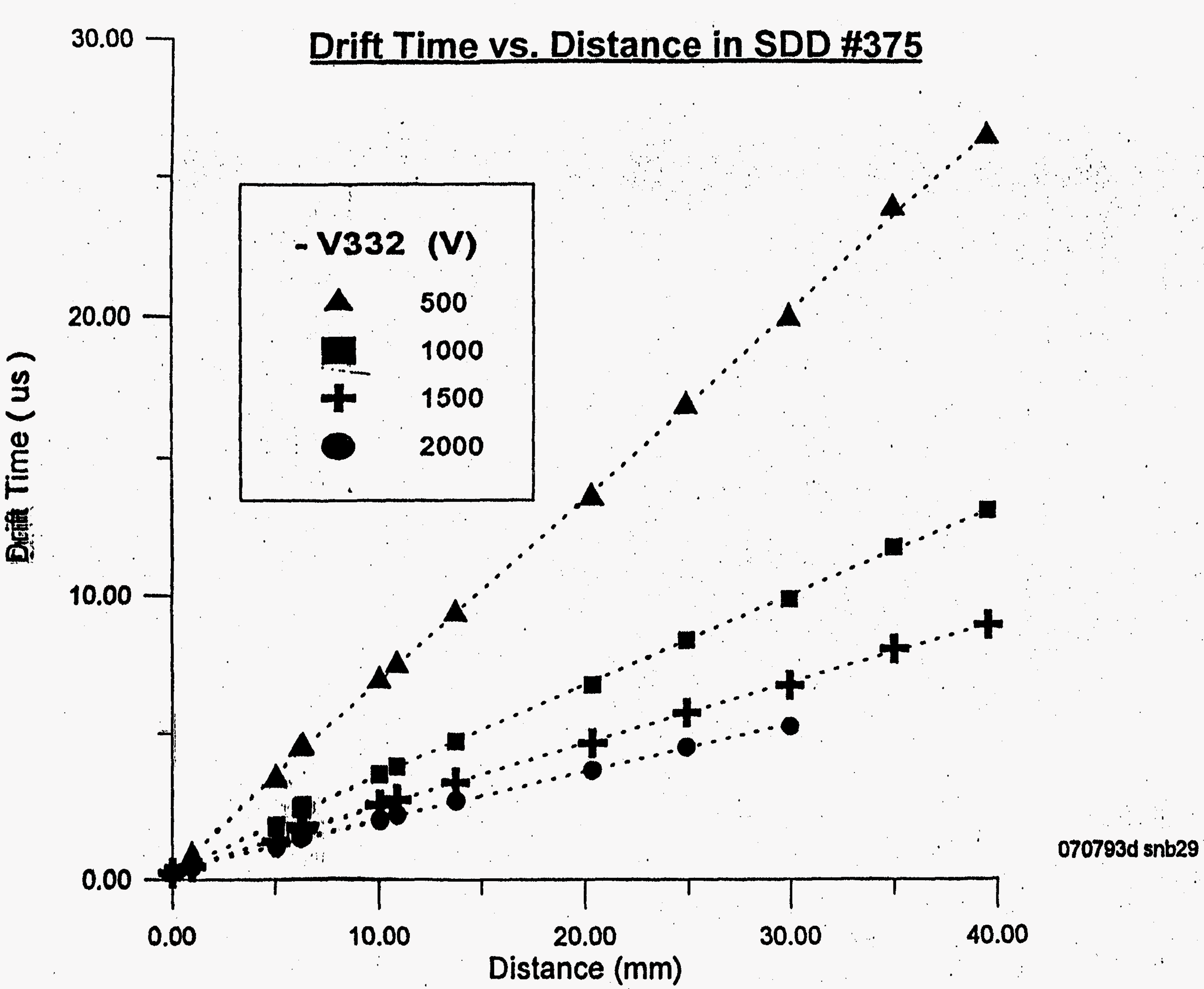
Drift Time vs. Distance in SDD #375
- V332 (V)
500
1000
1500
2000
Drift Time (us)
30.00
20.00
10.00
0.00
0.00
10.00
20.00
30.00
40.00
Distance (mm)
070793d snb29

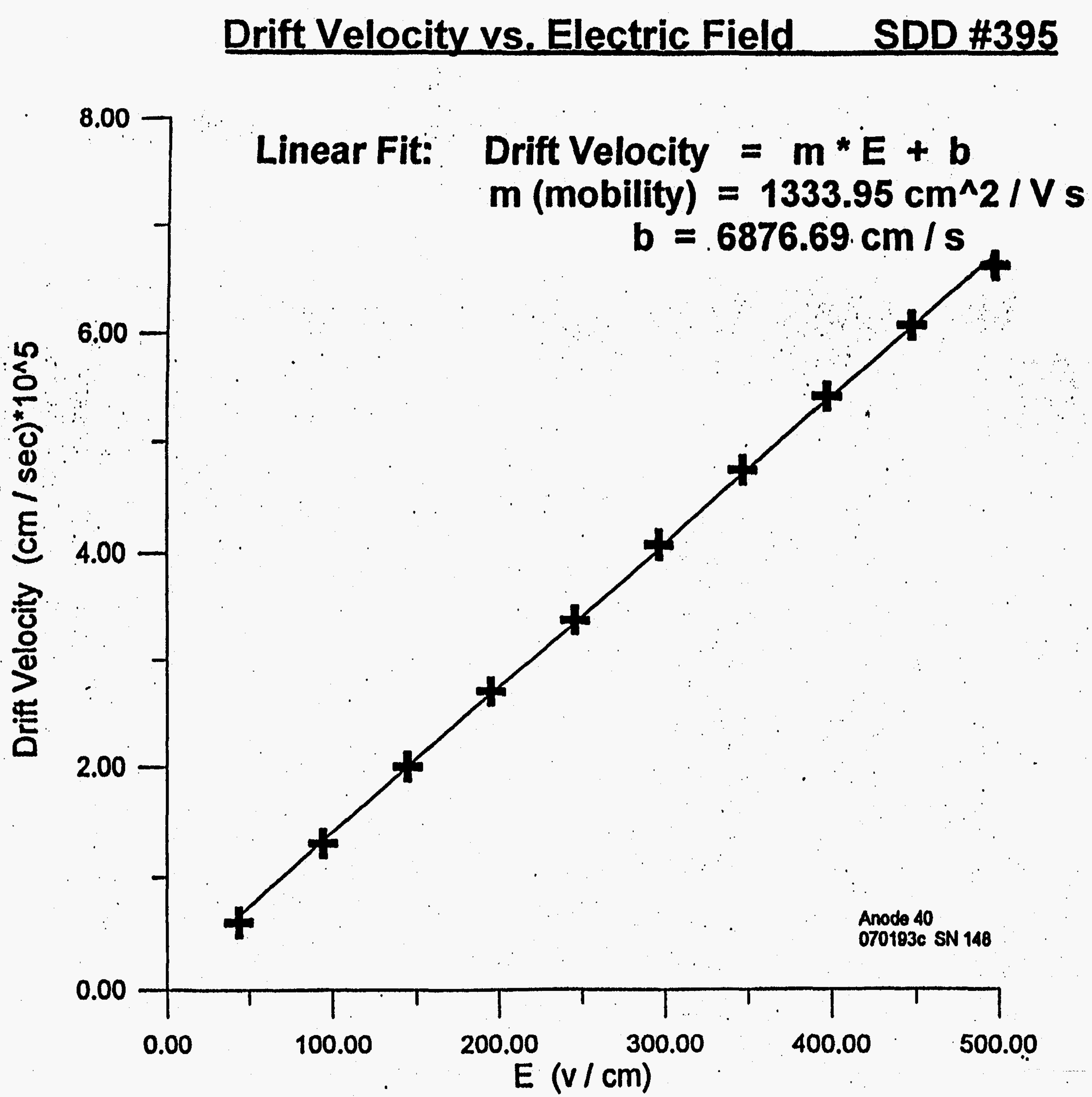
Drift Velocity vs. Electric Field SDD #395
Linear Fit: Drift Velocity = m * E + b
m (mobility) = 1333.95 cm^2 / V s
b = 6876.69 cm / s
Drift Velocity (cm / sec)*10^5
8.00
6.00
4.00
2.00
0.00
0.00
100.00
200.00
300.00
400.00
500.00
E (v / cm)
Anode 40
070193c SN 148

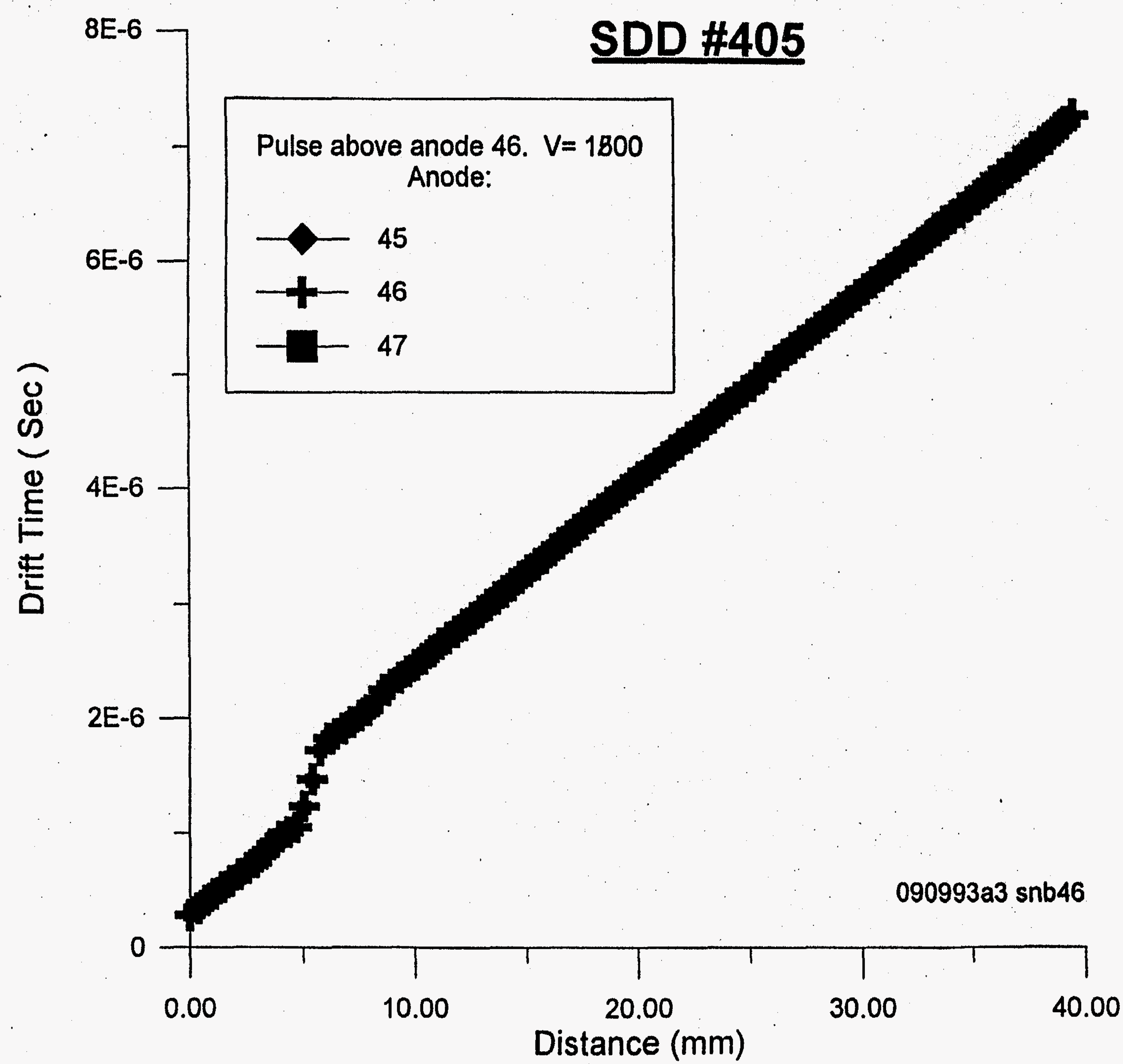
SDD #405
Pulse above anode 46. V= 1800
Anode:
45
46
47
8E-6
6E-6
4E-6
2E-6
0
Drift Time (Sec)
0.00
10.00
20.00
30.00
40.00
Distance (mm)
090993a3 snb46

X-RAY GAS PROPORTIONAL DETECTOR DEVELOPMENT AT BNL

G.C. Smith
Brookhaven National Laboratory
Upton, NY 11973

1. Basic characteristics of two-dimensional, gas proportional chambers with delay line readout:
   - 100μm FWHM position resolution
   - ±4% differential non-linearity
   - few times 10^5 s^{-1} count rate
   - high throughput TDC
   - results from X12B, NSLS
   - new, 0.5 mm wire pitch detector

2. Some measurements illustrating fundamental limit to position resolution in Ar, Kr, Xe

3. Development of next generation proportional chamber, using interpolating cathode pads. Design for count rate capability of 10^8 s^{-1}

Co-workers:
J. Fischer, J. A. Harder, V. Radeka, L.C. Rogers, B. Yu

2D Gas Proportional Detector Data Flow

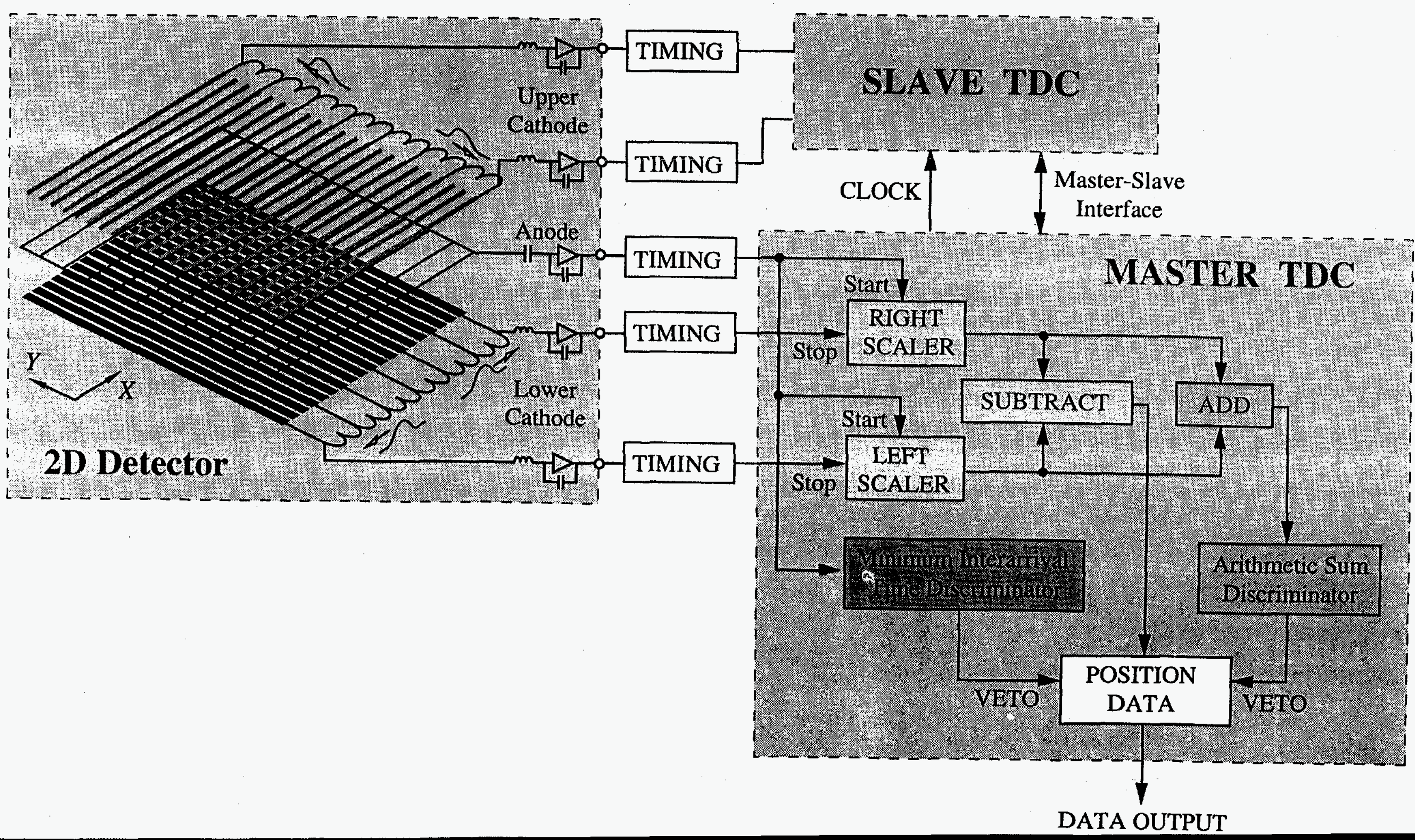

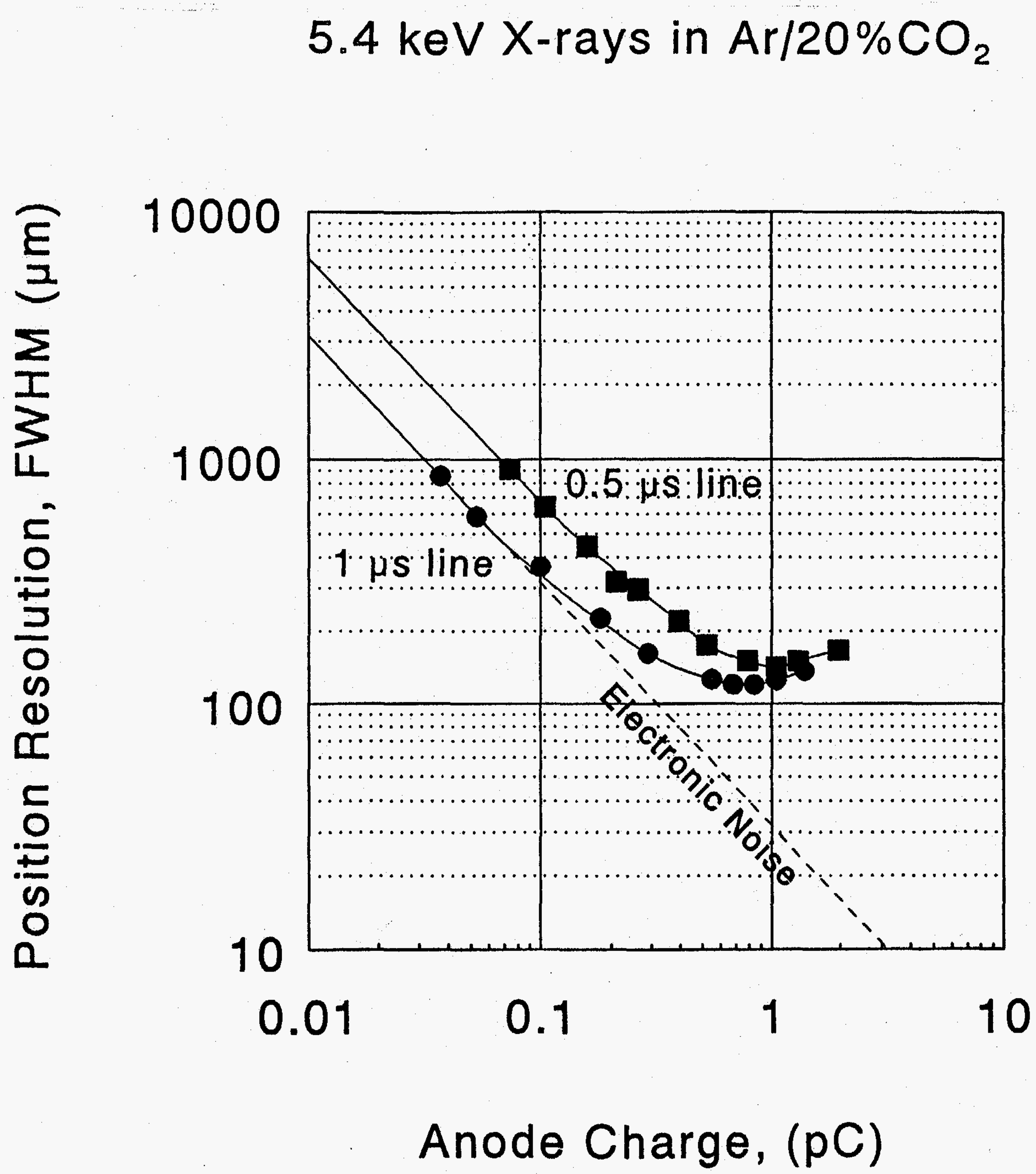
5.4 keV X-rays in Ar/20%CO2
Position Resolution, FWHM (µm)
10000
1000
100
10
0.01
0.1
1
10
Anode Charge, (pC)
0.5 µs line
1 µs line
Electronic Noise

BEAM LINE X12B, NSLS (Time resolved studies)

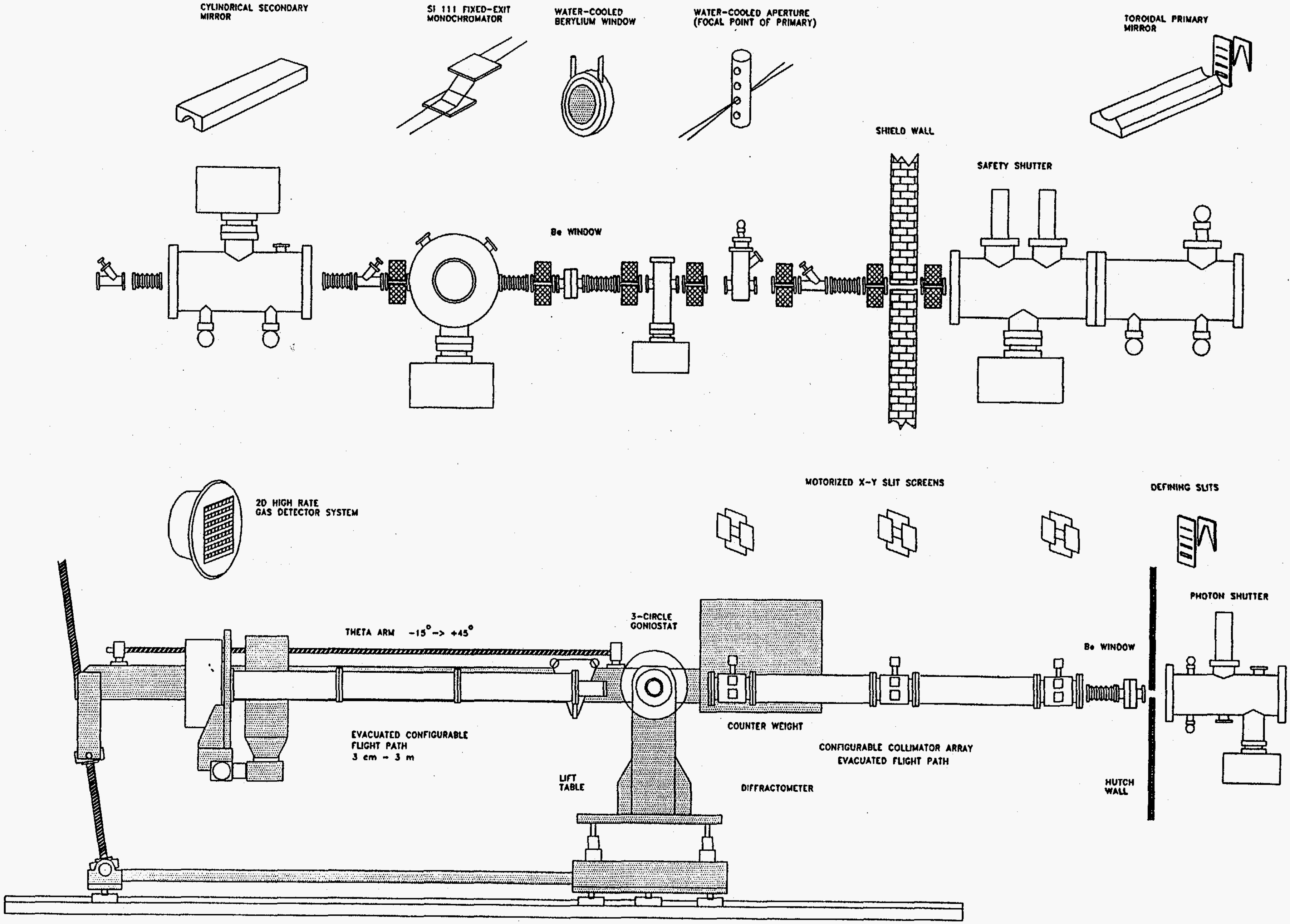

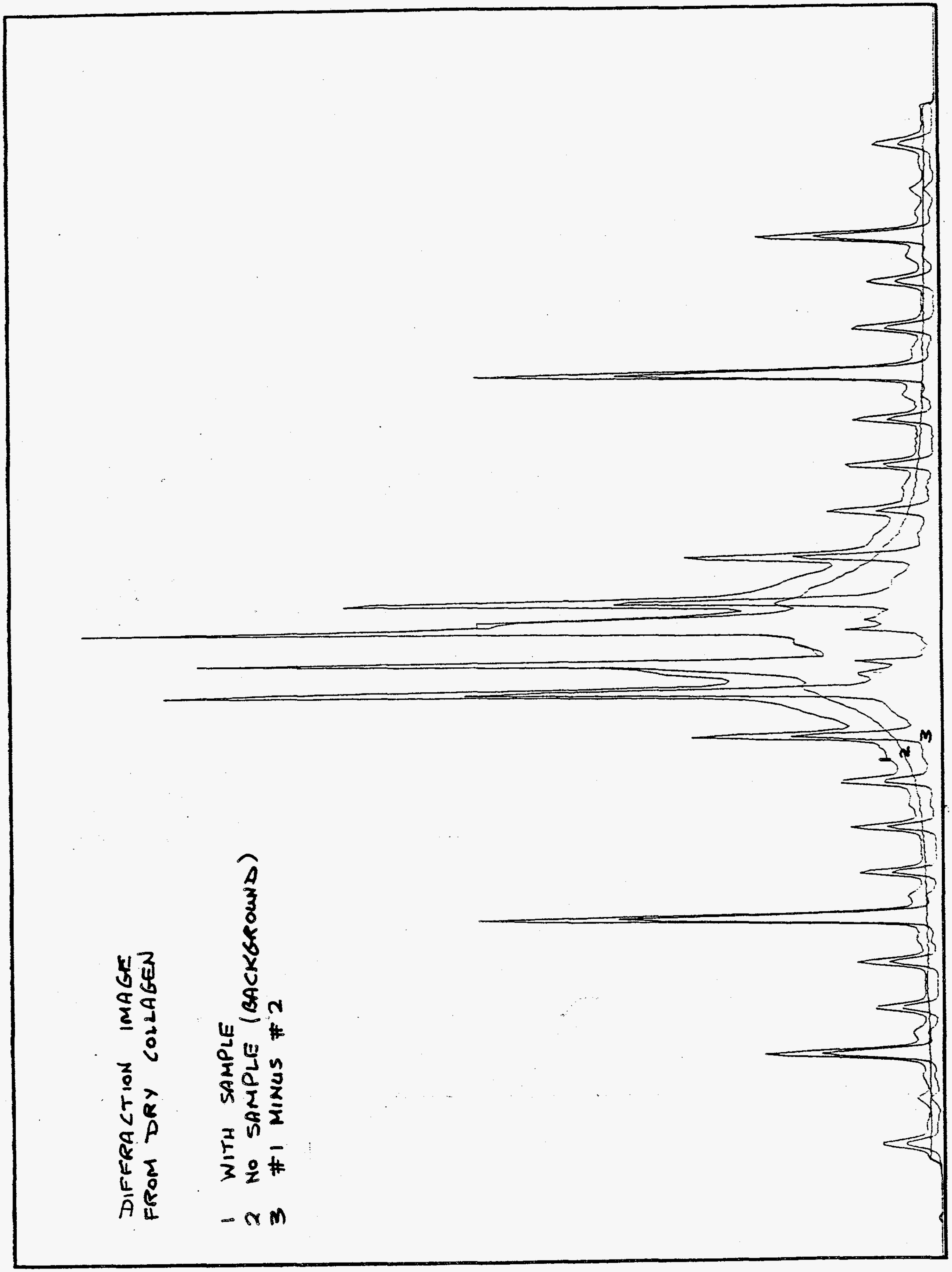
DIFFRACTION IMAGE
FROM DRY COLLAGEN
1 WITH SAMPLE
2 No SAMPLE (BACKGROUND)
3 #1 MINUS #2
1
2
3

2D Gas Proportional Detector with Delay Line Encoding

Anode Wire Pitch = 1 mm

Meridional diffraction pattern from two dried collagen fibers at right angles to each other (9keV, Ar/20%CO_2)

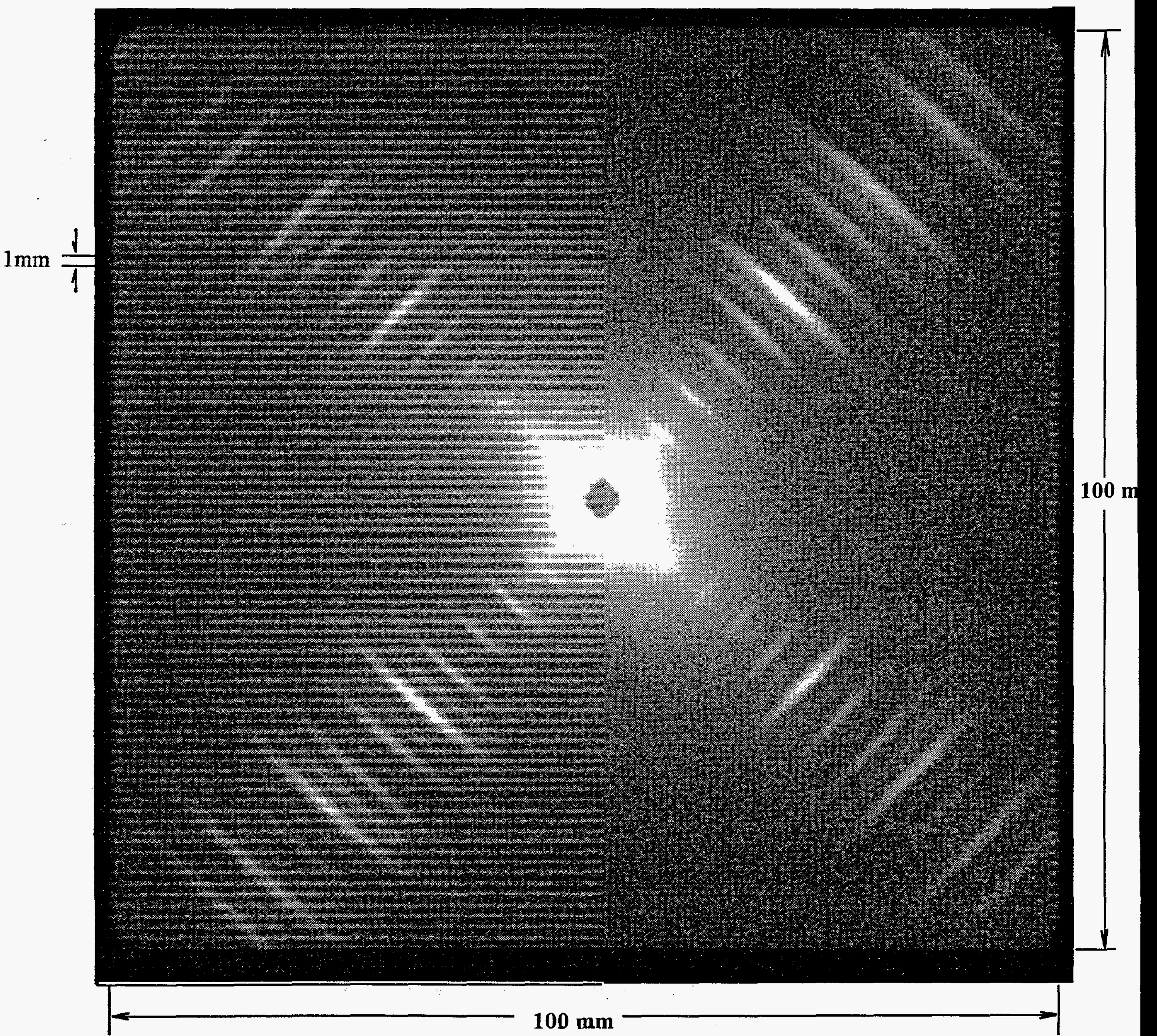

2D Gas Proportinal Detector with Delay Line Encoding

Anode Wire Pitch = 0.5mm

Image of a plastic gear wheel, 15 mm diameter (5.4 keV, Ar/20%CO_2)

RAW DATA

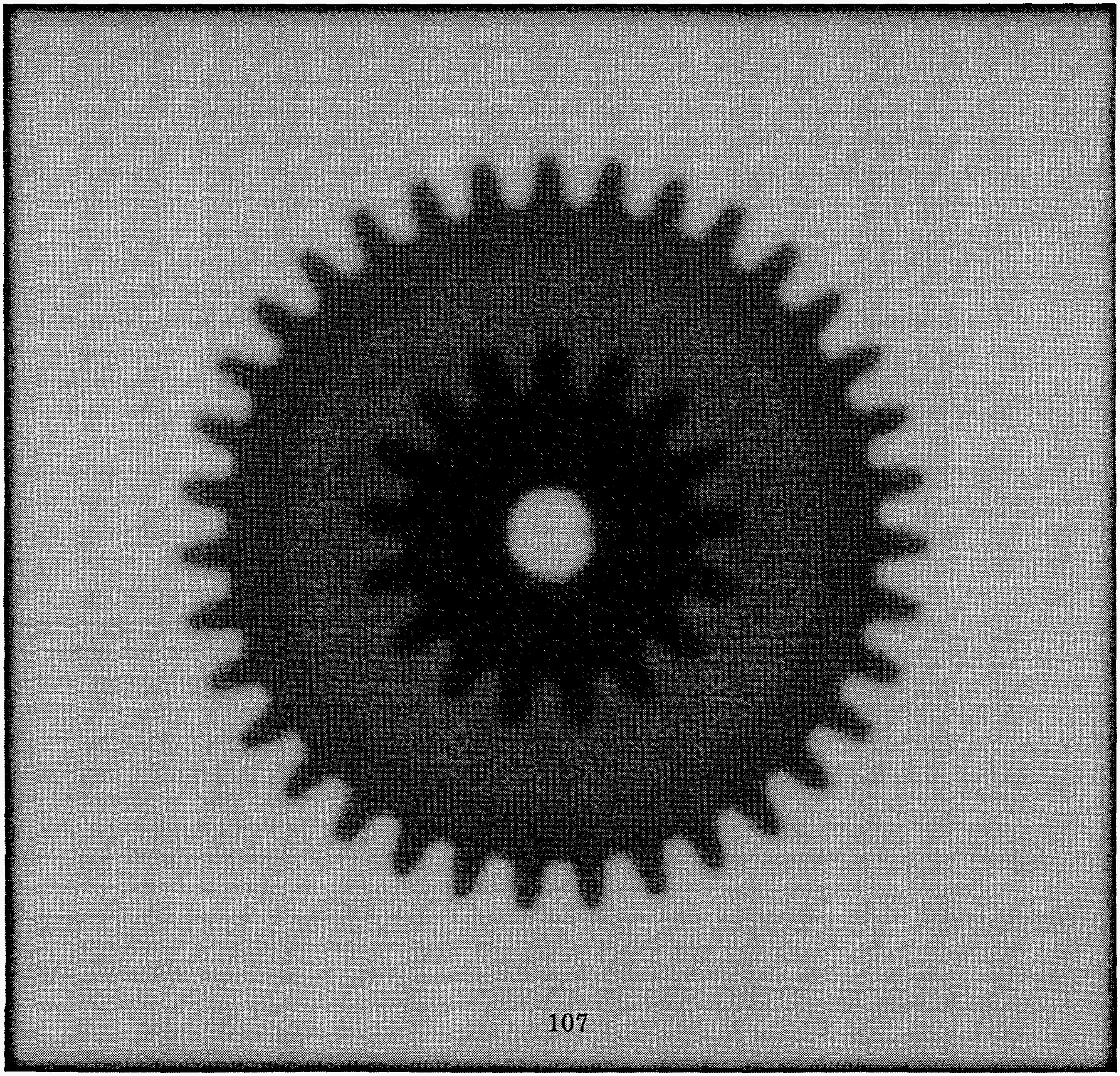

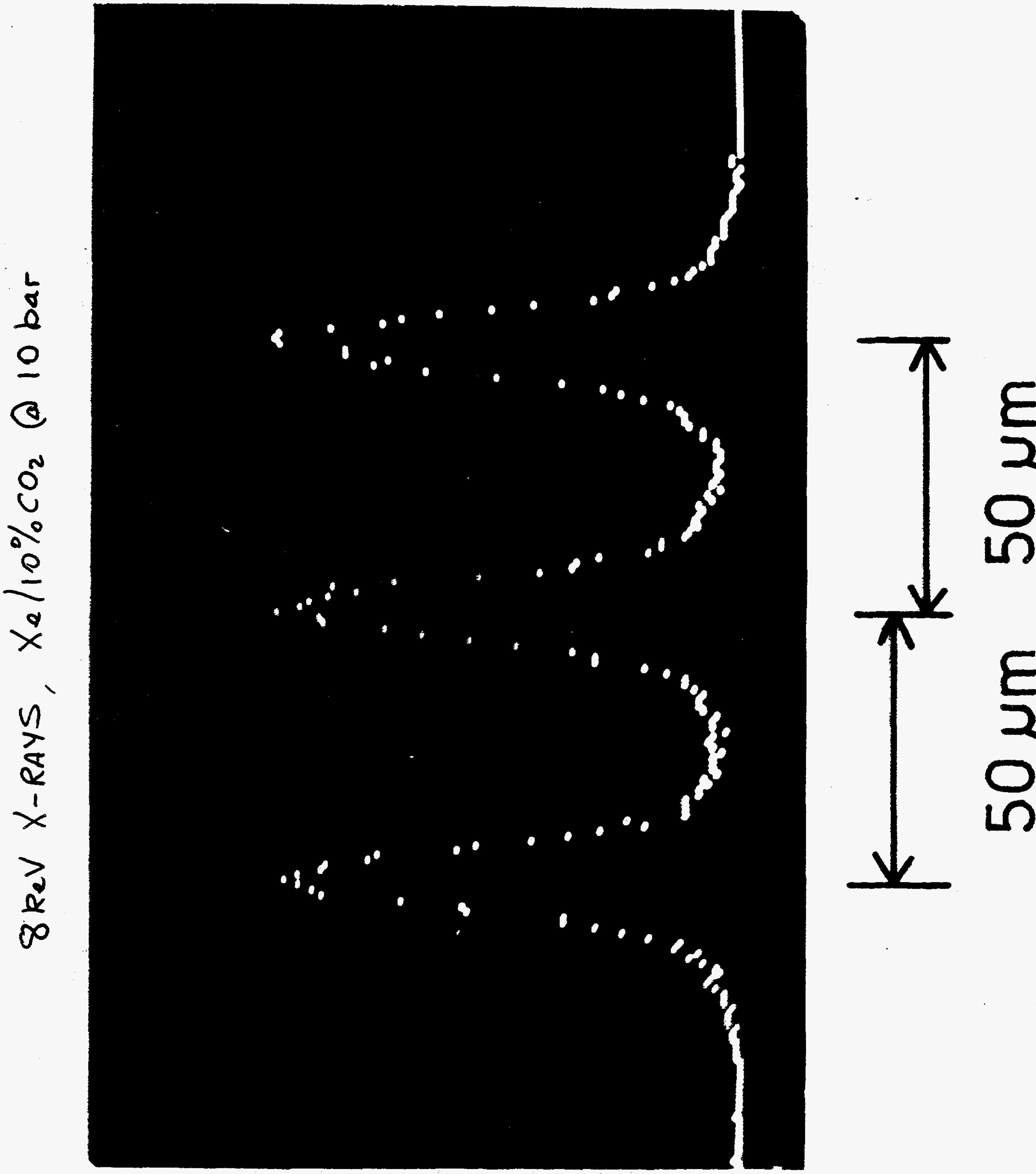
8 keV X-RAYS, Xe/10%CO2 @ 10 bar
50 μm
50 μm

X-ray Position Resolution, Xe/10%CO_2

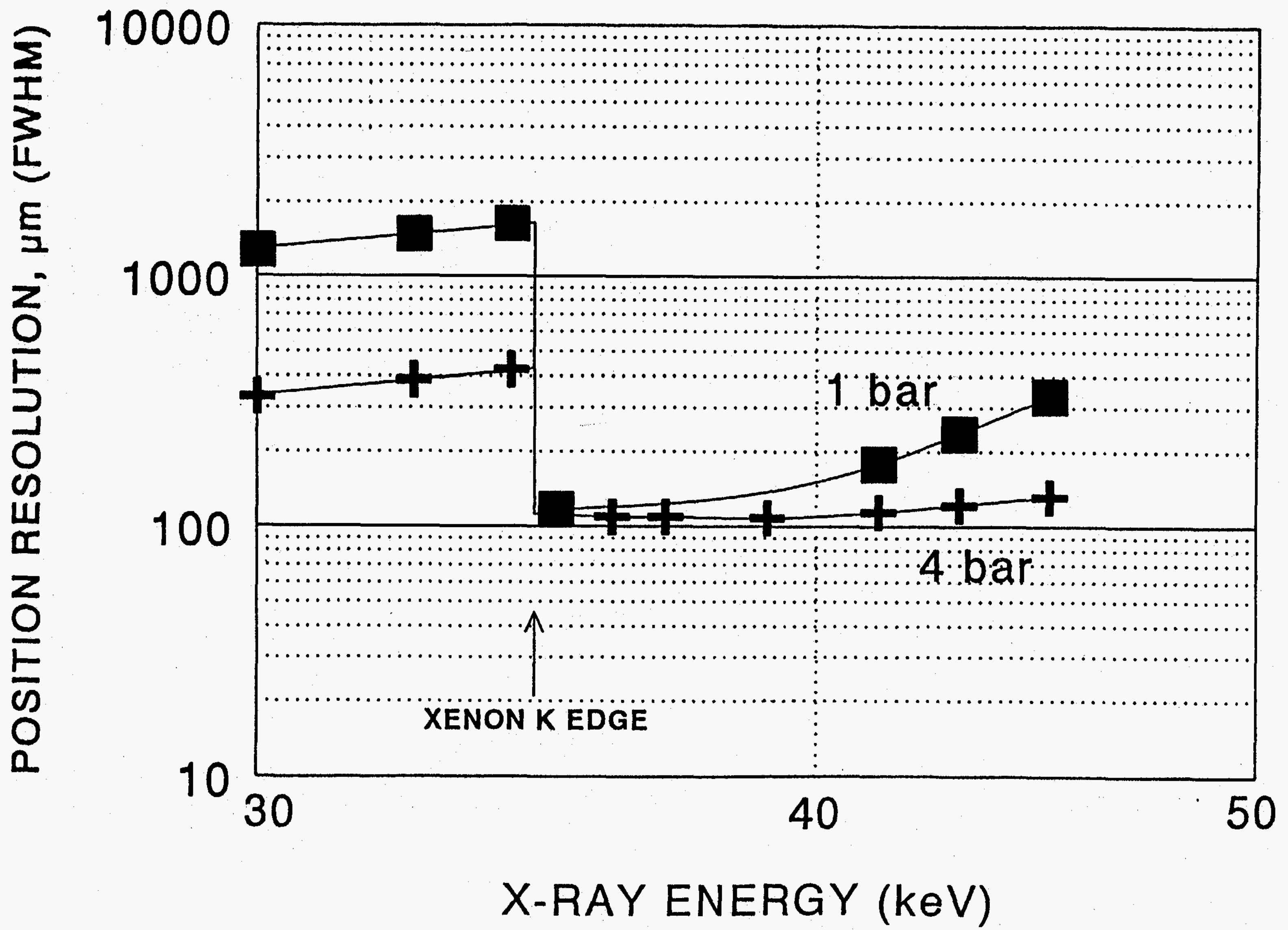

2D DETECTOR, 10^8 ph s^{-1}

PROPORTIONAL CHAMBER CROSS-SECTION

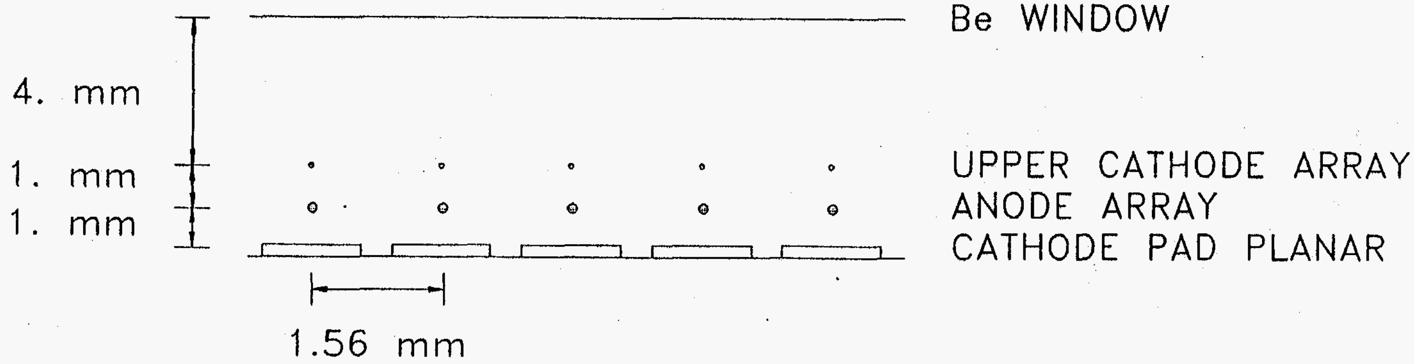

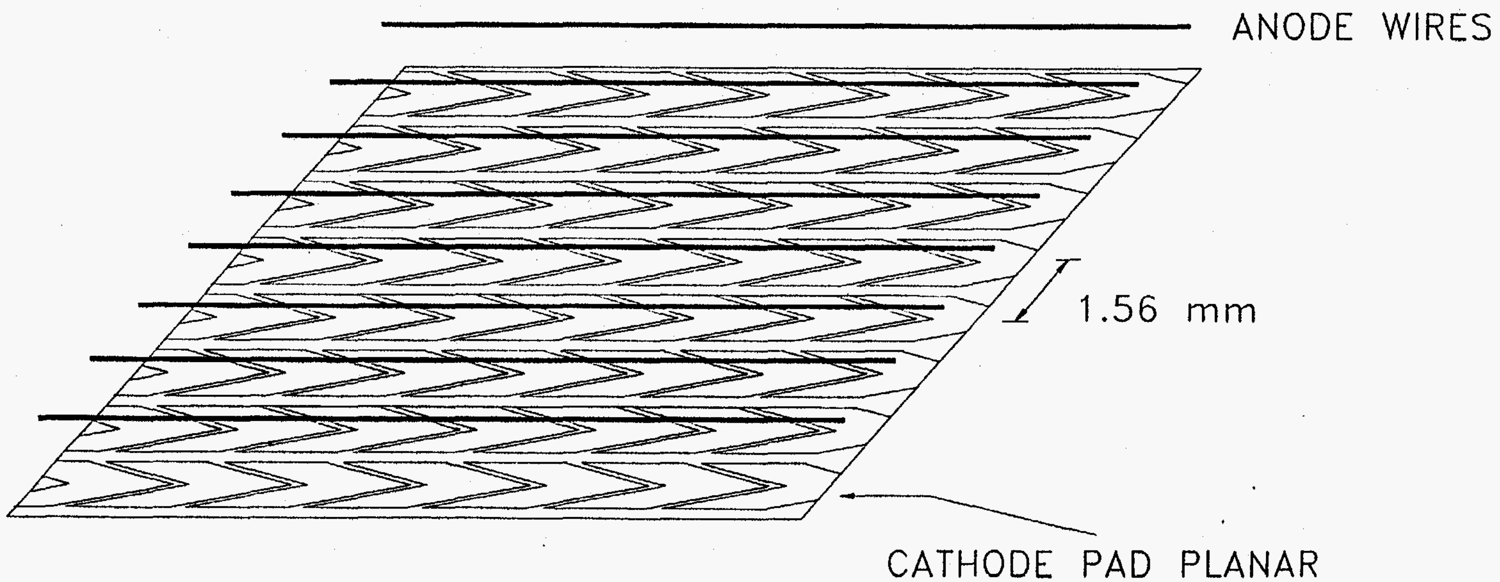

PERSPECTIVE VIEW

CATHODE PAD ARRAY FOR PROTOTYPE ULTRA-HIGH RATE 2D DETECTOR

16 pads × 128 pads = 2048 channels

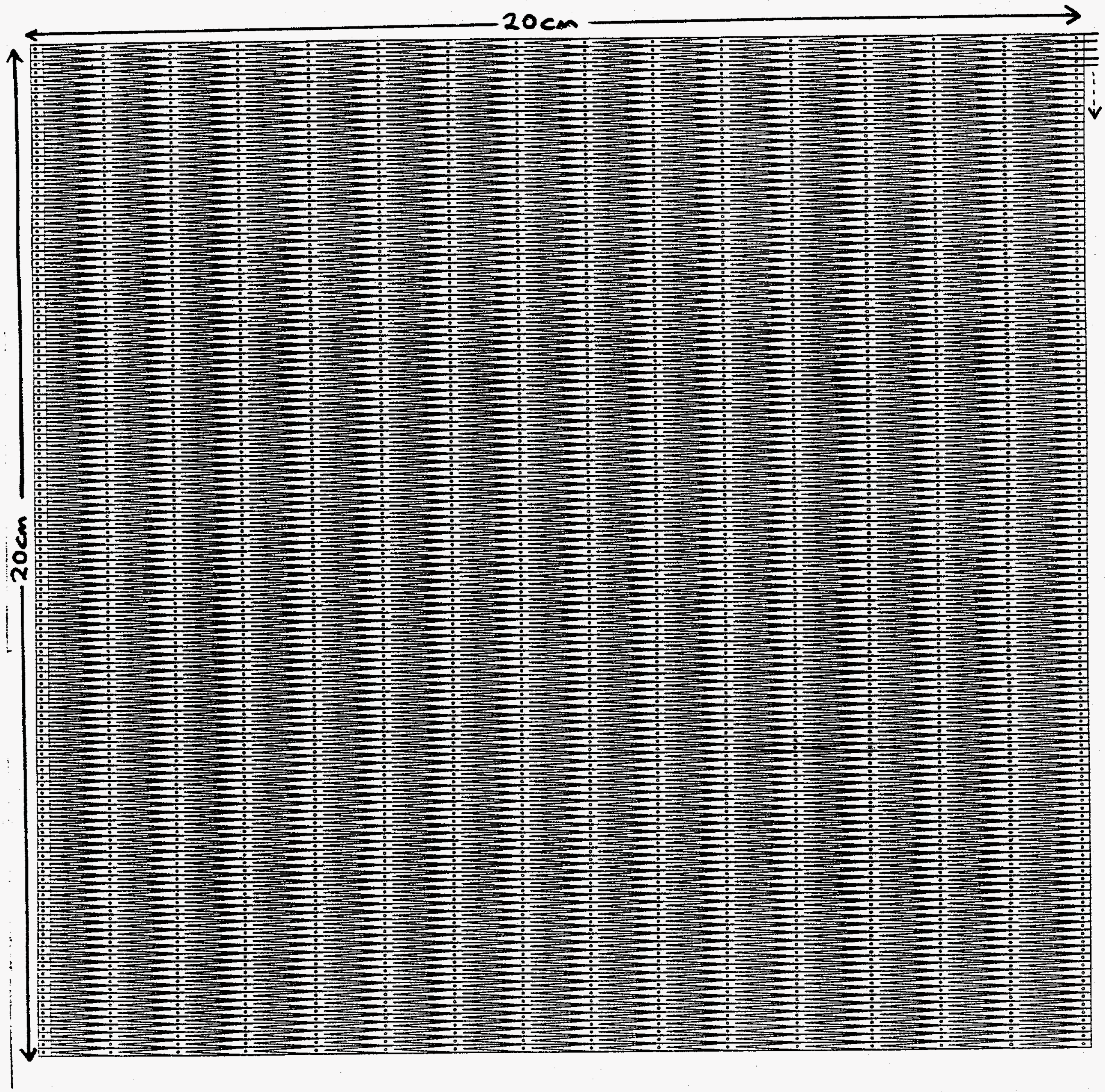

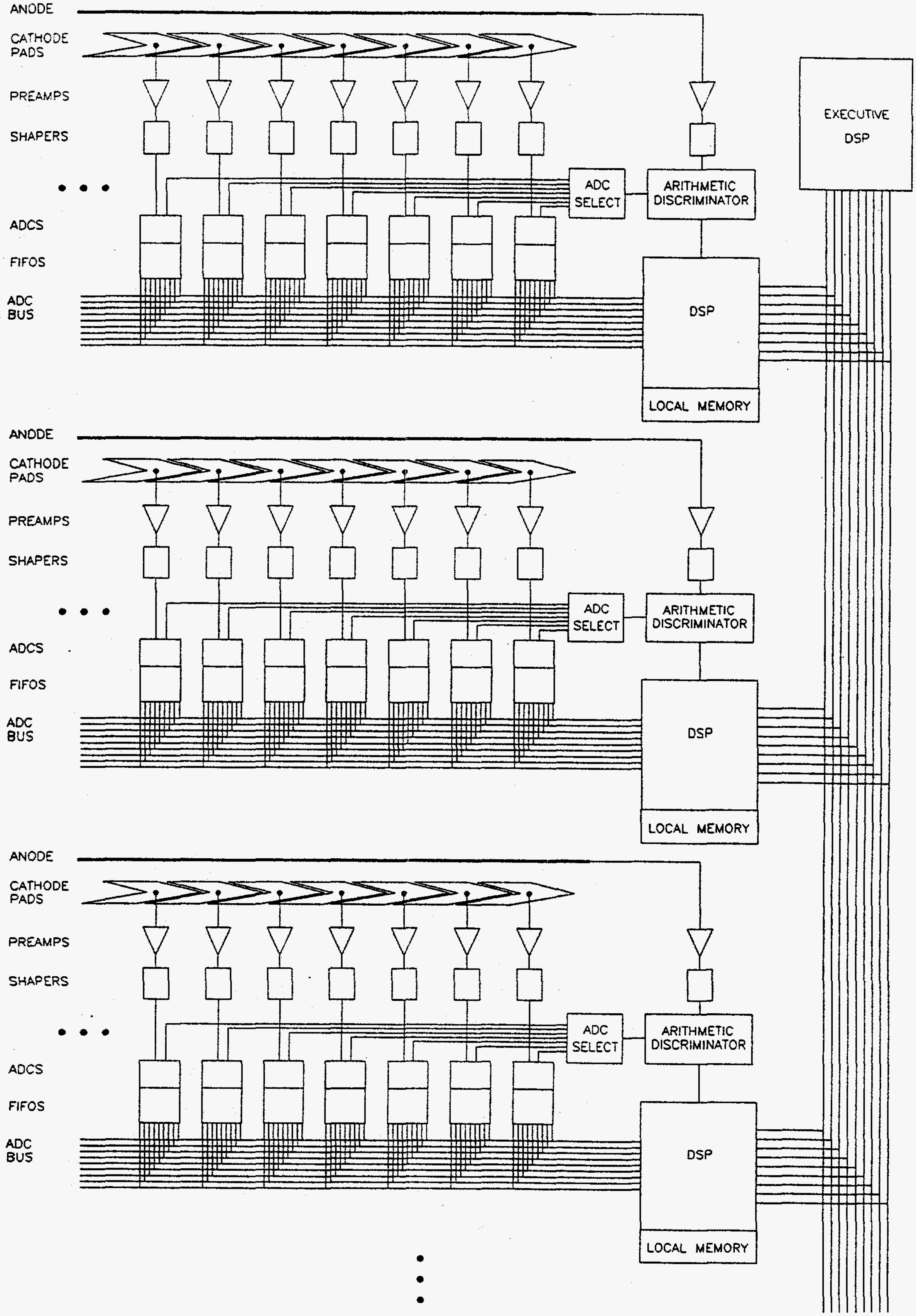
ANODE
CATHODE PADS
PREAMPS
SHAPERS
ADCS
FIFOS
ADC BUS
ADC SELECT
ARITHMETIC DISCRIMINATOR
DSP
LOCAL MEMORY
EXECUTIVE DSP
ANODE
CATHODE PADS
PREAMPS
SHAPERS
ADCS
FIFOS
ADC BUS
ADC SELECT
ARITHMETIC DISCRIMINATOR
DSP
LOCAL MEMORY
ANODE
CATHODE PADS
PREAMPS
SHAPERS
ADCS
FIFOS
ADC BUS
ADC SELECT
ARITHMETIC DISCRIMINATOR
DSP
LOCAL MEMORY

Deming Shu and Tuncer M. Kuzay

Advanced Photon Source

The Advanced Photon Source High Power Density X-ray Beam Position Monitor*

Synthetic diamond is being used for the s-ray beam position monitor blades subject to very high heat flux at the Advanced Photon Source at Argonne National Laboratory. The design and preliminary test results for the monitor are discussed in this presentation.

* This work supported by U.S. DOE BES Materials Science, under contract no. W-31-109-Eng-38.

1. Introduction

2. APS Insertion Devices X-ray Beam Parameters

3. X-ray Beam Position Monitor Design for APS Front End

4. Pre-prototype Beam Position Monitor Test at CHESS (Cornell Univ.) and NSLS (Brookhaven National Lab.)

5. X-ray Transmiting Beam Position Monitor Tests at NSLS

6. Discussion and Conclusions

Photon Beam Position Monitors

Design Goal:

Sensing 10% of undulator beam opening angle and beam spatial size.

For β_x and β_y of 10 m,

$$\partial\sigma_y < 8 - 30\ \mu m$$

$$\partial\sigma_{y'} < 1 - 2\ \mu rad$$

The detection of such changes is achieved by using two photon BPMs with a spatial resolution of $\pm$ 1μ and separated by 3 - 4 m.

DESIGN CRITERIA

1. USING PHOTON - ELECTRON EMISSION TYPE

   - UHV COMPATIBILITY
   - HIGH SENSITIVITY
   - EASY MAINTANENCE

2. USING CVD DIAMOND AS A BLADE BASE MATERIAL FOR SUPERIOR PERFORMANCE IN BLADE MATERIAL STRENGTH, THERMAL CONDUCTIVITY THERMAL EXPANSION AND STIFFNESS UNDER HEAT

3. USING METAL COATING MATERIAL, WHICH IS COMPATIBLE WITH DIAMOND FOR A GOOD BOND AND ALSO TO PROVIDE A GOOD PHOTO EMISSION SIGNAL

4. USING ROLLING WEDGE STRUCTURE TO PROVIDE HORIZONTAL BLADE ADJUSTMENT TO SUIT UNDULATOR OR WIGGLER OPERATION

5. USE OF A THREE PAIR GEOMETRIC ARRANGEMENT TO SOLVE THE "SHADOWING" PROBLEM

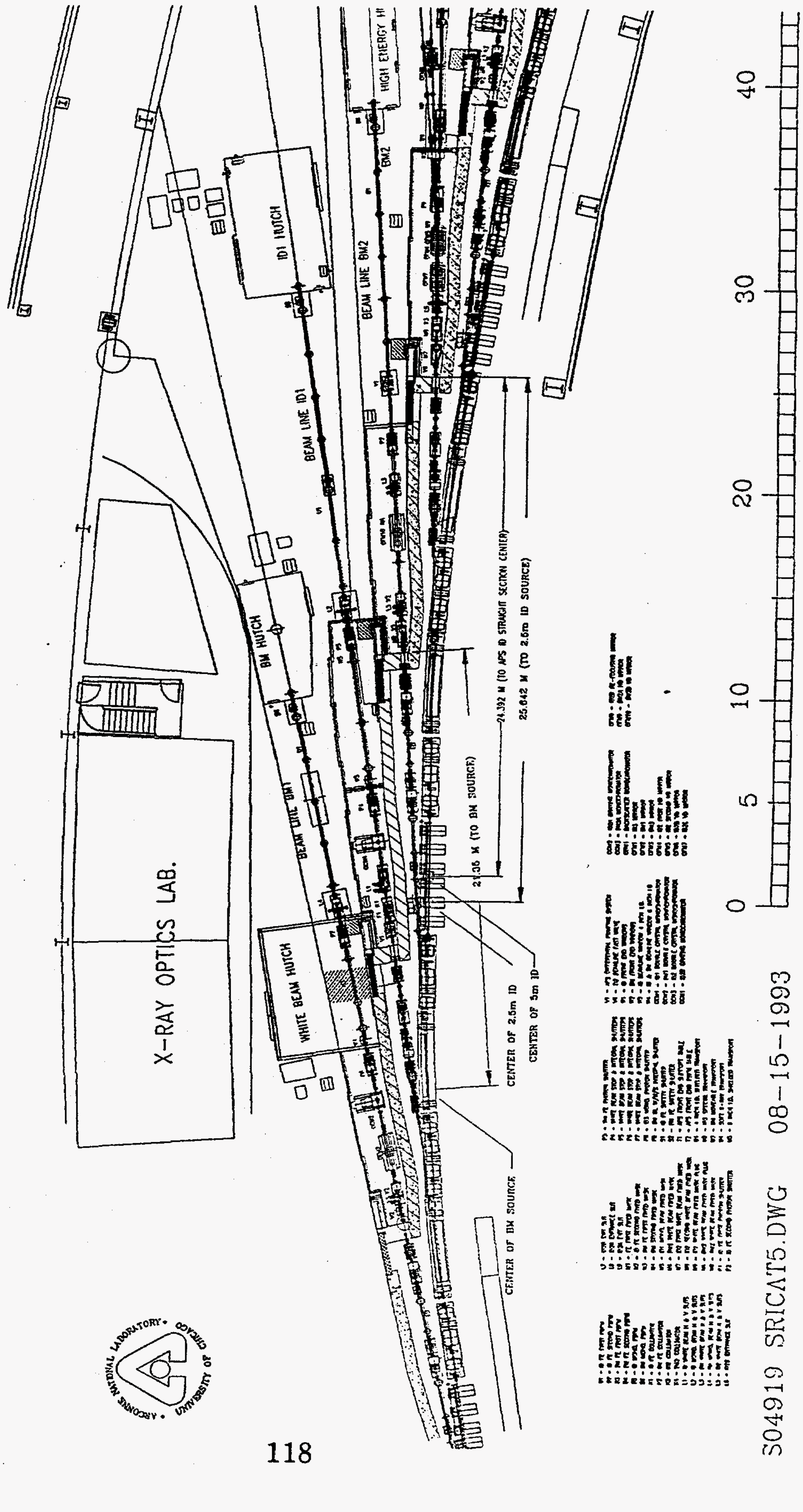
X-RAY OPTICS LAB.
WHITE BEAM HUTCH
BM HUTCH
ID1 HUTCH
BEAM LINE ID1
BEAM LINE BM2
BM2
HIGH ENERGY H
21.36 M (TO BM SOURCE)
24.392 M (TO APS ID STRAIGHT SECTION CENTER)
25.642 M (TO 2.5m ID SOURCE)
CENTER OF BM SOURCE
CENTER OF 2.5m ID
CENTER OF 5m ID
0
5
10
20
30
40
504919 SRICAT5.DWG
08-15-1993

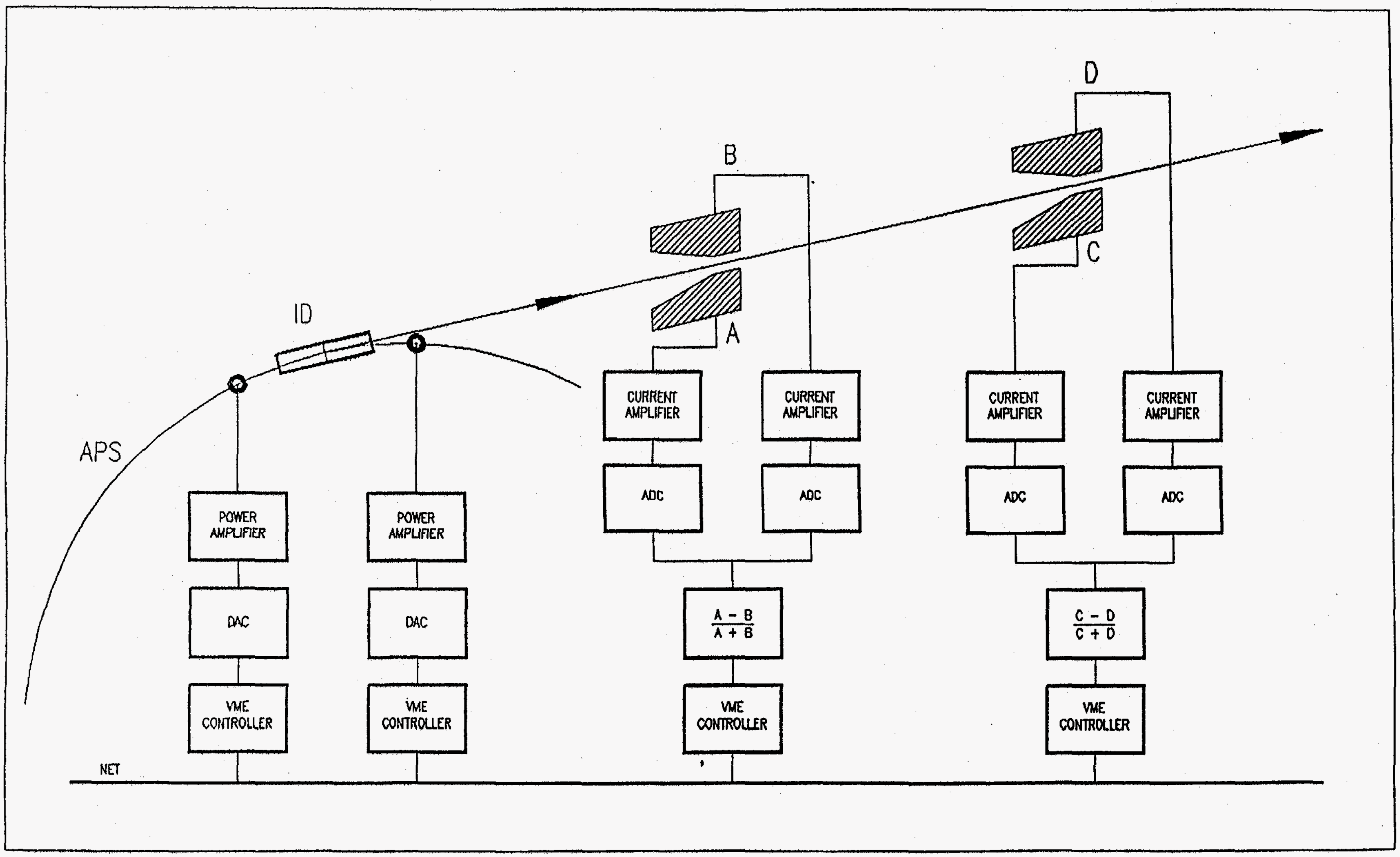
D
B
C
A
ID
APS
CURRENT AMPLIFIER
CURRENT AMPLIFIER
CURRENT AMPLIFIER
CURRENT AMPLIFIER
ADC
ADC
ADC
ADC
POWER AMPLIFIER
POWER AMPLIFIER
DAC
DAC
$\frac{A - B}{A + B}$
$\frac{C - D}{C + D}$
VME CONTROLLER
VME CONTROLLER
VME CONTROLLER
VME CONTROLLER
NET

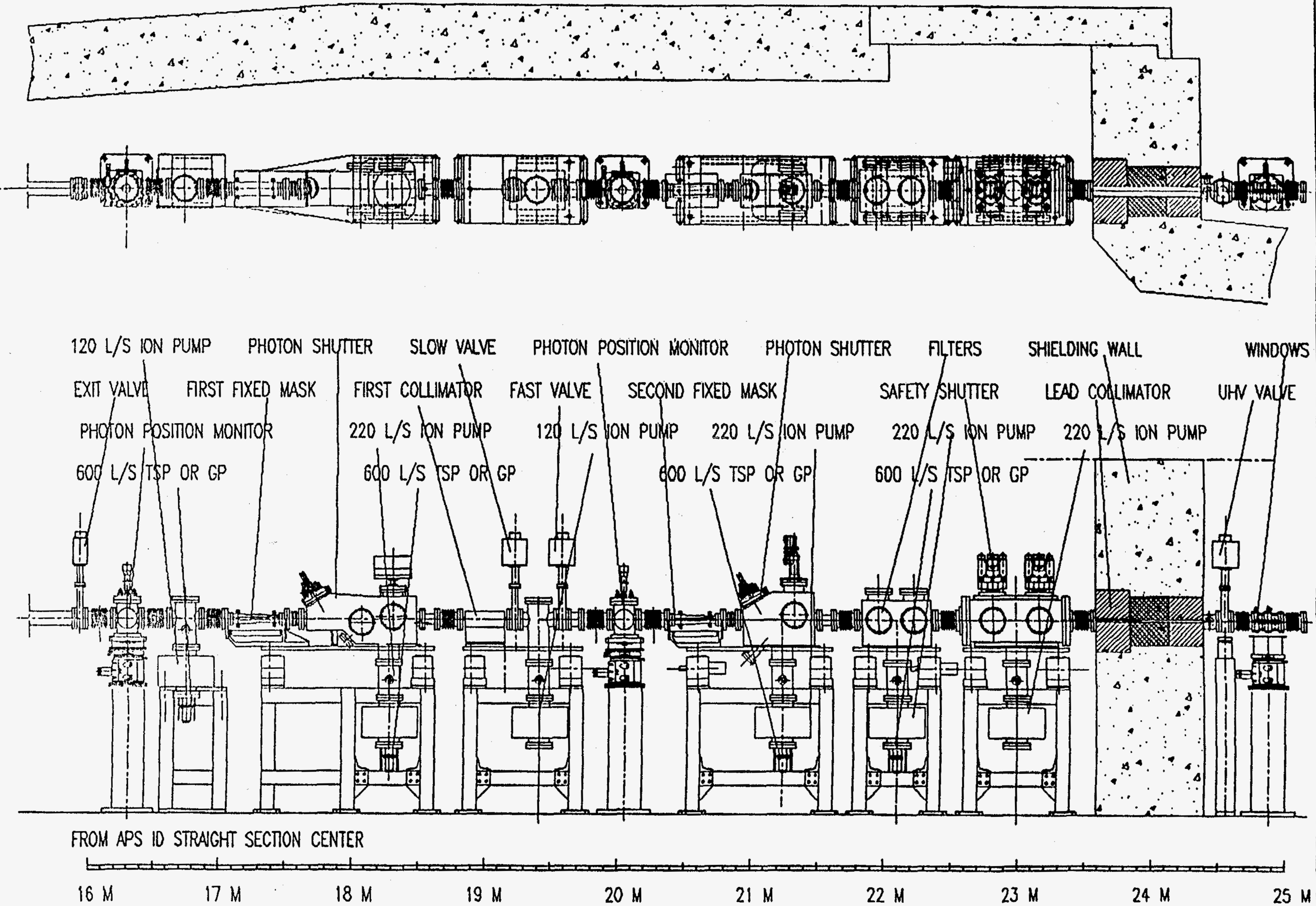

APS INSERTION DEVICE FRONT END GENERAL LAYOUT

S05490 IDF5.DWG 11-28-1992

ADVANCED PHOTON SOURCE

TABLE 1

Design Parameters for Various APS Insertion Devices

(E_r = 7 GeV; I = 100 mA, and $1/\gamma$ = 73 μrad. Quantities at the indicated gap position.)

Parameters	Undulator A (at closed gap of 11.5 mm)	Wiggler A (at 21 mm gap)
Period length [cm]	3.3	8.5
Device length [m]	2.40	2.40
Number of periods	72	28
Max. magnetic field B_0 [T]	0.72	1.0
Critical energy E_c [keV]	23.6	32.6
Max. deflection parameter, K	2.23	7.9
K/γ [μrad]	163	577
Total power [kW]	3.8	7.4
Peak power [kW/mrad^2]	134	73
ID-photon shutter distance (m)	16.9	18.1
Peak heat flux @ photon shutter (W/mm^2)	469	223

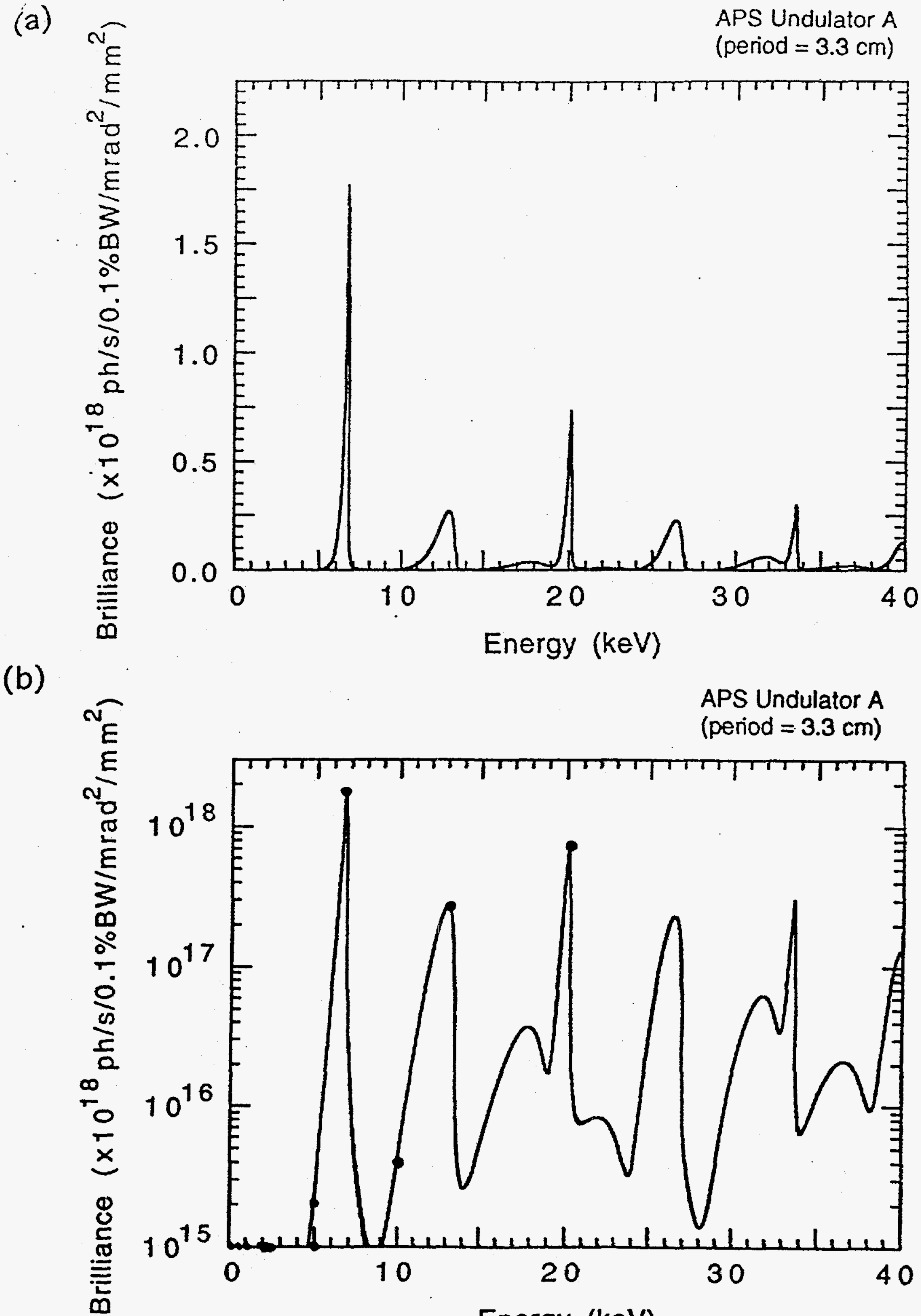

(a) Linear and (b) logarithmic plot of the on-axis brilliance spectrum for Undulator A at the initial gap of 1.55 cm (K=1.48). Note the presence of even and higher harmonics. (Operation at 7 GeV, 100 mA).

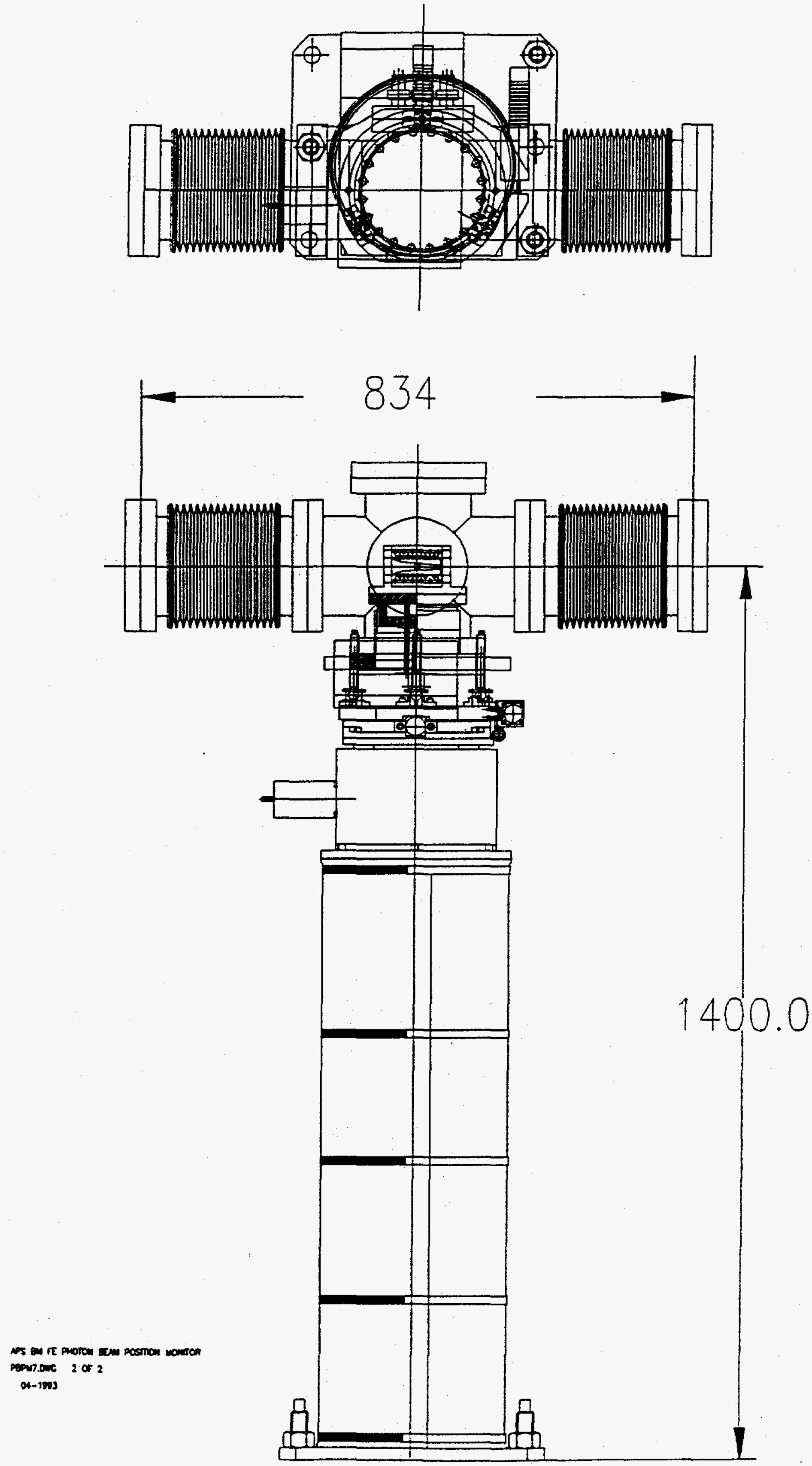
834
1400.0
APS BM FE PHOTON BEAM POSITION MONITOR
PBPM7.DWG 2 OF 2
04-1993

ADVANCED PHOTON SOURCE

W.B.S. 1.4.1.2.1.1.4

ID Front End Photon Beam Position Monitor

Technical Specifications

1.4.1.2.1.1.4 - 200000

ID Front End First Photon Beam Position Monitor

1. Location : 16.3 m from ID Straight Section Center
2. Aperture Size : 70 mm (H) x 27 mm (V)
3. Vertical Maximum Acceptance : 1.6 mrad
4. Horizontal Maximum Acceptance : 4.29 mrad
5. Input Flange O.D. : 150 mm (6 inch)
6. Output Flange O.D. : 150 mm (6 inch)
7. Monitor Type : Six Blade Photoelectron Emission
7. Monitor Blades Material : CVD Diamond
   with Thermal Conductivity > 1200 W/mk
8. Monitor Blade Thermal Limit : < 600 °C
9. Monitor Cooling Base Material : OFHC
10. Cooling Method: Water Cooling
11. Cooling Water Supply : < 0.5 GPM and 5 PSI Total Pressure Drop
12. Monitor Position Sensitivity : < 0.5 micron
16. Flange to Flange Device Length : 660 mm
17. Vacuum : UHV Compatible
18. Maximum Heat Load : Planned APS 2.4 m Undulator or Wiggler with
    7 GeV and 100 mA

ADVANCED PHOTON SOURCE

W.B.S. 1.4.1.2.1.1.4

ID Front-End Photon Beam Position Monitor

Technical Specifications

1.4.1.2.1.1.4 - 300000

ID Front-End Second Photon Beam Position Monitor

1. Location : 20.1 m from ID Straight Section Center
2. Aperture Size : 70 mm (H) x 18 mm (V)
3. Vertical Maximum Acceptance : 0.9 mrad
4. Horizontal Maximum Acceptance : 3.48 mrad
5. Input Flange O.D. : 150 mm (6 inch)
6. Output Flange O.D. : 150 mm (6 inch)
7. Monitor Type : Six Blade Photoelectron Emission
7. Monitor Blades Material : CVD Diamond with Thermal Conductivity > 1200 W/mk
8. Monitor Blade Thermal Limit : < 600 ^{o}C
9. Monitor Cooling Base Material : OFHC
10. Cooling Method: Water Cooling
11. Cooling Water Supply : < 0.5 GPM and 5 PSI Total Pressure Drop
12. Monitor Position Sensitivity : < 0.5 micron
16. Flange to Flange Device Length : 660 mm
17. Vacuum : UHV Compatible
18. Maximum Heat Load : Planned APS 2.4 m Undulator or Wiggler with 7 GeV and 100 mA

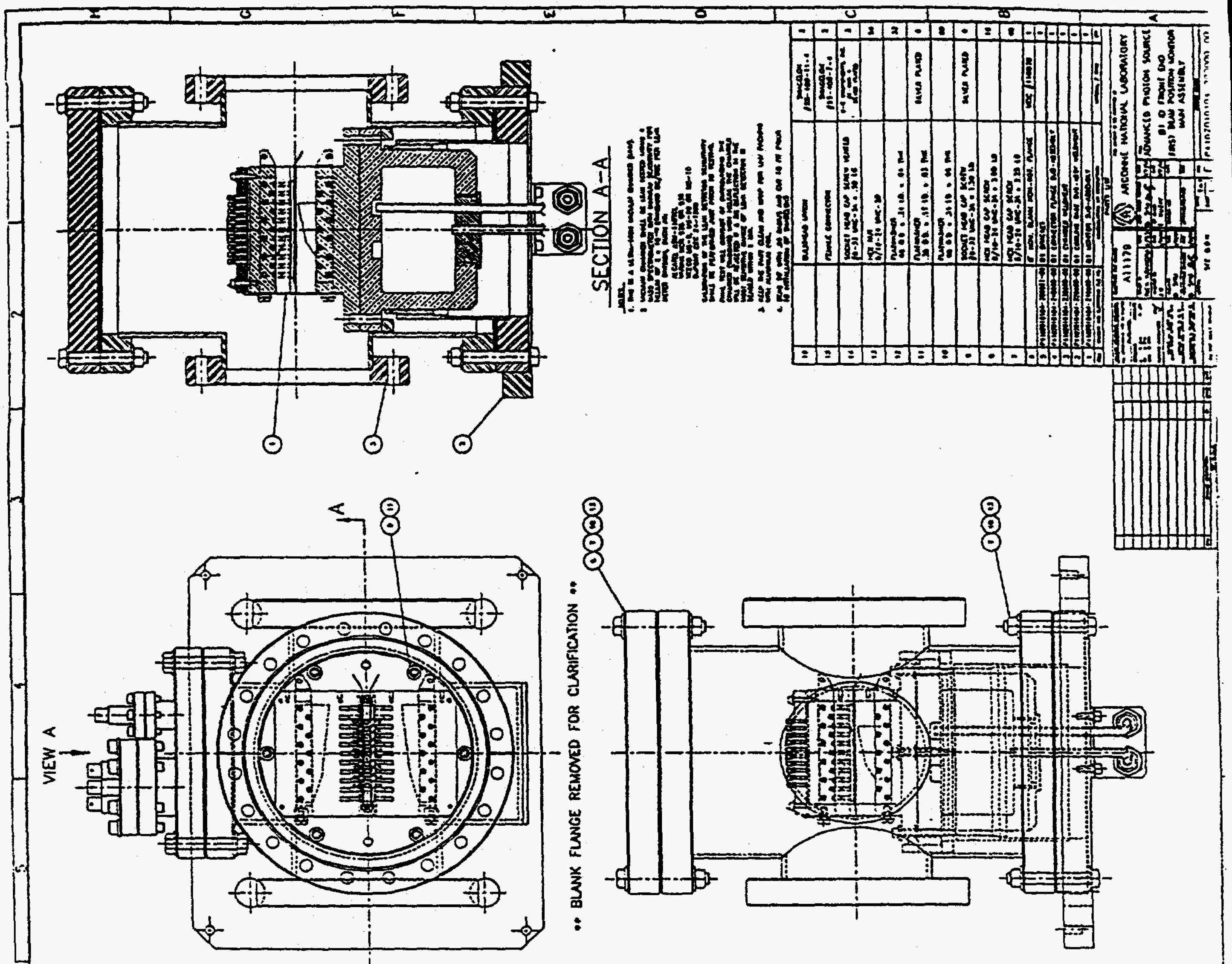
SECTION A-A
VIEW A
** BLANK FLANGE REMOVED FOR CLARIFICATION **
BEAM
SECTION B-B
VIEW A
ARGONNE NATIONAL LABORATORY
ADVANCED PHOTON SOURCE

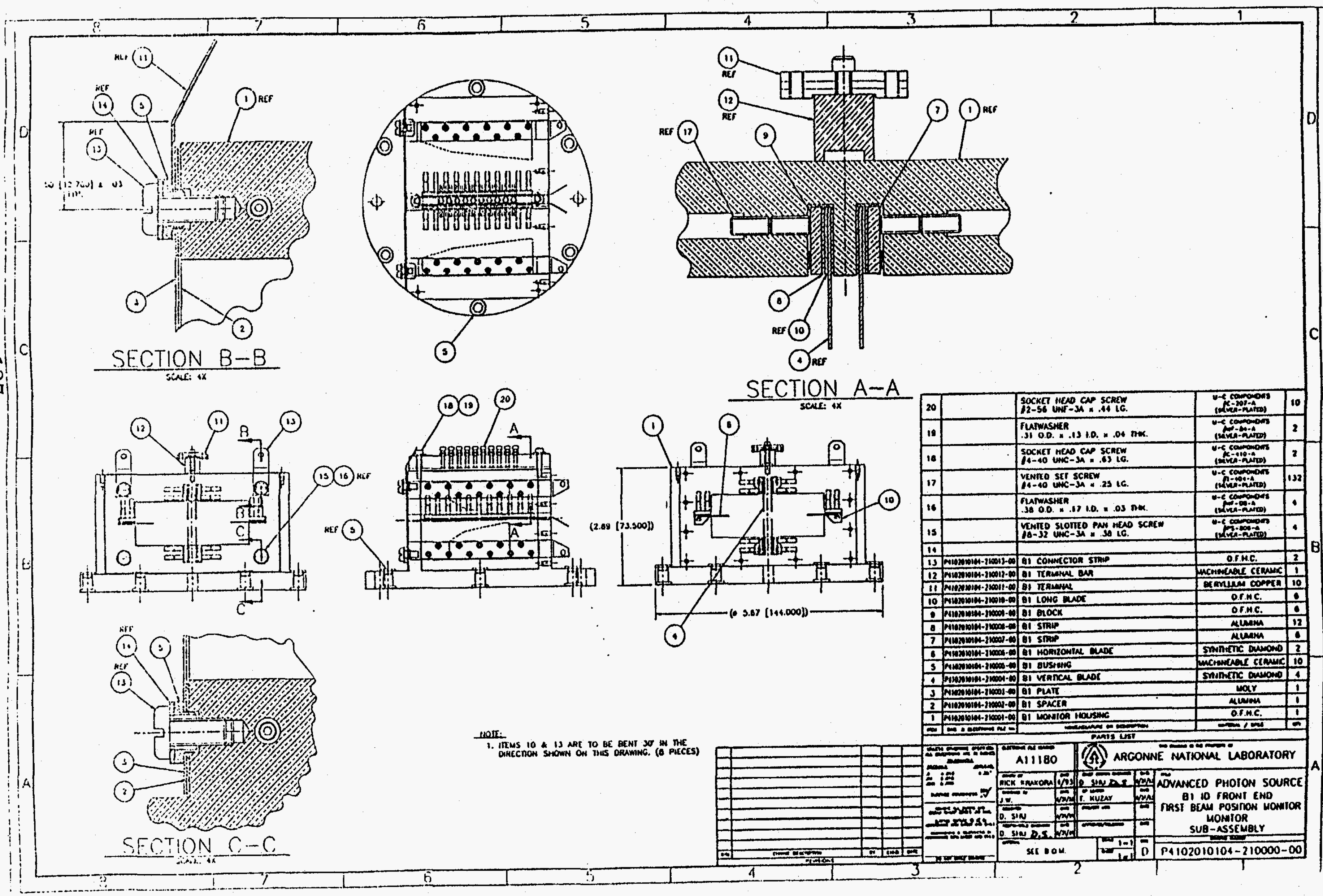

PARTS LIST

20		SOCKET HEAD CAP SCREW #2-56 UNF-3A x .44 LG.	U-C COMPONENTS #C-207-A (SILVER-PLATED)	10
19		FLATWASHER .31 O.D. x .13 I.D. x .04 THK.	U-C COMPONENTS #WF-04-A (SILVER-PLATED)	2
18		SOCKET HEAD CAP SCREW #4-40 UNC-3A x .63 LG.	U-C COMPONENTS #C-410-A (SILVER-PLATED)	2
17		VENTED SET SCREW #4-40 UNC-3A x .25 LG.	U-C COMPONENTS #1-404-A (SILVER-PLATED)	132
16		FLATWASHER .38 O.D. x .17 I.D. x .03 THK.	U-C COMPONENTS #WF-08-A (SILVER-PLATED)	4
15		VENTED SLOTTED PAN HEAD SCREW #8-32 UNC-3A x .38 LG.	U-C COMPONENTS #PS-806-A (SILVER-PLATED)	4
14				
13	P4102010104-210013-00	B1 CONNECTOR STRIP	O.F.H.C.	2
12	P4102010104-210012-00	B1 TERMINAL BAR	MACHINEABLE CERAMIC	1
11	P4102010104-210011-00	B1 TERMINAL	BERYLLIUM COPPER	10
10	P4102010104-210010-00	B1 LONG BLADE	O.F.H.C.	8
9	P4102010104-210009-00	B1 BLOCK	O.F.H.C.	6
8	P4102010104-210008-00	B1 STRIP	ALUMINA	12
7	P4102010104-210007-00	B1 STRIP	ALUMINA	6
6	P4102010104-210006-00	B1 HORIZONTAL BLADE	SYNTHETIC DIAMOND	2
5	P4102010104-210005-00	B1 BUSHING	MACHINEABLE CERAMIC	10
4	P4102010104-210004-00	B1 VERTICAL BLADE	SYNTHETIC DIAMOND	4
3	P4102010104-210003-00	B1 PLATE	MOLY	1
2	P4102010104-210002-00	B1 SPACER	ALUMINA	1
1	P4102010104-210001-00	B1 MONITOR HOUSING	O.F.H.C.	1

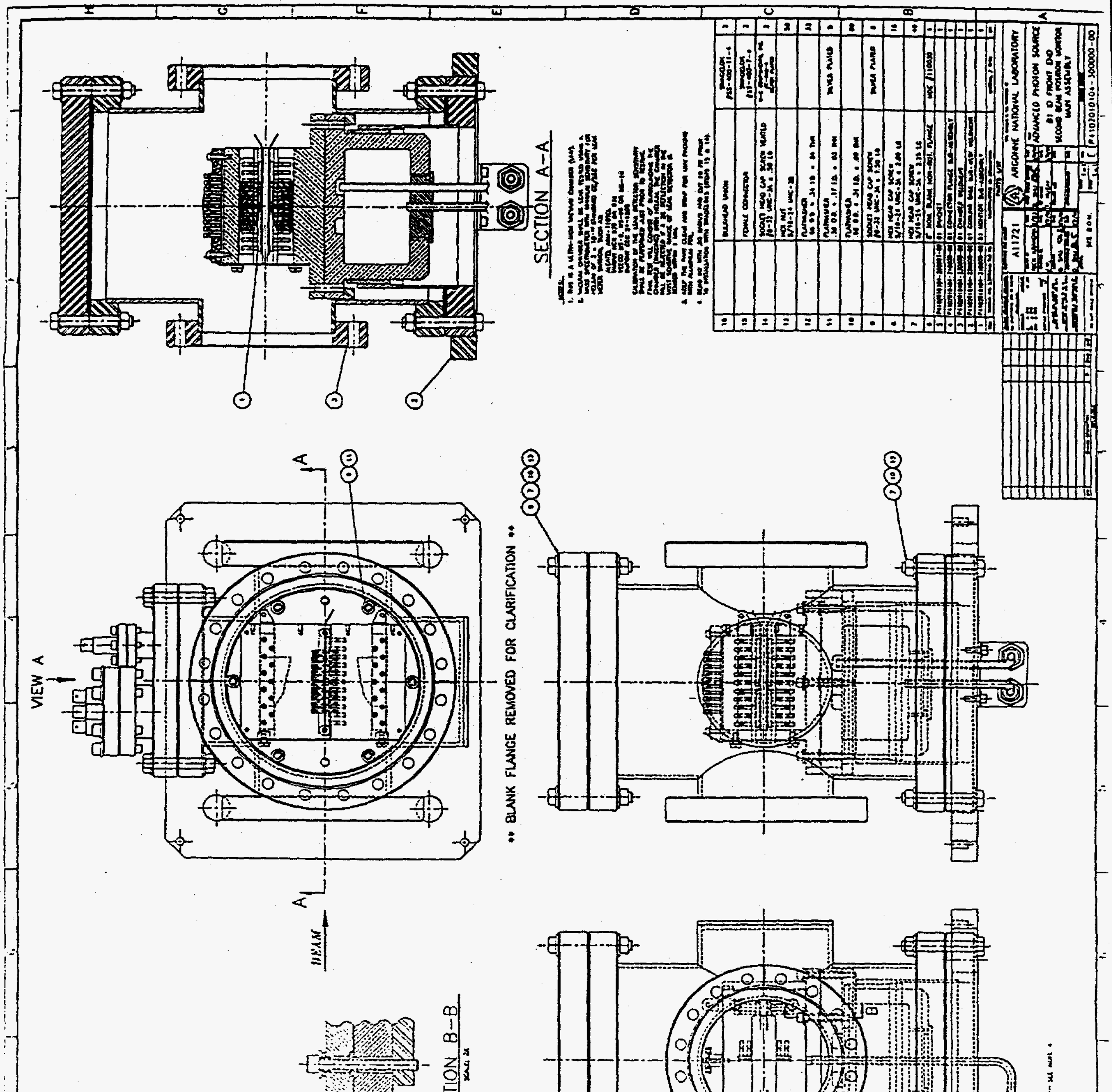
SECTION A-A
VIEW A
** BLANK FLANGE REMOVED FOR CLARIFICATION **
BEAM
SECTION B-B
VIEW A
ARGONNE NATIONAL LABORATORY
ADVANCED PHOTON SOURCE

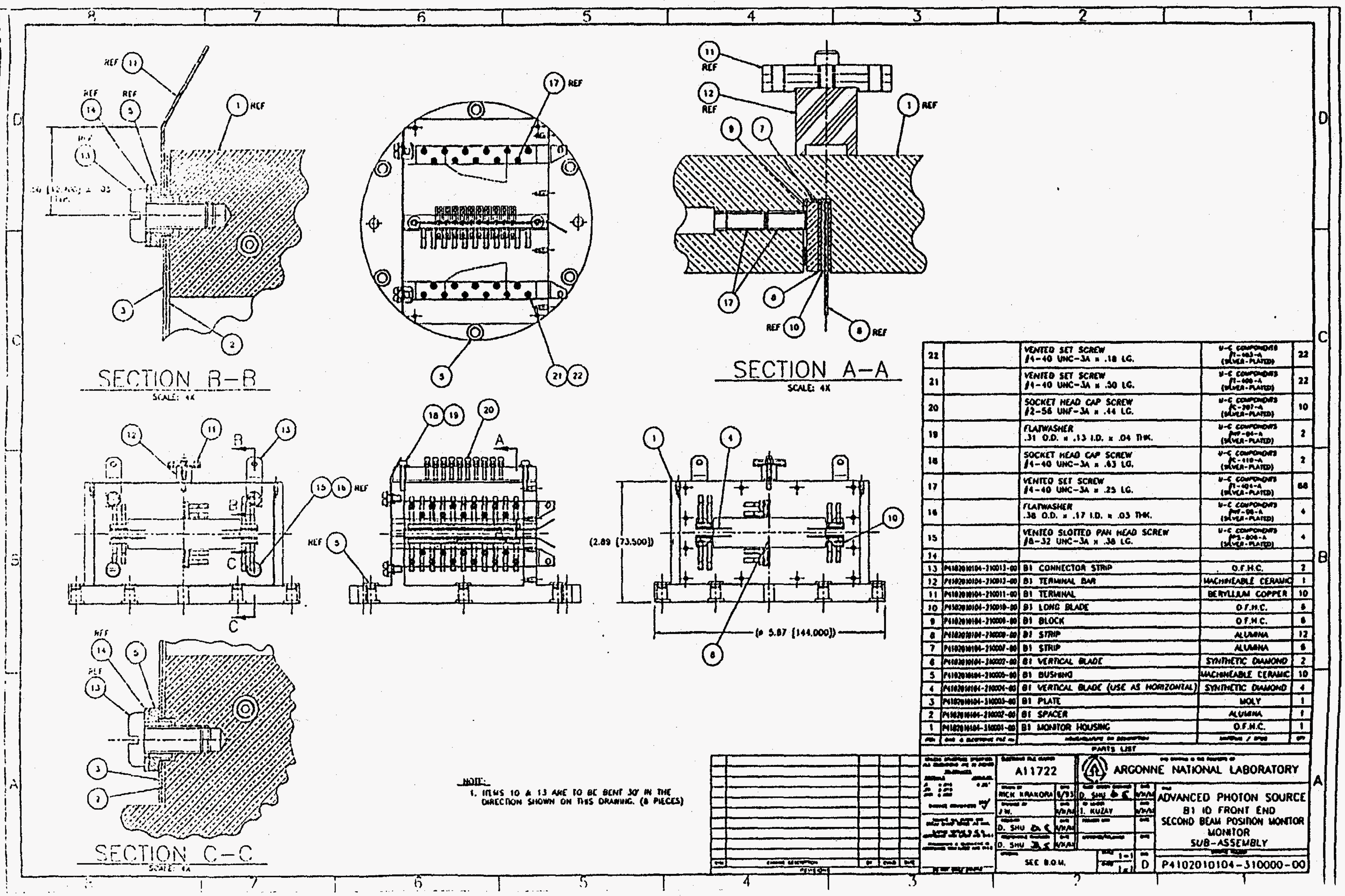
SECTION B–B
SCALE: 4X
SECTION A–A
SCALE: 4X
SECTION C–C
SCALE: 4X
(2.89 [73.500])
(⌀ 5.87 [144.000])
NOTE:
1. ITEMS 10 & 13 ARE TO BE BENT 30° IN THE DIRECTION SHOWN ON THIS DRAWING. (8 PIECES)
22 VENTED SET SCREW #4-40 UNC-3A x .18 LG. U-C COMPONENTS (SILVER-PLATED) 22
21 VENTED SET SCREW #4-40 UNC-3A x .30 LG. U-C COMPONENTS (SILVER-PLATED) 22
20 SOCKET HEAD CAP SCREW #2-56 UNF-3A x .44 LG. U-C COMPONENTS (SILVER-PLATED) 10
19 FLATWASHER .31 O.D. x .13 I.D. x .04 THK. U-C COMPONENTS (SILVER-PLATED) 2
18 SOCKET HEAD CAP SCREW #4-40 UNC-3A x .63 LG. U-C COMPONENTS (SILVER-PLATED) 2
17 VENTED SET SCREW #4-40 UNC-3A x .25 LG. U-C COMPONENTS (SILVER-PLATED) 68
16 FLATWASHER .38 O.D. x .17 I.D. x .03 THK. U-C COMPONENTS (SILVER-PLATED) 4
15 VENTED SLOTTED PAN HEAD SCREW #8-32 UNC-3A x .38 LG. U-C COMPONENTS (SILVER-PLATED) 4
14
13 B1 CONNECTOR STRIP O.F.H.C. 2
12 B1 TERMINAL BAR MACHINEABLE CERAMIC 1
11 B1 TERMINAL BERYLLIUM COPPER 10
10 B1 LONG BLADE O.F.H.C. 8
9 B1 BLOCK O.F.H.C. 8
8 B1 STRIP ALUMINA 12
7 B1 STRIP ALUMINA 8
6 B1 VERTICAL BLADE SYNTHETIC DIAMOND 2
5 B1 BUSHING MACHINEABLE CERAMIC 10
4 B1 VERTICAL BLADE (USE AS HORIZONTAL) SYNTHETIC DIAMOND 4
3 B1 PLATE MOLY 1
2 B1 SPACER ALUMINA 1
1 B1 MONITOR HOUSING O.F.H.C. 1
PARTS LIST
A11722
ARGONNE NATIONAL LABORATORY
ADVANCED PHOTON SOURCE
B1 ID FRONT END
SECOND BEAM POSITION MONITOR
MONITOR
SUB-ASSEMBLY
NICK KRAKORA
D. SHU
I. KUZAY
SEE B.O.M.
D
P4102010104-310000-00

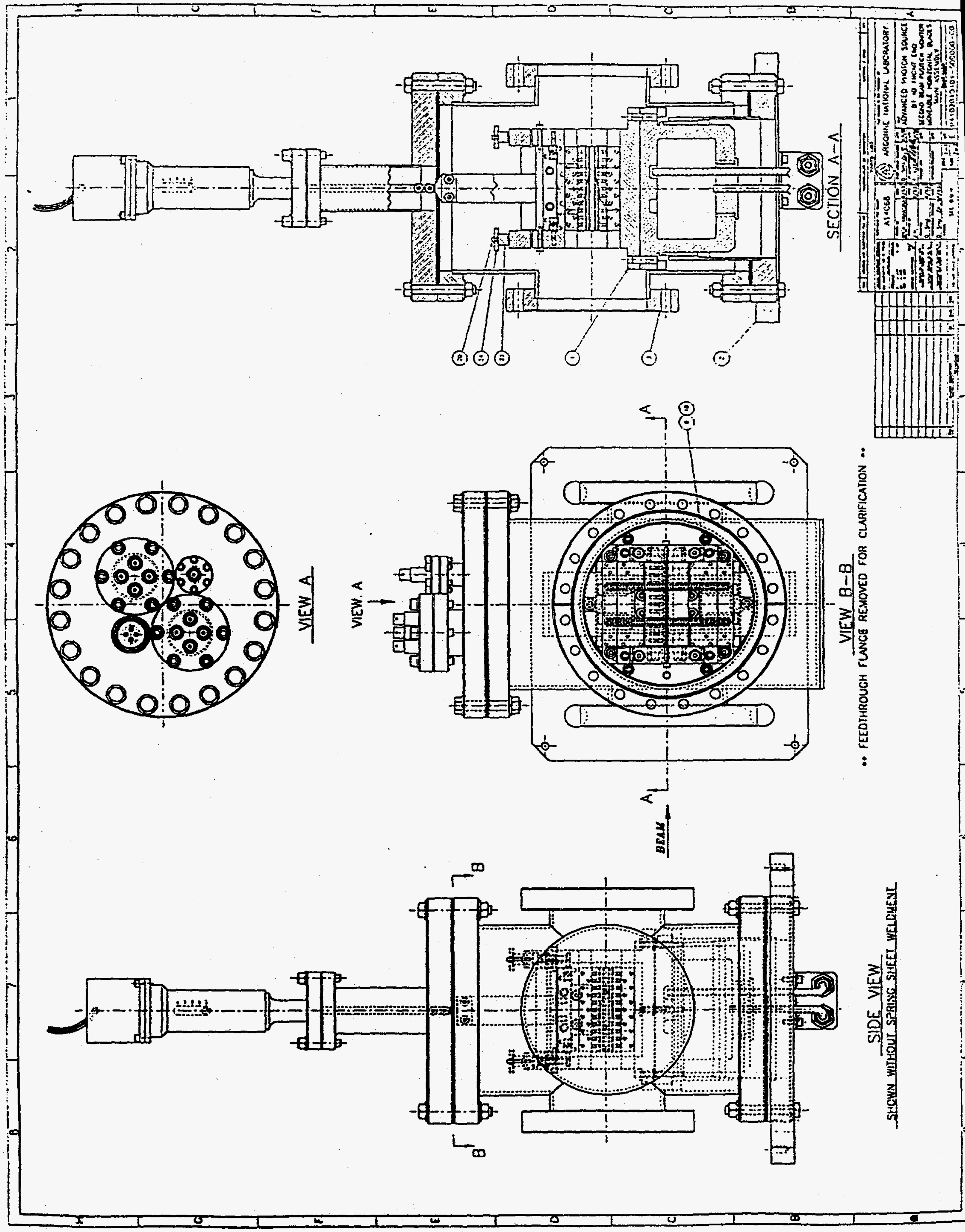
SECTION A-A
VIEW A
VIEW A
VIEW B-B
•• FEEDTHROUGH FLANGE REMOVED FOR CLARIFICATION ••
BEAM
SIDE VIEW
SHOWN WITHOUT SPRING SHEET WELDMENT
ARGONNE NATIONAL LABORATORY
ADVANCED PHOTON SOURCE

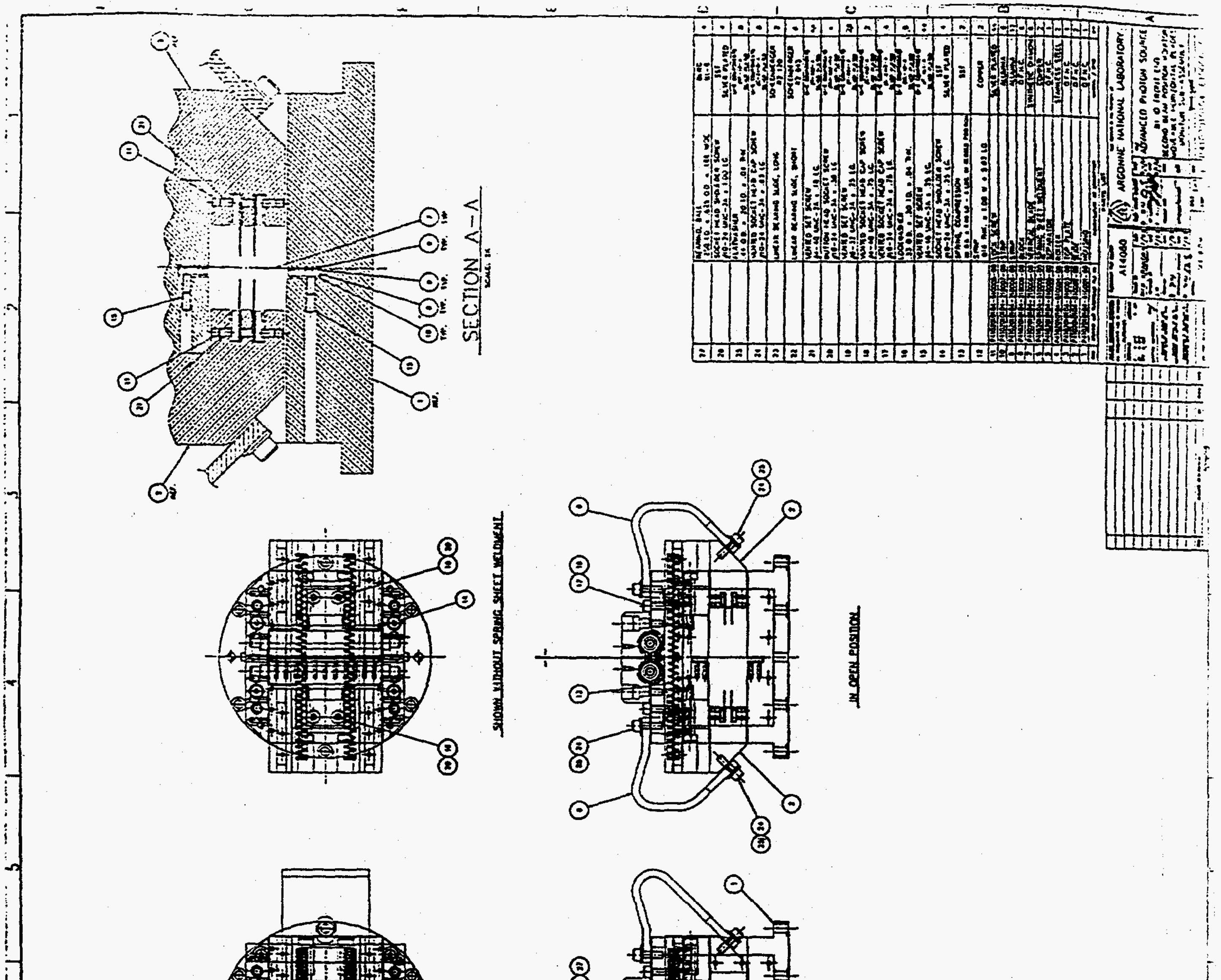
SECTION A-A
SHOWN WITHOUT SPRING SHEET WELDMENT
IN OPEN POSITION
SHOWN WITHOUT SPRING SHEET
ARGONNE NATIONAL LABORATORY
ADVANCED PHOTON SOURCE

TABLE 2 BPM Support Stages Specifications

Load Capacity	90 kg
Travel Range	+/- 5mm
Angular Range	+/- 2 deg
Linear Resolution	0.2 μm
Angular Resolution	0.5 arc second
Repeatability:	
Horizontal	+/- 5 μm
Vertical	+/- 2 μm
Angular	5 arc second
Straightness of Trajectory	$1x10^{-5}$rad/25mm

PURPOSE OF THE PRE-PROTOTYPE TEST

1. EXPERIMENTALLY PROVE THAT USING THE SOFT X-RAY PART OF THE HARD X-RAY UNDULATOR BEAM WILL DETERMINE THE BEAM CENTER POSITION

2. TEST THE DEVICE SENSITIVITY

3. ASSESS THE BENDING MAGNET SYNCHROTRON RADIATION CONTAMINATION

4. CHECKOUT BLADE GAP IN ADJUSTMENT IN UHV AND REPRODUCIBILITY

5. ASSESS IF TWO VERTICAL PAIR OF BLADES WILL PROVIDE A GOOD HORIZONTAL POSITION INFORMATION

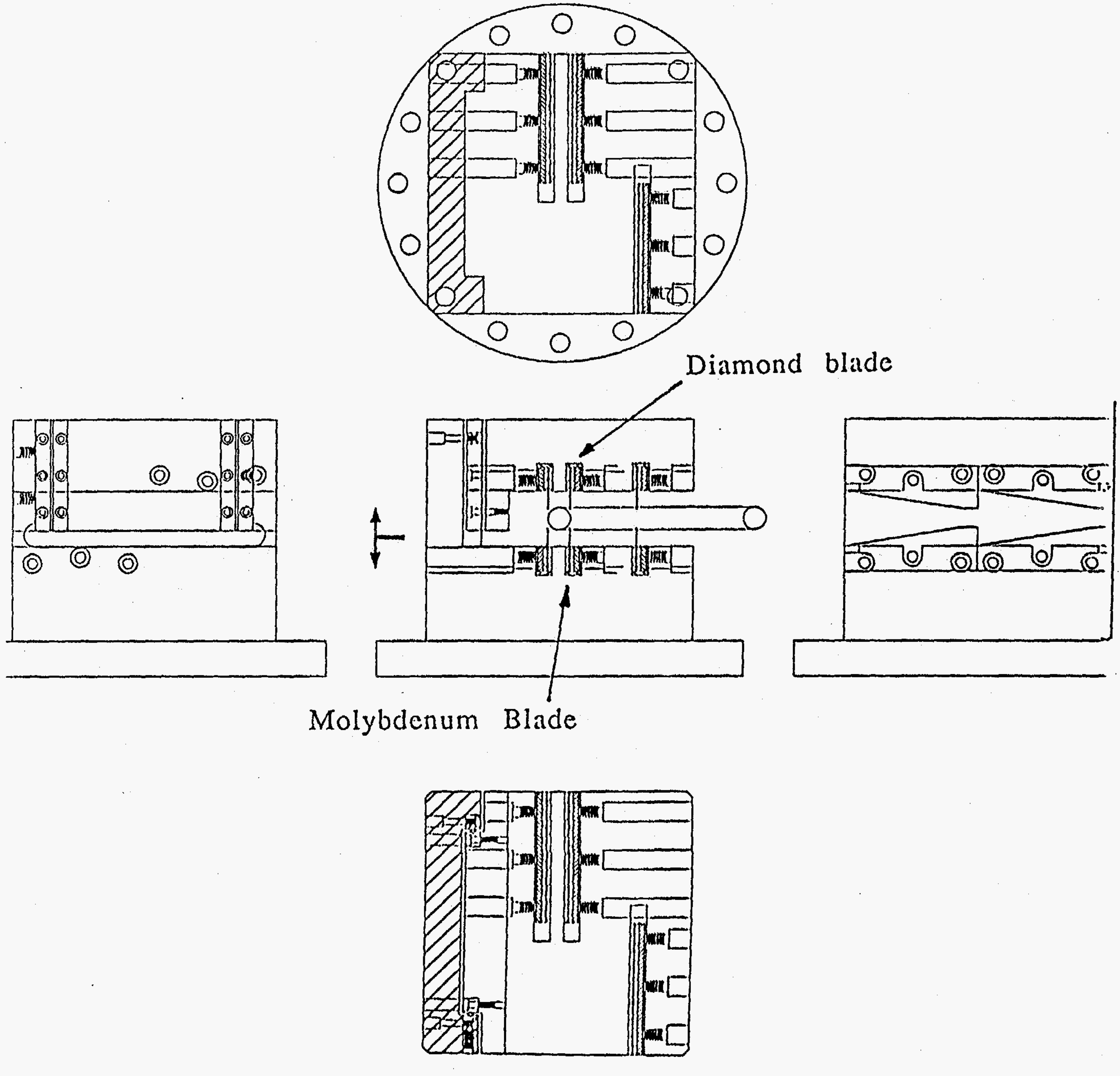

Assembly drawing of the Photon Beam Position Monitor
Tested at CHESS, Cornell University

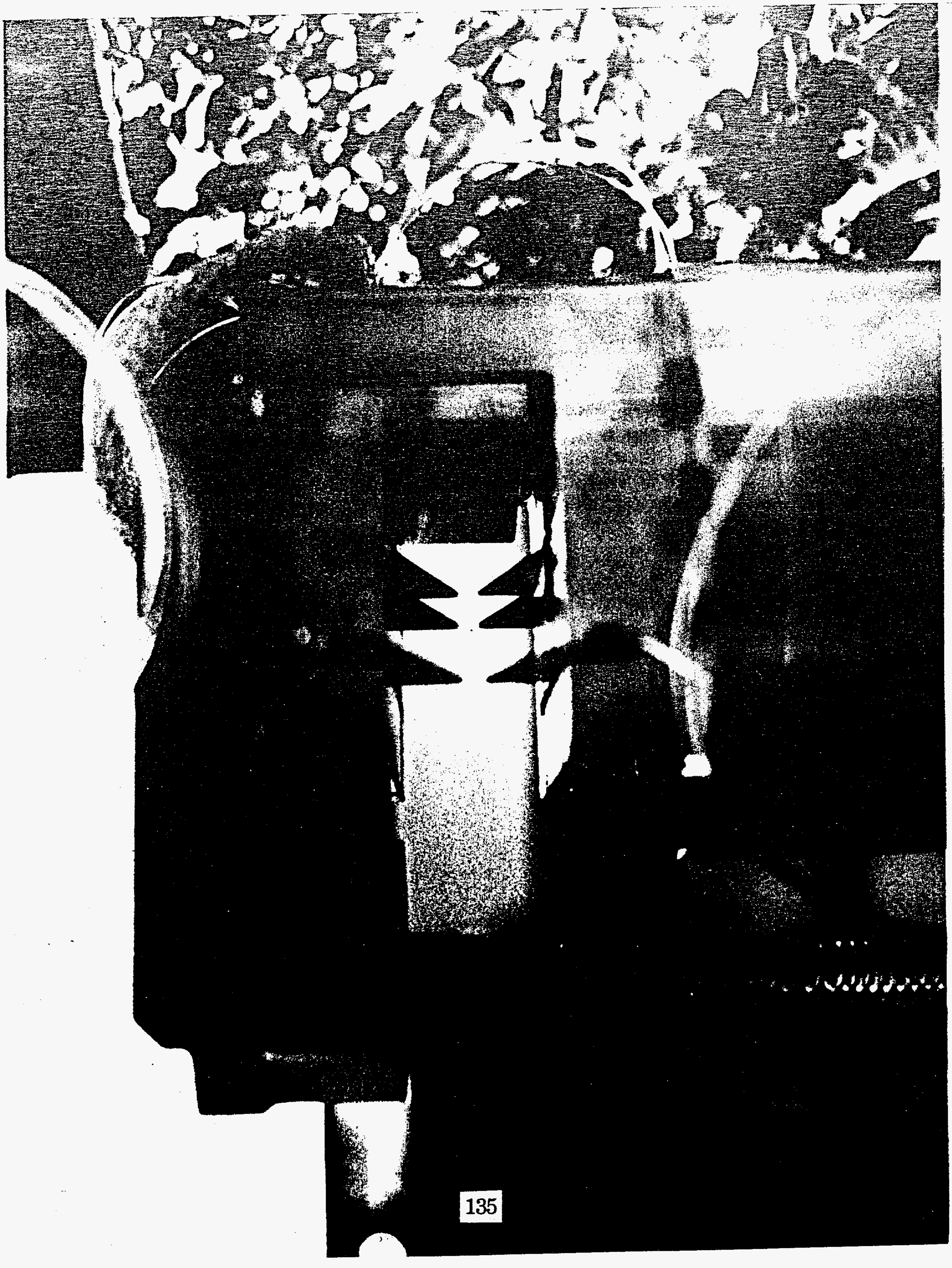

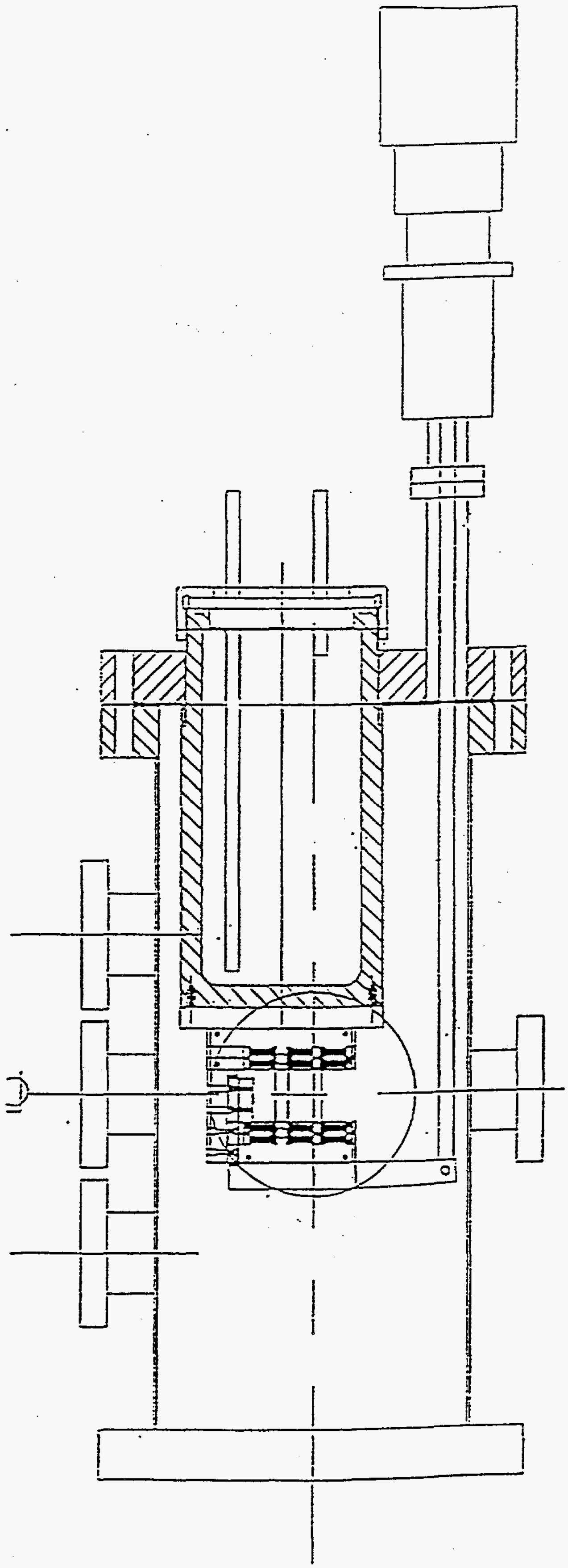

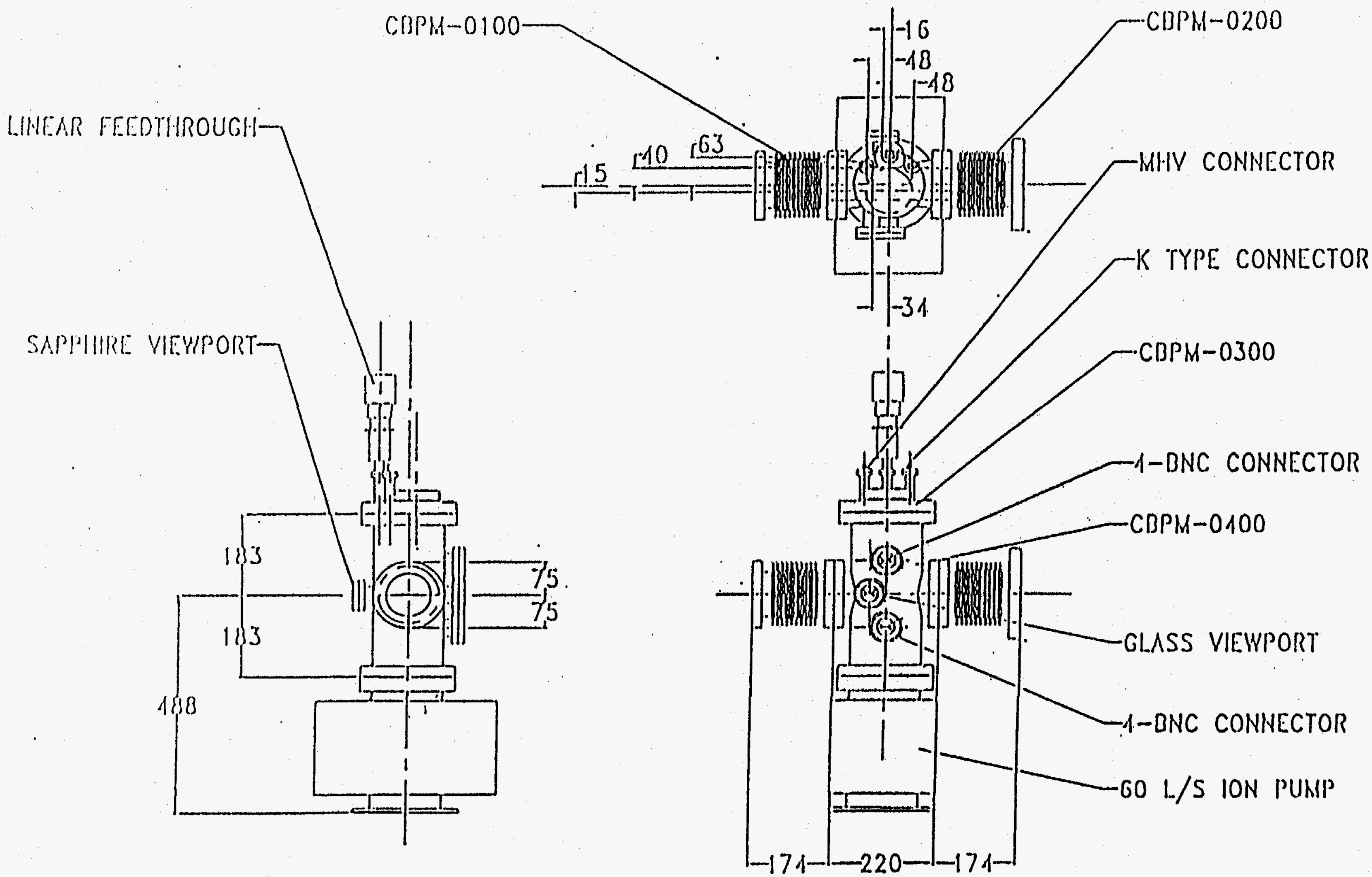

Layout of the APS Photon Beam Position Monitor for the APS/CHESS Undulator Runs

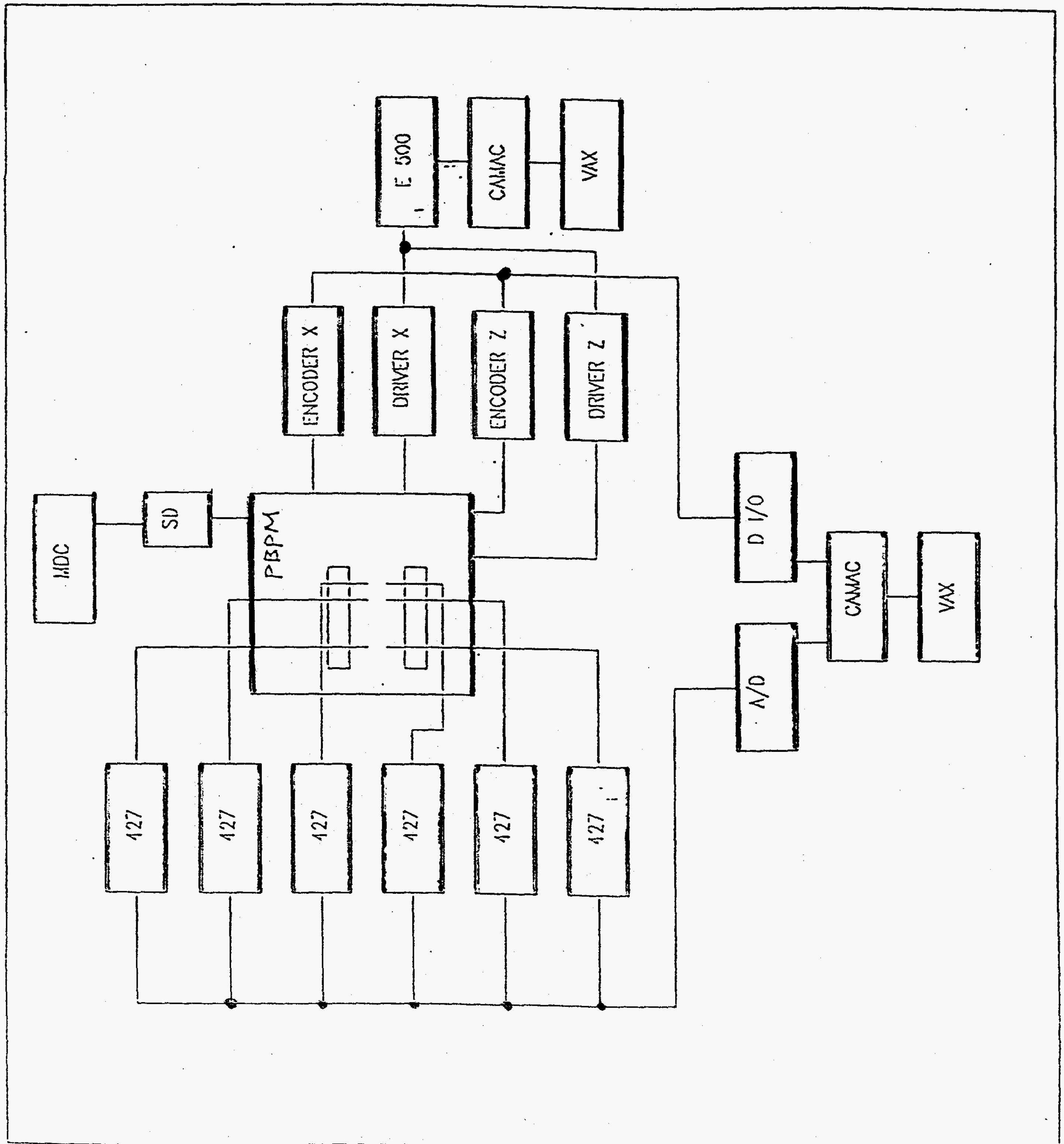

E 500
CAMAC
VAX
ENCODER X
DRIVER X
ENCODER Z
DRIVER Z
MDC
SD
PBPM
D I/O
CAMAC
VAX
A/D
427
427
427
427
427
427

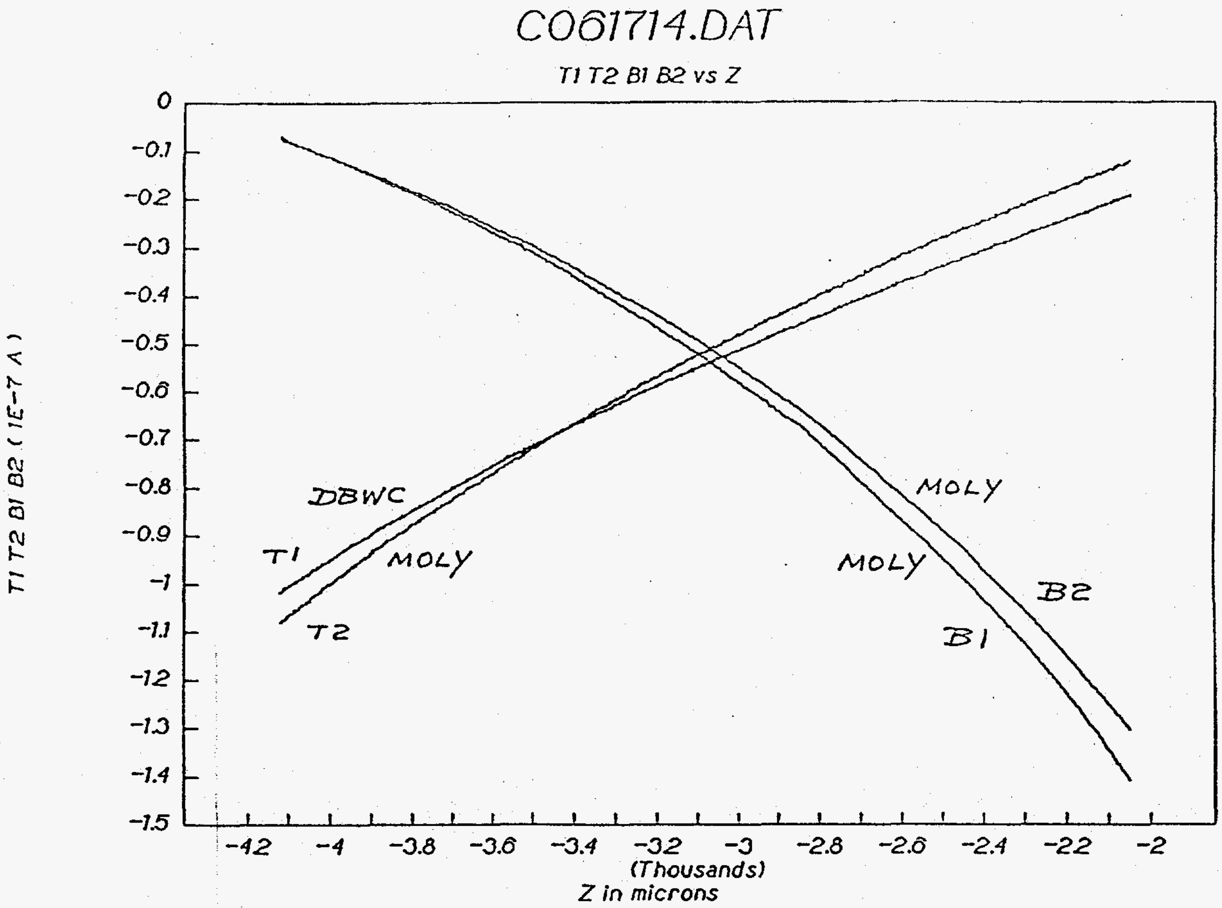

Diamond Blade and Molybdenum Blade Tests at CHESS

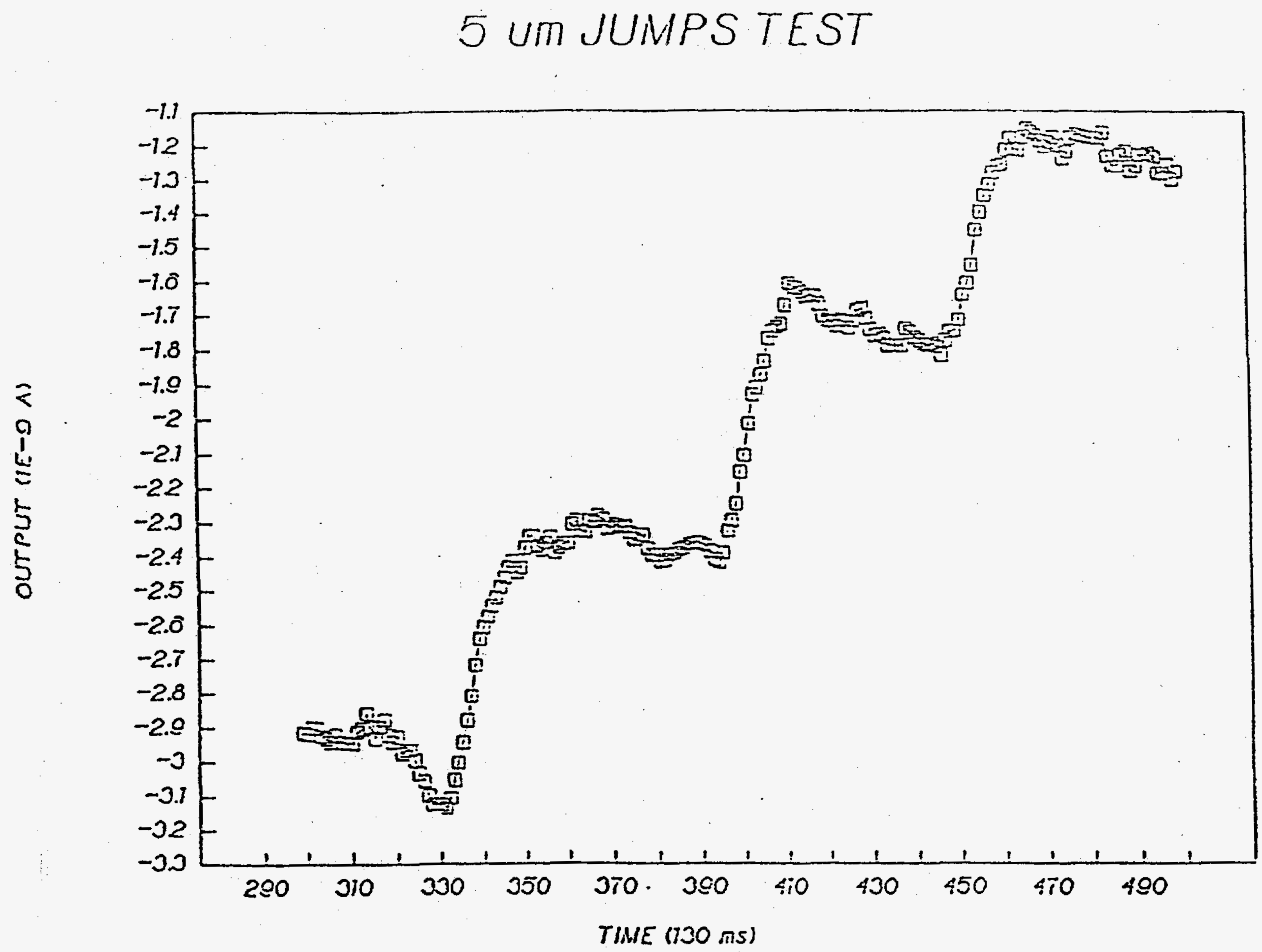

Diamond Blade sensitivity tests to 5 µm step change at CHESS

"WORST CASE" TEST.

July 15, 1991

ANL / CHESS UNDULATOR (GAP = 15 mm)

5.4 GEV

120 MA

POWER DENSITY AT 8.3 m 280 W/mm^2

BLADES WERE DIRECTLY IMPINGED BY THE CENTRAL PART OF THE WHITE BEAM.

THE MONITOR WAS STILL FULLY FUNCTIONAL.

NO VISUAL CHANGES WERE FOUND ON THE CVD DIAMOND BASE TUNGSTEN COATED BLADE.

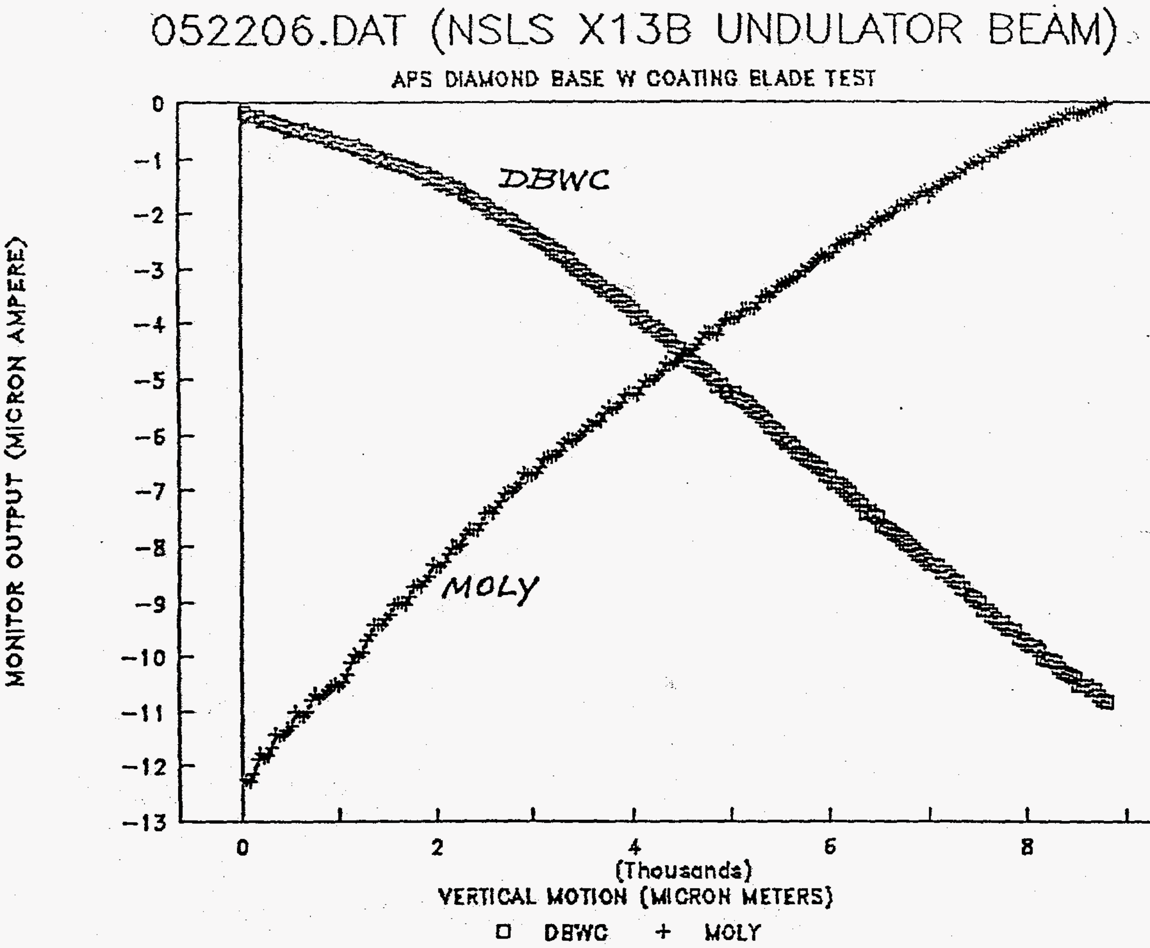

Diamond Blade and Molybdenum Blade Tests at NSLS X-13

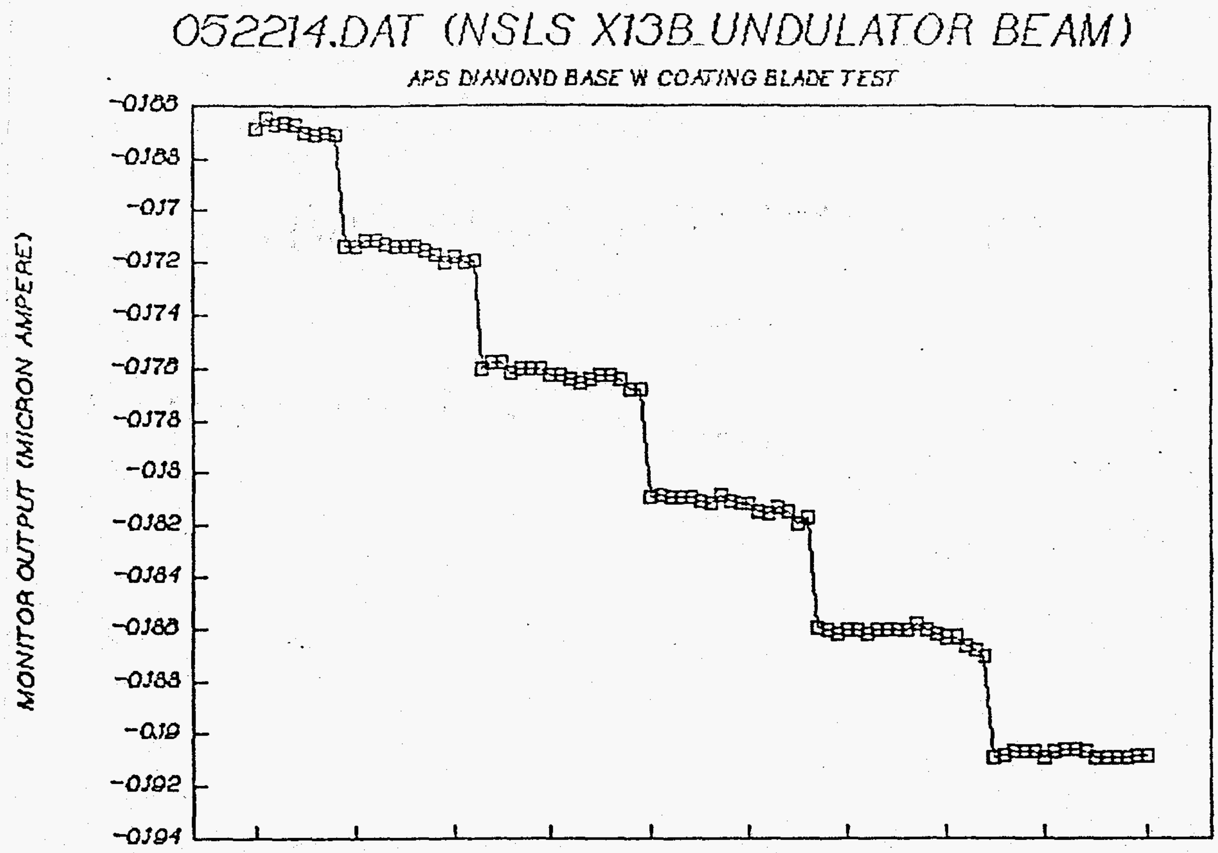

Diamond Blade Sensitivity Tests to 5 μm Step Change at NSLS X-13

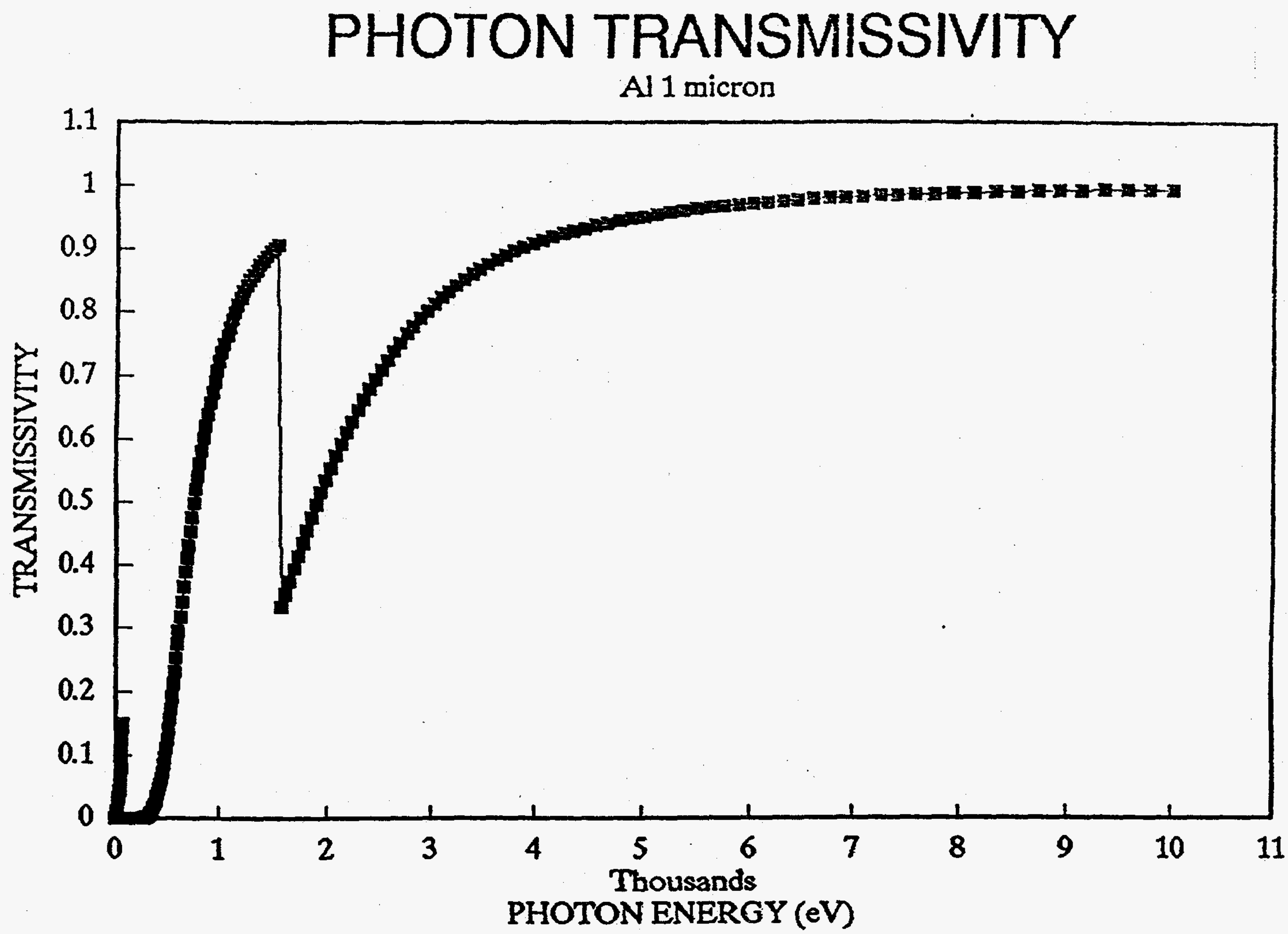

PHOTON TRANSMISSIVITY
Al 1 micron
TRANSMISSIVITY
1.1
1
0.9
0.8
0.7
0.6
0.5
0.4
0.3
0.2
0.1
0
0 1 2 3 4 5 6 7 8 9 10 11
Thousands
PHOTON ENERGY (eV)

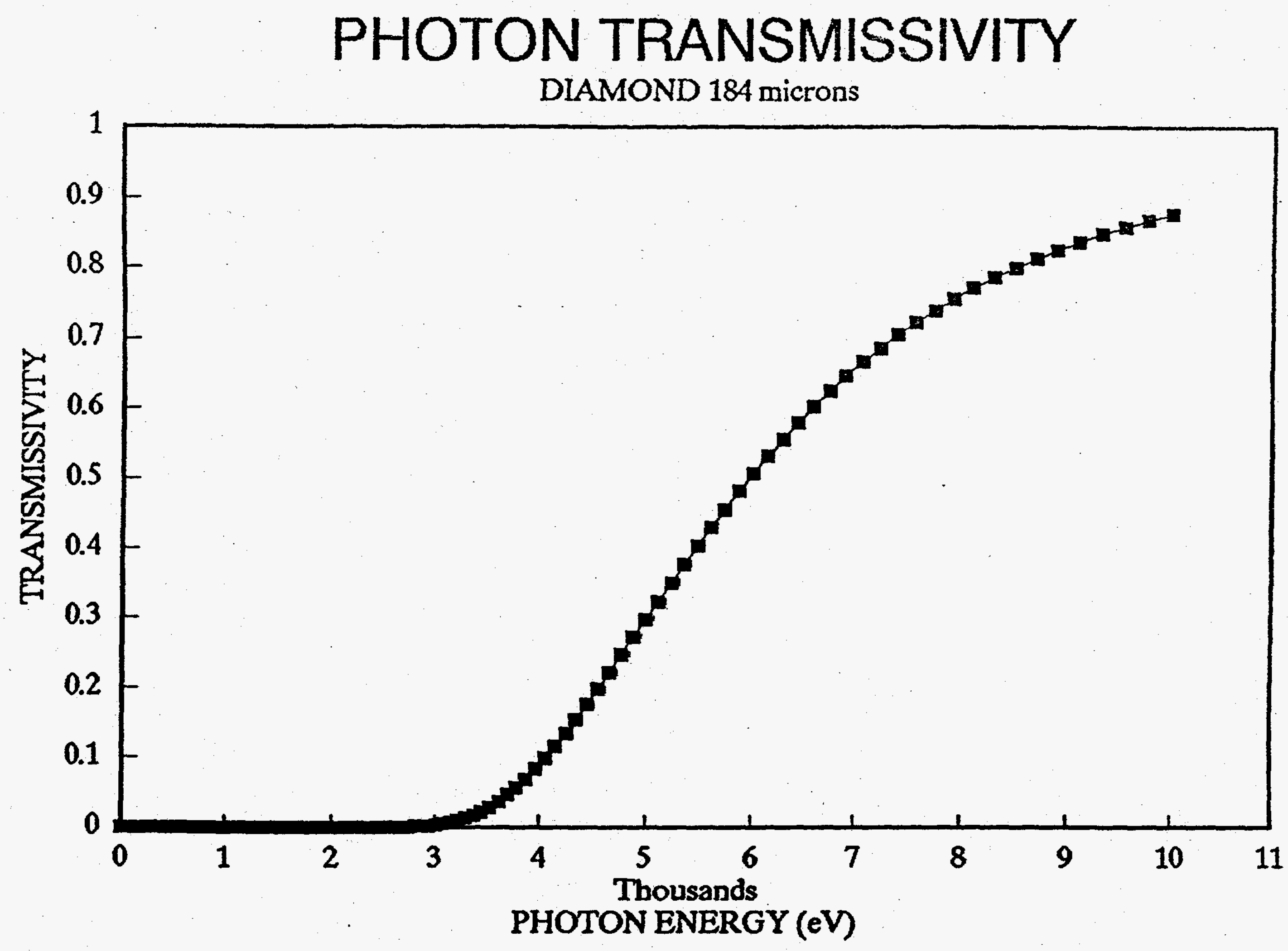

PHOTON TRANSMISSIVITY
DIAMOND 184 microns
TRANSMISSIVITY
0
0.1
0.2
0.3
0.4
0.5
0.6
0.7
0.8
0.9
1
0
1
2
3
4
5
6
7
8
9
10
11
Thousands
PHOTON ENERGY (eV)

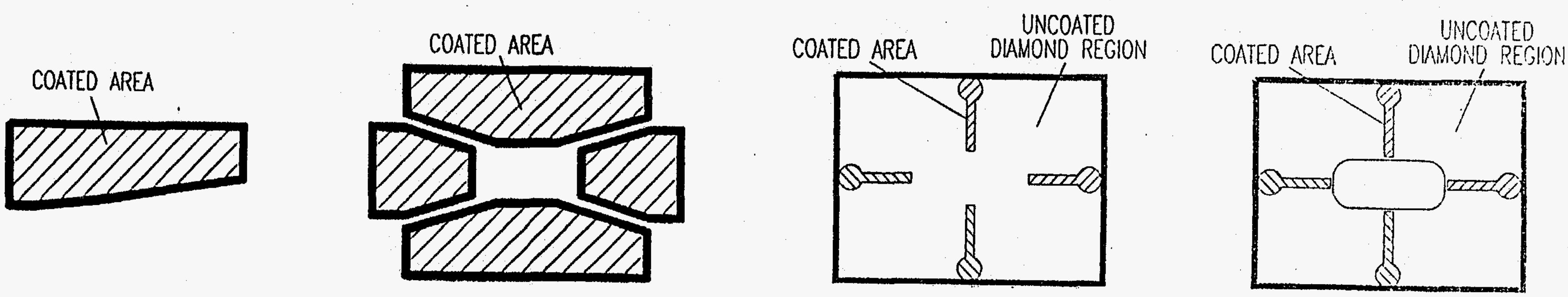

FIG.1a FIG.1b FIG.1c FIG.1d

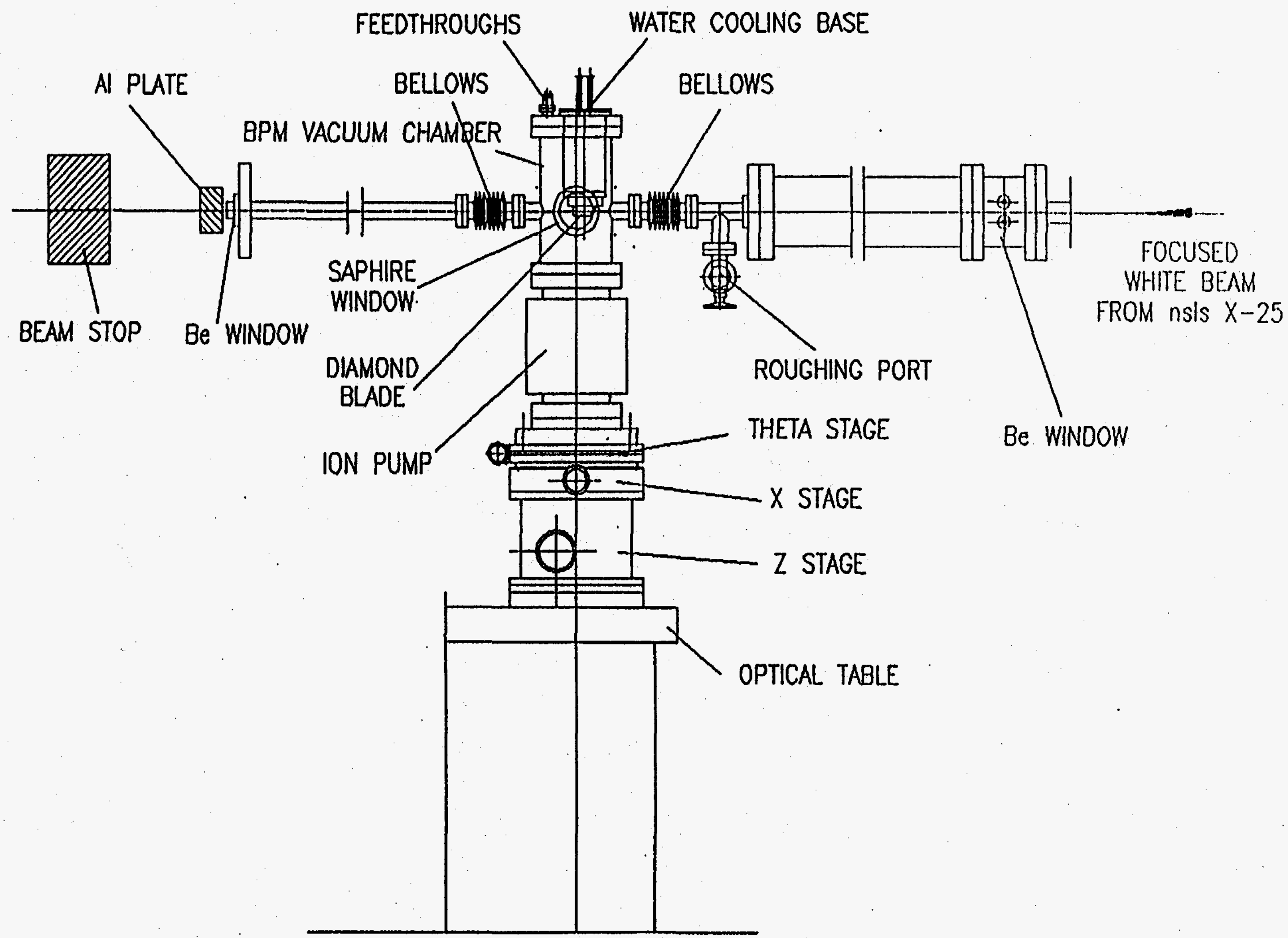

APS PTBPM TEST SET-UP SCHEMATIC AT NSLS X-25

NSLS X−25 POWER SPECTRA

2.5Gev 200ma 70w total AT FOCAL POINT

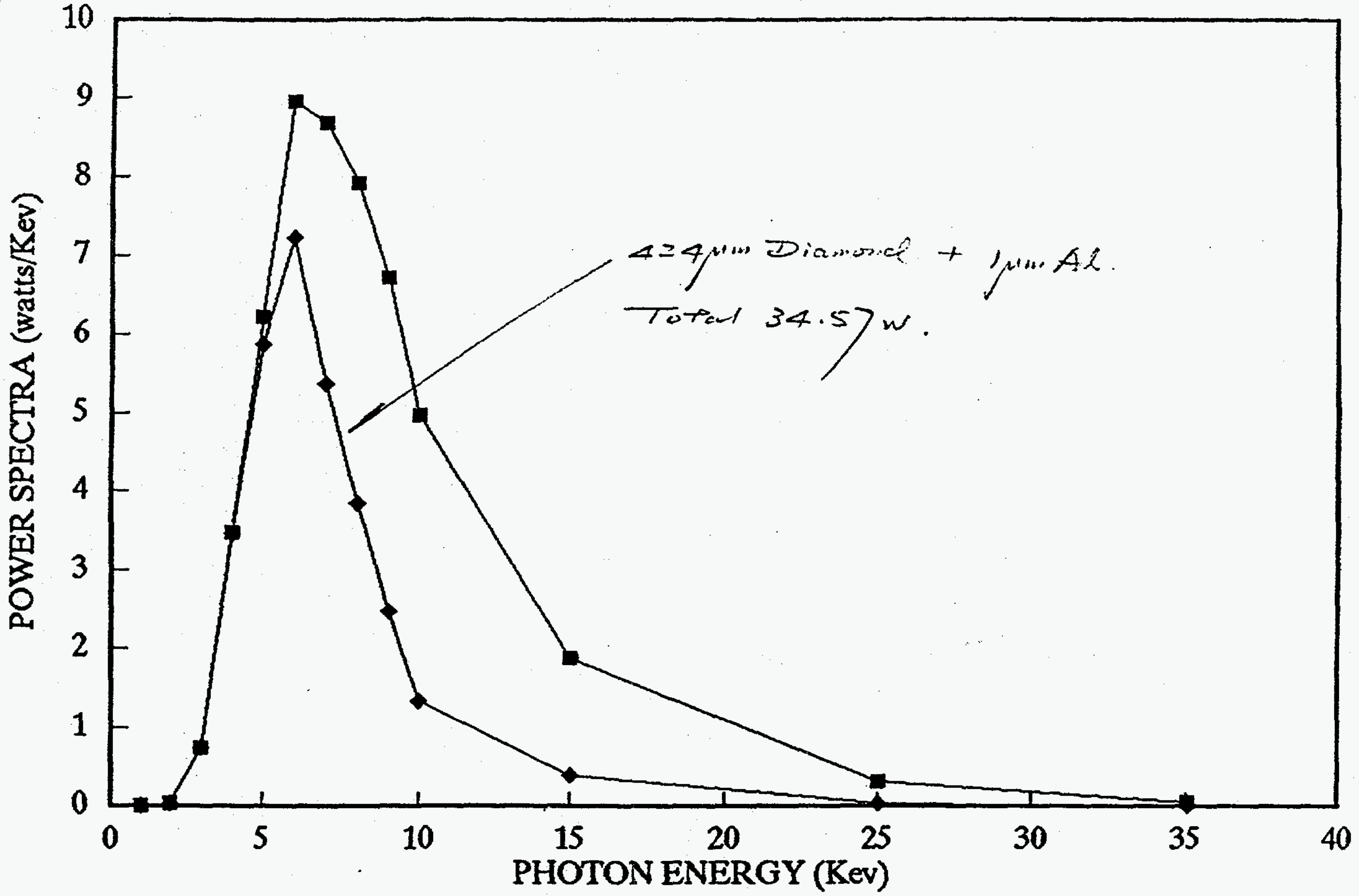

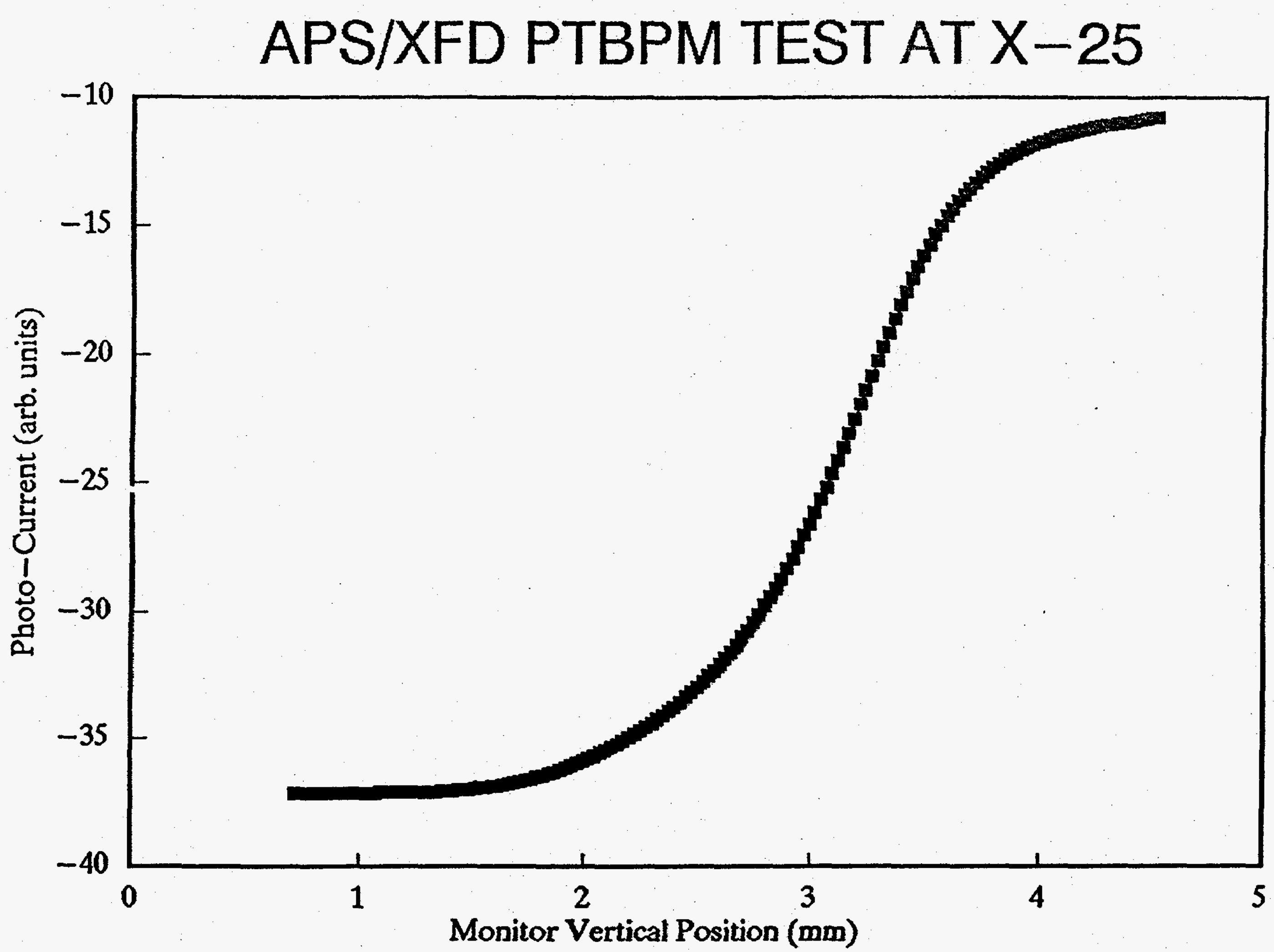
APS/XFD PTBPM TEST AT X−25
Photo−Current (arb. units)
Monitor Vertical Position (mm)
−10
−15
−20
−25
−30
−35
−40
0
1
2
3
4
5

ADVANCED PHOTON SOURCE

Vertical Stepping Tests at NSLS-X25

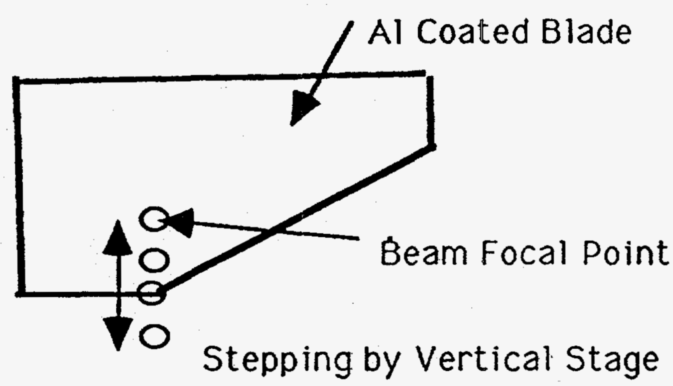

Stepping of the Test Blade 1 with Respect to the Beam with the Vertical Stage

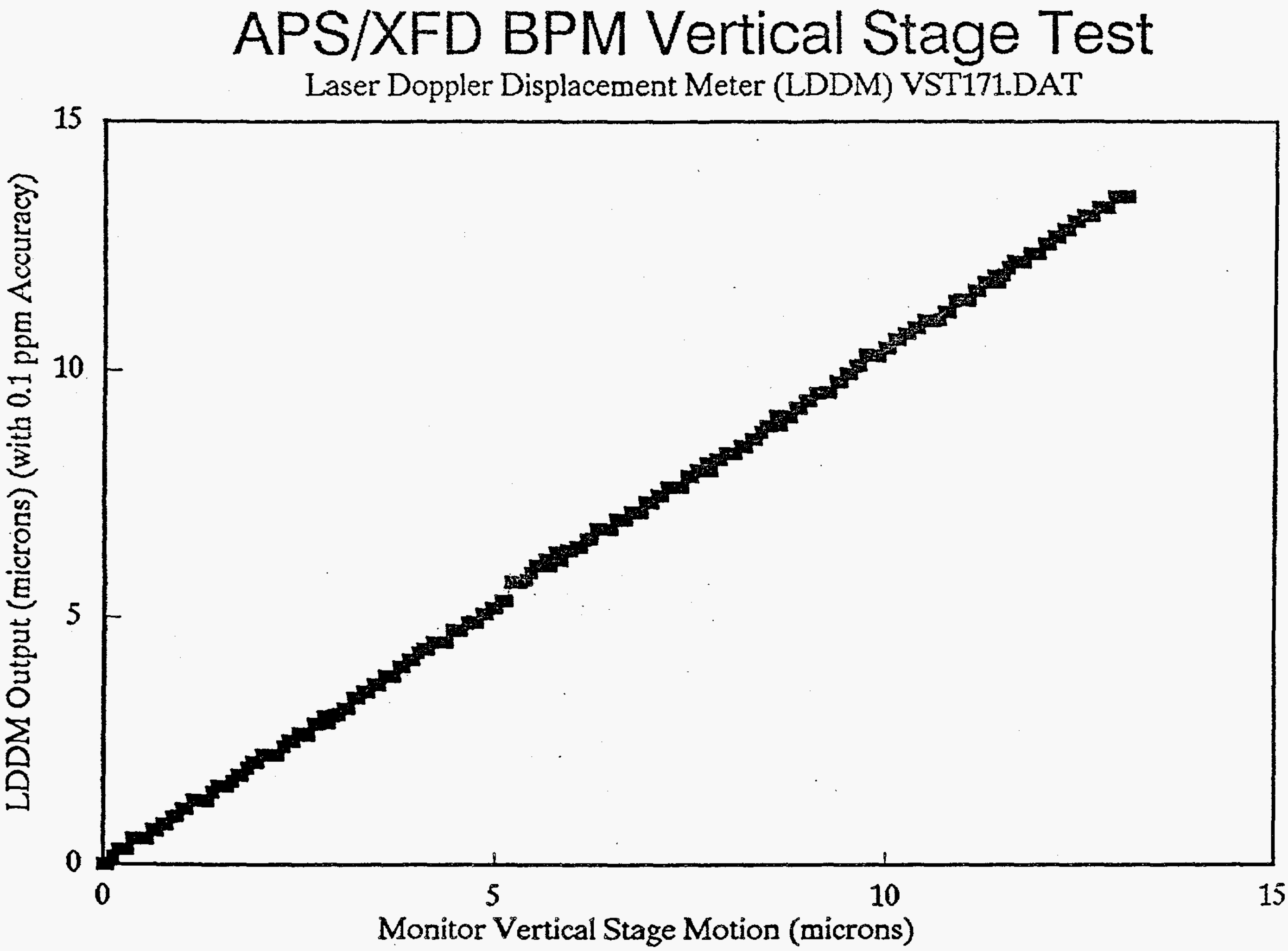

APS/XFD BPM Vertical Stage Test
Laser Doppler Displacement Meter (LDDM) VST171.DAT
LDDM Output (microns) (with 0.1 ppm Accuracy)
15
10
5
0
0
5
10
15
Monitor Vertical Stage Motion (microns)

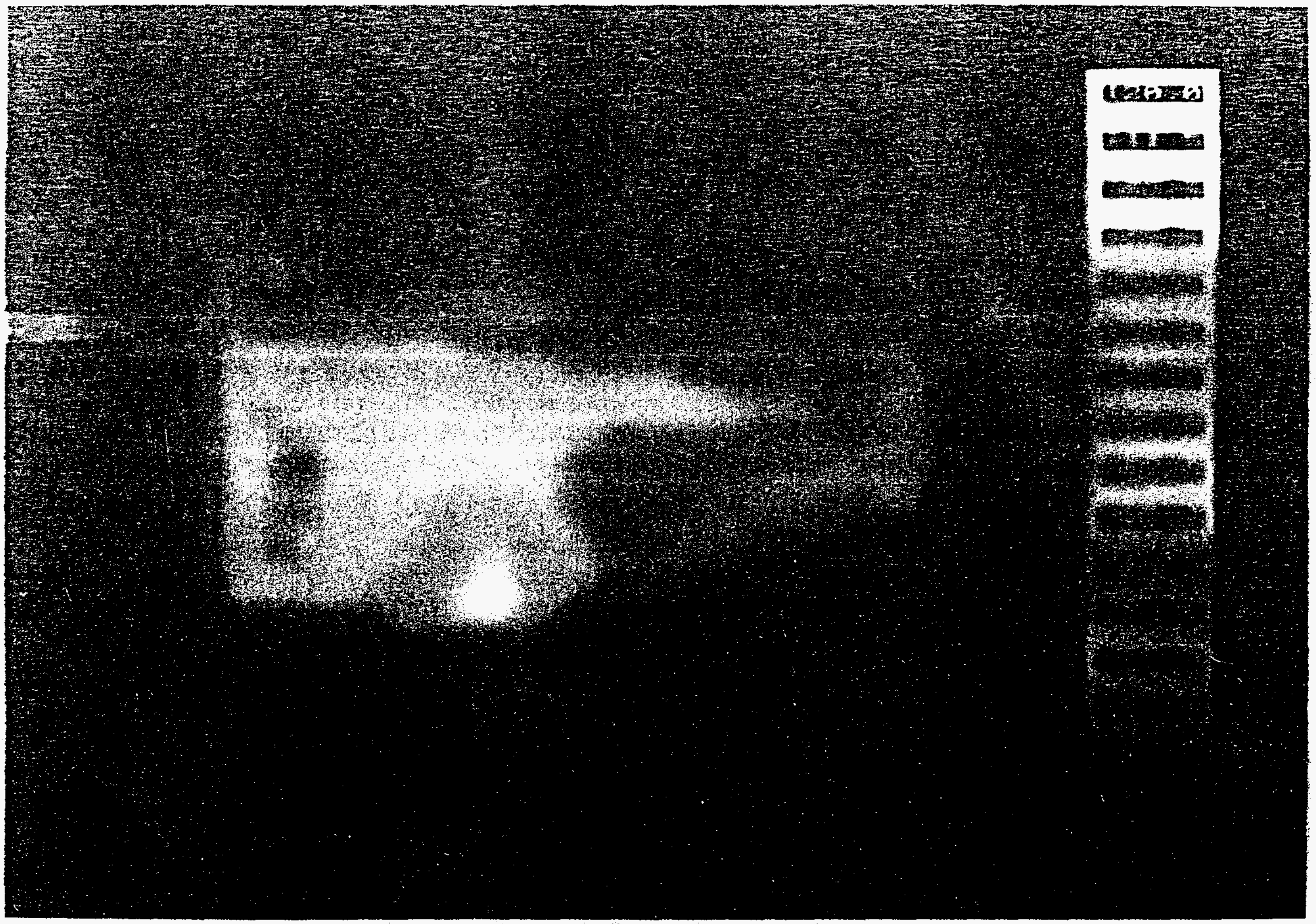

100504 TCG 2:40 E=.8
Tmax ~ 112 °C

Andrew Harrison

Edinburgh University

Physical and Technological Aspects of Storage Phosphor Plates Made of BaFBr:Eu^{2+}

In recent years, two-dimensional x-ray detectors have been developed that are based upon the use of BaFBr phosphor. This phosphor stores the x-ray image in the form of trapped charge, the charge having been produced by the x-ray ionization. The image may be read by exposing the plate to red light and observing the stimulated, blue luminescence. In this article, we describe the mechanisms of photostimulated luminescence (PSL) in BaFBr and show how this affects the material's use as a detector of x-ray diffraction images. Our research indicates that all our observations can be rationalized by postulating that one of the trapped species hops randomly in two dimensions until it finds itself in close proximity to a filled recombination center. Once they are in proximity, sub-condition band recombination can occur via photostimulation. This random lattice migration affects the image stability, the effective detector sensitivity, and the ability to zero the image, and it causes the recuperation of partially zeroed PSL signals. These effects will be described, and their implication for high-precision x-ray measurements will be examined. We have also been engaged in making phosphor plates specifically designed for x-ray diffraction applications. We describe the progress we have made towards developing the technology for making fully erasable image plates with improved spatial resolution.

PHYSICAL AND TECHNOLOGICAL ASPECTS OF STORAGE PHOSPHOR PLATES.

ANDREW HARRISON + RICHARD TEMPLER*

Department of Chemistry, Edinburgh

* Department of Chemistry, Imperial College, London

with -

A. SYRYKH + G.P. KEOGH, IMPERIAL

M.T. HARRISON + A.S. WILLS, OXFORD

C. HALL + R. LEWIS DARESBURY

C. WILKINSON EMBL, GRENOBLE

• STORAGE PHOSPHORS

WHAT HAPPENS WHEN IONIZING RADIATION IMPINGES ON AN INSULATING SOLID?

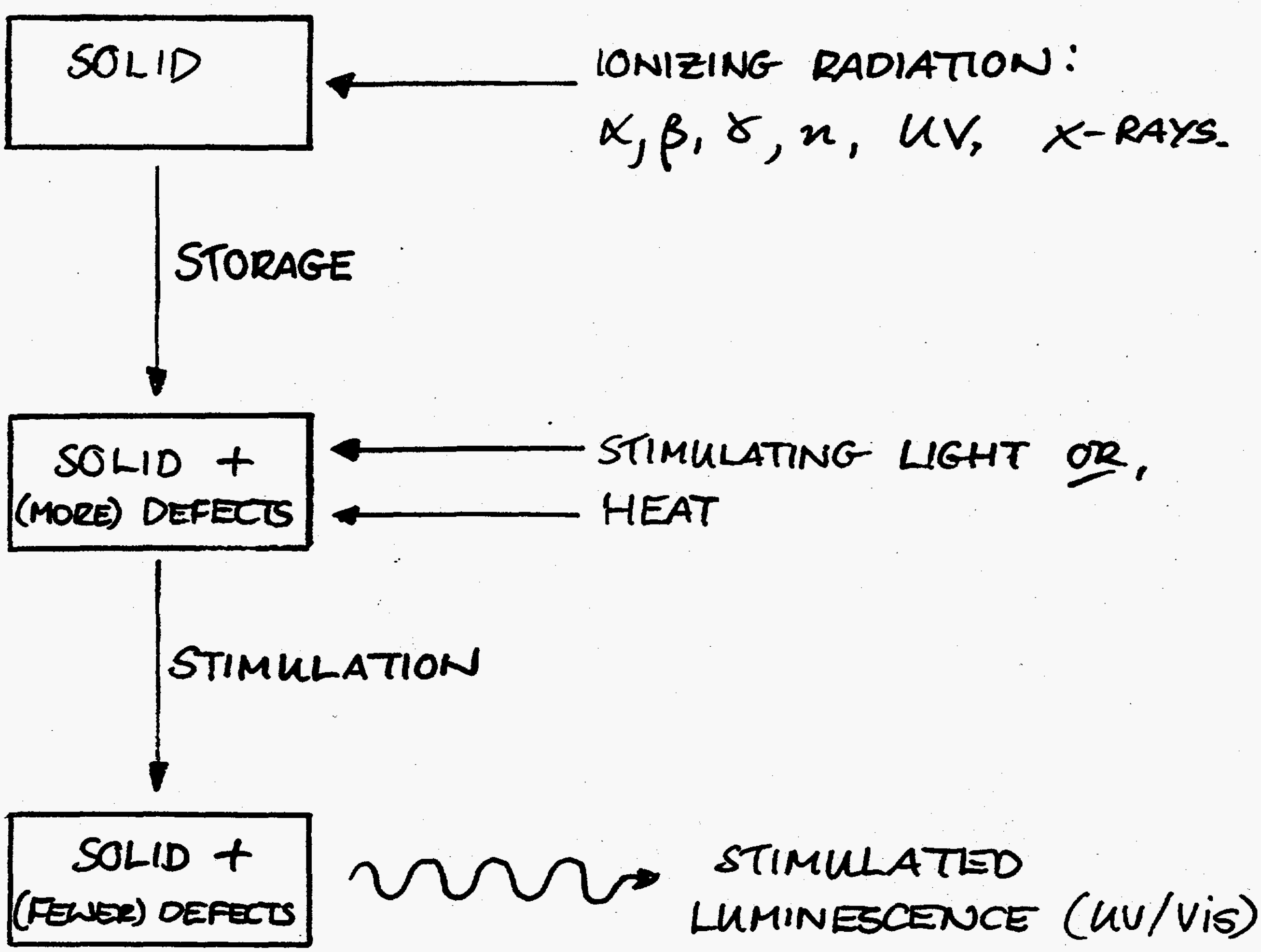

IF LUMINESCENCE IS STIMULATED BY LIGHT IT IS CALLED PHOTOSTIMULATED LUMINESCENCE (PSL).

IF STIMULATED BY HEAT IT IS CALLED THERMOLUMINESCENCE (TL).

P.S.L. RADIOGRAPHY MACHINE

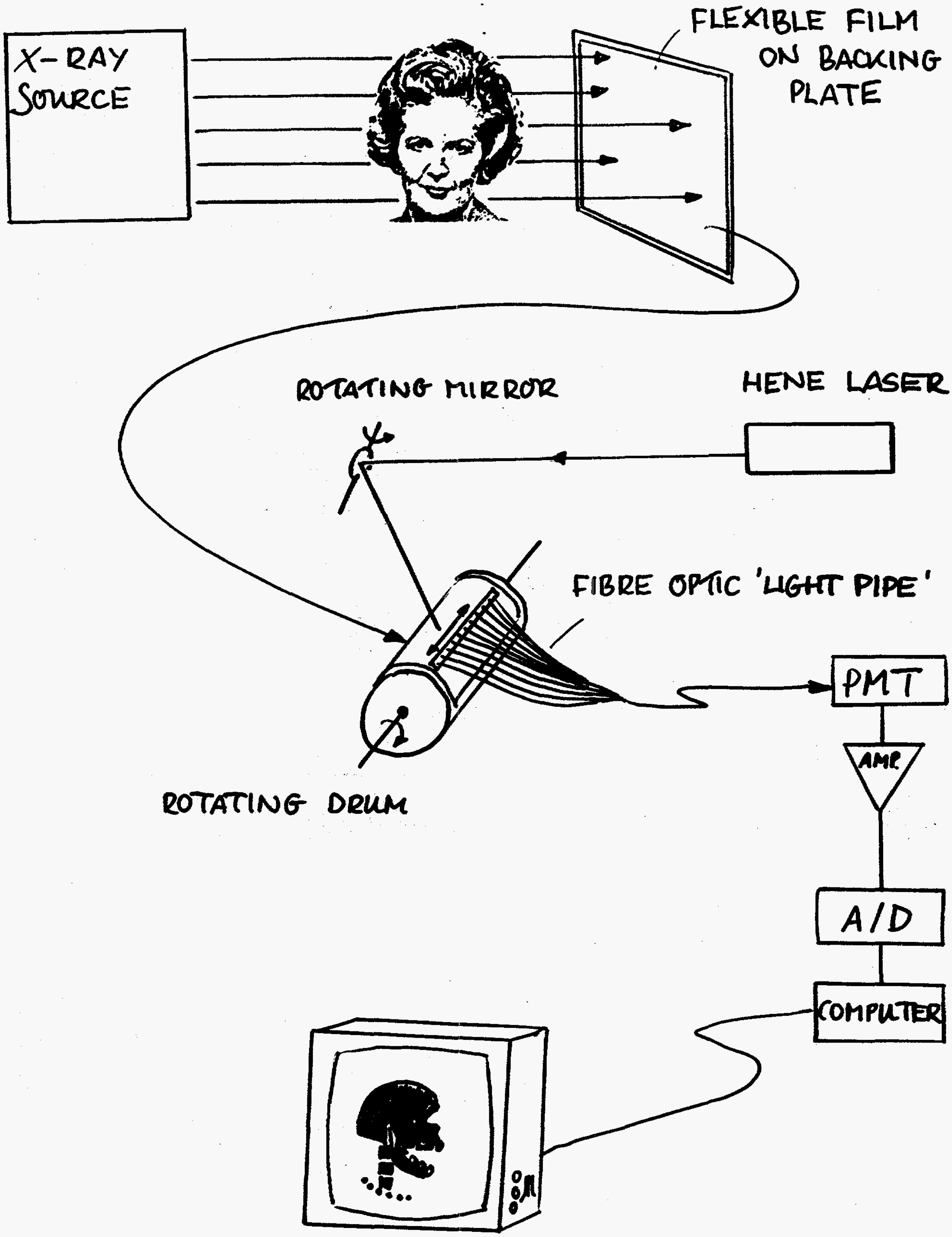

PREVIOUS WORK

PHILIPS, FUJI, KODAK, SIEMENS, du PONT

Takahashi et al, J. Lumin 31 832 (1984) 266

Amemiya et al, Nucl. Inst. & Methods A266 (1988) 645

Von Seggen et al, J. Appl. Phys. 64 (1988) 1405

Crawford et al, J. Appl. Phys. 66 (1989) 3758

Koschnick et al, Phys. Rev. Lett. 67 (1991) 3571

Templer et al, Acta Cryst (In Press)

Almost exclusively on $BaFBr:Eu^{2+}$

OUTLINE OF THE TALK

- 'CLASSICAL' MODEL FOR STORAGE, STIMULATION + ERASURE
- OUR MEASUREMENTS OF STORAGE AND STIMULATION KINETICS IN $BaFBr:Eu^{2+}$
- A REFINED MODEL AND ITS TECHNOLOGICAL IMPLICATIONS
    - STORAGE STABILITY
    - SENSITIVITY
    - DYNAMIC RANGE
    - RESOLUTION
    - ERASURE

BaFBr + EuFBr.

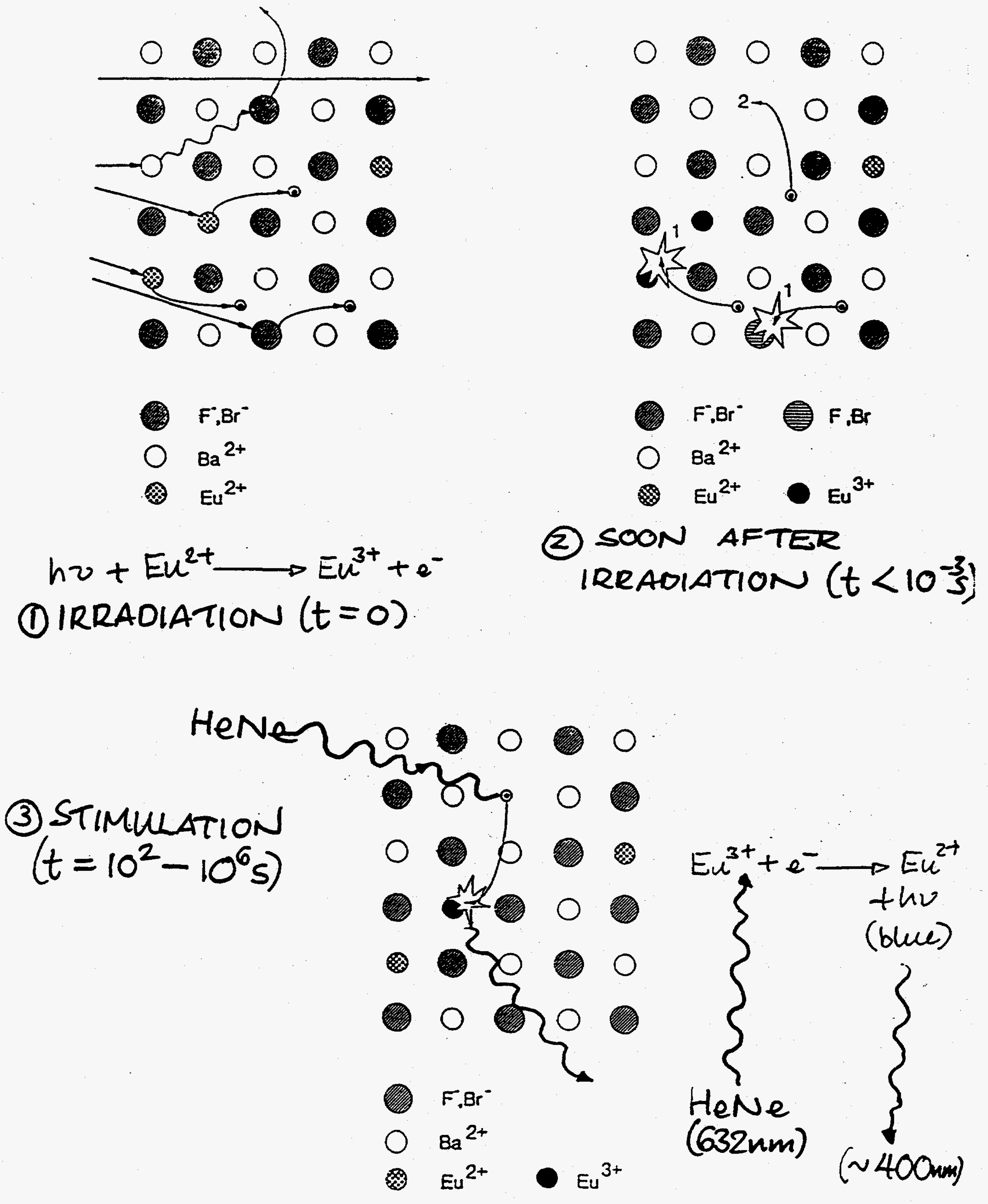

F⁻,Br⁻
Ba 2+
Eu 2+
hν + Eu2+ → Eu3+ + e⁻
① IRRADIATION (t = 0)
2
1
1
F⁻,Br⁻
F ,Br
Ba 2+
Eu 2+
Eu 3+
② SOON AFTER IRRADIATION (t < 10⁻³ s)
HeNe
③ STIMULATION (t = 10² – 10⁶ s)
Eu3+ + e⁻ → Eu2+ + hν (blue)
HeNe (632nm)
(~400nm)
F⁻,Br⁻
Ba 2+
Eu 2+
Eu 3+

THE CLASSICAL PICTURE

- IRRADIATION

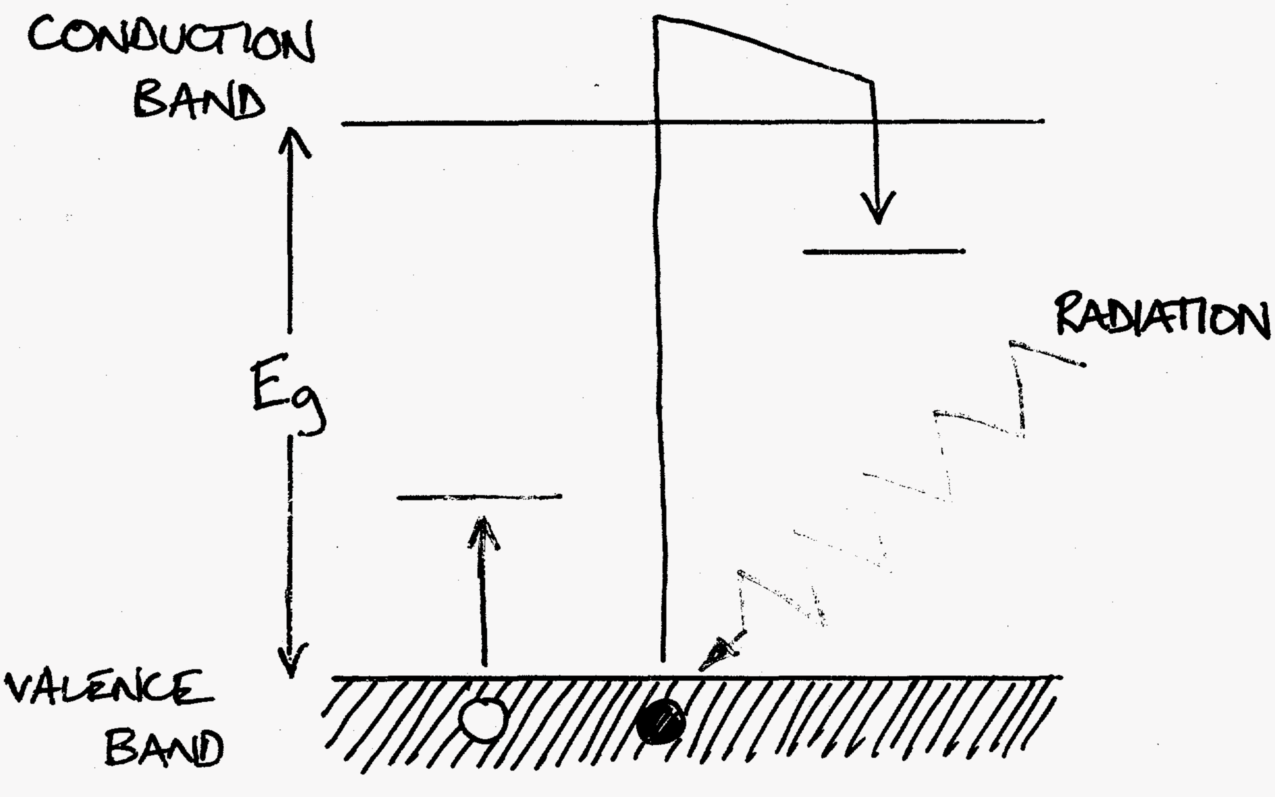

THE CLASSICAL PICTURE

- STORAGE

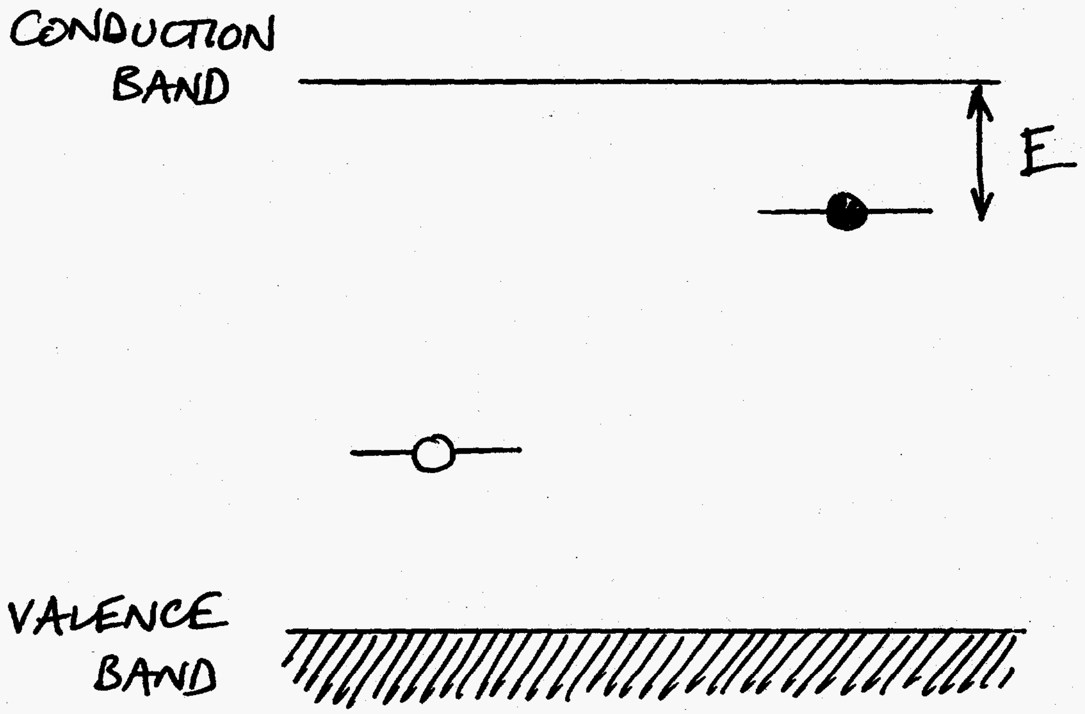

$$\tau = s^{-1} e^{E/kT}$$

THE CLASSICAL PICTURE

- READOUT

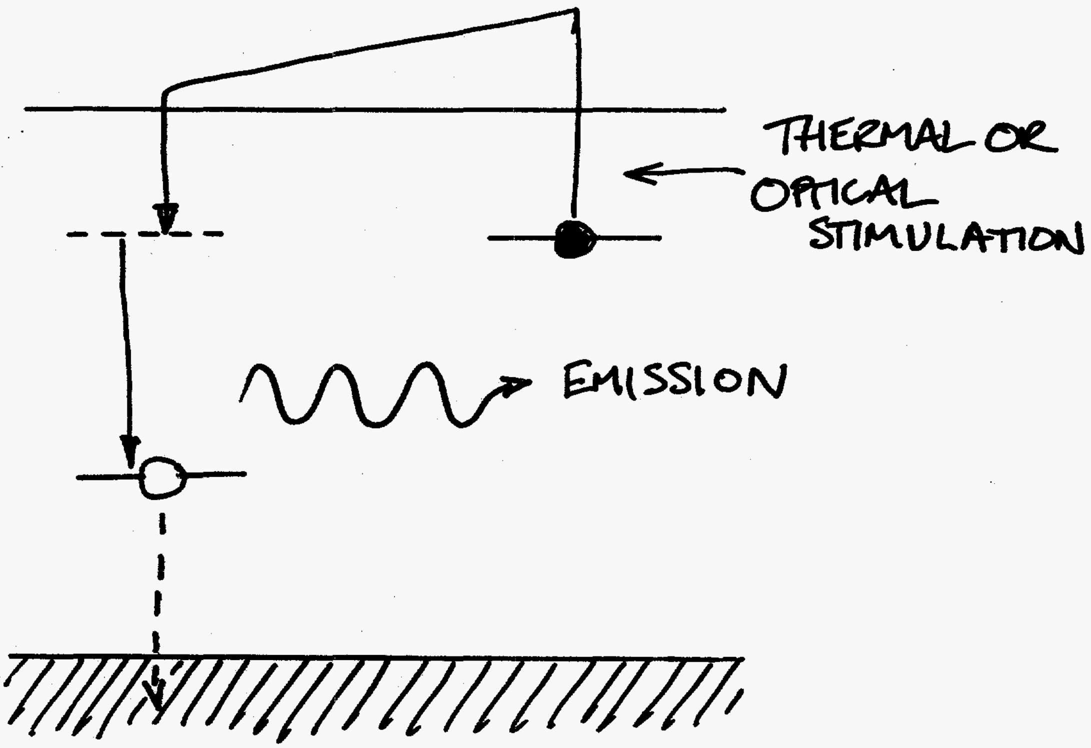

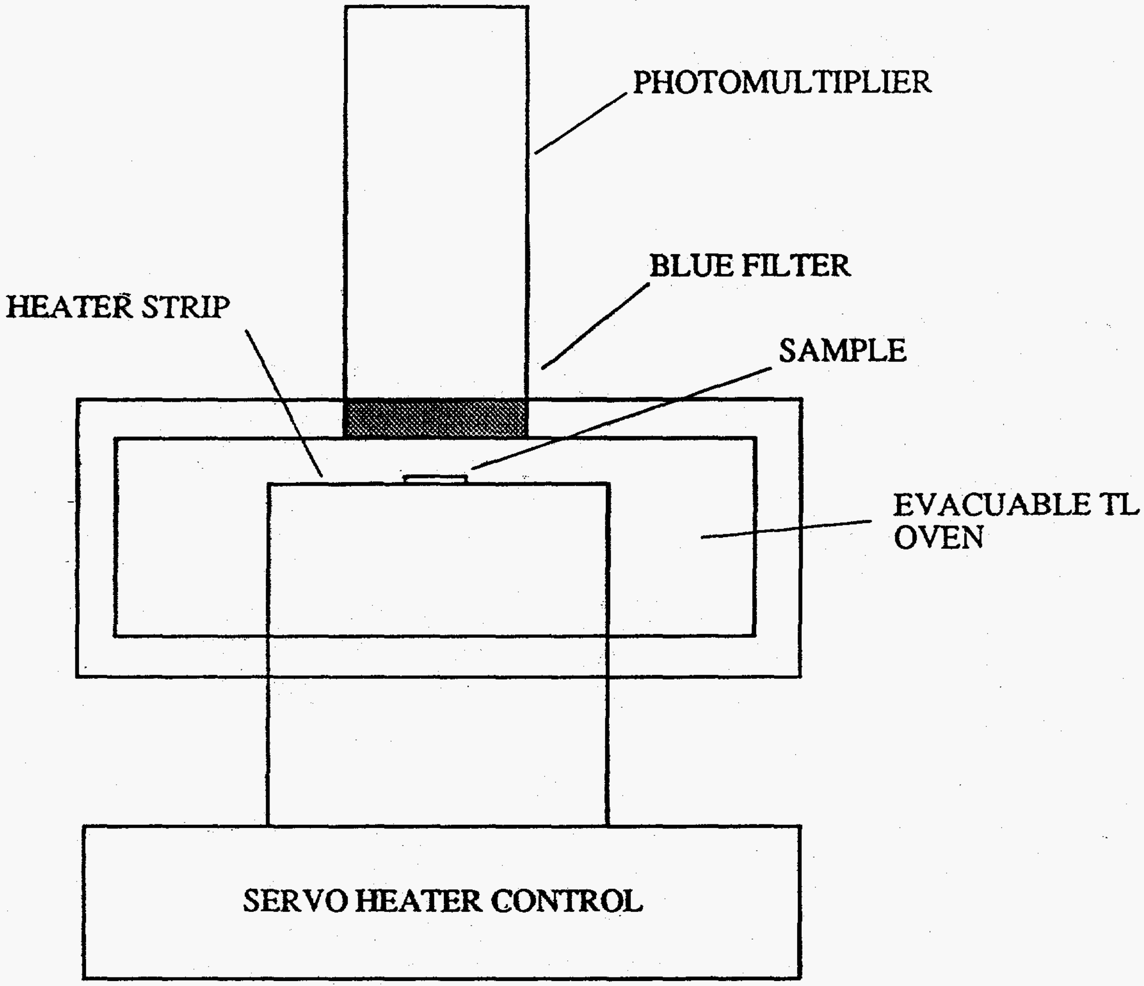
PHOTOMULTIPLIER
BLUE FILTER
HEATER STRIP
SAMPLE
EVACUABLE TL OVEN
SERVO HEATER CONTROL

TL FROM $BaFBr:Eu^{2+}$

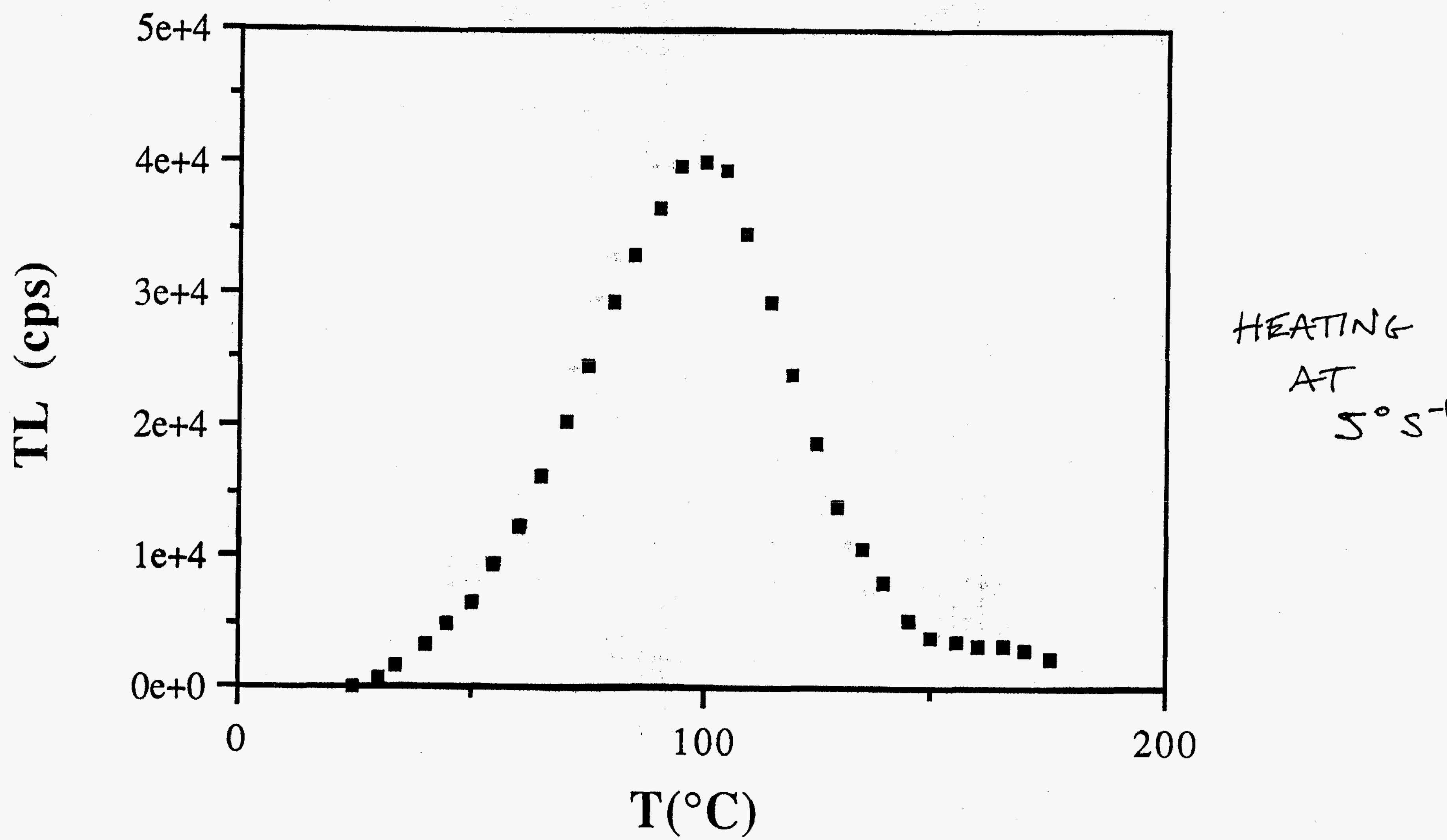

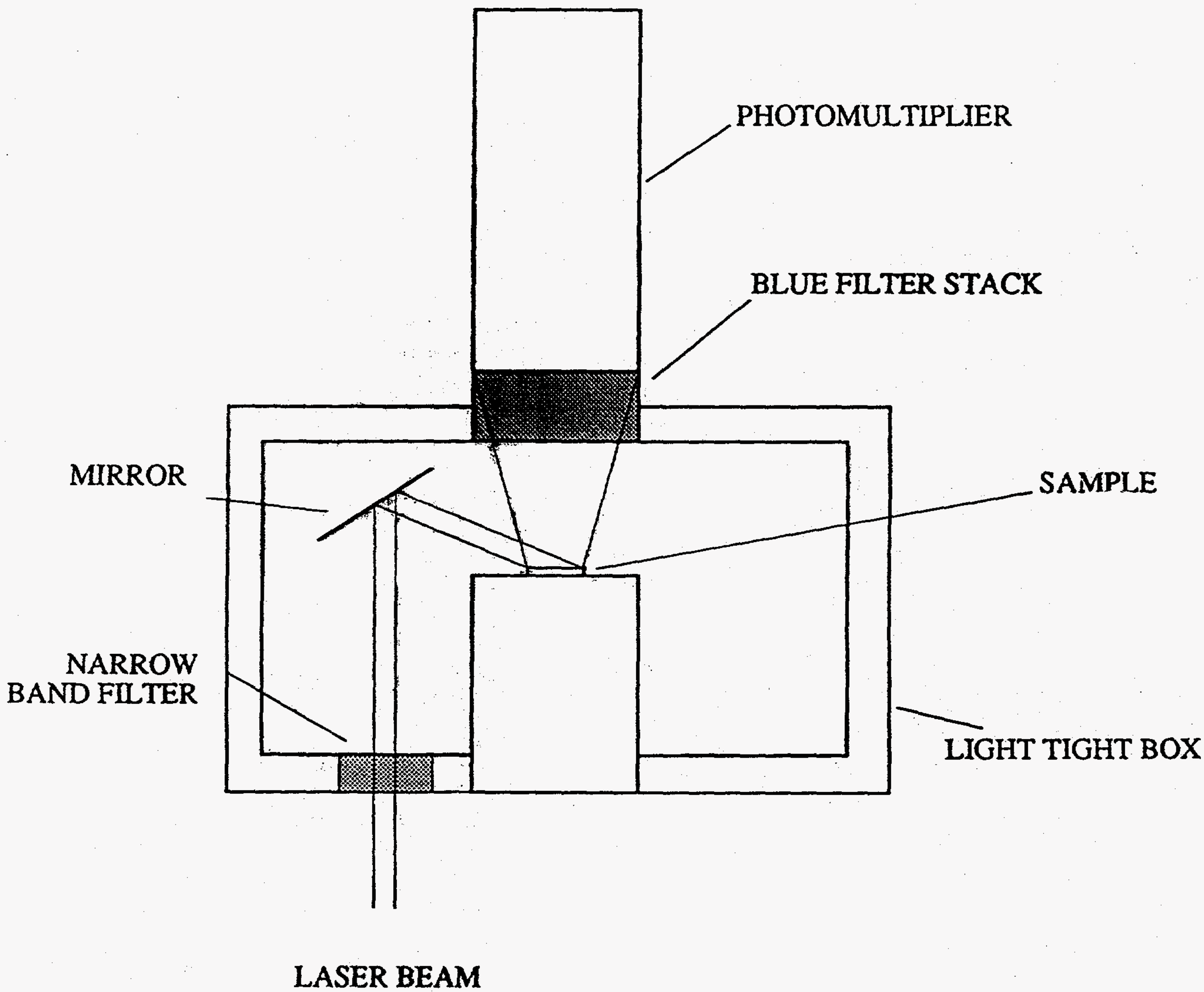
PHOTOMULTIPLIER
BLUE FILTER STACK
MIRROR
SAMPLE
NARROW
BAND FILTER
LIGHT TIGHT BOX
LASER BEAM

PSL FROM $BaFBr:Eu^{2+}$

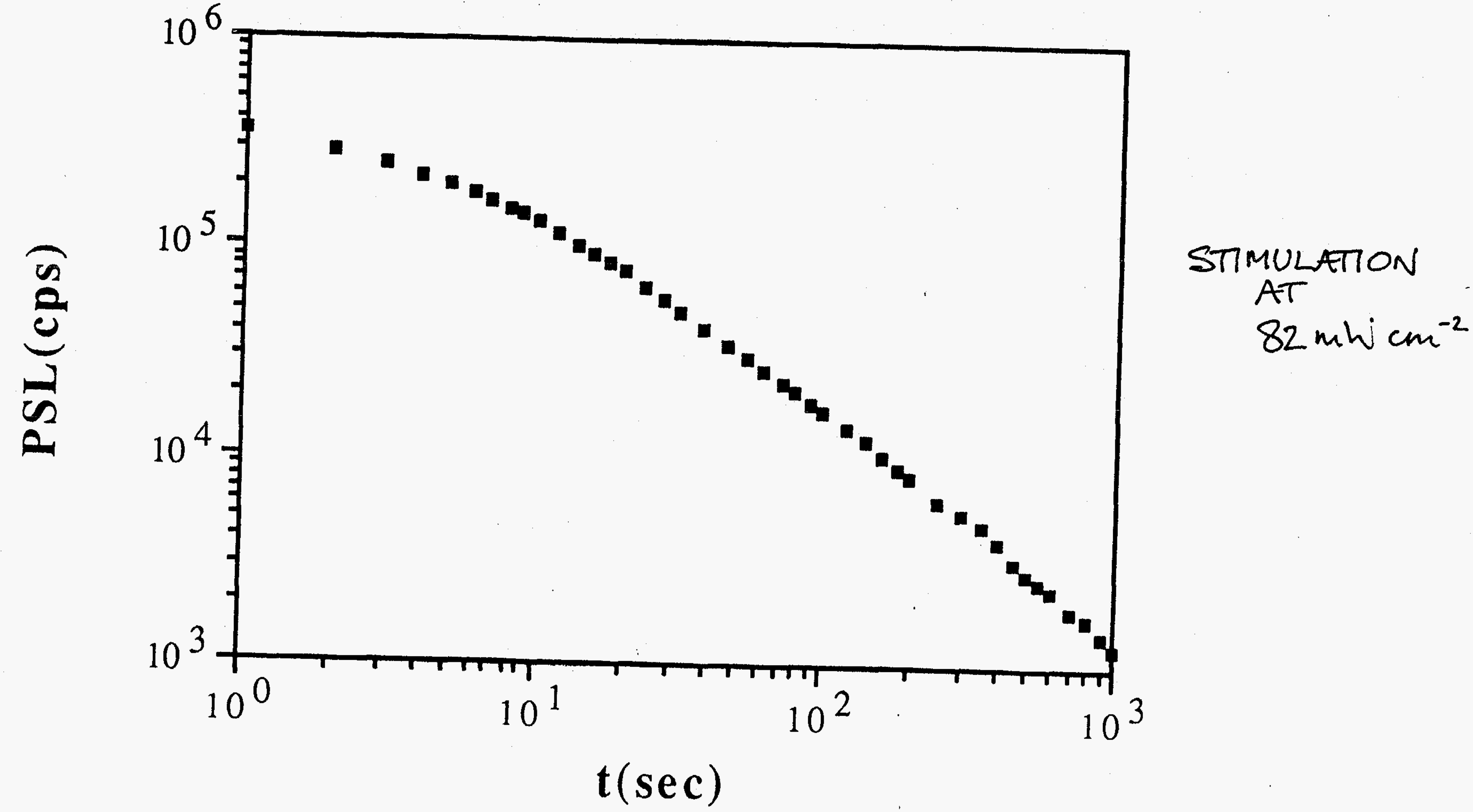

FAILURE OF THE CLASSICAL PICTURE

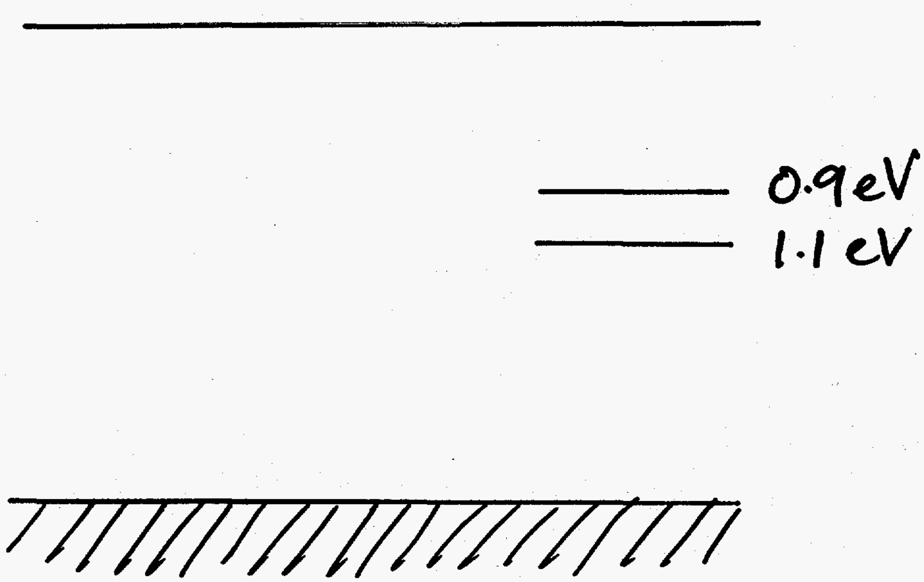

$$\frac{E_0}{E} = \frac{k_0}{k}$$

For BaFBr $\frac{k_0}{k} \doteq 3.1 \quad \therefore \; E_0 = 2.7\text{eV}$

for $E = 0.9\text{eV}$.

LOCALIZED TRANSITIONS

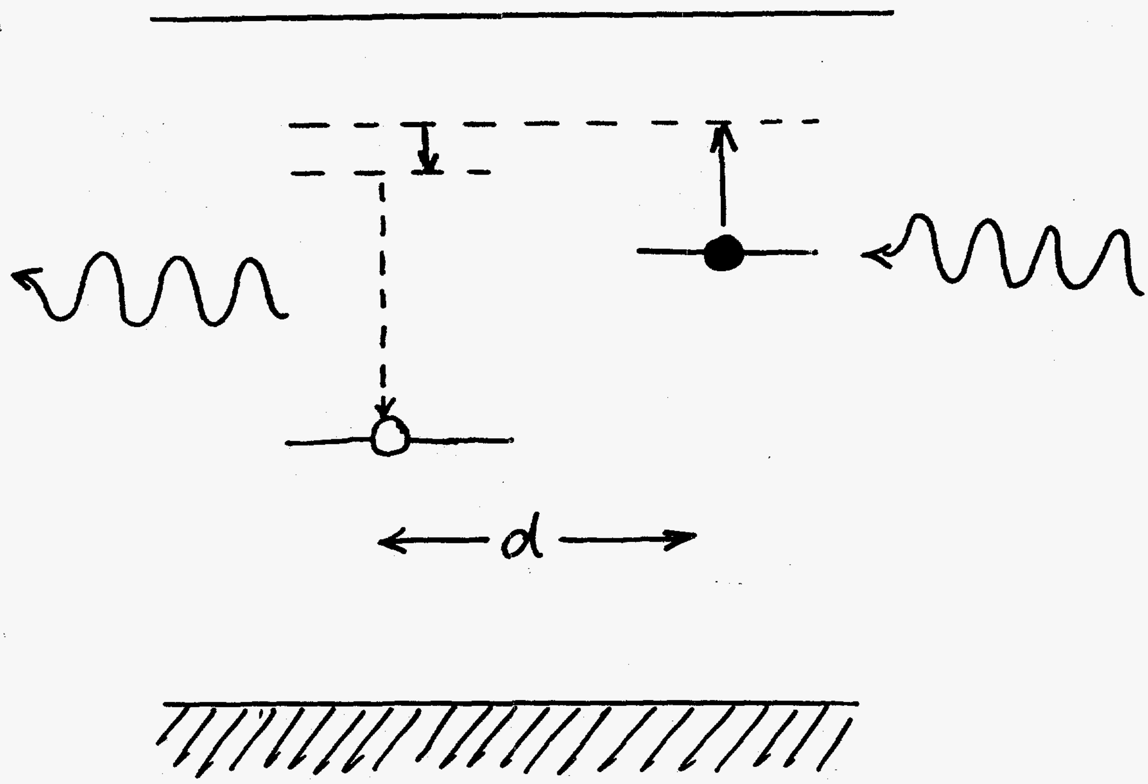

$d \lesssim 15 Å$

ANNEALING THE PSL

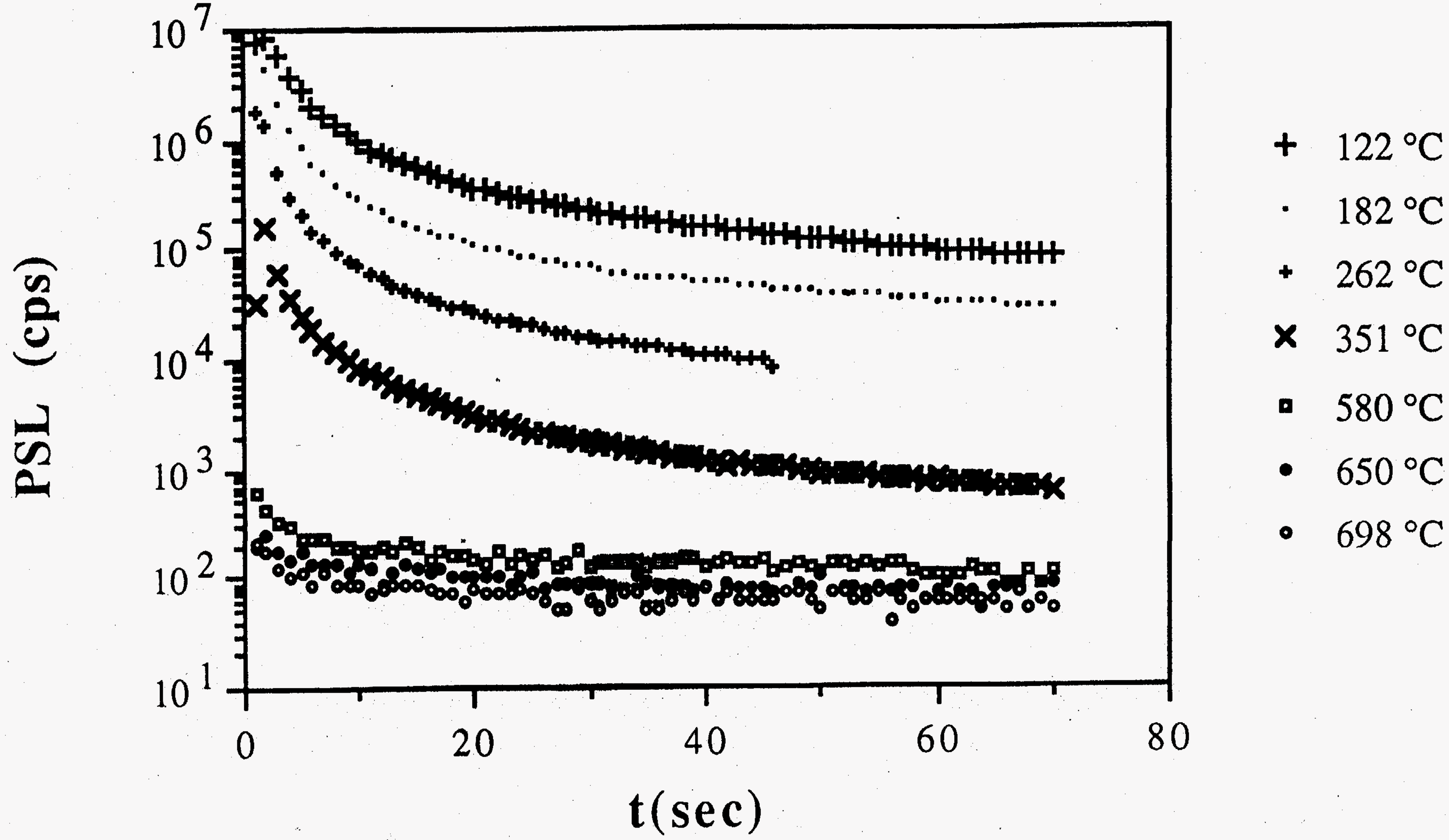

SELF SIMILARITY AFTER ANNEALS

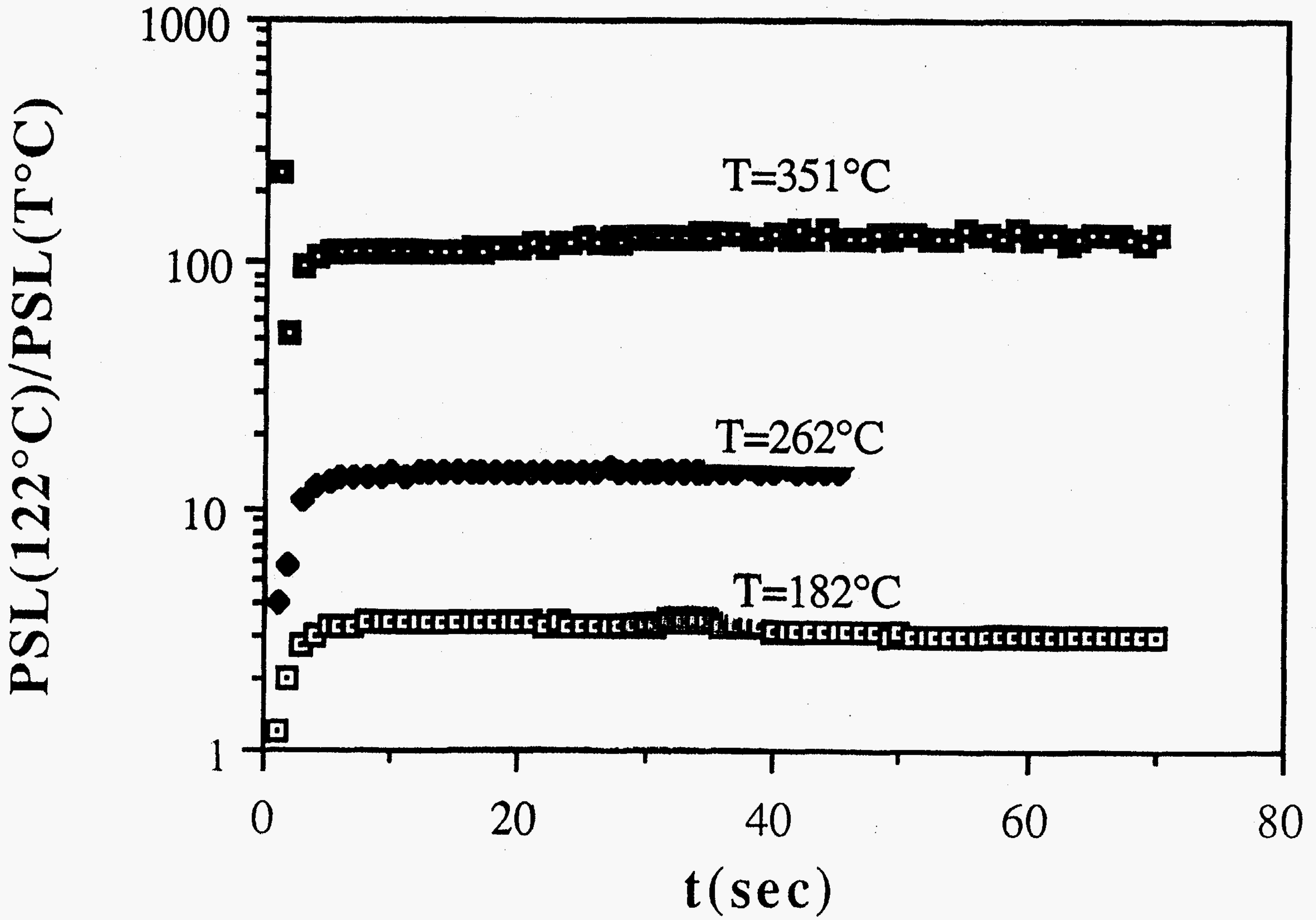

BaFBr STRUCTURE

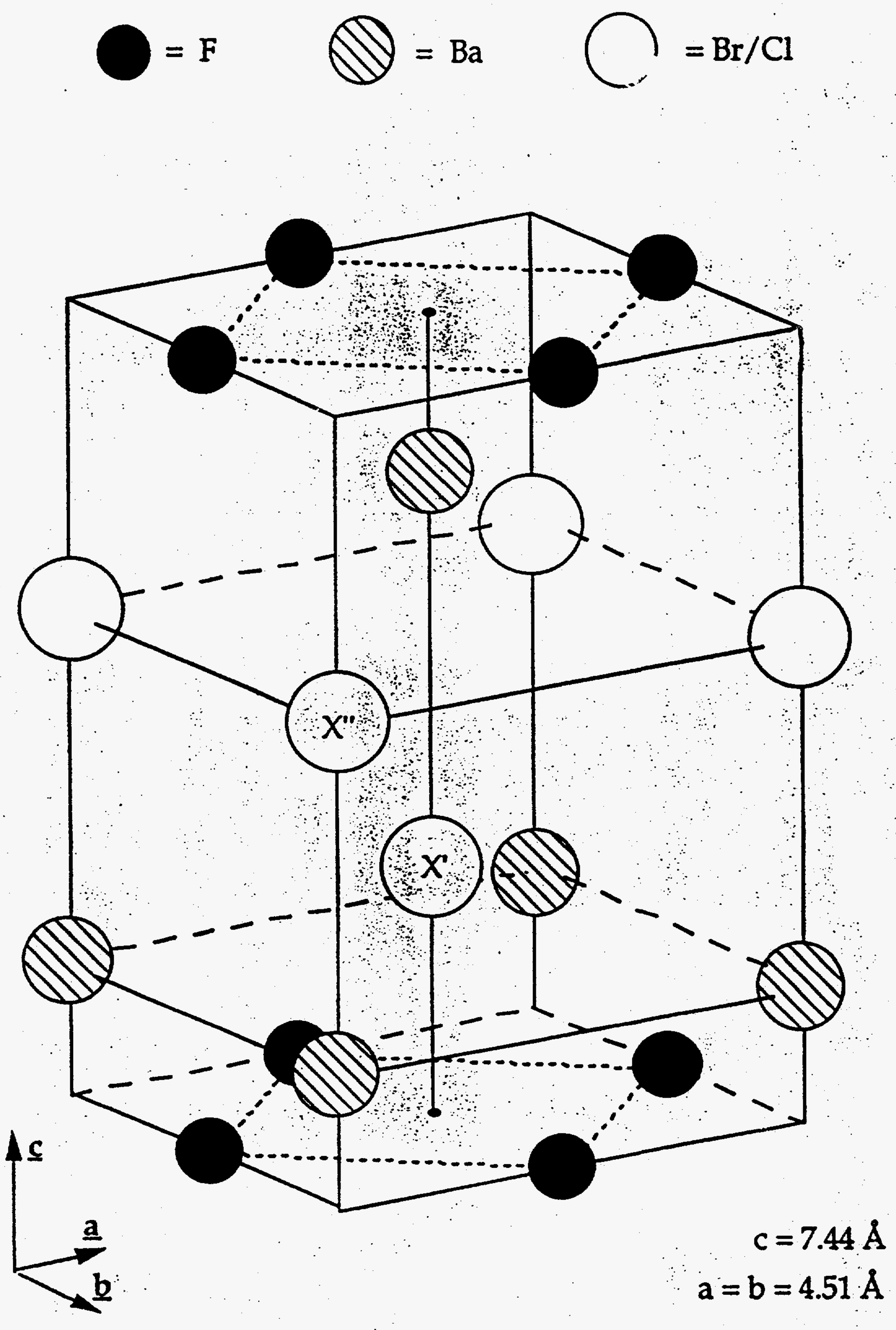

RANDOM WALK MODEL OF PSL

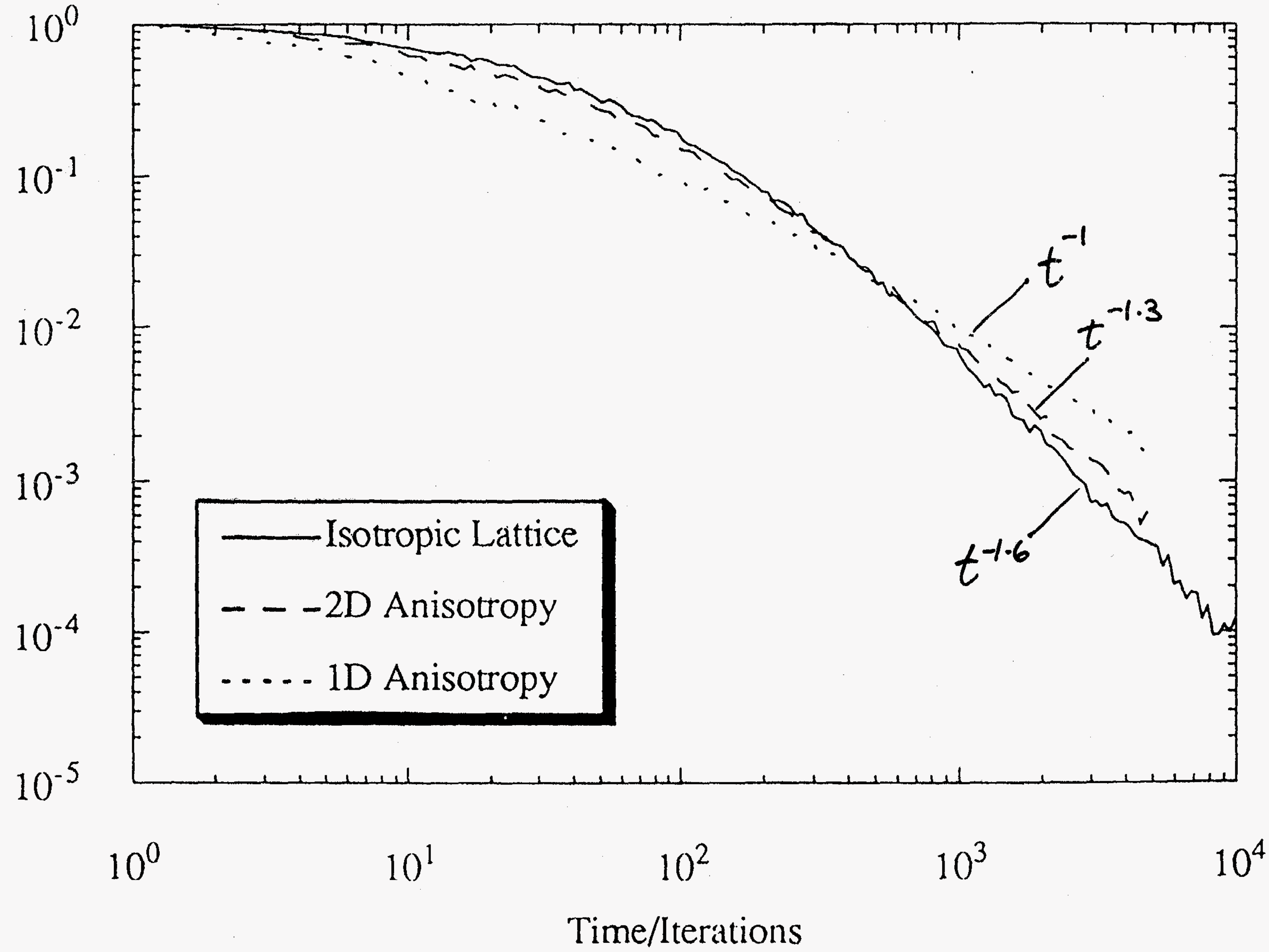

PSL AS A FUNCTION OF T

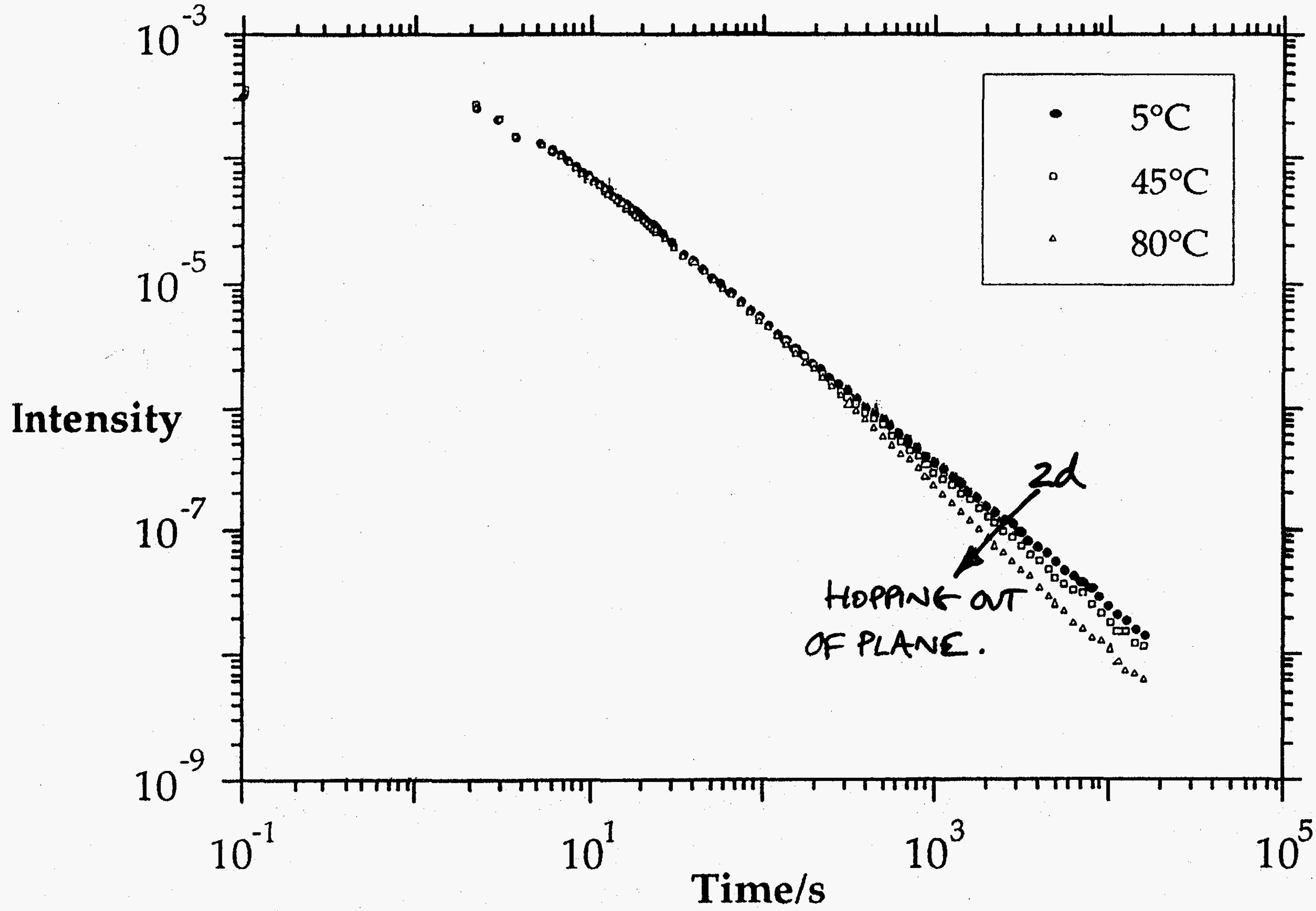

PSL RECUPERATION

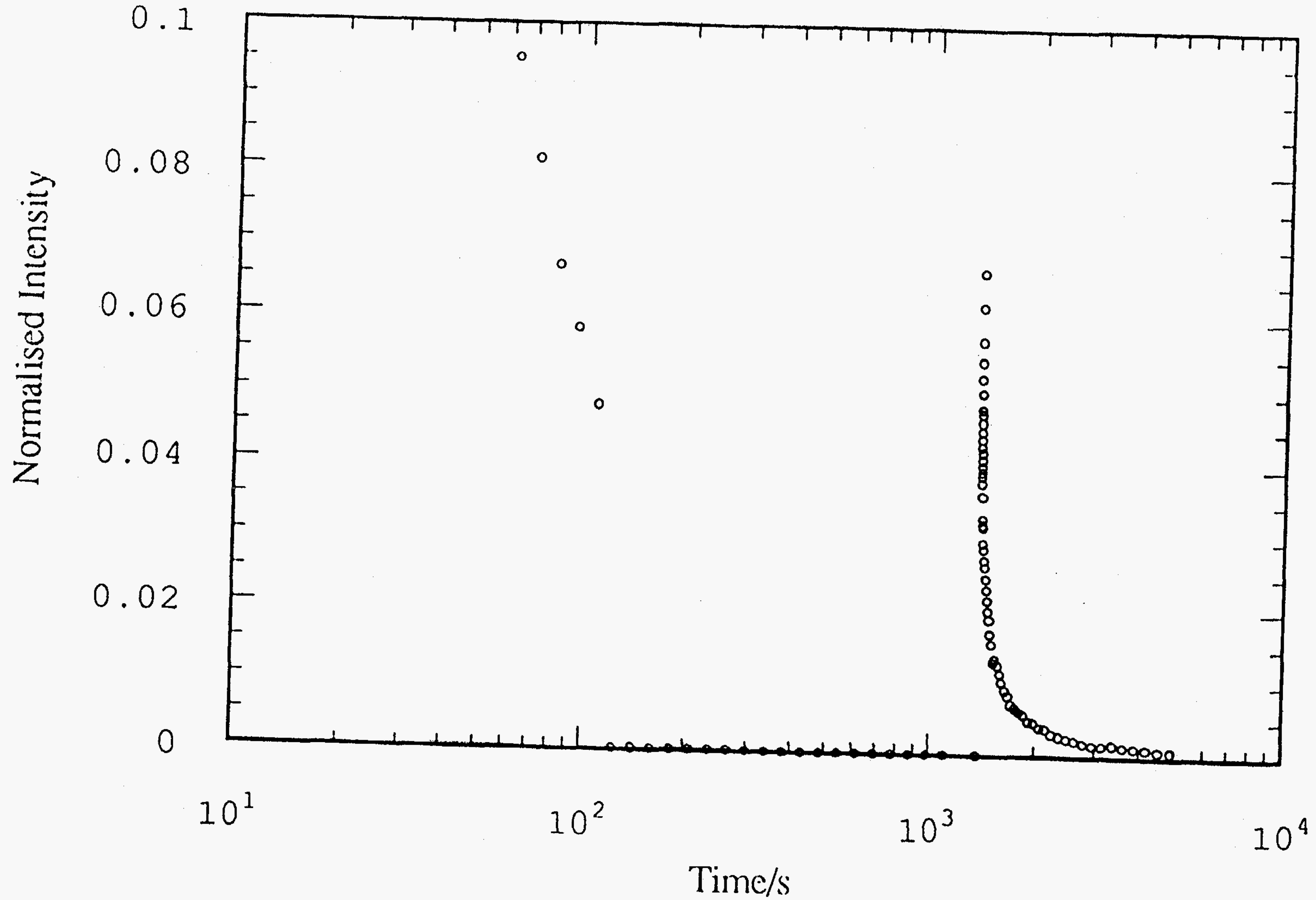

T=45°C

RECUPERATION AT 45°C

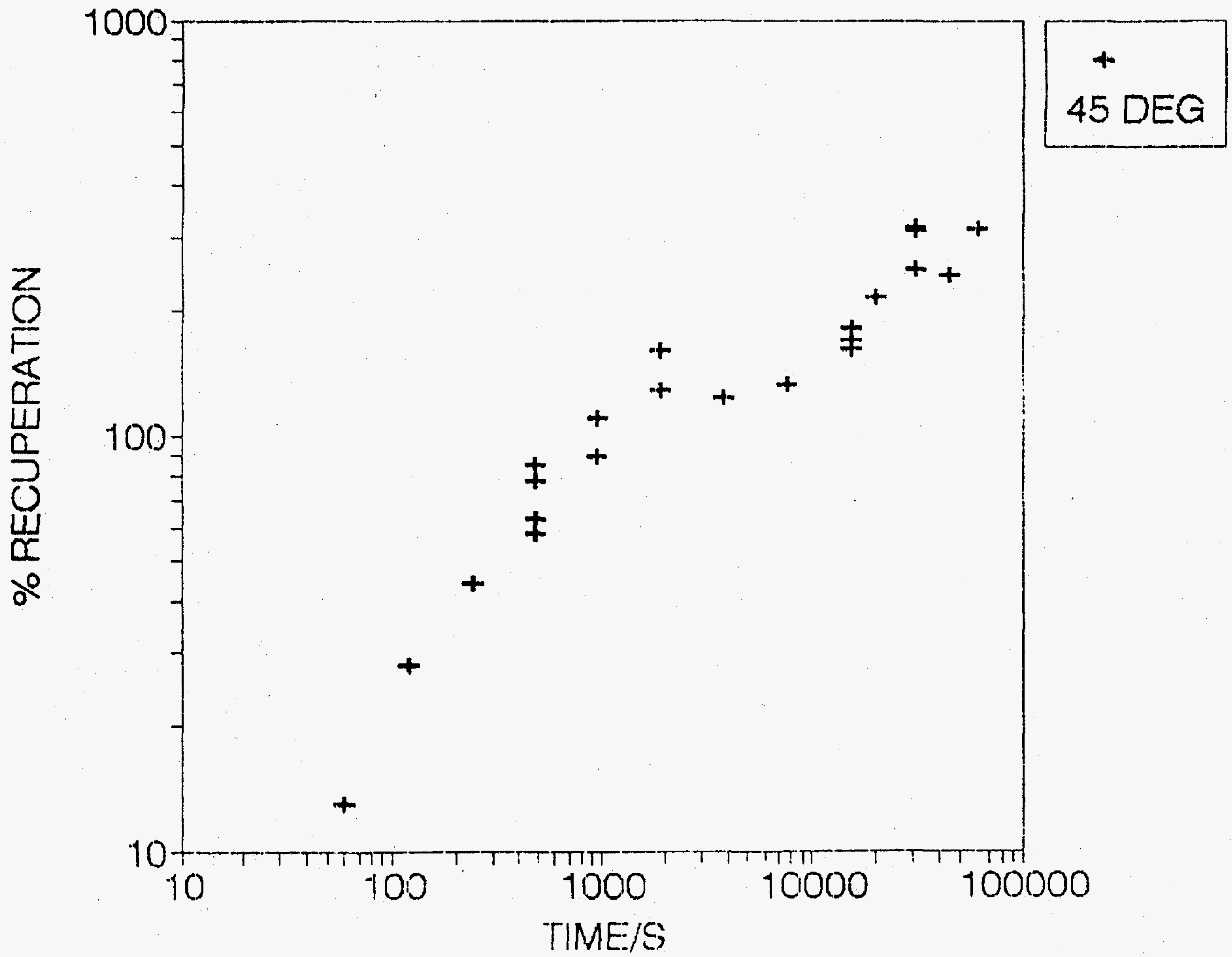

RECUPERATION AT 65°C

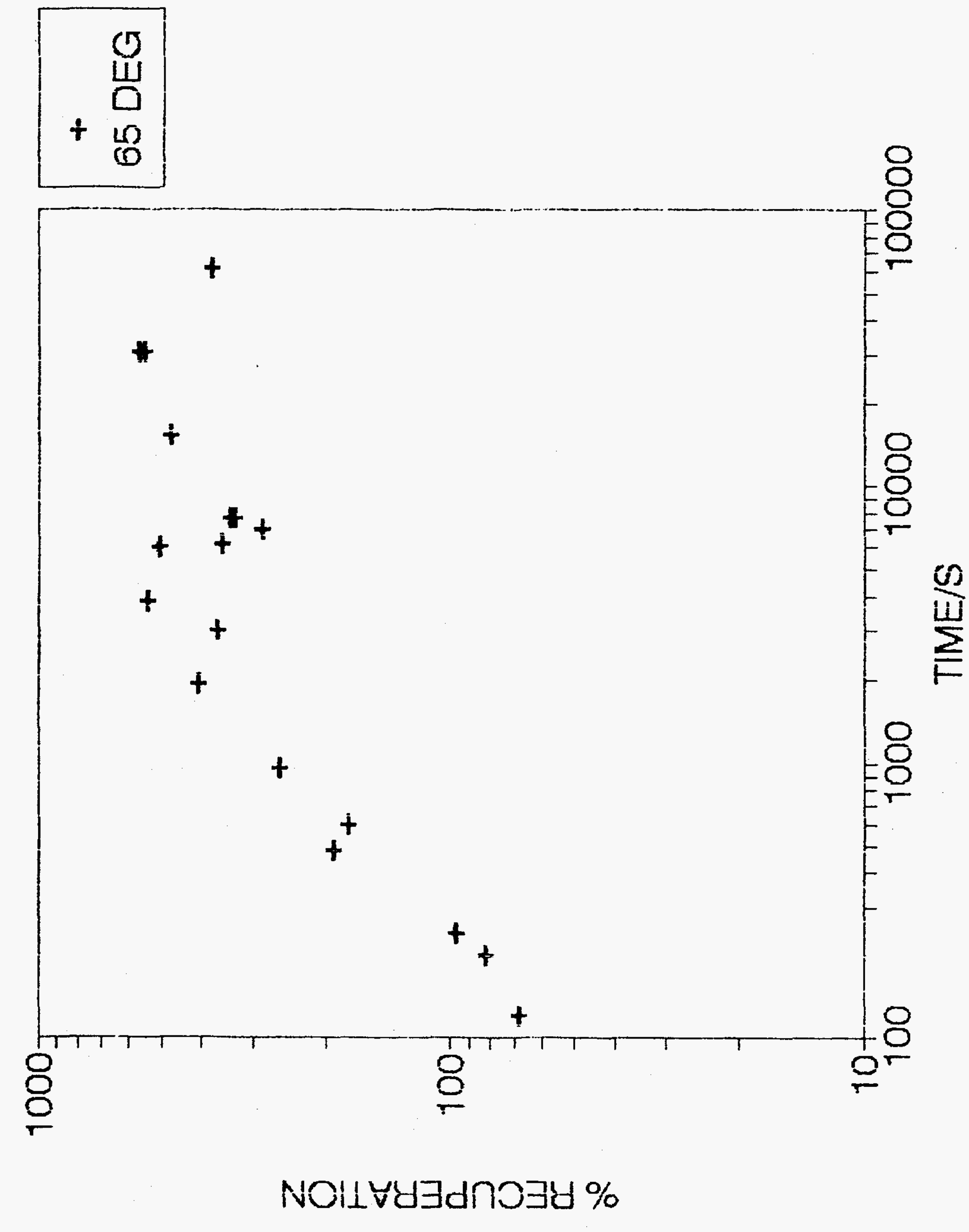

TECHNOLOGICAL IMPLICATIONS

EVOLUTION OF LUMINESCENCE WITH TIME

IMAGE STABILITY

10% drop in image intensity in 2-4 mins.

PROBLEM:

Relative intensities wrong

SOLUTION(S):

1. Leave to fade 1st.
2. Calibrate plate
3. Cool
4. New materials

ERASURE

Ghosts may appear overnight after optical bleach

PROBLEM:

Is a weak spot real?

SOLUTION(S):

1. Stronger optical bleach
2. Thermal bleach (>500°C)
3. Bleach just before use.

THE EFFECT OF NON-ZERO OPTICAL BLEACHING & SIGNAL RECUPERATION

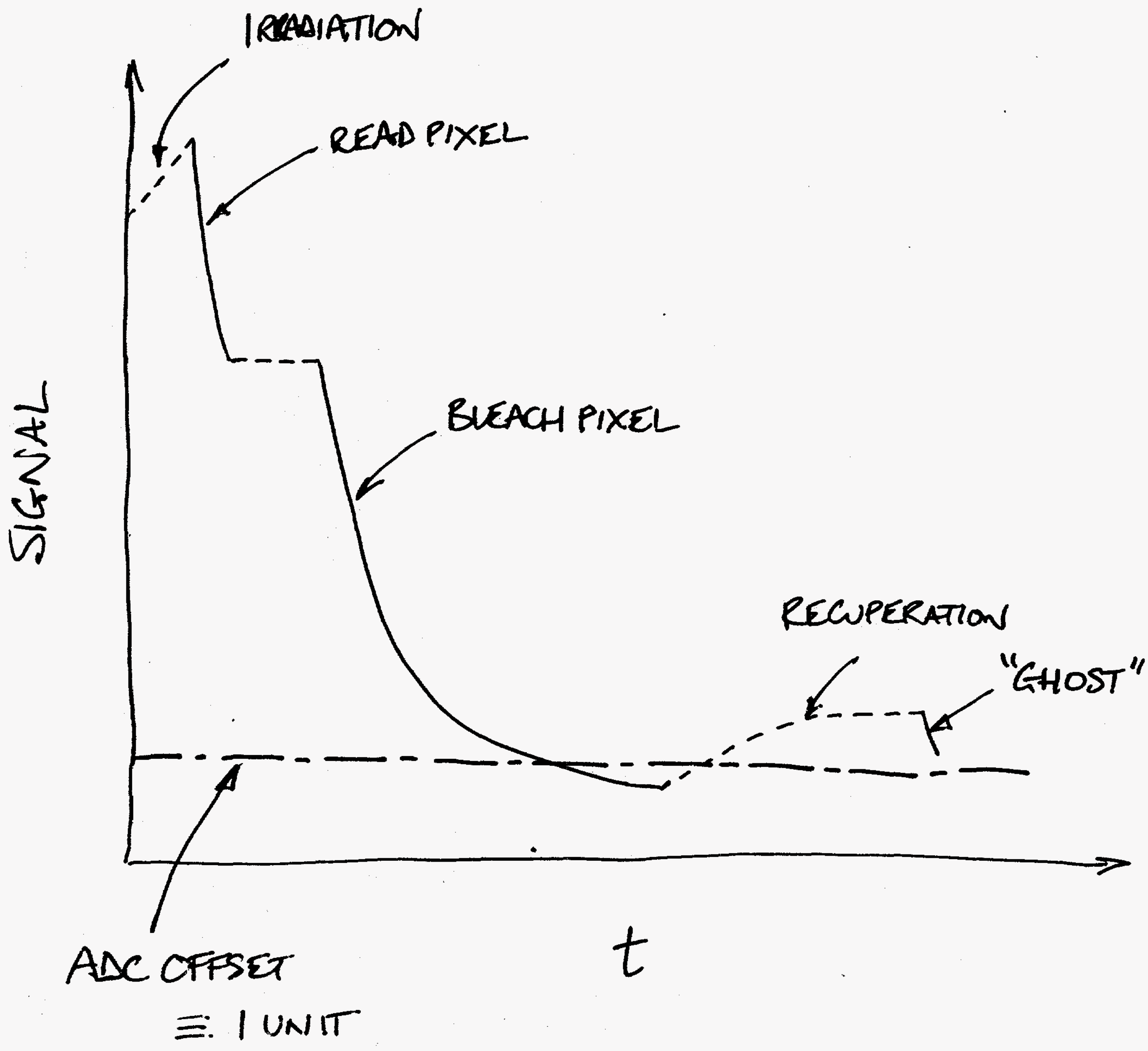

SIGNAL STORAGE INSTABILITY

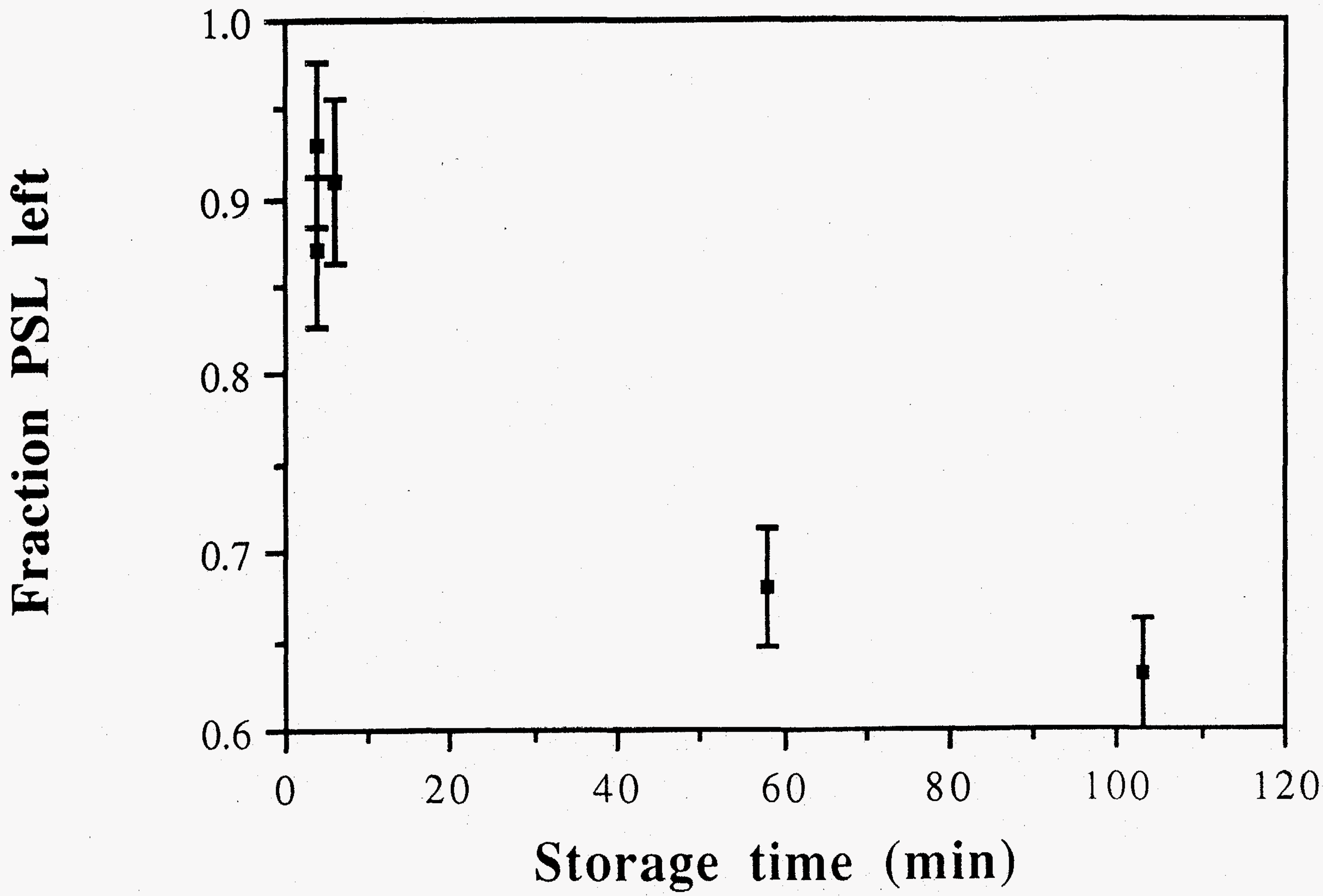

SENSITIVITY

Maximum no e⁻/CuKα X-Ray (~ 33%).	< 325
Maximum no. recd for 8 mJ.cm⁻² (~ 10%)	< 32.5
Efficiency of light collection (~ 40%).	< 13
Absorbance of filters. (-20%).	< 10
Q.E. of PMT (~15%).	< 1.5

Marginal !!

Experience at Daresbury shows problems detecting signals < 20-50 photons CuKα.

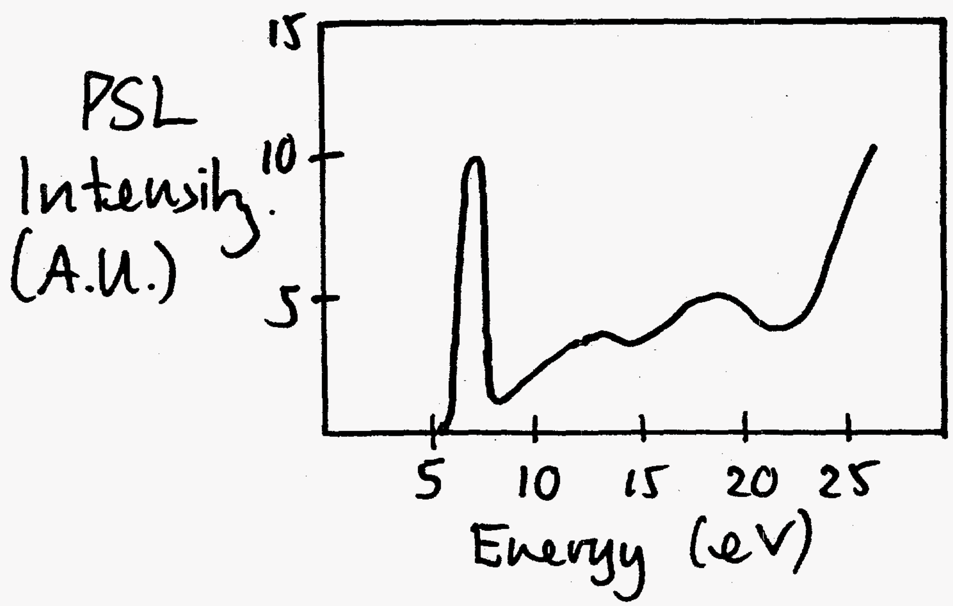

RESOLUTION

Plate dimensions ≃ 250 × 200 mm
Pixel size ≃ 100 × 100 μm

Typical resolution ≃ 180 μm FWHM.

BUT

Appreciable spread as far as 1 mm.

PROBLEM

Preview strong reflections

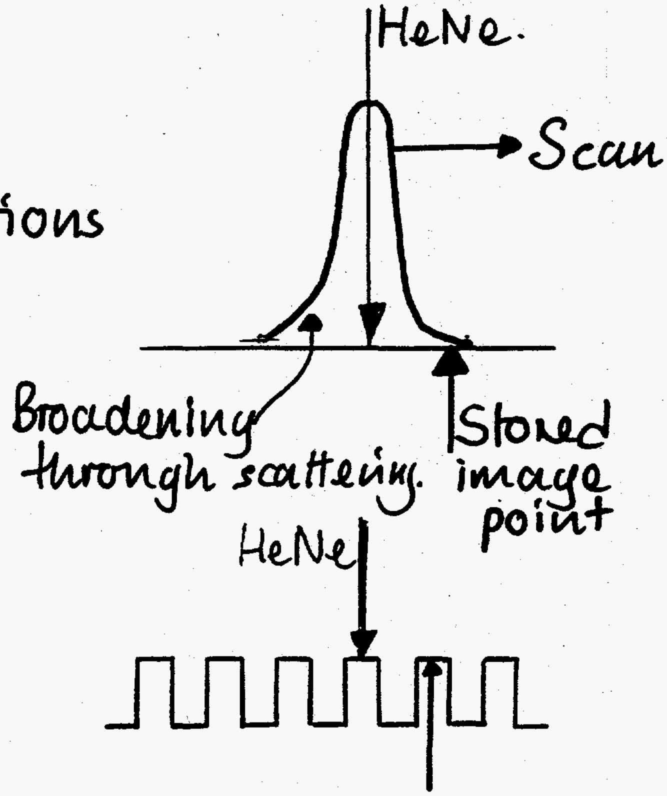

SOLUTION?

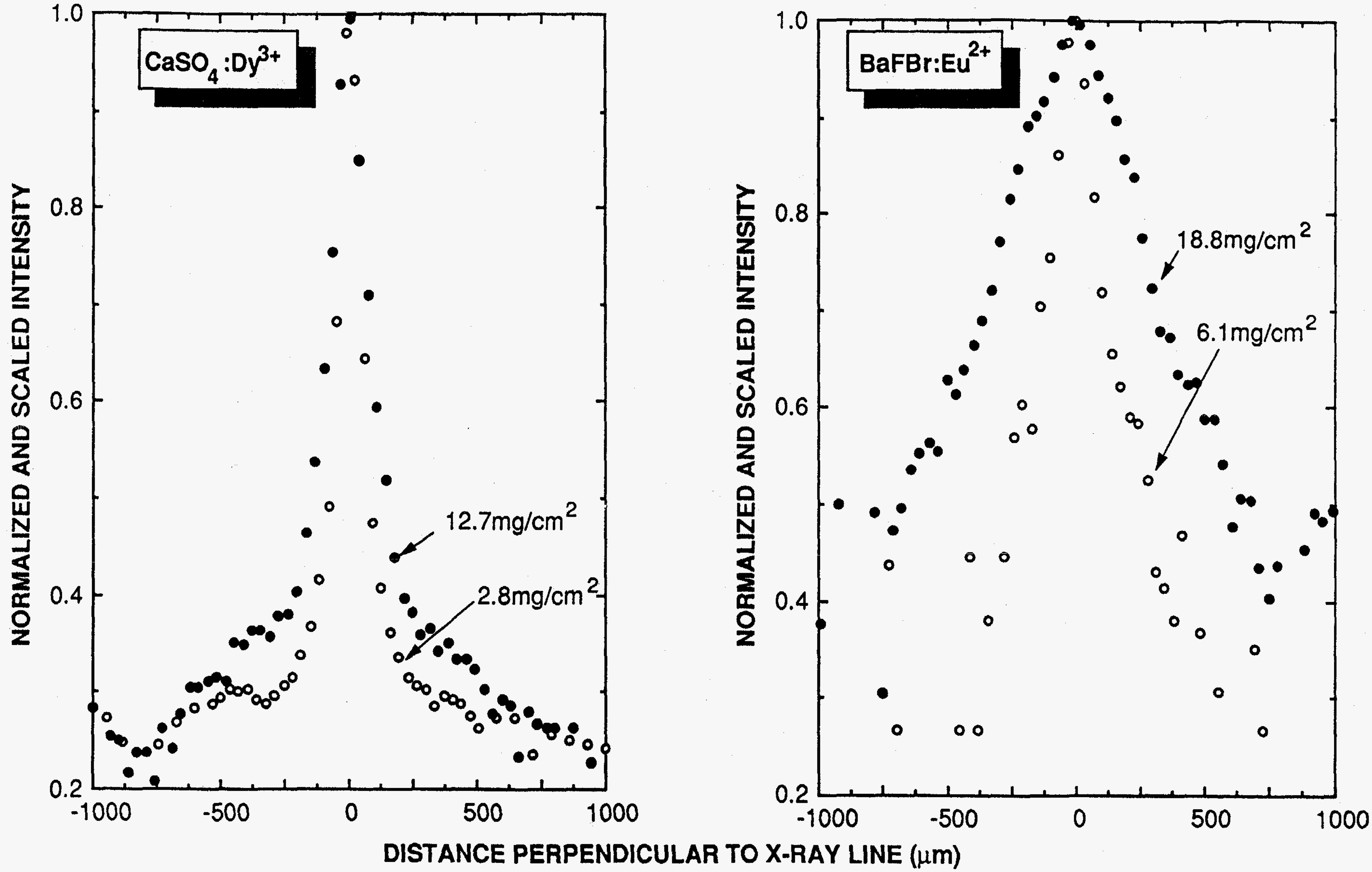
CaSO4 :Dy3+
12.7mg/cm2
2.8mg/cm2
BaFBr:Eu2+
18.8mg/cm2
6.1mg/cm2
NORMALIZED AND SCALED INTENSITY
DISTANCE PERPENDICULAR TO X-RAY LINE (µm)
1.0
0.8
0.6
0.4
0.2
-1000
-500
0
500
1000

DYNAMIC RANGE

We find sublinear response for doses > 10^7 CuKα photons / $100 \times 100\,\mu m$ pixel

Probably due to signal loss at longer exposures

⟹ Dynamic range ≃ 2×10^5

PERFORMANCE SUMMARY

Sensitivity ≃ 10-50 CuKα.

Resolution 100-200 μm FWHM

Dynamic range > 10^5.

PROBLEMS	SOLUTIONS
Signal fading	Cool plate
Zeroing/erasure incomplete	Heat plate
	Stronger bleach

LOOKING AHEAD

Better plate design

- Thermally stable binder
- Isolated pixels

Better materials

- What makes a good storage phosphor?

ACKNOWLEDGEMENTS

Richard Templer Gary Keogh Alexei Synykh	Imperial College, London
Mike Harrison Andrew Wills	Oxford University
Chris Hall Rob Lewis	Daresbury Synchrotron
Clive Wilkinson	EMBL, Grenoble

SERC, Royal Society + Paul Instrument Fund.

A. R. Faruqi

MRC Laboratory of Molecular Biology

Time-Resolved Experiments on Muscle Using Synchrotron Radiation

A monochromatized and focused high-flux x-ray beam obtained from a synchrotron radiation source provides a unique tool for reducing exposure times sufficiently to make time-resolved measurements with submillisecond time resolution on many biological specimens. One of the major applications of the technique has been in making dynamic studies on vertebrate muscle undergoing different types of mechanical or chemical activity during contraction. The main aim of such studies is to determine the details of structural changes that lead to force generation. The high intensities in the x-ray pattern to be recorded by the detector impose quite difficult and often conflicting requirements, and for these reasons the development of adequate detectors has been a slow process that needs to be continued, perhaps with increased effort, as sources are being developed relatively more rapidly than detectors.

The talk will be divided into two main parts:

1. What have we learned from time-resolved measurements on muscle and what further information can we reasonably hope to acquire given the increased technical specifications of the APS, ESRF, and other new generation of high-brilliance storage rings, and

2. What special requirements are there for detectors for use in time-resolved measurements and which type of detectors are likely to be the most readily applicable.

X-Ray Studies on Muscle

Sliding Filament Model:

Relative sliding movement between actin & myosin filaments

Main Aims of Current Research

(1) Give explanations of details of muscle contraction at molecular level.

(2) Control or Regulation of Contraction: A more detailed explanation

For Dynamic processes a useful technique:

'Time Resolved X-ray Diffraction from contracting muscle'.

Main Difficulties: Technical. Small physical size of cross-bridges and rapid movement

Time-Resolved X-ray Diffraction from Muscle

Molecular mechanisms involved in muscle contraction & force generation.

Sl. Actin - Myosin interactions → Force
Muscle small angle pattern dominated by myosin & actin. Changes in pattern during contraction very informative re- structural changes.

Sl. Difference Pattern (from Huxley, et al at SRS, Dares.)

Kinetics of cross-bridge cycling with MWLD shows that at fast
Sl. shortening cross-bridges take 15-20 ms to diffuse back to myosin. (Poster)

Muscle Sarcomere

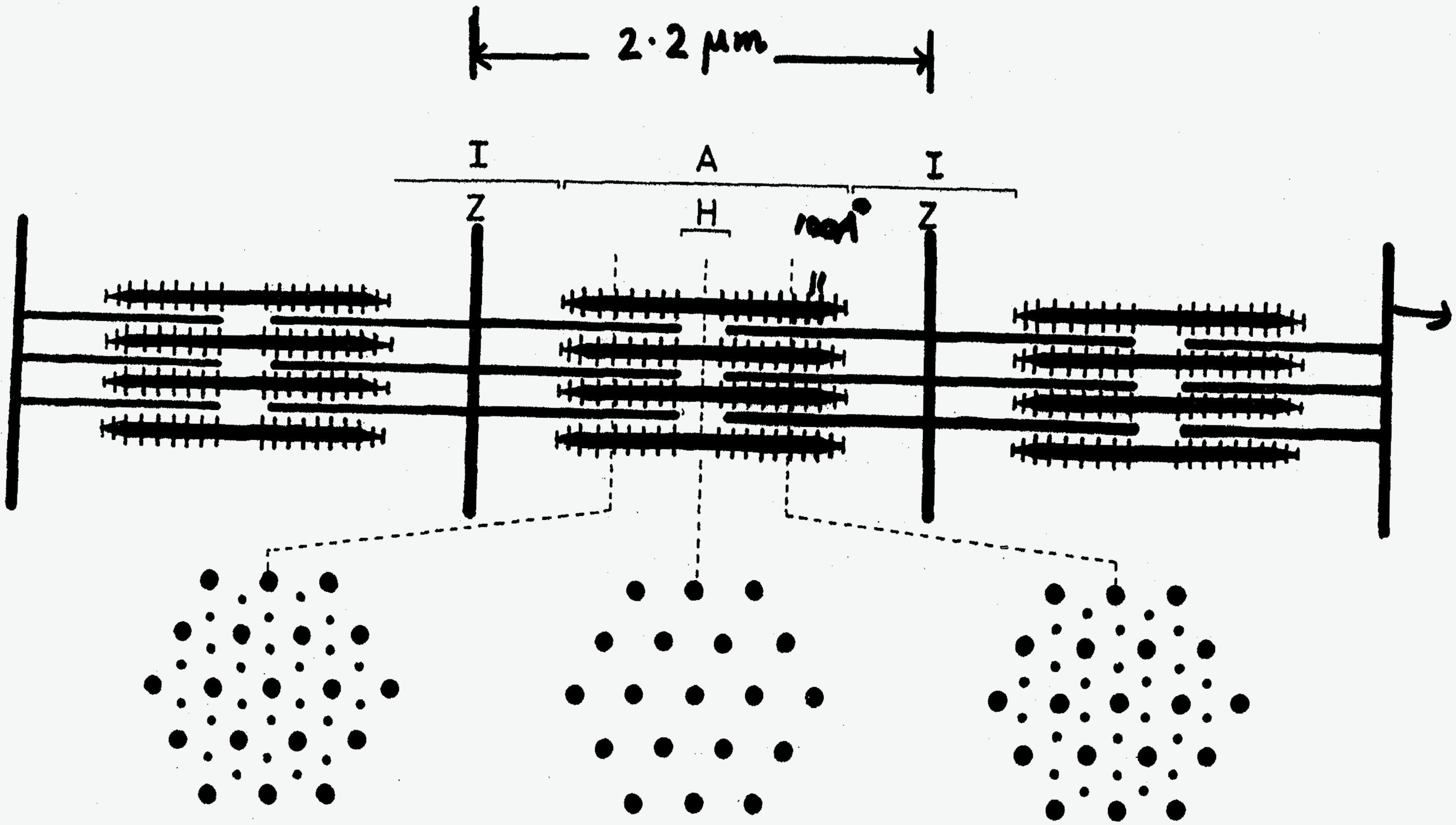

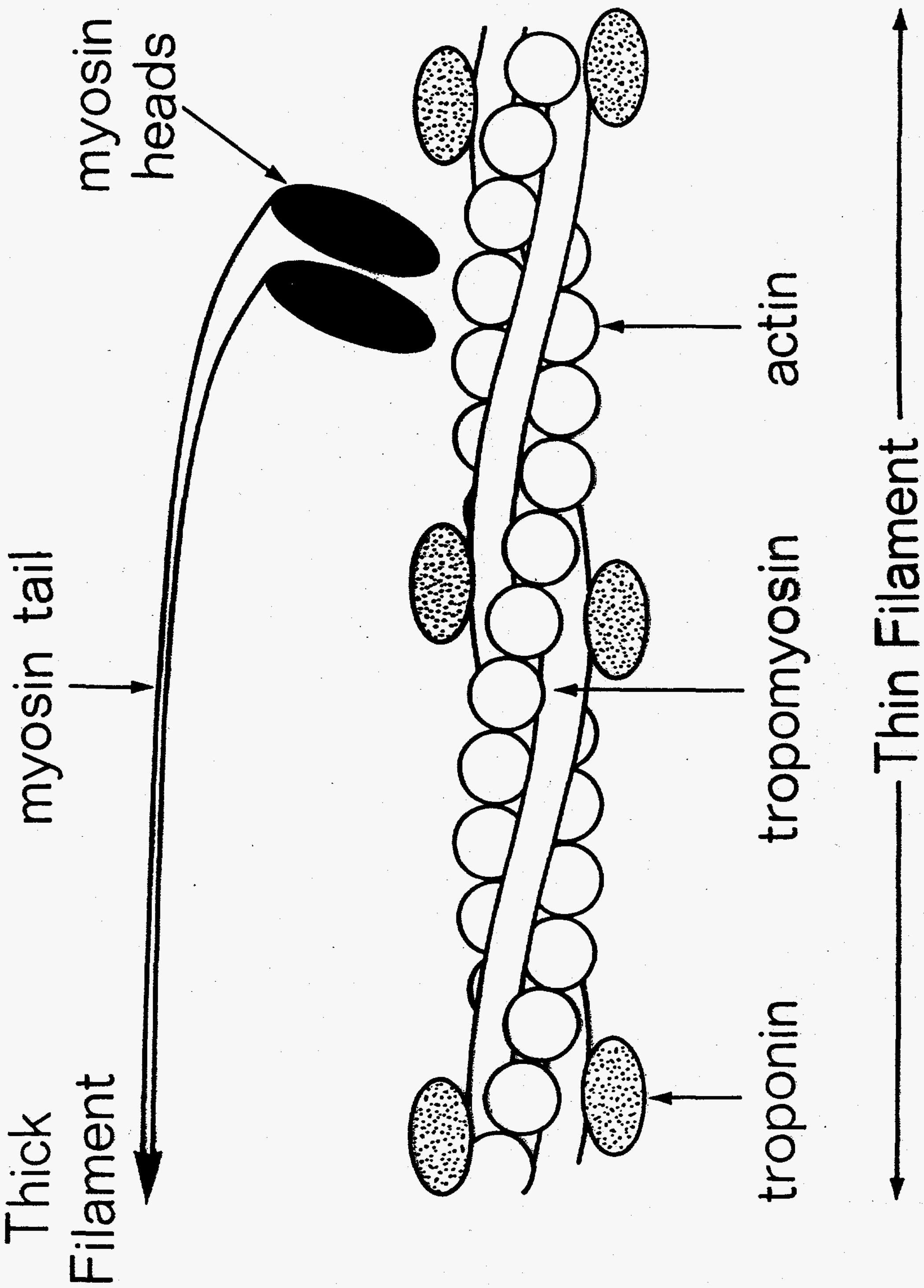
myosin heads
myosin tail
Thick Filament
actin
tropomyosin
troponin
Thin Filament

ACTIN Layer Lines

Kress et al J. Mol Biol 188 (1986) 325-342

2nd layer line : axial 179Å
(tropomyosin) radial $\cdot 023 Å^{-1}$
(43Å)

At 6°C, large changes in the intensity of the 2nd LL both in 'normal' & 'overstretched muscle with no overlap between thick and thin filaments.

Ca^{++} binding to troponin → movement (no axial change) of tropomyosin, which is the first step (structurally) in muscle contraction. (See Fig. 2)

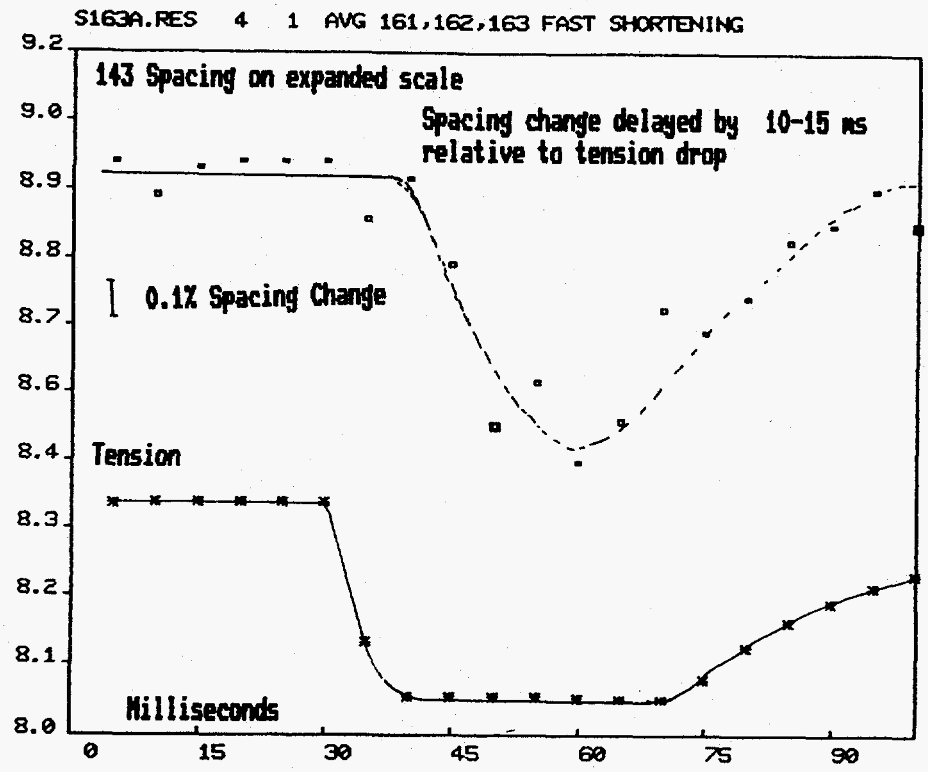

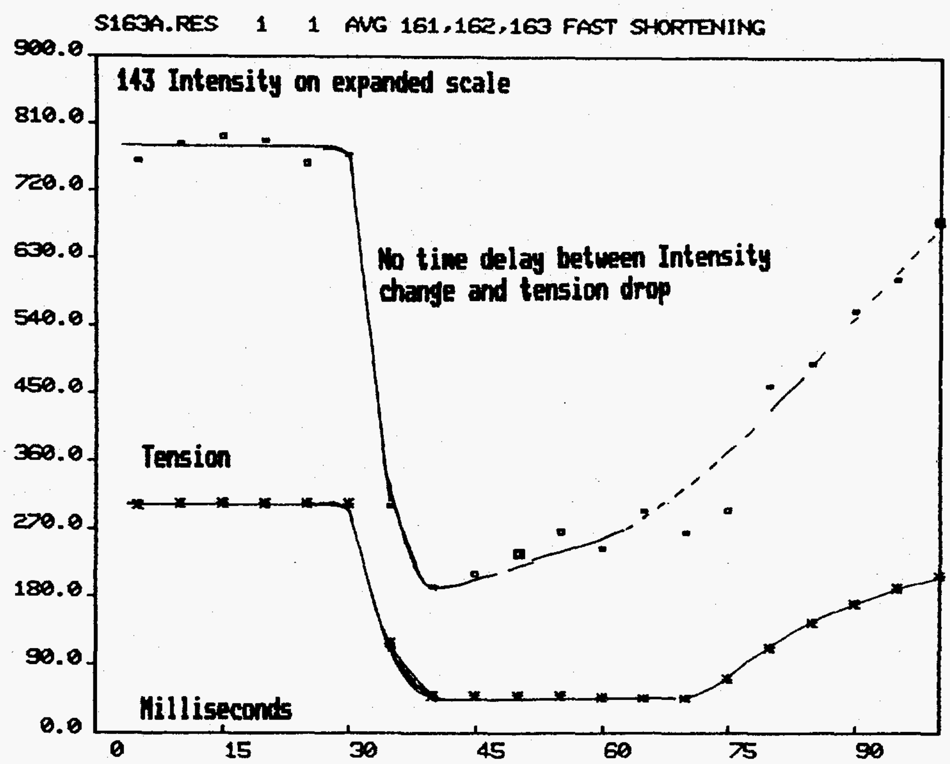

A. R. Faruqi et al. Nucl Instr & Meth A310 (1991) 359 – 361

X-ray Detectors

(A) Integrating Detectors

(i) Film

(ii) Image Plate

(iii) TV- based

(iv) CCD

(B) 'Pulse' Counting Detectors

(i) Multiwire Chambers

(ii) Scintillation Detectors

POSITION SENSITIVE DETECTOR

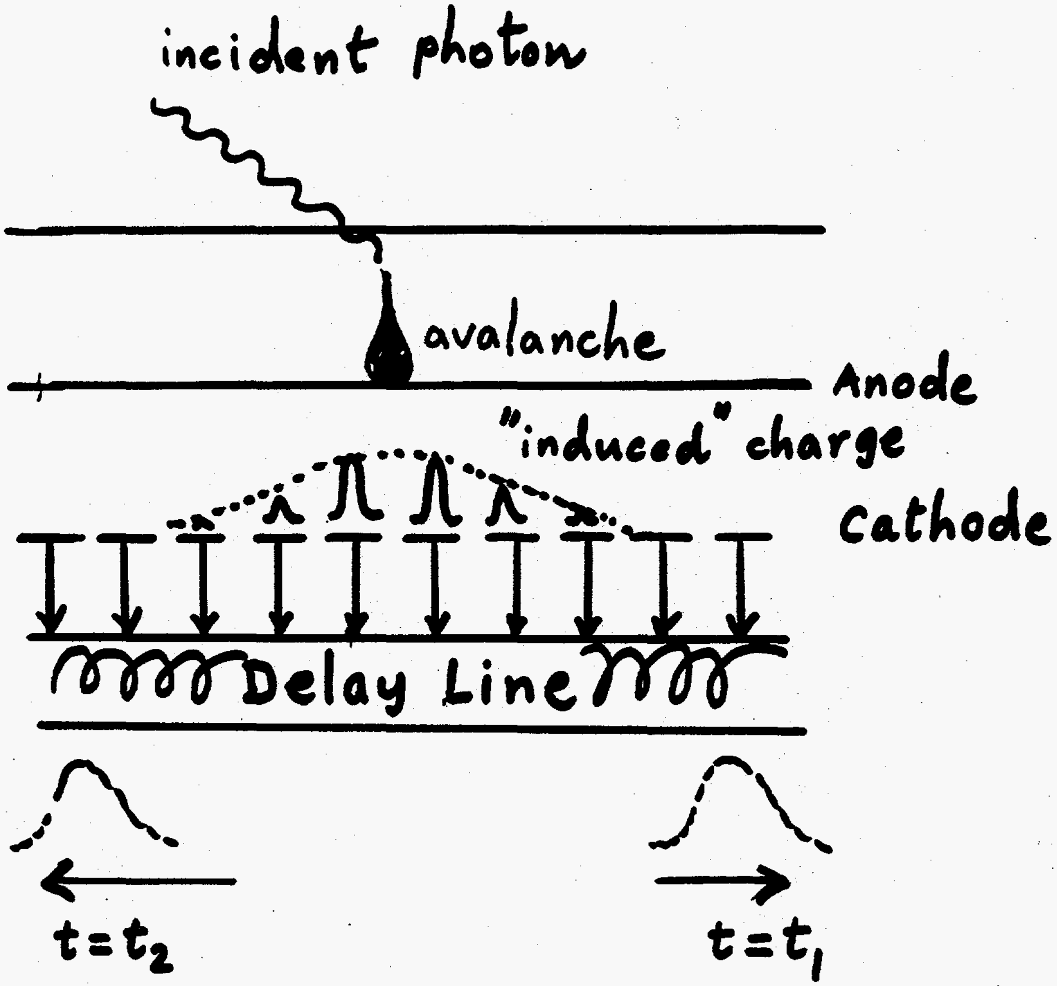

Position $\propto |t_1 - t_2| \times$ velocity

Transmission Velocity 1-10 ns/mm

MULTIWIRE PROPORTIONAL CHAMBERS

ADVANTAGES

(1) High Quantum Efficiency for 8 keV x-rays

(2) Time-Resolved Work possible due to relatively rapid readout

(3) Good Dynamic Range

(4) Good Linearity

(5) Adequate Spatial Resolution

(6) Geometry (i.e size) well matched to muscle specimen & synchrotron source size

DISADVANTAGES

(1) Counting Rates not high enough (SR)

(2) Radiation Damage limits lifetime (SR)

(3) High Angles: Parallax

MULTIWIRE LINEAR DETECTOR

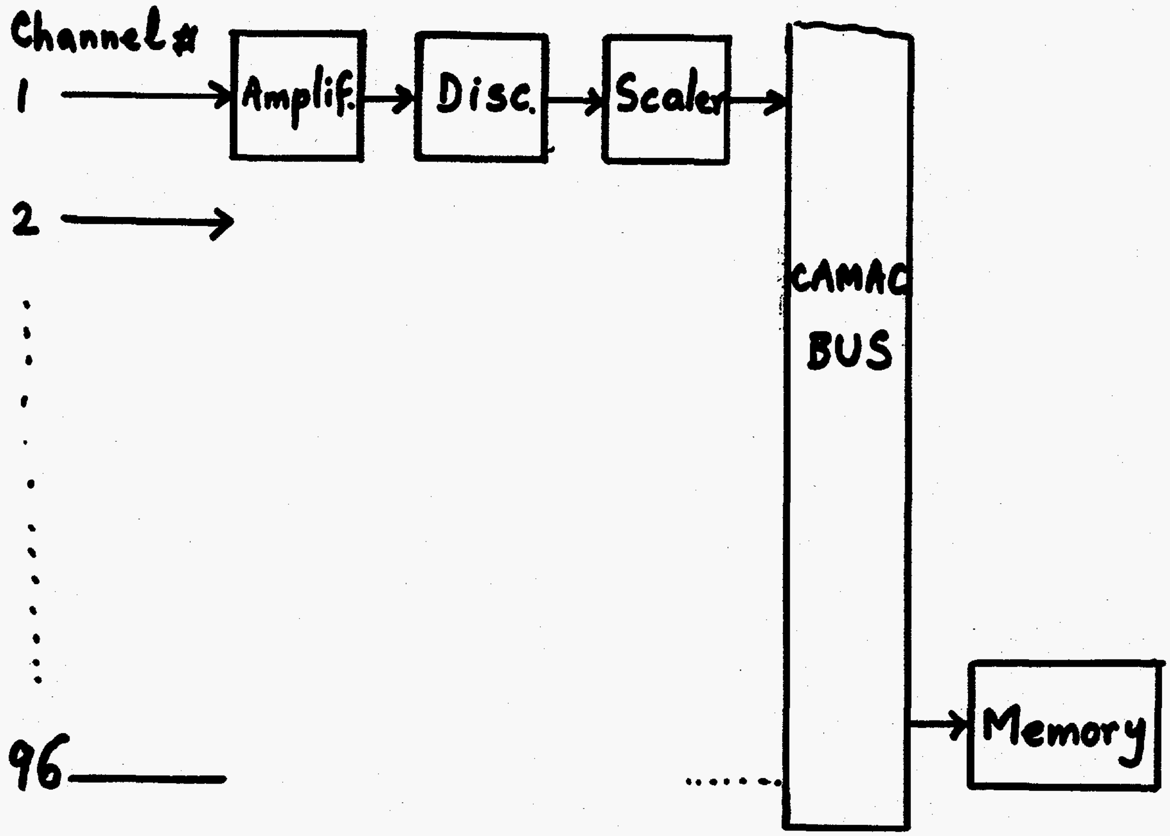

Efficiency ~ 90%

Spatial Resolution ~ 1 mm wire spacing ≲ 50 μm

Precision of 'Spatial' Measurements: v. good

Count Rates : local 10^4 mm^{-2} sec^{-1}

global 10^7 sec^{-1}

Linearity : few percent

'Time Resolution 0.1 ms → seconds

slide
results (1,1)

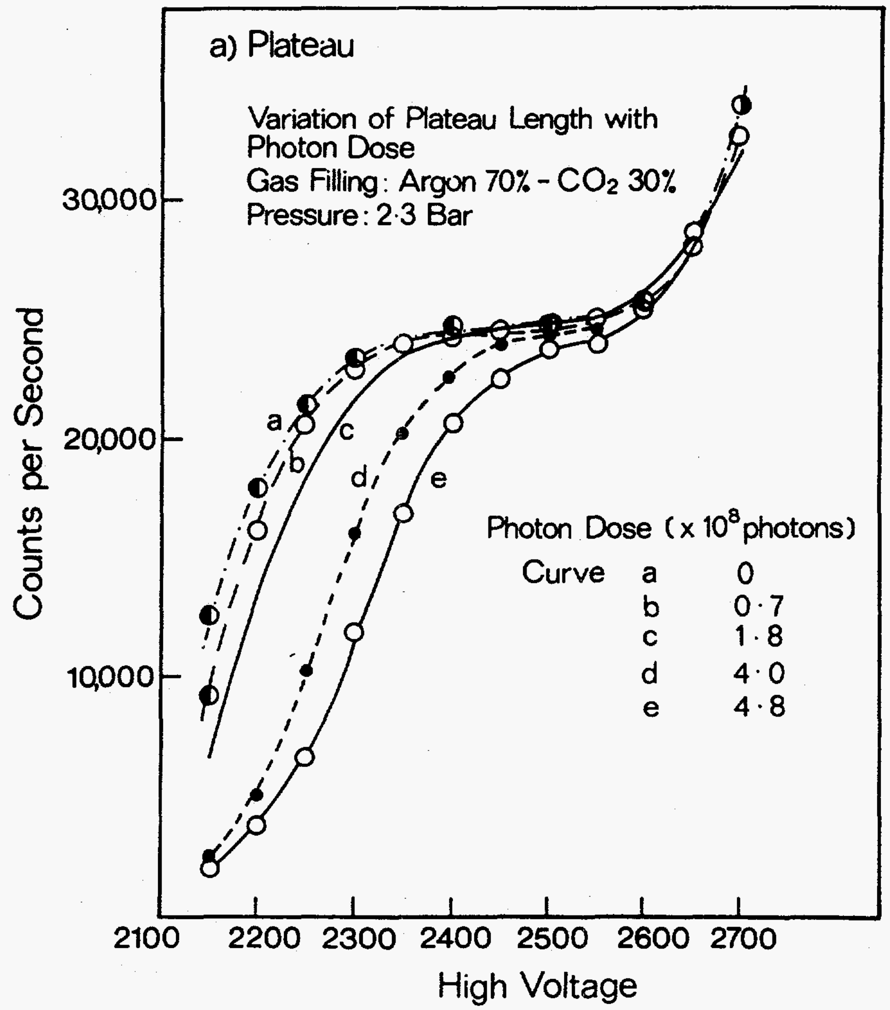

A R Faruqi IEEE Trans Nucl Sci NS-27 (1980) 644

F.Angelini, R.Bellazzini, A.Brez, M.M.Massai, R.Raffo,
G.Spandre, M.A.Spezziga
INFN-Pisa and University of Pisa
Via Livornese 582-I-56010 S.Piero a Grado,Pisa,ITALY

NIM A323 (1992) 229-235

MicroStrip Gas Chambers with true two-dimensional and pixel read-out

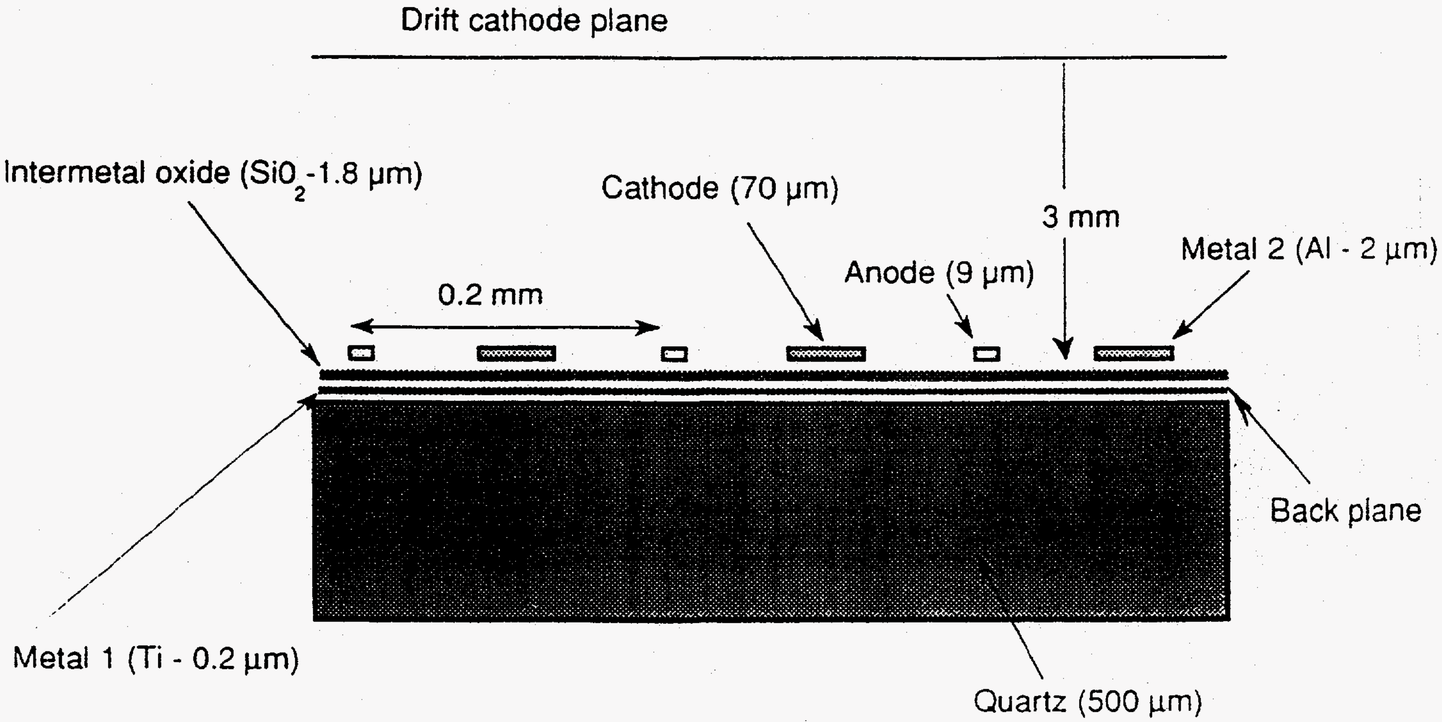

F.Angelini, R.Bellazzini, A.Brez, M.M.Massai, R.Raffo,
G.Spandre, M.A.Spezziga
INFN-Pisa and University of Pisa
Via Livornese 582-I-56010 S.Piero a Grado,Pisa,ITALY

NIM A323 (1992) 229 - 235

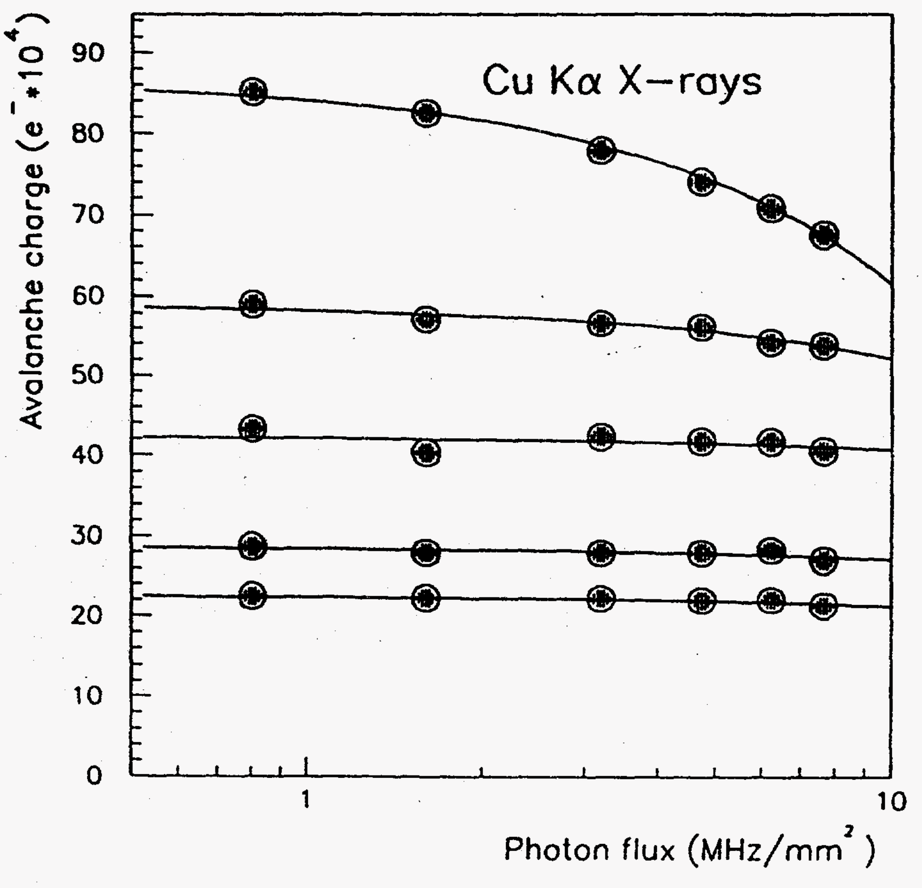

Gas : Argon 90% DME 10%

Radiation Damage $\frac{\delta G}{G}$ ~ -15% @ .016 C/cm

F.Angelini, R.Bellazzini, A.Brez, M.M.Massai, R.Raffo,
G.Spandre, M.A.Spezziga
INFN-Pisa and University of Pisa
Via Livornese 582-I-56010 S.Piero a Grado,Pisa,ITALY

NIM A323 (1992) 229-235

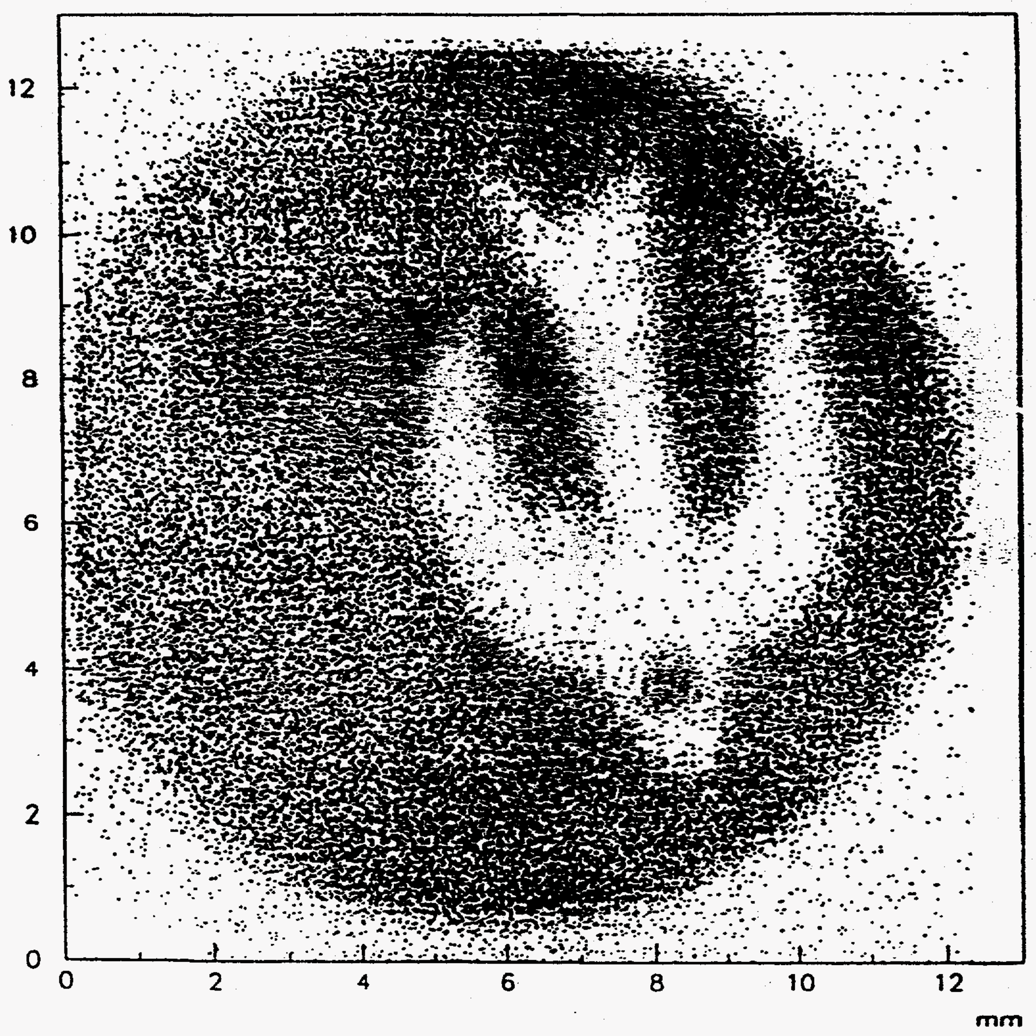

F.Angelini, R.Bellazzini, A.Brez, M.M.Massai, R.Raffo,
G.Spandre, M.A.Spezziga
INFN-Pisa and University of Pisa
Via Livornese 582-I-56010 S.Piero a Grado,Pisa,ITALY

NIM A335 (1993) 69-77

The Micro-Gap Chamber

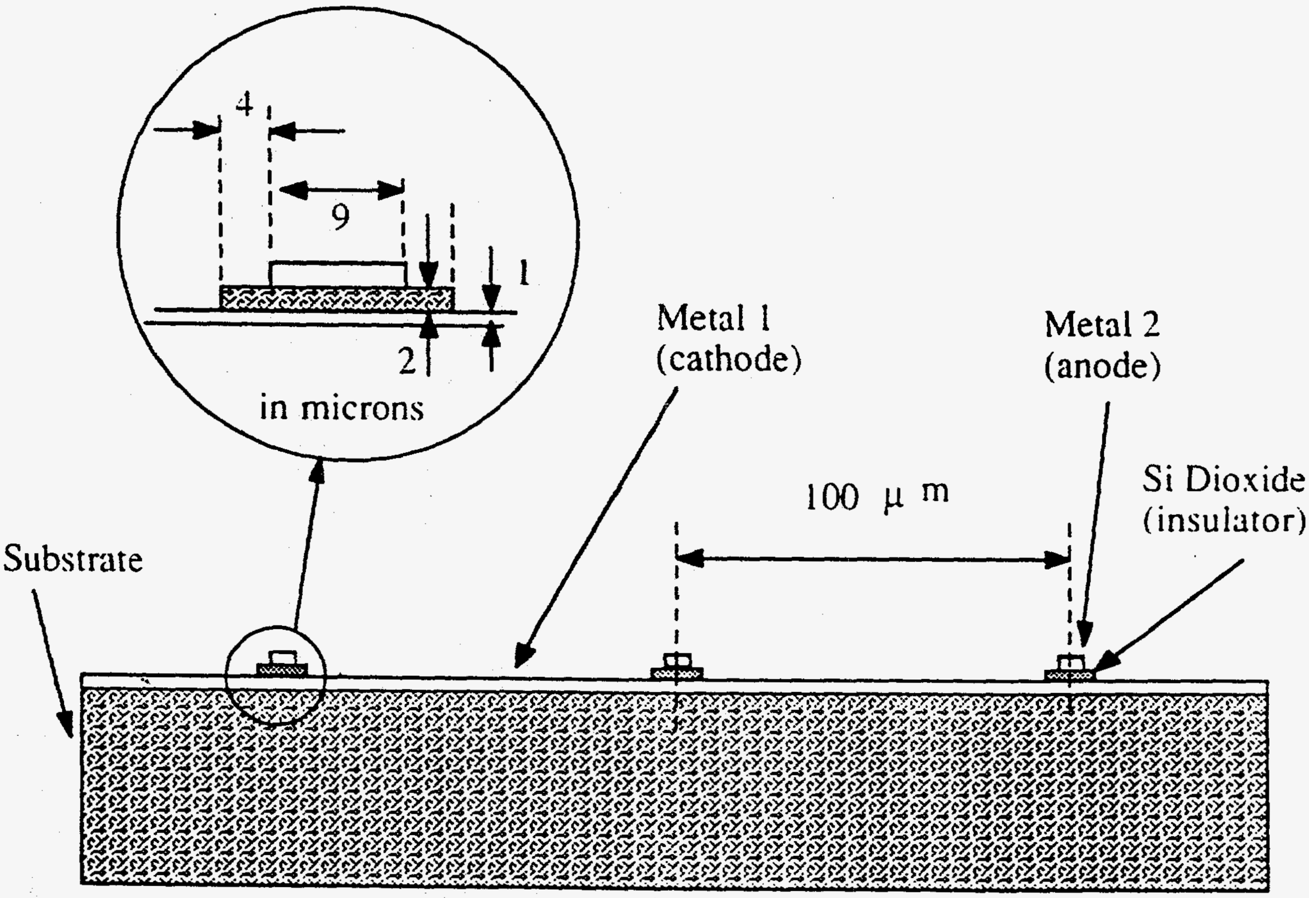

F.Angelini, R.Bellazzini, A.Brez, M.M.Massai, R.Raffo,
G.Spandre, M.A.Spezziga
INFN-Pisa and University of Pisa
Via Livornese 582-I-56010 S.Piero a Grado,Pisa,ITALY

NIM A335 (1993) 69-77

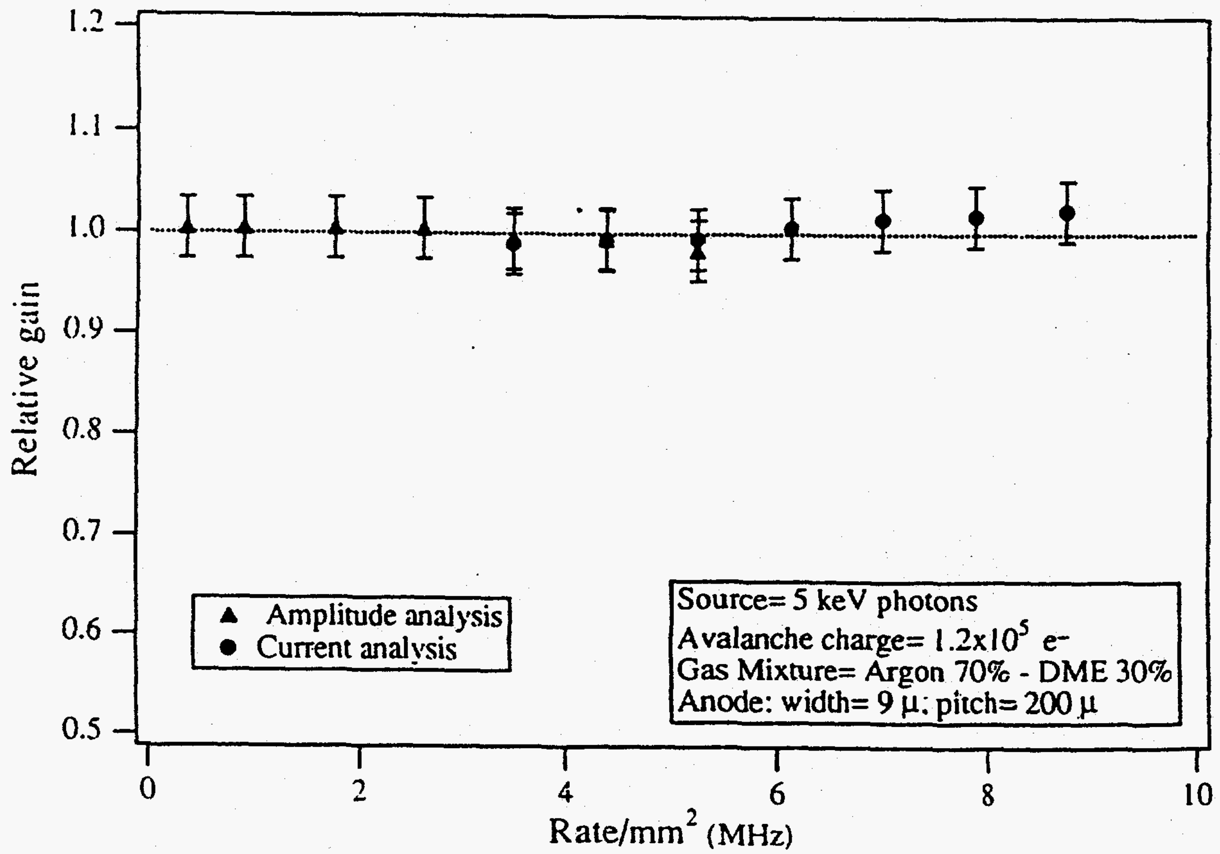

Microstrip Gas Detectors

Microstrip gas detectors, first proposed by Oed (ILL), circumvent some of the problems associated with conventional multiwire proportional chambers. Both anode and cathode are 'etched' on the surface of a high resistivity material like glass or ceramic and does not use delicate wires which may break easily (LMB chamber has 10 μm anode wires stretched with 12 gm tension and breaking tension is ~18 gm). Anode size is similar, i.e. 10 μm seperated from the cathode by only ~50 μm (compared to 3-6 mm in conventional chambers). X-ray photon is absorbed in the gas which also has a drift field, but multiplication takes place close to the anode. The back plane has strips running at right angles to pick up the orthogonal coordinate.

Main Advantages

1. More uniform gas gain - better energy resolution.
2. Very good spatial resolution in one direction.
3. Lower operating voltages.
4. Higher count rates should be possible as positive ions can be removed more quickly.
5. Substrate may be made of flexible material which can be rolled up, for example, into a cylindrical shape detector.

Main Disadvantages

1. Anodes can still be destroyed by minor sparks - repair not possible.
2. Choice of substrate quite tricky as gas gain appears variable (probably) due to charge build up.

Reference

Budt-Jorgensen, *et al* Nucl Instr & Meth. A310 (1991) pp82-87

How to reduce parallax

1. Radial Drift Field
2. Pressure
3. Multiple Detectors

4

G. CHARPAK N.I.M. 156, (1978), 1-1

Kahn, Fourme .... Rev Sci Instr (1992) 63 655-65

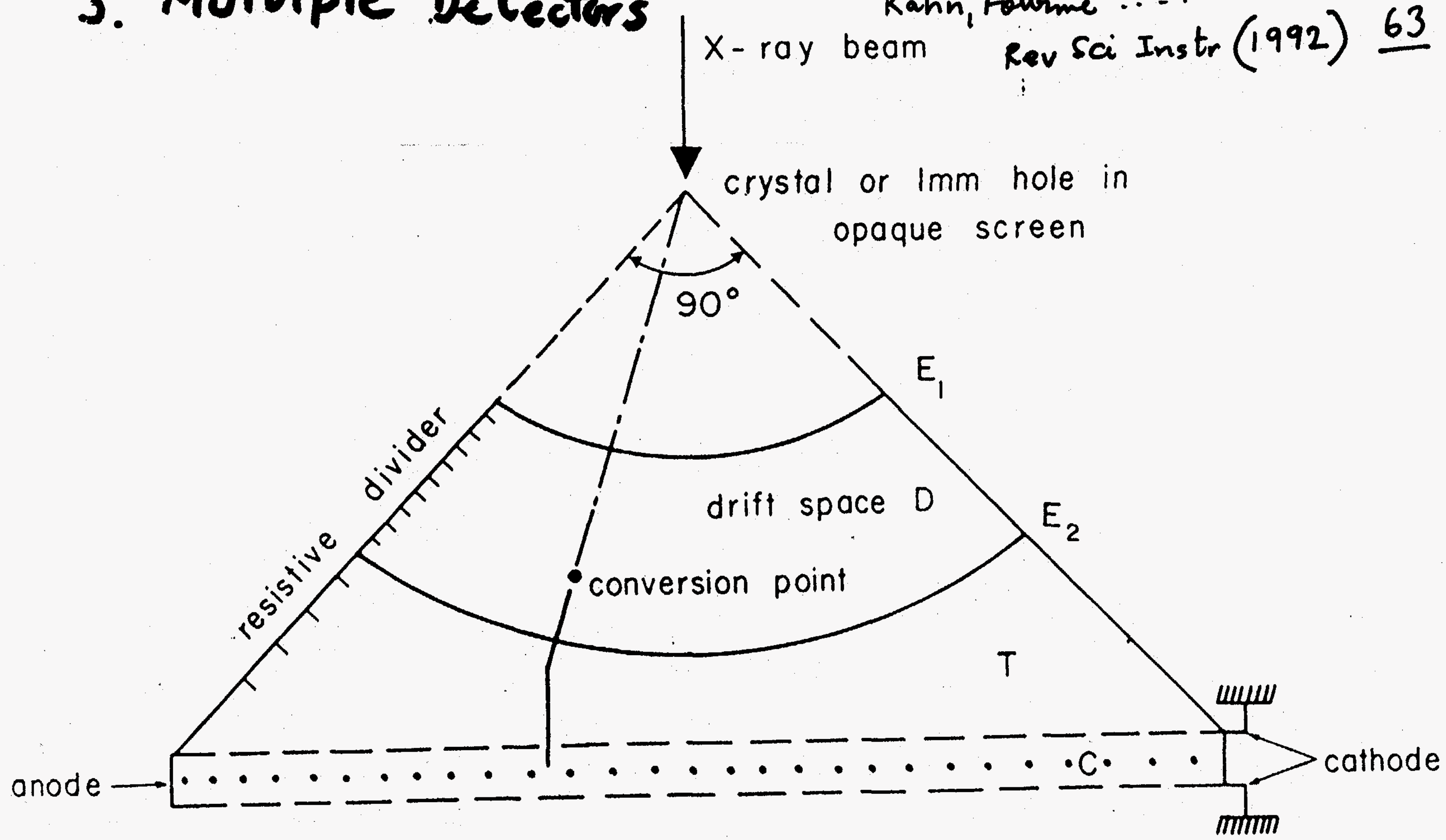

DETECTOR REQUIREMENTS - A SUMMARY

Resolution 2000 * 2000 pixels

Size 150 - 200 mms

Count Rates global 10 - 1000 MHz
local 100 kHz

Detective Quantum Efficiency 'high' for 0.5 - 1.5 Angstrom

Linearity and Uniformity should be correctable

Dynamic Range 1000 - 10000

Radiation Damage should be able to withstand few months

Time Framing desirable

General Reviews:

1.Proceedings of the Europeon Workshop on
X-ray Dtectors for Synchrotron Radiation Sources
Aussois France 1991
Ed. A.H.Walenta

2. Detector Applications in biology and condensed matter physics
A.R.Faruqi
Nucl. Instr and Methods A310 (1991) 14-23

Basic Parameters - Summary (PX)

Resolution		~ 2000×2000 pixels
Size		150 - 200 mms
Count Rates :	global	~10^7 – 10^9 Hz
	local	~ 10^5 Hz
DQE (1Å)		'High'
Linearity (& Uniformity)		'correctable'
Dynamic Range		10^3 – 10^4
Radiation Damage		'100 days'
Time Framing		desirable (PX)
		essential (TRXD)

Model of Myosin S1 consisting of three domains

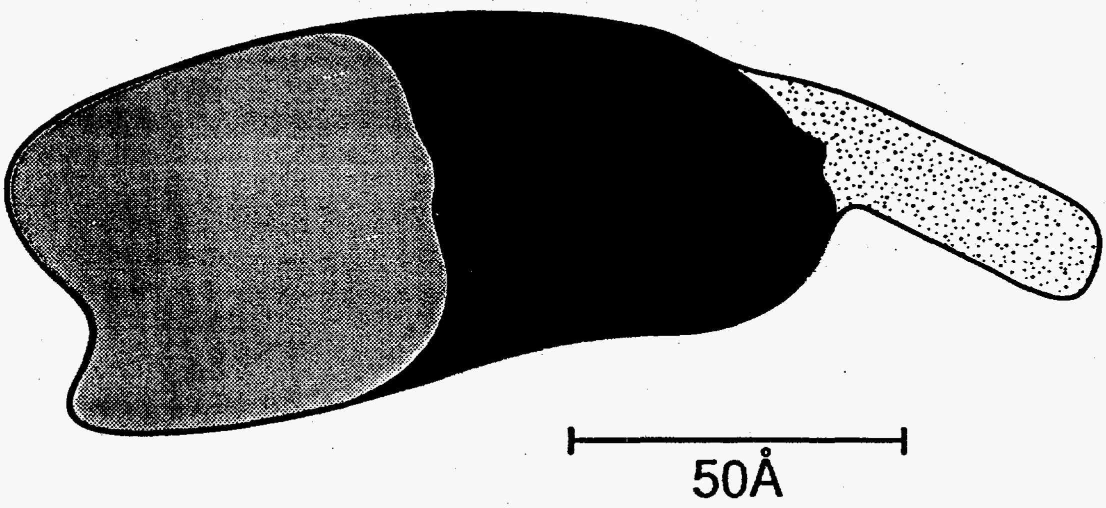

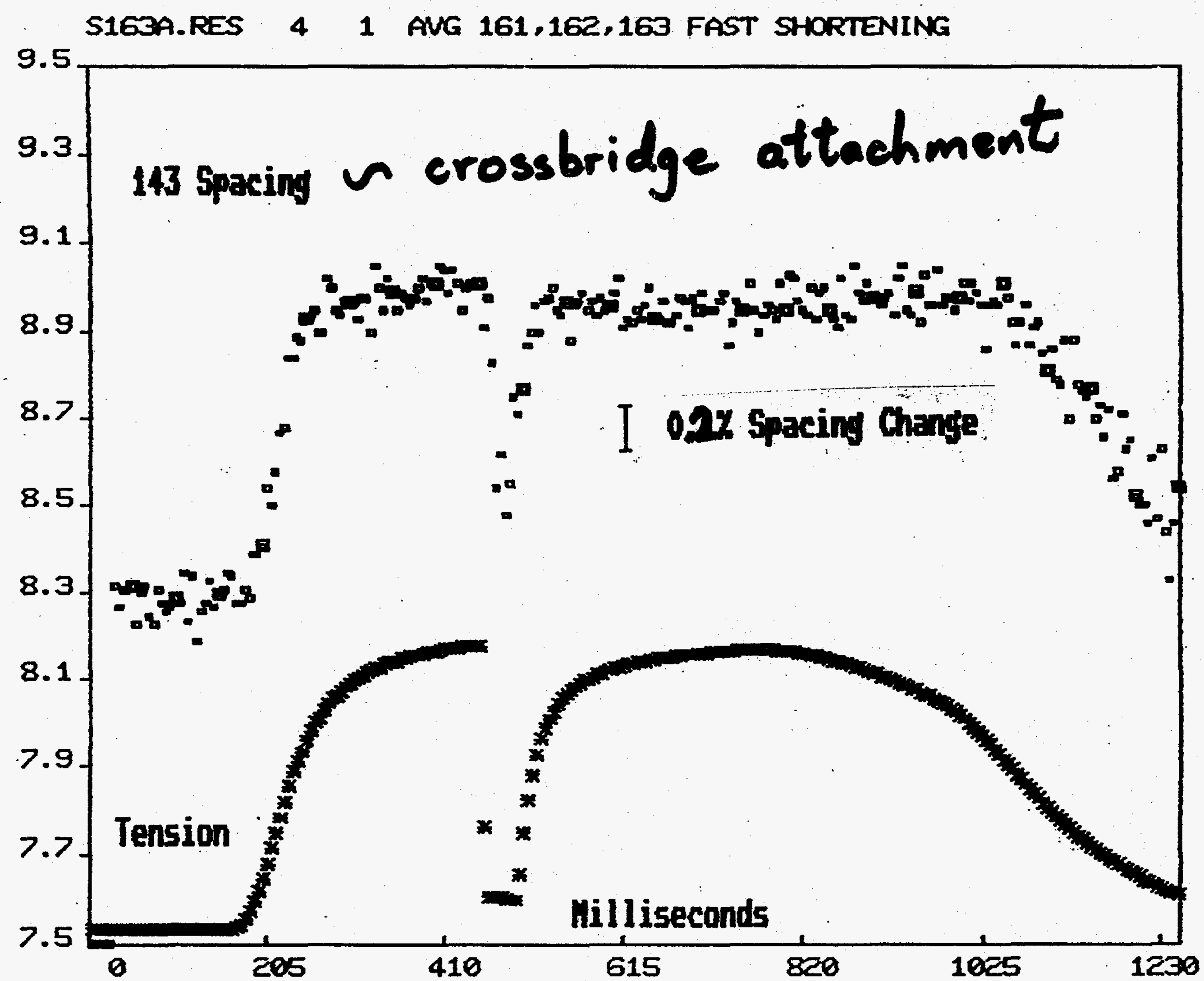
S163A.RES 4 1 AVG 161,162,163 FAST SHORTENING
143 Spacing
crossbridge attachment
0.2% Spacing Change
Tension
Milliseconds
9.5
9.3
9.1
8.9
8.7
8.5
8.3
8.1
7.9
7.7
7.5
0
205
410
615
820
1025
1230

Sol M. Gruner

Princeton University
Department of Physics

CCD Area X-ray Detectors: Experiments and Possibilities

CCD-based area x-ray detectors are capable of solving many of the quantitative imaging and diffraction problems expected to be encountered at the APS. These detectors are under development by a small number of groups for a variety of problems. The capabilities and limitations of existing detectors are reviewed, with an emphasis on the experiences of our group in applying these devices at the NSLS and at CHESS. Future capabilities are also discussed.

GOAL:

DEVELOP 2-D DETECTORS FOR STORAGE RINGS TO
-- ENHANCE CAPABILITIES
-- INCREASE EFFICIENCY

SPECIFICATIONS:

A) HIGH DQE (QUANTUM LIMITED)
B) AREA > 10 CM ACROSS
C) FORMAT > 2000 x 2000 PIXELS
D) COUNT-RATE INSENSITIVE
E) DYNAMIC RANGE > 10,000
F) ROBUST IN DEMANDING ENVIRONMENT
G) EXPERIENCE TESTED, USER FRIENDLY, FLEXIBLE AND APPLICATION INTEGRATED

STRATEGY:

1) LARGE FORMAT, 1 CCD DETECTORS
2) MOSAIC ARRAY OF SMALLER CCDs
3) PIXEL ARRAY DETECTORS

GOAL.STR

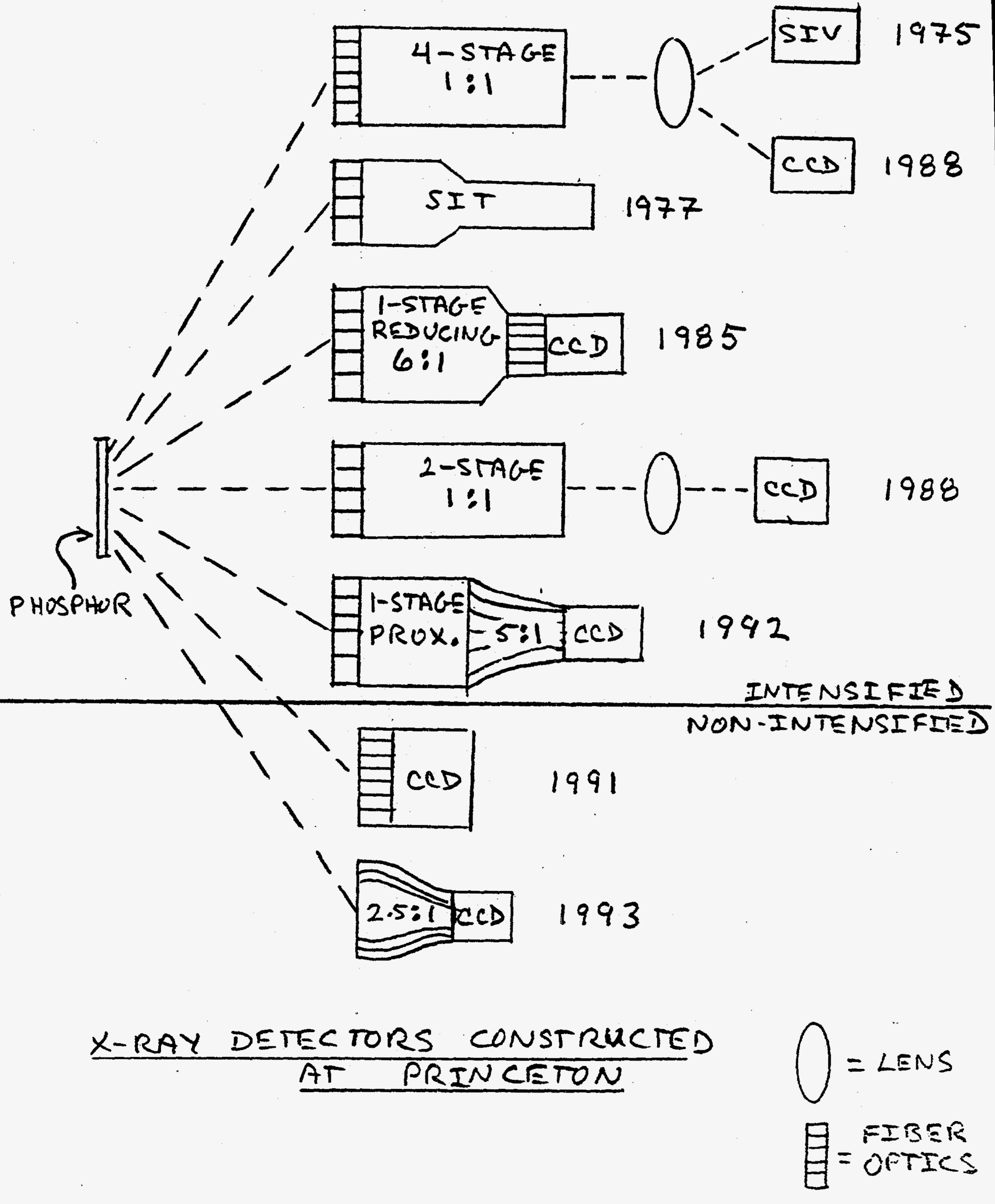

X-RAY DETECTORS CONSTRUCTED AT PRINCETON

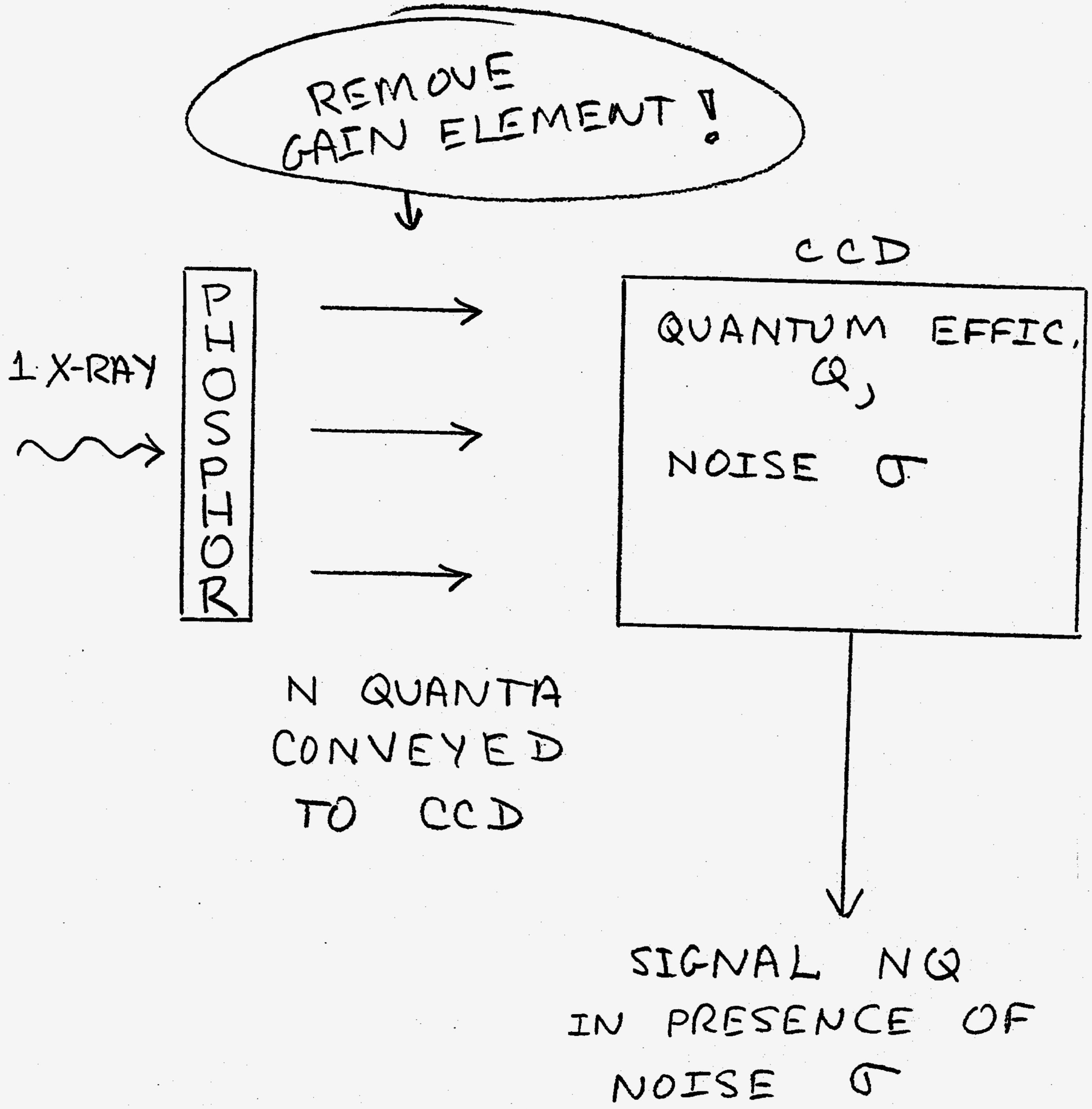

IDEALLY $NQ > \sigma$

BUT TO MAXIMIZE DYNAMIC RANGE

$$NQ \simeq \sigma$$

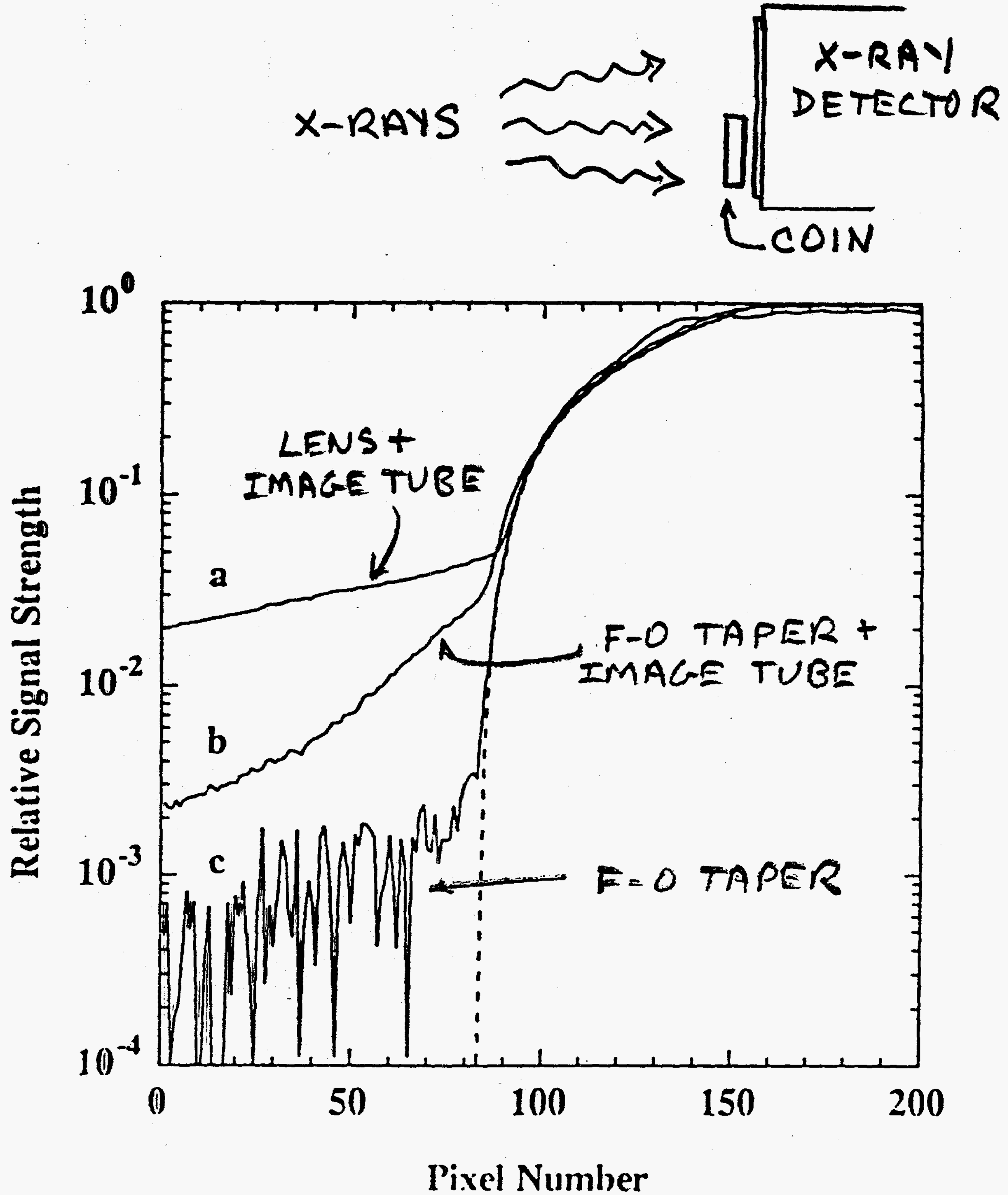
X-RAYS
X-RAY DETECTOR
COIN
LENS + IMAGE TUBE
F-O TAPER + IMAGE TUBE
F-O TAPER
a
b
c
Relative Signal Strength
Pixel Number
10^0
10^{-1}
10^{-2}
10^{-3}
10^{-4}
0
50
100
150
200

USEFUL NUMBERS *

1) **EFFICIENT INORGANIC PHOSPHOR HAVE**

EFFICIENCIES ≡ (X-RAY ENERGY/LIGHT ENERGY)

= 10-20 %.

FOR 5-10 KeV X-RAYS:

5-15 PHOTOELEC./X-RAY

33-~~100~~ 140 PHOTONS DELIVERED

(P-45, P-43, CsI (Na OR Tl), P-11) ! FOOT NOTE !

2) **LENS COUPLING EFFICIENCY ≤ FEW %**

$$C = \left(\frac{M}{2\mathcal{F}(1+M)}\right)^2$$

M = IMAGE/OBJECT (MAGNIFICATION)

$\mathcal{F}$ = "$\mathcal{F}$" **NUMBER**

---

* SEE: GRUNER, "CCD & VIDICON X-RAY DETECTORS: THEORY AND PRACTICE" REV. SCI. INSTR. 60 (1989) 1545.

3) **FIBER-OPTIC TAPER EFFICIENCY (GREEN LIGHT)**

M	$C_{F.O.}$	C_{LENS} (f/1.0)
1	**75%**	6%
0.5	**20%**	3%
0.3	**13%**	1.3%
0.25	**9%**	1%

(COLEMAN, ADV. E.E.P. 64B (1985) 649)

C = 75% ACROSS A FIBER-OPTIC INTERFACE

4) **OPTICAL QUANTUM EFFICIENCY OF Si**

Q_S = **35 - 80%**

80% ← **BARE Si**

35 ← **OVERLAID STRUCTURES**

5) 3.65 eV OF X-RAY ENERGY IN Si PRODUCES 1 e^--hole PAIR.

IMPORTANT X-RAY CHARACTERISTICS

(1) ROBUST & STABLE
(2) EFFICIENTLY CONVERT X-RAYS TO LIGHT
(3) SPECRAL MATCHING TO TAPER & CCD
(4) PROMPT EMISSION W/LOW PERSISTENCE
(5) HIGH X-RAY STOPPING POWER/RESOLUTION
(6) LINEARITY OF OUTPUT W/DOSE & INTENSITY

NO SINGLE KNOWN PHOSPHOR EMBODIES THE BEST OF THESE CHARACTERISTICS.

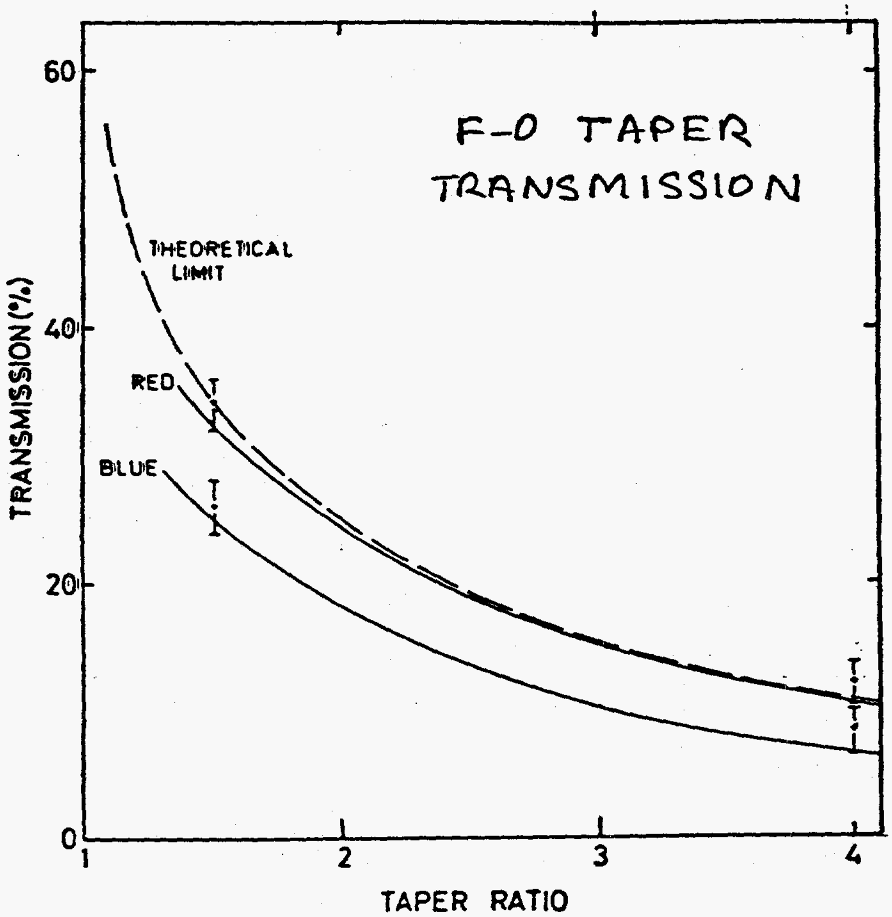

COLEMAN
ADV. EEP
64B (1984) 649

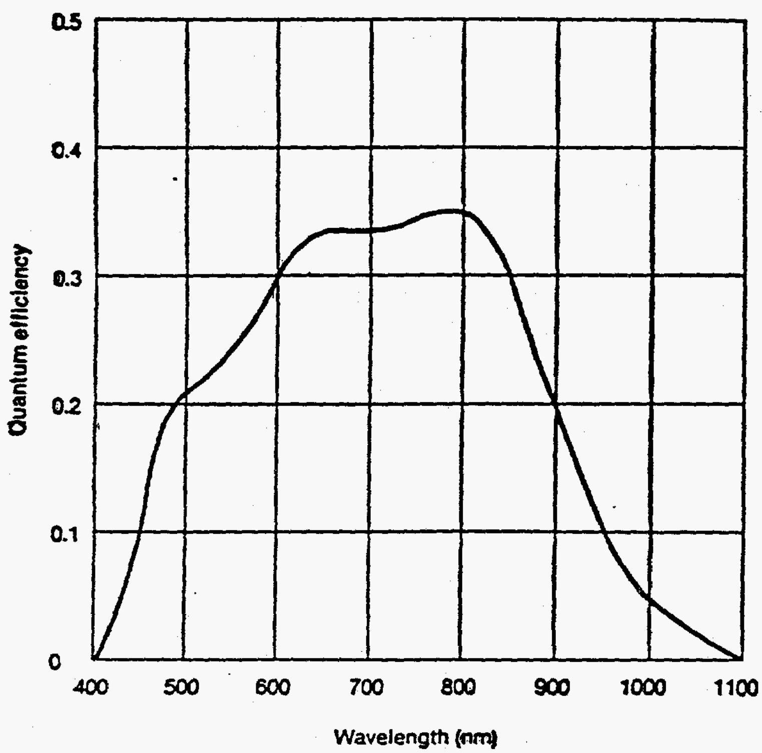

FIGURE 7 : TYPICAL SPECTRAL RESPONSE.

SPECTRAL
RESPONSE

THOMSON
TH7896A
CCD.
(FRONT ILLUM.)

rbhdl - $Zn_2SiO_4:Mn$ (0.3)

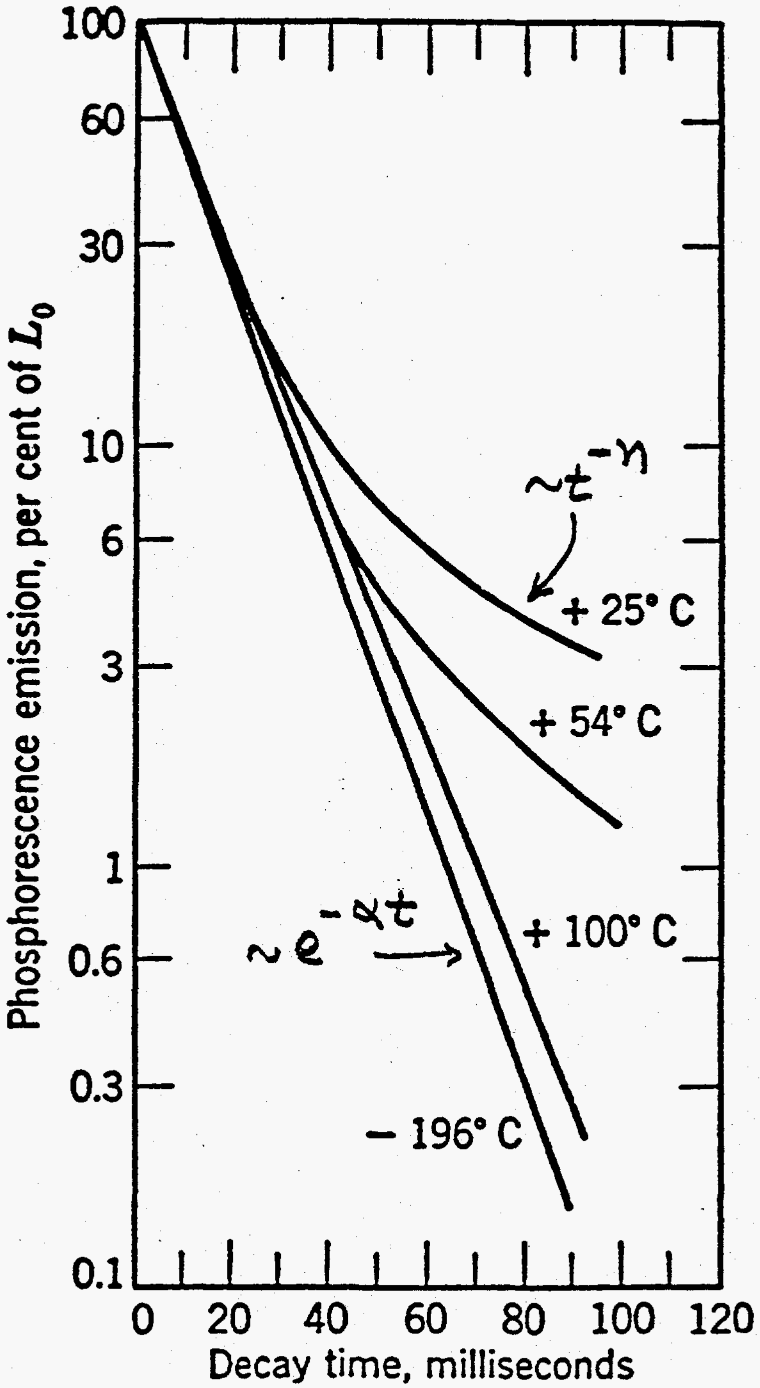

LEVERENZ, AN INTRO. TO LUMINESCENCE OF SOLIDS
(JOHN WILEY, NY, 1950)

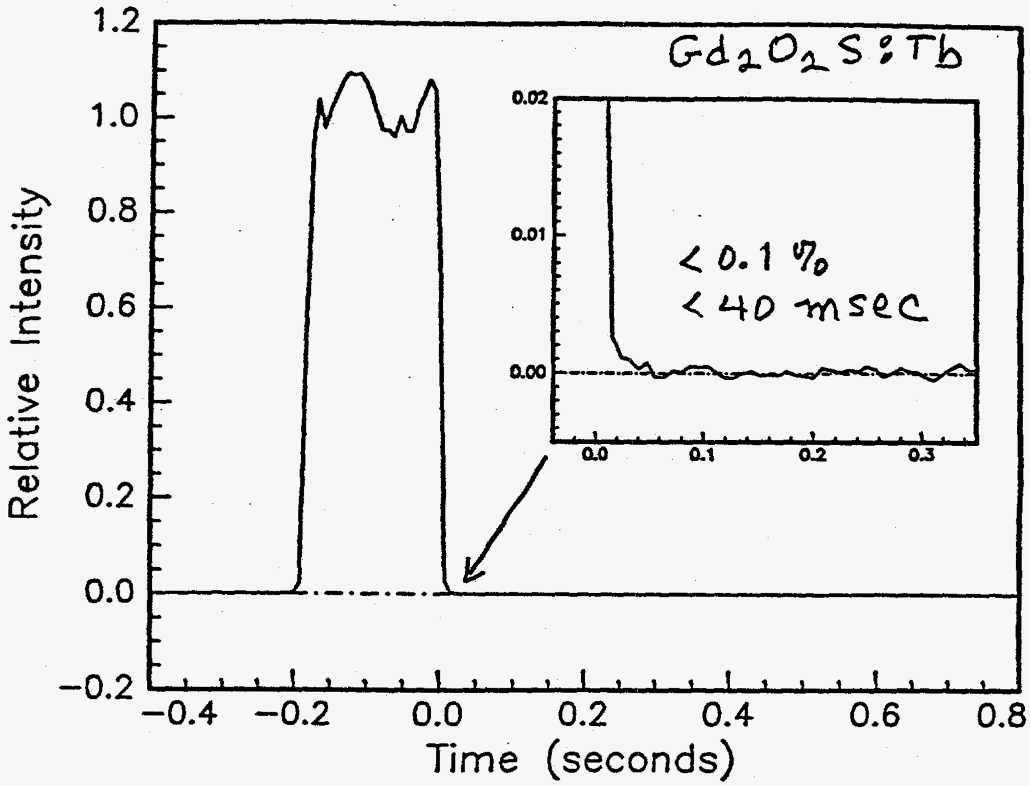

Gd2O2S:Tb
< 0.1 %
< 40 msec
Relative Intensity
Time (seconds)

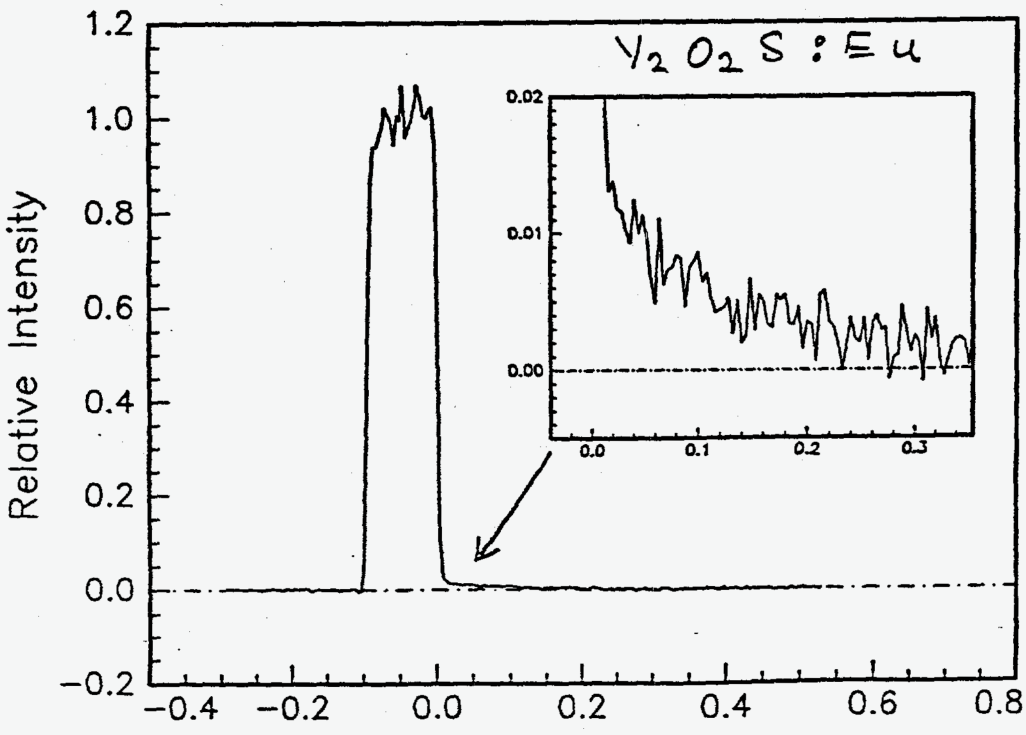

Y2O2S:Eu
Relative Intensity

	$CsI:Na$ (1)	$CsI:Tl$ (1)	$Gd_2O_2S:Tb$ (2)	$La_2O_2S:Eu$ (2)
ROBUSTNESS	VERY HYGROSCOPIC	HYGROSCOPIC	STABLE	STABLE
X-RAY STOPPING POWER	VERY HIGH	VERY HIGH	HIGH	HIGH
EFFICIENCY	GOOD	GOOD	GOOD	GOOD
SPEED PERSISTENCE (TO 10^{-3})	FAST NO LAG	FAST LAG	SLOW A LITTLE LAG	SLOW SOME LAG
SPECTRUM	BLUE	GREEN	GREEN	RED
LINEARITY	?	?	?	?

(1) EVAPORATED
ALLOWS TEXTURED GROWTH

(2) SETTLED POWDER

QUESTION:

GIVEN THAT NO SINGLE PHOSPHOR IS IDEAL, HOW WELL CAN WE DO USING SIMPLE, SETTLED SCREENS OF COMMERCIALLY AVAILABLE PHOSPHOR POWDERS?

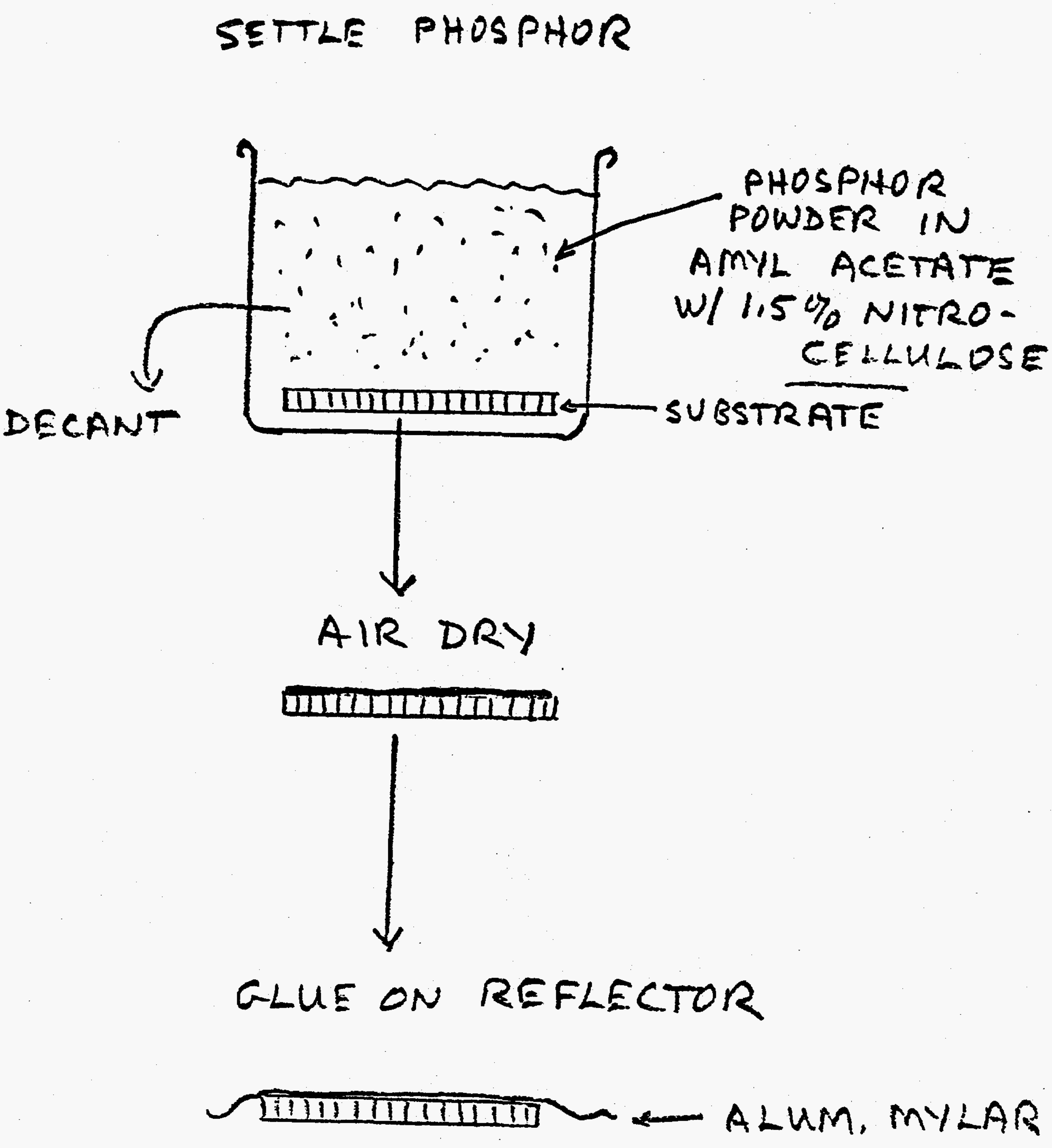

RESULTS:

6 μm $Gd_2O_2S{:}Tb$

10 mg/cm^2

32 μm THICK

41% CRYSTAL DENSITY

Phosphor	Density	Efficiency*	Decay Time**	Stopping Power for 10 mg/cm^2	
				5.9 keV	13.6 keV
Y_2O_2S:Tb	8-11 mg/cm^2	50-140	-	92%	23%
Y_2O_2S:Eu	8-12 mg/cm^2	130-150	-	92%	23%
La_2O_2S:Eu	11 mg/cm^2	170	300 ms	100%	54%
Gd_2O_2S:Tb	10-15 mg/cm^2	50-70	10 ms	91%	66%

* Photons/^{55}Fe x-ray, guided through the fiber optic plate.
** To 0.2%

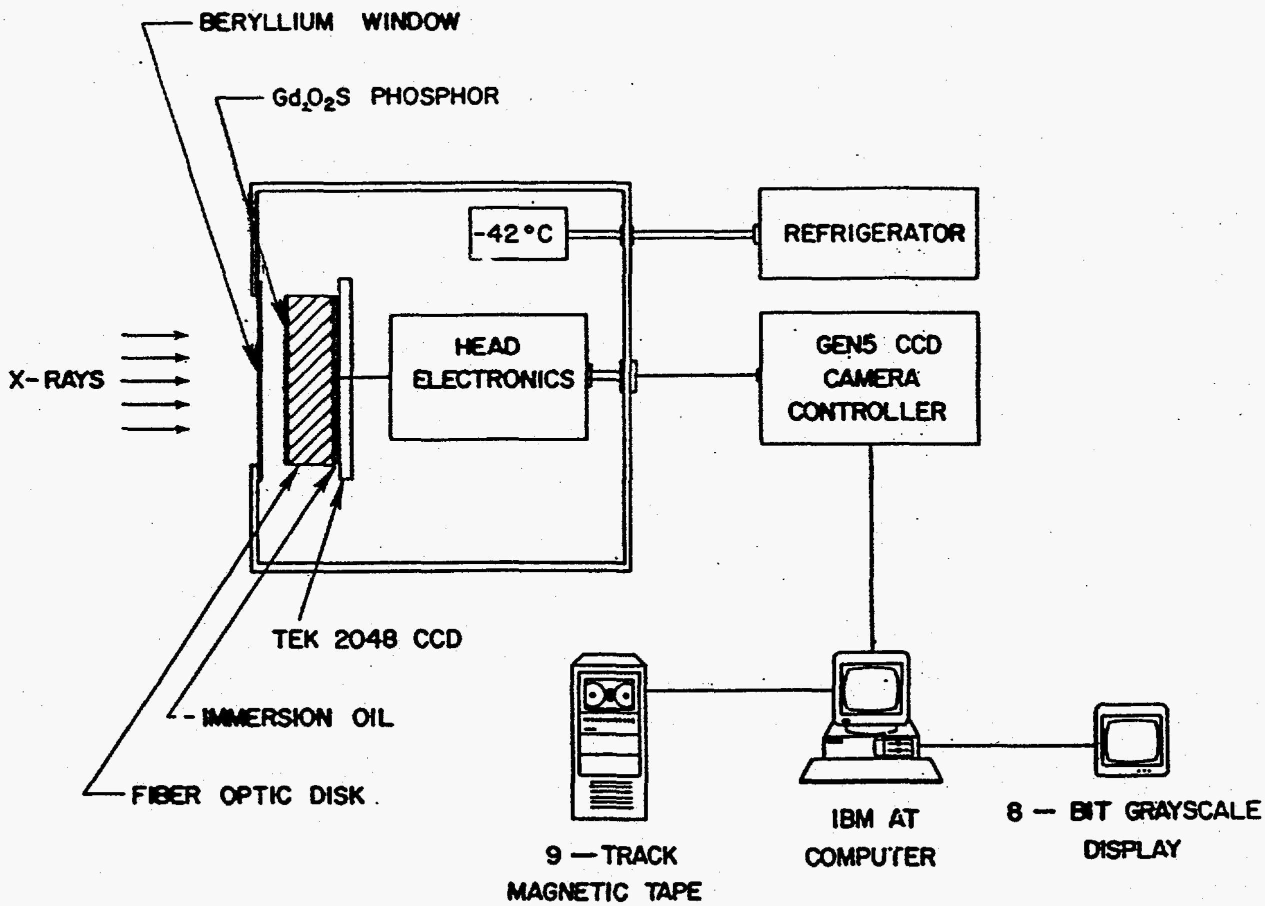

2048 X 2048 PIXEL CCD X-RAY DETECTOR

EIKENBERRY, TATE, BELMONTE, LOWRANCE, BILDERBACK & GRUNER. IEEE TRANS. NUC. SCI. 38 (1991) 110-118.

2K CCD X-RAY DETECTOR

CCD	TEK 2K, 2048 x 2048 pixels
Pixel Size	27 μm x 27 μm
Phosphor	Gd_2O_2S, 9 mg/cm^2 on 50 mm fiber optic
PSF	45 μm, FWHM
Sensitivity	24 e^-/x-ray, ^{55}Fe
Saturation	3×10^4 x-rays/pixel
Dark Current	0.56 x time @ -42 °C
Dark Current Noise	$0.2 \times \sqrt{time}$ @ -42 °C
Readout Noise	1 x-ray
Linearity	Excellent
Distortion	< 0.35 pixel
Zinger Rate	4×10^{-7}/pix/s on phosphor 6×10^{-8}/pix/s off phosphor

EIKENBERRY, TATE, BELMONTE, LOWRANCE, BILDERBACK & GRUNER, "A DIRECT-COUPLED DETECTOR FOR SYNCHROTRON X-RADIATION USING A LARGE FORMAT CCD"

IEEE TRANS. NUC. SCI. 38 (1991) 110-118.

GALLIUM ARSENIDE, LAUE
20 μm INCIDENT BEAM

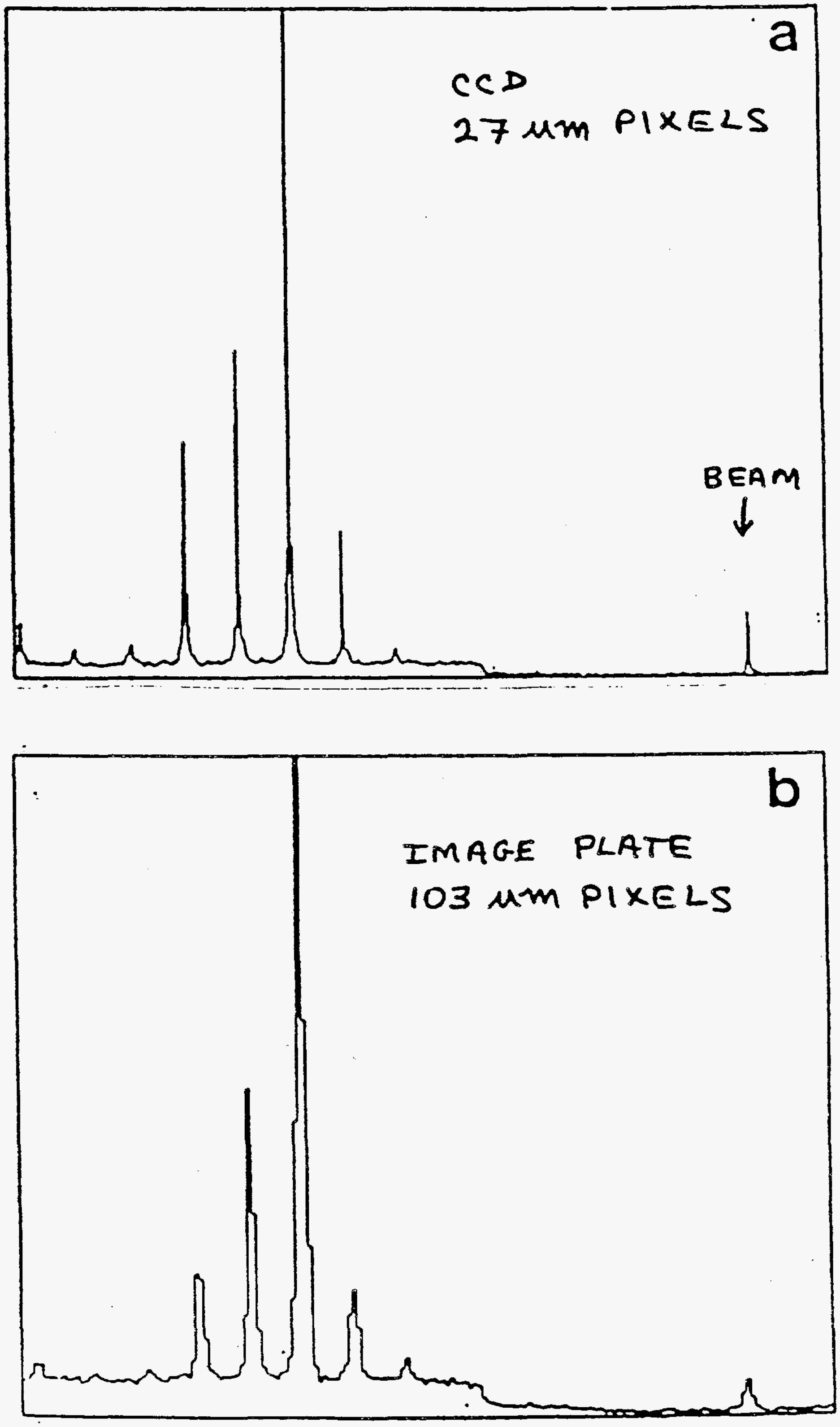

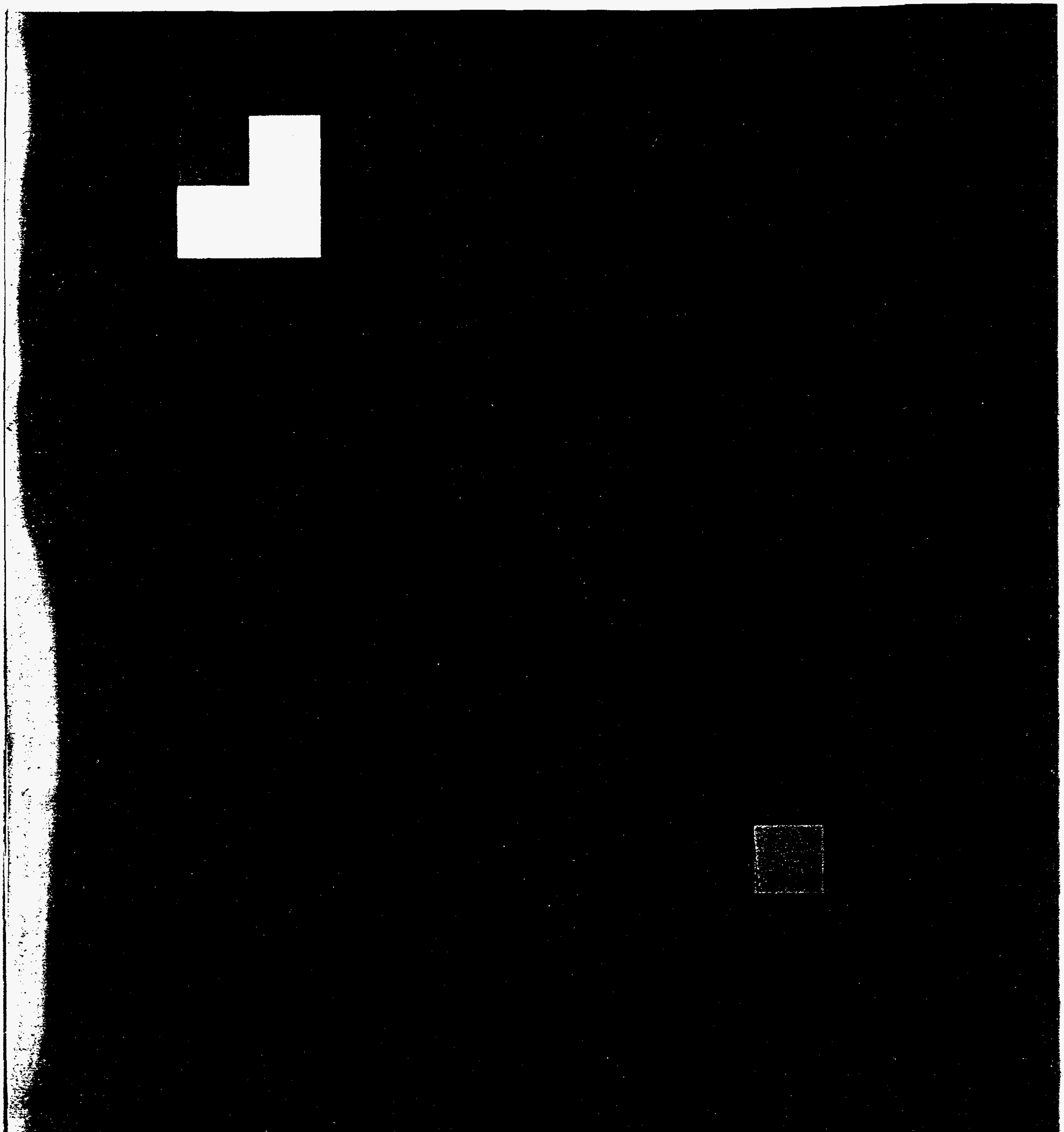

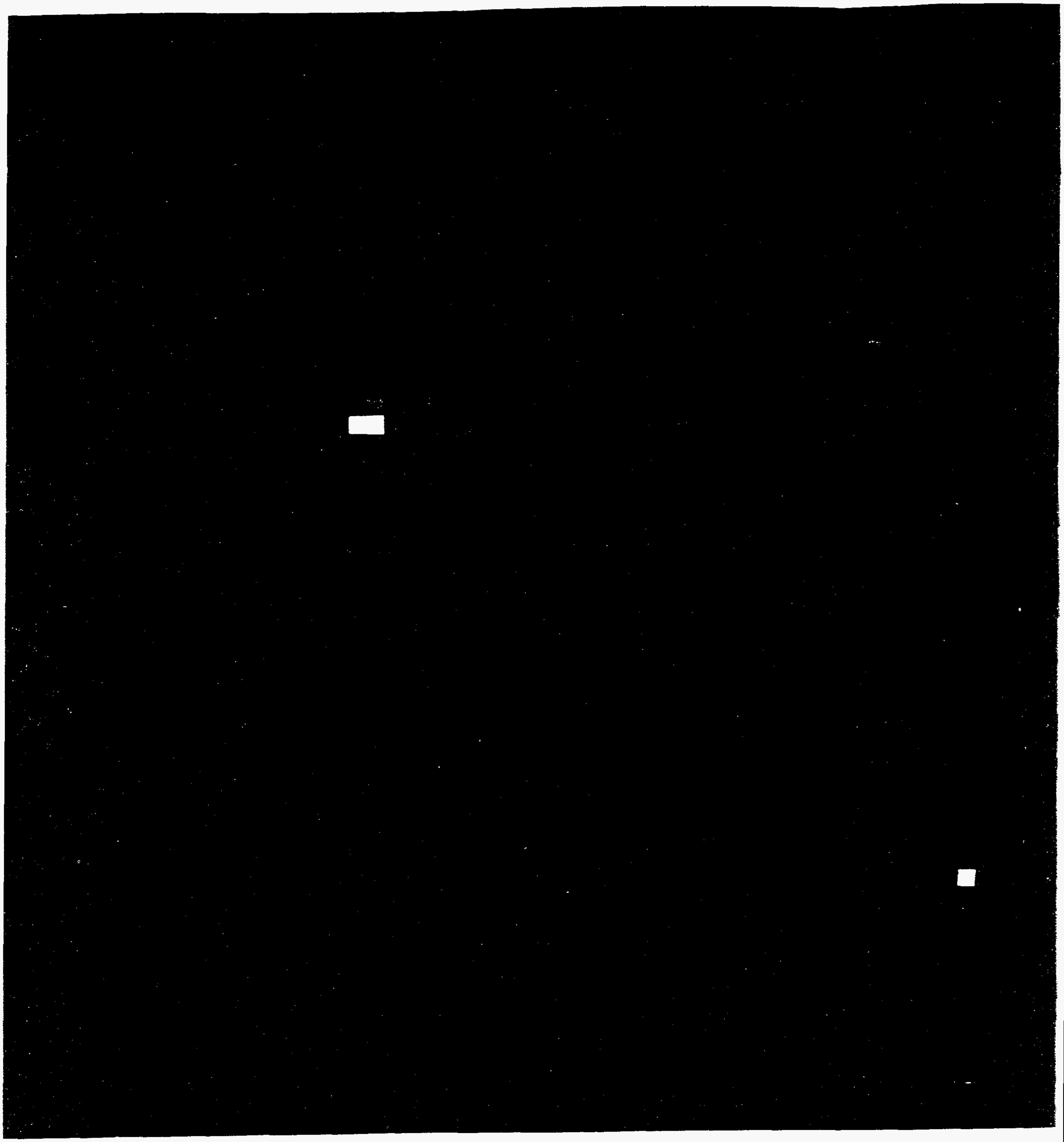

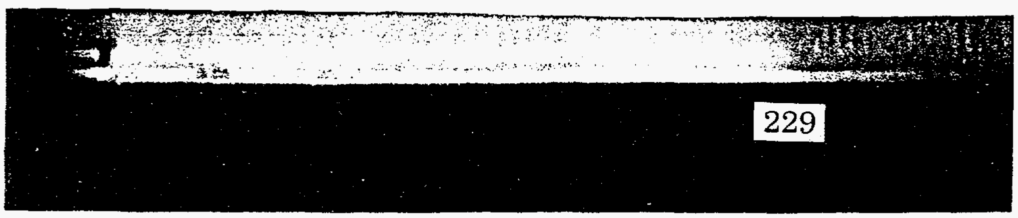

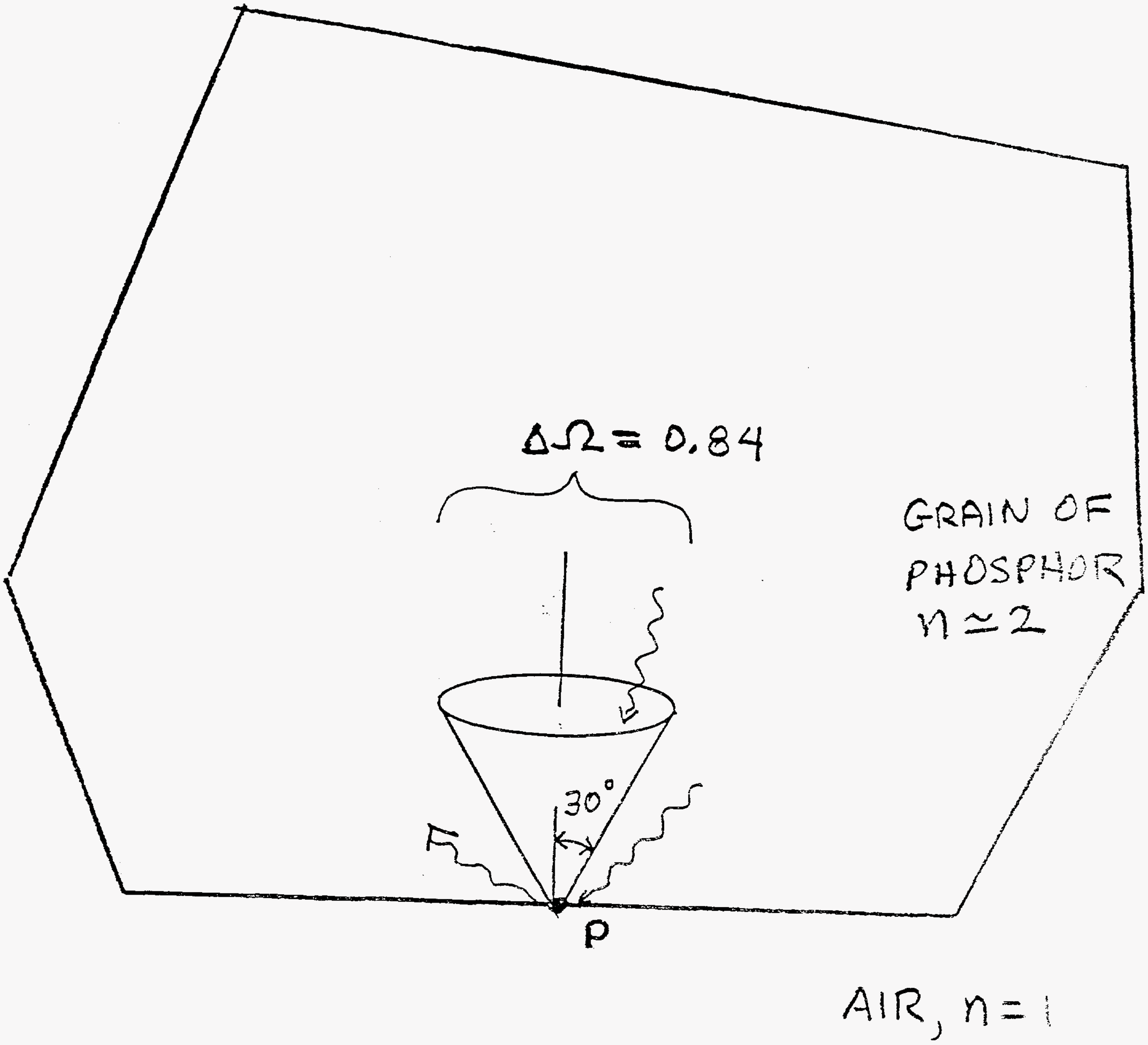

PROBABILITY FOR ESCAPE AT POINT P $= \dfrac{\Delta\Omega \text{ (STERAD)}}{2\pi \text{ (STERAD)}} = 0.13 \simeq \dfrac{1}{7.5}$

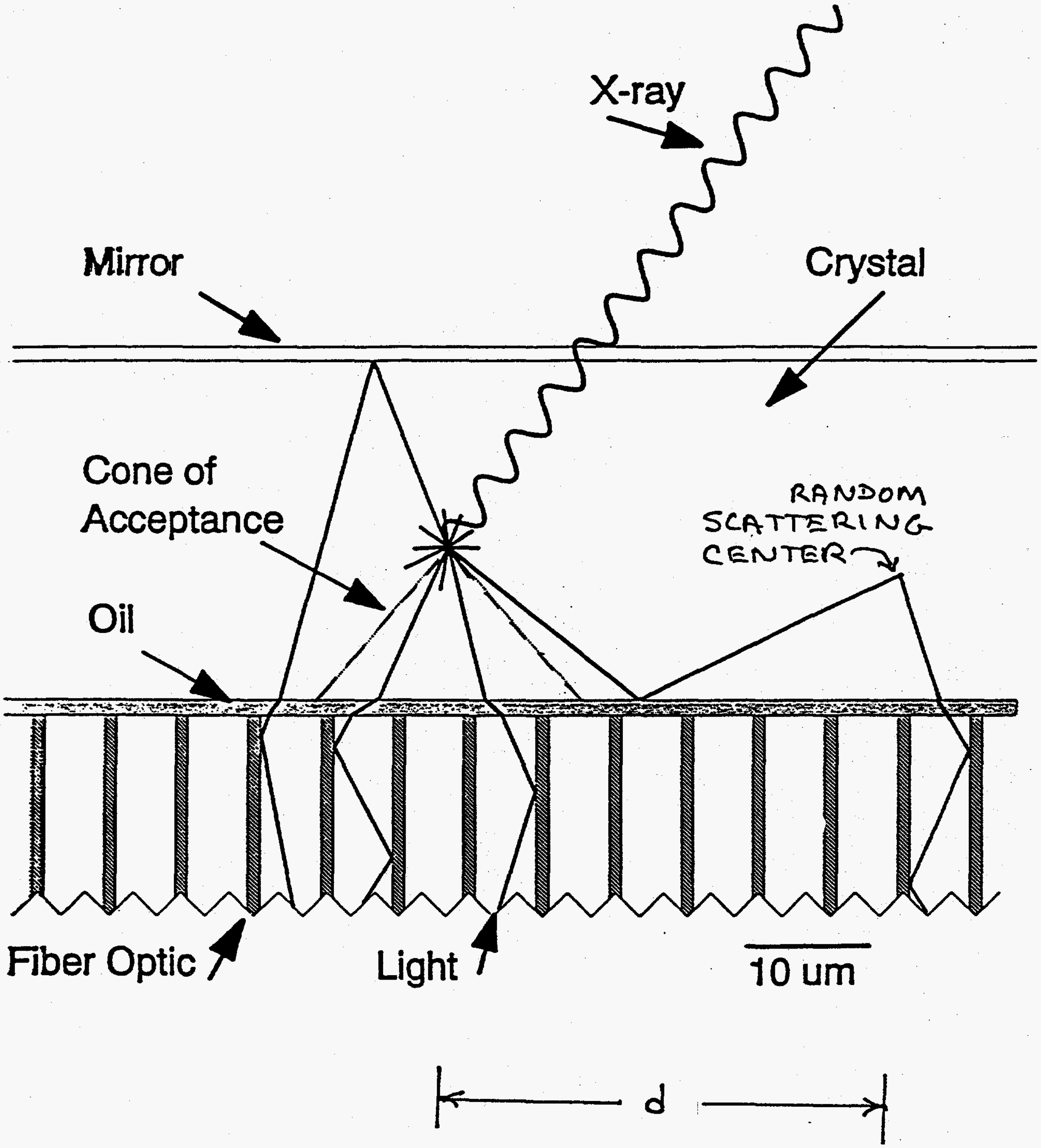

ATTENUATION $\sim e^{-Pd/c}$

C = XTAL ABSORP. LENGTH

$P \simeq 1$

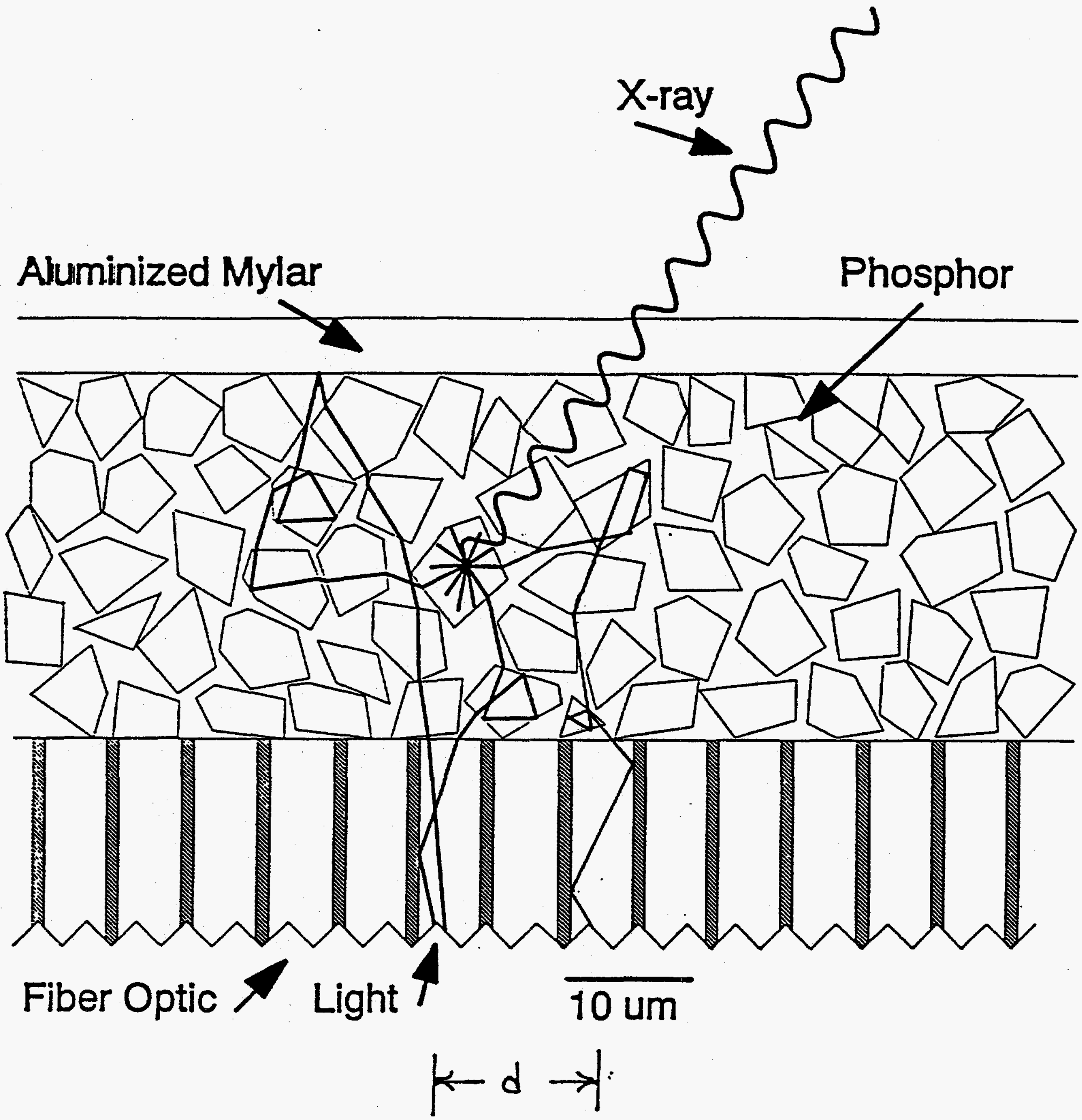

$d \simeq S\sqrt{N}$ S = STEP SIZE

N = # STEPS

$d_{TOT} = SN$

ATTENUATION $\sim e^{-\frac{d_{TOT}}{c}} = e^{-d^2/cS}$

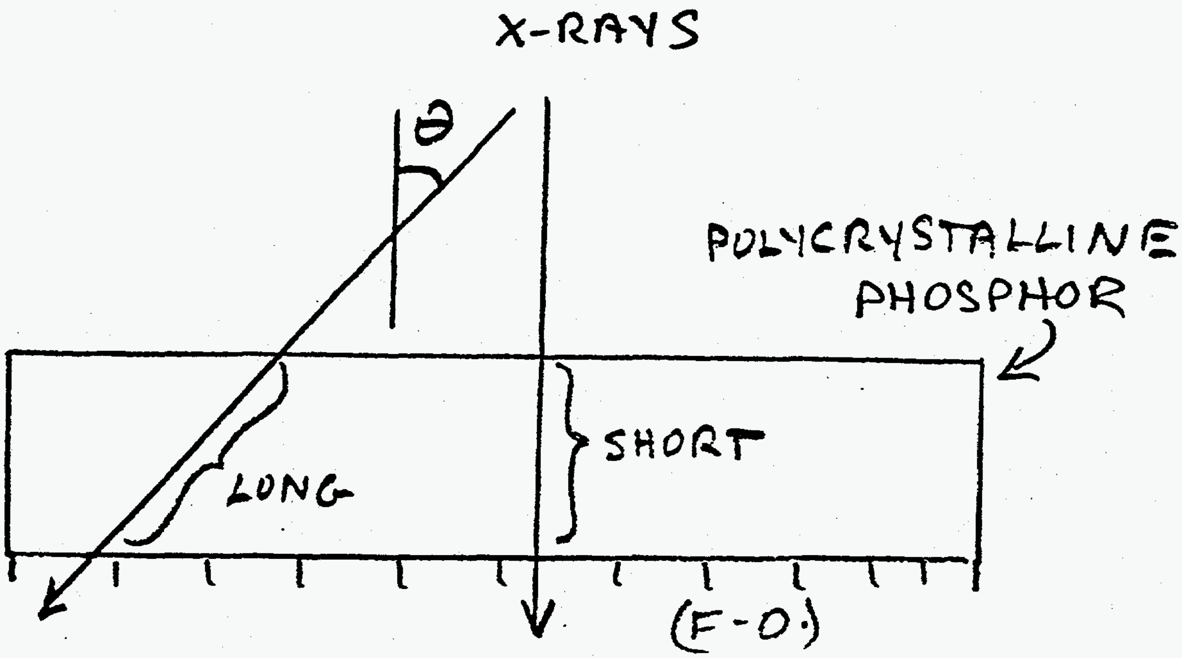

X-RAY TRANSPARENT LIMIT (λ SHORT)
STOPPING POWER INCREASES
∴ EFFICIENCY GOES <u>UP</u> AS θ <u>INCREASES</u>

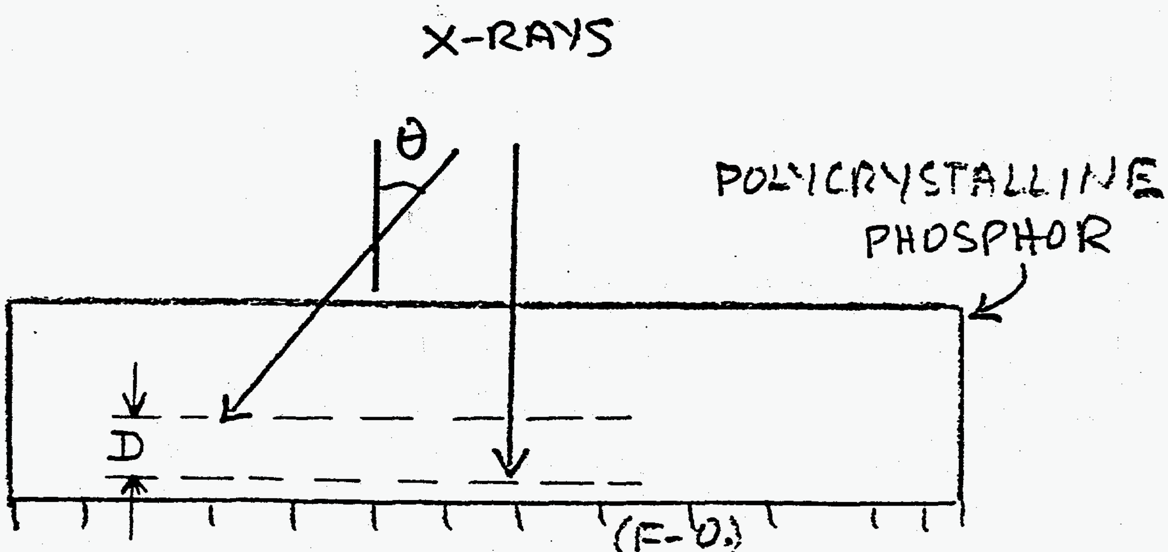

X-RAY OPAQUE LIMIT (λ LONG)
LIGHT PASSED TO F-OPTICS DECREASES
AS D INCREASES, i.e., AS θ INCREASES.
∴ EFFICIENCY GOES <u>DOWN</u> AS θ <u>INCREASES</u>

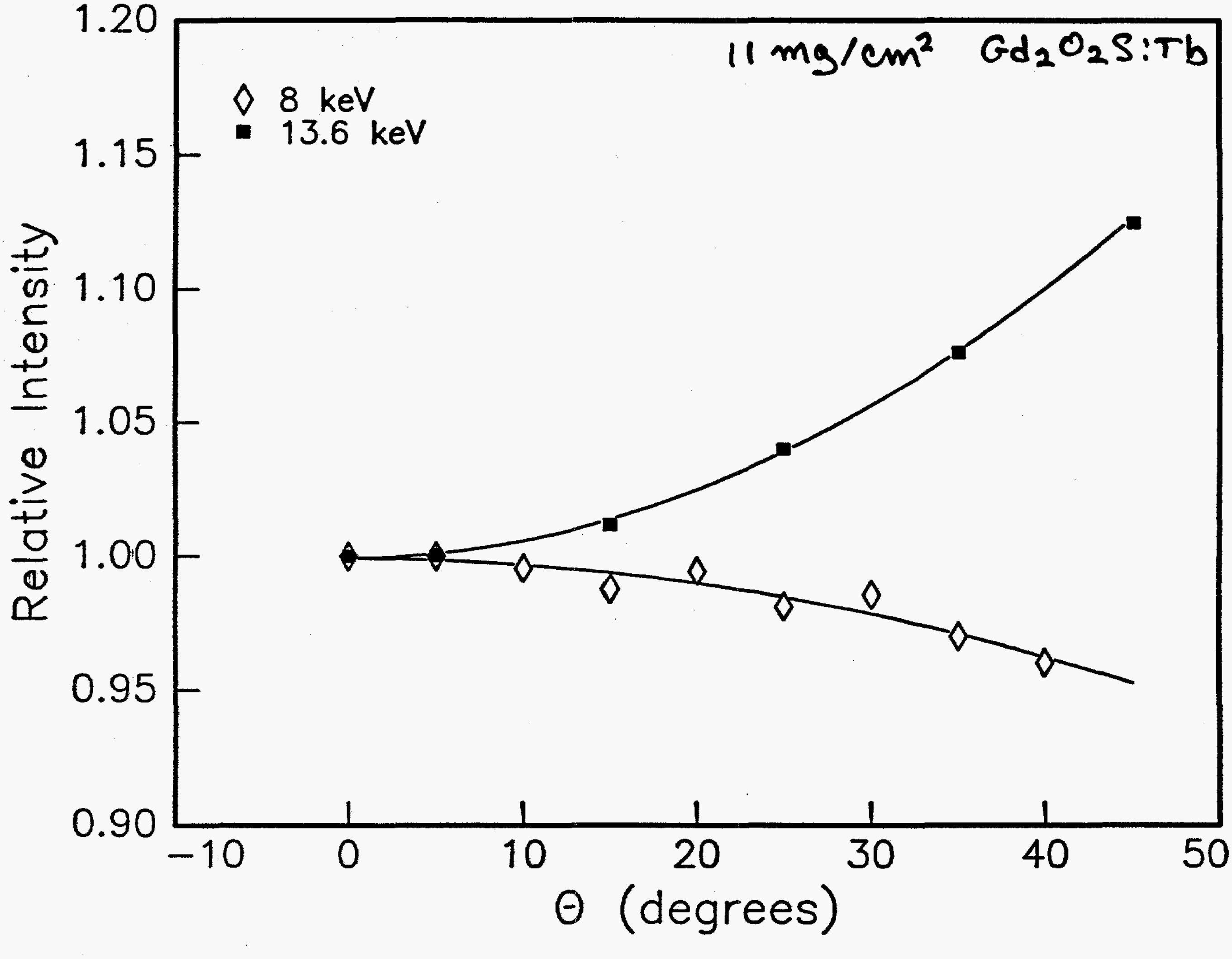

11 mg/cm² Gd₂O₂S:Tb
8 keV
13.6 keV
Relative Intensity
1.20
1.15
1.10
1.05
1.00
0.95
0.90
−10
0
10
20
30
40
50
Θ (degrees)

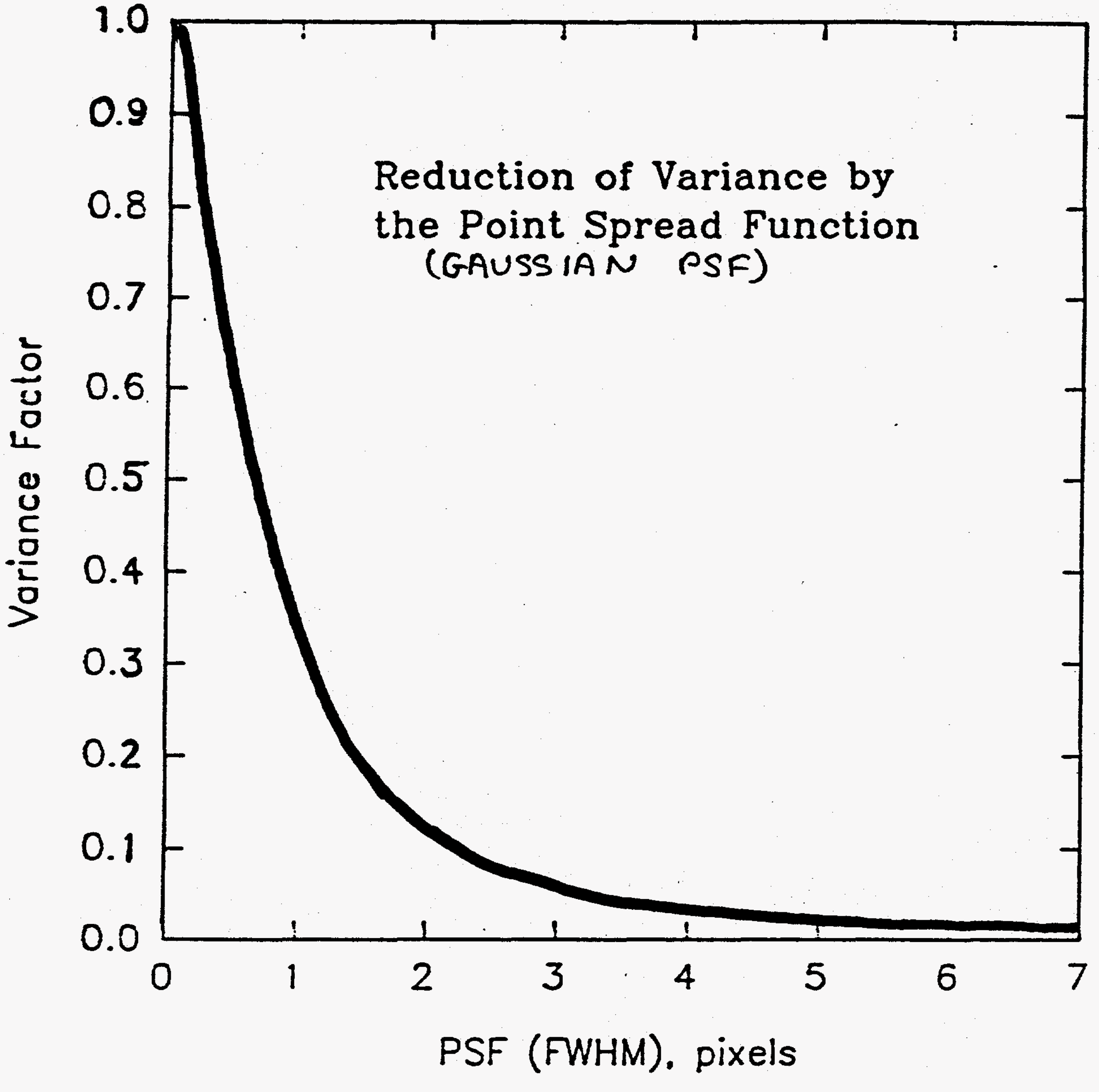

Reduction of Variance by
the Point Spread Function
(GAUSSIAN PSF)
1.0
0.9
0.8
0.7
0.6
0.5
0.4
0.3
0.2
0.1
0.0
Variance Factor
0
1
2
3
4
5
6
7
PSF (FWHM), pixels

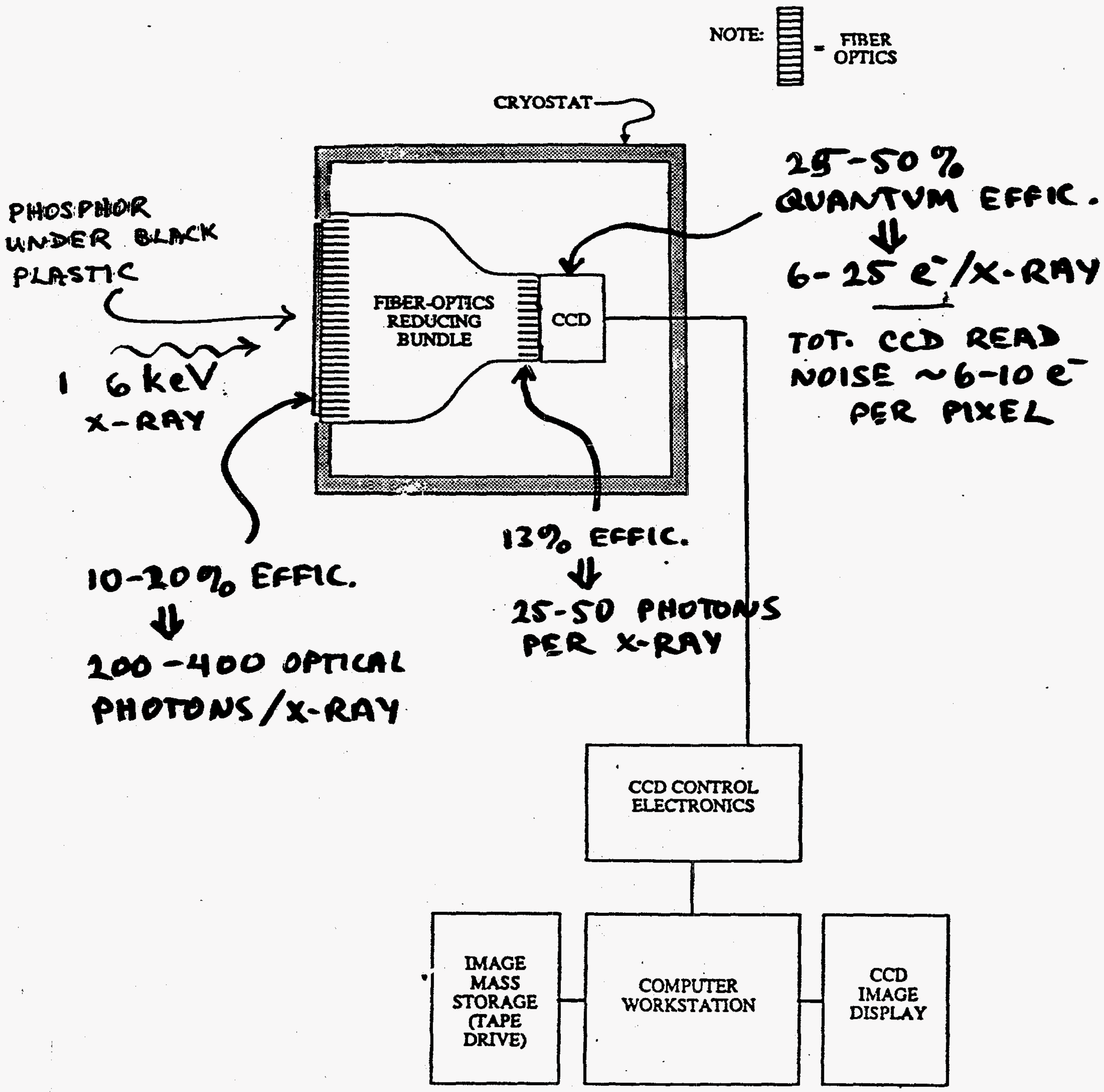
NOTE: = FIBER OPTICS
CRYOSTAT
PHOSPHOR UNDER BLACK PLASTIC
1 6keV X-RAY
FIBER-OPTICS REDUCING BUNDLE
CCD
25-50 % QUANTUM EFFIC.
6-25 e⁻/X-RAY
TOT. CCD READ NOISE ~6-10 e⁻ PER PIXEL
10-20% EFFIC.
200-400 OPTICAL PHOTONS/X-RAY
13% EFFIC.
25-50 PHOTONS PER X-RAY
CCD CONTROL ELECTRONICS
IMAGE MASS STORAGE (TAPE DRIVE)
COMPUTER WORKSTATION
CCD IMAGE DISPLAY

CCD	Thomson TH7896AVRNF
Pixel format	1024 × 1024
Fiber optic reduction ratio	2.6:1
Active input area	51 × 51 mm^2
Pixel size at phosphor (microns)	50.1
Phosphor	Gd_2O_2S:Tb
Operating temperature	−60 °C
A/D resolution (bits)	16
Gain (e^-/ADU)	4.6
Sensitivity (e^-/5.9 keV x-ray)	4.6
Read noise (e^-/pixel) RMS	8
Dark accumulation (e^-/pixel/s)	0.8 at −60 °C
Full well (e^-/pix)	4×10^5
Point spread (microns)	
full width half maximum	80
full width tenth maximum	165
full width hundredth maximum	230

TABLE II
Detector sensitivity vs. x-ray energy

X-ray energy (keV)	5.9	8.0	8.9	11.0	13.5	18.0
Fraction of x-rays stopped[1]	0.932	0.986	0.975	0.878	0.703	0.430
Signal/incident x-ray (e^-)	4.6	7.1	7.7	10.3	11.1	10.3
Signal/stopped x-ray (e^-)	4.9	7.2	7.9	11.7	15.8	24.0
Signal/stopped x-ray/Energy (e^-)	0.83	0.90	0.89	1.06	1.16	1.33
Quadratic response coefficient[2]	—	-3.5×10^{-5}	-2.2×10^{-5}	2.0×10^{-5}	6.0×10^{-5}	1.2×10^{-4}

[1] For 11.5 mg/cm^2 Gd_2O_2S:Tb phosphor.

[2] Quadratic coefficient, B, characterizing the change in detector response, R, as a function of angle as $R = 1 + B \times \theta^2$, where θ is given in degrees.

Thomson 1k DQE - 75 and 300 micron spots

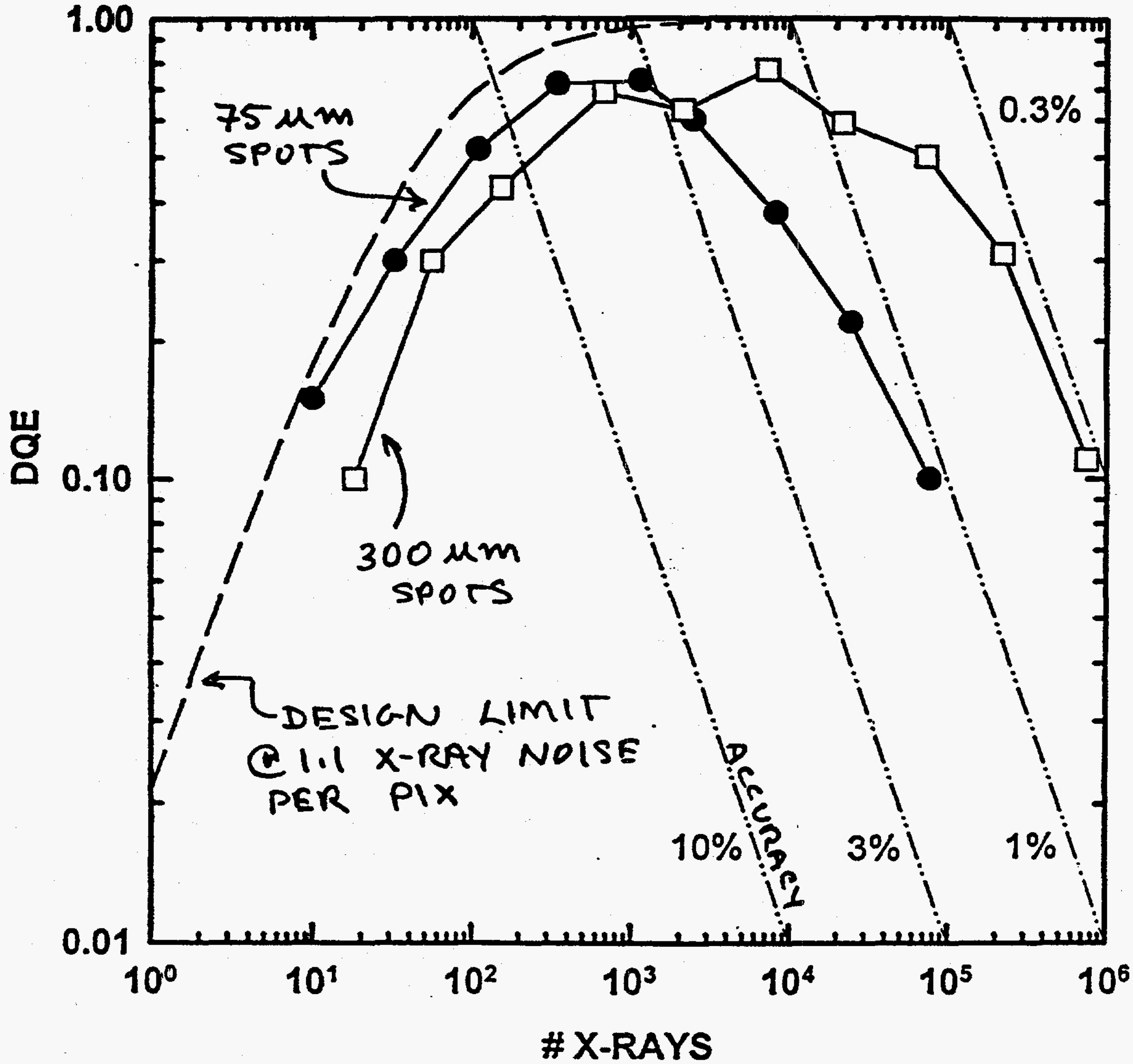

TBSV

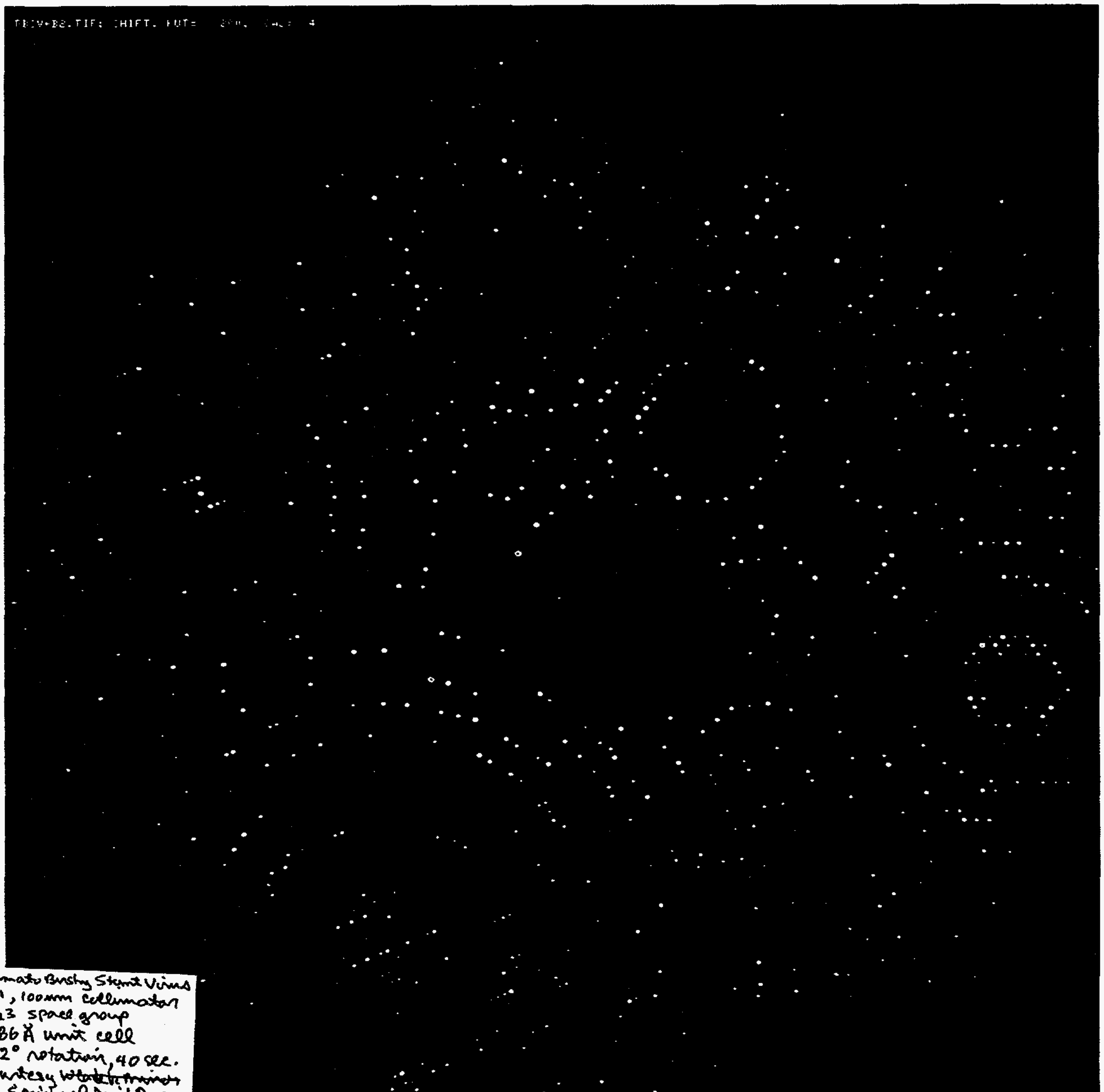

Tomato Bushy Stunt Virus
F1, 100mm collimator
I_23 space group
386 Å unit cell
0.2° rotation, 40 sec.
Courtesy ~~[illegible]~~
& ~~Michael~~ David Rogers
and Steve Harrison

PHI_X

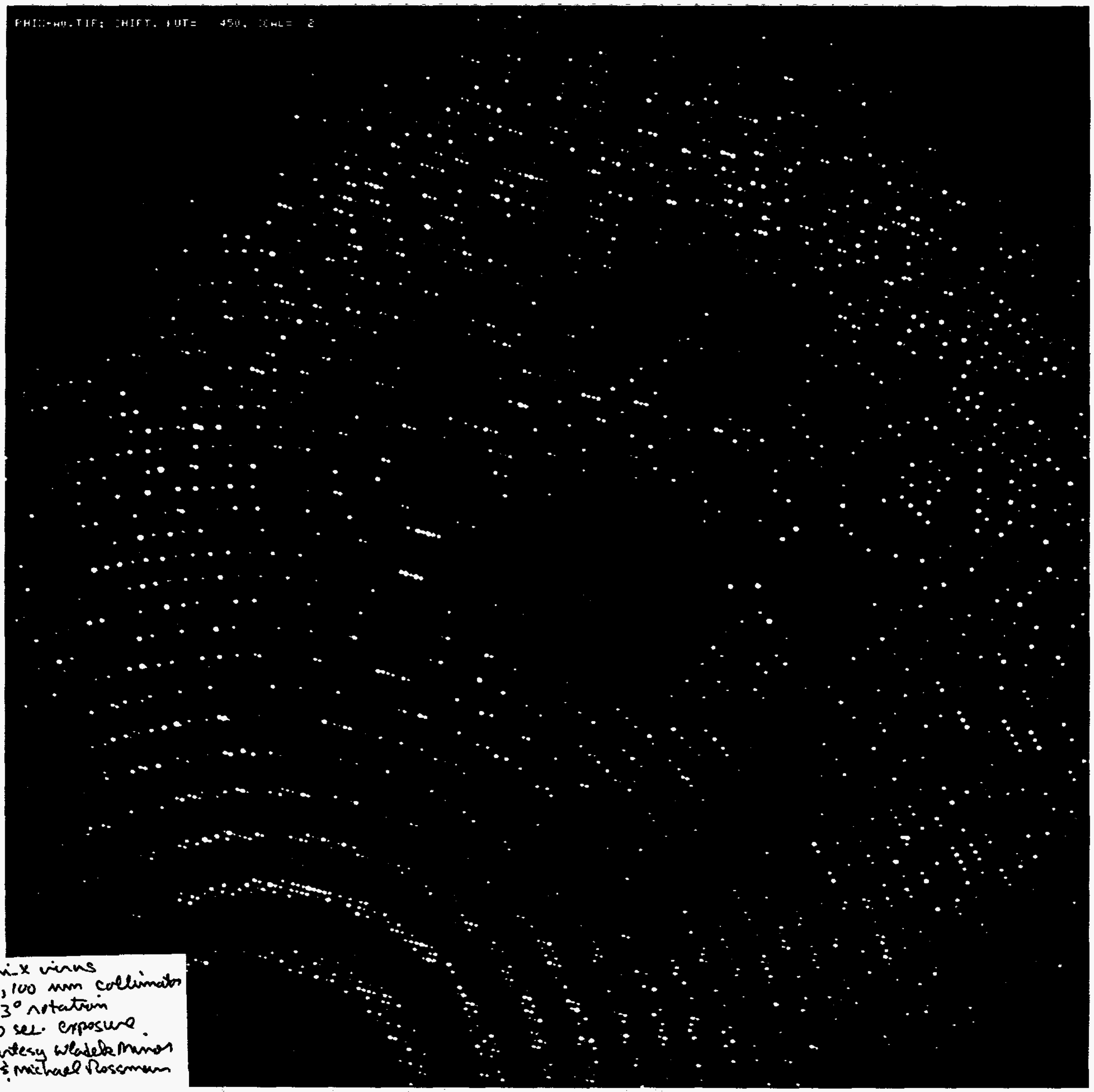

Phi_X virus
F', 100 mm collimator
0.3° rotation
30 sec. exposure.
Courtesy Wladek Minor
& Michael Rossmann

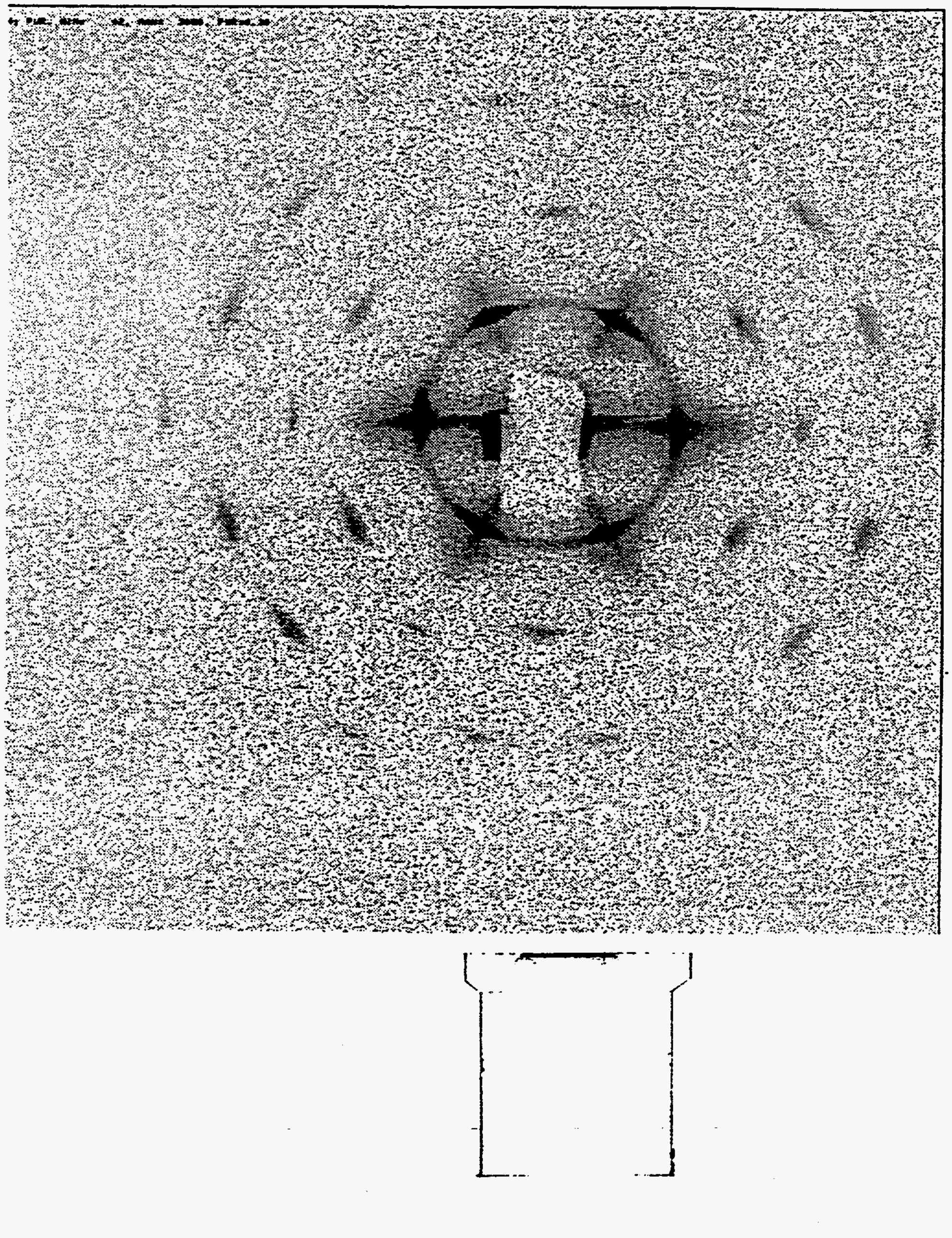

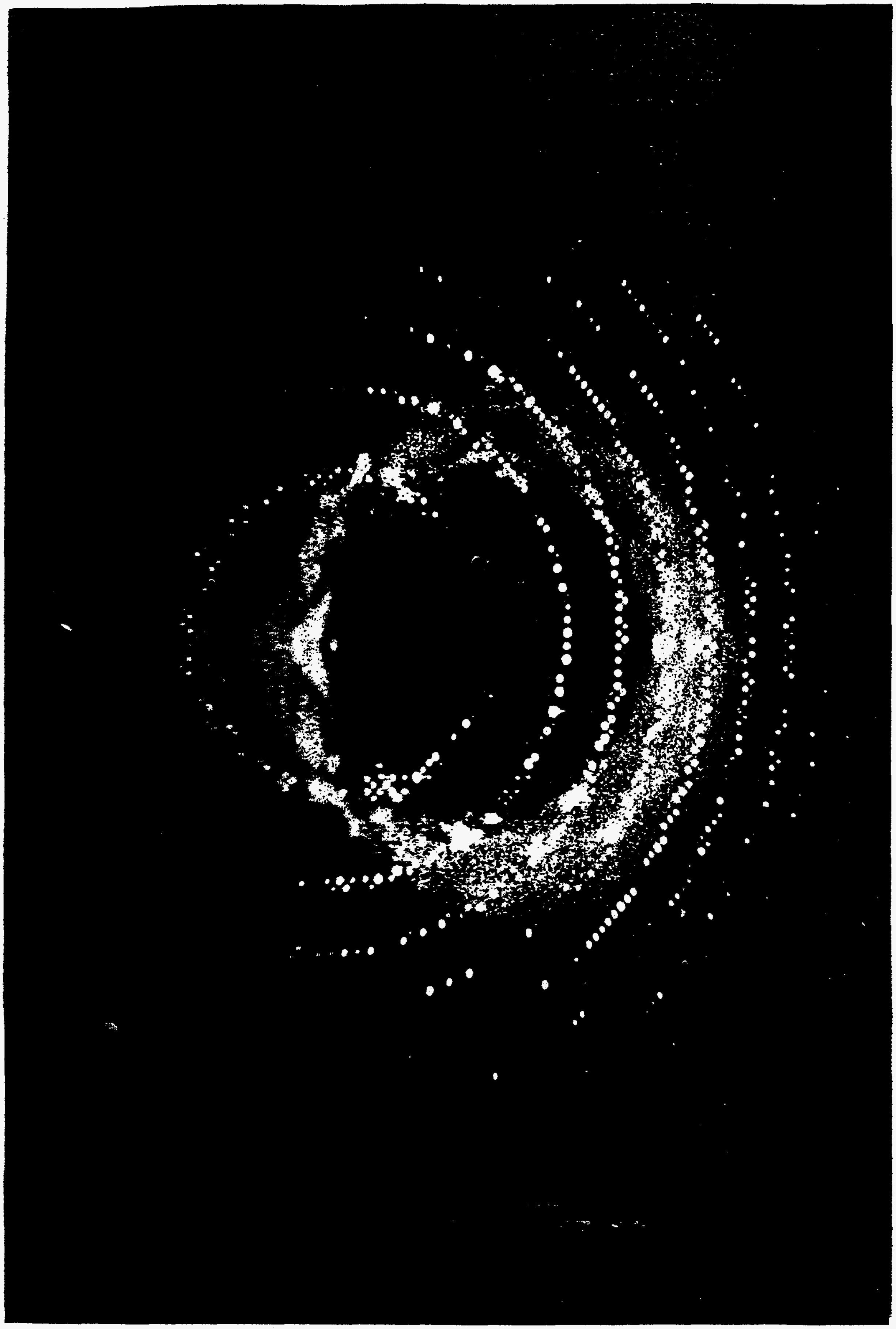

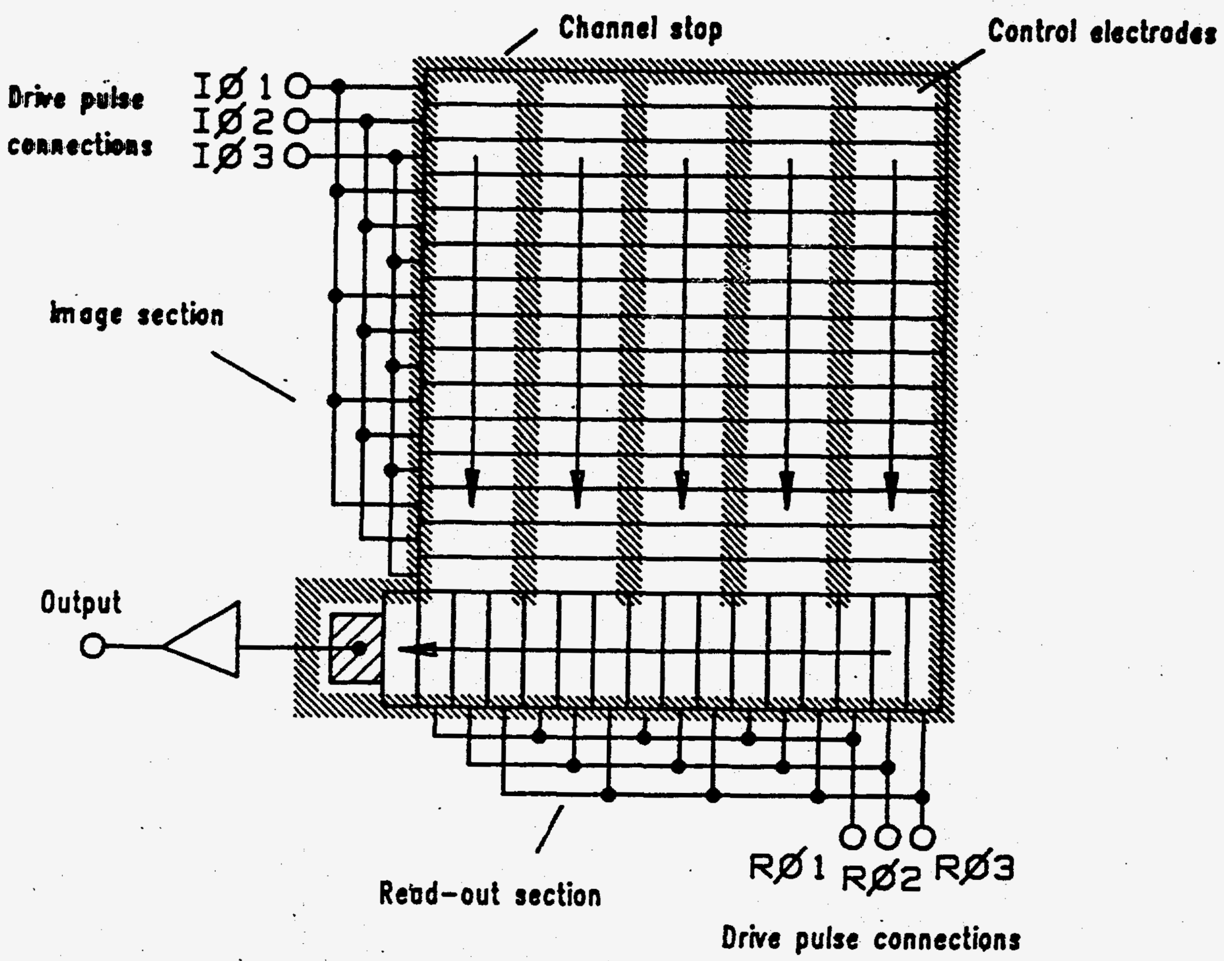

Fig. 1. Diagram of a basic CCD array.

D.J. BURT
NIM A305 (1991) 564

OSTERBERG, KRIECHBAUM, POLCYN, SKITA, TATE, SO, GRUNER & SHYAMSUNDER ERRAMILLI

Sample used in p-jump studies:

DOPE (Dioleoyl-phosphatidylethanolamine) in excess water. The morphology as a function of temperature T and pressure p includes two lamellar phases (gel phase L_β and the liquid crystalline phase L_α) and the inverted-hexagonal (H_{II}) phase as shown in the p-T phase diagram below. Static measurements have shown the existence of additional phases at high pressure in the L_β phase regime (P.T.C. So, Thesis, Princeton University, 1992)

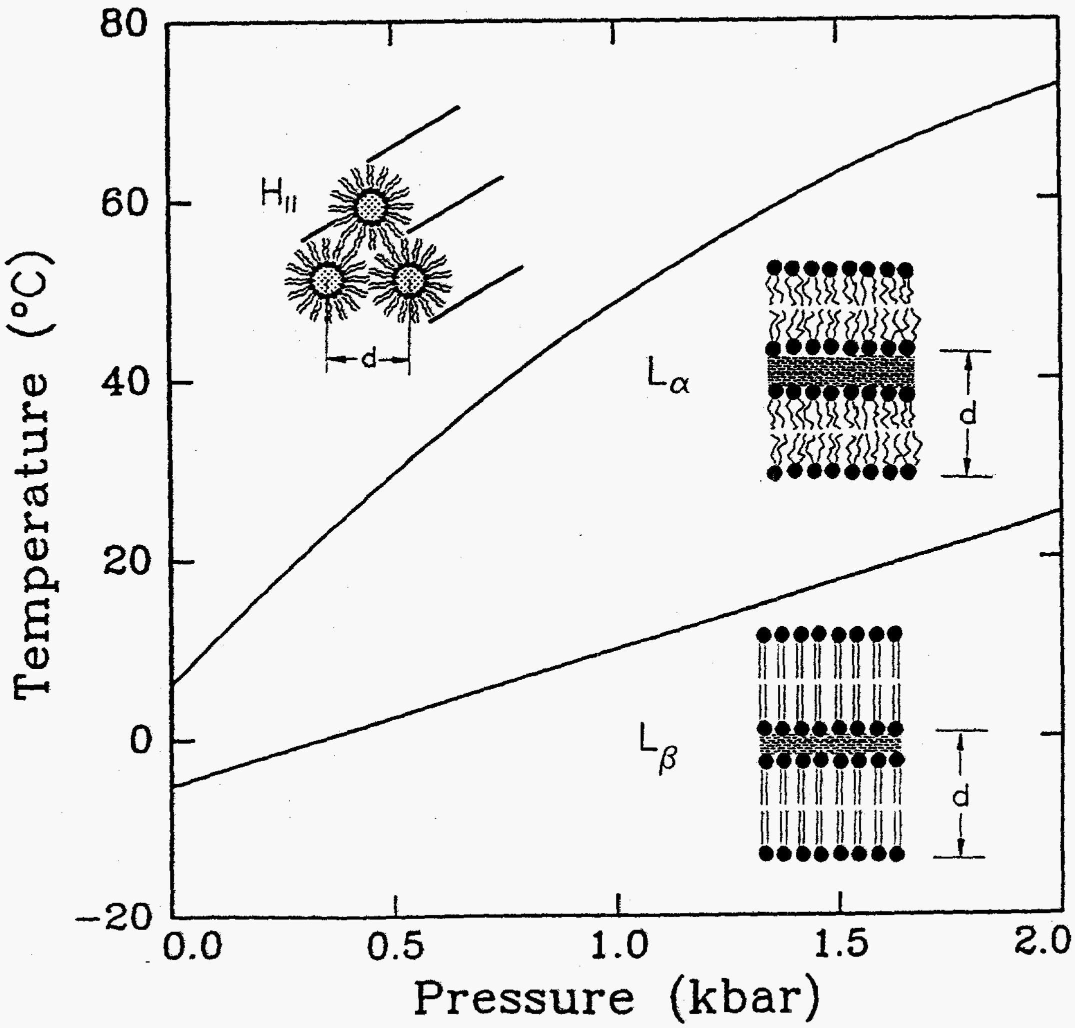

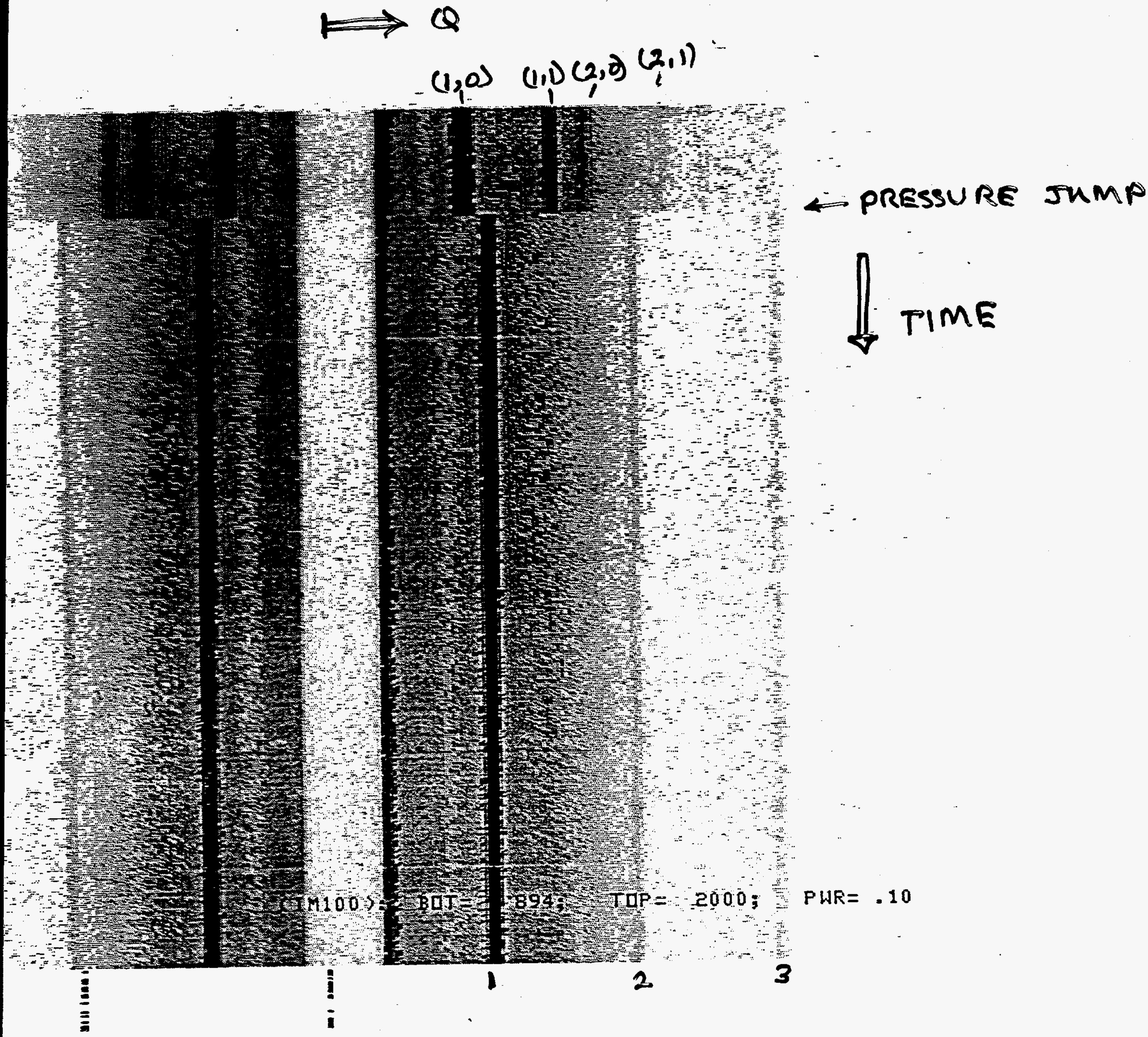

DOPE, EXCESS WATER, $H_{II} \rightarrow L_{\alpha}$
25°C, 102 BAR → 1935 BAR
9 ms/LINE

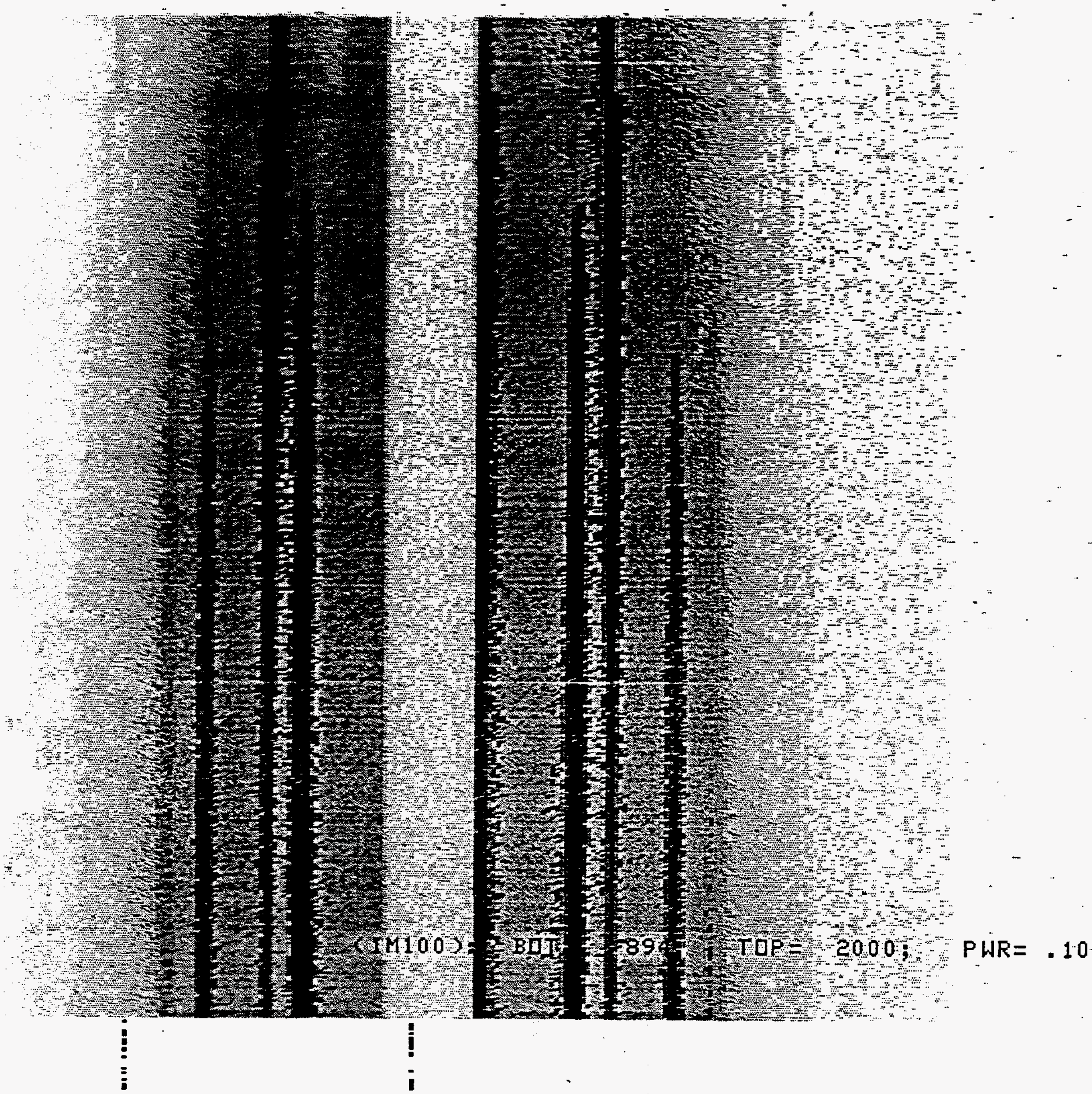

DOPE, EXCESS WATER, $L_\alpha \rightarrow H_{II}$
25 °C, 1895 BAR → 222 BAR
9 ms/LINE

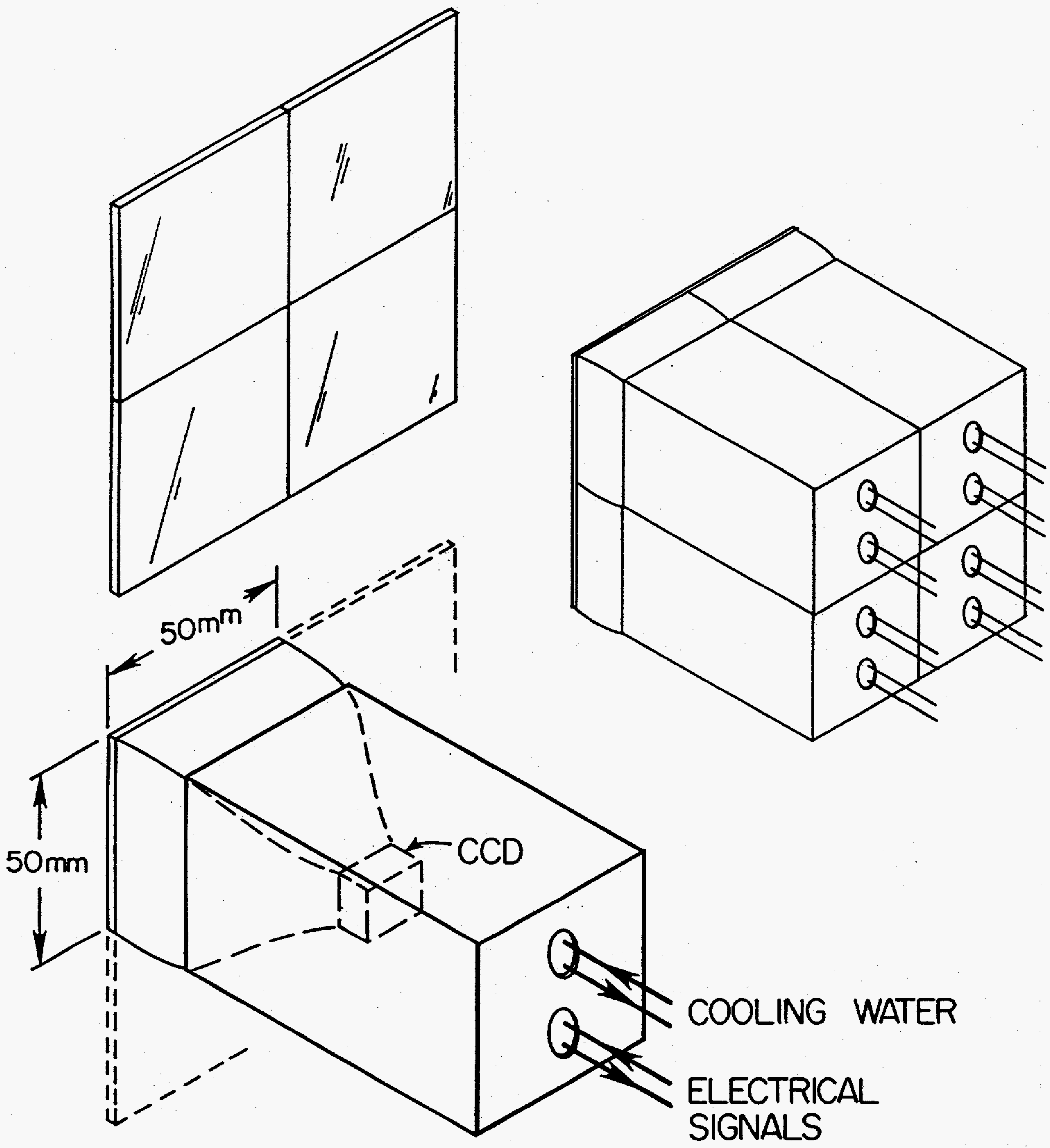
50mm
50mm
CCD
COOLING WATER
ELECTRICAL
SIGNALS

MOSAIC CONCEPT

ADVANTAGES

1) AVAILABILITY OF PARTS
2) MPP-CCDs REQUIRE LESS COOLING
3) AREA AND FORMAT ARE UNLIMITED
4) FLEXIBLE GEOMETRY OF AREA
5) NO NEW BASIC TECHNOLOGY NEEDED
6) HOME LAB/NAT. LAB TRANSITIONS EASED

TO DO

1) PACKAGING
2) CONTROL ELECTRONICS
3) SOFTWARE INTERFACE
4) DATA HANDLING
5) CALIBRATIONS
6) COST CONTAINMENT

mosaic1.doc

HOW FAST CAN WE DRIVE THE CCD?
1 MPIX/SEC IS DIFFICULT, BUT FEASIBLE.

CCD OUTPUT AMP LIMITS

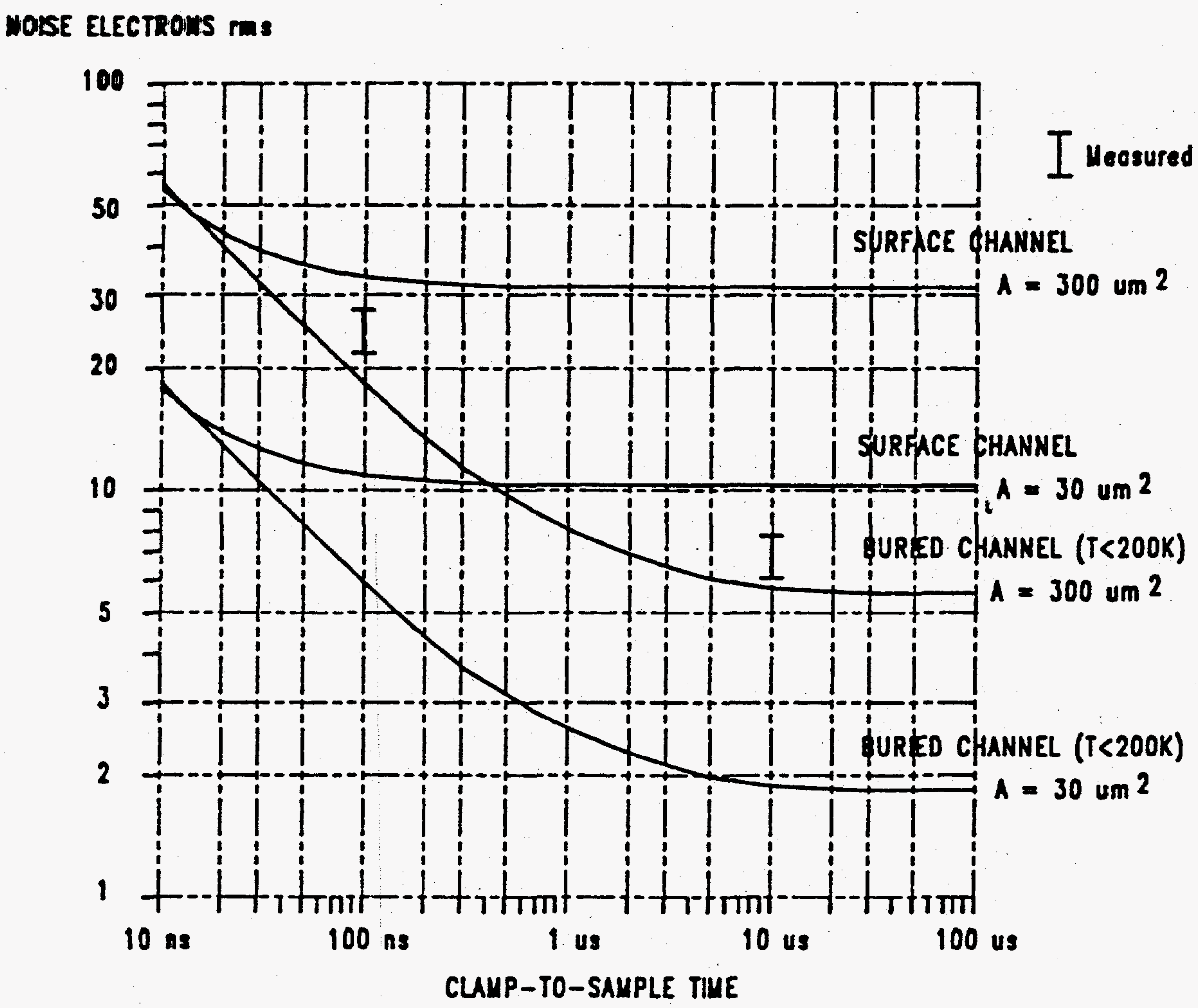

A = OUTPUT TRANSISTOR AREA.
300 μm^2 IS TYPICAL. IN PRACTICE 1MHz LOW NOISE OPERATION IS HARD TO ACHIEVE.

D.J. BURT
NIM A305 (1991) 564

NEEDED FUTURE WORK

1) BETTER PHOSPHORS

2) IMPROVED FIBER OPTICS

3) BETTER CALIBRATIONS

4) BETTER DATA HANDLING METHODS
(2000 x 2000 PIX/10 SEC) x (2 BYTES/PIX) x
(24 HRS/DAY) = 70 GBYTES/DAY

5) BETER USER EDUCATION

6) NEWER CCDs

7) MOSAIC DEVICES AND STRATEGIES

8) MORE BEAMLINE EXPERIENCE

FUTURE.APS

PRIMARY PARTICIPANTS:

SOL GRUNER -- PRINCETON U.
MARK TATE -- PRINCETON U.
ERIC EIKENBERRY -- RWJ MEDICAL SCHOOL

PETER EISENBERGER -- PRINCETON U.
JOHN SHEPHERD -- PRINCETON U.
SANDOR BARNA -- PRINCETON U.
MARTIN NOVAK -- PRINCETON U.
JOHN LOWRANCE -- PRINCETON SCI. INSTR.
STEVE EALICK -- CHESS
DON BILDERBACK -- CHESS
BRIAN RODRICKS -- APS

SUPPORT:

DoE -- MOSTLY
NSF -- A LITTLE BIT

FRIENDS.END

Istevan Naday

Argonne National Laboratory

and

Robert Street

Xerox

Amorphous Silicon-Based Imaging Detectors for Protein Crystallography

Two-dimensional amorphous silicon arrays have been developed in recent years primarily for liquid crystal displays and optical imagers. The novel aspect of the technology is the large size and low cost of the image sensor array. Present techniques allow an array size of about 10 in. x 10 in., but it is anticipated that 24 in. x 24 in. or larger will be possible in the future. Page size arrays with pixel sizes of 127 μm^2 have been made, although the technology is capable of even higher resolution. The arrays are made possible by the successful integration of field-effect thin film transistors (TFTs) and light sensors in large-area devices. Each pixel contains an amorphous silicon photodiode, connected to a TFT, controlled by the matrix of gate and data lines that cross the whole array. The parameters of the imager and readout electronics have been studied by computer simulation. The two most significant sources of the readout noise are the thermal noise of the "on" resistance of the TFT and the noise of the readout electronics. The simulation confirmed the already demonstrated 1000-2000 electron read noise figure. The intrinsic dynamic range of the imaging array is about 10^5. The minimum readout time of about 25 msec allows real-time imaging.

X-ray images are obtained by exposing arrays that are in contact with a phosphor/scintillator. Contact imaging allows the imager to collect light very efficiently, making it well suited to x-ray imaging. Medical applications of this technology for imaging during radiation therapy, fluoroscopic, and radiographic procedures appear very promising. In protein crystallography, the large size and high conversion gain of the imager will offset the effect of the higher read noise. The expected Detective Quantum Efficiency of a large-area amorphous silicon x-ray detector for protein crystallography will be better than 50%.

Amorphous Silicon Detectors for Protein Crystallography

Robert STREET, XEROX Electronics Materials Labs.
Istvan NADAY, ANL Electronics and Computing Technologies
Stephen ROSS, ANL Electronics and Computing Technologies

254

APS Workshop

Detectors for Third-Generation Synchrotron X-Ray Sources

February 14-15, 1994
Argonne National Laboratory

Amorphous Silicon detectors for Protein Crystallography

- **Advantages compared to CCD detectors:**
  - much lower cost of basic detector
  - can be made physically large
  - no fiber optics, less spatial distortion
  - tolerant of higher dosages of radiation (direct detection)
- **Disadvantages**
  - limited availabilty -- its a new material
  - higher readout noise
  - larger pixels, lower resolution
  - concern over longterm stability of material
  - small amount of image lag

Goals of initial ANL a:Si-H Detector work

- **Establish its reliablity at a working protein crystallography synchrotron beamline.**
- **Perform basic studies of how the imager behaves**
  - develop general performance (especially noise) models and measure device parameters
  - determine to effect of direct phosphor deposition
  - measure effects of temperature
- **Get experience with the engineering aspects of making an a:Si-H detector**
  - reliable connections to glass plate
  - trial designs and packaging of the many parallel readout amplifiers
  - possible integration of readout electronics using custom integrated circuited (e.g. MOSIS foundry)

Amorphous silicon has been previously used or proposed for various nuclear detectors.

- U. Michigan/Xerox collaboration to develop the array for radiation oncology diagnostics (Antonuk et. al.)
- X-ray and beta detection with CsI + a-Si photodiodes (Fujieda et. al., Xerox)
- Neutron detection (proposed), (Mireshighi et. al., LBL)

Status of a:Si-H work at ANL

- **Models developed to predict performance of a -Si based detector for crystallography**
  - Analytical and PSPICE detector plus electronics noise models.
  - Spreadsheet to predict DQE, SNR given electronics noise, allow quick trades involving exposure times, detector placement, temperature.
- **Consideration given to layout of the detector**
  - electrical connection to the glass substrate
  - means to cool and support the array
- **Phosphor deposition studied**
  - deposition on array or on fiberoptic faceplate
- **Consideration given to readout electronics**
  - circuitry necessary to optimize readout to improve SNR via changes in filtering and timing
  - physical layout of the large numbers of readout amplifiers

Requirements for Protein crystallography drive the performance of the detector.

- Crystal structure R factor requirement sets minimum SNR
- Total Radiation Dose to Crystal sets total exposure time to X-ray beam
- Crystal unit cell size sets pixel resolution
- Maximum Bragg angle of interest sets the total sampled area

Dominant Noise Sources

- Thin film a:Si-H FET "on" resistance thermal noise during reset of the sensor capacitance (kTC noise)
  - may be removed by double sampling of video at the expense of additional operational amplifier read noise.
- Thin film FET "on" resistance thermal noise during the readout of the sensor charge (modified by readout bandwidth)
  - may be filtered at the expense of circuit complexity
- Operational amplifier voltage read noise.
  - may be filtered at the expense of circuit complexity

Gold CCD vs. a:Si-H

• array size cm	15	28
• pixel size, um	50	120
• xray/sec/pix	50	120
• exposure time, sec	1	3.5
• exposures/xtal	3.5	1
• signal in, xrays	50	420
• electron out/xray in	13.2	188
• electron out/pixel	660	78000
• electronic noise/pixel	15	3000
• binning of pixels	5x5	2x2
• binned signal out, electrons	16500	314000
• binned electronic noise eRMS	75	6000
• binned dark electrons	150	1100
• noise w/o electronics eRMS	525	11800
• total noise out eRMS	530	13300
• SNR out (Binned pixels)	31	24
• SNR in (Binned pixels)	35	41
• DQE (Binned pixels)	.77	.33

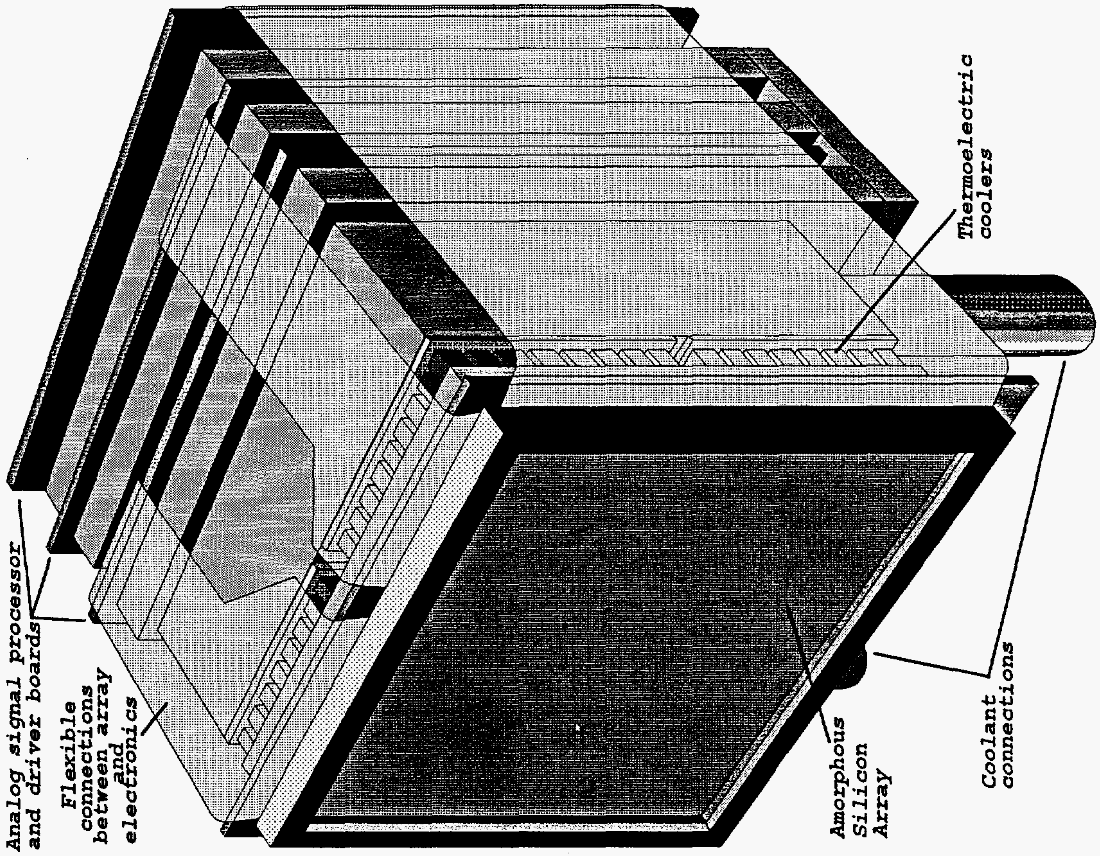
Analog signal processor and driver boards
Flexible connections between array and electronics
Amorphous Silicon Array
Coolant connections
Thermoelectric coolers

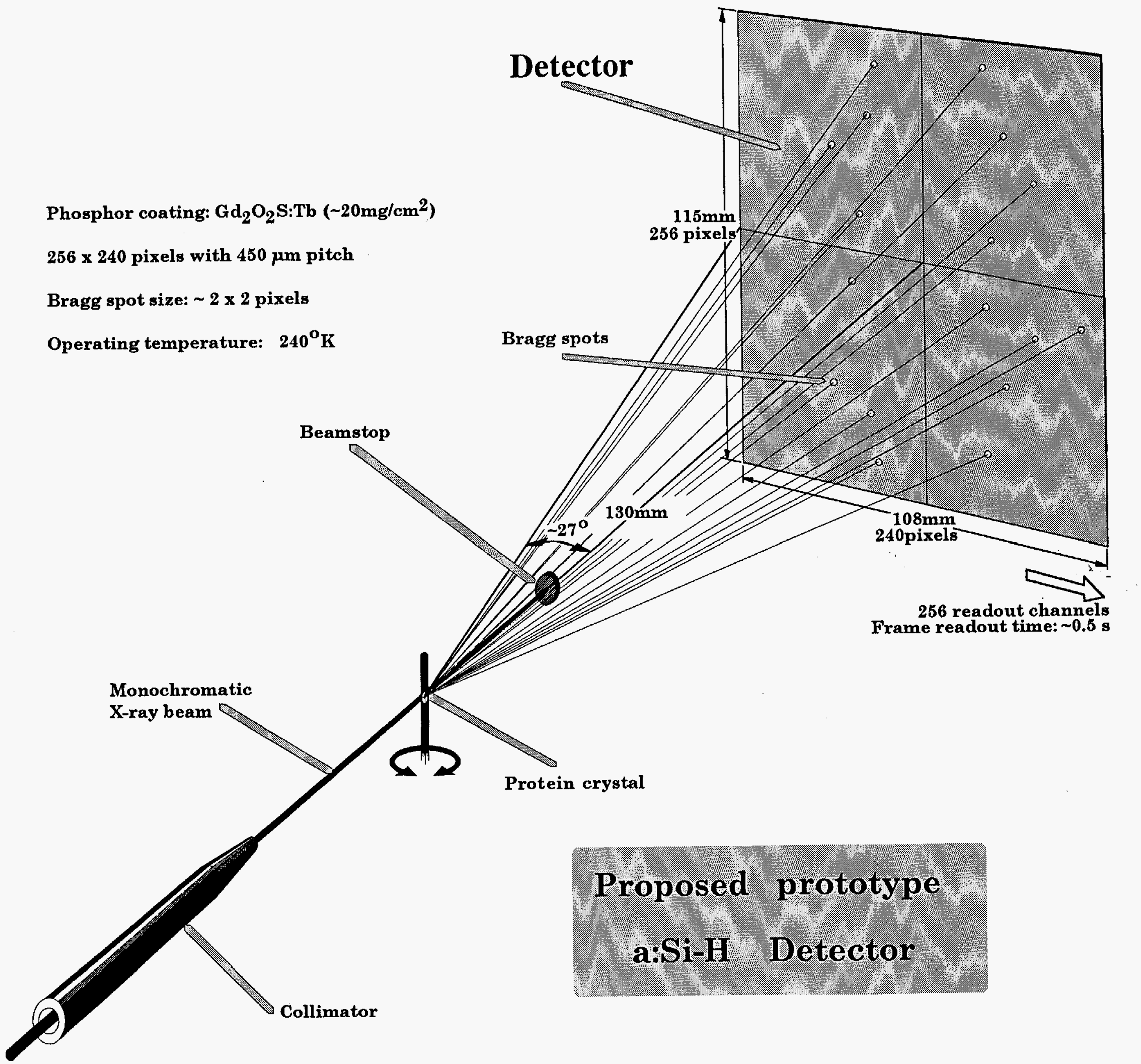
Detector
Phosphor coating: Gd_2O_2S:Tb (~20mg/cm^2)
256 x 240 pixels with 450 μm pitch
Bragg spot size: ~ 2 x 2 pixels
Operating temperature: 240^{o}K
115mm
256 pixels
Bragg spots
Beamstop
~27°
130mm
108mm
240pixels
256 readout channels
Frame readout time: ~0.5 s
Monochromatic
X-ray beam
Protein crystal
Collimator
Proposed prototype
a:Si-H Detector

AMOR10.XLS Chart 26

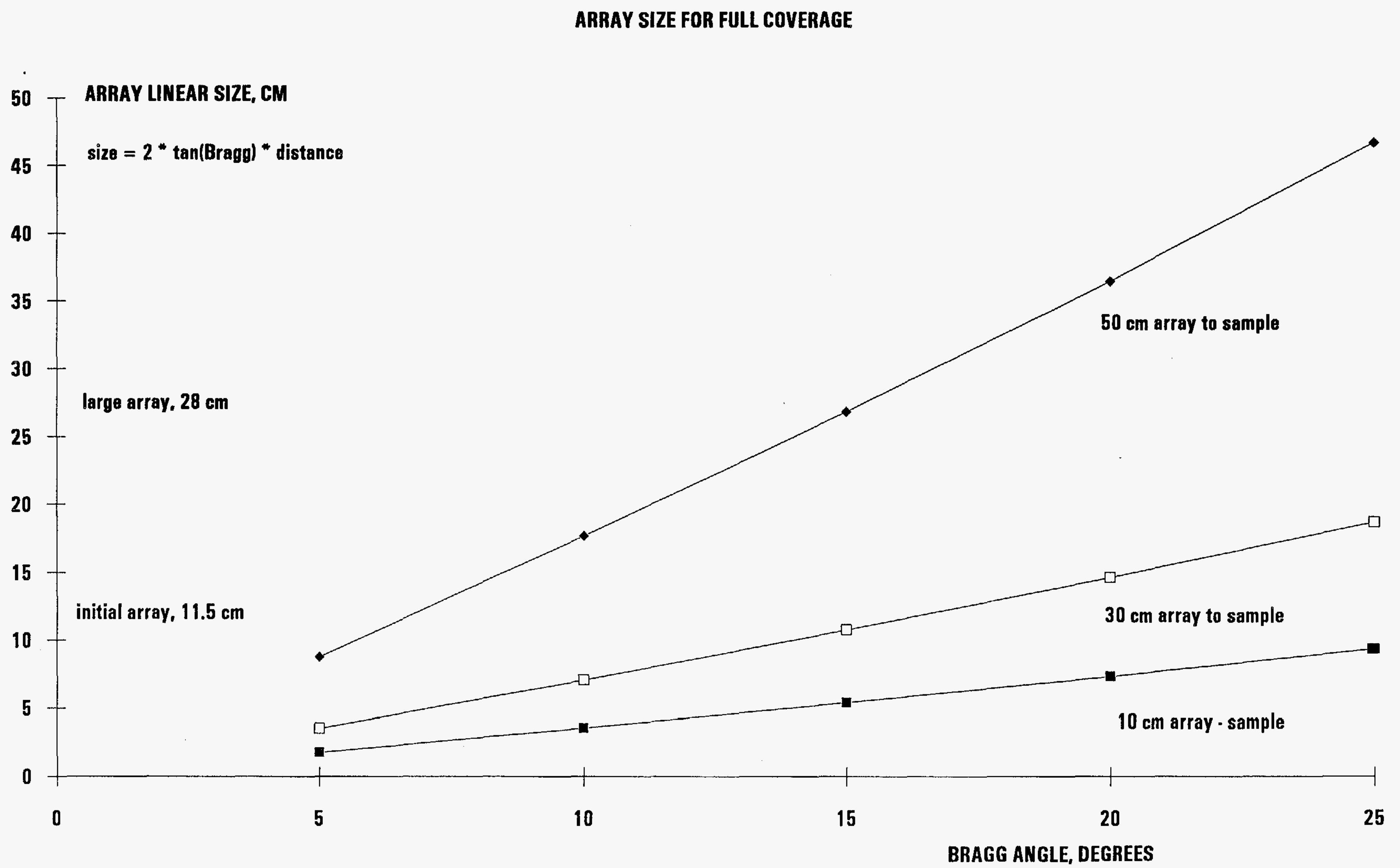

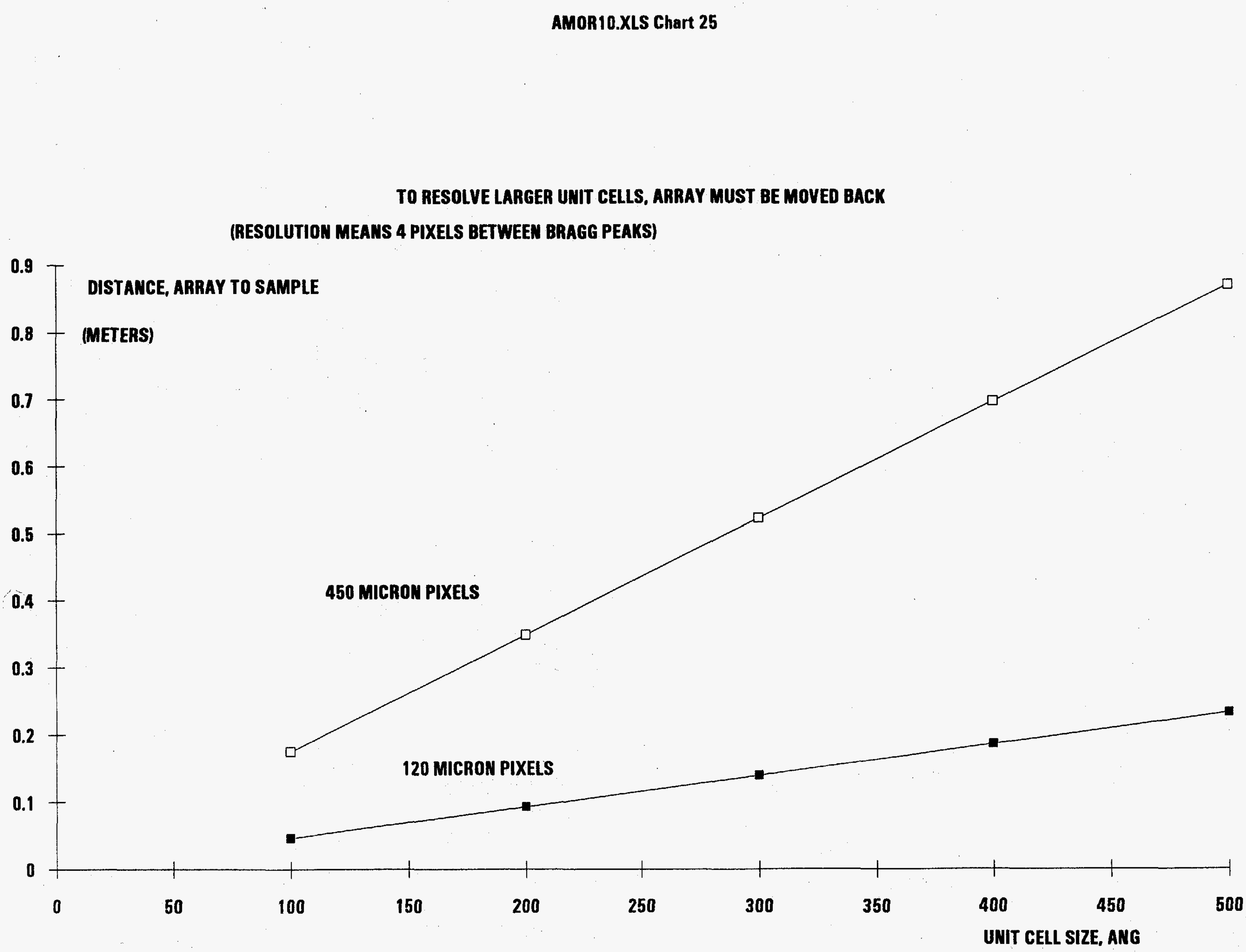
AMOR10.XLS Chart 25
TO RESOLVE LARGER UNIT CELLS, ARRAY MUST BE MOVED BACK
(RESOLUTION MEANS 4 PIXELS BETWEEN BRAGG PEAKS)
DISTANCE, ARRAY TO SAMPLE
(METERS)
450 MICRON PIXELS
120 MICRON PIXELS
0.9
0.8
0.7
0.6
0.5
0.4
0.3
0.2
0.1
0
0
50
100
150
200
250
300
350
400
450
500
UNIT CELL SIZE, ANG

AMOR10.XLS Chart 28

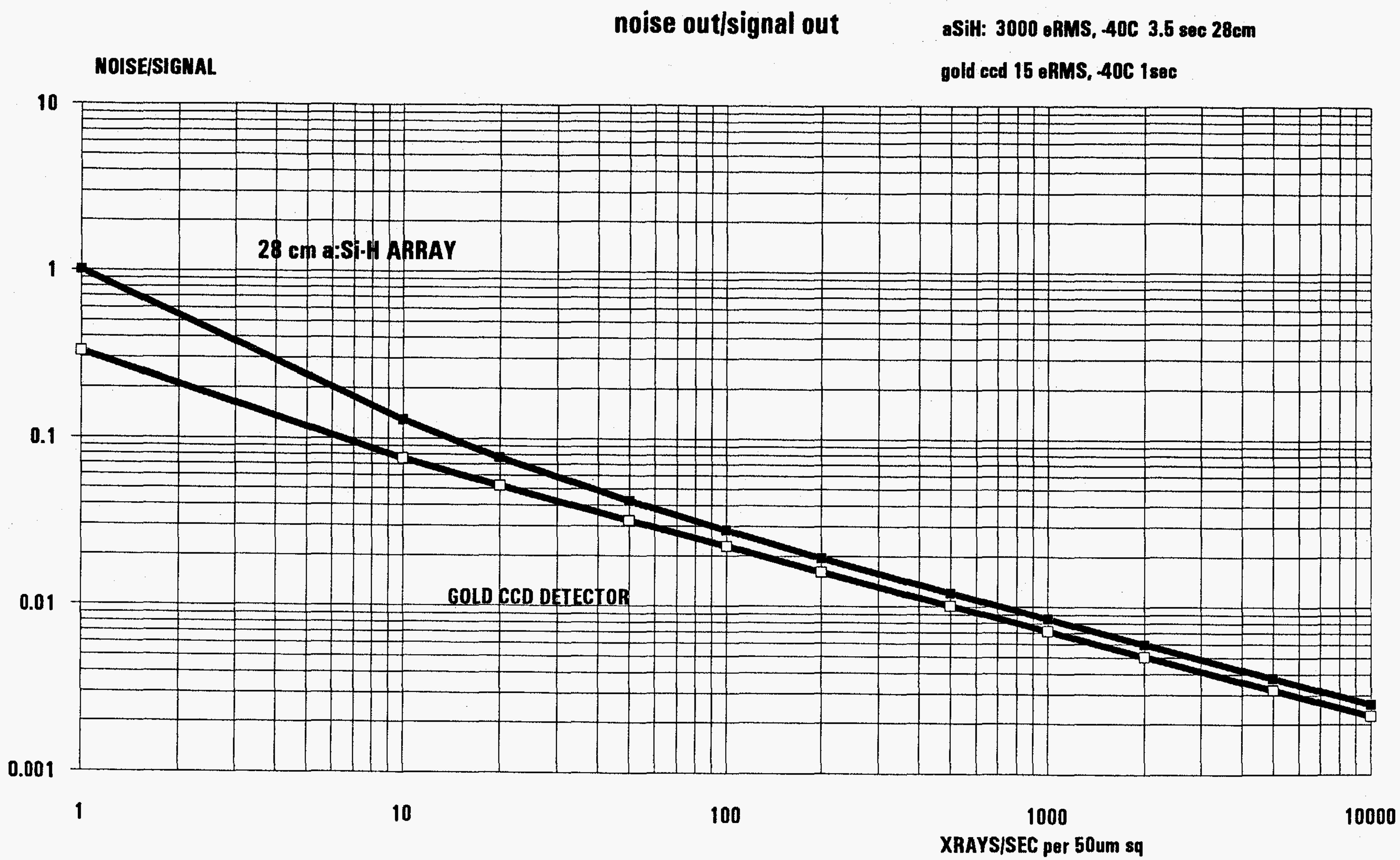

AMOR10.XLS Chart 23

Relative Variance is determined by Xray counts and DQE

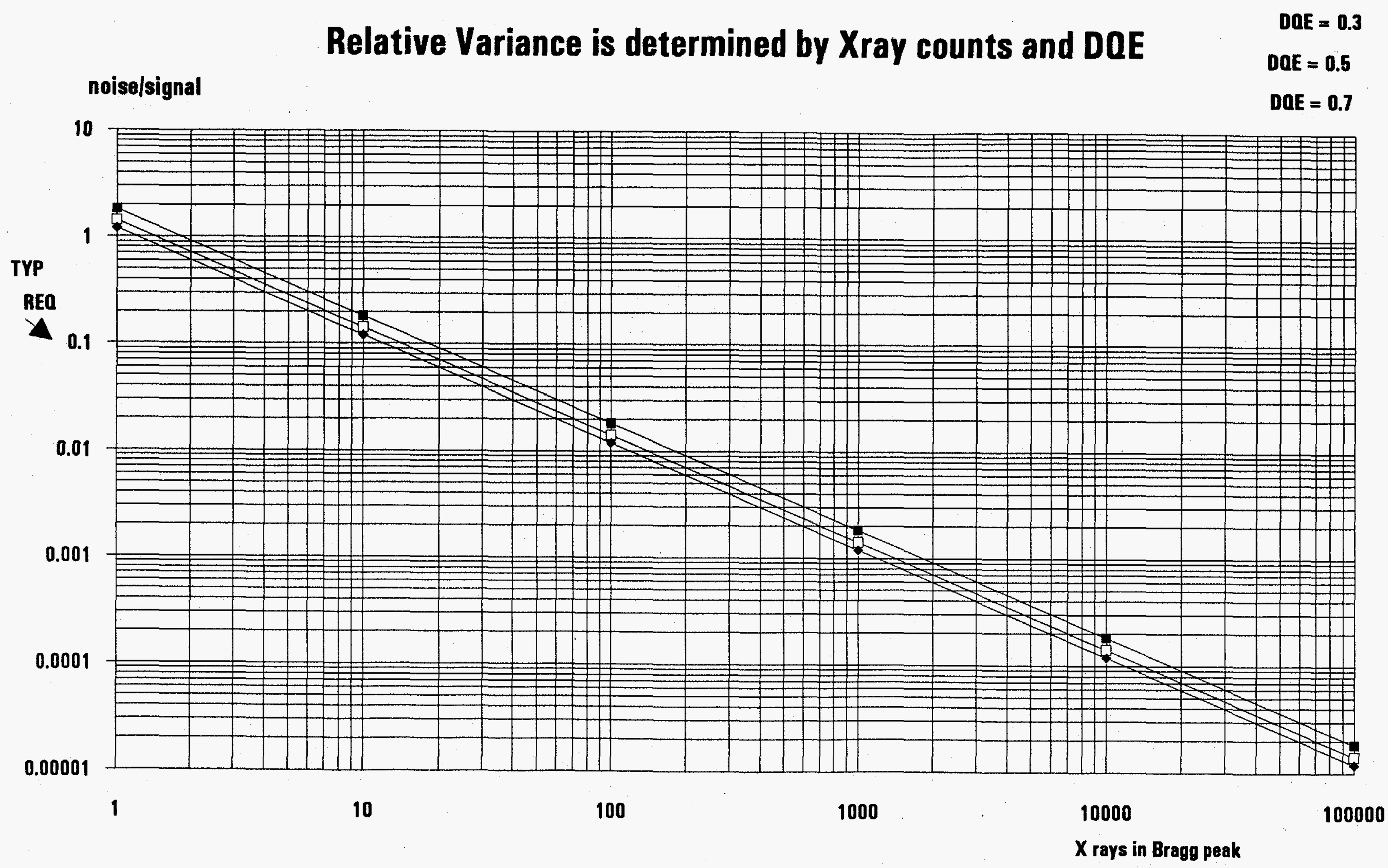

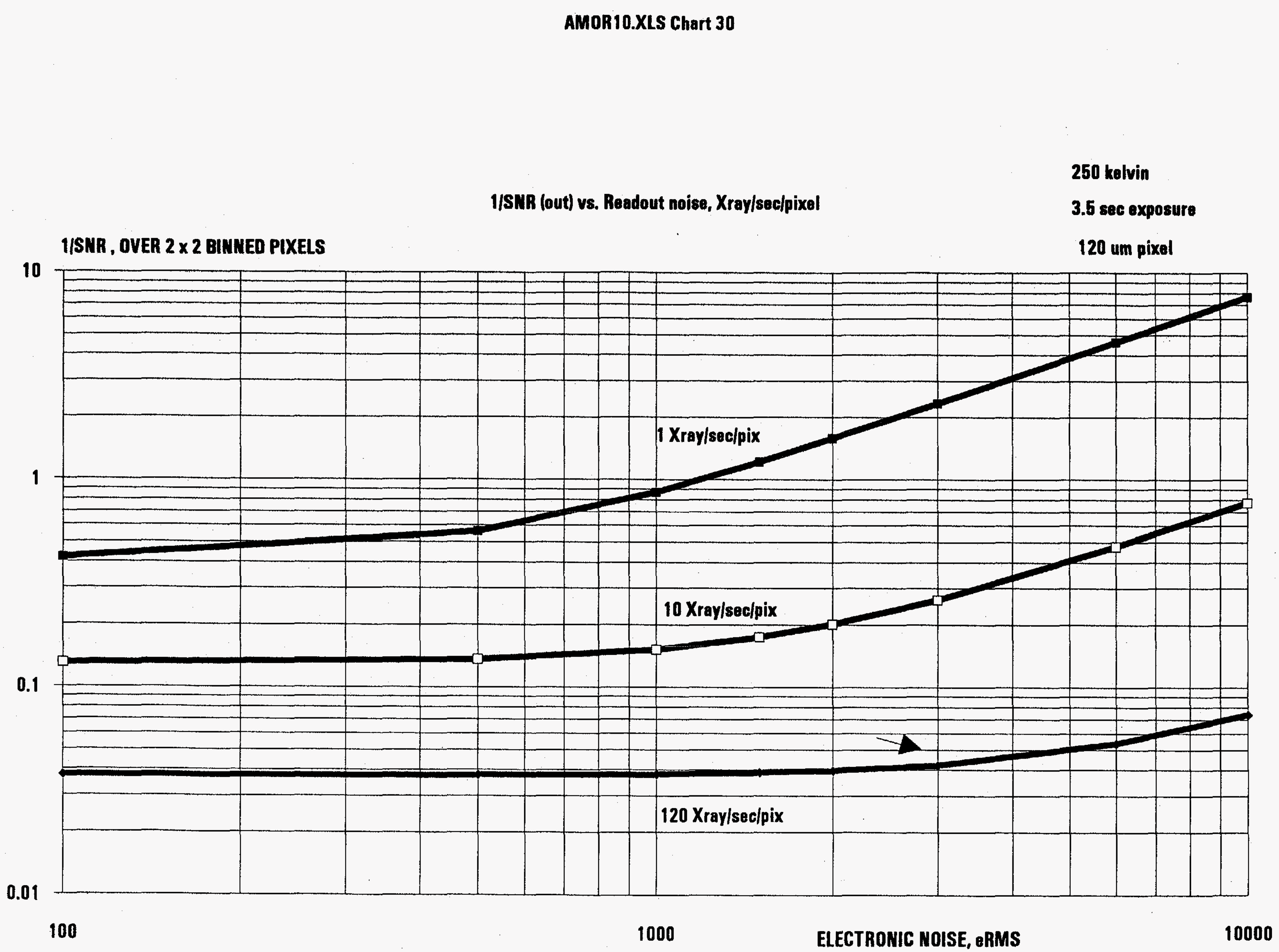

AMOR10.XLS Chart 30
1/SNR (out) vs. Readout noise, Xray/sec/pixel
250 kelvin
3.5 sec exposure
120 um pixel
1/SNR , OVER 2 x 2 BINNED PIXELS
10
1
0.1
0.01
100
1000
10000
ELECTRONIC NOISE, eRMS
1 Xray/sec/pix
10 Xray/sec/pix
120 Xray/sec/pix

Amorphous silicon detectors

Bob Street, Xerox PARC; Steve Naday, ANL

- Large area amorphous silicon matrix addressed arrays

- Applications to Protein Crystallography

XEROX PARC

The Sensor Array is Matrix Addressed

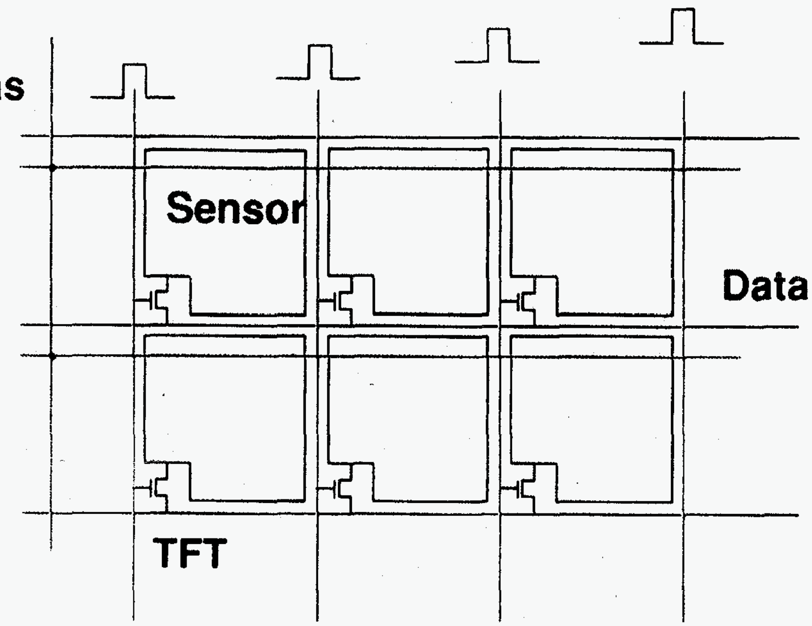

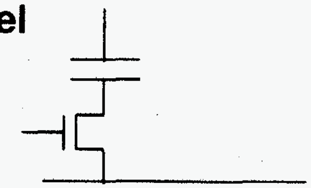

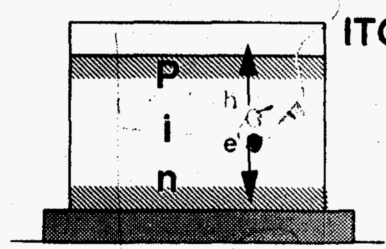

The same addressing structure is used for:

- Liquid crystal display
- Optical imagers
- Linear arrays (FAX)

XEROX PARC
Electronic Materials Laboratory

Amorphous silicon devices

sensor

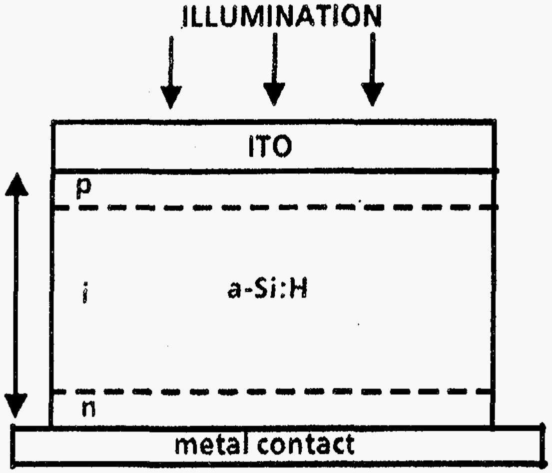

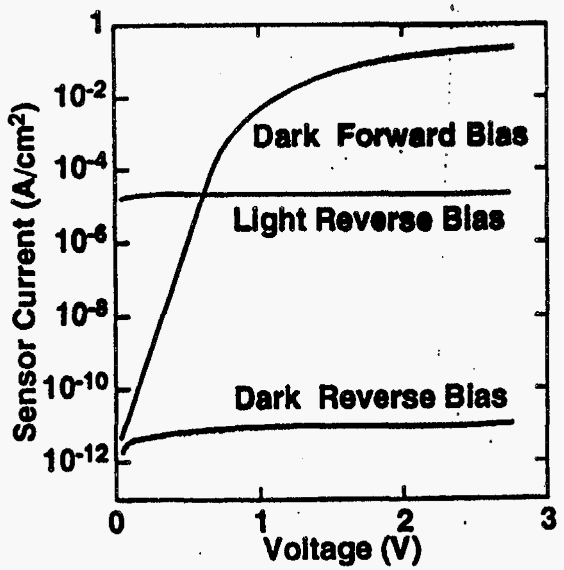

TFT

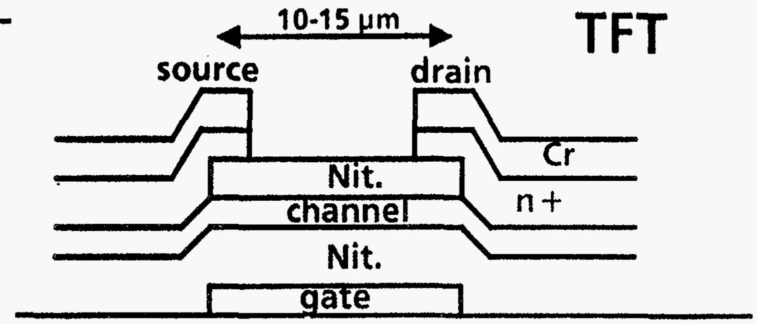

n-channel accumulation mode

mobility 0.5-1.0 cm^2/Vsec

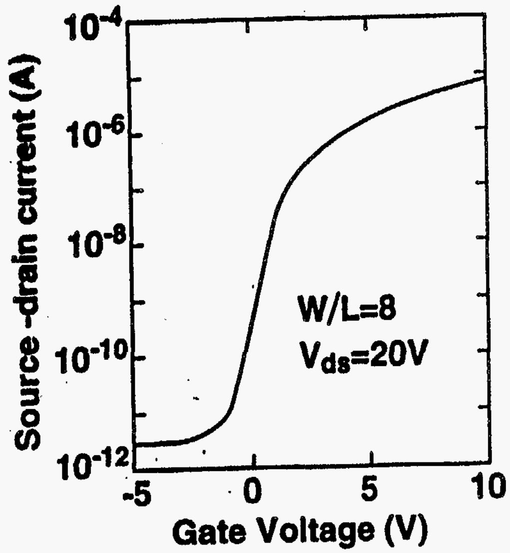

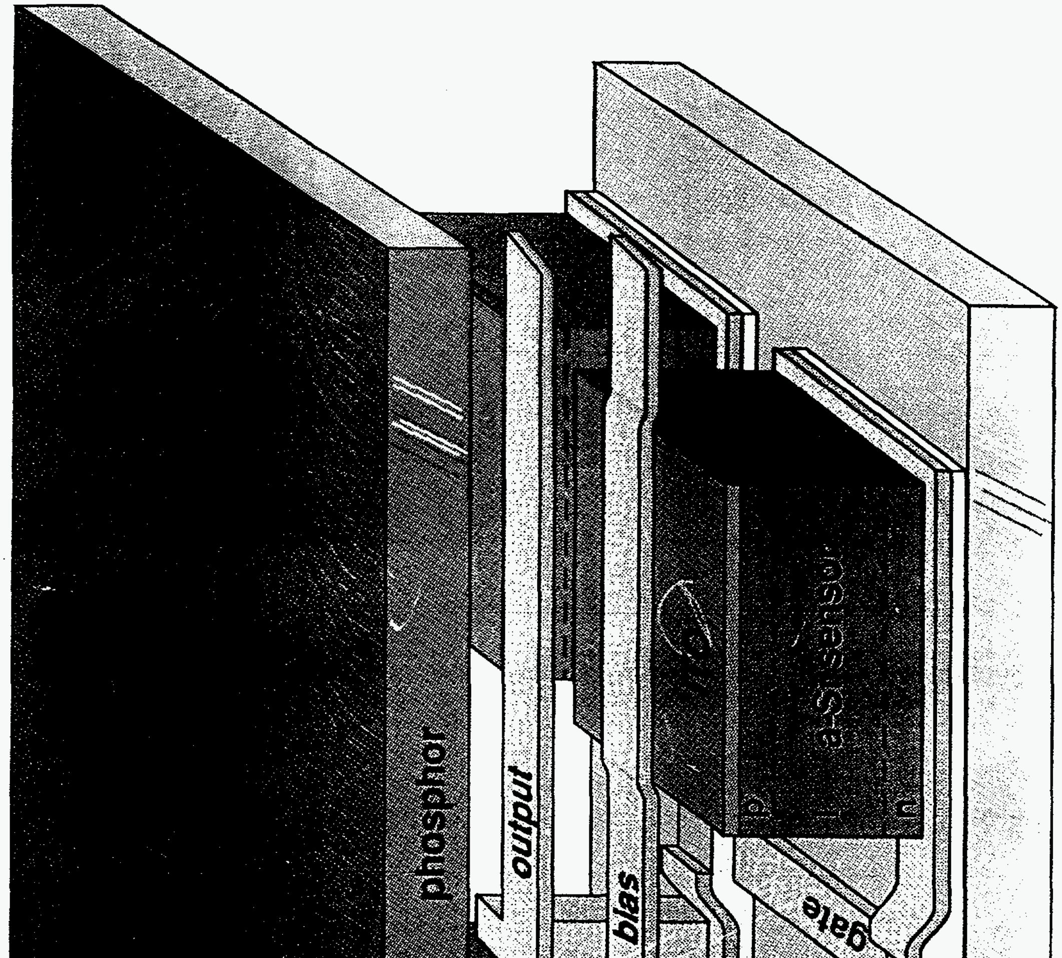
phosphor
output
bias
gate
TFT
light
p
n

Emission spectra of phosphors

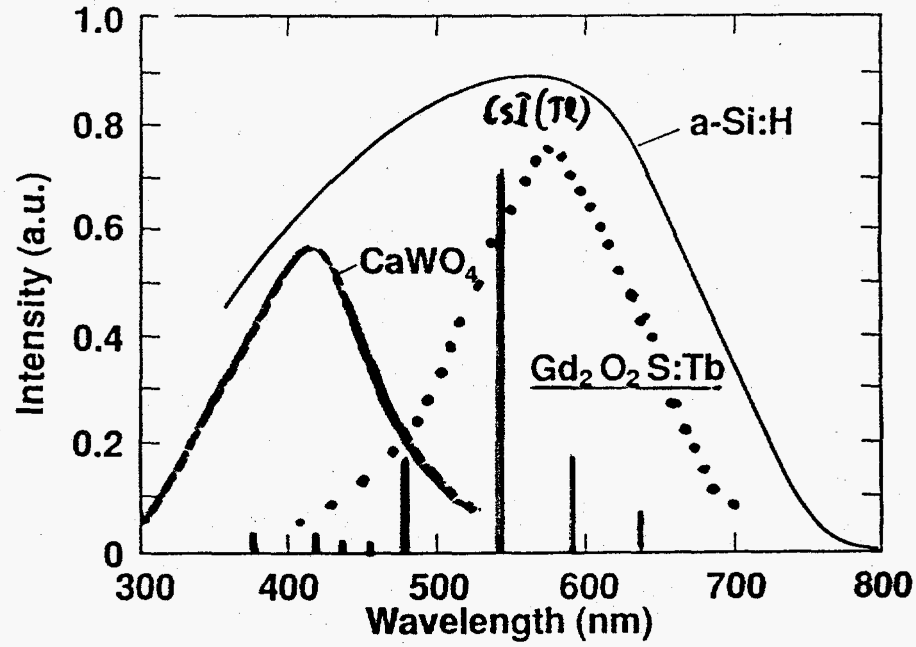

- Gd_2O_2S:Tb is well suited to the a-Si:H collection efficiency spectrum
- Alternative phosphors include, CsI, NaI and many others

Pixel design

For higher resolution:

- reduced design rules
- sensor over metal lines

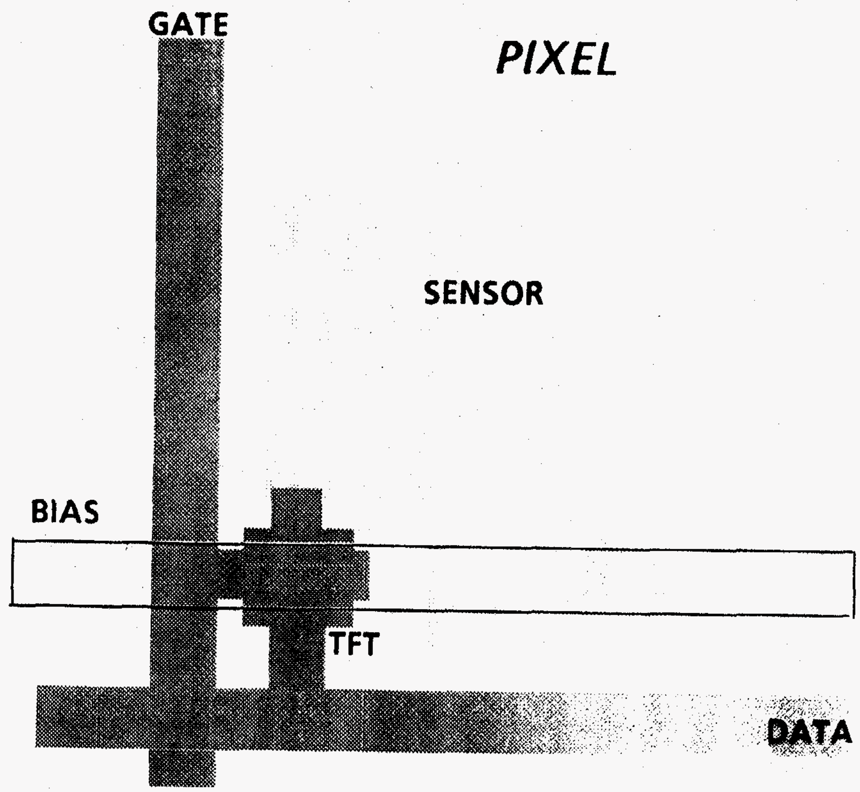

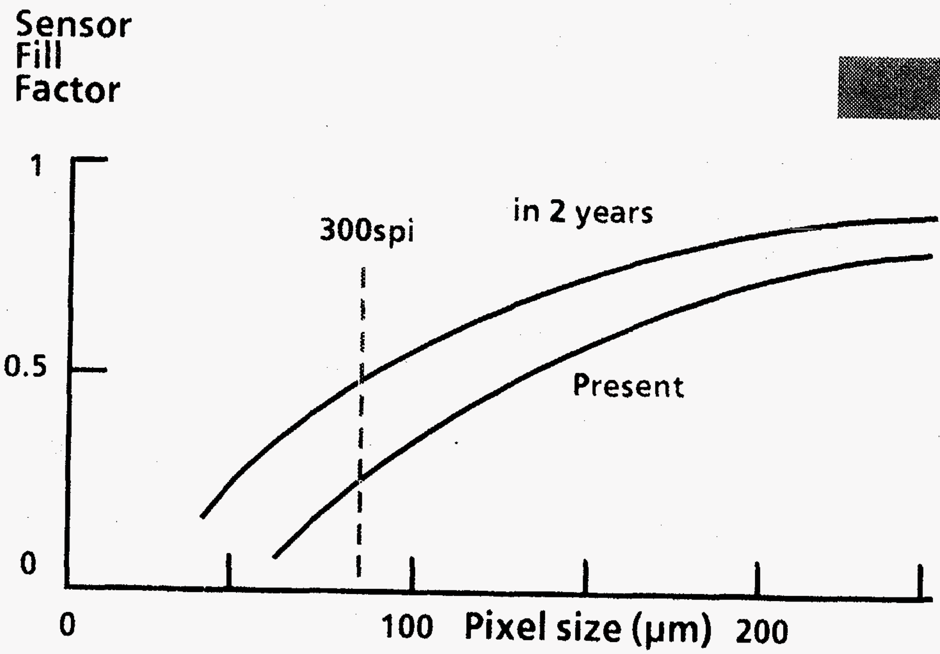

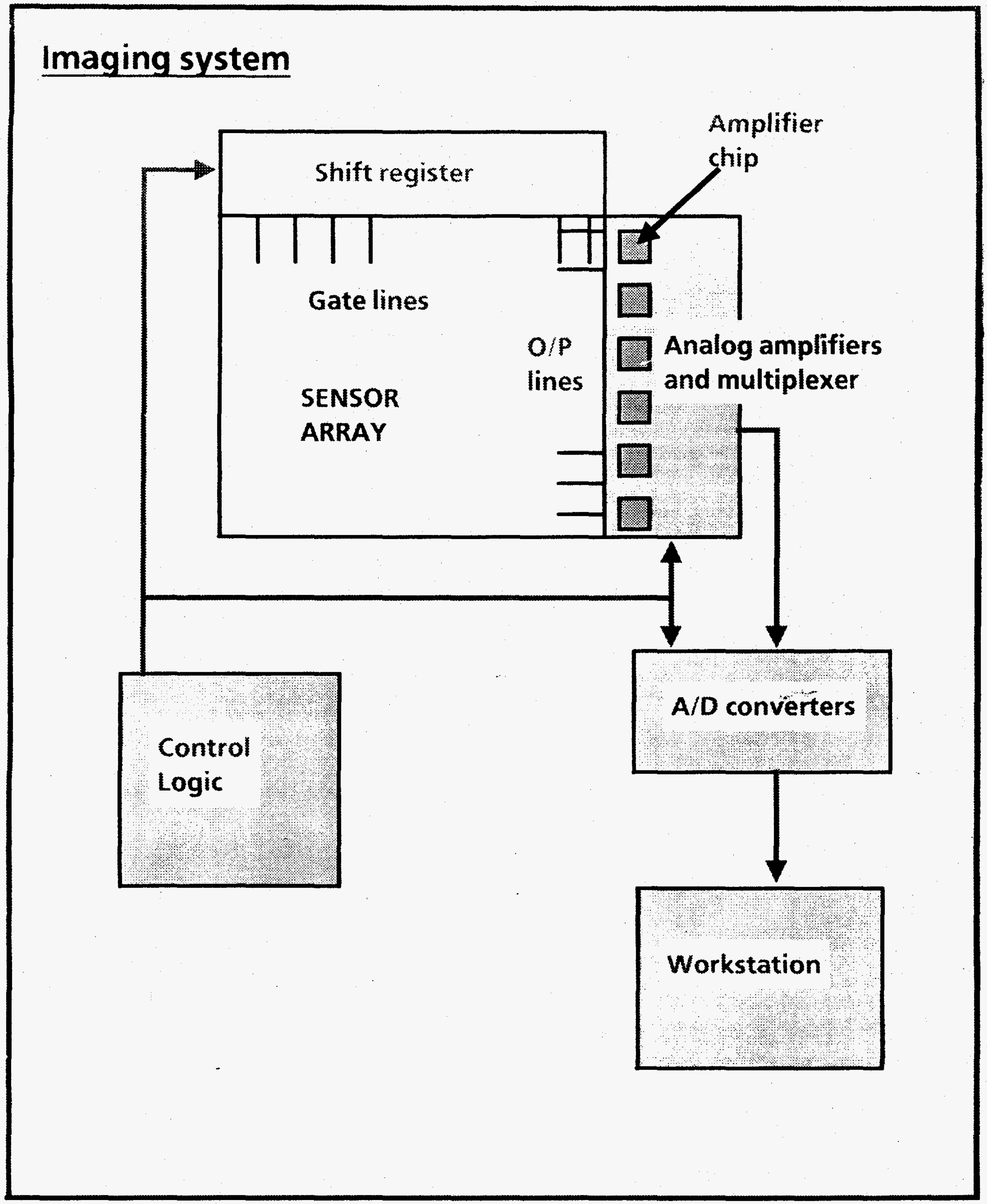
Imaging system
Amplifier chip
Shift register
Gate lines
O/P lines
SENSOR ARRAY
Analog amplifiers and multiplexer
A/D converters
Control Logic
Workstation

Specifications of a 200 spi Array

Physical:

Array size:	7.7" x 9.6"
Number of pixels:	1536 x 1920
Sensor fill factor:	36%
Transparent region:	20%

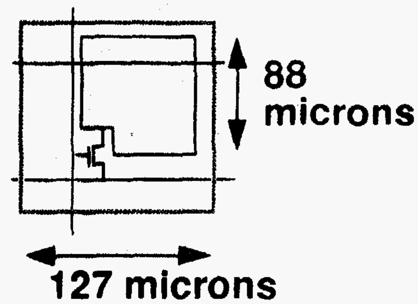

Electrical:

Sensor capacitance:	0.8 pF
Max pixel charge:	4 pC ~ 1 cd/m^2 in light intensity
TFT on-resistance (10V):	4 MOhm
Array frame time:	1920 x 5 $R_{on}C_{sens}$ = 30 msec -> 33 pages/sec
Sensor dynamic range:	10^4~10^5
System dynamic range:	500 ~ 1000
Responsivity uniformity:	10%

XEROX PARC
Electronic Materials Laboratory

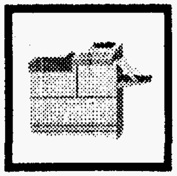

Back Illumination Allows Contact Imaging

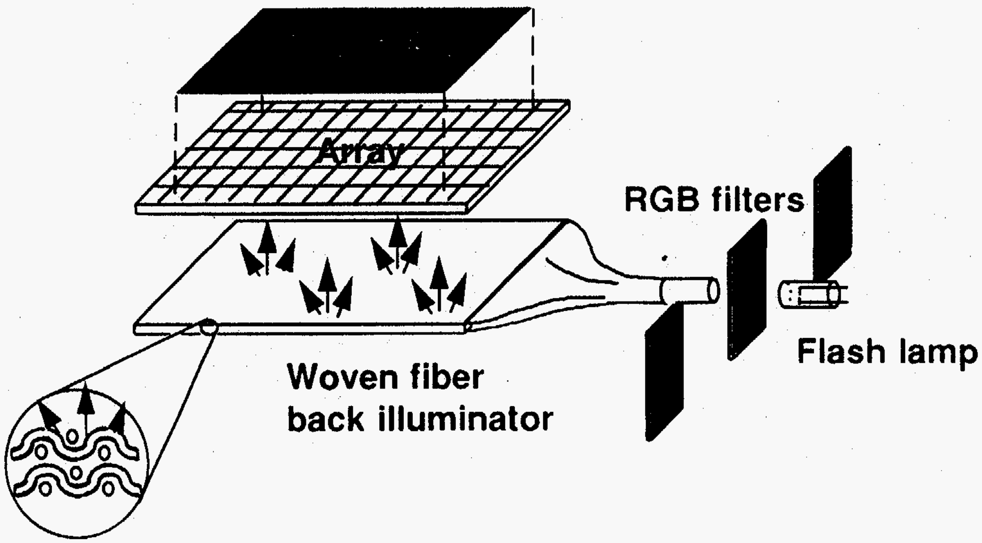

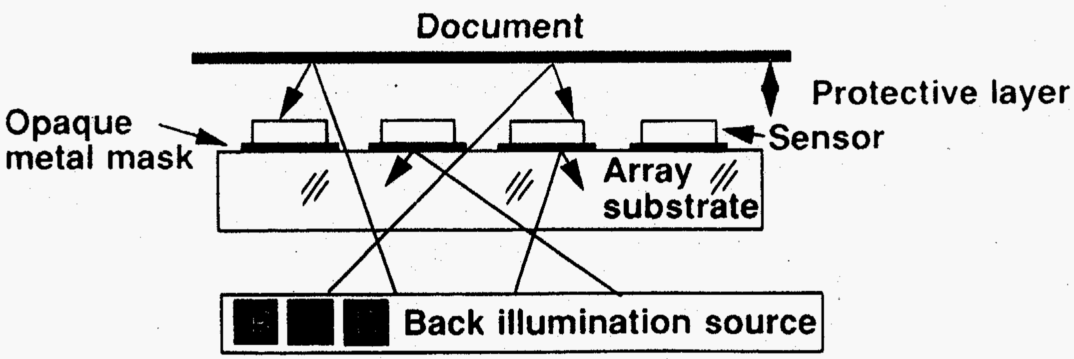

- Illumination through transparent glass substrate and between sensors.
- Contact imaging has an efficient optical transfer.

XEROX PARC
Electronic Materials Laboratory

Technology progression

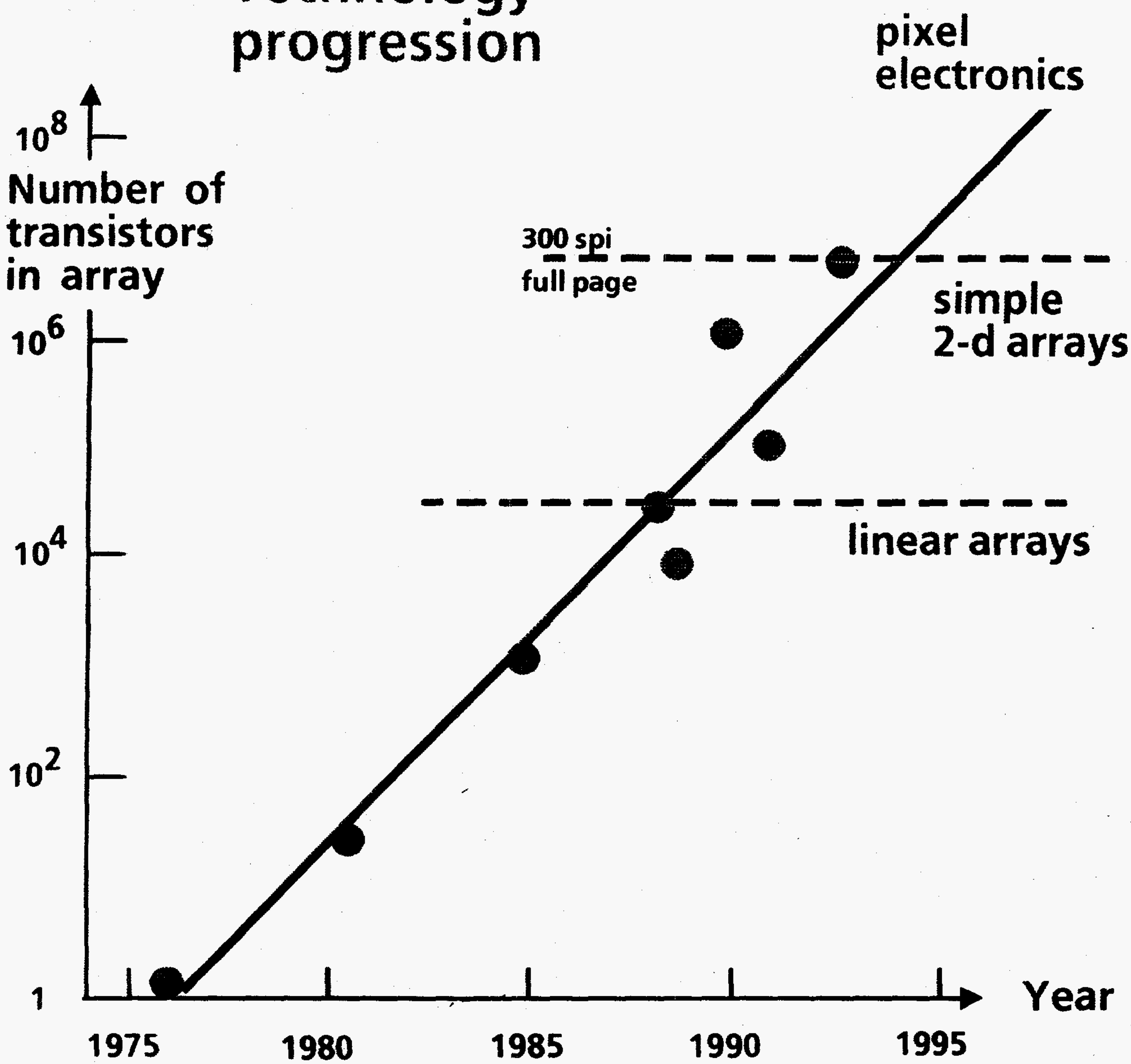

Pixel electronics;

Amplifiers, image processing, 3-d structures

EML/EIL
PARC

Wladek Minor

Purdue University
Department of Biological Sciences

Crystallographic Data Handling and Reduction in Experiments with Extremely High Data-Acquisition Rates

As in many experimental sciences, data acquisition and data processing are often the most critical steps in x-ray crystallographic studies and dictate the success or failure of the entire process. The successful synchrotron experiment requires high photon brilliance, a very fast x-ray detector, and a computing environment that can handle very high rates of data collection effectively. Although data acquisition may not be computationally intensive even for very high data-acquisition rates, the experiment evaluation procedures and robust data reduction at rates comparable to the data collection rate will require not only a very fast computer but also software designed for the synchrotron environment.

In anticipation of an increase in data-acquisition rates due to more intense synchrotron sources and new fast detectors, modular software tools should be developed with the goal of speeding up the entire crystallographic experiment and optimizing the use of beam time. The software modules should be unified by a flexible, rapid and easy to use graphical user interface. These modules should provide the ability to evaluate and control a crystallographic experiment in conditions close to real time, at all currently expected rates of data acquisition. Among the most important tools will be those that allow the rapid evaluation of diffraction images, fast crystal alignment and/or indexing, and real-time reduction of two- or three-dimensional diffraction data to indexed intensities. The effective management of the very high rate of data acquisition, experimental data base setup and access, long-term data storage, and effective use of networking must also be addressed.

Wild West approach:

Shoot first and ask questions later.

Let them shoot crystals and send them home with data (any data) and they will ask themselvs questions later (when at home).

East coast approach:

W. Hendrickson (Science 254(1991)54) :

The challenge is to produce at existing and developing synchrotron sources both the necessary instrumentation and also convenient modes of access and use. A long-awaited trip to the synchrotron used to yield packs of films to be processed; now one can return from a few synchrotron centers with processed diffraction amplitudes. In the future, the hope is to return from an on-call trip to one of several MAD beam lines with both the amplitudes and phases needed to solve another exciting biological problem.

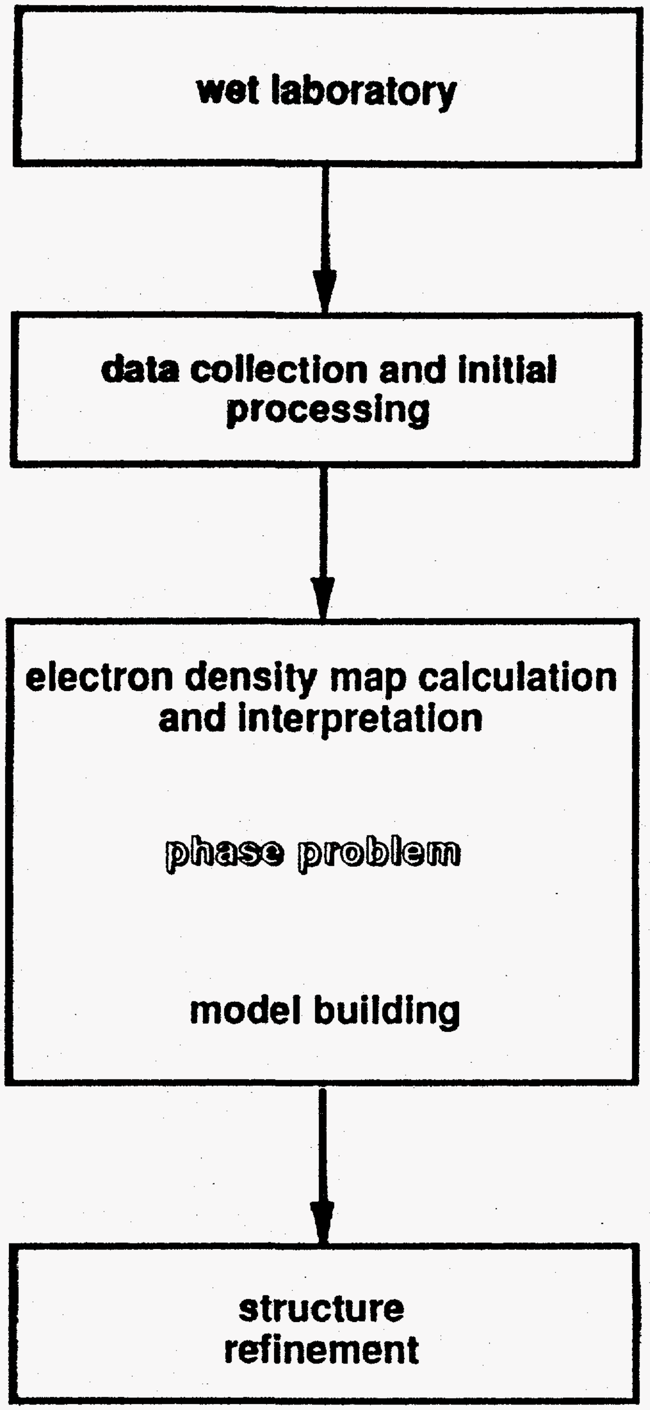
wet laboratory
data collection and initial processing
electron density map calculation and interpretation
phase problem
model building
structure refinement

Software role from the synchrotron user point of view:

Design of Experiment

Data acquisition

- evaluation and on the fly monitoring
- reduction - *in real time*
- storage and/or transmission

User requirements:

Instrument and experiment independent

Computer independent

Network transparent

User friendly graphical interface

The strength of the chain is determined by it's weakest link

Detector from the software point of view:

Low intristic noise

High spatial and time resolution

High dynamic range

Reproducibility

Software has to understand the nature of the detector hardware

Software type of callibration

COMPUTING STANDARDS at APS

The hallmark of computing environment is FLEXIBILITY.

- **modular and powerful computing tools for very convenient, rapid control and monitoring of the experiment**

- **effective management of the very high rate of data acquisition**

- **easily adaptable**

- **easy addition of new features by people other than the program author**

- **operating system independent, powerful and easy to use user interface**

- **portable to a "standard" laboratory environment**

- **flexible to the rapidly advancing computer industry**

- **real-time computer response
store and reliably process diffraction data at a rate comparable to the rate at which they will be recorded.**

This is one of the biggest challenges of the computing effort, and it can not be seen as a substitute for storage of raw data images.

USER INTERFACE

Powerful user interfaces that allow the user to concentrate on the experiment with minimal concern about how to run the support software.

- **management of the experiment**
- **rapid, graphical and flexible**
- **flexibility for addition of new experiments.**
- **ability to interact with all phases of the experiment**
    - **crystal evaluation and alignment,**
    - **set-up and running of data collection**
    - **on line experiment monitoring**
    - **real-time data processing**

MANAGEMENT OF THE EXPERIMENT

- Extremes of organization

- electronic notebook for the experimenter.

- some information from the database of the APS

- Example of items
  - time and date
  - ring current and energy
  - wavelength or wavelength range
  - settings of insertion device
  - positions and settings of beamline optical elements
  - type and Bragg reflection of the monochromator crystal
  - positions of slits, attenuators and filters in the beam
  - shutter condition
  - instrument alignment angles
  - incident beam intensity
  - detector count rate
  - position of the beam and beamstop
  - hutch temperature
  - actual and set temperatures for sample cooling
  - Helium and cooling gas flows to the experiment
  - instrument angles at the aligned position of the sample
  - instrument setting
  - angular range and scan speed for the current image
  - exposure time and dose of current image
  - fiducial marking on the image.

Ideal data reduction package:

Source	-	any
Crystal	-	any space group any cell dimensions (5 - 2000 Å)
Diagnostics	-	everything
Feedback	-	real time
Speed	-	real time
Goniostat	-	any
Detector	-	any
Computer	-	any (with full graphics support)
OS	-	any
Cost	-	public domain

Data processing:

MADNES

MOSFILM

XENGEN - POLYDET

XDS

OSC

DENZO

HKL package:

- Denzo
- Xdisplayf
- Scalepack

Tasks:

- Indexing
- *Callibration*
- Prediction
- Refinement
- Integration

Processing time:

Lipoxygenase (2.1 A)

MAC-Science scanner: 180/25 sec/frame
(95.6, 94.3, 50.3, 90.0 91.3, 90.0)

Rotavirus (8.0 A)

FUJI scanner (CHESS): 180/40 sec/frame
(692, 993, 1395, 90, 90,90)
Steve Harrison - Brenda Temple

Bovine PNP (1.7 A)

CCD detector (CHESS): 180/50 sec/frame
(92.7, 92.7, 92.7, 90, 90, 90)
Steve Ealick

primitive cubic	44.52%	82.59	82.59	82.59	90.00	90.00	90.00
		50.29	94.11	95.29	90.02	91.45	89.95
I centred cubic	38.72%	116.46	116.46	116.46	90.00	90.00	90.00
		106.74	106.61	133.91	128.87	127.68	77.78
F centred cubic	25.82%	142.76	142.76	142.76	90.00	90.00	90.00
		142.22	143.86	142.19	96.45	97.13	138.83
primitive rhombohedral	44.52%	82.59	82.59	82.59	89.64	89.64	89.64
		50.29	95.29	94.11	89.98	89.95	88.55
primitive hexagonal	15.27%	101.11	101.11	94.11	90.00	90.00	120.00
		106.61	95.29	94.11	89.98	89.99	151.86
primitive tetragonal	1.25%	94.70	94.70	50.29	90.00	90.00	90.00
		94.11	95.29	50.29	91.45	90.05	89.98
I centred tetragonal	8.17%	138.11	138.11	50.29	90.00	90.00	90.00
		142.19	133.91	50.29	89.00	109.64	89.68
primitive orthorhombic	0.59%	50.29	94.11	95.29	90.00	90.00	90.00
		50.29	94.11	95.29	90.02	91.45	89.95
C centred orthorhombic	0.74%	133.91	133.94	50.29	90.00	90.00	90.00
		133.91	133.94	50.29	91.07	89.00	90.72
I centred orthorhombic	5.92%	50.29	133.91	142.19	90.00	90.00	90.00
		50.29	133.91	142.19	89.68	70.36	91.00
F centred orthorhombic	5.20%	50.29	194.78	195.87	90.00	90.00	90.00
		50.29	194.78	195.87	93.44	103.42	75.08
primitive monoclinic	0.02%	50.29	94.11	95.29	90.00	91.45	90.00
		50.29	94.11	95.29	90.02	91.45	89.95
C centred monoclinic	0.66%	133.94	133.91	50.29	90.00	91.07	90.00
		133.94	133.91	50.29	91.00	91.07	89.28
primitive triclinic	0.00%	50.29	94.11	95.29	89.98	88.55	89.95

autoindex unit cell 50.29 94.11 95.29 90.00 91.45 90.00

Volume of the primitive cell 450846.

Autoindex Xbeam, Ybeam 99.38 99.82

```
primitive cubic          34.86%1209.381209.381209.38  90.00  90.00  90.00
                               1205.861395.00 993.82  89.89 144.93  89.99

I centred cubic          33.06%1607.821607.821607.82  90.00  90.00  90.00
                               1697.311395.001711.25 144.50 109.67  89.91

F centred cubic          28.18%1845.381845.381845.38  90.00  90.00  90.00
                               1848.271844.171843.71  81.68 114.86 135.91

primitive rhombohedral   16.47%1560.631560.631560.63  37.04  37.04  37.04
                               1559.601711.251395.00  35.50  26.38  43.39

primitive hexagonal      13.57%1104.941104.941395.00  90.00  90.00 120.00
                               1205.86 993.821395.00  90.11  90.01 144.93

primitive tetragonal     14.87% 856.69 856.691395.00  90.00  90.00  90.00
                                692.94 993.821395.00  90.11  90.18  89.43

I centred tetragonal     17.07%1782.571782.57 692.94  90.00  90.00  90.00
                               1848.271714.35 692.94  90.48 112.20 107.42

primitive orthorhombic    0.23% 692.94 993.821395.00  90.00  90.00  90.00
                                692.94 993.821395.00  90.11  90.18  89.43

C centred orthorhombic    6.83% 692.942098.421395.00  90.00  90.00  90.00
                                692.942098.421395.00  90.04  89.82  71.29

I centred orthorhombic   12.22% 692.941844.172195.41  90.00  90.00  90.00
                                692.941844.172195.41  89.78 128.66  68.11

F centred orthorhombic    6.20% 692.942098.422872.61  90.00  90.00  90.00
                                692.942098.422872.61  94.48 103.78  71.29

primitive monoclinic      0.12% 993.821395.00 692.94  90.00  90.57  90.00
                                993.821395.00 692.94  90.18  90.57  89.89

C centred monoclinic      6.83% 692.942098.421395.00  90.00  90.18  90.00
                                692.942098.421395.00  90.04  90.18 108.71

primitive triclinic       0.00% 692.94 993.821395.00  89.89  89.82  89.43

autoindex unit cell 692.90 993.771394.99  90.00  90.00  90.00

crystal rotx, roty, rotz -40.648 176.335   2.546

Volume of the primitive cell960614720.

 Autoindex Xbeam, Ybeam  122.67   99.18
```

Networking:

The World of Multiple Standards

Internet: Collection of voluntary participants

Transparent for users - easy to realize within short distances.

Now:	Ethernet, TCP/IP, NFS
Future:	FDDI - Fiber Distributed Data Interface
Future:	OSI - Open System Interconnect

Long-Distance

Link	Speed [Mb/s]
T1	1.5
T3	45
NREN	100

Data Storage:

Right combination of adequate capacity, functionality, long-term value and economy

On-line storage of data on RAID (Redundant Array of Inexpensive Disks) and migration to cheaper off-line storage with relatively high capacity and relatively slow access time.

Data compression ??????

very fast compression, speed of decompression less important

CS type of compression not applicable - *nature of crystallographic data*

Diffraction Industry	-	nightmare
MRC Cambridge	-	J.P. Abrams
NIST	-	P. Klosowski

Off - line storage:

Media	Capacity [GB]	Cost [GB/s]	Speed [MB/s]	Investment [k$]
8 mm	2.3 / 5.0	1.40	0.5	2.5
4mm (DAT)	1.3	1.75	0.2	2.5
VHS	14.0	1.40	3.0	250.0 (600GB)
D1 / D2	165.0	2.50	15.0	700.0 (6TB)
WORM	6.6	140.00	0.5	10.0
RWOD	0.6	400.00	0.5	15.0
Opt. tape	50.0	~1.00	?	?

Hardware requirements:

CPU	as fast as possible (ALPHA)
Memory	> 128MB (at least 5 x diffraction image)
Disk space	> 10GB
Network	internet, fast NFS - FDDI
Graphics	> 1024 x 1248, fast
OS	Unix (OSF/1), VMS, Windows NT, ...
Vendor	DEC, SGI, Sun, HP, IBM ....
Cost	< 40k$

Michael Campbell

CERN

Silicon Pixel Detector Development at CERN

Future experiments at the proposed Large Hadron Collider at CERN will study particle collision events generating thousands of particles every 25 ns. Silicon pixel detectors could yield enormous benefits by providing unambiguous two-dimensional images of particle tracks at the center of these experiments. The CERN RD 19 Collaboration has developed a hybrid pixel detector covering a 53 mm x 56 mm plane with two staggered arrays. The design of the readout chip will be presented, along with practical aspects of the construction of such a system. I will attempt to emphasize the lessons we learned from this exercise, which could help in designing pixel detectors for the APS. Finally, I will present the excellent results we obtained in 1993, which make us believe that pixel detectors have a very promising future in such experiments.

Silicon pixel detector development at CERN

Michael Campbell

representing the

CERN RD-19 Collaboration

Chicago, February 1994

- **The particle physics environment**
- **The Omega2 pixel readout chip**
- **Development of a 5cm x 5cm array**
- **Experimental results**
- **Conclusions**

Future high energy physics experiments at CERN

- bunch crossing interval 25 ns
- no. of particles generated per bunch crossing >> 1000
- Radiation dose 1 MRad/year and 1 e ^{13} n/cm^{2}/year
- detector types:

  muon

  calorimeter

  tracking

CMS
A Compact Solenoidal Detetor for LHC

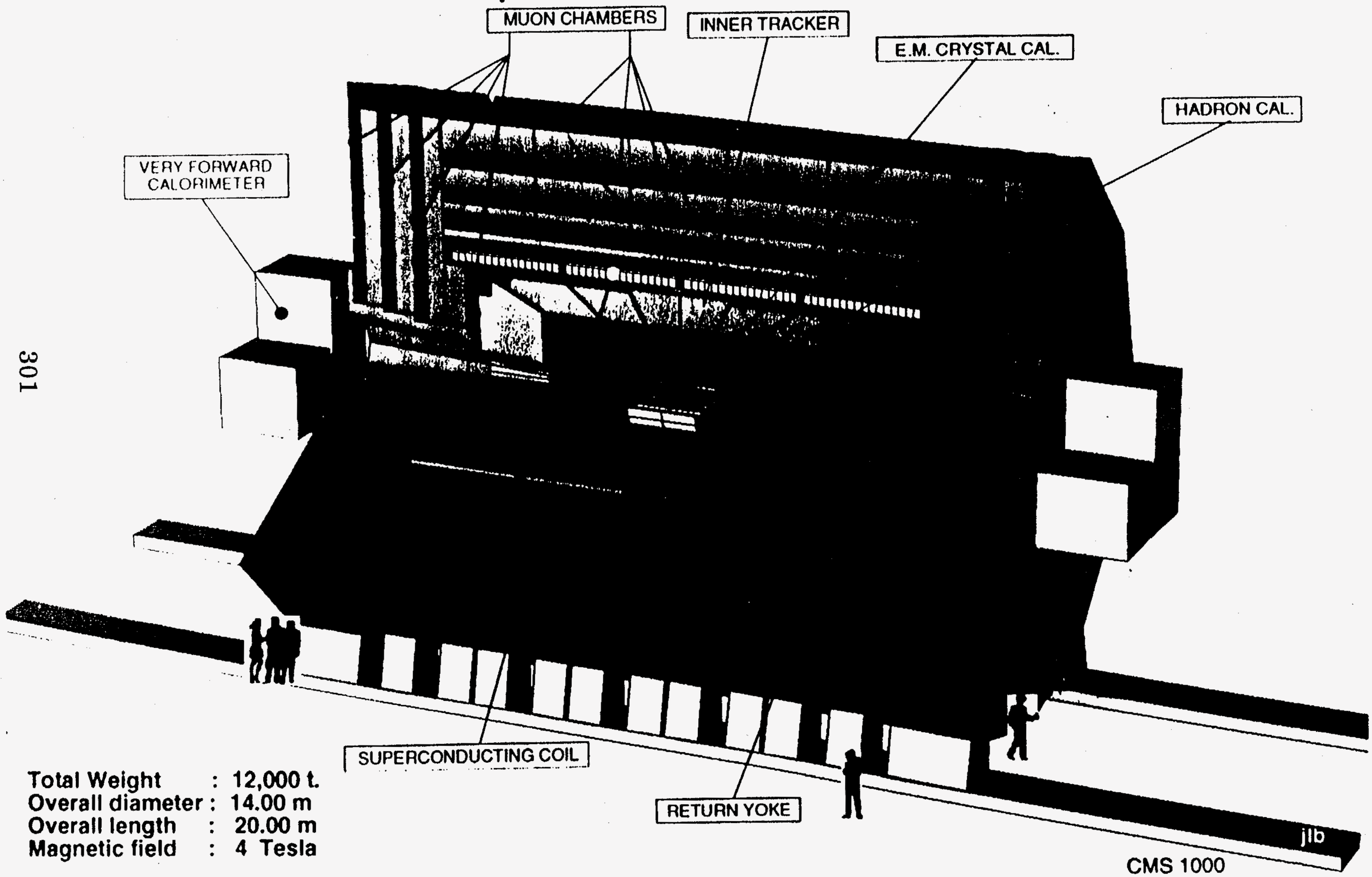

Total Weight : 12,000 t.
Overall diameter : 14.00 m
Overall length : 20.00 m
Magnetic field : 4 Tesla

Two dimensional detectors:

CCD

- low readout speed, but well developed technology

Pixel detectors

- high speed but new approach
- readout can be analog or binary

Silicon Pixel Detector - 3 possible approaches

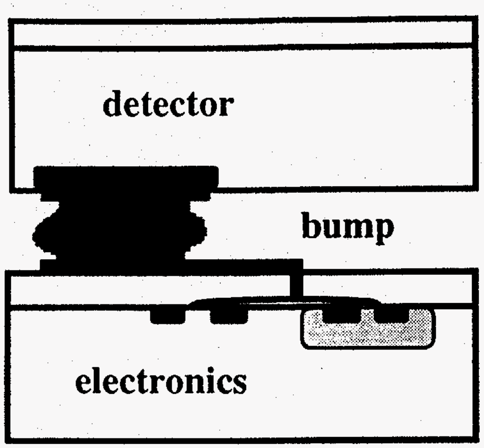

Hybrid

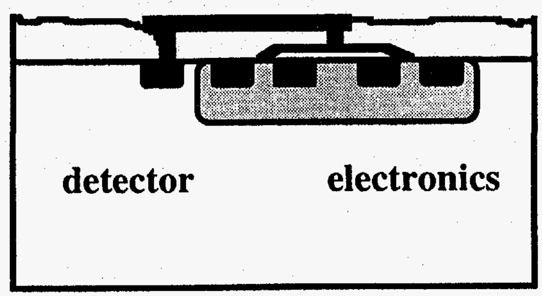

Monolithic

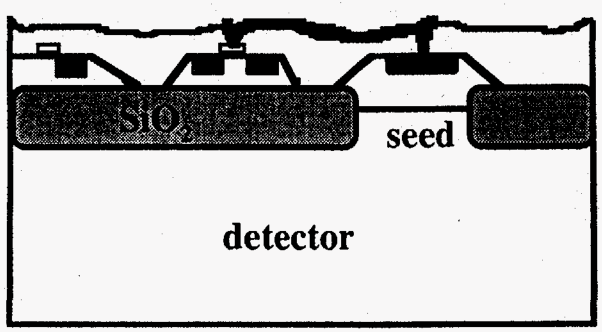

SOI

Advantages of the hybrid approach:

- Well mastered CMOS technology

-Simple detector structure

-Reliable bump-bonding procedure

-Electrical isolation

Omega2 pixel cell and timing

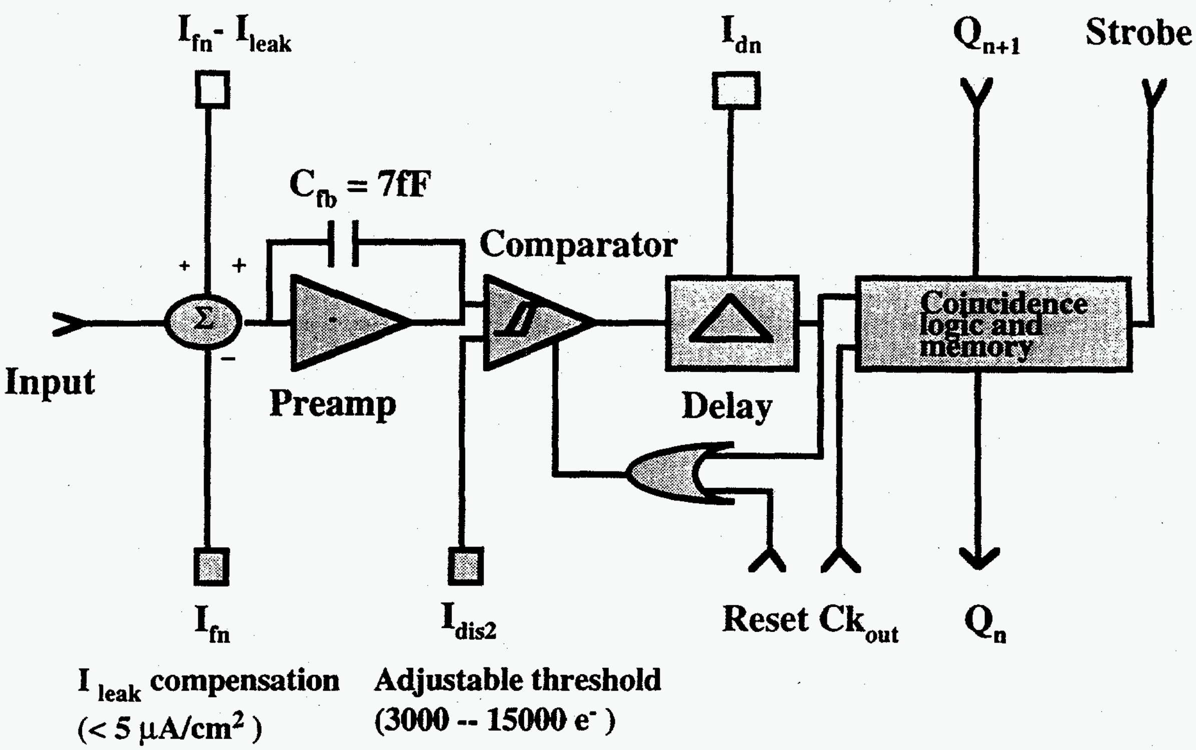

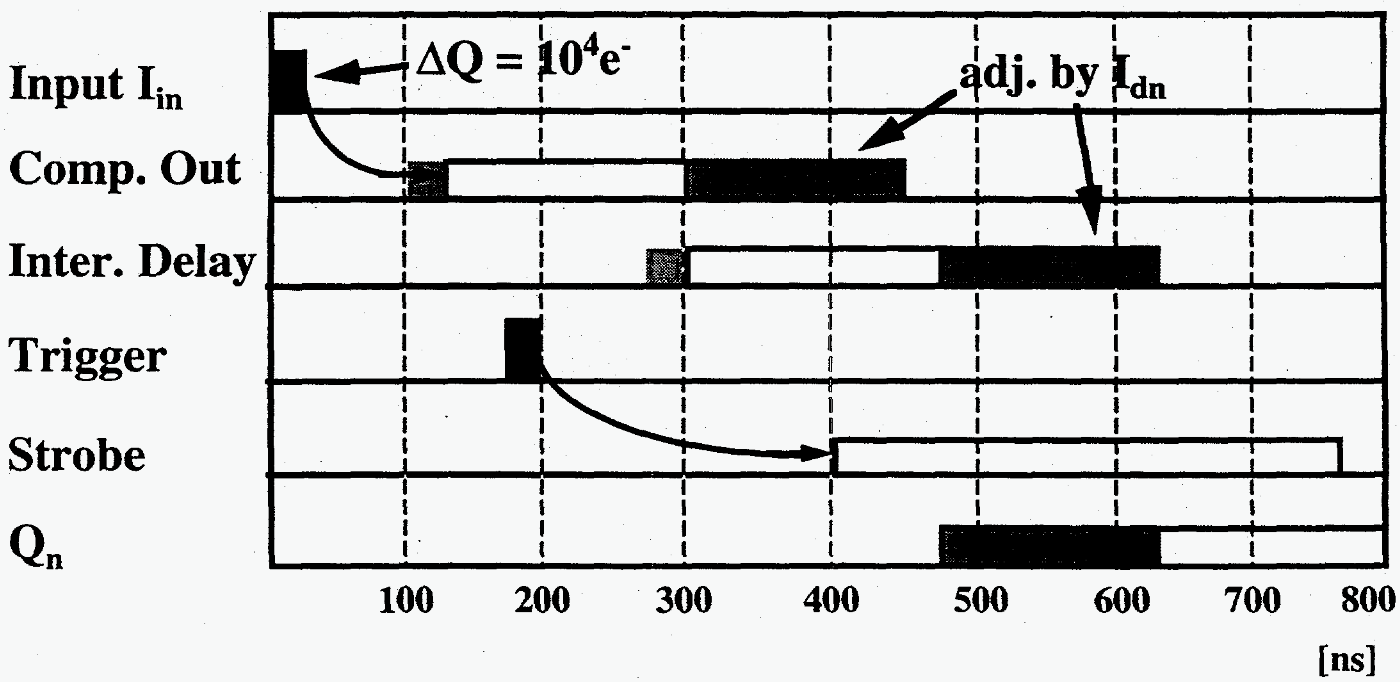

Simple Readout architecture

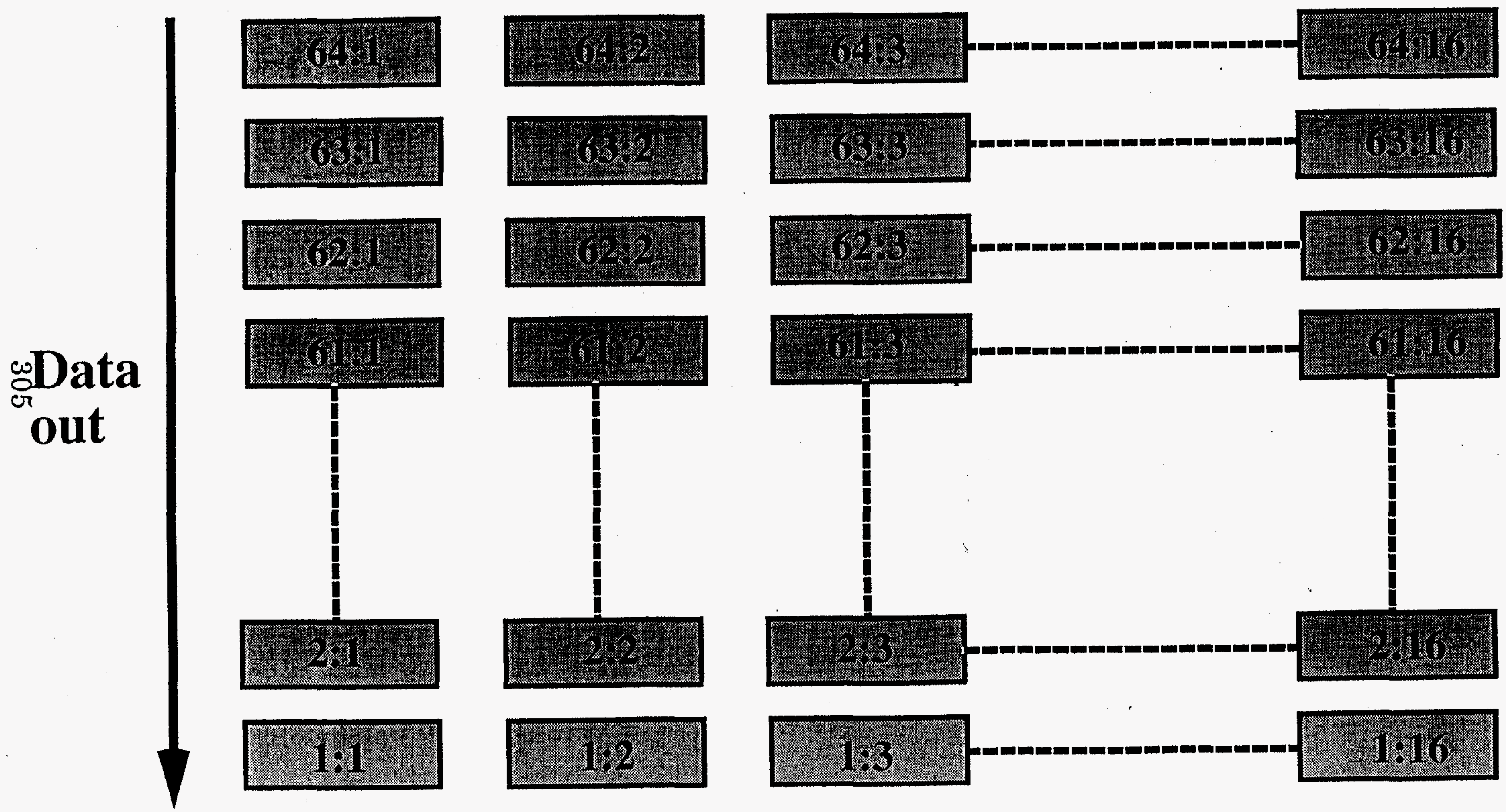

64 x 16 - bit words

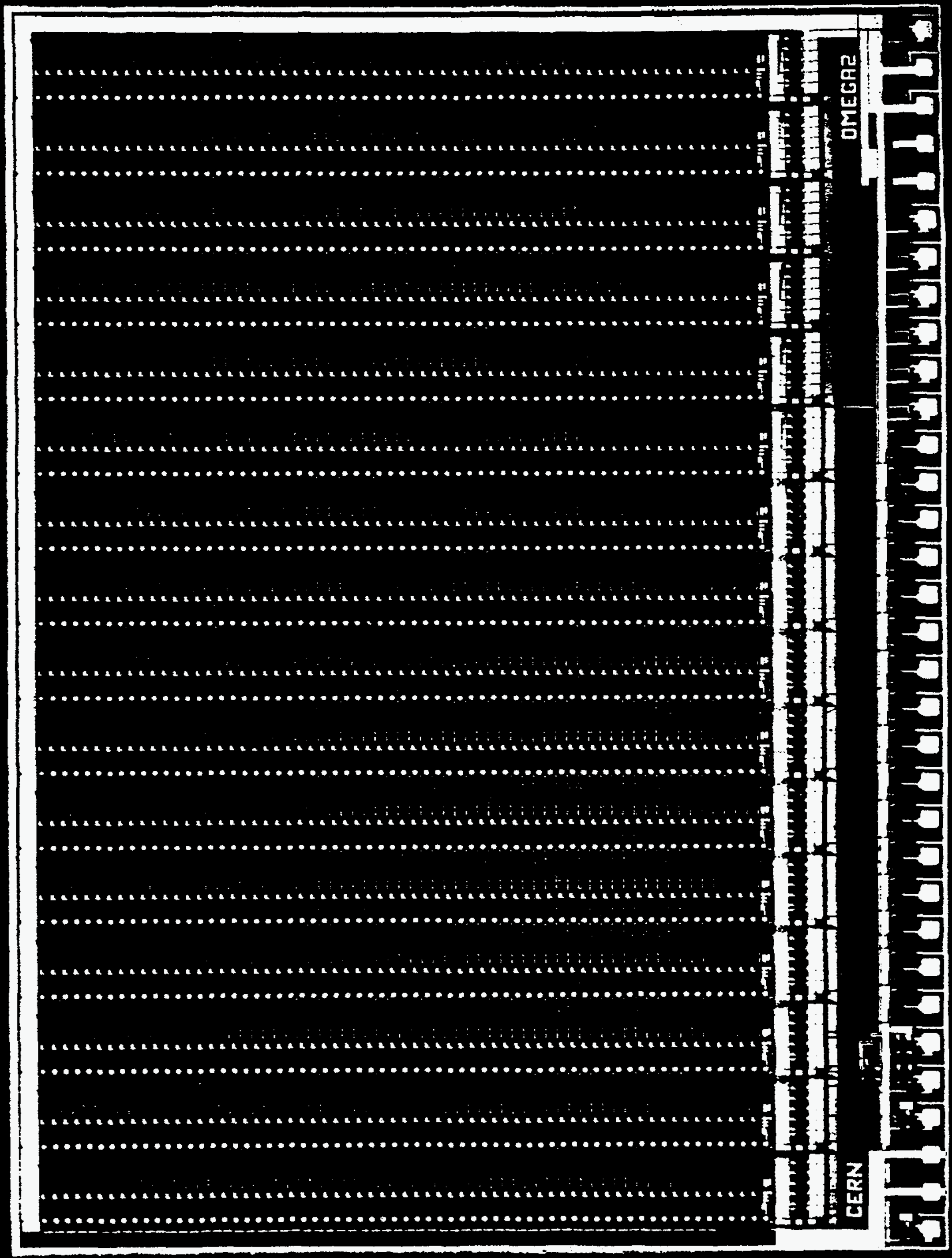
OMEGA2
CERN

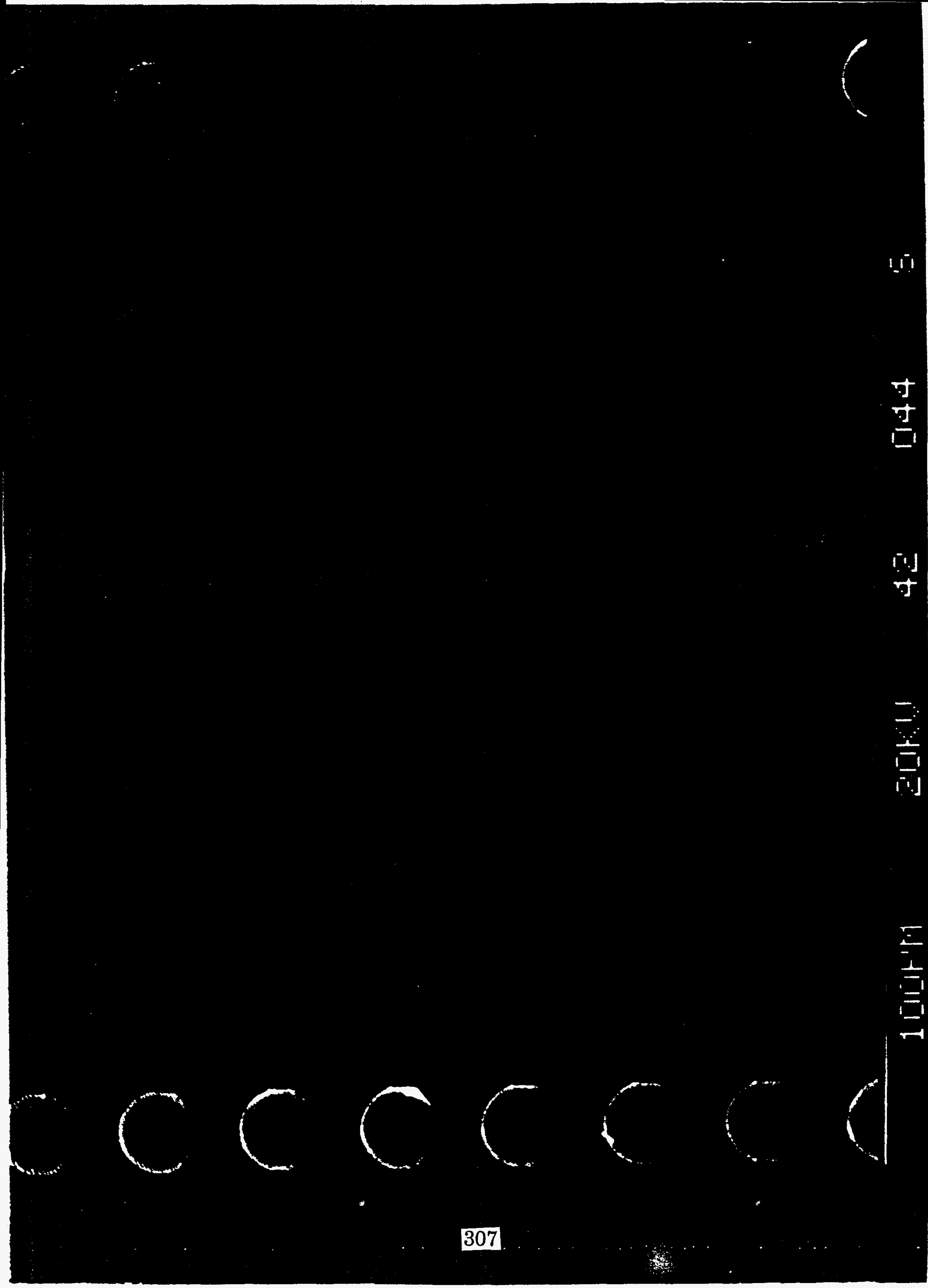
100μm 20KV 42 044 5

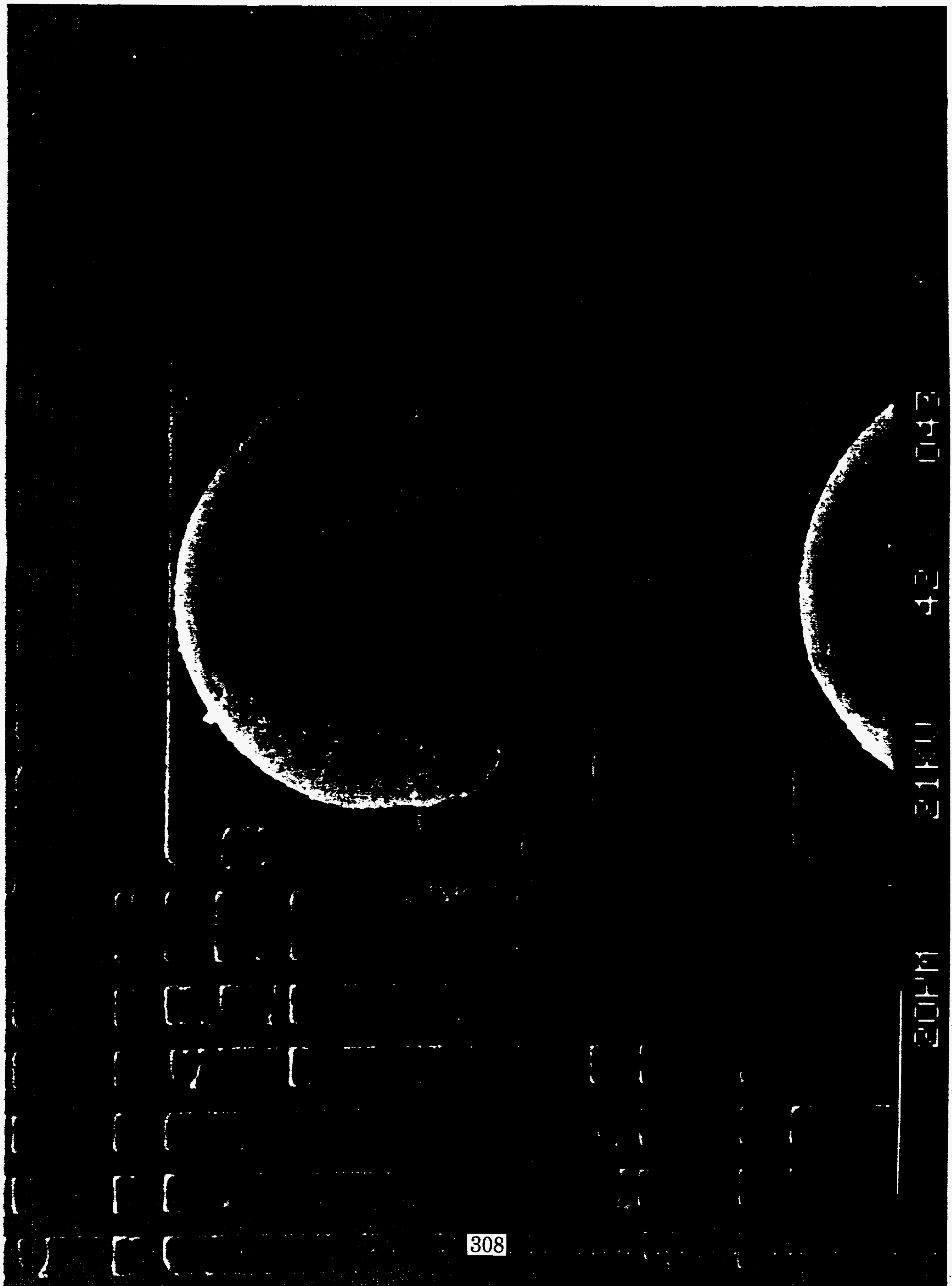

Development of a 5 cm x 5 cm logical plane

- **Detector ladders with 6 readout chips**

  detector dimensions 53 mm x 4.8 mm

  no insensitive regions between readout chips

- **Ceramics containing 6 ladders**

  ladder spacing < 4.8 mm

- **Two ladders staggered**

Logical Plane

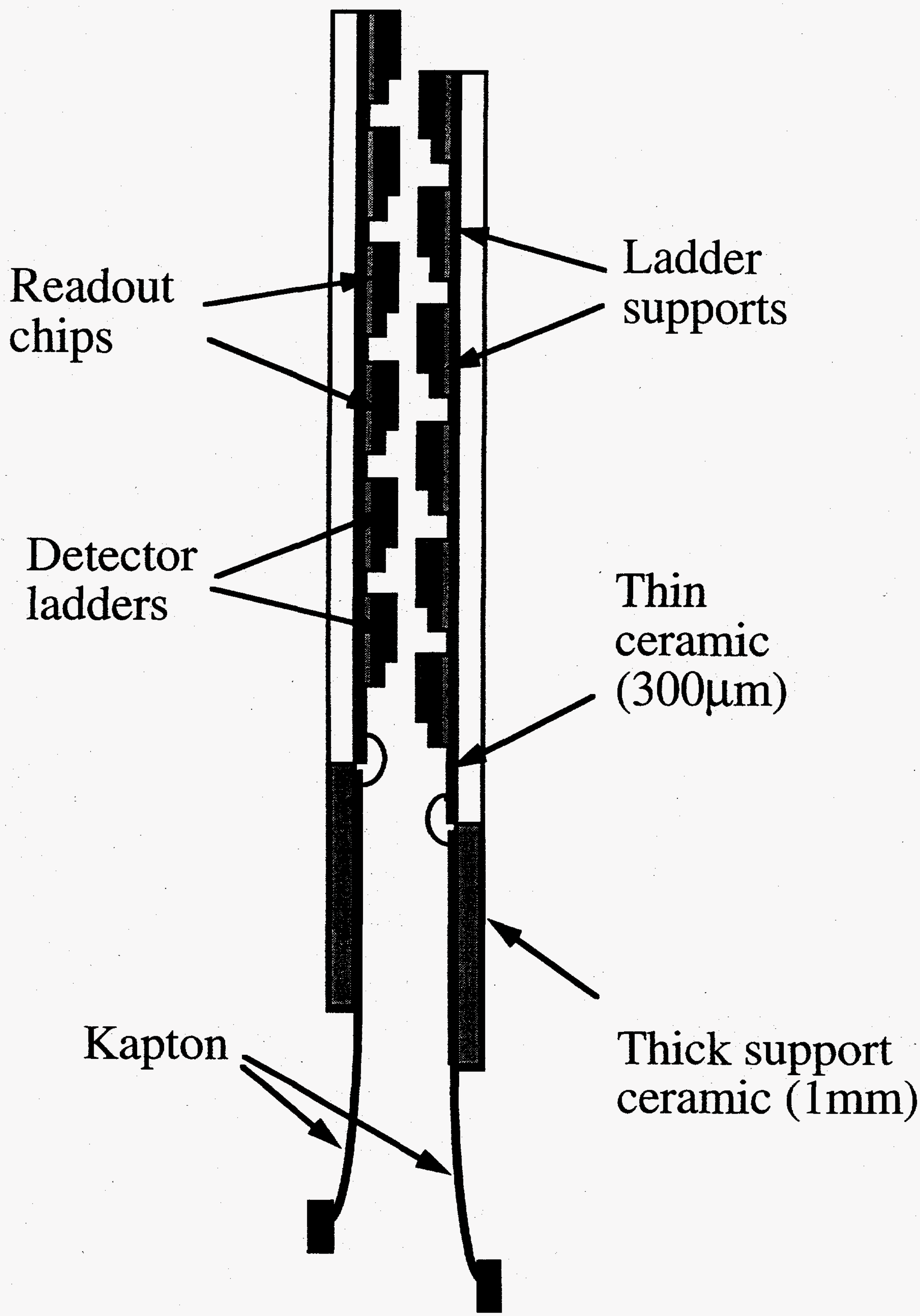

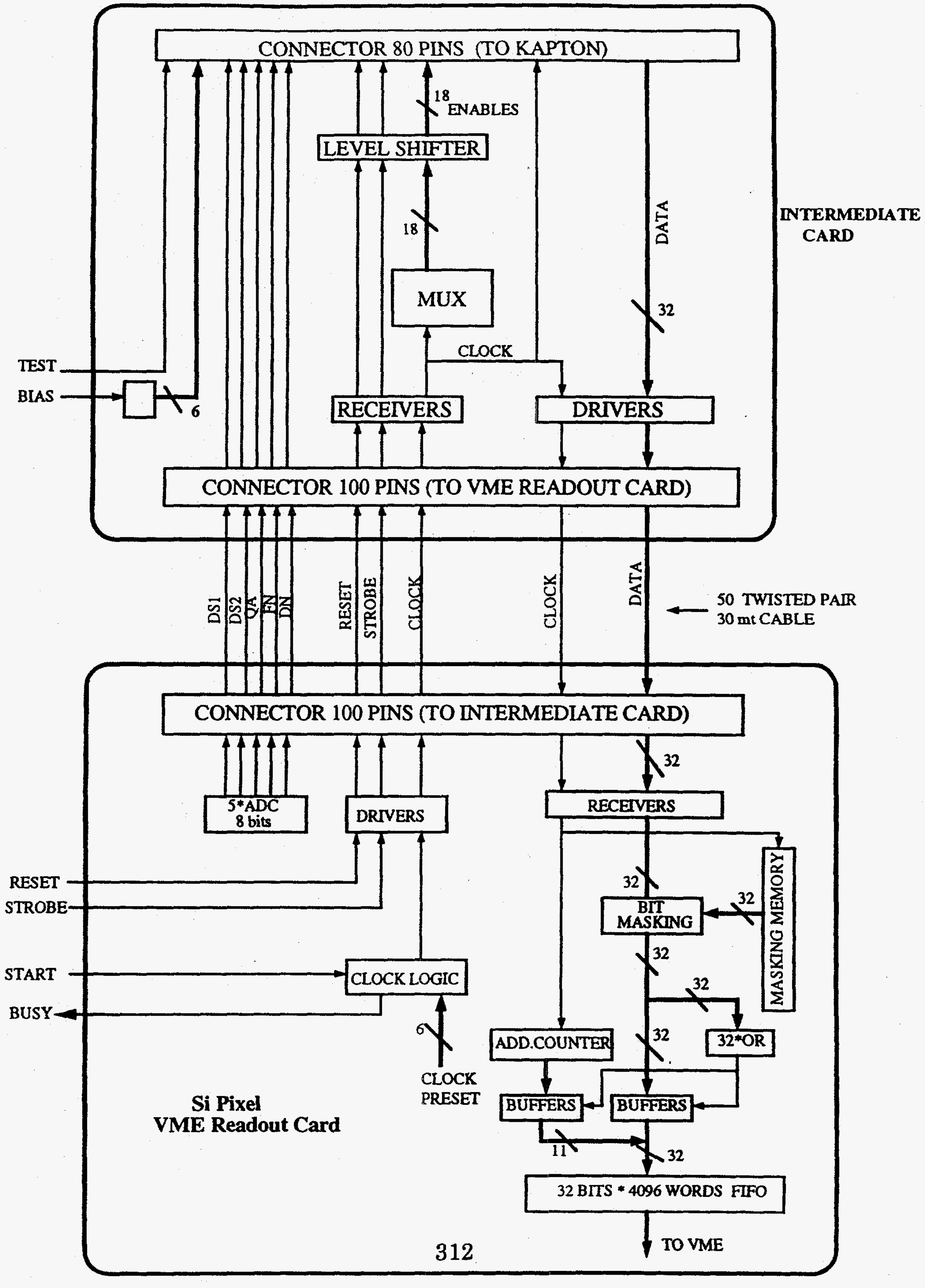
CONNECTOR 80 PINS (TO KAPTON)
18
ENABLES
LEVEL SHIFTER
18
DATA
INTERMEDIATE
CARD
MUX
32
CLOCK
TEST
BIAS
6
RECEIVERS
DRIVERS
CONNECTOR 100 PINS (TO VME READOUT CARD)
DS1
DS2
QA
EN
DN
RESET
STROBE
CLOCK
CLOCK
DATA
50 TWISTED PAIR
30 mt CABLE
CONNECTOR 100 PINS (TO INTERMEDIATE CARD)
32
5*ADC
8 bits
DRIVERS
RECEIVERS
RESET
STROBE
32
BIT
MASKING
32
MASKING MEMORY
32
START
CLOCK LOGIC
32
BUSY
6
ADD.COUNTER
32
32*OR
CLOCK
PRESET
Si Pixel
VME Readout Card
BUFFERS
BUFFERS
11
32
32 BITS * 4096 WORDS FIFO
TO VME

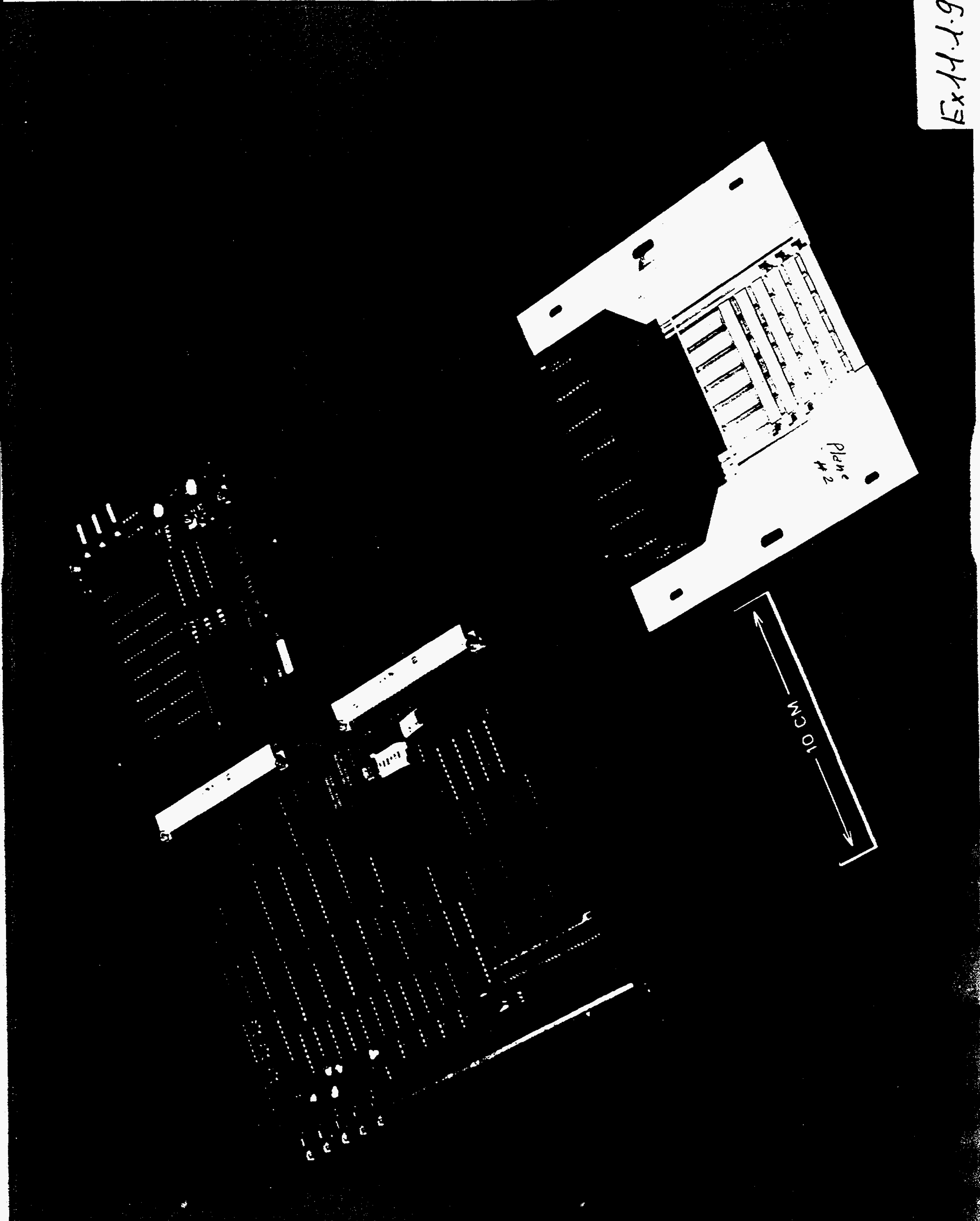
Plane #2
10 CM

Electrical characterisation

- Each chip contains 16 test pixels which can be used for timing and threshold measurements
- Minimum effective strobe width is 100 ns per chip and ~1 μs for the array
- Threshold variable from 3 000 to 15 000 e^-
- Large threshold variation ~ 750 e^- rms
- Very low noise 100 e^- rms
- Digital to analog cross-talk limits strobe width
- Test channels essentail for commisioning

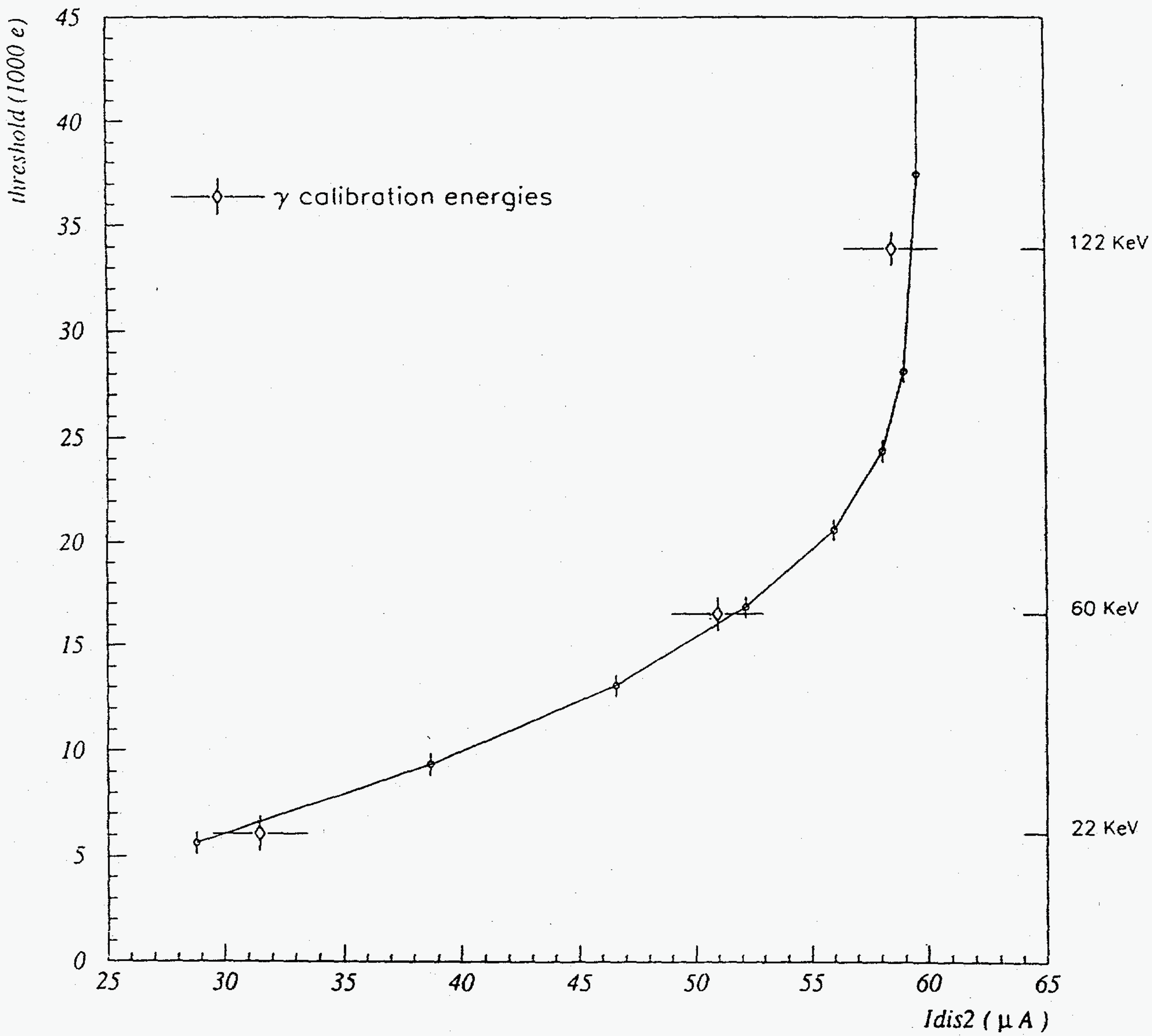

threshold (1000 e)
γ calibration energies
122 KeV
60 KeV
22 KeV
Idis2 (μ A)
0
5
10
15
20
25
30
35
40
45
25
30
35
40
45
50
55
60
65

CD Spectrum with 22 KeV and 25 KeV line

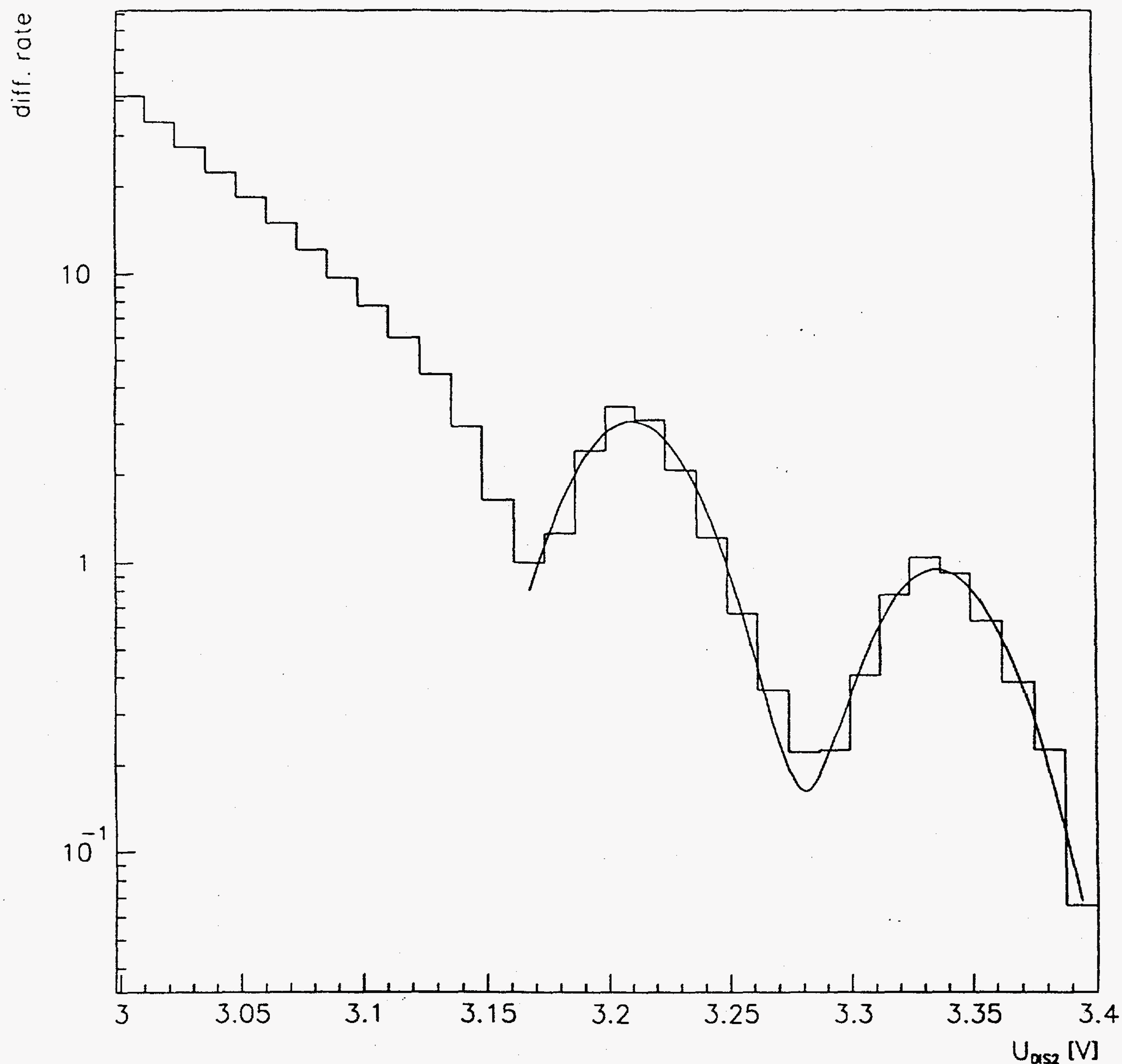

σ = 170 ± 25 e^-, FWHM = 1,4 ± 0,2 KeV

Test Beam Setup

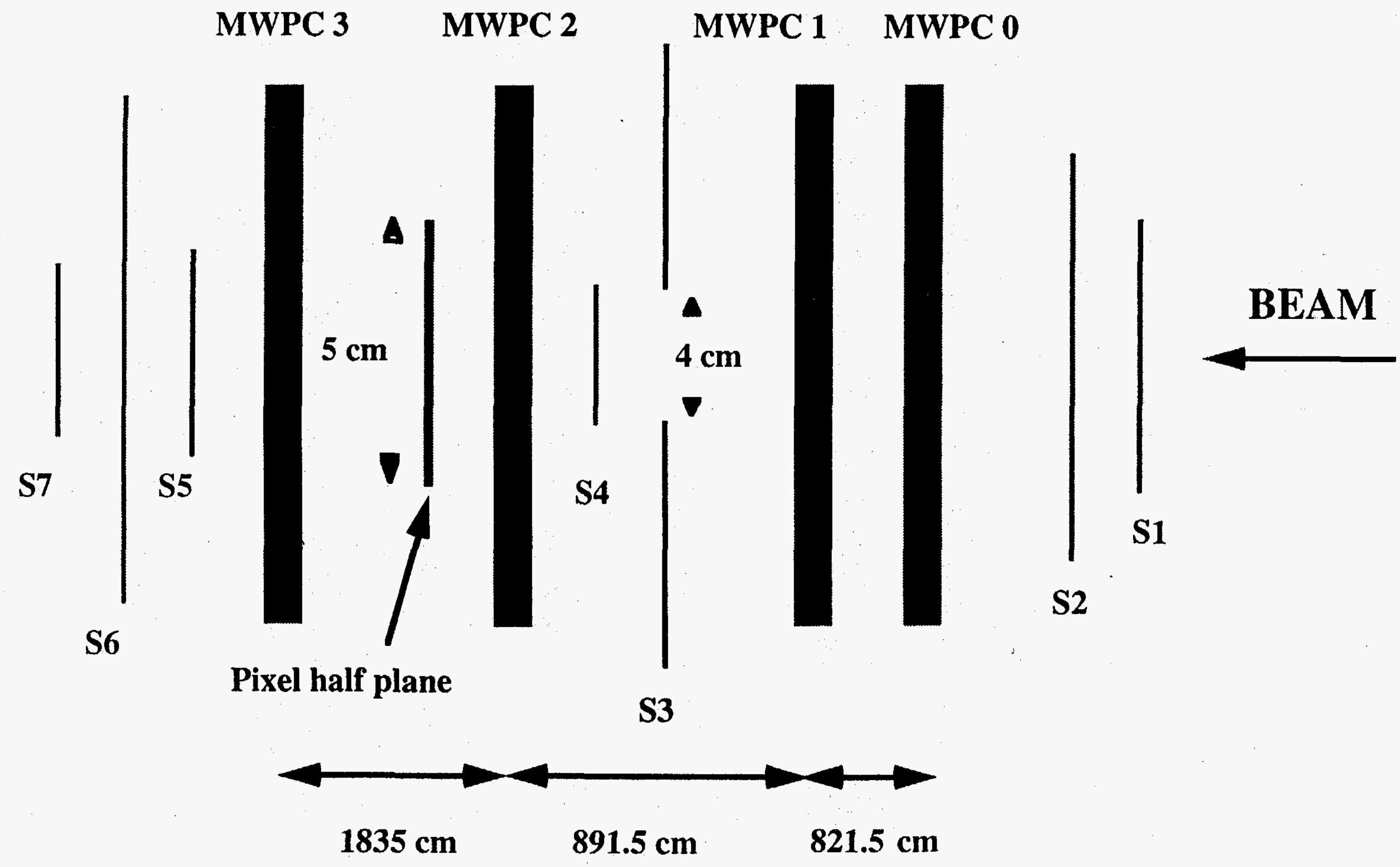

PIXELS SCATTER PLOT

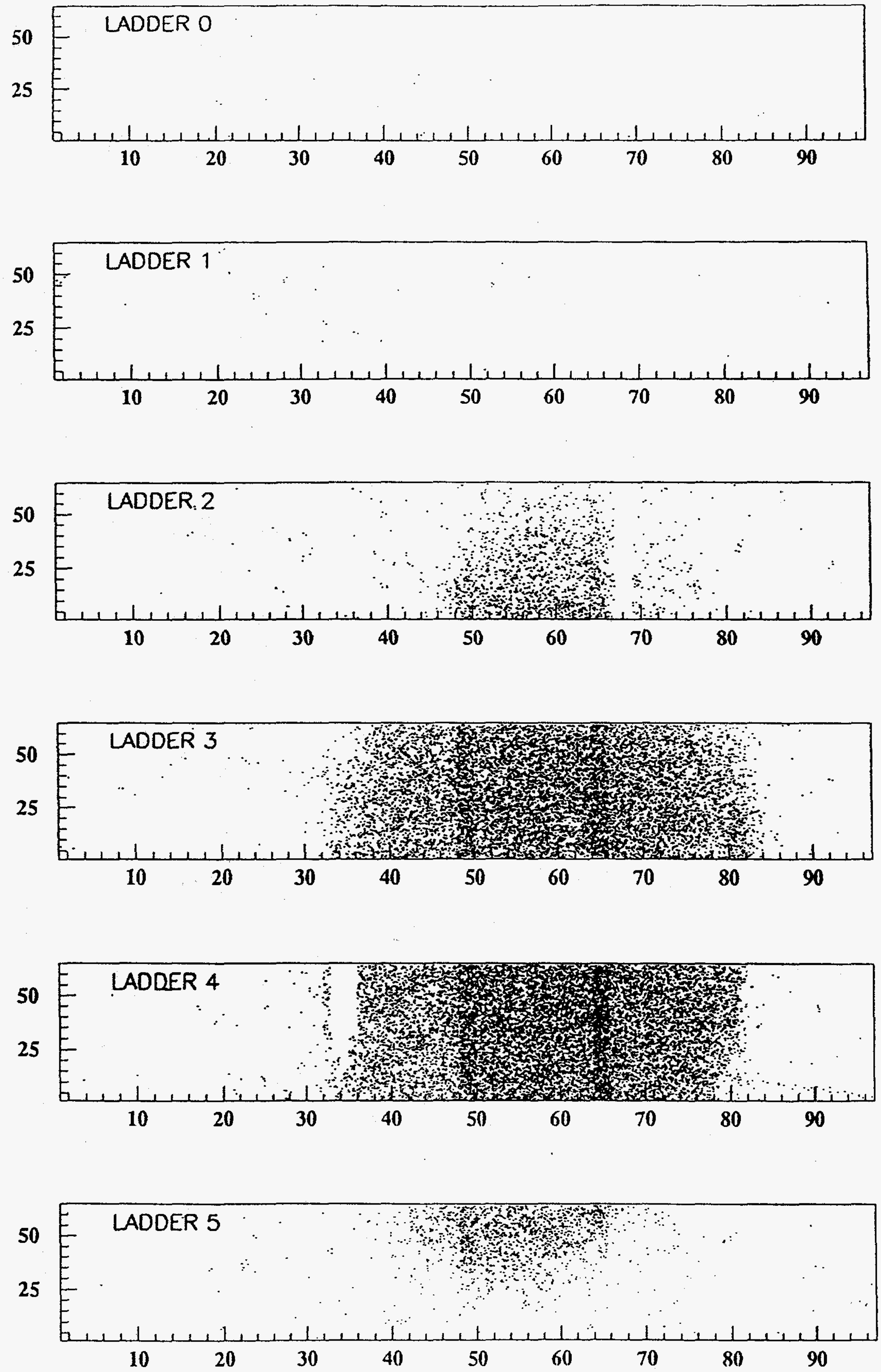

PIXEL COLUMNS PROFILE

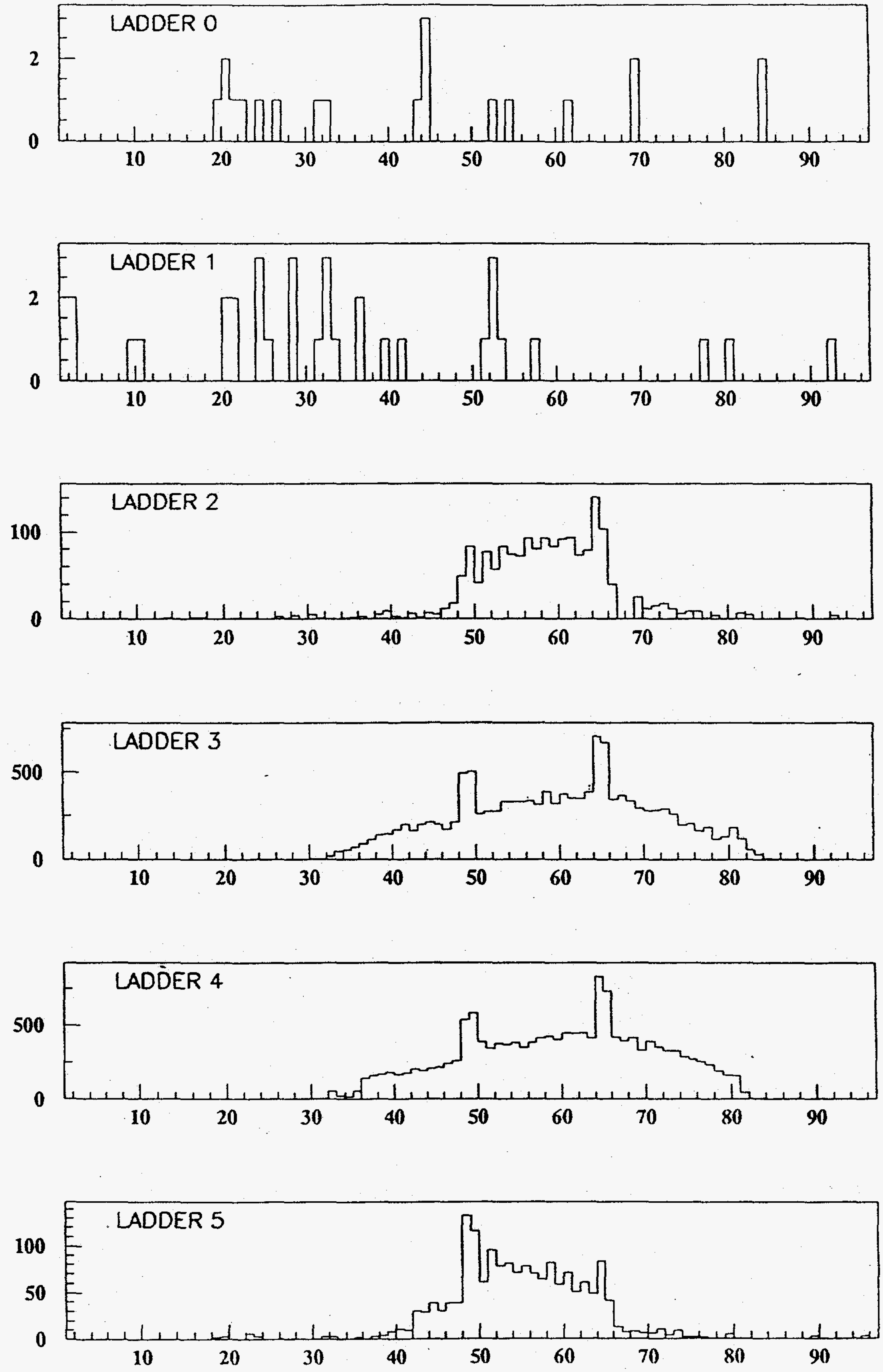

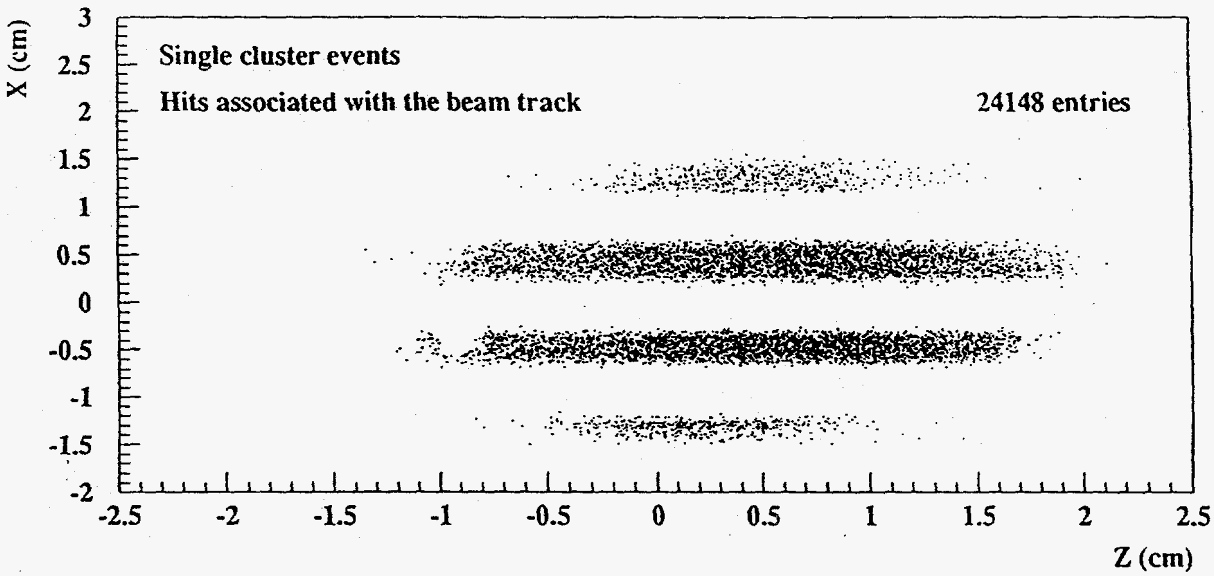
Single cluster events
Hits associated with the beam track
24148 entries
X (cm)
Z (cm)

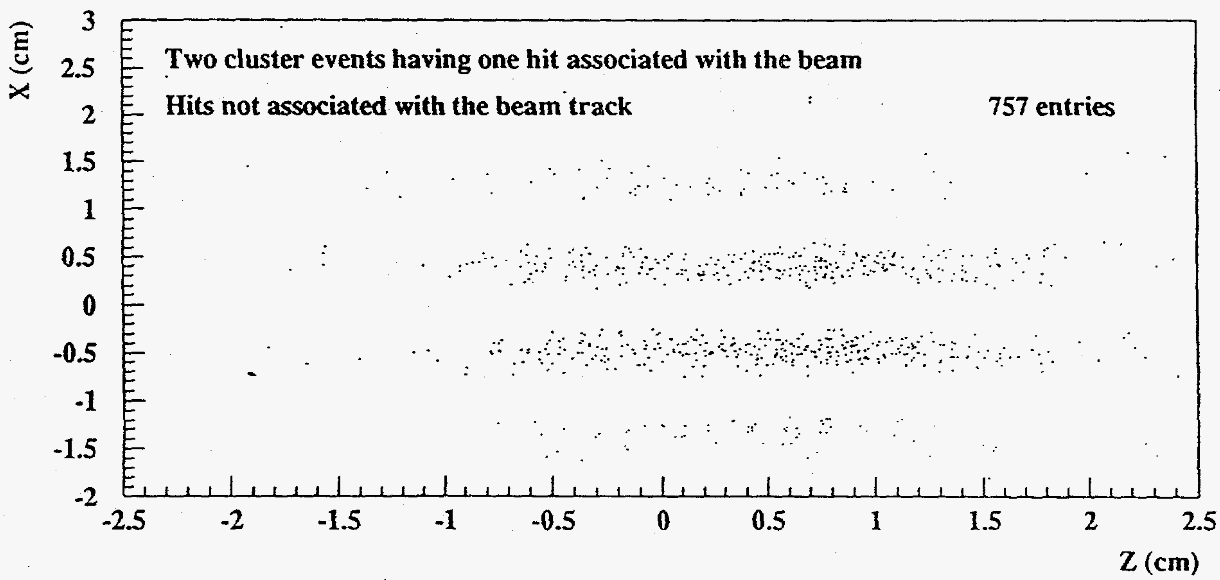
Two cluster events having one hit associated with the beam
Hits not associated with the beam track
757 entries
X (cm)
Z (cm)

WA97 Test Beam Setup

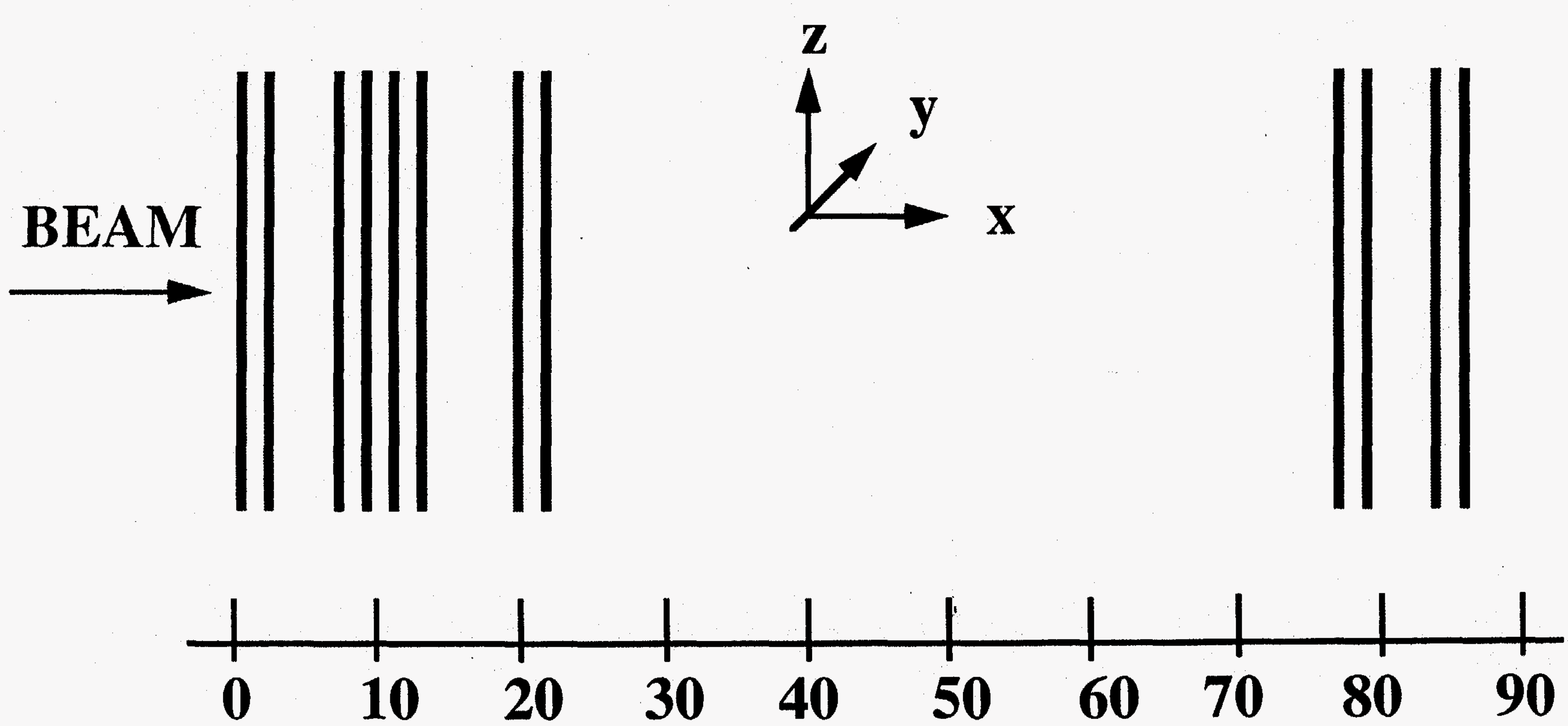

| = Y direction microstrips (50 μm pitch)

| = Z direction microstrips (50 μm pitch)

| = Pixel plane (75 μm x 500 μm)

OMEGA WA97 PIXEL TEST (1993)

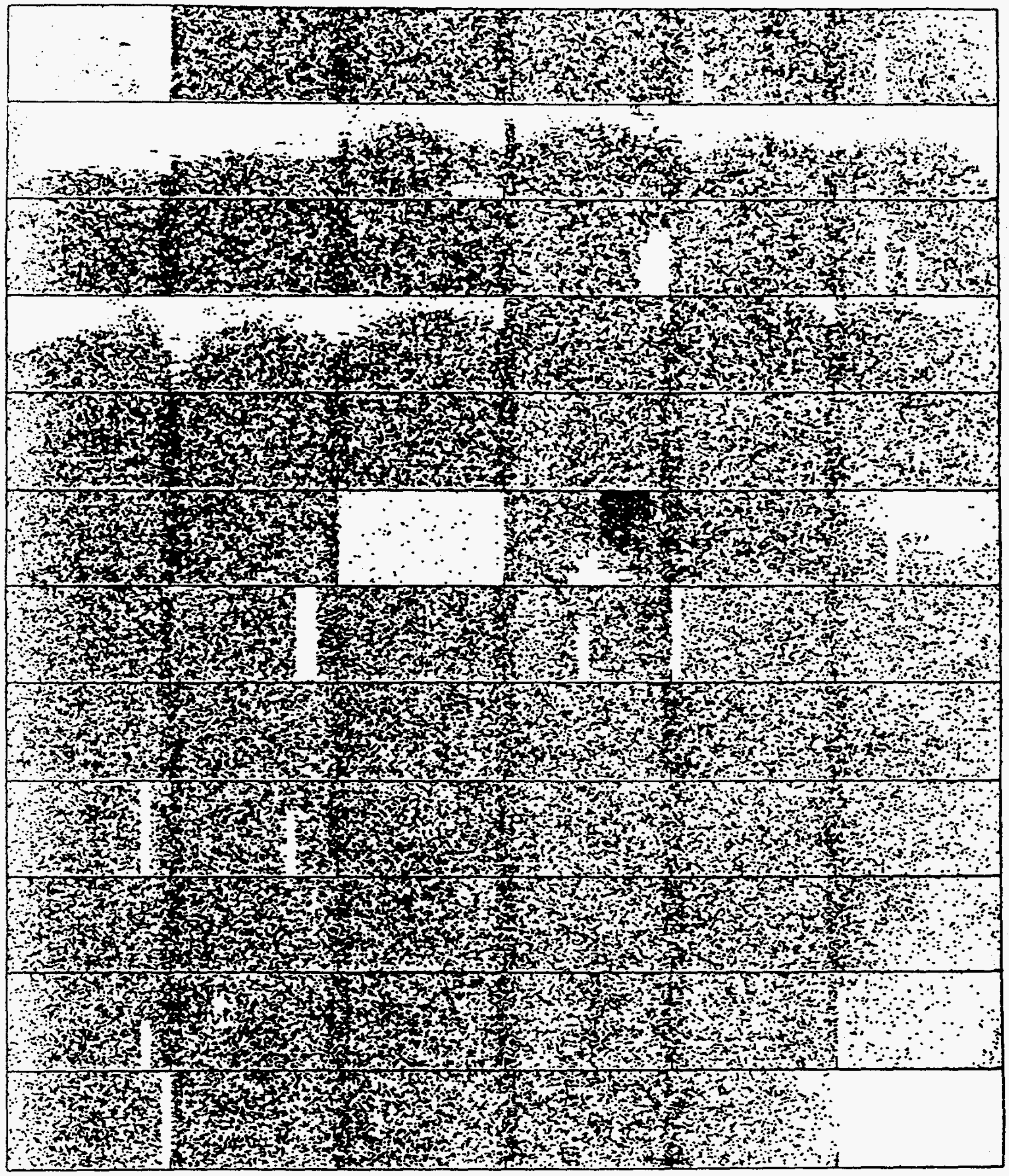

PIXEL RESOLUTION

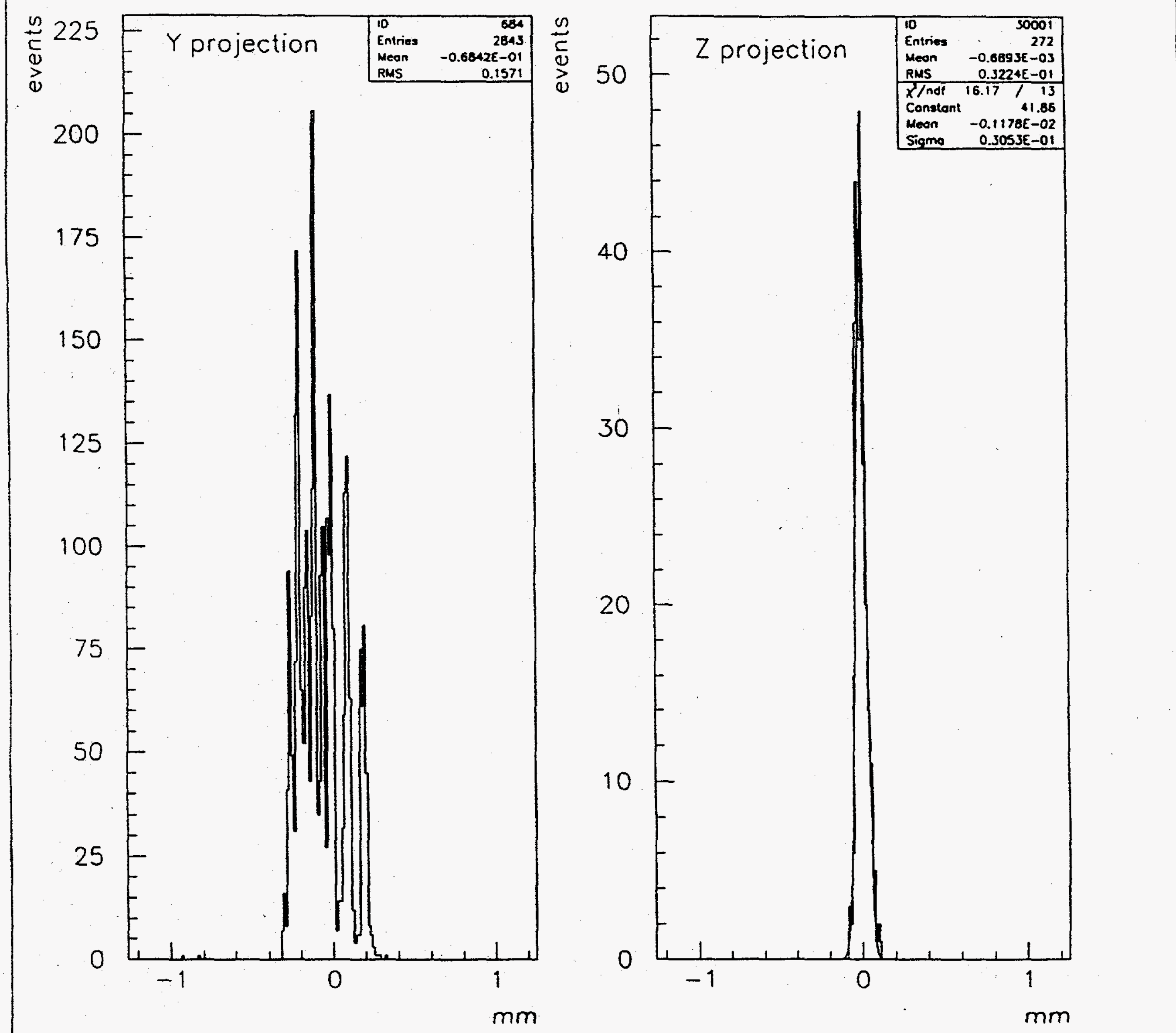

Conclusions

- A silicon pixel detector has been developed for high energy physics applications
- A logical plane of 5 cm x 5 cm has been constructed comprising 2 physical planes and containing 72 000 sensitive elements
- The equivalent noise charge has been measured to be 170 e^-
- Clean data has been obtained in several beam tests
- Pixel detectors hold great potential for future HEP experiments and may be of interest for the APS

Applications to photon imaging

- Different detector material to improve detection efficiency eg GaAs
- Tiling an area with one plane could be difficult
- Present readout scheme well adapted for HEP - may need to be changed
- Already tested for visible detection

Key references:

F. Anghinolfi et al.

A 1006 element hybrid silicon pixel detector with strobed binary output

IEEE trans Nucl. Sci. NS-39 (1992) 654.

E.H.M. Heijne et al.

First operation of a 72 k element hybrid silicon micropattern pixel detector array

to be submitted to,

Nuclear Instruments and Methods A, February 1994.

copies and preprints available from:

M. Campbell

ECP Division

CERN

1211 Geneva 23

Switzerland

Wolfgang Sturhahn

Advanced Photon Source
Argonne National Laboratory

APDs - Large Dynamic Range Detectors for Hard X-rays†

The ultrahigh brilliance of the third-generation synchrotron radiation sources will increase count rates by several orders of magnitude if compared to existing synchrotron radiation sources. Detectors that allow one to exploit this advantage should have a linear range of operation that reaches from very high count rates to their intrinsic noise level. We investigated APDs (Avalanche Photo Diodes) with respect to linearity, efficiency, time resolution, and dynamic range by the use of 8.4-keV and 14.4-keV synchrotron radiation. We observed linear behavior up to count rates of 10^8 Hz. The intrinsic noise level was below 10^{-2} Hz. Efficiencies of about 50% at 8.4 keV and about 14% at 14.4 keV were achieved. The time resolution was about 1 ns. We will present the experimental data and discuss the performance of APD detectors.

---

† in collaboration with T. Toellner, E. E. Alp, P. Montana, and M. Ramanathan. This work is supported by US - DOE, BES Materials Science, under contract No.: W-31109-ENG-38.

APDs - Large Dynamic Range Detectors for Hard X-Rays

by

Wolfgang Sturhahn

Argonne National Laboratory

Advanced Photon Source

(1) Introduction

(2) Multiphoton Counting

(3) Linearity

(4) Time Resolution and Dynamic Range

(5) Efficiency

(6) Conclusion

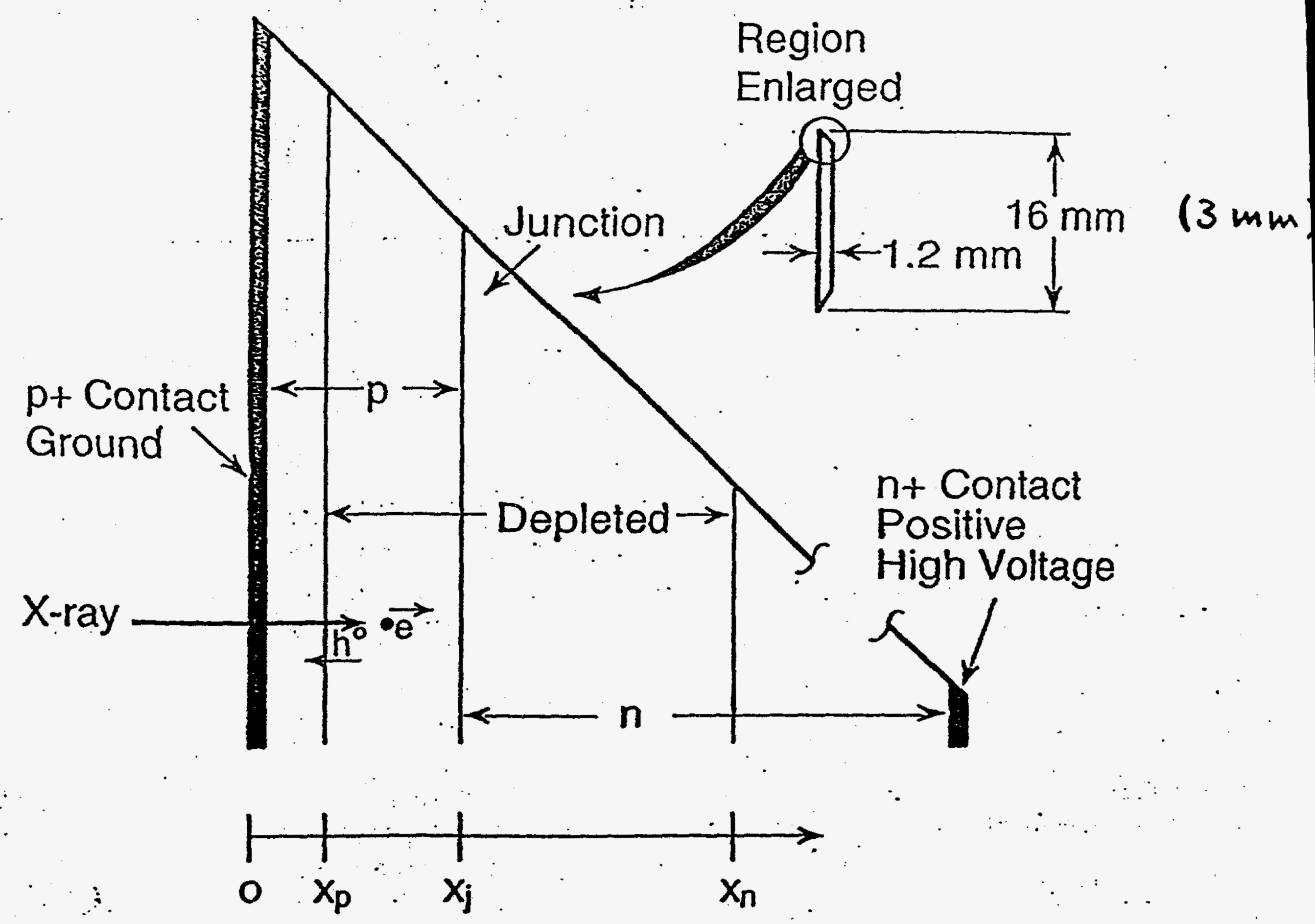

APD operational setup:

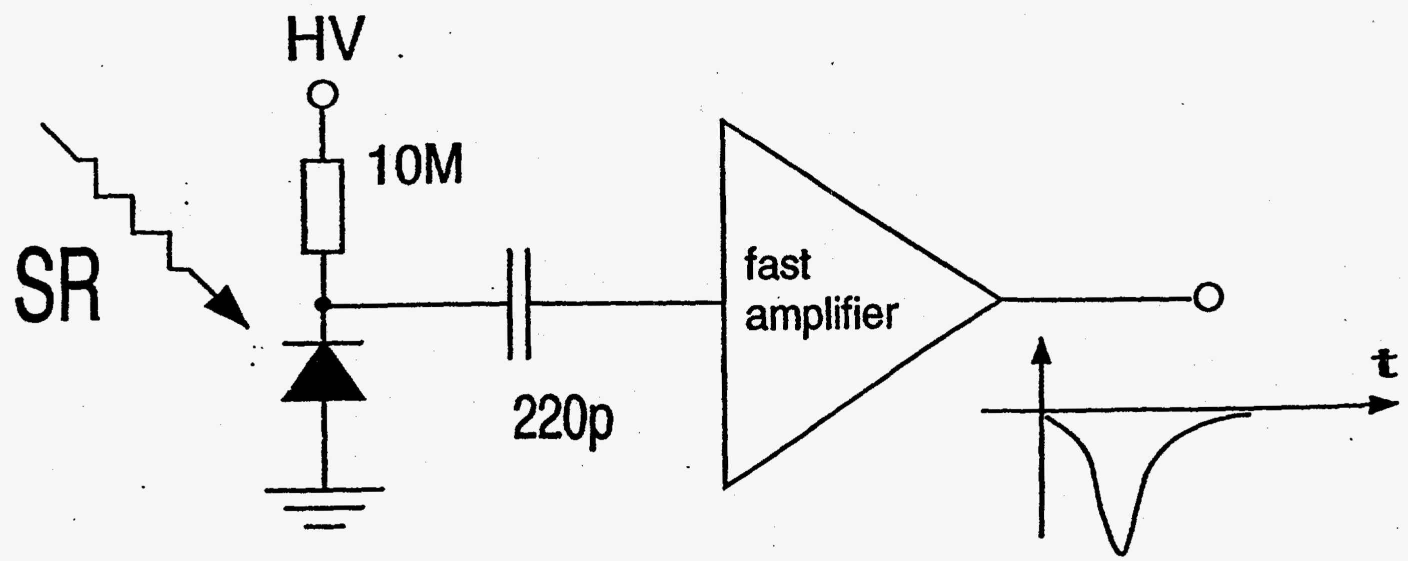

Multiphoton counting

- the average number of photons per SR flash may come close to one or at high intensities exceed one considerably

- the APD output pulse height increases in steps with the step size proportional to the amount of charge one photon is releasing

  (energy resolution: 10% @ 6 keV)

2.1

100 KHz

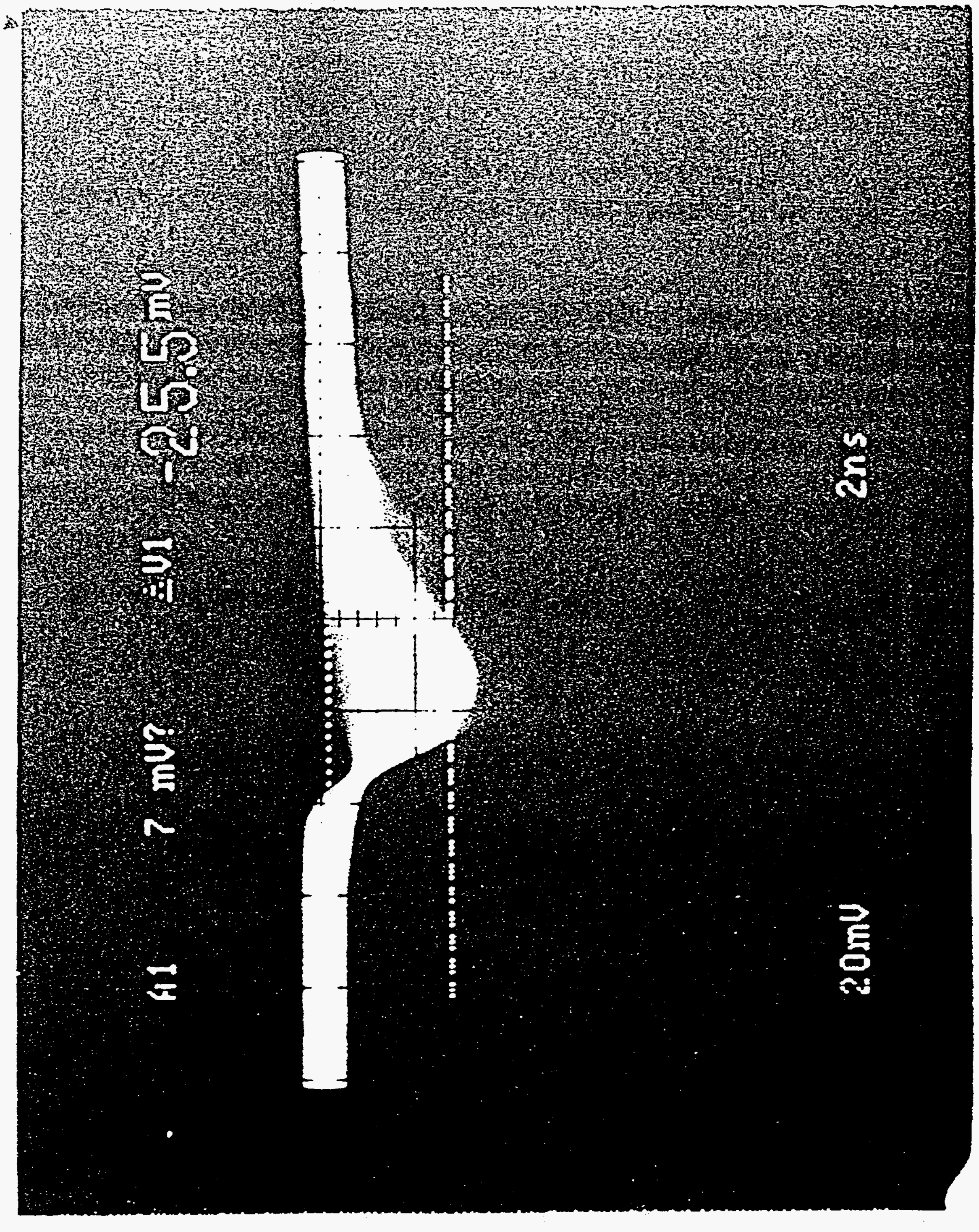

2.2

$1.4 \cdot 10^6$ Hz

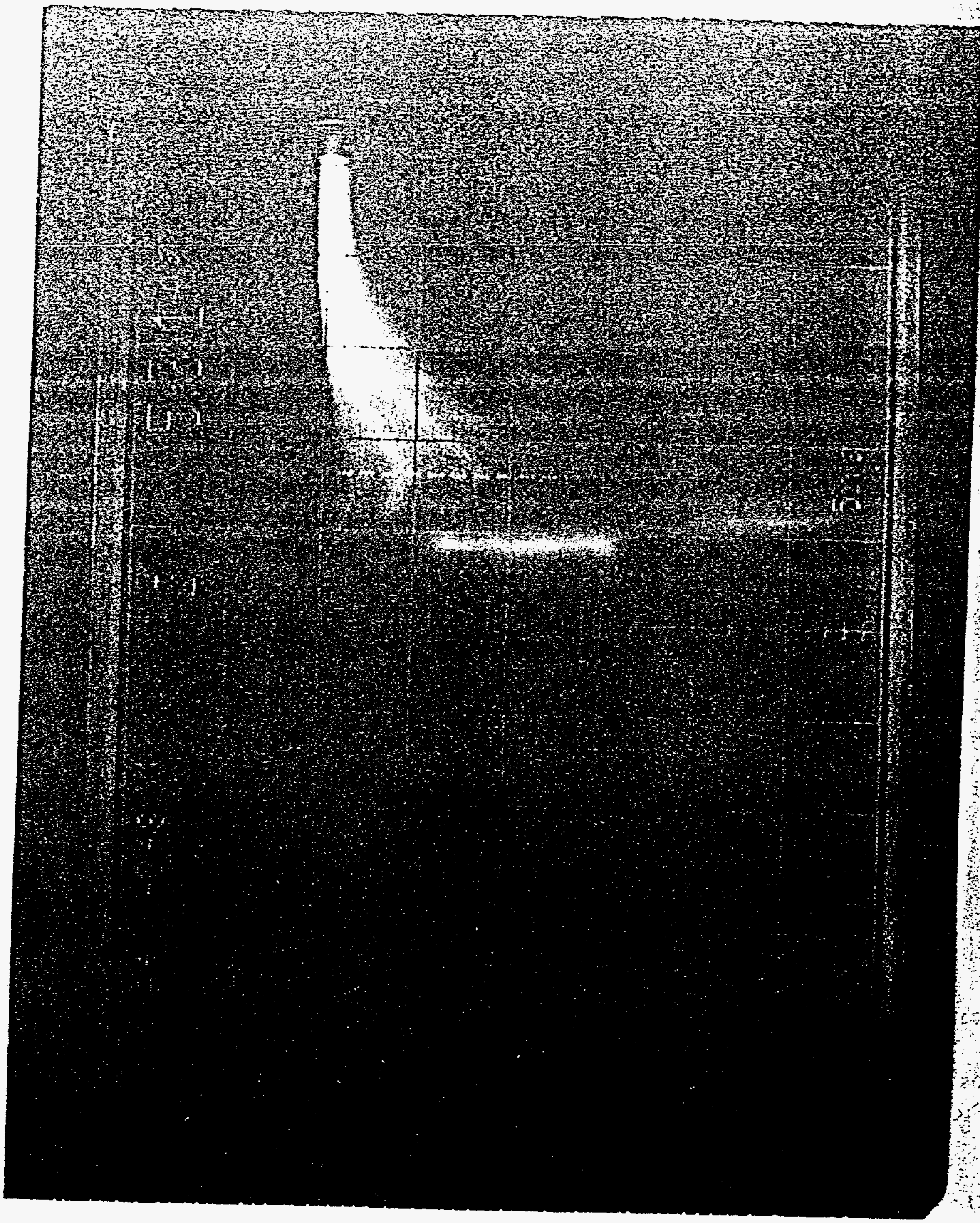

2.3

$9.6 \cdot 10^7$ Hz 54 photons/flash

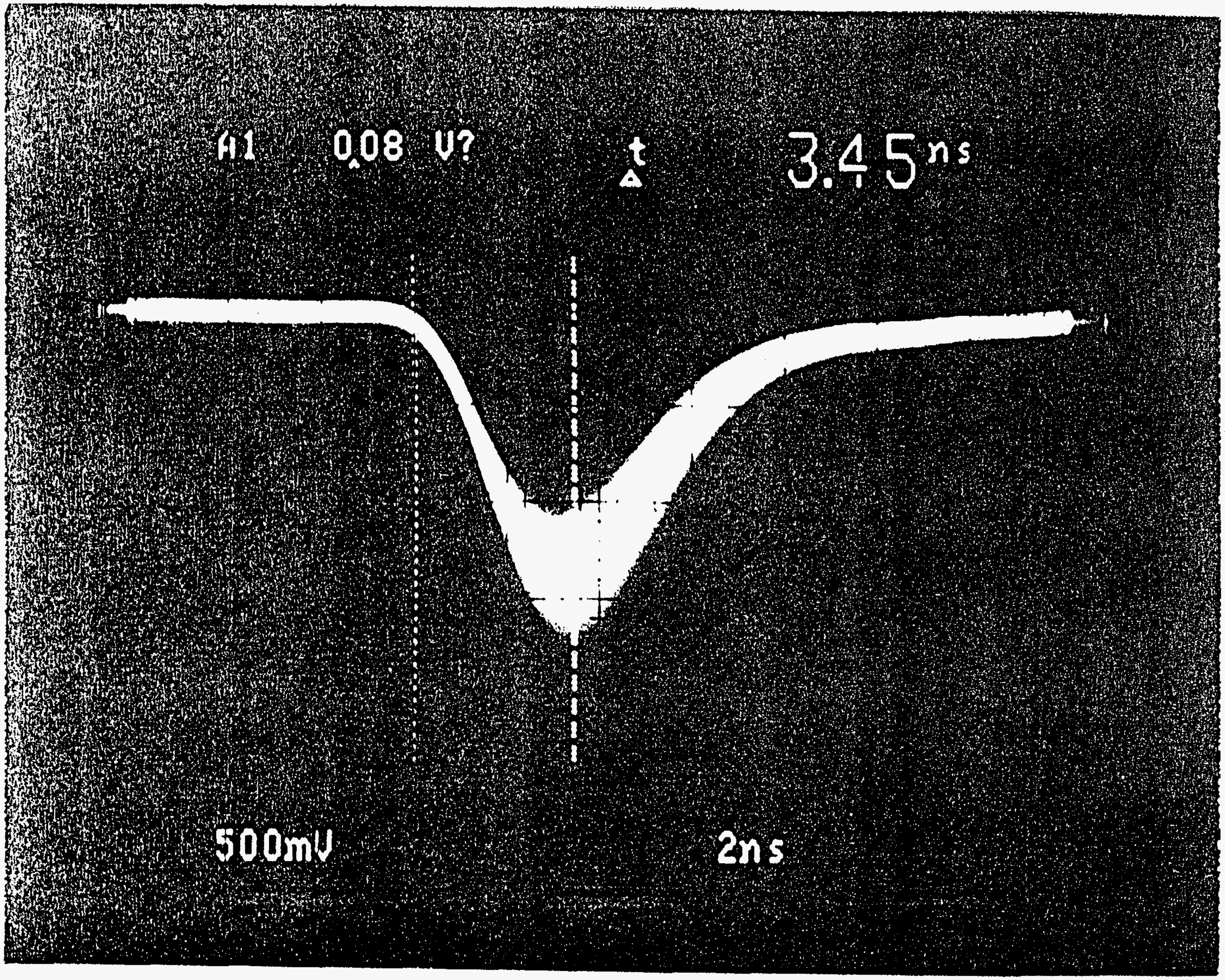

$3 \cdot 10^9$ Hz photons/flash

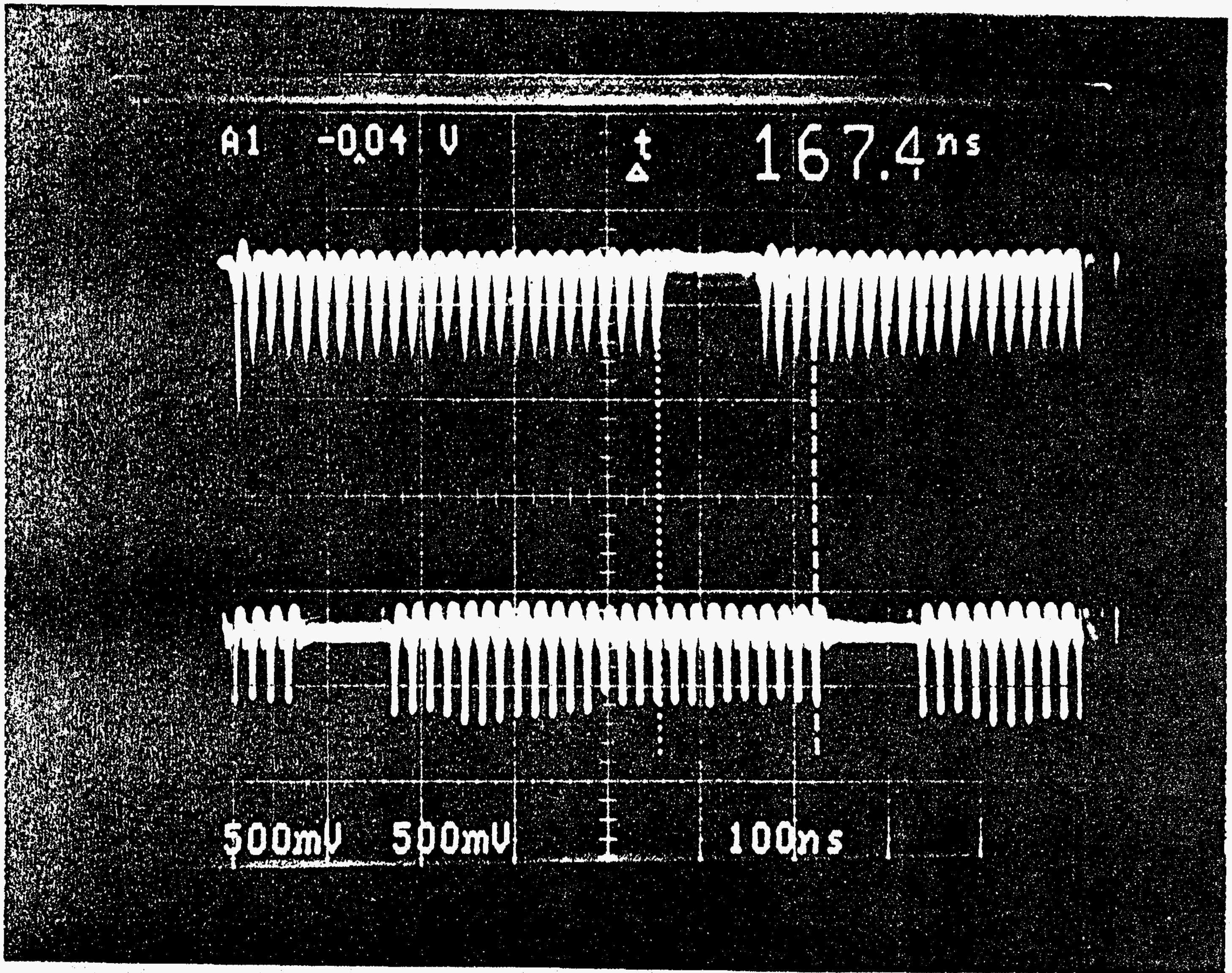

Multiphoton counting

The probability to observe n photons in a SR flash is given by

$$p_n(\lambda) = e^{-\lambda} \frac{\lambda^n}{n!} \qquad \text{(Poisson distr.)}$$

with $\lambda = I \cdot \tau$

- τ — separation of SR pulses
- I — average intensity

If the detector can detect j photons in the same flash the measured intensity evaluates to

$$N_j = I - \underbrace{\frac{1}{\tau} \sum_{n=j+1}^{\infty} (n-j)\, p_n(\lambda)}_{\text{small for } I \ll \frac{1}{\tau}\{(j+1)!\}^{1/j}}$$

Linearity

experimental setup for linearity measurement

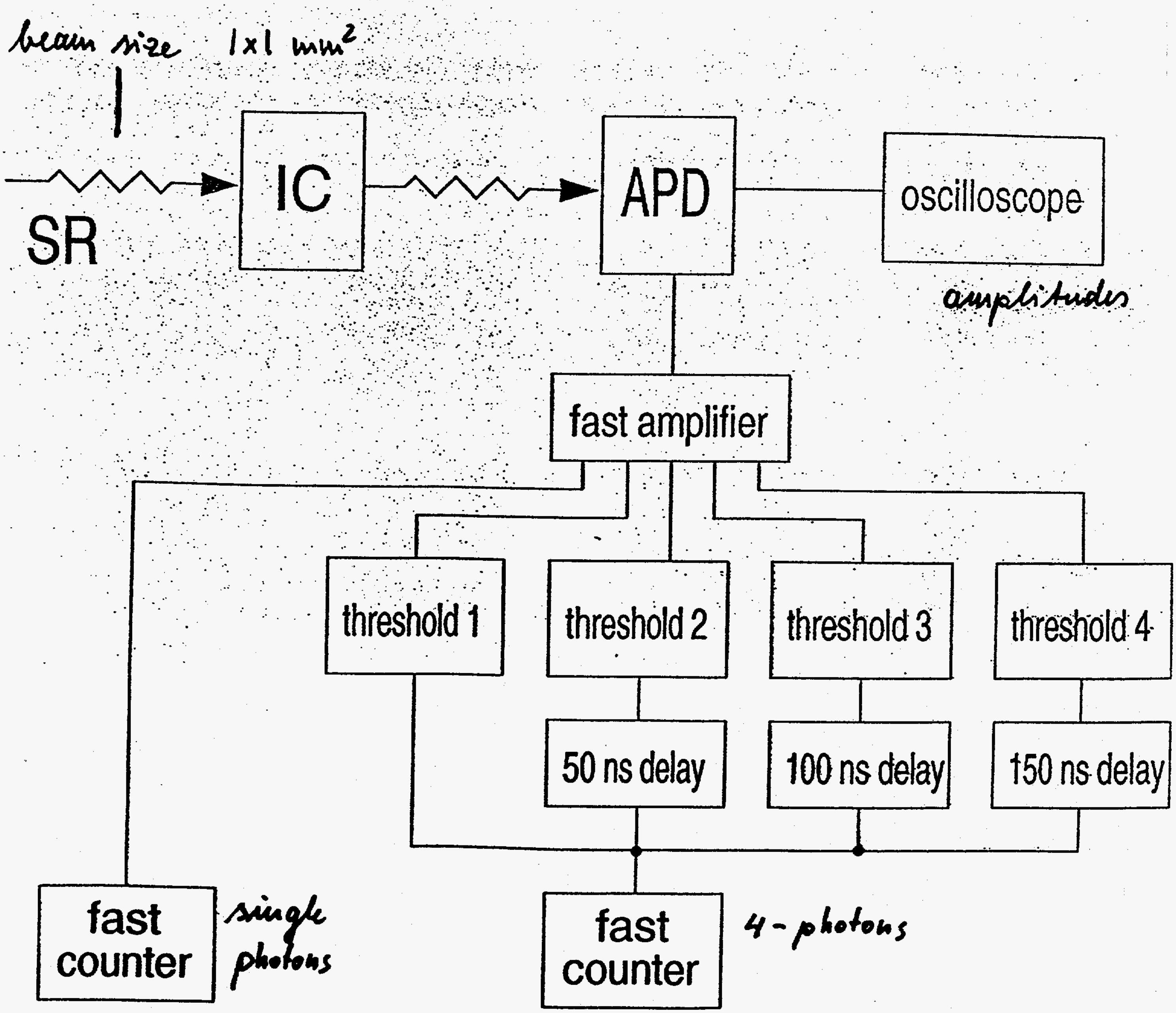

Linearity of APD to 8.4 keV photons

Ar_2 filled, 8.5 cm chamber, 1050 V

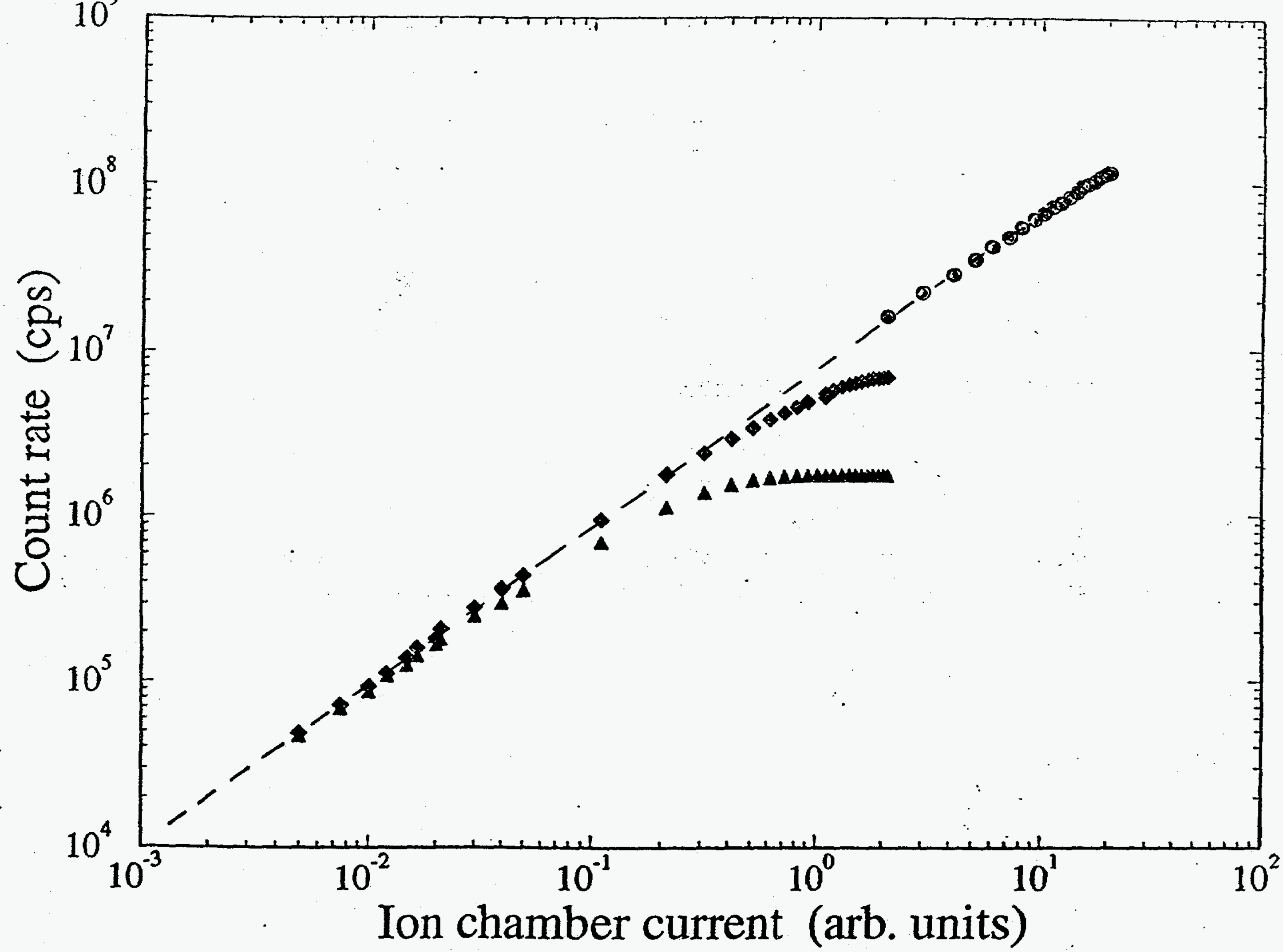

one photon counter
4 - photon counter
amplitude measurement

Time resolution and dynamic range

experimental setup for timing experiments:

- analyze the ability of an APD to count single photons after a SR flash

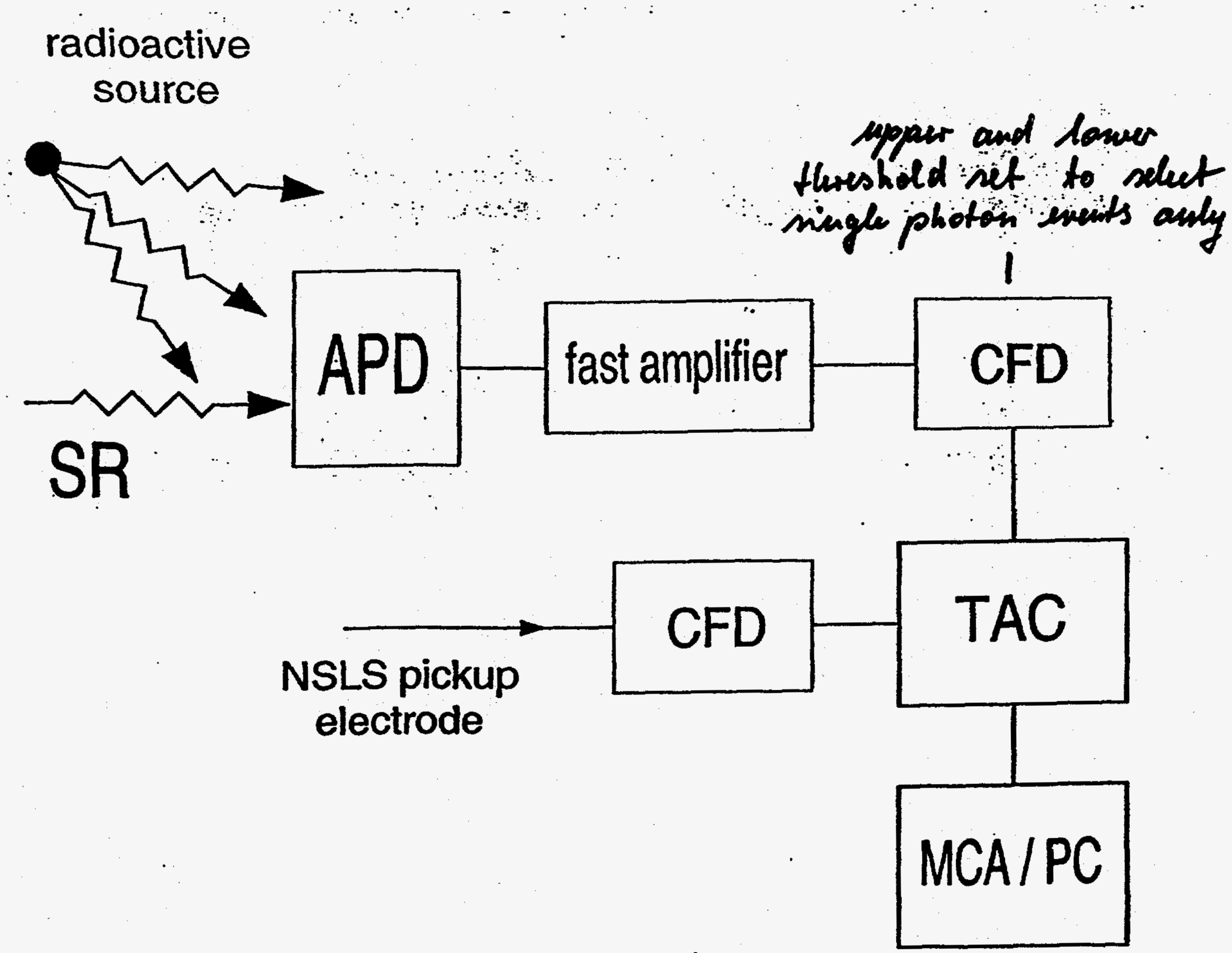

APD time response to single 8.4 keV photons

total count rate (@ 90% trigger): 260 kHz, FWHM: 0.92 ns

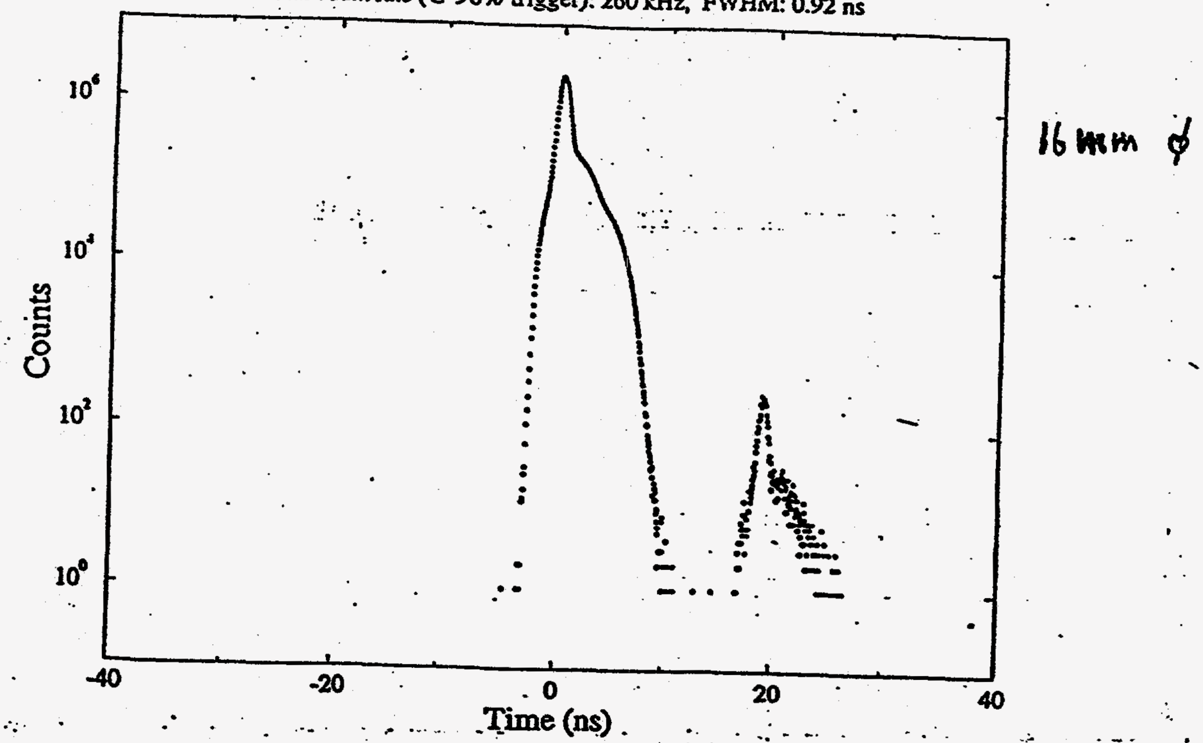

APD time response to single 8.4 keV photons

total count rate (@ 80% trigger): 250 kHz, FWHM: 1.1 ns

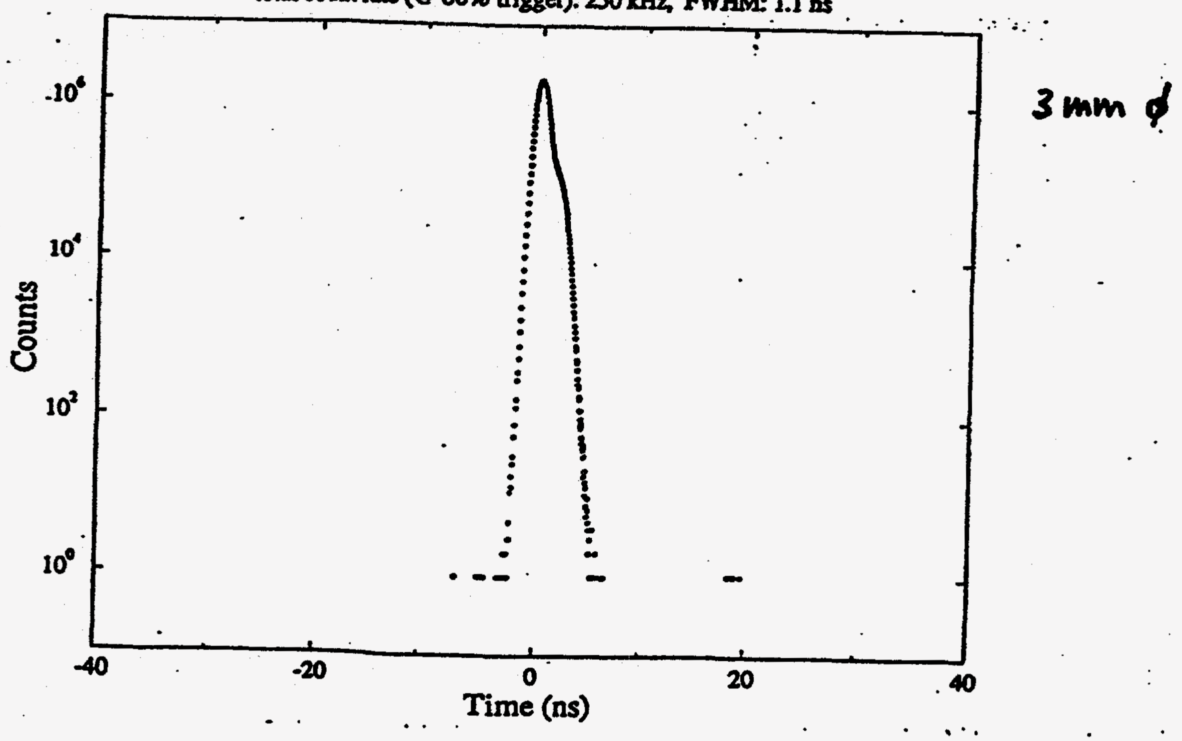

8.4 keV pulsed SR time spectrum

total count rate (@ 90% trigger): 100 kHz, single photon events only

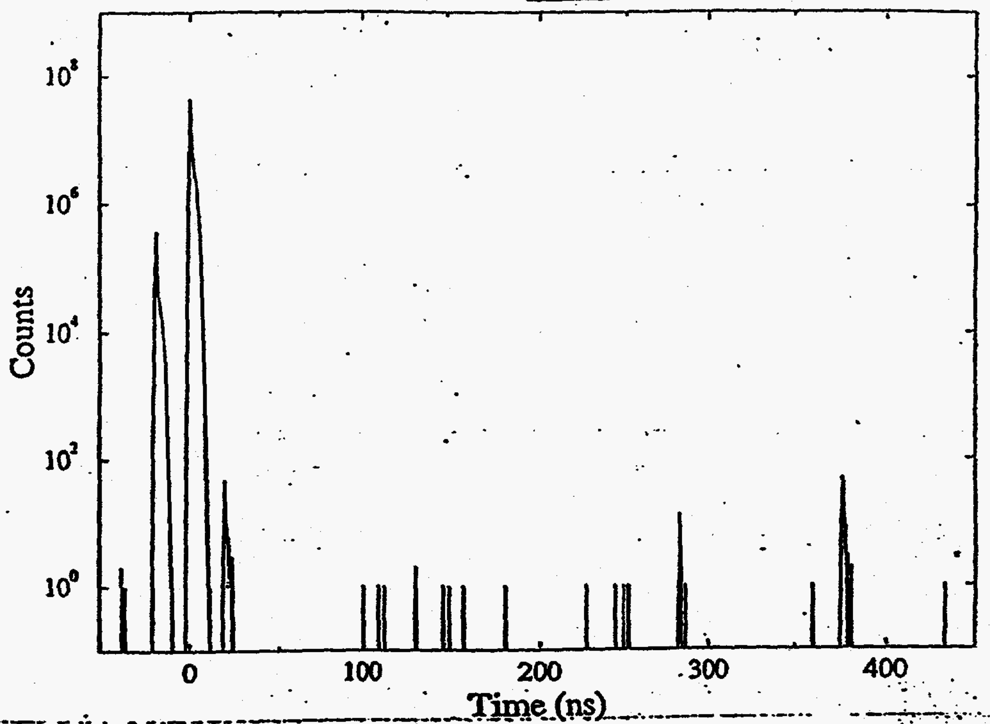

~ 30 min

8.4 keV pulsed SR time spectrum

total count rate (@ 90% trigger): 26 MHz, single photon events only

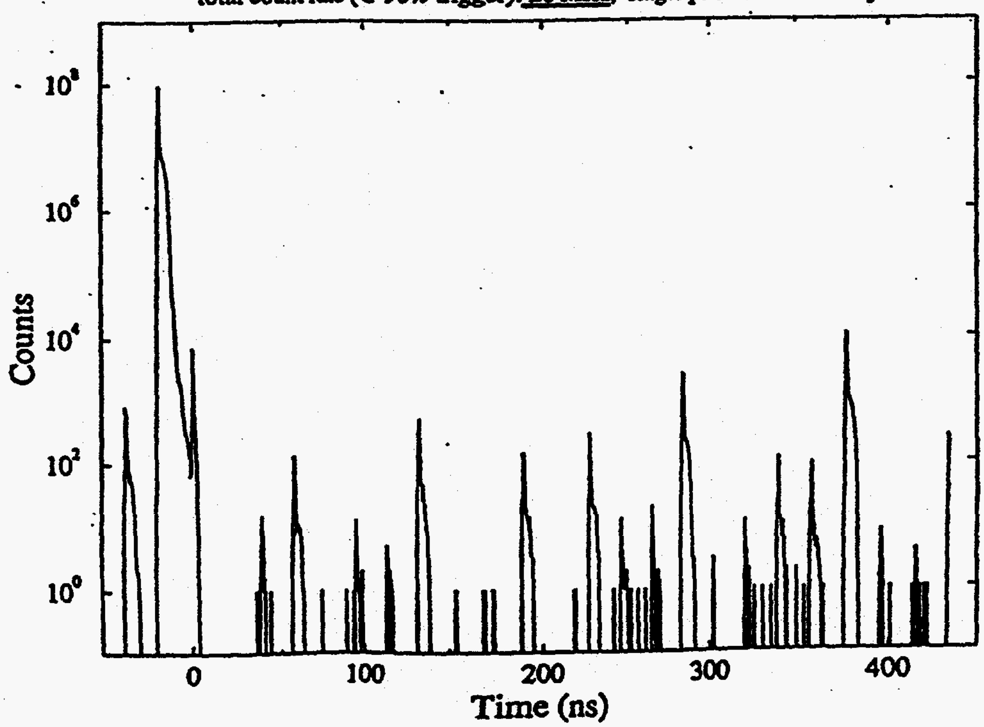

8.4 keV pulsed SR and CuK (8 keV) source

total count rate (@ 90% trigger): 70 kHz, single photon events only

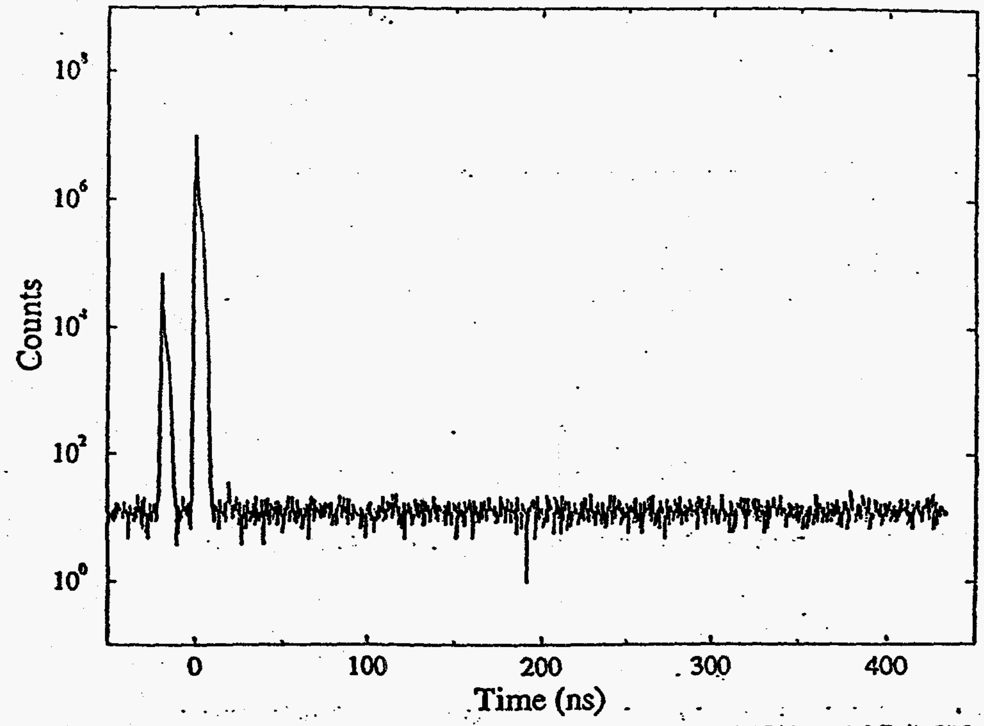

8.4 keV pulsed SR and CuK (8 keV) source

total count rate (@ 90% trigger): 26 MHz, single photon events only

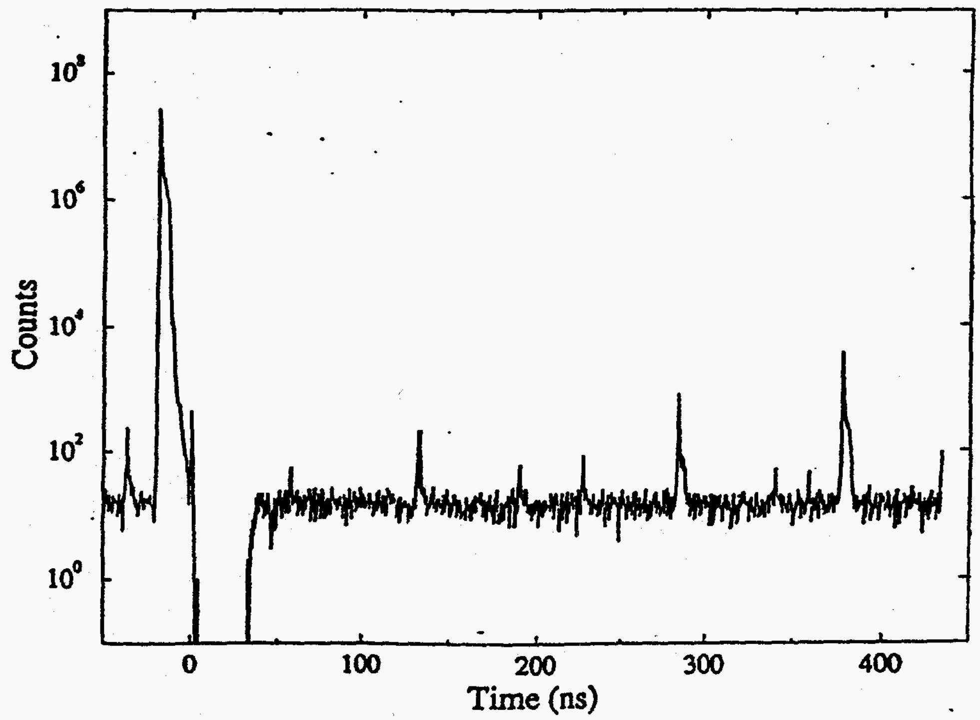

Efficiency

- the efficiency is determined by the thickness of the active zone and by the substrate material

here: active zone ~ 50 μm
substrate silicon

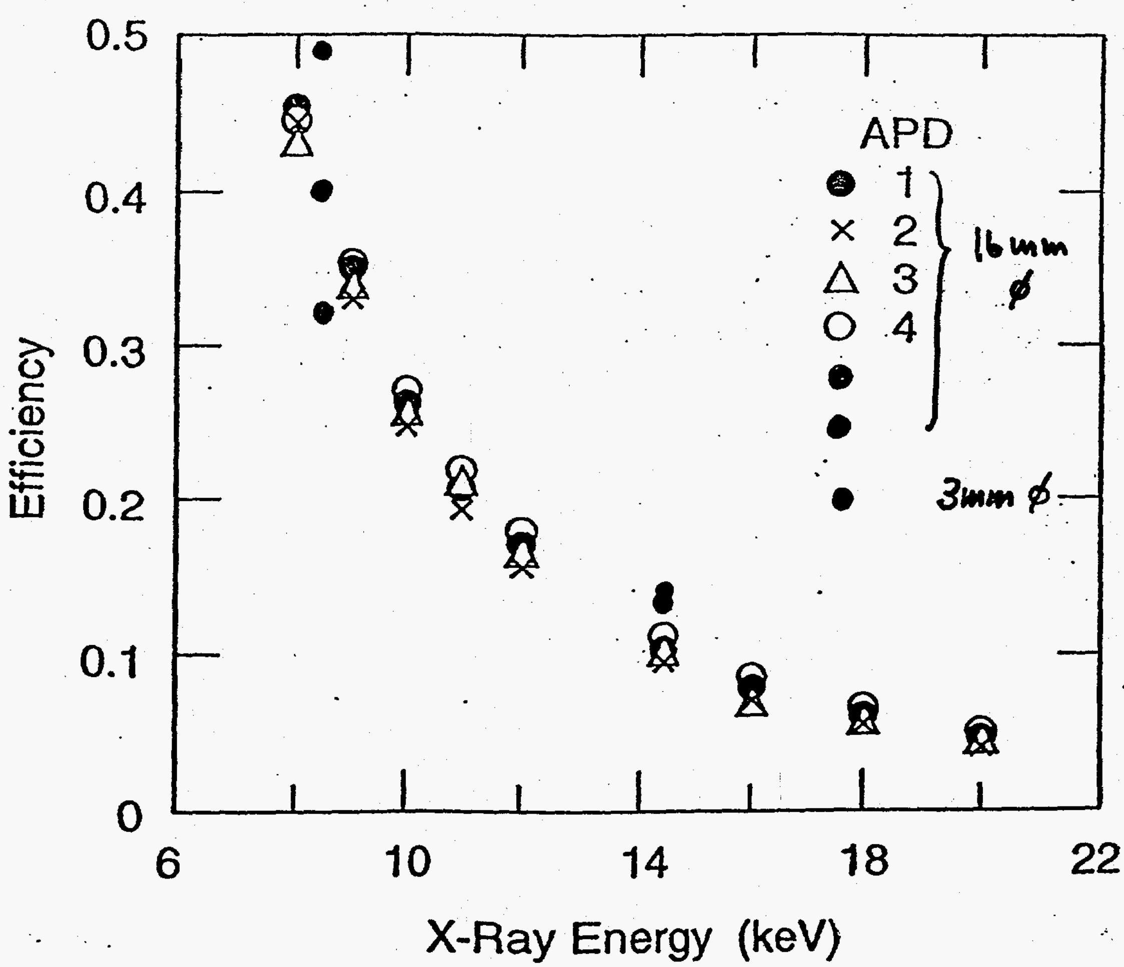

1...4 A.Q.R. Baron et al.

Conclusion

- APDs have a very good time resolution and a good energy resolution

- APDs were used for multiphoton counting and thus linear behaviour up to 10^8 Hz was demonstrated

- the noise level was well below 0.01 Hz

- reasonable efficiencies can be achieved up to 20 keV

Richard C. Schirato

Science Applications International Corporation

Application of Bulk-Grown $Cd_{1-x}Zn_xTe$ Alloys to Single-Photon X-ray Imaging

Richard C. Schirato, Raulf M. Polichar
and John H. Reed

We have fabricated monolithic x- and gamma-ray detector arrays using various $Cd_{1-x}Zn_xTe$ alloys in both linear and area geometries with associated read-out systems. Advantages of these materials include relatively high stopping power and room-temperature operation. The arrays have been operated in a pulse-counting mode with photon energy discrimination. So far, we have fabricated arrays with a pixel pitch as small as 0.8 mm. Our results show that even smaller pitches should be possible. The effects of material properties and array geometry on spatial and energy resolution will be discussed, with emphasis upon charge carrier transport. Results from calculational models and experimental measurements of pulse height vs event interaction position within a pixel will be presented, along with images obtained with these arrays. The experimental results include data from arrays recently fabricated from new High-Pressure Bridgeman-grown $Cd_{0.9}Zn_{0.1}Te$ material with improvements in both electron and hole mobility lifetime products. Possible areas of application for systems based on this technology include nuclear medicine, low-dose simultaneous dual-energy radiography, nonproliferation inspection, NDE, and x-ray astronomy.

SAIC

Science Applications International Corporation

APPLICATION OF BULK-GROWN $Cd_{1-X}Zn_{X}Te$ ALLOYS TO SINGLE-PHOTON X-RAY IMAGING

Presented to:

ADVANCED PHOTON SOURCE WORKSHOP ON DETECTORS FOR THIRD GENERATION SYNCHROTRON SOURCES
Argonne National Laboratory

Presented by :

R.C. Schirato, R.M. Polichar, J.H. Reed
SCIENCE APPLICATIONS INTERNATIONAL CORPORATION
4161 Campus Point Court, San Diego, California 92121
(619) 458-3779

February 14 and 15, 1994

SAIC-94PRSNT-6 SAIC-94RS-5

Science Applications International Corporation

ADVANTAGES OF SOLID STATE IONIZATION DETECTORS

- HIGH EFFICIENCY POSSIBLE
- LARGE SIGNAL CURRENTS (Relative to Scintillators - Photodiodes)
- FAST COLLECTION TIME
- ADAPTABLE TO BOTH PULSE COUNTING AND CURRENT MODE
- CAN BE MADE AS MONOLITHIC ARRAYS

SAIC-93RS-42

USE OF MONOLITHIC ARRAYS FOR X-RAY AND GAMMA-RAY IMAGING DEVICES

- GOOD DIRECTIONAL CHARGE COLLECTION IN HIGH-FIELD MONOLITHIC DEVICES GIVES CROSSTALK PERFORMANCE COMPETITIVE WITH DISCRETE DEVICES
- VACUUM DEPOSITION OF CONTACTS MAKES LARGER AND MORE COMPLEX DEVICES PRACTICAL
- FABRICATION COSTS OF MONOLITHIC ARRAYS ARE LESS THAN COMPARABLE MULTIPLE DISCRETE DEVICE ARRAYS
- READOUT FOR BOTH LINEAR AND AREAL ARRAYS DEMONSTRATED
- TECHNOLOGY OF MONOLITHIC CONSTRUCTION DEMONSTRATED AND AVAILABLE NOW

SAIC®

ADVANTAGES OF USING HIGH PRESSURE BRIDGMAN GROWN CdTe AND CdZnTe FOR DETECTORS AND ARRAYS

- LARGE AREA BOULE CROSSECTION ALLOWS FLEXIBLE USE OF MATERIALS
- NEW REFINING METHODS RESULT IN HIGHER RESISTIVITIES (>10" OHM-cm) AND LONGER CARRIER LIFETIMES
- UNIFORMITY OVER CROSSECTION PERMITS FABRICATION OF LARGE MONOLITHIC ARRAYS
- SEVERAL RELIABLE SOURCES OF MATERIALS ALLOW ONE TO FOCUS ON DETECTOR FABRICATION AND SYSTEMS
- NEW PROCESSING METHODS ARE ALREADY LEADING TO LOWER COSTS AND HIGHER PERFORMANCE DEVICES

SAIC-94RS-10

Science Applications International Corporation

APPLICATION OF MONOLITHIC CdTe and CdZnTe DETECTOR ARRAYS TO NUCLEAR AND X-RAY IMAGING

COMPARISON OF GAMMA RAY EFFICIENCY FOR DIFFERENT THICKNESS OF CdZnTe AND A STANDARD NaI ANGER PLATE

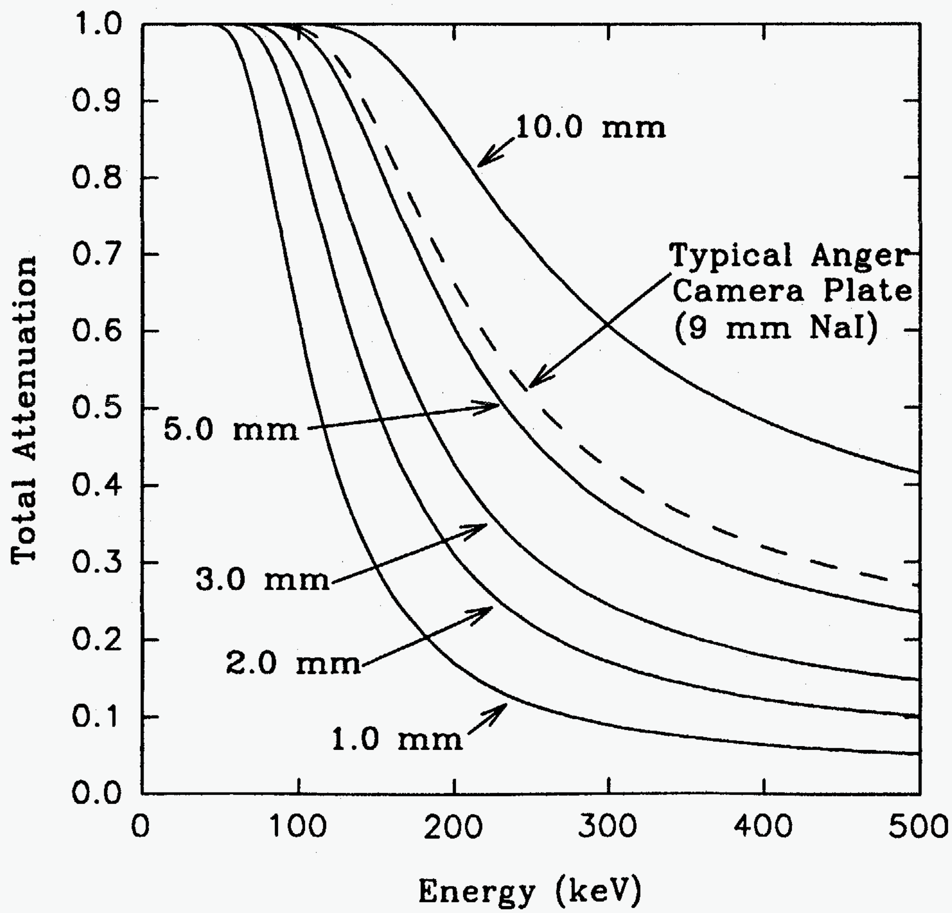

SAIC-93RP-114

Science Applications International Corporation

CALCULATION OF RELATIVE CHARGE OUTPUT, Q AS A FUNCTION OF INTERACTION POSITION

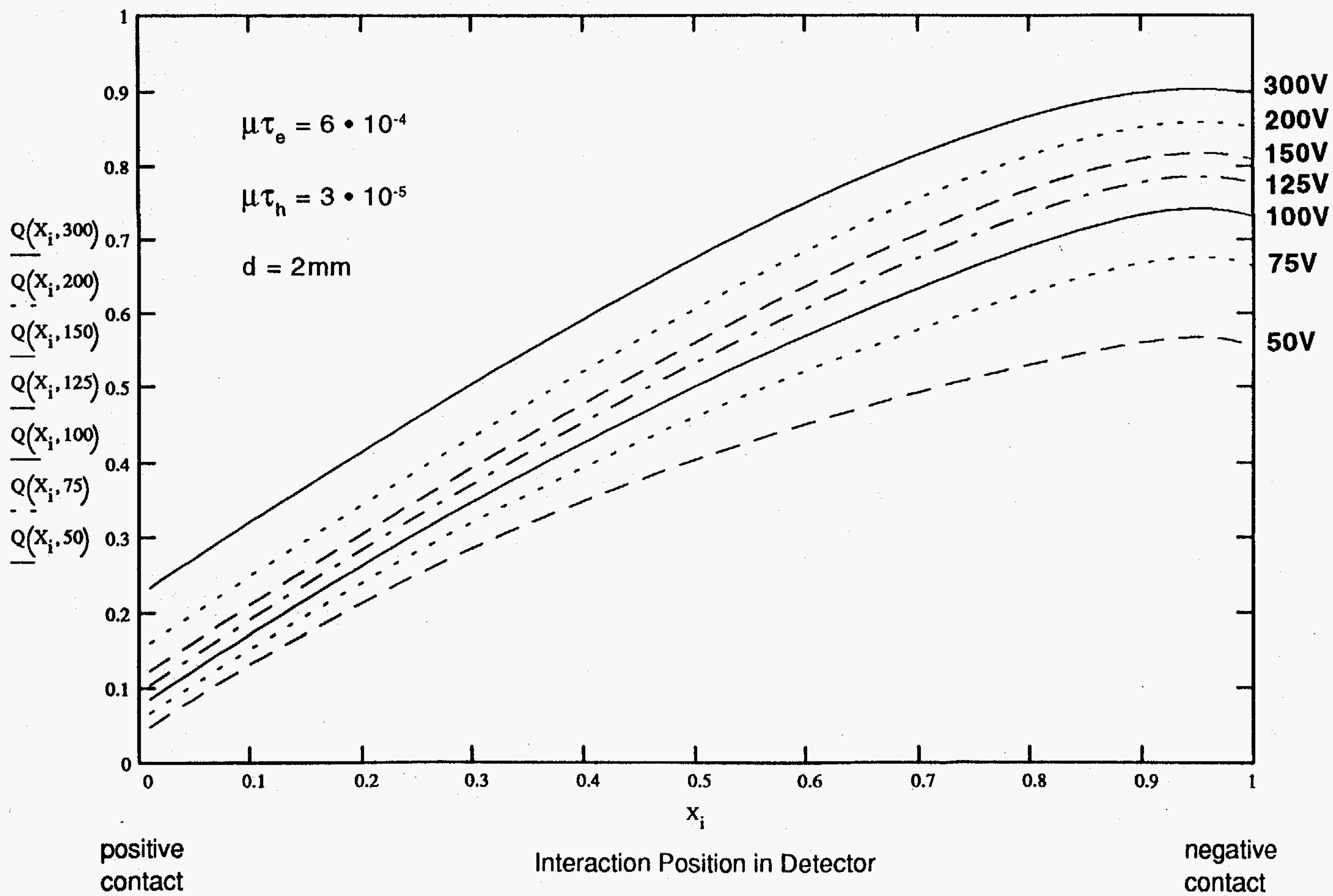

SAIC-94RP-2

Science Applications International Corporation

CALCULATION OF RELATIVE CHARGE OUTPUT, Q AS A FUNCTION OF INTERACTION POSITION

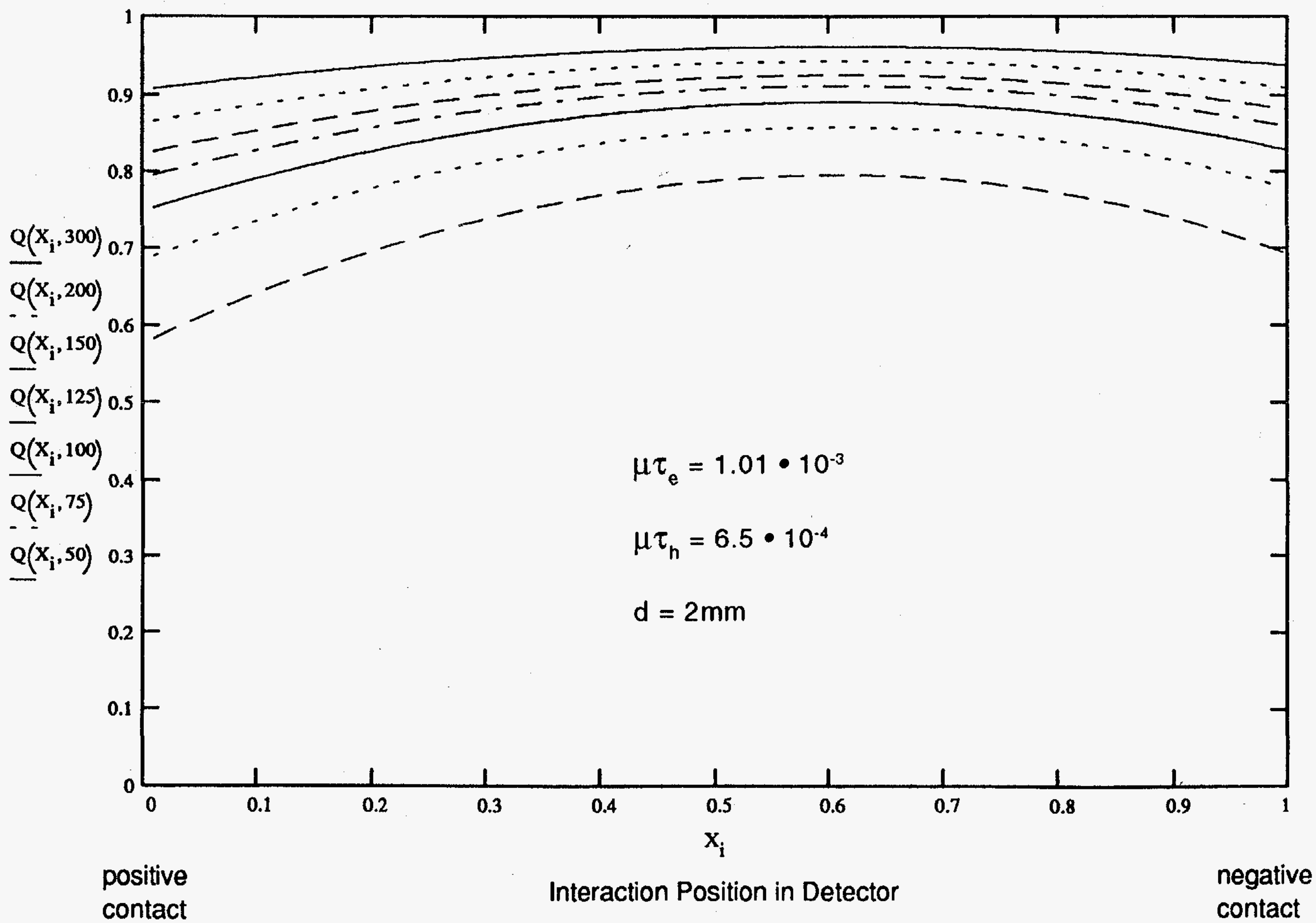

SAIC-94RP-1

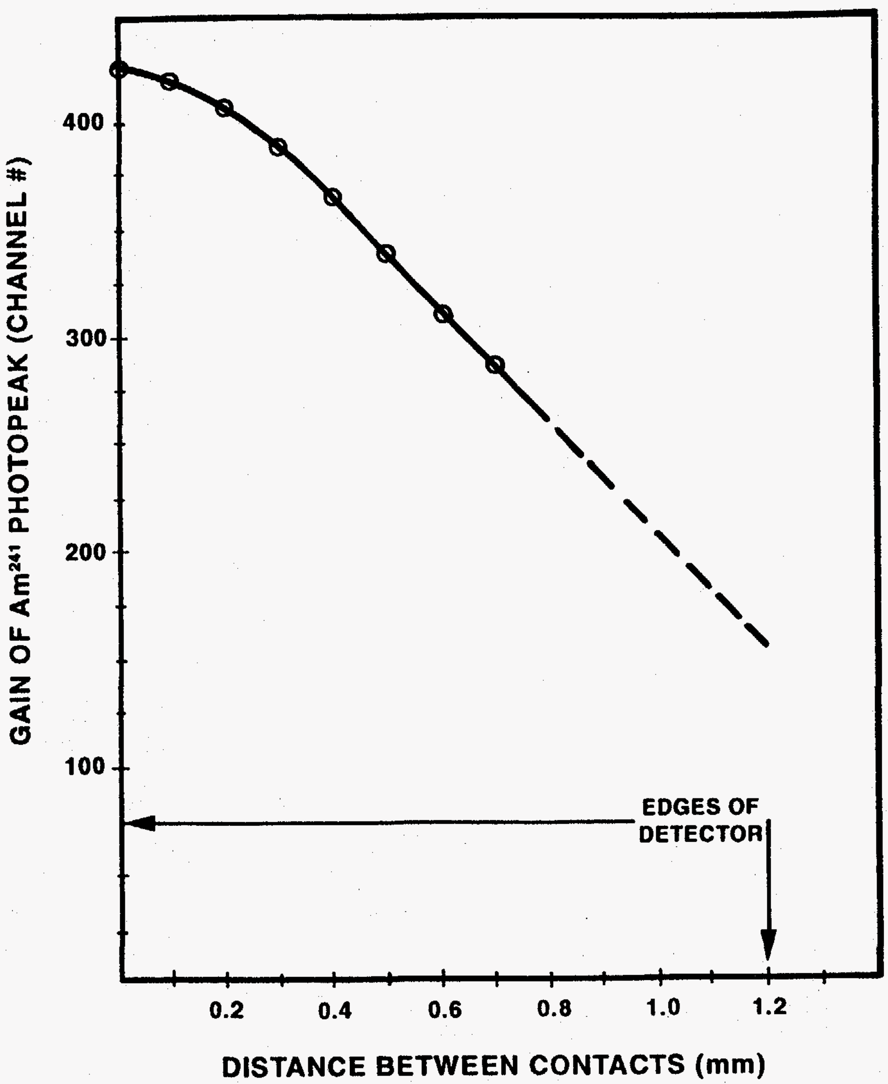

MEASURED VARIATION OF DEVICE GAIN ACROSS DETECTOR WIDTH IS DUE TO CHARGE TRAPPING OF HOLE CARRIERS IN EARLY CdZnTe WHEN VIEWED BY SIDE-ENTRANCE GEOMETRY

SAIC-92RP-192

Science Applications International Corporation

APPLICATION OF MONOLITHIC CdTe and CdZnTe DETECTOR ARRAYS TO NUCLEAR AND X-RAY IMAGING

SENSOR MATERIALS EVALUATED

$Cd_{0.8}Zn_{0.2}Te$	[AURORA TECH. EARLY HPB DEVELOPMENT MATERIAL]
CdTe	[eV PRODUCTS / II/VI: ULTRAPURE HPB, UNDOPED MATERIAL]
$Cd_{0.9}Zn_{0.1}Te$	[eV PRODUCTS / II/VI: ALLOYED, HPB MATERIAL WITH LOWER LEAKAGE AND IMPROVED CHARGE COLLECTION]

SAIC-93RP-118

PULSE HIEGHT SPECTRUM OF ^{57}Co (122 keV) USING A 2.5 cm THICK $Cd_{0.9}Zn_{0.1}Te$ DETECTOR

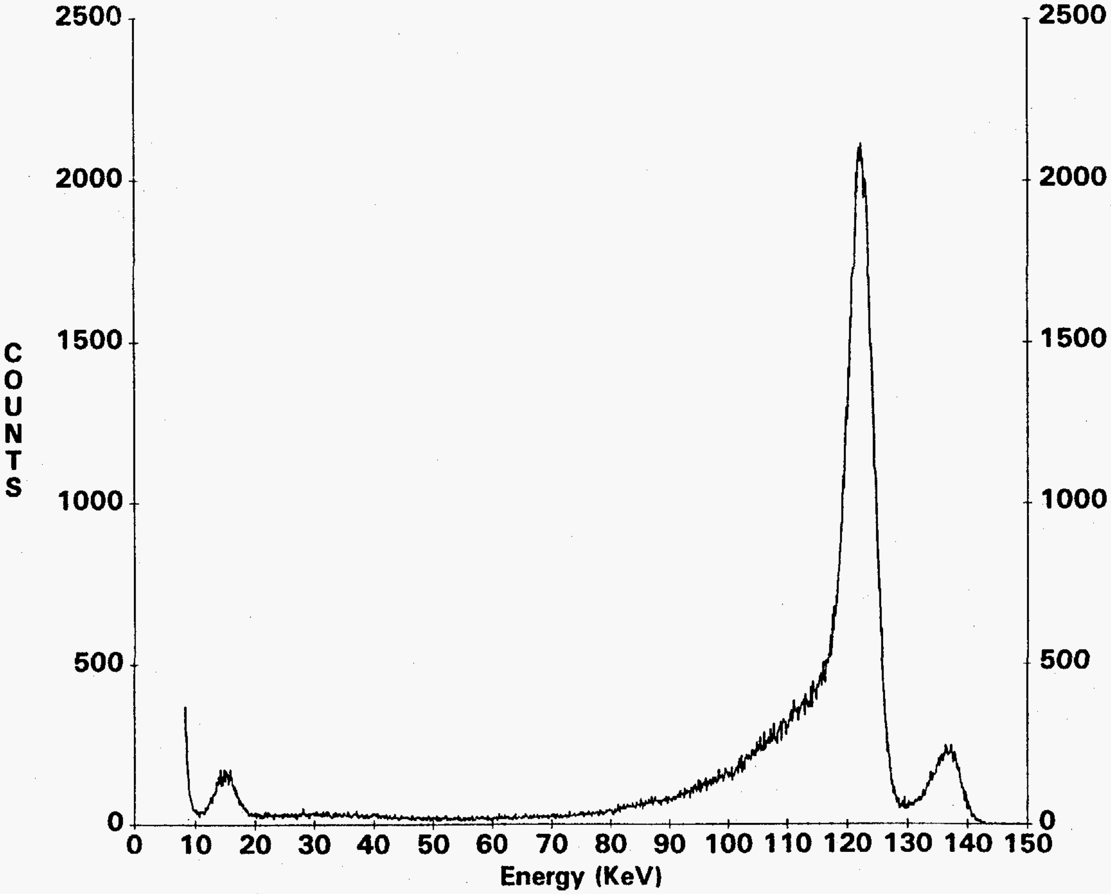

Source	^{57} Co
Crystal Size	10mm x 10mm x 25mm
Bias Voltage	+2000 VDC
Shaping time	2 μsec
Oper. temp.	+25º C
FWHM	4.7 %

Spectrum Courtesy eV Products

SAIC-94RS-11

Science Applications International Corporation

CdZnTe LINEAR SCANNER ILLUMINATION GEOMETRY

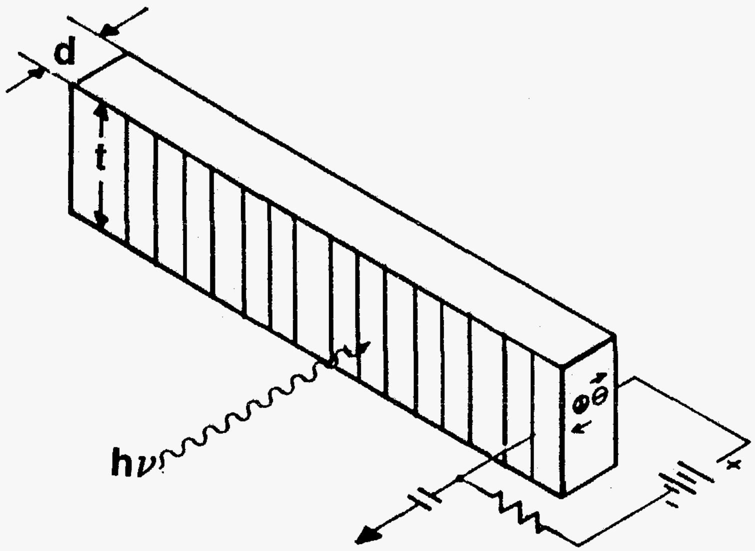

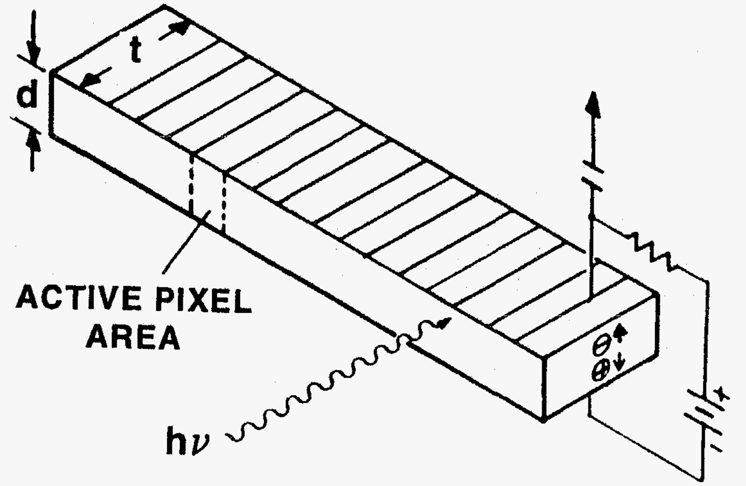

Standard Geometry
Gammas Enter Neg Contact
Best Energy Resolution for Low-Energy Radiation
Limited Stopping Power Because
Charge Collection Limits Depth

Side Illuminated Geometry
Poorer Resolution for Low-Energy Gammas
Enhanced Efficiency for Higher Energies
Shows Promise for High-Energy Spectrometers

Science Applications International Corporation

16- ELEMENT CdZnTe LINEAR ARRAY MOUNTED ON PLUG-IN HEADER ASSEMBLY

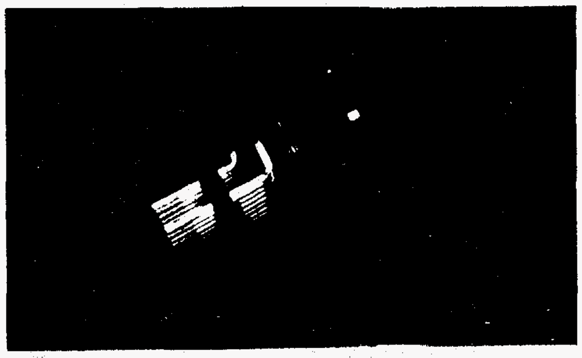

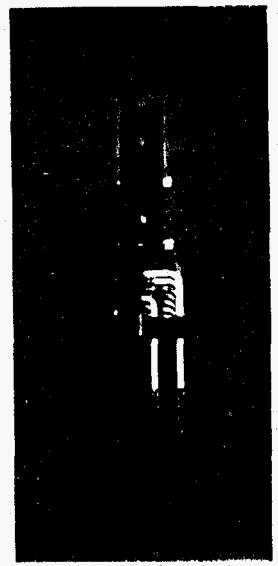

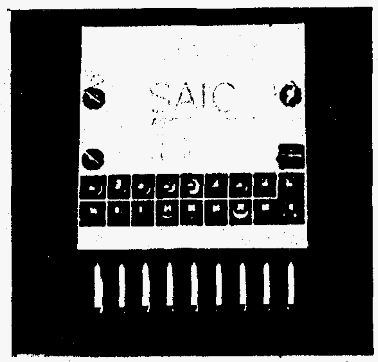

SAIC-92RP-185

Science Applications International Corporation

UNIQUE DC BIASING OF MULTI-ELEMENT DEVICE REDUCES NOISE FROM BIAS RESISTOR, BUT DEPENDS ON LOW-LEAKAGE CURRENT DEVICES SUCH AS CdZnTe

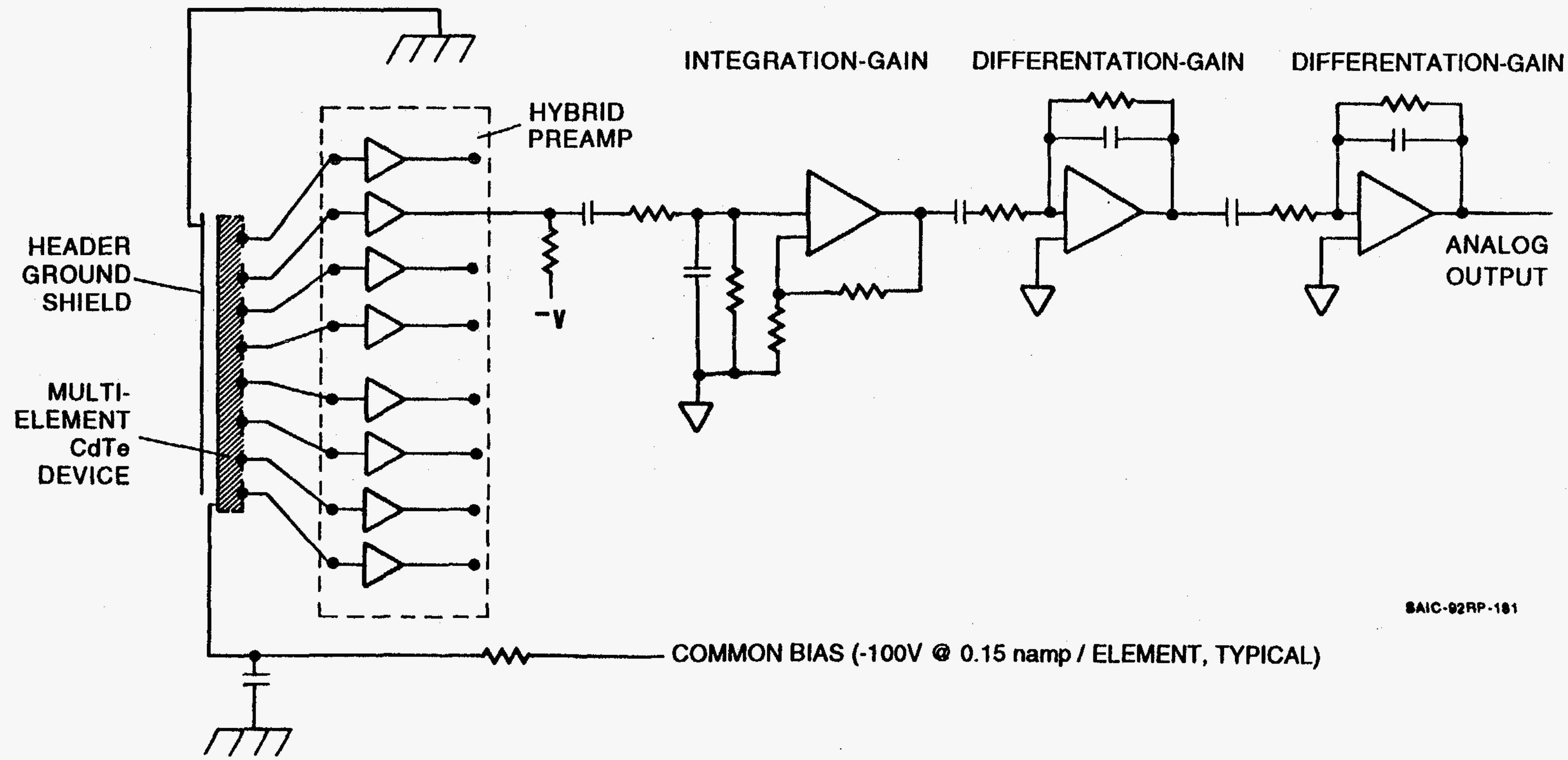

Science Applications International Corporation

COMPLETED 16-CHANNEL READOUT SYSTEM INCLUDES ALL ANALOG PULSE SHAPING, COMPARITORS AND BUFFERED DIGITAL OUTPUTS

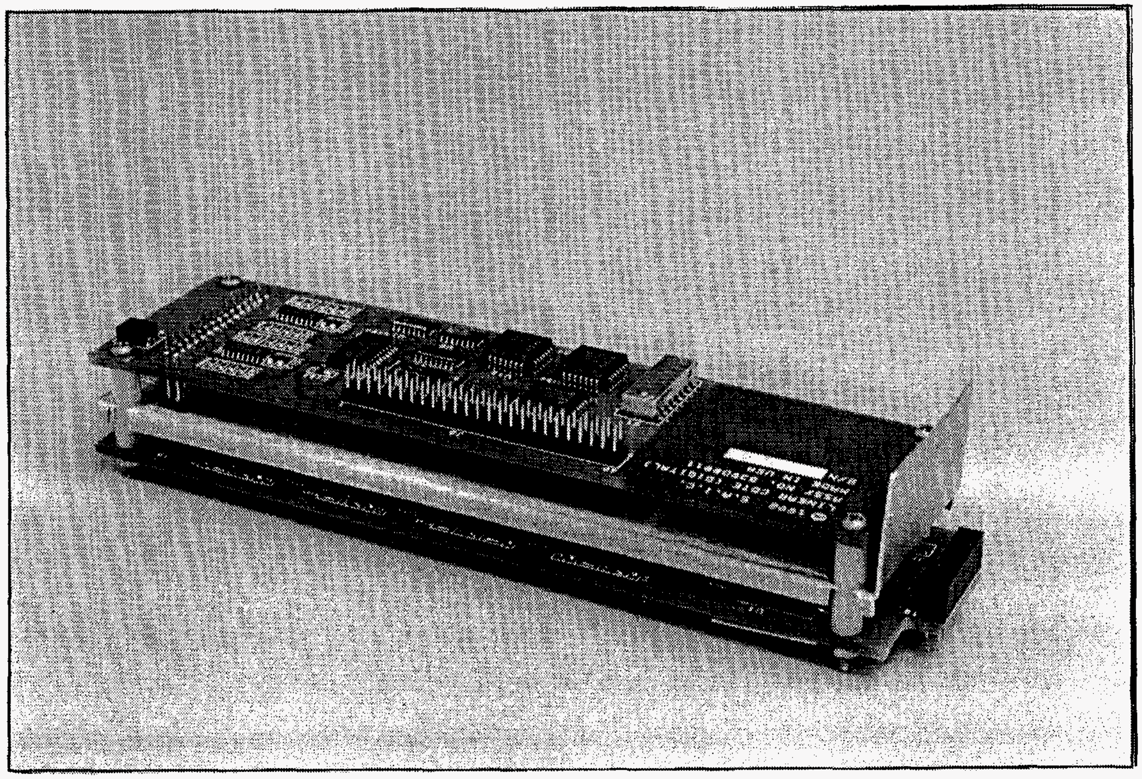

SAIC-92RP-189

Science Applications International Corporation

64-CHANNEL LINEAR SCANNER PROTOTYPE USING FOUR CASCADED ARRAYS

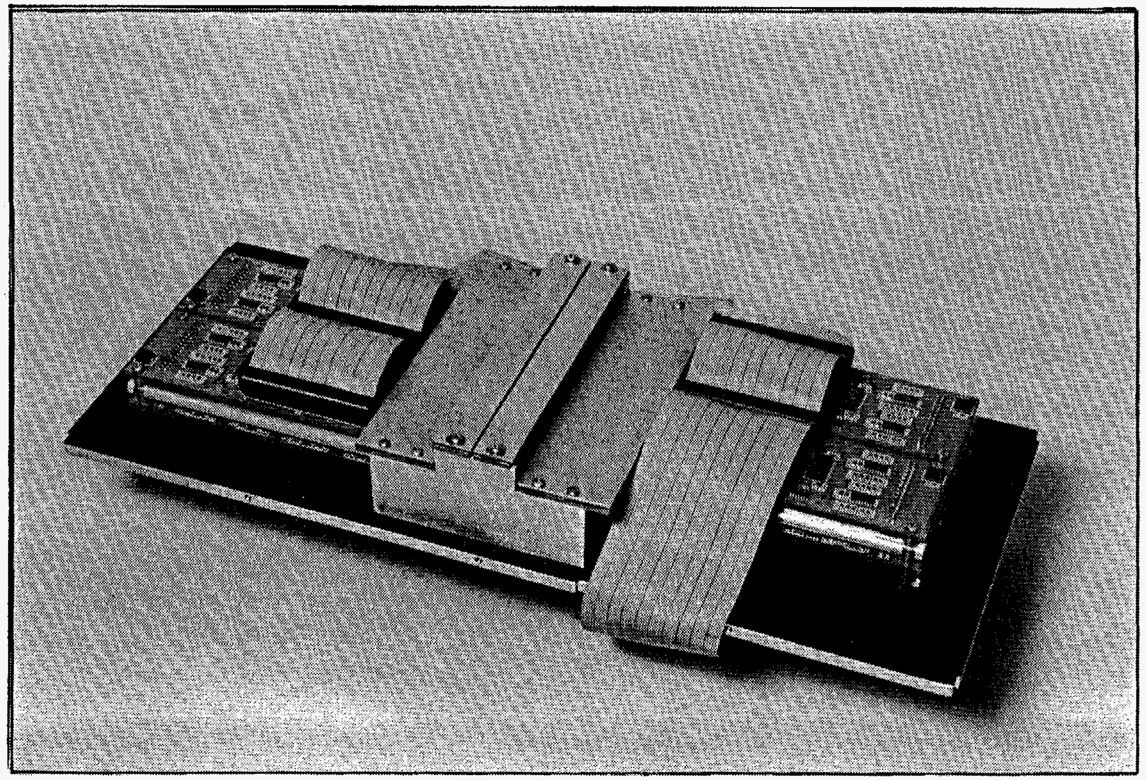

SAIC-92RP-190

Science Applications International Corporation

LINEAR SCANNER TRANSMISSION RADIOGRAPHY

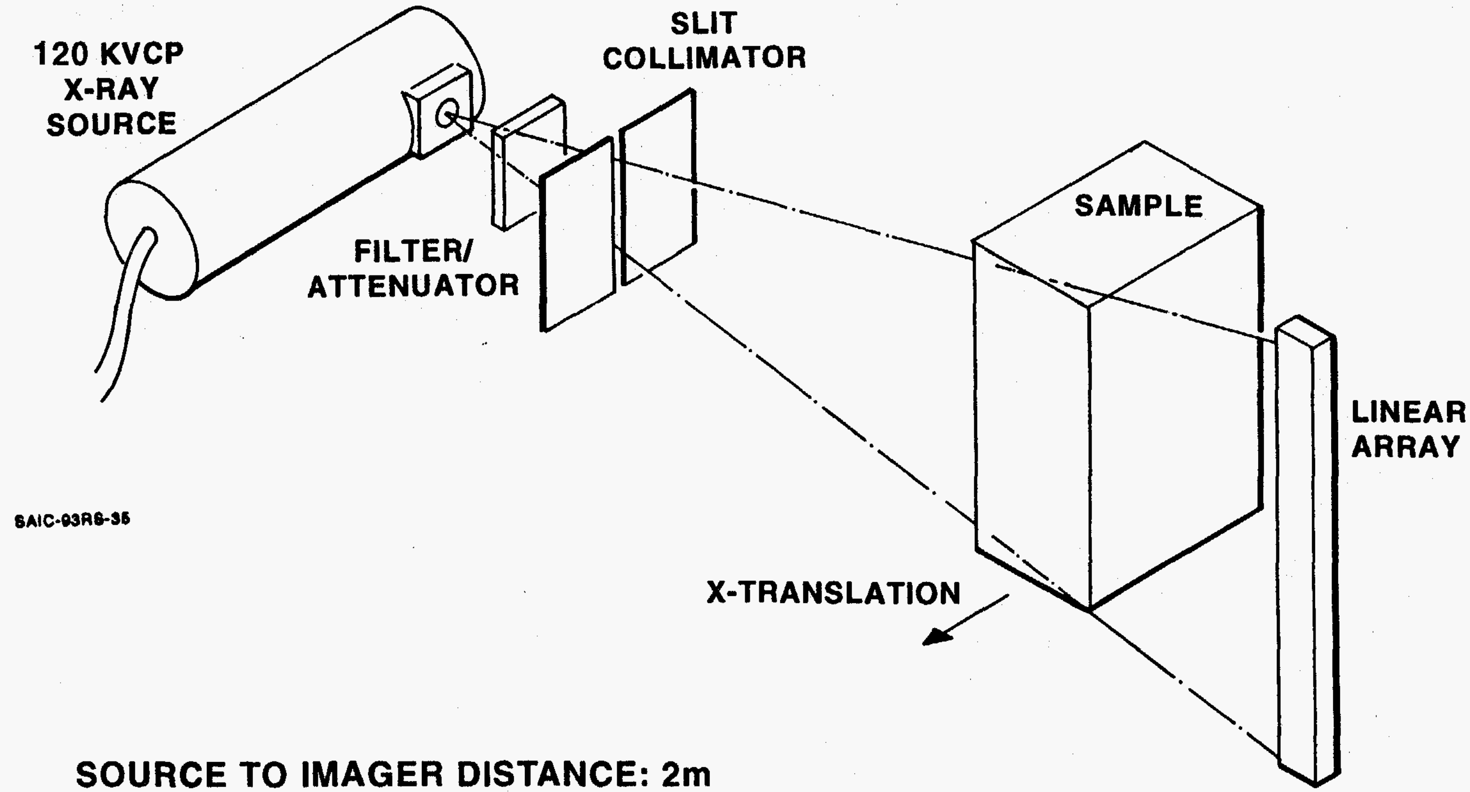

SOURCE TO IMAGER DISTANCE: 2m
ATTENUATOR: 0.22cm Cu
SOURCE PARAMETERS: 120 kV POTENTIAL, <0.5mA CURRENT

SAIC-93RS-35

Science Applications International Corporation

COUNTS AS A FUNCTION OF POSITION CdZnTe LINEAR ARRAY #109

120V Bias, DAC Threshold = 50, 125kV CP X-Ray Source, Slit Size = 5 mils, 88 mil Cu Filter.

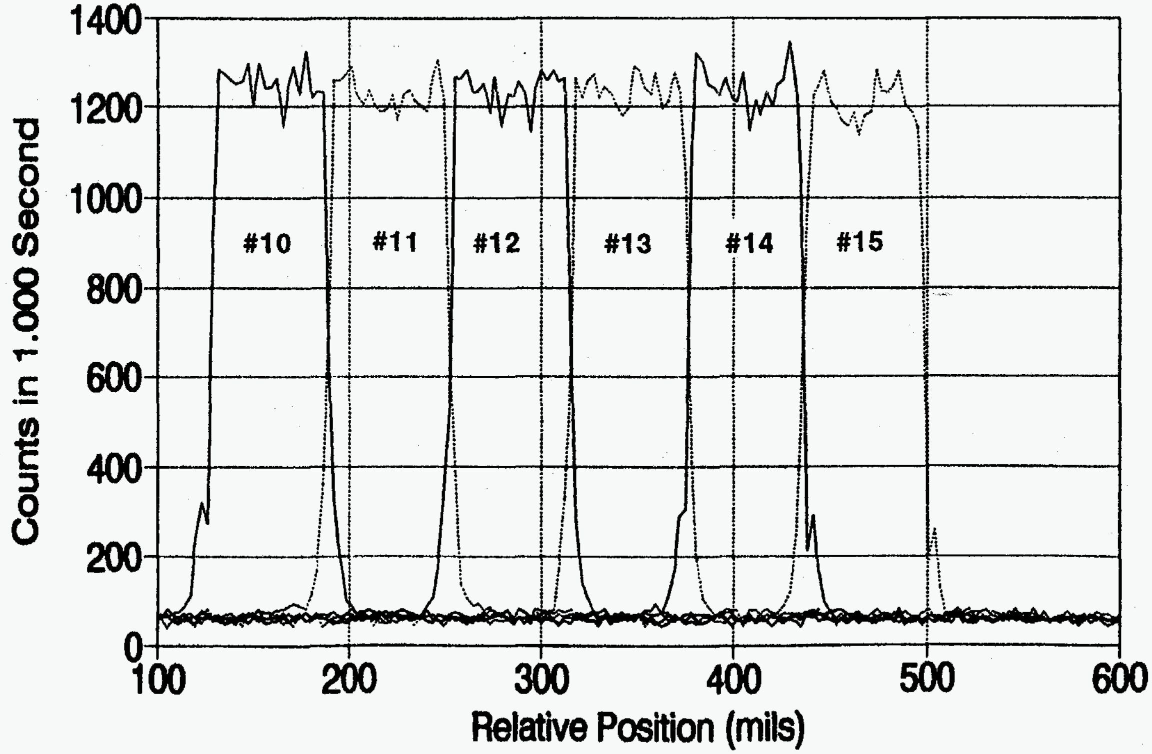

SAIC-94RS-4

LOW-DOSE, LINE-SCAN X-RAY IMAGE OF FOOT PHANTOM

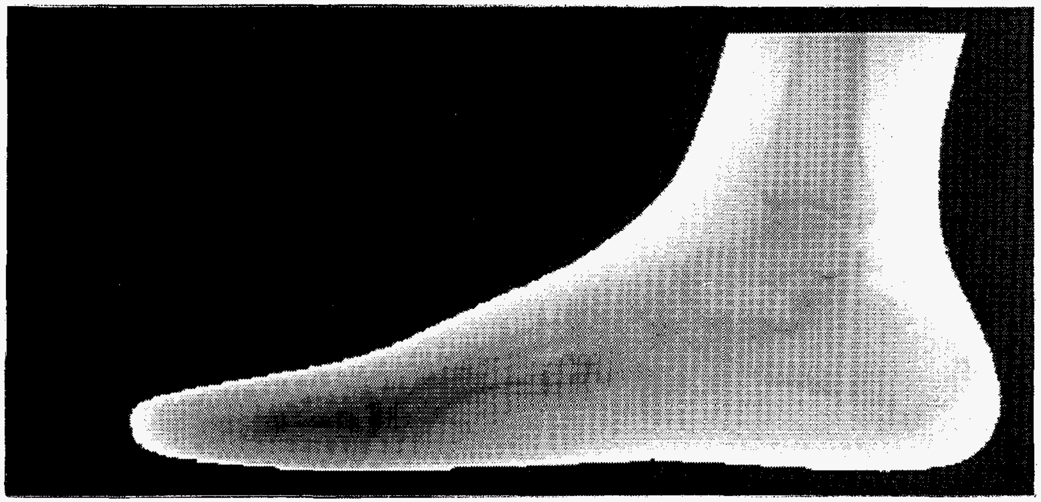

SAIC-94RS-7

SAIC®

LOW-DOSE, LINE-SCAN X-RAY IMAGE OF LABORATORY OSCILLOSCOPE

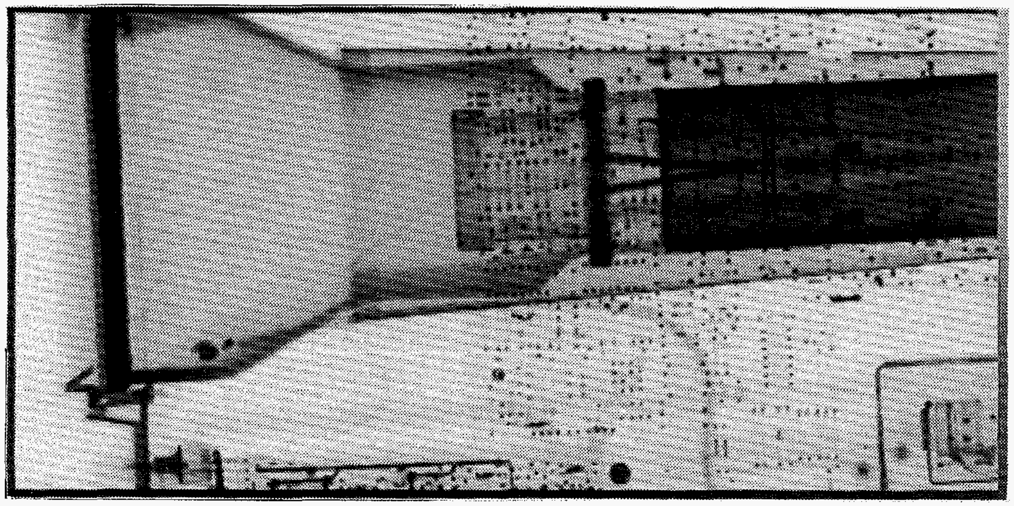

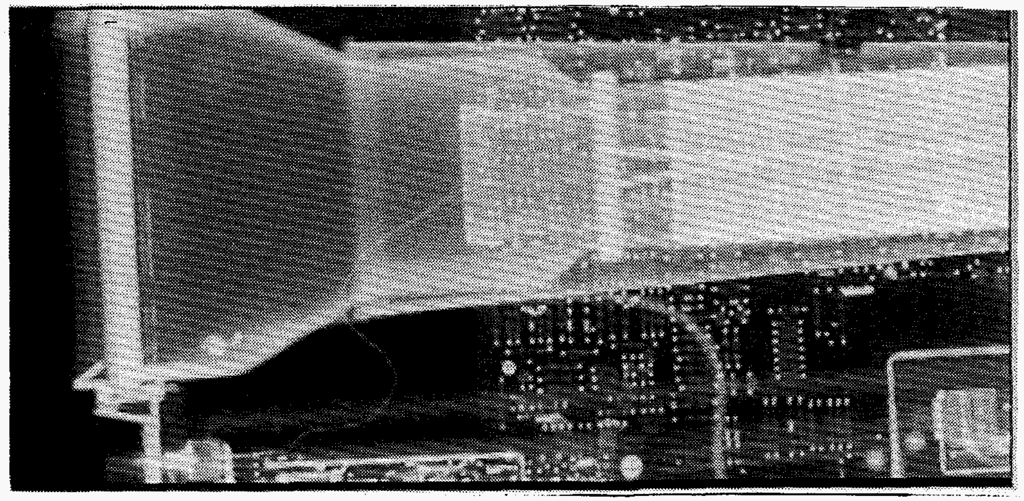

LOW-DOSE, LINE-SCAN X-RAY IMAGE OF CLOCK AND THERMAL CONTROLLER

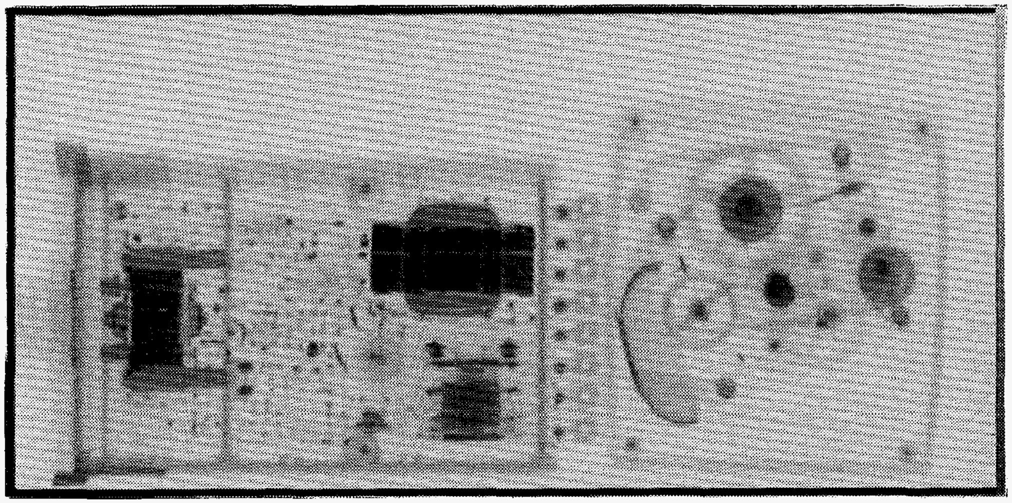

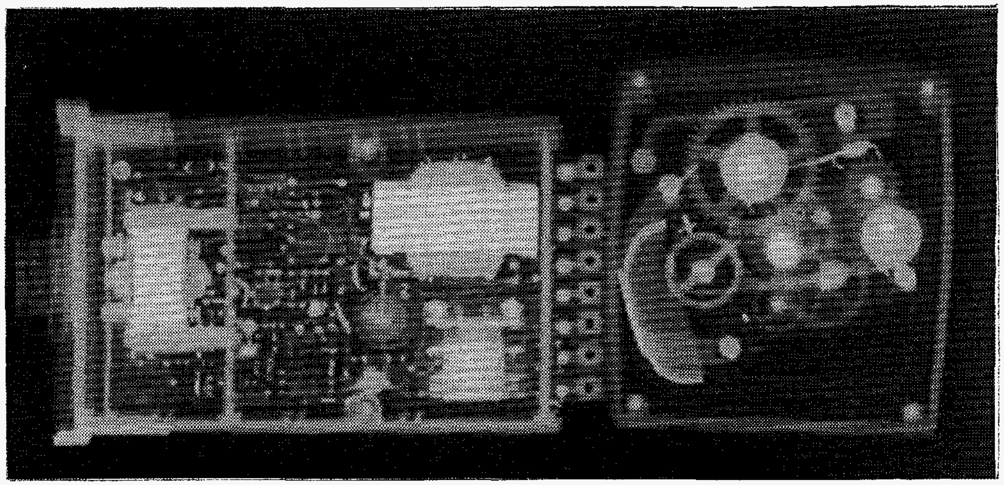

SAIC-94RS-8

Science Applications International Corporation

10 x 10 ELEMENT CdZnTe AREA ARRAY

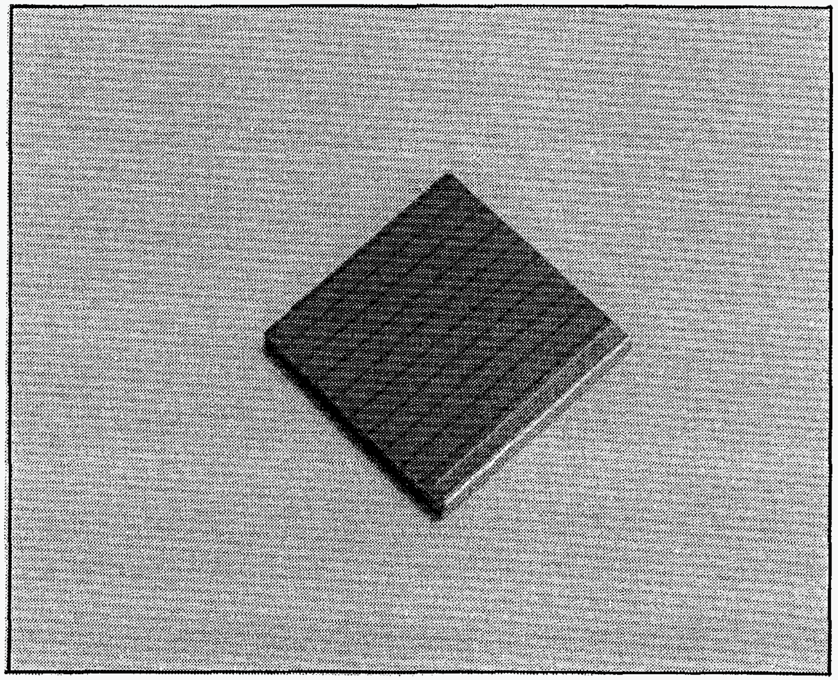

SIZE: 1 X 1 cm

PITCH: 1.0 mm

THICKNESS: 1.8 mm

SAIC-92RP-187

Science Applications International Corporation

COINCIDENT CHARGE READOUT FOR A CdZnTe DETECTOR ARRAY

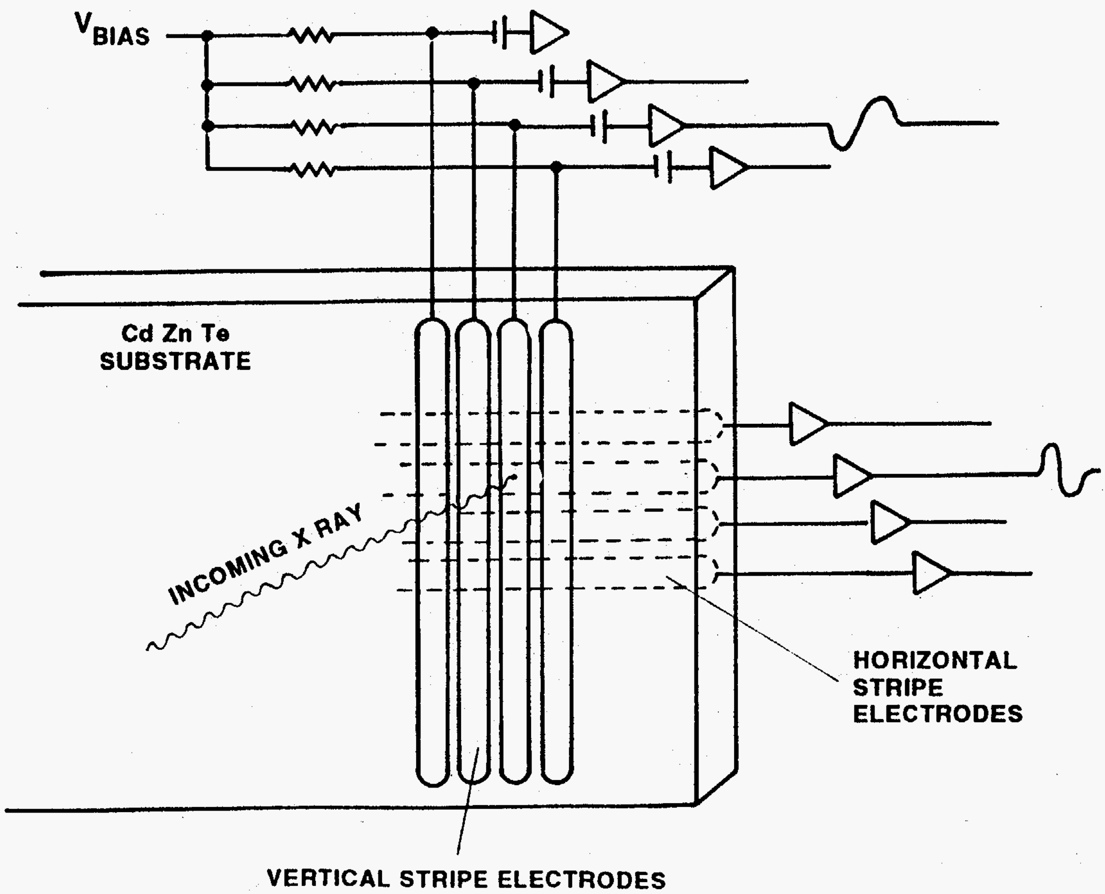

SAIC-92RP-164

PULSE ACQUISITION AND PROCESSING USED FOR "AREA" ARRAYS

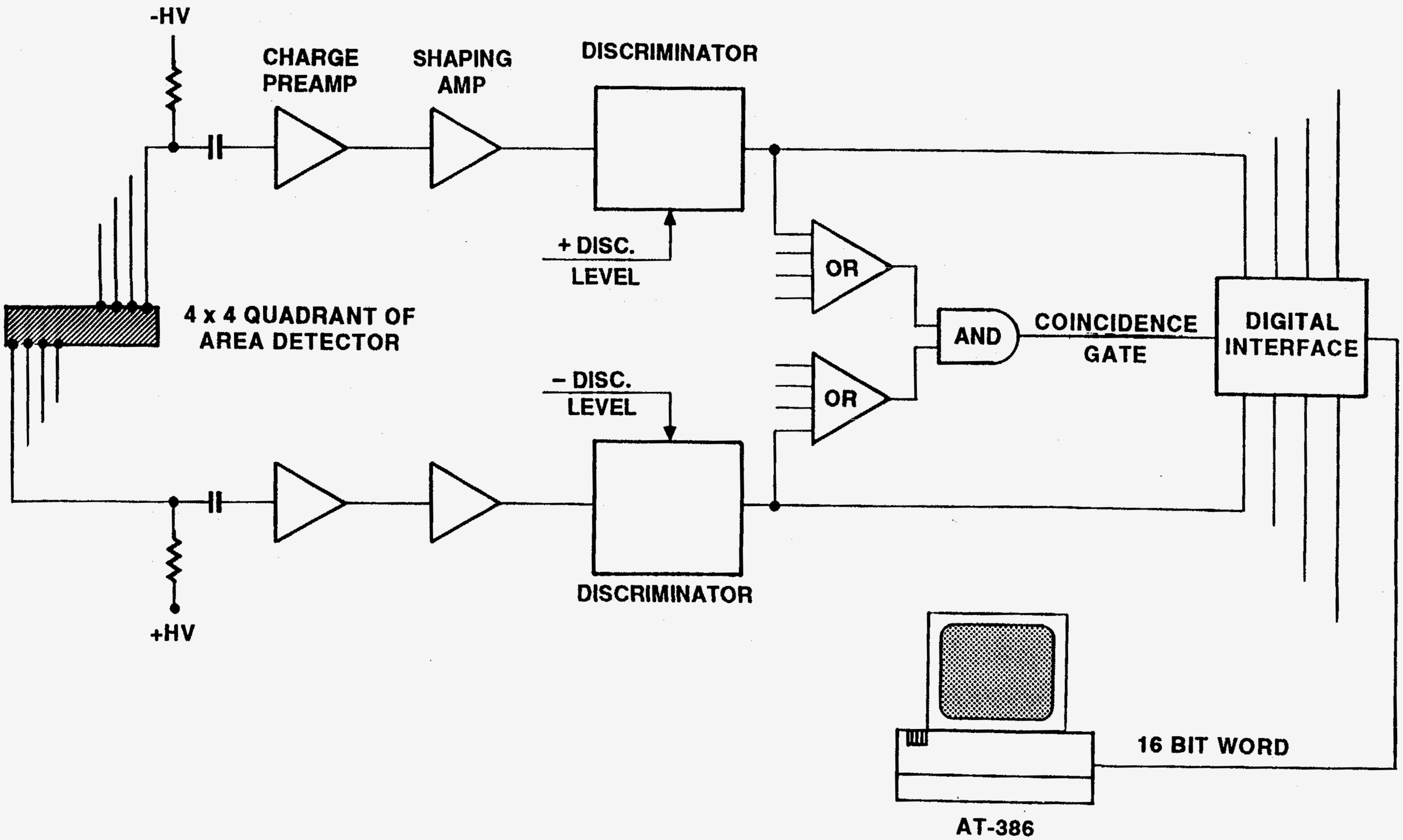

SAIC-92RS-41

Science Applications International Corporation

GAMMA-RAY IMAGING DATA FROM PROTOTYPE CdTe ARRAY

8 x 8 Array Pinhole Image
1 mCi Am-241 Source, 1 mm Diameter

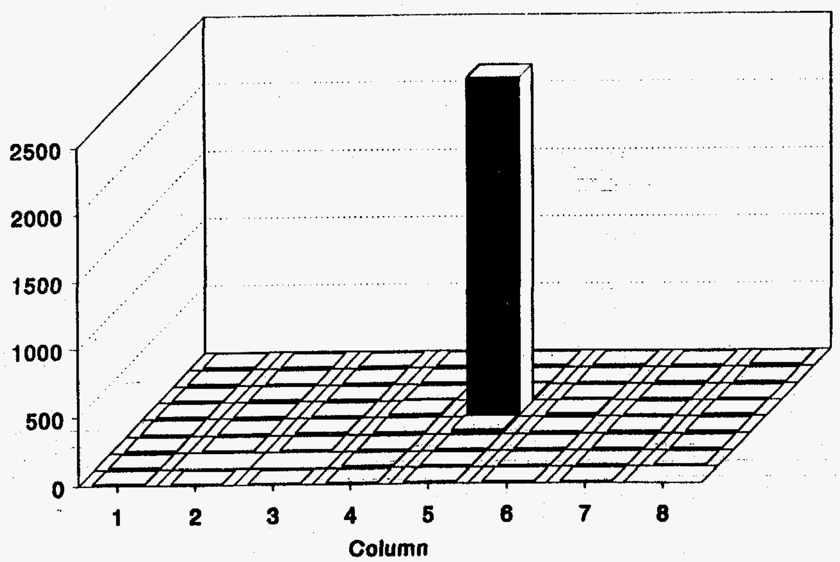

8 x 8 Array Pinhole Image
Two Am-241 Sources

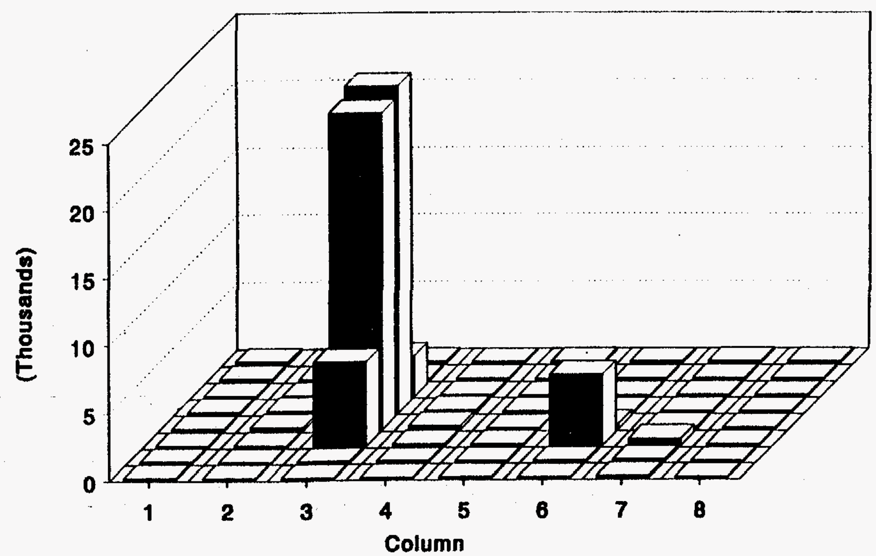

SAIC-92VO-206

Science Applications International Corporation

GAMMA-RAY DATA ILLUSTRATES ENERGY DISCRIMINATION CAPABILITIES

8 x 8 Array Pinhole Image
1.0 mCi Am-241, 1.6 mCi Cd-109

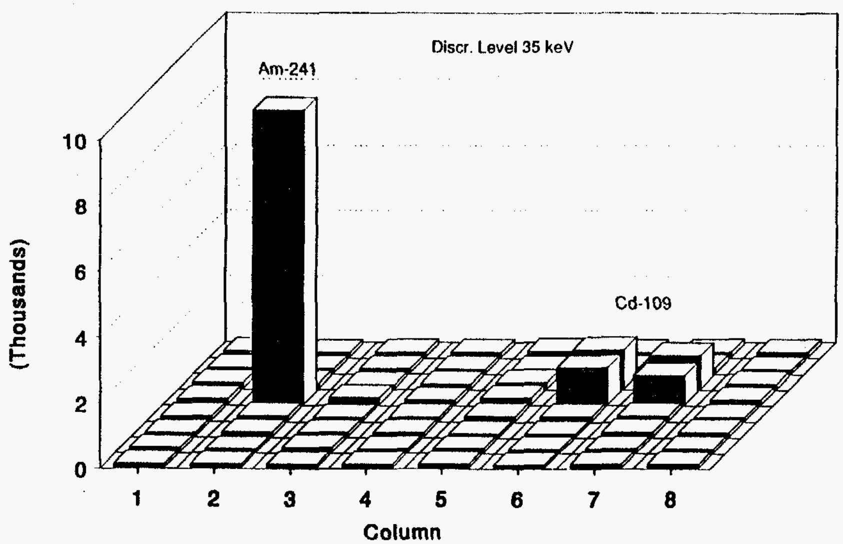

DISCRIMINATING LEVEL ≈ 35 keV

8 x 8 Array Pinhole Image
1.0 mCi Am-241, 1.6 mCi Cd-109

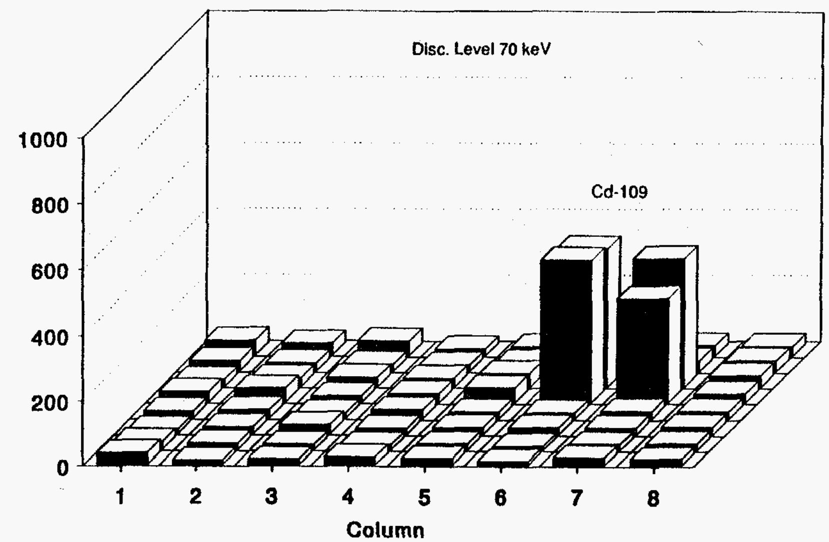

DISCRIMINATING LEVEL ≈ 70 keV

SAIC-92VO-207

Sung Shik Yoo

Department of Physics
University of Illinois

MBE CdTe Photoconductive Position Sensitive X-ray Detectors*

The group II-VI compound semiconductors, such as CdTe, are very attractive for x-ray detectors because of their large atomic numbers. Since the band gap is fairly large (1.46 eV), the dark current is small enough to operate the devices at room temperature. MBE growth of CdTe has been greatly improved to provide high-quality crystals. To date, 125 arcsec of DCRC FWHM has been obtained on Si substrates. We fabricated 10-20 μm thick MBE CdTe layers for application as x-ray detectors. Thirty-two or sixty-four element linear photoconductor arrays were fabricated on MBE CdTe layers. The photoconductor gap size varies from 5 to 50 μm with 50-μm width and 100-μm pitch sizes.

The temporal response was measured by using 100 fsec Ti:Sapphire laser pulses, values of 25 psec rise time and 35 psec pulse width were measured on the devices. The spatial response was measured by using a Nd:YAG laser, x-rays from a rotating anode, and synchrotron x-rays (NSLS). We also measured the energy response of the device over a wide range of energies (7-18 keV). The image of the beam profile was obtained for the direct and the partially attenuated beams by rastering a single photoconductor around the x-ray beam. In the synchrotron direct beam, no saturation response was observed. The noise was small enough so that the dynamic range reaches three decades at room temperature in spite of the small size of the active area. The photoconductor was exposed to the synchrotron beam for 60 hours without any observable deterioration of the device.

* Work supported by the US DOE.

MBE CdTe PHOTOCONDUCTIVE POSITION SENSITIVE X-RAY DETECTORS*

S. S. Yoo[1], B. Rodricks[2], S. Sivananthan[1], J. Bai[3,4], J. P. Faurie[1], and P.A. Montano[1,4]

[1]Department of Physics
Microphysics Laboratory
University of Illinois at Chicago
Chicago, IL 60607

[2]Advanced Photon Source
Argonne National Laboratory
Argonne, IL 60439

[3]Department of Physics,
Brooklyn College of CUNY,
Brooklyn, NY

[4]Material Science Division
Argonne National Laboratory
Argonne, IL 60439

* Work supported by the US DOE

MOTIVATION

1. Diagnosis for Ultrashort X-ray Pulses
   * 72 psec pulsewidth
   * 184 nsec period

2. Position Sensitive Detector
   * 5-50 x 50 μm sensitive area
   * 100 μm pitch size
   * High spatial resolution

CdTe FOR X-RAY DETECTION

1. Large Atomic Number
   * Cd:48, Te:52
   * Large absorption coefficient
     (μ = 500 - 1000 cm^{-1} for 5 - 20 KeV)

2. Wide Band Gap
   * Eg = 1.48 eV
   * $\rho = 10^{8} - 10^{11} \Omega\text{-cm}^{-3}$

3. Excellent Carrier Transportation Property
   * μ_e = 1000 cm^2/V-sec
   * μ_h = 200 cm^2/V-sec

4. Room Temperature Operation

MOLECULAR BEAM EPITAXY OF CdTe

1. High Quality Crystal
   * DCRC FWHM of 125 arcsec on Si substrate

2. Thin Film Growth
   * 10 - 20 μm Thickness
   * Increased spatial resolution

3. Flexible Choice of Substrates
   * Insulating
   * Conducting
   * Semiconducting

FABRICATION

1. Molecular Beam Epitaxy of CdTe
   * High quality of CdTe on Si substrate
   * 10 - 20 μm thickness

2. Mounting on Insulating Substrate
   * Removal of Si Substrate
   * Surface etching of CdTe

3. 1st Photolithography
   * Device isolation

4. Device Isolation
   * Etching between elements

FABRICATION

5. 2nd Photolithography
 * 5-50 µm photoconductor gap
 * 50µm wide and 100 µm pitch
 * 32 or 64 element linear array
 * Fan-out metal strip for bonding

6. Metal Deposition and Liftoff
 * Electroless Au
 * Sputtered Au or Ni

7. Mounting and Bonding
 * Mounted on 64 leadless chip carrier
 * Gold wire bonding on 32 elements

SCHEMATIC DIAGRAM OF LINEAR ARRAY STRUCTURE

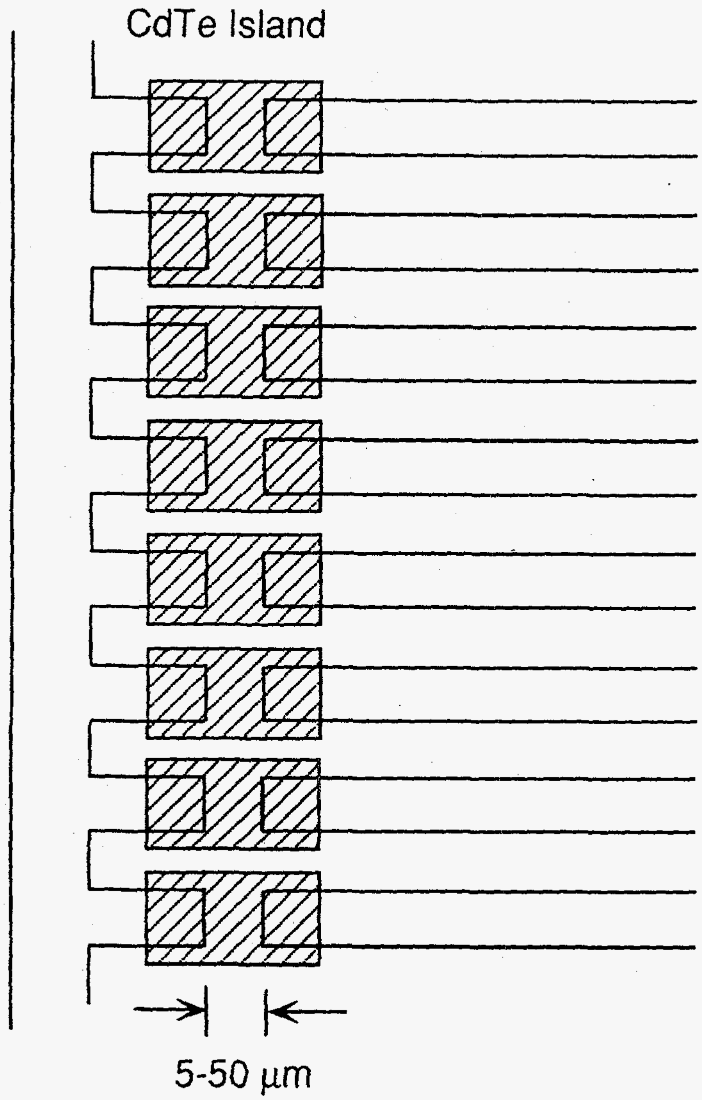

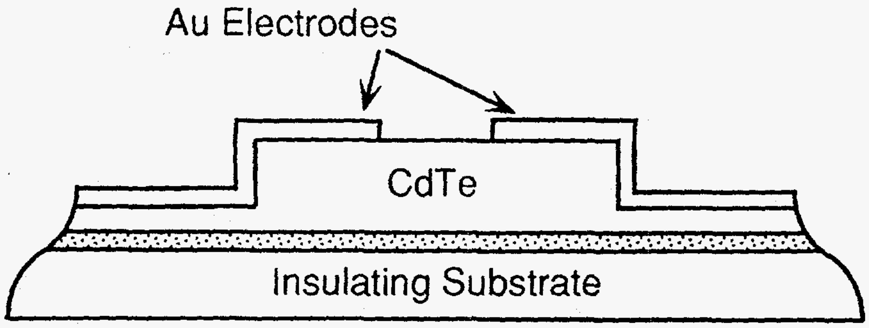

MEASUREMENTS

1. Electrical Measurement
   * Current-Voltage

2. Laser Response
   * Nd:YAG laser (0.53um)
   * Ti:Sapphire (0.875um)
   * Tektronix CS803 Sampling Digital Scope (20 GHz Bandwidth)

3. Rotating Anode X Ray (Cu)
   * White beam
   * Monochromatic beam

4. Synchrotron Source (NSLS/X18B)
   * Monochromatic beam (7 - 18 KeV)

CURRENT-VOLTAGE CHARACTERISTICS

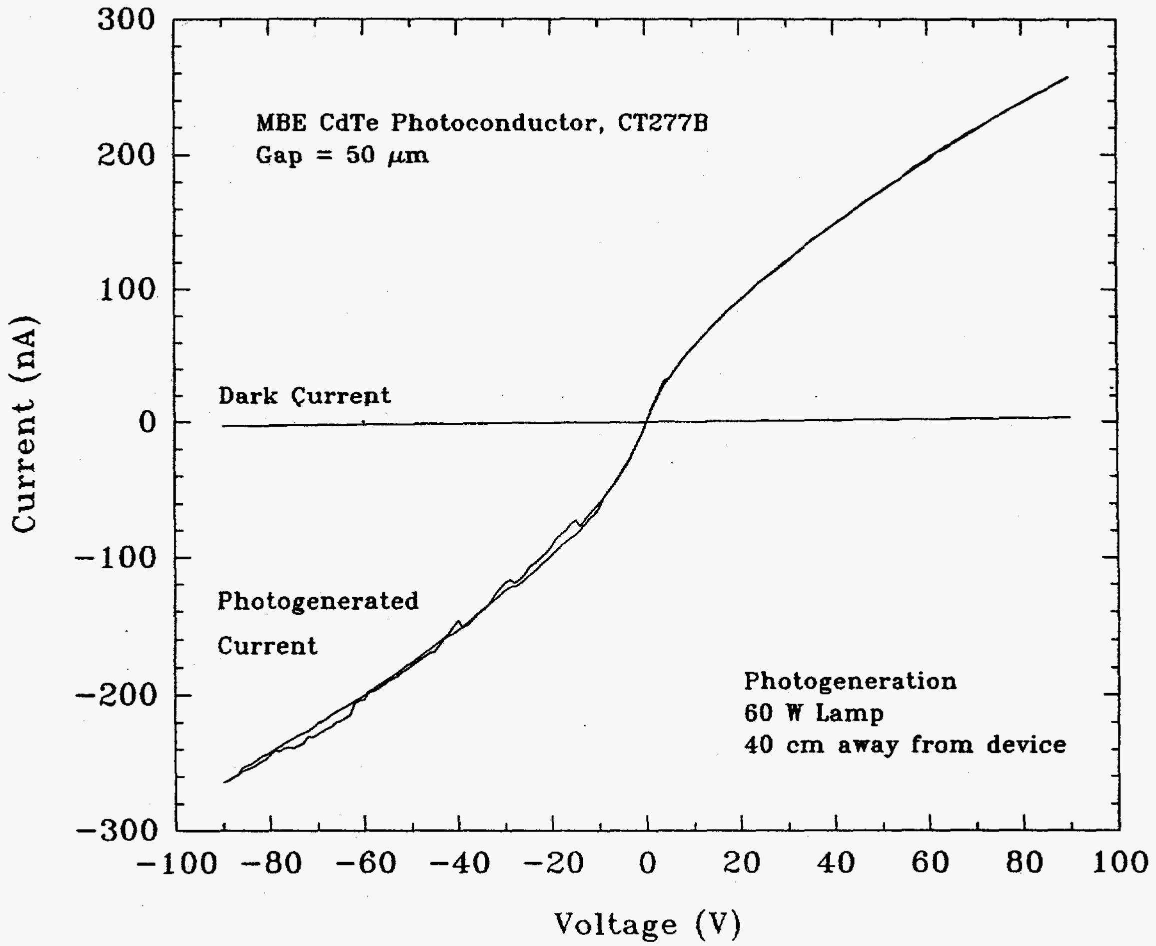

UNIFORMITY OF LINEAR ARRAY

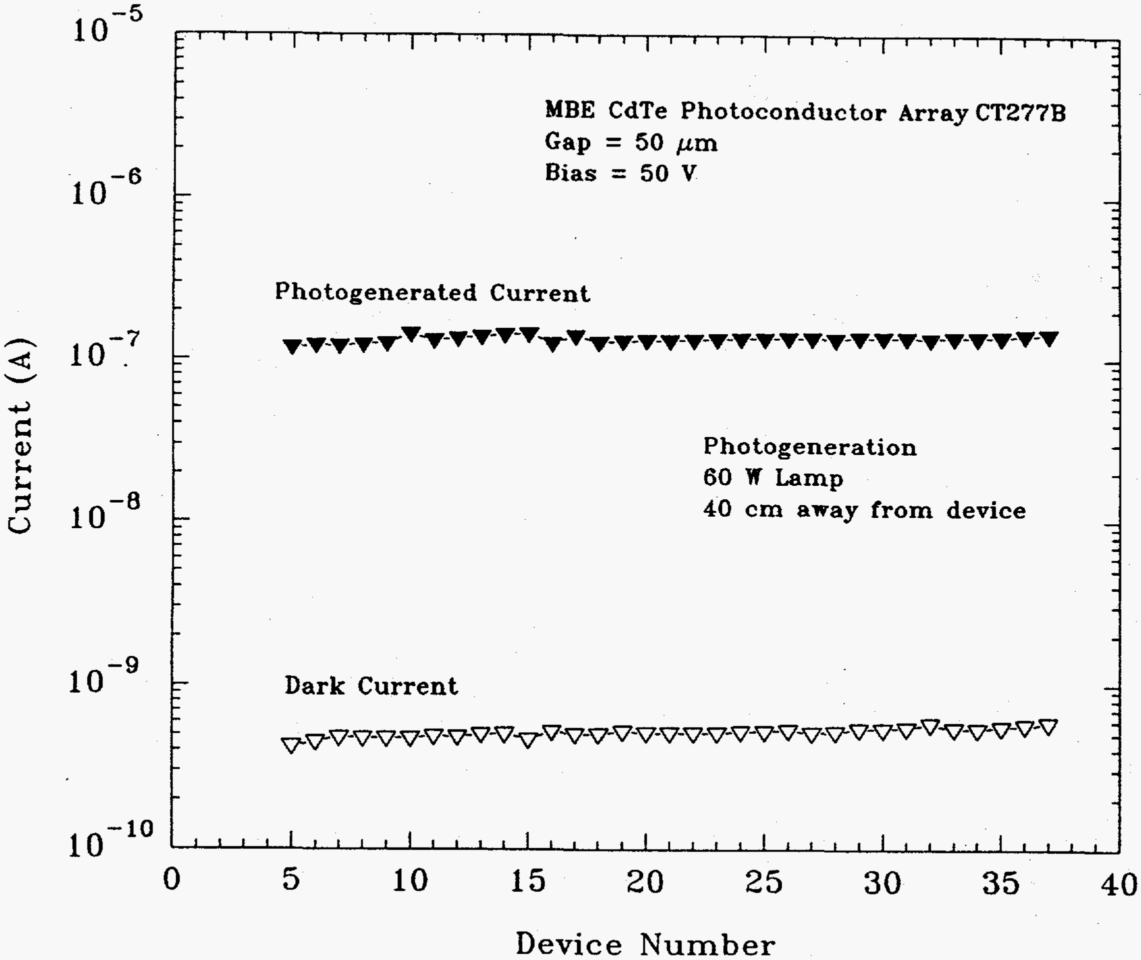

SCHEMATIC DIAGRAM OF TEMPORAL RESPONSE MEASUREMENT

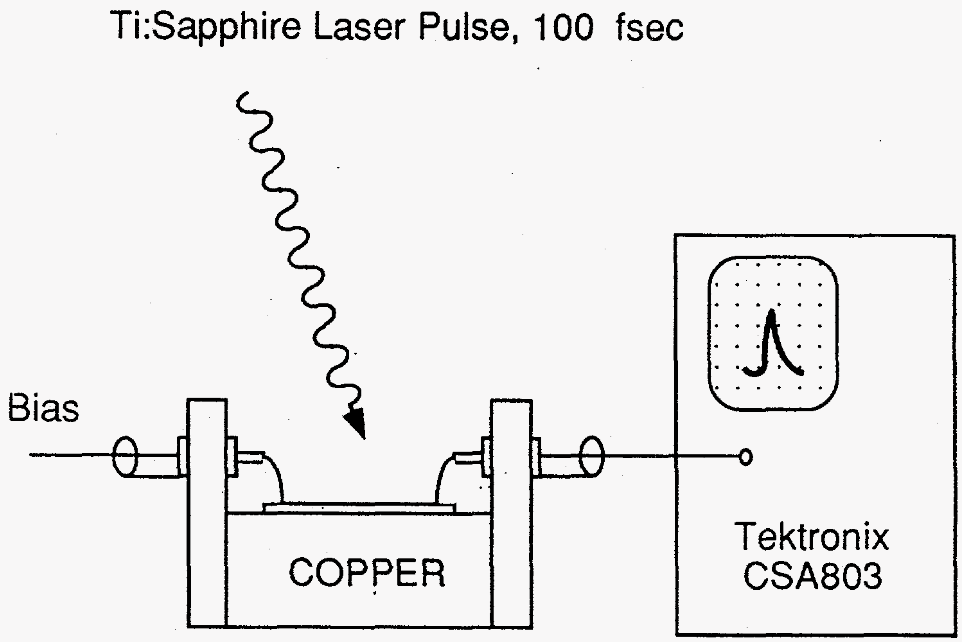

TEMPORAL RESPONSE TO Ti:Sapphire LASER PULSE

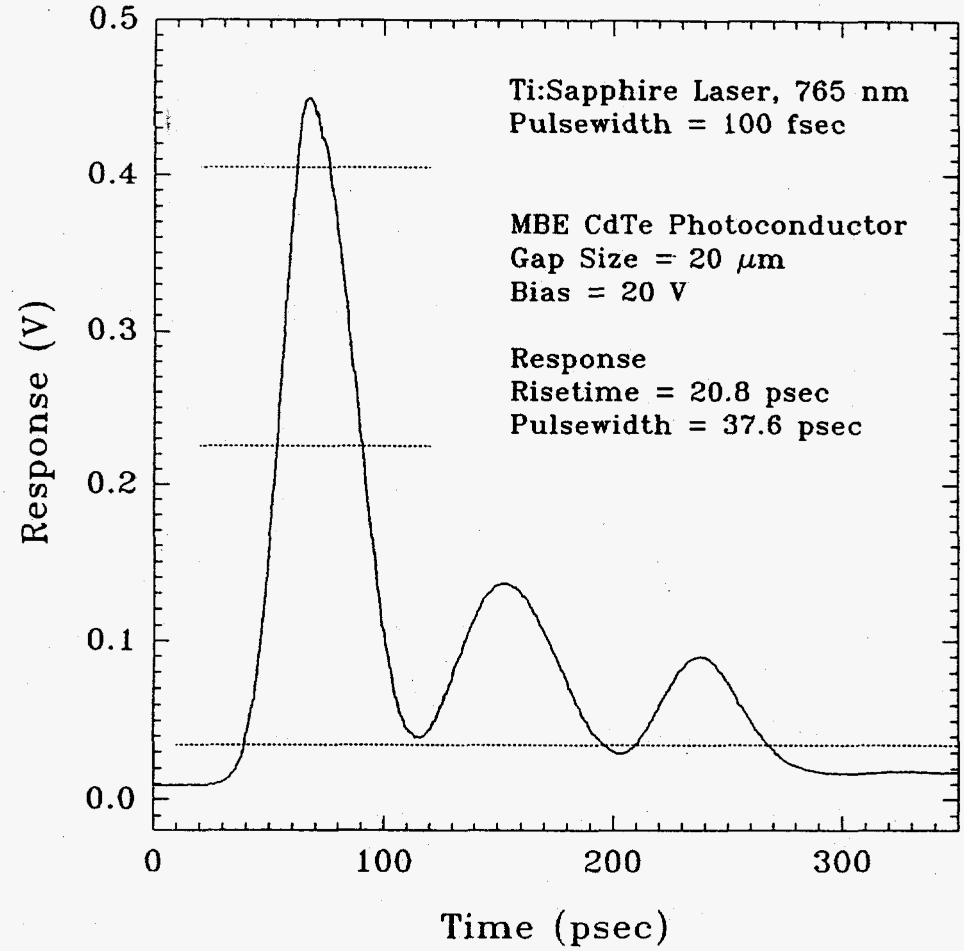

SPATIAL RESPONSE TO Nd:YAG LASER PULSE

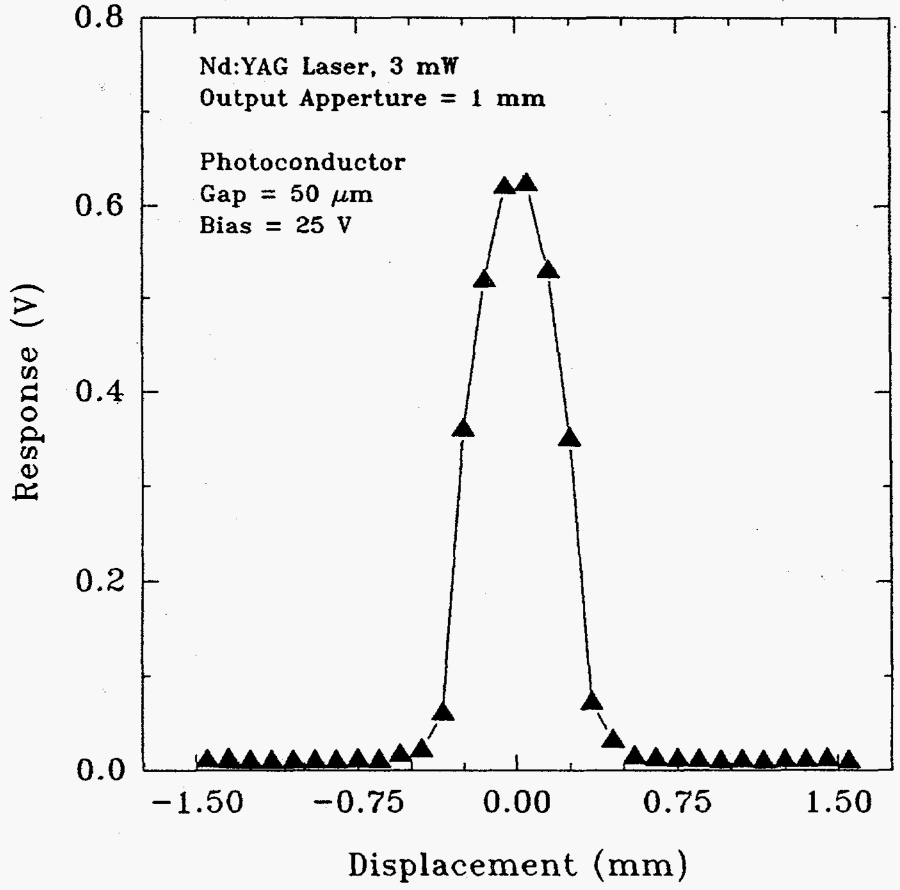

LINEAR RESPONSE TO ROTATING ANODE X RAY
(WHITE BEAM)

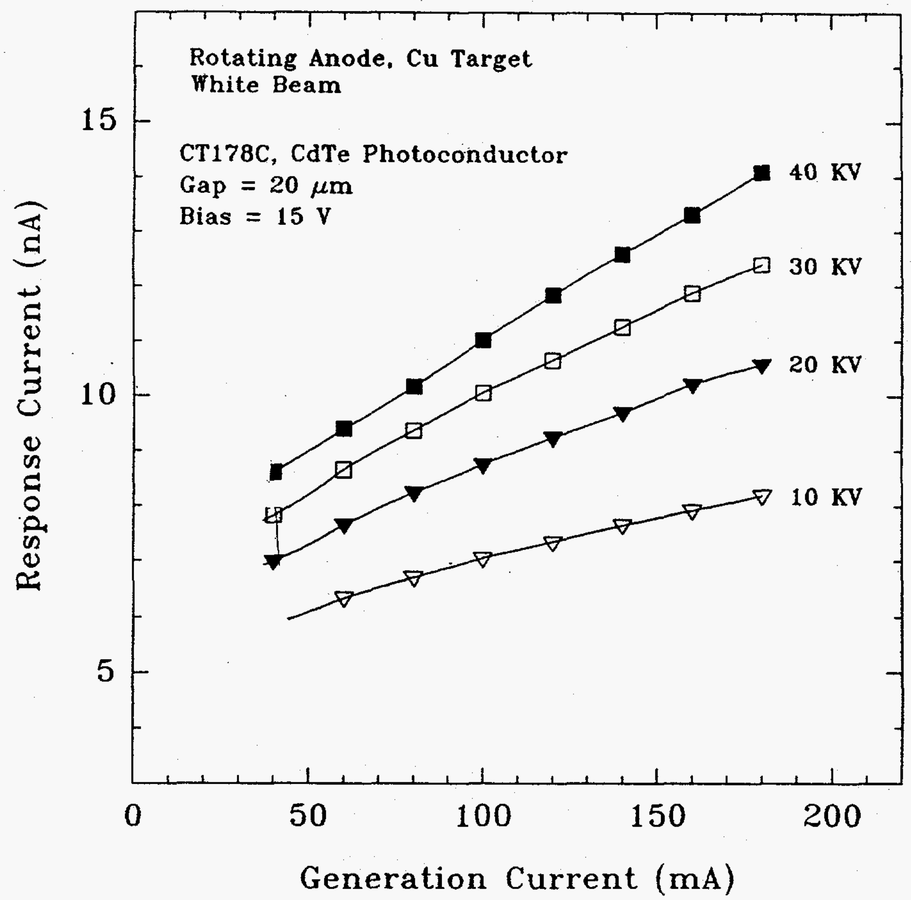

SCHEMATIC DIAGRAM OF SPATIAL RESPONSE MEASUREMENT

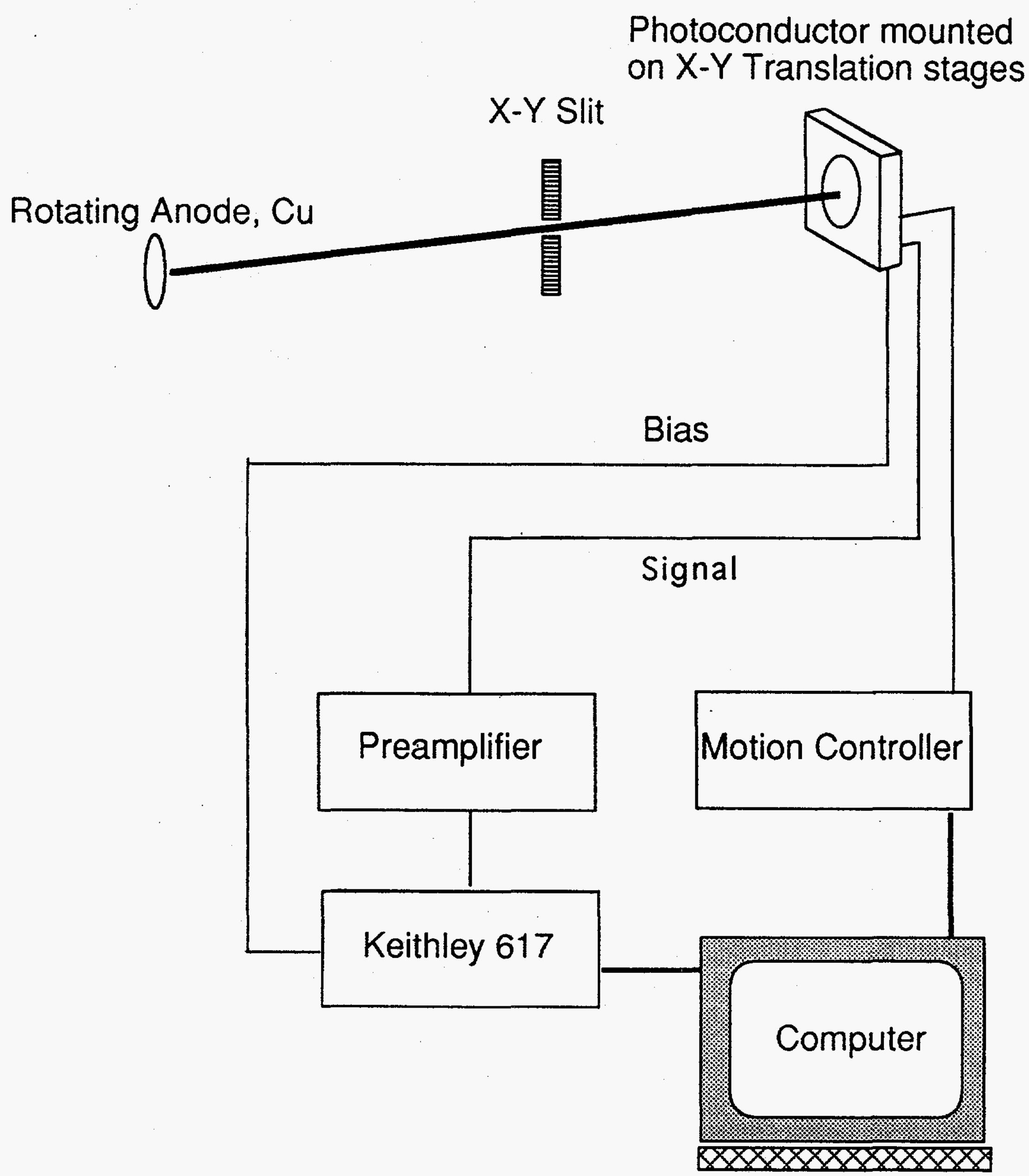

Spatial Response To Sychrotron Source
(NSLS/X18B)

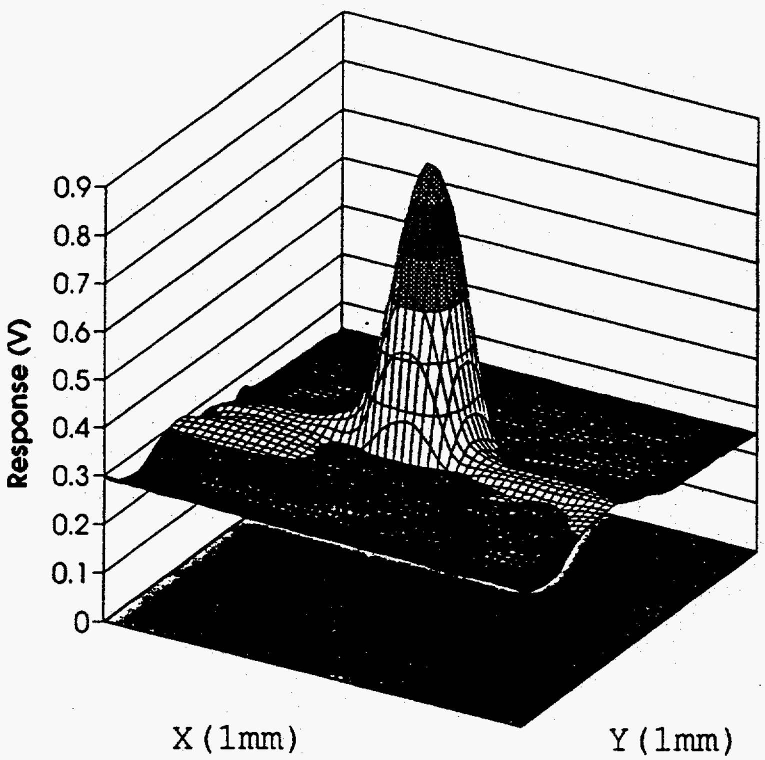

Synchrotron Source: I=206 mA
E=16 KeV
I_0=1436

CdTe Photoconductor: 20 μm gap, 5 V

CONCLUSION

1. Utilized MBE CdTe for X-ray Detection
   * 10-20 μm thickness, 50 μm wide
     Position Sensitive Detector

2. Fast Temporal Response Achieved.
   * 20 psec risetime and 35 psec pulsewidth

3. Linear Response to X-Ray Photon Flux
   * Rotating Anode

4. Demonstrated X-ray Beam Profiling
   * Rotating Anode X Ray
   * Synchrotron Source (NSLS)

5. Room Temperature Operation

SPATIAL RESPONSE TO ROTATING ANODE (Cu, White Beam)

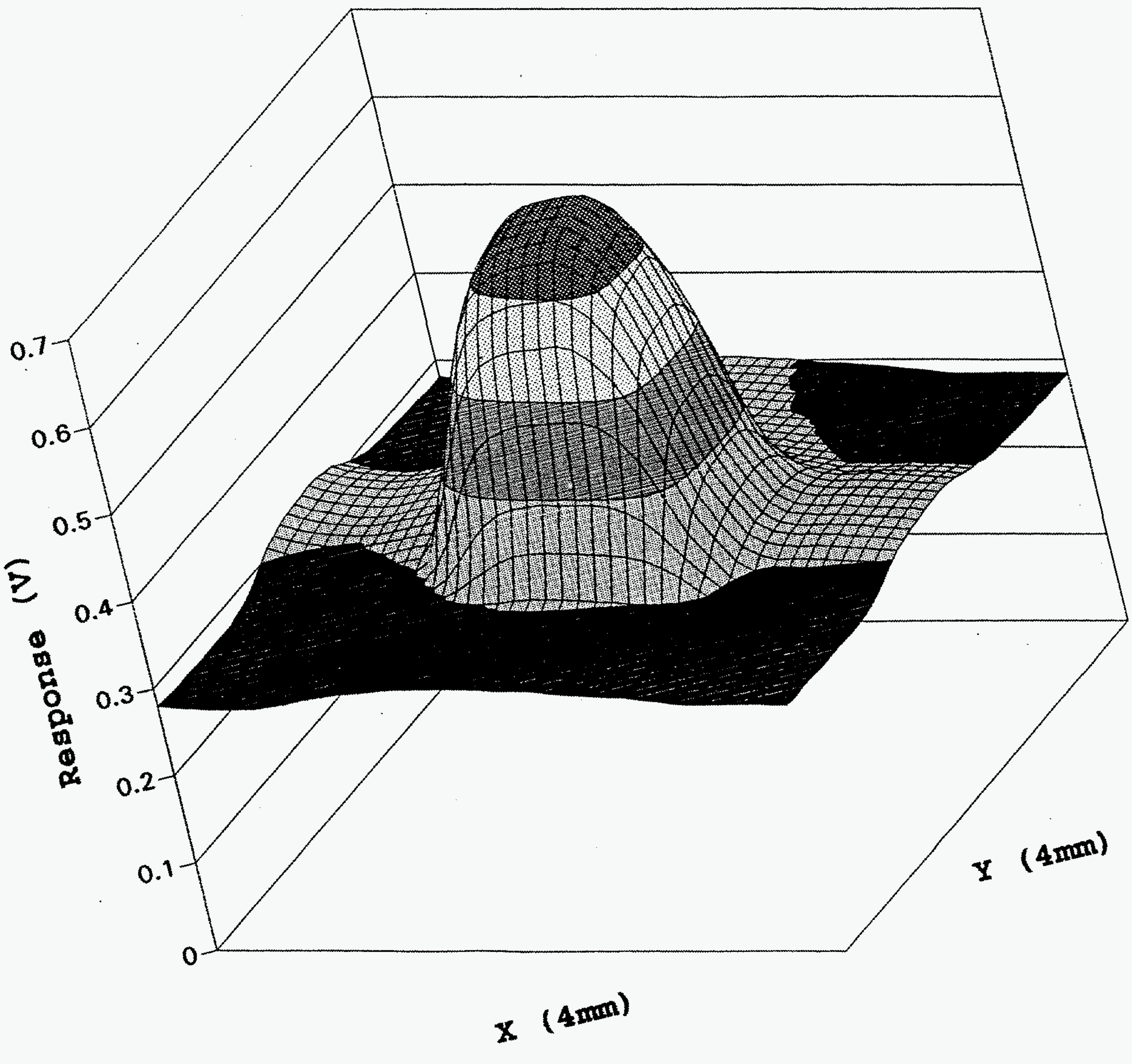

X-Ray Source:	**20 KV, 100 mA**
Slit Size:	**1500 X 1500 μm**
CdTe Photoconductor:	**15 μm, 5 V**

SPATIAL RESPONSE TO ROTATING ANODE (Cu, White Beam)

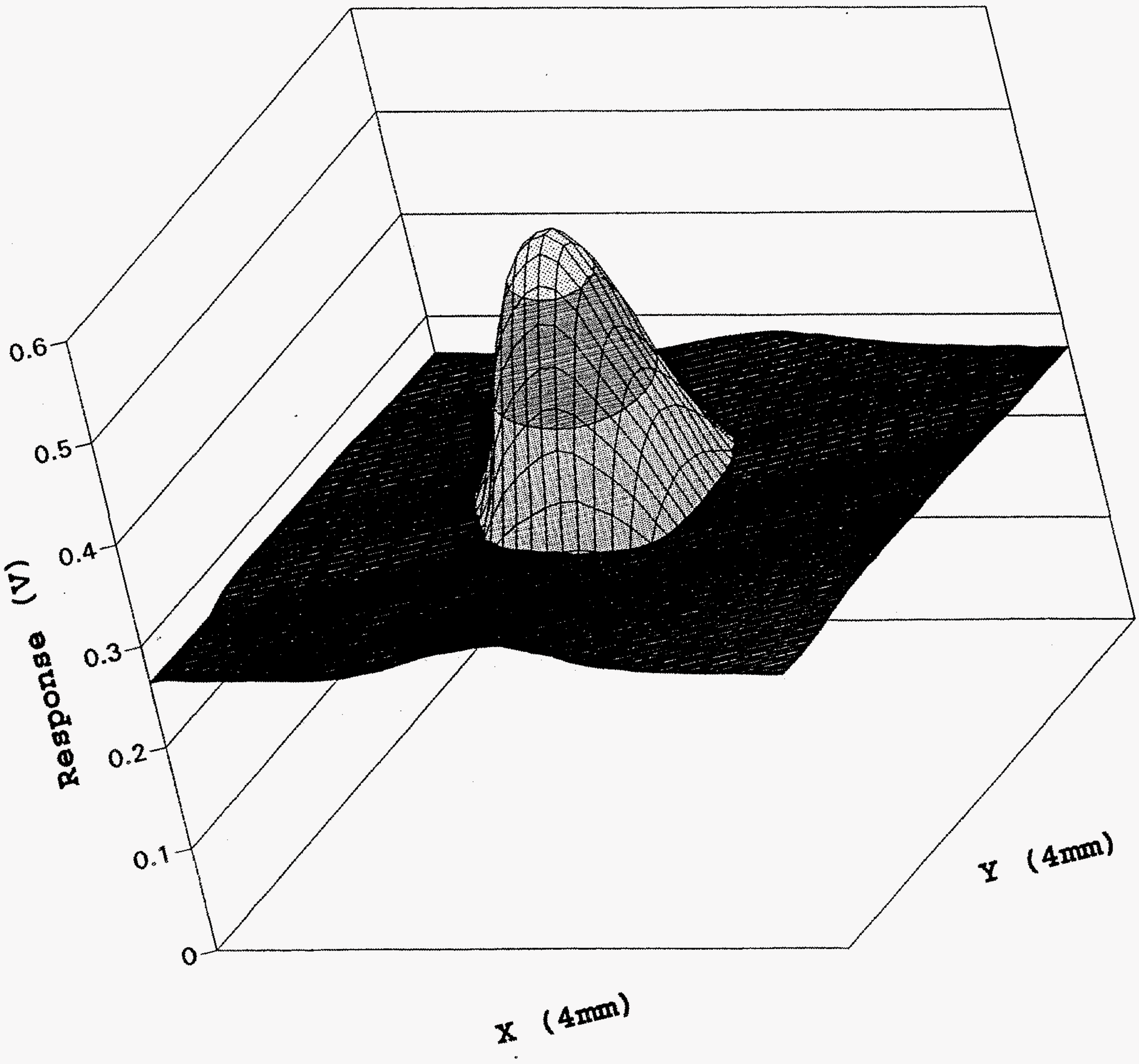

X-Ray Source: 20 KV, 100 mA
Slit Size: 600 x 600 μm
CdTe Photoconductor: 15 μm, 5 V

SPATIAL RESPONSE TO ROTATING ANODE
(8 KeV Monochromatic and Focuced Beam)

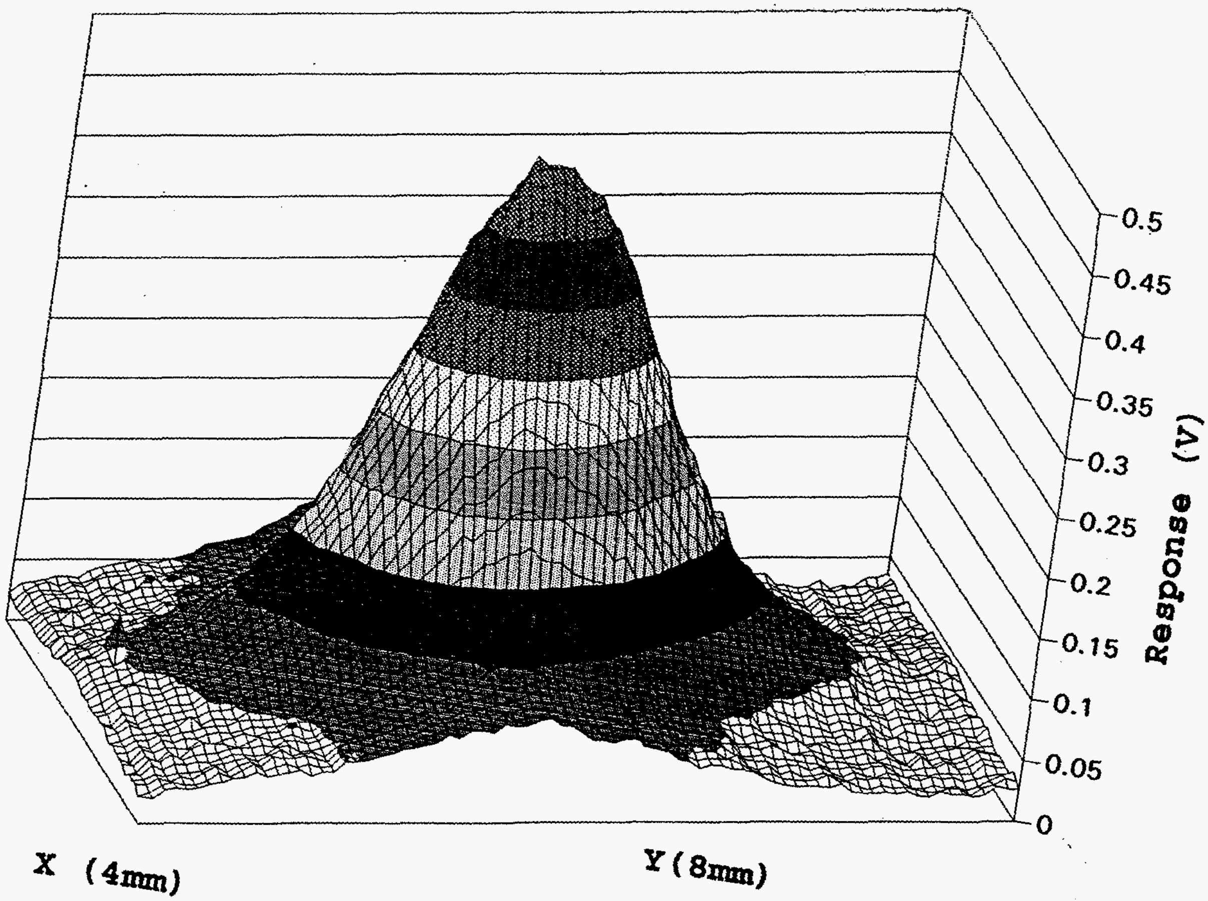

X-Ray Source:	20 KV, 20mA
X-Y Slit:	3 X 3 mm
CdTe Photoconductor:	15 um, 5 V

SPATIAL RESPONSE TO SYNCHROTRON SOURCE (NSLS/X18B)

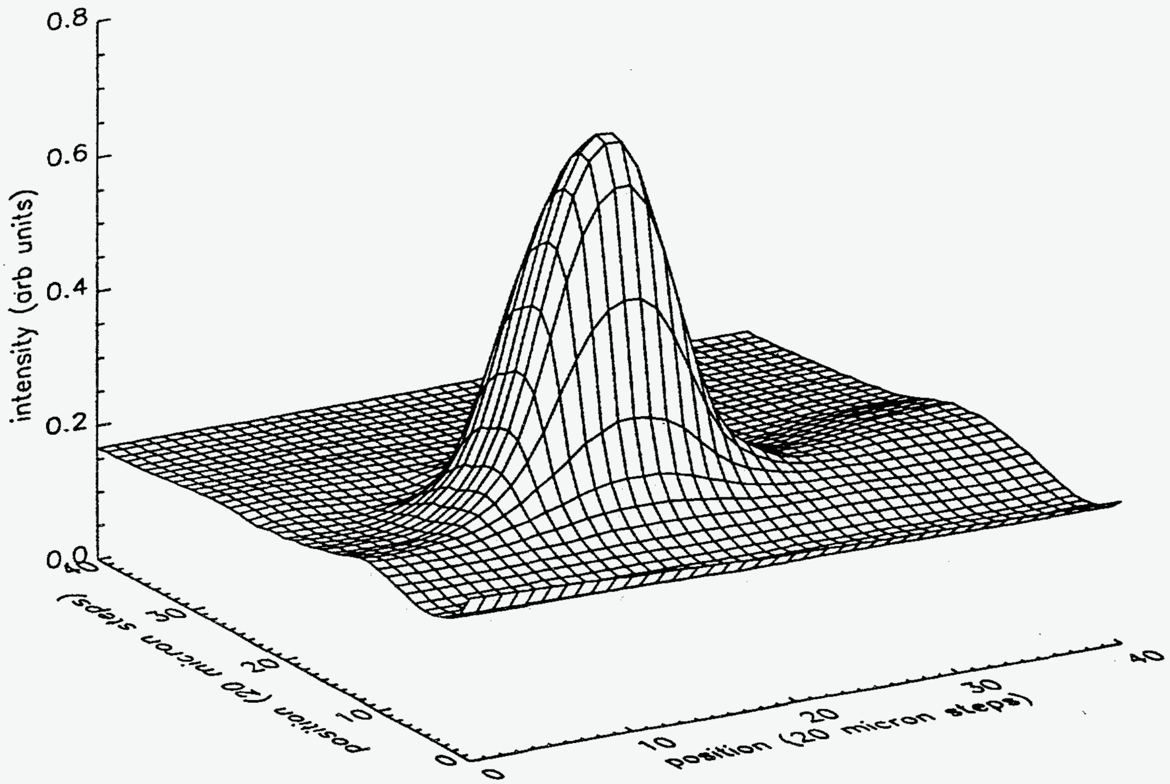

Synchrotron Source:	**I=206 mA**
	E=16 KeV
	I_0=1436
Beam Size:	**100x100 µm**
CdTe Photoconductor:	**20 µm gap, 5 V**

SPATIAL RESPONSE TO SYNCHROTRON SOURCE (NSLS/X18B)

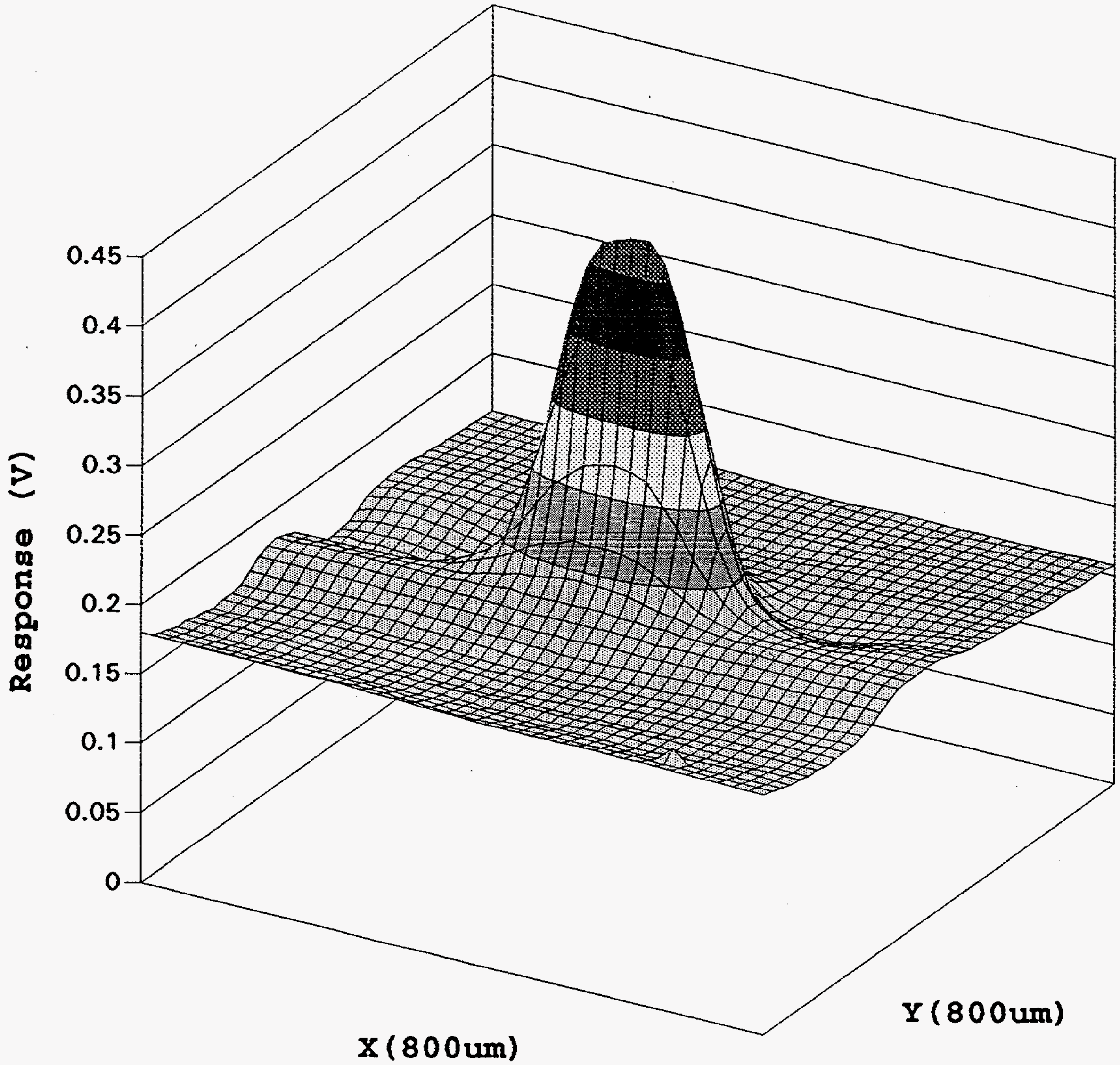

Synchrotron Source:	**I=141mA**
(Direct Beam)	**E=8 KeV**
	I_0=982
Slit Size:	**200(X) x 50(Y) μm**
CdTe Photoconductor:	**20 μm gap, 5 V**

SPATIAL RESPONSE TO SYNCHROTRON SOURCE (NSLS/X18B)

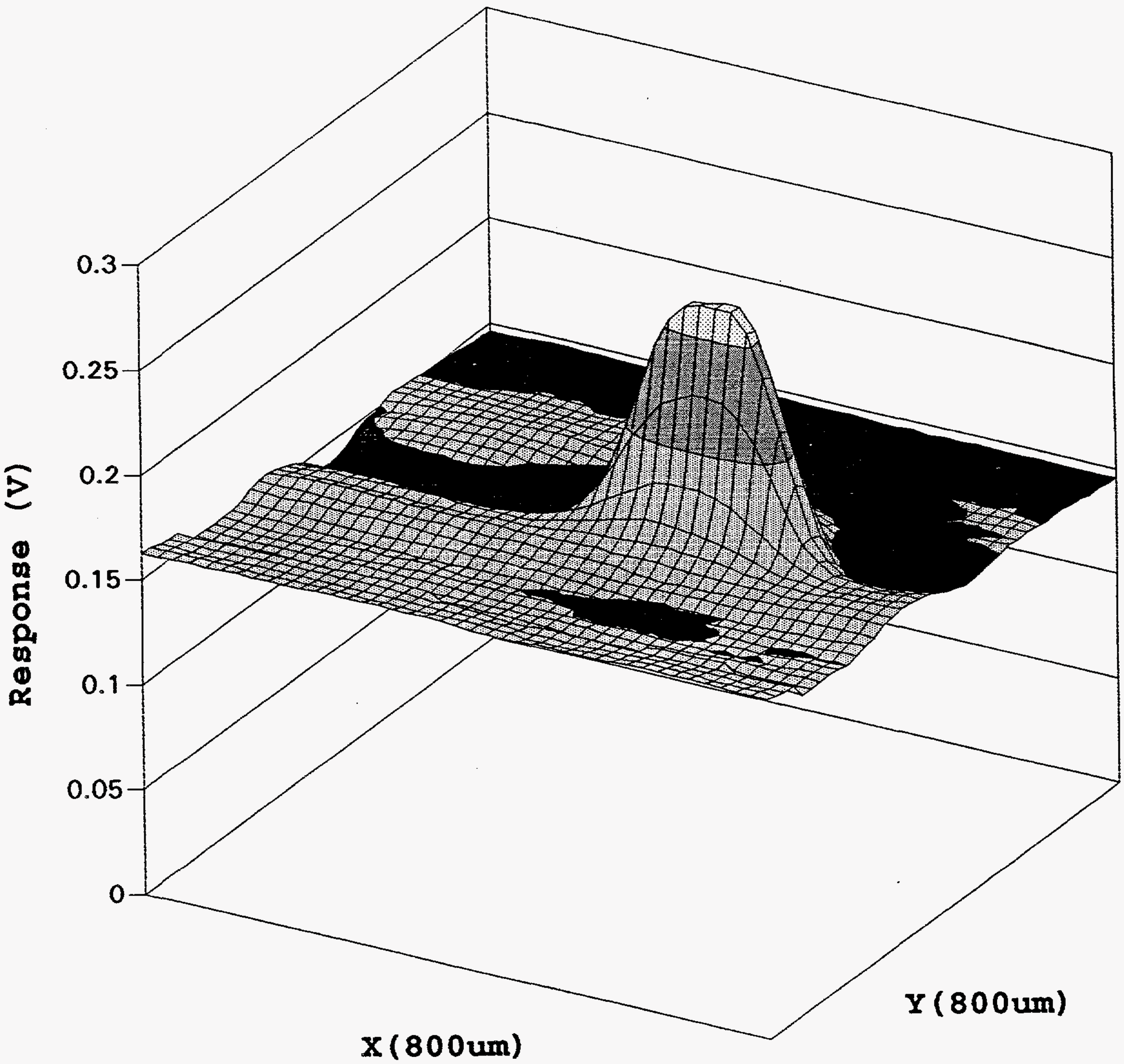

Synchrotron Source:	**I=120 m**
(Partially Absorbed Beam)	**E =8 KeV**
	I0=302
Slit Size:	**200(X) x 50(Y) µm**
CdTe Photoconductor:	**20 µm gap, 5 V**

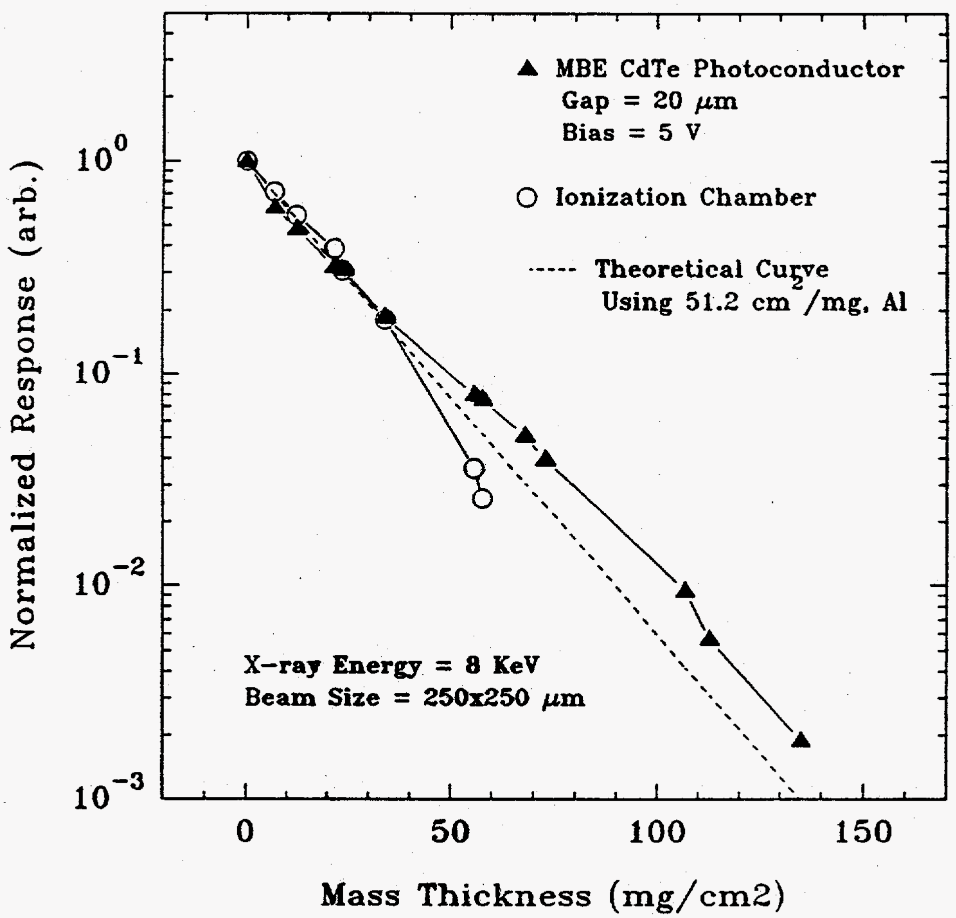

MBE CdTe Photoconductor
Gap = 20 μm
Bias = 5 V
Ionization Chamber
Theoretical Curve
Using 51.2 cm2/mg, Al
X-ray Energy = 8 KeV
Beam Size = 250x250 μm
Normalized Response (arb.)
Mass Thickness (mg/cm2)

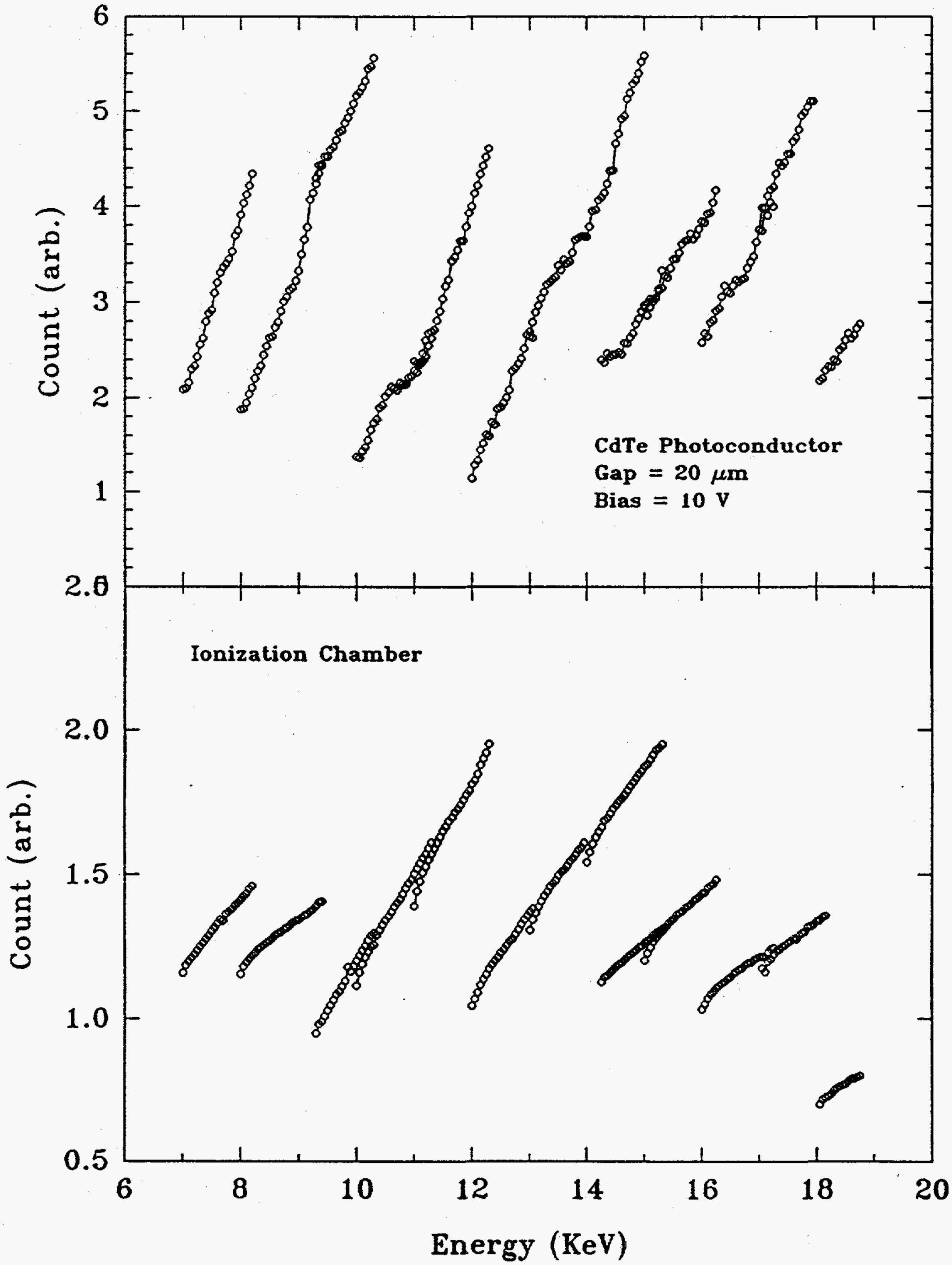
CdTe Photoconductor
Gap = 20 μm
Bias = 10 V
Ionization Chamber
Count (arb.)
Count (arb.)
Energy (KeV)
0
1
2
3
4
5
6
0.5
1.0
1.5
2.0
2.5
6
8
10
12
14
16
18
20

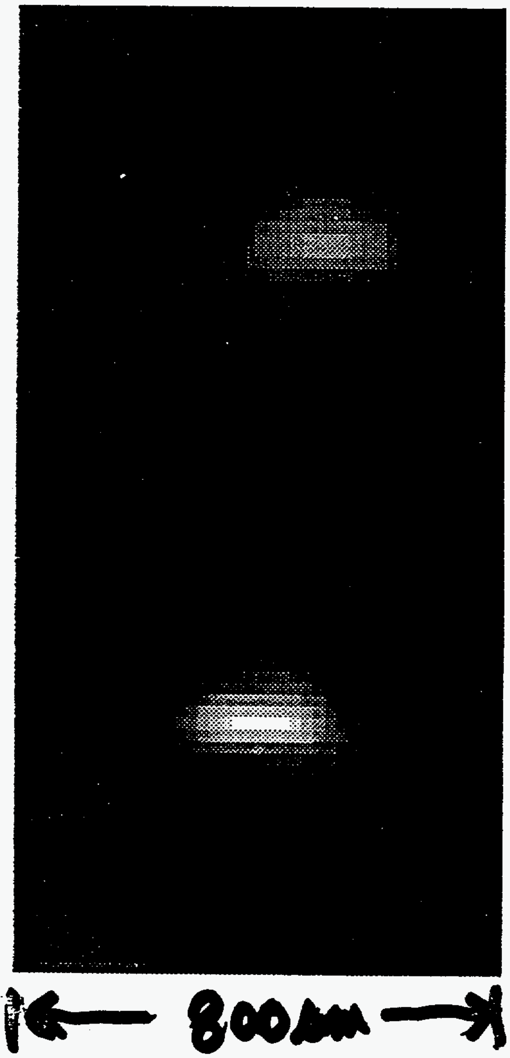
800 μm